Mathematical Problems in Engineering

Mathematical Modeling for Resources and Environmental Systems

Guest Editors: Y. P. Li, G. H. Huang, S. L. Nie, B. Chen, and X. S. Qin

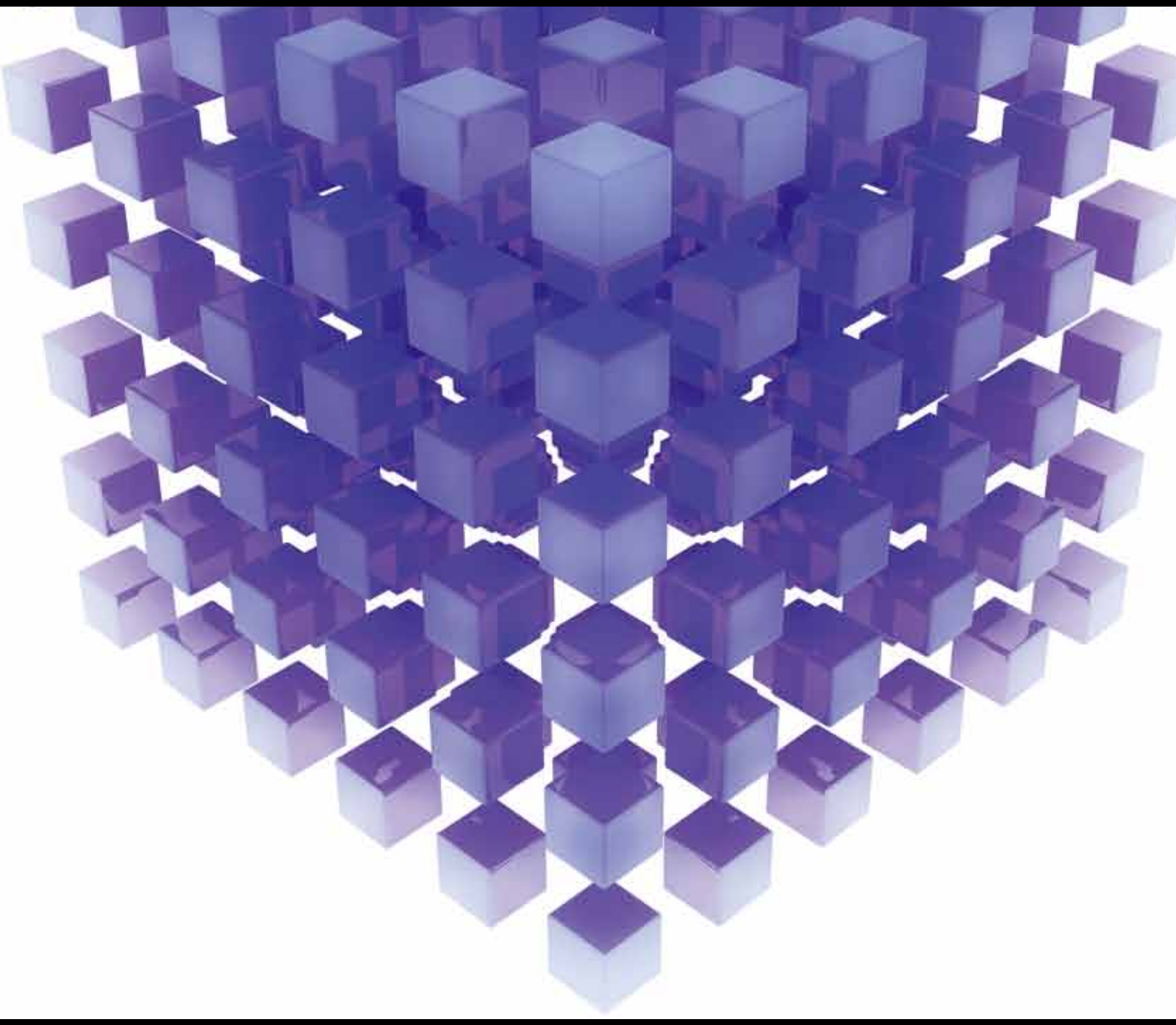

Mathematical Modeling for Resources and Environmental Systems

Mathematical Problems in Engineering

Mathematical Modeling for Resources and Environmental Systems

Guest Editors: Y. P. Li, G. H. Huang, S. L. Nie, B. Chen, and X. S. Qin

Editorial Board

Contents

Hindawi Publishing Corporation
Mathematical Problems in Engineering
Volume 2013, Article ID 674316, 4 pages
http://dx.doi.org/10.1155/2013/674316

Editorial

Mathematical Modeling for Resources and Environmental Systems

Y. P. Li,[1] G. H. Huang,[2] S. L. Nie,[3] B. Chen,[4] and X. S. Qin[5]

[1] *MOE Key Laboratory of Regional Energy Systems Optimization, S-C Resources and Environmental Research Academy, North China Electric Power University, Beijing 102206, China*
[2] *Environmental Systems Engineering Program, Faculty of Engineering and Applied Science, University of Regina, Regina, SK, Canada S4S 0A2*
[3] *College of Mechanical Engineering and Applied Electronics Technology, Beijing University of Technology, Beijing 100124, China*
[4] *Faculty of Engineering & Applied Science, Memorial University, St. John's, NL, Canada A1B 3X5*
[5] *School of Civil & Environment al Engineering, Nanyang Technological University, Blk N1-01c-82, 50 Nanyang Avnue, Singapore 639798*

Correspondence should be addressed to Y. P. Li; yongping.li@iseis.org

Received 28 October 2013; Accepted 28 October 2013

Effective management and planning of resources and environmental systems have been of concerns in the past decades since contamination and resource-scarcity problems have led to a variety of impacts and liabilities. However, achieving a reasonable and efficient management strategy is difficult since many conflicting factors have to be balanced due to complexities of the real-world problems. In resources and environmental systems, there are a number of factors that need to be considered by planners and decision-makers, such as social, economic, technical, legislational, institutional, and political issues, as well as environmental protection and resources conservation. Moreover, a variety of processes and activities are interrelated to each other, resulting in complicated systems with interactive, dynamic, nonlinear, multiobjective, multistage, multilayer, and uncertain features. These complexities may be further amplified due to their association with economic consequences if the promises of expected targets are violated. Mathematical models are recognized as effective tools that could help examine economic, environmental, and ecological impacts of alternative pollution-control and resources-conservation actions, and thus aid planners or decision-makers in formulating cost-effective management policies.

Therefore, to facilitate more robust management and planning of resources and environmental systems, innovative mathematical tools that are able to reflect various combinations of these complexities are desired. This special issue is devoted to provide a forum for facilitating discussions of emerging technologies for supporting decisions of resources and environmental management. It focuses on exposition of innovative methodologies for tackling challenges in modeling a variety of resources and environmental problems, as well as successful case studies. A number of state-of-the-art mathematical modeling studies related to resources and environmental systems are presented, which can help analyze the relevant information, simulate the related processes, implement pollutant mitigations, evaluate the resulting impacts, and generate sound decision alternatives.

The paper "*Experimental study and modeling of fouling in immersed membrane bioreactor operating in constant pressure filtration*" by M. Hosseinzadeh et al. proposed a new mathematical model to predict fouling in an airlift immersed membrane bioreactors. With experimental verification, the results showed that the ultimate filtration resistance and the initial rate of cake formation are more sensitive to the aeration rate at lower superficial velocities. It was also found that the ultimate filtration resistance has a linear relation with mixed liquor suspended solid (MLSS) concentration.

The paper "*Hydrological design of nonstationary flood extremes and durations in Wujiang River, south china: changing properties, causes, and impacts*" by X. H. Chen et al. analyzed the flood duration frequency (QDF) using annual maximum streamflow series of 1–10-day durations observed at Pingshi and Lishi stations in Wujiang River, southern China. The trends and change point of annual maximum flood flow and flood duration were also investigated by statistical tests. The results indicated that the annual maximum flood flow has a marginally increase trend, whereas the flood duration exhibits a significant decrease trend at the 0.10 significant level. A nonstationary frequency analysis taking account of change point in the data series is highly recommended for future studies.

The paper "*Application of MM5-CAMx-PSAT modeling approach for investigating emission source contribution to atmospheric SO_2 pollution in Tangshan, northern China*" by L. Li et al. introduced an integrated MM5-CMAx-PSAT modeling approach to identify the variation of emission contribution from each modeling grid to regional and urban air quality per unit emission rate change. The method was applied to a case study in Tangshan, a typical industrial region in northern China. Principal component analysis, canonical correlation analysis, and Pearson correlation analysis indicated that there was an obvious negative correlation between the grid-based variation of emission contribution to regional air quality and planetary boundary layer height as well as wind speed, while terrain data presented insignificant impacts on emission contribution variation.

The paper "*Numerical solution of advection-diffusion equation using a sixth-order compact finite difference method*" by G. Gurarslan et al. conducted a study to produce numerical solutions of one-dimensional advection-diffusion equation using a sixth-order compact difference scheme in space and a fourth-order Runge-Kutta scheme in time. The suggested scheme was a very accurate and relatively flexible solution approach in solving the contaminant transport equation for $Pe \leq 5$. The accuracy and validity of the numerical model were verified through the presented results and the literature. The computed results showed that the use of the current method in the simulation is very applicable for the solution of the advection-diffusion equation.

The paper "*Numerical study on initial field of pollution in the Bohai Sea with an adjoint method*" by C. H. Wang et al. introduced a marine ecosystem dynamical model to simulate the dispersion process of the pollution in the Bohai Sea, where routine monitoring data were assimilated to study the initial field of pollution by using the adjoint method. The model could help reduce the misfit between inversion results and observations significantly and make the simulated results closer to reality. The results illustrated that the adjoint method can make use of the existing observations to the maximum extent, where not only the values and locations of the observations but also the sampling time can be taken into consideration.

The paper "*Simulation of multiphase flow of the oil-water separation in a rotating packed bed for oil purification*" by X. J. Zhang et al. investigated the optimal operating conditions and configurations on the hydraulic performance of rotating packed bed (RPB). The operating conditions and configuration on the hydraulic performance of the RPB are investigated. The results indicated that the separation efficiency of high gravity rotary device rotating oil purifier is affected by the configuration, especially the layout of liquid inlet, oil outlet, and water outlet in the RPB. The mathematical models used in the study could contribute to a better understanding of the hydraulic characteristics of the RPB with the fast development of the computer technology.

The paper "*Modified palmer drought severity index based on distributed hydrological simulation*" by D. H. Yan et al. modified the Palmer drought severity index (PDSI) based on a distributed hydrological model for Luanhe River basin, North China. The proposed method could not only reflect the spatial heterogeneity of regional drought and improve the physical mechanism of PDSI but also provide technical support for comprehensive understanding of drought and effective preventing and relieving of drought disasters.

The paper "*Effect of land use and climate change on runoff in the Dongjiang basin of south china*" by Y. H. He et al. identified the quantitative impacts of land use and climate change on the runoff through soil conservation service (SCS) monthly model. With the real case study for four subbasins in the Dongjiang basin of south China, their results disclosed that approximately 20~30% runoff change was contributed by land-use modification. Besides, the effect of climate change on runoff variation had a different inner-annual distribution even under same annual precipitation.

The paper "*Guidance of autonomous amphibious vehicles for flood rescue support*" by S. Ragi et al. advanced a path-planning algorithm to guide autonomous amphibious vehicles (AAVs) for flood rescue support missions. An approximation method called nominal belief-state optimization (NBO) was proposed for solving the partially observable Markov decision process (POMDP) problems. Results showed that the NBO technique outperforms the greedy approach significantly.

The paper "*Nonsmooth dynamic behaviors inherited from an ecohydrological model: mutation, bifurcation, and chaos*" by M. Lin et al. advanced an ecohydrological model with the pulsed atmospheric forcing to analyze the nontrivial dynamic behaviors in a coupled ecohydrological system qualitatively and numerically. The developed mathematical model could help identify existence of multiple stationary states, study parameter bifurcation, and obtain the chaotic characteristic of the system state under some specific parameters.

The paper "*Analysis of variation trends in precipitation in an upstream catchment of Huai River*" by P. Shi et al. analyzed the variation trends in precipitation based on the linear regression method and Mann-Kendall test. With real application in Shaying River catchment, the upstream of the Huai River, China, the results suggested that the changing trends in precipitation for different time series in the whole catchment were relatively complex and not obvious. The annual precipitation series showed positive trends in the northern region and negative trends in the southern region.

The paper "*Detecting abrupt change of streamflow at Lintong station of Wei River*" by J. J. Fan et al. introduced two methods of moving approximate entropy and moving

permutation entropy to analyze the abrupt year of the daily river runoff at Lintong station of Wei River in Loess Plateau, China. With the analysis of hydrological characters of different stages, the result showed that the proposed methods are useful for analyzing runoff series and identifying points of abrupt change. The results also disclosed that the attribution of abrupt change at the Lintong runoff series was primarily due to a number of factors such as reduced precipitation, increased water-conservancy project, boosted water consumption, decreased groundwater table, and raised evaporation.

The paper "*A sustainability-oriented multiobjective optimization model for siting and sizing distributed generation plants in distribution systems*" by G. Chen et al. proposed a multiobjective optimization model for siting and sizing distributed generation plants in distribution systems. With numerical study based on the modified IEEE 33-node system, the results indicated that benefits for environmental sustainability of using DG plants can be effectively reflected by the proposed model, which helps the planner to make rational decision towards sustainable development of the distribution system.

The paper "*A model for urban environment and resource planning based on green GDP accounting system*" by L. Y. Xu et al. proposed a model to identify the key factors in urban environment and resources regulation based on a green GDP accounting system. With real application in the City of Wuyishan, China, the results showed that energy use was a key factor that influenced the urban environment and resources development. It was also found that biodiversity and air quality were the most sensitive factors that influenced the value of green GDP in the study city. The proposed model is helpful for decision-makers in improving the urban environment and resources planning and promoting sustainable development.

Although many simulation and optimization models are developed for management and planning of resources and environmental systems, it is still difficult for decision-makers to gain an in-depth insight into the tradeoffs when uncertainties exist in many system components and their interrelationships. There are many sources of uncertainty in modelling resources and environmental systems due to complexities in parameter estimation, data availability, and model structure. In detail, uncertainties may be derived from random feature of many related natural processes as well as errors in estimated modeling parameters; uncertainties can also arise due to human-induced imprecision or fuzziness, such as lack of available data and biased judgment (or preferences) in assigning priority factors (weighting levels) to multiple management objectives. Moreover, uncertainties may exist in multiple levels: vagueness and/or impreciseness in the outcomes of a random sample and randomness and/or fuzziness in the lower and upper bounds of an interval. The various uncertainties that exist in real-world resources and environmental systems have essentially placed them beyond the conventional mathematical methods. Thus, simulation and optimization methodologies that can reflect uncertainties are desired for enhancing applicability of the modeling efforts.

The paper "*A hybrid stochastic-interval analytic hierarchy process approach for prioritizing the strategies of reusing treated wastewater*" by L. Jing et al. proposed a hybrid stochastic-interval analytic hierarchy process (SIAHP) approach for prioritizing the strategies of reusing treated wastewater. SIAHP can address uncertainty in group decision making by integrating interval judgment, probabilistic distribution, lexicographic goal programming, and Monte Carlo simulation. A case study related to wastewater treatment plant effluent reuse was conducted to demonstrate that the SIAHP approach can aid group decision making by accommodating linguistic information and dealing with insufficient information or biased opinions.

The paper "*Modelling snowmelt runoff under climate change scenarios in an ungauged mountainous watershed, northwest China*" by Y. G. Ma et al. introduced an integrated modeling system for analyzing the impact of climate change on snowmelt runoff in Kaidu Watershed, Northwest China. The system coupled Hadley Centre Coupled Model version 3 (HadCM3) outputs with snowmelt runoff model (SRM), where statistical downscaling model (SDSM) was used to downscale coarse outputs of HadCM3. Different scenarios were considered for analyzing the climate change impact on snowmelt flow in the Kaidu Watershed under uncertainty. The results indicated that watershed hydrology would alter under different climate change scenarios, which could provide useful decision support for water resources management in the arid region.

The paper "*Generalized likelihood uncertainty estimation method in uncertainty analysis of numerical eutrophication models: take BLOOM as an example*" by Z. J. Li et al. introduced an eutrophication and algal bloom model BLOOM for investigating the applicability of the GLUE method to quantify the uncertainty in numerical eutrophication models. The results demonstrated that GLUE is effective for uncertainty analysis of complex dynamic ecosystem models. The method was found to be able to provide a solid foundation for the use of the model predictions in decision making.

The paper "*An inventory-theory-based inexact multistage stochastic programming model for water resources management*" by M. Q. Suo et al. introduced one integrated optimization method to address multiple forms of uncertainties incorporating inventory theory within an inexact multistage stochastic programming framework. The developed method can not only handle uncertainties represented as probability density functions and discrete intervals but also reflect dynamic features of system conditions under different water flow levels within a multistage context. The model is helpful for decision-makers in seeking optimal water transfer schemes when they are facing tradeoff problems with high complexities.

The paper "*RSW-MCFP: a resource-oriented solid waste management system for a mixed rural-urban area through Monte Carlo simulation-based fuzzy programming*" by P. Li et al. introduced a resource-oriented solid waste management system for a mixed rural-urban area through Monte Carlo simulation-based fuzzy programming. The developed system was tested by a real-world case with consideration of various resource-oriented treatment technologies and the associated

uncertainties. The results indicated that the community-based biocoal and household-based CH_4 facilities are necessary and become predominant in the waste management system.

The paper "*Suitable environmental flow release criteria for both human and riverine ecosystems: accounting for the uncertainty of flows*" by J. Tang et al. proposed a new method to determine the optimal environmental flow (e-flow) release criteria under flow uncertainty accounting for both the human and riverine ecosystem needs. Scenario-tree analysis method was utilized to generate the possible scenarios of flows and the range of variability approach (RVA) was refined by incorporating the uncertain flows. With the real application to Tang River of northern China and comparison of the previous method, the results indicated that the advanced can get more suitable criteria that are suitable for both human and riverine ecosystems.

The paper "*Uncertainty assessment of hydrological frequency analysis using bootstrap method*" by Y.-M. Hu et al. put forward a bootstrap-based method to analyze the impact of sampling uncertainty on hydrological design value. Using bootstrap resampling technique, a large number of bootstrap samples were constructed from the original flood extreme observations; the corresponding design value or quantile was estimated for each bootstrap sample, such that the sampling distribution of design value was constructed; based on the sampling distribution, the uncertainty of quantile estimation could be quantified. Compared with the conventional deterministic approach, the proposed method improved the estimation and evaluated quantitatively the uncertainty of estimation for the design of hydraulic engineering works.

The paper "*Applying an extended fuzzy parametric approach to the problem of water allocations*" by T. Y. Xu and X. S. Qin advanced an extended fuzzy parametric programming (EFPP) model for planning water resources allocation problems under uncertainty. A numerical example and a water resources management case were used to demonstrate the applicability of the proposed method. The obtained results could assist decision-makers in understanding the balance between the system benefit and system-failure risk. By comparing with fuzzy chance-constrained programming model, EFPP could better reflect uncertainties and generate more optimal solutions and had a potential to be applied to the other environmental problems.

The paper "*Development of optimal water-resources management strategies for Kaidu-kongque watershed under multiple uncertainties*" by Y. Zhou et al. advanced an interval-stochastic fractile optimization (ISFO) model for supporting water resources management under coupled forms of probability and possibility. With real application in Kaidu-kongque watershed, China, the model was found to be able to help decision-makers alleviate the water supply-demand conflict and achieve better socioeconomic and ecological sustainability. The results suggested that this hybrid technique is effective and can be extended to other environmental problems that involve policy analysis and uncertainty reflection.

The paper "*Bilevel multiobjective programming applied to water resources allocation*" by S. Q. Fang et al. proposed a bilevel mutiobjective linear programming (BLMOLP) model for water resource allocation. Fuzzy goal programming approach was employed to minimize the group regret of degree of satisfactions for all decision-makers. The proposed method was also applied to a case study for water resources allocation in Wuwei Basin, China. Based on analysis of multiple scenarios, the model was found to be able to balance the benefits among all regions and sections according to the priority of the upper level decision-makers.

The paper "*An interval-parameter fuzzy linear programming with stochastic vertices model for water resources management under uncertainty*" by Y. Han et al. introduced an integrated optimization method for handling uncertainties presented as interval parameter with stochastic vertices in both of the objective functions and constraints. A hybrid intelligent algorithm based on genetic algorithm and artificial neural network was proposed to solve the formulated model. The developed method was applied to water resources allocation in Beijing, China. The results indicated that reasonable solutions were obtained, which could help water resources managers to not only make decisions of water allocation but also gain insight into the tradeoffs between environmental and economic objectives.

In summary, the effective mathematical models for managing resources and environmental systems are becoming one of the most important goals pursued by governments, industries, communities, and researchers. These 25 papers formulated a variety of mathematical models for supporting natural resources allocation, flooding prevention and control, environmental pollution control, ecological protection, and sustainable development improving, where a number of innovative perspectives and findings are advanced. These mathematical models can (i) describe complex environmental processes and interactions, characterize the spatial and temporal variations, and predict the fate and transport of the contaminants; (ii) assess potential risks existing in various resources-related activists and the associated socioeconomic and environmental impacts under a variety of system conditions; (iii) generate sound decision alternatives for generating desired policies that target on more effective resources and environmental management. This special issue reports the latest research results in mathematical modeling for resources and environmental systems.

Acknowledgment

We wish to extend our thanks to those who contributed to this issue.

Y. P. Li
G. H. Huang
S. L. Nie
B. Chen
X. S. Qin

Hindawi Publishing Corporation
Mathematical Problems in Engineering
Volume 2013, Article ID 685452, 8 pages
http://dx.doi.org/10.1155/2013/685452

Research Article

Dynamics of a Bioreactor with a Bacteria Piecewise-Linear Growth Model in a Methane-Producing Process

Luz A. Melo Varela,[1] Simeón Casanova Trujillo,[1] and Gerard Olivar Tost[2]

[1] *Departamento de Matemáticas y Estadística, Facultad de Ciencias Exactas y Naturales, Universidad Nacional de Colombia-Sede Manizales, Carrera 27 No. 64-60 Manizales, Caldas, Colombia*
[2] *Departamento de Ingeniería Eléctrica, Electrónica y Computación, Percepción y Control Inteligente-Bloque Q, Facultad de Ingeniería y Arquitectura, Universidad Nacional de Colombia-Sede Manizales, Bloque Q, Campus La Nubia, Manizales 170003, Colombia*

Correspondence should be addressed to Simeón Casanova Trujillo; scasanovat@unal.edu.co

Received 13 December 2012; Revised 20 August 2013; Accepted 4 October 2013

Academic Editor: Bing Chen

This paper shows a study, both analytical and numerical, of a continuous-time dynamical system associated with a simple model of a wastewater biorreactor. Nonsmooth phenomena and border-collision local bifurcations appear when the main parameters (dilution and biomass concentration at the inflow) are varied. We apply the Filippov methods following Kuznetsov's work.

1. Introduction

Currently, anaerobic methods are applied to reduce water contamination problems. With these methods, we can reduce the percentages of chemical oxygen demand (COD) and biological oxygen demand (BOD), which are measurements of water quality. Depuration through anaerobic treatments converts organic matter in wastewater into methane (CH_4—biogas) and carbonic gas (CO_2). Methane can be used as an energetic component because it offers good calorific power, and CO_2 can be recirculated to the bioreactor to improve the percentages of biogas yield, thus decreasing organic loads. Organic loads contain high concentrations of organic matter that originates from water circulation in garbage, which dissolves the elements present in it when running through the waste. The result is an environmentally damaging liquid that contaminates the soil and superficial and subterranean waters in their path. For this reason, leachates, among others, are one of the most significant contaminating agents in a landfill as has been extensively discussed in the literature (see, e.g., [1–3]).

In this paper, we are mainly interested in leachates since our experimental secondary data comes from this sort of wastewaters. The most used systems for leachate treatment are the so-called high-rate systems, such as the UASB reactor (Figure 1). This bioreactor separates different phases: biological (sludge bed), liquid (sludge blanket), and gas (upper section). The wastewater enters the reactor through its lower section and exits through the upper section. The reactor has no filling to support biological growth. The sludge created in the reactor can be divided into two regions: region one, the sludge bed, and region two, the sludge blanket, which is composed of granules or particles in addition to the wastewater, as discussed in [4–6].

The upper section of the reactor contains the solid-liquid-gas (SLG) separator, which prevents the discharge of solids from the reactor and separates them from the produced gas and effluent liquid. This section acts as a sludge sedimenter and gas collector because the gases produced under anaerobic conditions cause internal recirculation, which helps in the creation and sustainment of bacteria. The upper piece (so-called screen) generates a low-turbulence region, where 99% of the sludge in the suspension settles and returns to the reactor. The screen also serves to recover the gas that exits through the center region, as discussed by Kjeldsen et al. [5]. Therefore the SLG separator is fundamental in order to maintain settled sludge, a clarified effluent (gas-free), and properly separated gases.

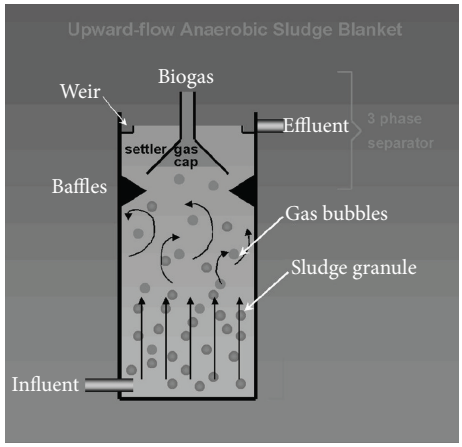

Figure 1: UASB reactor.

Anaerobic leachates depuration uses a combination of several processes. One of the most important is the so-called anaerobic digestion, which is a fermentation of organic matter. This is performed by bacteria when oxygen is not present. Fermentation subproducts are a mixture of gases (mainly CO_2 and CH_4, biogas) and also some biomass, which is kept in the process. Anaerobic digestion can be applied to leachates from cattle, forest and agroindustry, and disposal from transformation industries, either one by one, or together (codigestion). The method reported in the paper could be applied not only to leachates but also to a methanisation process that treats glucose or acetate residues.

Many mathematical models for bioreactors have been obtained and there is a hugh literature on this topic (see e.g., [7–9]). Also, control of an anaerobic digester through normal form of smooth fold bifurcation has been implemented. This method has faster convergence rate and lower error than traditional methods. The idea is designing a nonlinear controller taking advantage of the knowledge of the bifurcation scenario [10]. Thus bifurcation diagrams and analytical results are important for a good design and control.

In this paper we take real data from the leachates in "Esmeralda" landfill, which is located in Manizales (Caldas), a medium-size city in Colombia. Numerical simulations were carried out with standard procedures in MATLAB.

The rest of the paper is organized as follows. Section 2 is devoted to an overview of Filippov and Kuznetsov theory on nonsmooth systems and nonsmooth bifurcations. This theory will be applied to our model. In Section 3 we describe the model mathematically and we perform some basic algebraic computations following nonsmooth theory. Results are shown in Section 4, and they are compared with analytical computations. Also, nonsmooth bifurcations are reported. Finally, conclusions are stated in Section 5.

2. An Overview of Filippov Systems

Nonsmooth systems (continuous piecewise-linear, continuous piecewise-smooth, discontinuous piecewise-smooth, and so on) have been studied in the literature [11–14].

Through theory mainly developed by Filippov we can determine the solution of a system ruled by differential equations with discontinuous terms on the right-hand side. According to this method (Filippov method), the borders of all state-velocity vectors within the region of a point on a discontinuous surface must be complemented by a minimum convex set, and the state-velocity vector of the sliding motion must belong to this set, as discussed in [11].

For a dynamical system in the state-space where Filippov method can be applied, and assuming only two regions separated by the discontinuity, we can write

$$\dot{z} = \begin{cases} F^{(1)}(z), & z \in R_1, \\ F^{(2)}(z), & z \in R_2, \end{cases} \tag{1}$$

where

$$\begin{aligned} R_1 &= \left\{ z \in \mathbb{R}^2 : H(z) < 0 \right\}, \\ R_2 &= \left\{ z \in \mathbb{R}^2 : H(z) < 0 \right\}. \end{aligned} \tag{2}$$

The discontinuity boundary Σ separates the two regions R_1 and R_2 and is given by

$$\Sigma = \left\{ z \in \mathbb{R}^2 : H(z) = 0 \right\}, \tag{3}$$

where $H(z)$ is a smooth scalar function with a nonzero gradient over Σ. The boundary Σ is a closed set, and we must have that $F^{(1)} \neq F^{(2)}$ over Σ.

2.1. Sliding Solutions. Following [11], for $z \in \Sigma$, we define

$$\sigma(z) = \left\langle H_z(z), F^{(1)}(z) \right\rangle \left\langle H_z(z), F^{(2)}(z) \right\rangle, \tag{4}$$

where $\langle , \rangle$ denotes the standard scalar product, and $\sigma(z)$ defines the crossing or sliding region. The crossing set $\Sigma_c \subset \Sigma$ is defined by

$$\Sigma_c = \{ z \in \Sigma : \sigma(z) > 0 \} \tag{5}$$

which corresponds to the set of all points $z \in \Sigma$, where the two vectors $F^{(i)}(z)$ have nontrivial normal components of identical sign.

We also have the sliding set Σ_s, which complements Σ_c in Σ:

$$\Sigma_s = \{ z \in \Sigma : \sigma(z) \leq 0 \}. \tag{6}$$

The crossing set is open, whereas the sliding set is the union of the sliding closed segments and sliding isolated points.

The Filippov method associates the following convex combination $g(z)$ of the two fields $F^{(i)}(z)$ for each nonsingular sliding point $z \in \Sigma$, where $g(z)$ is the so-called the Filippov vector field [11]:

$$g(z) = \lambda F^{(1)}(z) + (1 - \lambda) F^{(2)}(z), \tag{7}$$

where $\lambda = \langle H_z(z), F^{(2)}(z) \rangle / \langle H_z(z), F^{(2)}(z) - F^{(1)}(z) \rangle$.

3. Bioreactor Mathematical Model

We used the model proposed by Muñoz (2006) [15] for anaerobic digestion in a UASB reactor, but an approximation by straight lines to the bacterial growth model is applied (Monod kinetics). The system, originally smooth, is converted into a nonsmooth one because it is modeled by a system of differential equations with a discontinuous right-hand side. For this approximation method by straight lines, only substrate concentrations from 0 to 6000 (mg/L COD) have been considered. This is because, in addition to achieving a good approximation, the values only have physical sense in this region and are consistent with the design conditions of the UASB bioreactor.

The assumptions in the model include that the operation temperature is 20°C, the constants in the model are those observed by Muñoz (2006) [15] $K_s = 5522.3$, (mg/L), $\mu_{\max} = 1.32\,\mathrm{d}^{-1}$, $Y = 3.35$, (mg COD/mg VSS), and acidogenesis and metanogenesis are considered to be the only processes governed by Monod kinetics, which assumes that the bacterial growth follows Michaelis-Menten kinetics for processes catalyzed by enzymes. Therefore,

$$\mu(S) = \mu_{\max}\frac{S}{K_s + S}, \tag{8}$$

where K_s is the substrate semisaturation constant.

According to this model, for the discussed biological process, the rate of microbial growth will asymptotically tend to the maximum value $\mu_{\max}$.

Accounting for the above, the proposed model is

$$\begin{aligned}\dot{S} &= D\left(S^{\mathrm{in}} - S\right) - Y\mu(S)X,\\ \dot{X} &= D\left(X^{\mathrm{in}} - (1-\eta)X\right) + \mu(S)X,\end{aligned} \tag{9}$$

where η is the SLG separator efficiency (and thus $\alpha = 1 - \eta$), D is the dilution factor (in d^{-1}) and represents the influent volumetric flow per unit of reactor volume (the inverse of the hydraulic retention time). S^{in} is the substrate concentration in the input flow (in mg/L COD); S is the substrate concentration in the reactor (in mg/L COD); Y is the substrate yield coefficient (in mg COD/mg VSS); $\mu(S)$ is the bacterial growth model; X is the biomass concentration in the reactor (in mg/L VSS); X^{in} is the biomass concentration in the input flow (in mg/L VSS); and η is the sedimentation efficiency of the separator (SLG).

We slightly modify this model by using an approximation to $\mu(S)$ by straight lines so that the originally smooth system is converted to a nonsmooth one. We take this approach after observing the experimental data in [15], which resembles much more to piecewise-linear than to a classical smooth Monod model. Zero is the minimum value for S (physically, negative concentrations cannot be observed) and 6000 [in mg/L COD] is the maximum (the maximum substrate concentration value at the input flow based on the operation conditions) [15].

Figure 2 corresponds to a continuous piecewise-linear approximation, but we will also consider discontinuous piecewise-linear approximations, taking into account the observed data in [15], as slight perturbations to the continuous one.

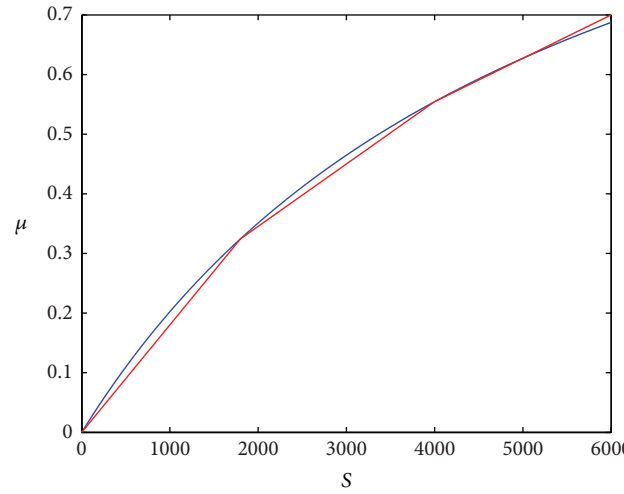

Figure 2: Piecewise-linear continuous approximation of Monod growth model. Nonsmooth points correspond to $S_1 = 1800$ and $S_2 = 4000$.

Thus we will consider $0 < p_1 < p_2$ as parameters, defining the nonsmooth discontinuous approximation $\overline{\mu}(S)$ to the Monod curve.

We have

$$\begin{aligned}\overline{\mu}(S) &= \frac{\mu_1}{S_1}S, \quad \text{for } 0 \le S < p_1,\\ \overline{\mu}(S) &= \mu_1 + \frac{\mu_2 - \mu_1}{S_2 - S_1}(S - S_1), \quad \text{for } p_1 \le S < p_2,\\ \overline{\mu}(S) &= \mu_2 + \frac{\mu_3 - \mu_2}{S_3 - S_2}(S - S_2), \quad \text{for } S \ge p_2,\end{aligned} \tag{10}$$

and thus the final proposed model is the following:

$$\begin{aligned}\dot{S} &= D\left(S^{\mathrm{in}} - S\right) - Y\overline{\mu}(S)X,\\ \dot{X} &= D\left(X^{\mathrm{in}} - (1-\eta)X\right) + \overline{\mu}(S)X,\end{aligned} \tag{11}$$

where $\alpha = 1 - \eta$ corresponds to the SLG separator deficiency, and η is the SLG separator efficiency, $\mu_1 = 0.32$, $S_1 = 1800$, $\mu_2 = 0.5544$, $S_2 = 4000$, $\mu_3 = 0.7$, and $S_3 = 6000$.

Each region is ruled by a system of differential equations, which can be discontinuous in the border of each region. When $p_1 = p_1^* = 1800$, $p_2 = p_2^* = 4000$, and $p_3 = p_3^* = 6000$, corresponding to the continuous piecewise-linear approximation of the Monod curve, our system of differential equations is piecewise-continuous, and thus no sliding regions are possible. But when parameters p_i slightly vary from the corresponding nominal values p_i^*, then the differential equations have discontinuous right-hand side, and Filippov methods can be applied.

However, only analyses of regions corresponding to mode one ($0 \le S < p_1$) and mode two ($p_1 < S < p_2$) were performed since these are the regions where a physically possible dynamic was observed when representing the positive

equilibrium points. Thus, equations to be analyzed are (11) in modes one and two.

In our case, $H(z) = S - p_1$, and when this is zero, the sliding region will be included in $S = p_1$.

The gradient for $H(z)$ is given by $\nabla H_z(z) = (0, 1)$, which is constant and different from zero for each $z \in \Sigma$.

When applying the Filippov method, following [11], we can distinguish some critical points.

Singular points are $z \in \Sigma_s$ such that

$$\left\langle H_z(z), F^{(1)}(z) - F^{(2)}(z) = 0 \right\rangle. \tag{12}$$

Pseudoequilibriums are $z \in \Sigma_s$ such that

$$g(z) = 0, \qquad F^{1,2}(z) \neq 0. \tag{13}$$

Boundary equilibriums are $z \in \Sigma_s$ such that

$$F^{(1)}(z) = 0, \qquad F^{(2)}(z) = 0. \tag{14}$$

Tangent points are $z \in \Sigma_s$ such that

$$\langle H_z(z), F^{(i)}(z) \rangle = 0, \qquad F^{1,2}(z) \neq 0. \tag{15}$$

From now on, we will be interested in the case of discontinuous piecewise-linear approximations, leading to the Filippov solutions.

3.1. Algebraic Computations. Boundary-node nonsmooth bifurcations were observed in this model, which are obtained when a node approaches the switching surface and collides with a pseudoequilibrium. This is considered a local bifurcation.

We consider again the two vector fields:

$$F^{(1)} = \begin{cases} D\left(X^{\text{in}} - \alpha X\right) + ASX \\ D\left(S^{\text{in}} - S\right) - YASX \end{cases}$$

$$F^{(2)} = \begin{cases} D\left(X^{\text{in}} - \alpha X\right) + \left[\mu_1 + B\left(S - S_1\right)\right] X \\ D\left(S^{\text{in}} - S\right) - Y\left[\mu_1 + B\left(S - S_1\right)\right] X, \end{cases} \tag{16}$$

where $A = \mu_1/S_1$ and $B = (\mu_2 - \mu_1)/(S_2 - S_1)$.

Some basic algebraic computations can be performed for this system and obtain the Filippov vector field. Then, for example, in order to obtain the pseudoequilibriums we have to impose

$$\begin{aligned} &\left(D\left(S^{\text{in}} - S\right) - YX\left[\mu_1 + B\left(S - S_1\right)\right]\right) \\ &\quad \times \left(D\left(X^{\text{in}} - \alpha X\right) + ASX\right) - \left(D\left(S^{\text{in}} - S\right) - YASX\right) \\ &\quad \times \left(D\left(X^{\text{in}} - \alpha X\right) + \left[\mu_1 + B\left(S - S_1\right)\right] X\right) = 0. \end{aligned} \tag{17}$$

Then we have

$$\begin{aligned} &X^2\left(YmD\alpha - YASD\alpha\right) \\ &\quad + X\left(DASK - YmDX^{\text{in}} - DmK + Y\text{ASD}\,X^{\text{in}}\right) = 0, \end{aligned} \tag{18}$$

where $m = \mu_1 + B(S - S_1)$, $K = S^{\text{in}} - S$.

Solutions to (18) correspond to pseudoequilibriums.

4. Results

We analyse the system given by (11), when the bacterial concentration in the input flow of the bioreactor, X^{in}, is varied to be 0, 240, and 320 (in mg/L VSS). Note that since the source was a leachate, the value of X^{in} is always different from zero, but $X^{\text{in}} = 0$ must be considered because bioreactor wash out can occur. The axis variables in the figures are S (the concentration of the substrate in the reactor) (in mg/L COD) and X (the concentration of the biomass in the reactor) (in mg/L VSS).

In the following, we plot a series of figures that resulted from the analytical calculations for the critical points, including equilibrium points, pseudoequilibriums, tangent points, and singular sliding points, which served as references for the numerical analysis.

Only figures corresponding to $X^{\text{in}} = 240$ were used (the average value of bacterial input in the bioreactor input flow, obtained by Muñoz (2006) [15], in its experimental part), since a similar behavior was observed for the other values.

Parameter α seems to be very important since a boundary-node bifurcation occurred when α is varied from 0.15 to 0.18 when $X^{\text{in}} = 0$ or when α changes from 0.19 to 0.24 for $X^{\text{in}} = 240$ and when α also changes from 0.24 to 0.27, for $X^{\text{in}} = 320$. This shows that the higher the biomass amount at the bioreactor input, the lower the sedimentation efficiency of the SLG separator. This lower efficiency blocks a good, previously stabilized sludge recirculation, which affects the bacterial performance and presents sludge mixture with the treated effluent.

When increasing the bacterial concentration at the bioreactor input, it is also expected that there will be different types of generated bacteria. This is due to the effluent coming from the landfill, other reactions, or the presence of toxic substances that avoid the proper functioning of the bioreactor.

4.1. Bifurcations with Parameter α. Figures 3(a)–3(d) show the analytical results obtained from the algebraic computations. An input flow biomass concentration of 240 (in mg/L VSS) was chosen. The system evolution shows how the equilibrium in region one was moved towards the switching boundary, approaching a collision. This results in a boundary-node bifurcation. However, the pseudoequilibrium also moved within the sliding segment between the tangent points and finally disappears when it collides with the left tangent point.

Figures 4(a)–4(e) show the system evolution when applying the Filippov convex method through numerical simulations. A change in the phase portrait is presented when parameter α is varied, keeping $X^{\text{in}} = 240$ (in mg/L VSS). Figure 4(b) shows that when α had a value of 0.203, the birth of a pseudo-equilibrium was observed in the sliding segment, and there was a node in the upper region. When the value of α was close to 0.23 (Figure 4(d)), the equilibrium in the lower region approached the switching surface and a collision of this equilibrium subsequently occurred. This process is similar to the one described before, generating a boundary-node bifurcation.

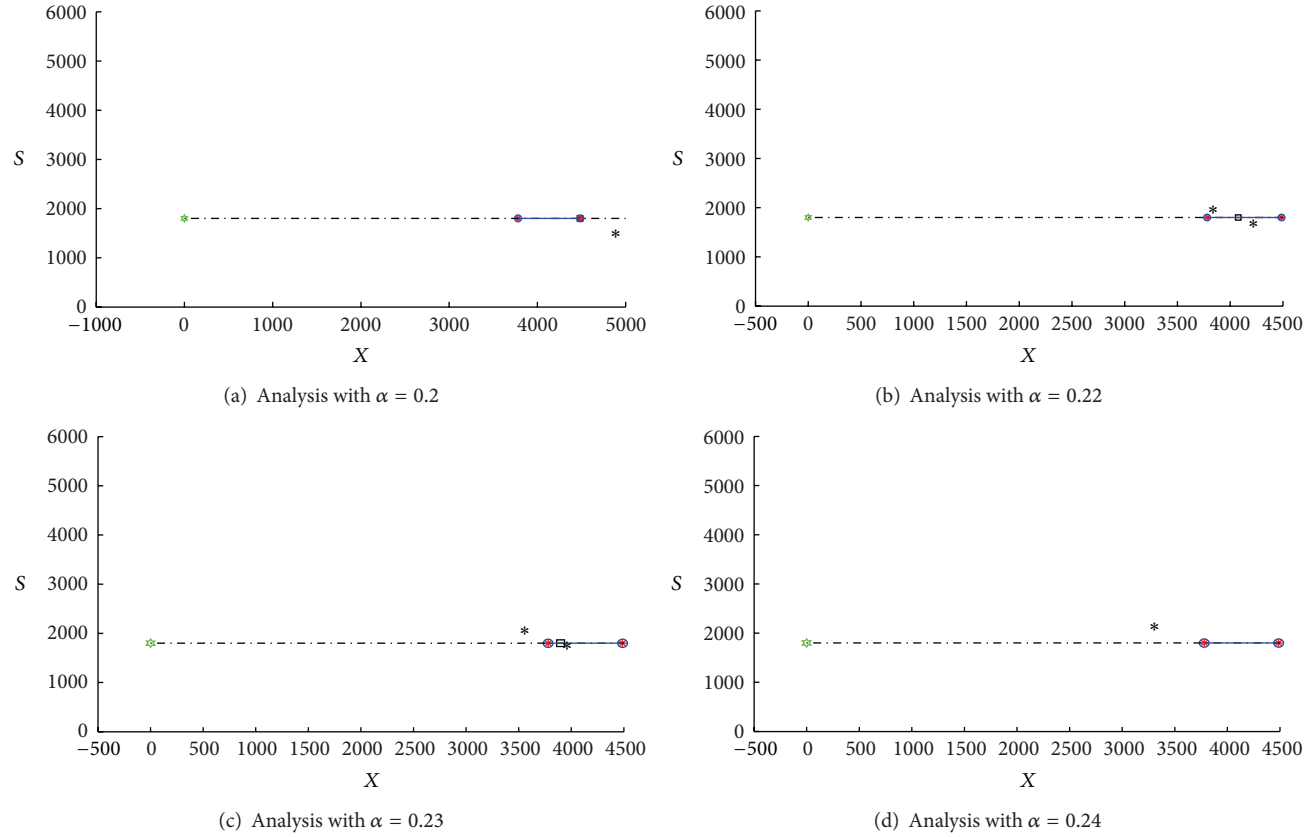

FIGURE 3: Algebraic computations when parameter α is varied. Equilibriums in *. Pseudoequilibriums in black square. Boundary points in red *. Tangent points in blue $^\circ$. Singular points in green star.

Therefore, when increasing the value of X^{in}, the α value for which the boundary-node bifurcation occurred also increased. This result shows that the SLG separator efficiency is inversely related to the type of water treated, since, at higher bacterial concentrations in the effluent, the SLG sedimenter is less efficient. This fact allows a good organic matter conversion into methane because the suspended sludge does not return to the reactor when a deficient sedimentation occurs, which affects biogas production.

4.2. Bifurcations with Parameter D. Bioreactor analysis when varying parameter D was also performed for input flow biomass concentrations X^{in} with 0, 240, and 320. For 240 and 320 (in mg/L VSS), it was observed that no interesting dynamics were present. However, richer dynamics were obtained for $X^{\text{in}} = 0$ (in mg/L VSS) (Figures 5(a) to 5(e)), where only one stable node exists in the lower region. When increasing parameter D from 2.0 to 2.45, a pseudo-equilibrium is created in the sliding segment, and when D is incresed further, another node appears in the upper region. When D approached 2.40, the equilibrium in the lower region approached the switching surface. Subsequently, a collision of the equilibrium point occurred within this boundary, which led to its catastrophic disappearance.

Basins of attraction can also be computed. For example, for $D = 2.1$ and $X^{\text{in}} = 0$ (shown in Figure 6), we observed that the pseudo-equilibrium only attracted the initial points that were in the switching surface, which was also recognized as an unstable sliding segment. The equilibriums within both regions are attractors.

A comparison between numerically and algebraically computed pseudo-equilibriums and the corresponding bifurcations was performed. Error rates were less than 0.02%.

5. Conclusions

When applying the Filippov convex method to a UASB, nonsmooth local boundary-node bifurcations with washout conditions in the reactor were shown. These bifurcations occur when parameter D or α is varied. When increasing the input biomass concentration, parameter α tends to increase the bioreactor inefficiency. This is due to the fact that it had more biomass in the input flow. Predator organisms, such as anaerobic ciliates or chemical products that generate biomass death in the reactor, can exist. In this case the leachates are not properly transformed into biogas. The comparison between the analytical section (algebraically computed from the Filippov vector field) and the numerical approximation yields an error close to 0.02%, which validates the performed calculations. The importance of parameter α was observed in the operation of the UASB bioreactor because the boundary-node bifurcation was present regardless of the biomass

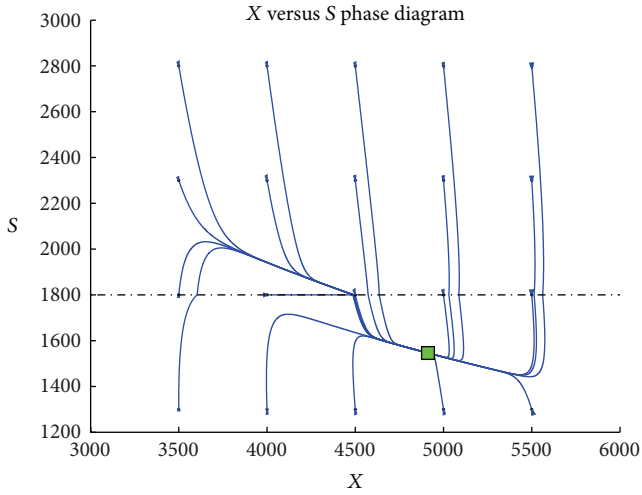

(a) Numerical computation with $\alpha = 0.198$

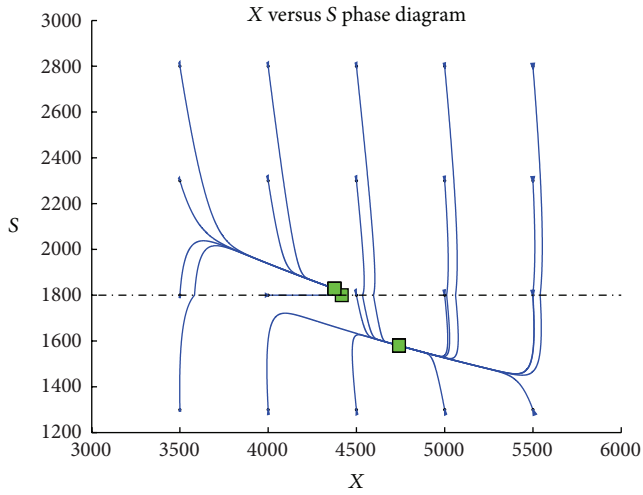

(b) Numerical computation with $\alpha = 0.203$

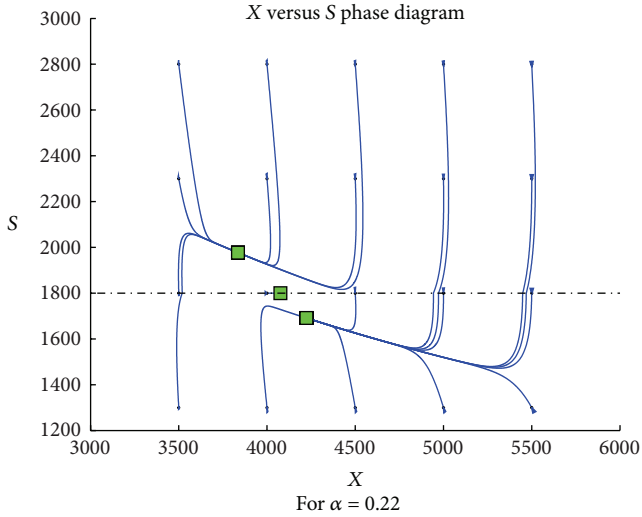

(c) Numerical computation with $\alpha = 0.22$

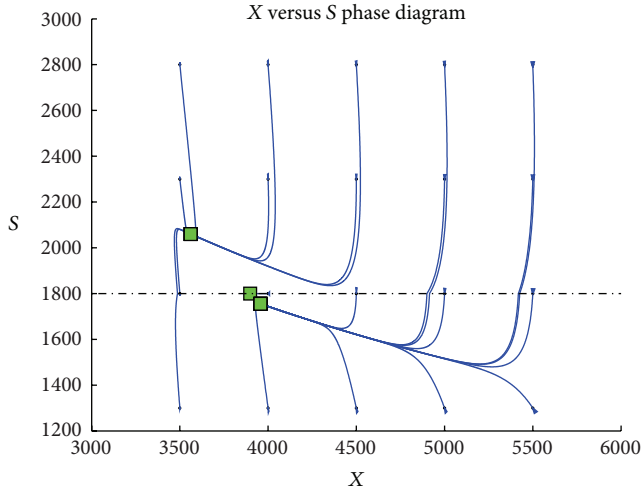

(d) Numerical analysis with $\alpha = 0.23$

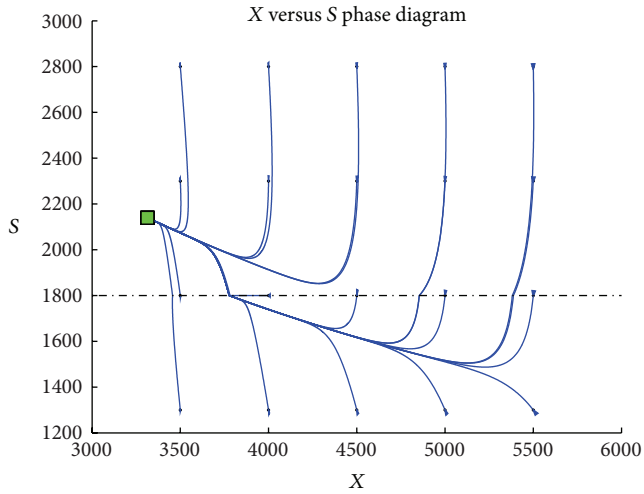

(e) Numerical computation with $\alpha = 0.24$

Figure 4: Numerically computed phase portraits when parameter α is varied.

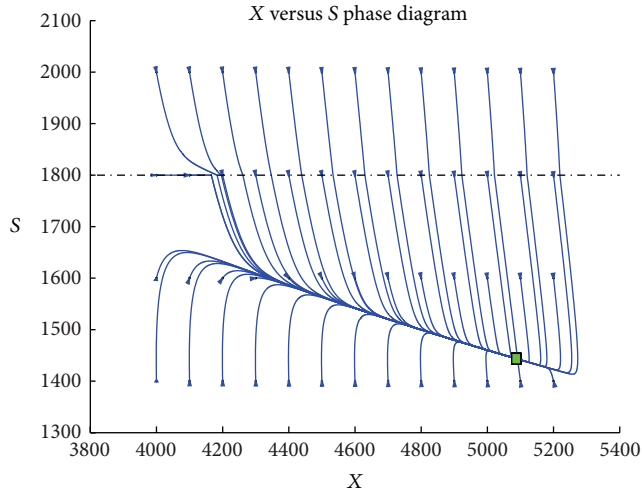

(a) Parameter $D = 2$

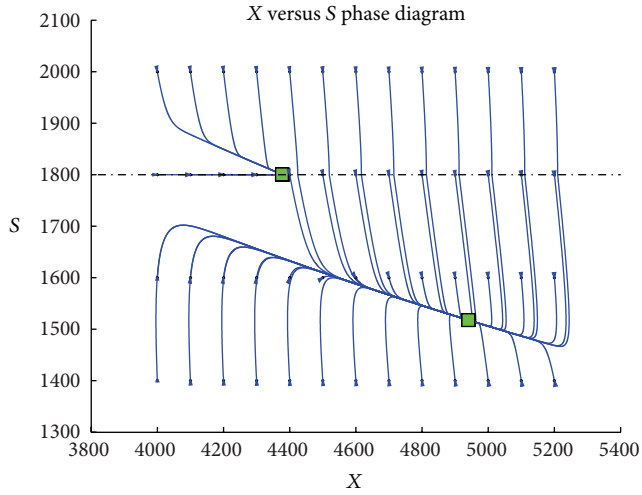

(b) Parameter $D = 2.05$

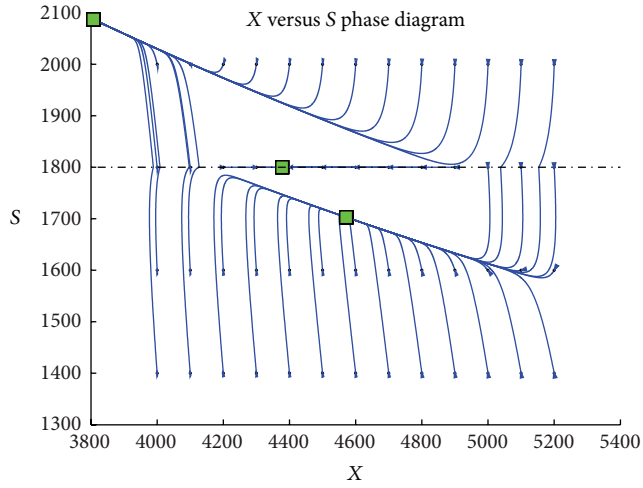

(c) Parameter $D = 2.3$

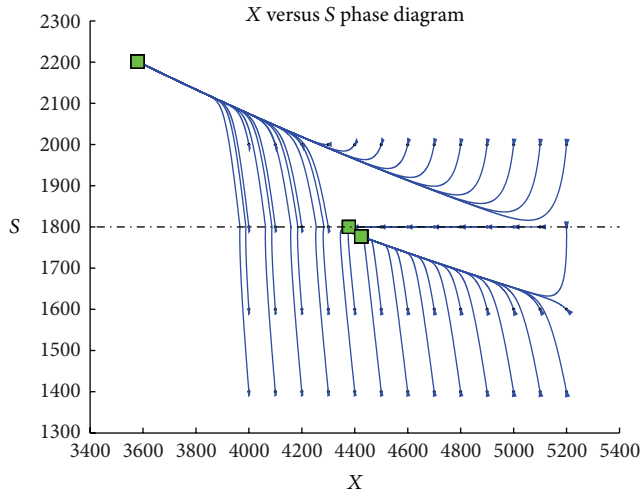

(d) Parameter $D = 2.4$

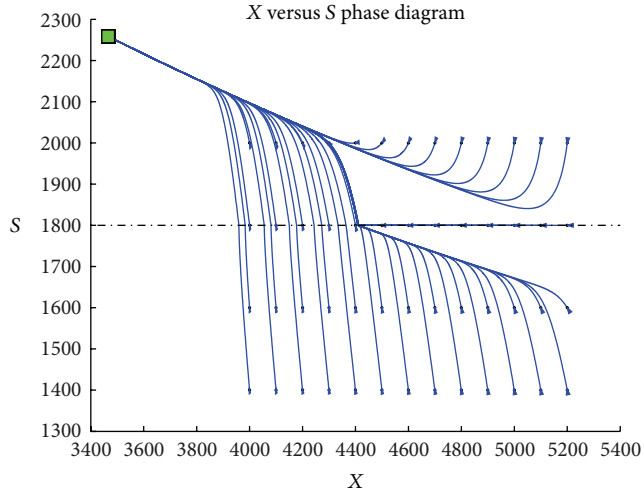

(e) Parameter $D = 2.45$

Figure 5: Numerical computations varying parameter D.

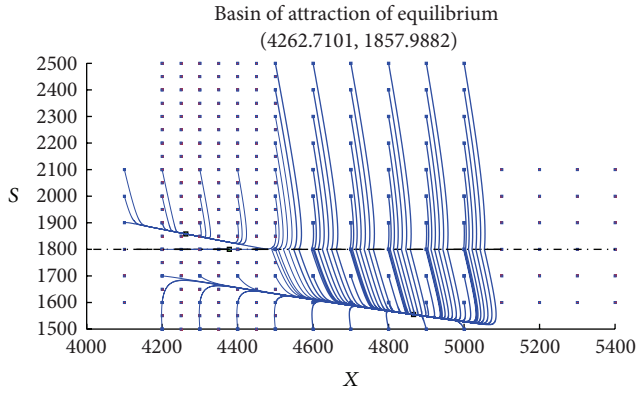

Figure 6: Numerically computed basins of attraction for parameter $D = 2.1$.

concentration at the bioreactor input. This shows that the equilibrium can be controlled with this parameter, either in region one or region two. The obtained results serve as a basis for bioreactor automatic control where a higher decontamination in the treated effluent and an improved conversion of the organic matter to biogas are expected.

Acknowledgments

This research was funded through project *Dynamic analysis of a continuous stirred tank reactor (CSTR) with biofilm formation for the treatment of residual waste*, Support Program for postgraduate theses, DIMA 2012 of Universidad Nacional de Colombia, and Project no. 20201007075 (VRI Universidad Nacional de Colombia).

References

[1] L. Borzacconi, I. López, and M. Ohanian, "Wastewater anaerobic treatment," in *Proceedings of the 5th Latin-American Workshop-Seminar on Wastewater Anaerobic Treatment*, Viña del Mar, Chile, 1998.

[2] H. D. Robinson and G. R. Harris, "Use of reed bed polishing systems to treat landfill leachates to very high standards," in *Proceedings of the Alternative Uses of Constructed Wetland Systems Conference*, pp. 55–68, Aqua Enviro Technology Transfer, Doncaster, UK, 2001.

[3] H. D. Robinson, M. S. Carville, and G. R. Harris, "Advanced leachate treatment at Buckden landfill, Huntingdon, UK," *Journal of Environmental Engineering and Science*, vol. 2, pp. 255–264, 2003.

[4] C. Campos and G. Anderson, "The effect of the liquid upflow velocity and the substrate concentration on the start-up and the steady state periods of lab-scale UASB reactors," in *Proceedings of the 6th International Symposium on Anaerobic Digestion*, Sao Paulo, Brazil, 1991.

[5] P. Kjeldsen, M. A. Barlaz, A. P. Rooker, A. Baun, A. Ledin, and T. H. Christensen, "Present and long-term composition of MSW landfill leachate: a review," *Critical Reviews in Environmental Science and Technology*, vol. 32, no. 4, pp. 297–336, 2002.

[6] S. R. Guiot, A. Pauss, and J. W. Costerton, "A structured model of the anaerobic granule consortium," *Water Science and Technology*, vol. 25, no. 7, pp. 1–10, 1992.

[7] D. M. Bagley and T. S. Brodkorb, "Modeling microbial kinetics in an anaerobic sequencing batch reactor—model development and experimental validation," *Water Environment Research*, vol. 71, no. 7, pp. 1320–1332, 1999.

[8] D. J. Costello, P. F. Greenfield, and P. L. Lee, "Dynamic modelling of a single-stage high-rate anaerobic reactor—II. Model verifiction," *Water Research*, vol. 25, no. 7, pp. 859–871, 1991.

[9] L. Fernandes, K. J. Kennedy, and Z. Ning, "Dynamic modelling of substrate degradation in sequencing batch anaerobic reactors (SBAR)," *Water Research*, vol. 27, no. 11, pp. 1619–1628, 1993.

[10] A. Rincon, F. Angulo, and G. Olivar, "Control of an anaerobic digester through normal form of fold bifurcation," *Journal of Process Control*, vol. 19, no. 8, pp. 1355–1367, 2009.

[11] Y. A. Kuznetsov, S. Rinaldi, and A. Gragnani, "One-parameter bifurcations in planar Filippov systems," *International Journal of Bifurcation and Chaos in Applied Sciences and Engineering*, vol. 13, no. 8, pp. 2157–2188, 2003.

[12] E. Freire, E. Ponce, F. Rodrigo, and F. Torres, "Bifurcation sets of continuous piecewise linear systems with two zones," *International Journal of Bifurcation and Chaos in Applied Sciences and Engineering*, vol. 8, no. 11, pp. 2073–2097, 1998.

[13] M. Di Bernardo and S. J. Hogan, "Discontinuity-induced bifurcations of piecewise smooth dynamical systems," *Philosophical Transactions of the Royal Society A*, vol. 368, no. 1930, pp. 4915–4935, 2010.

[14] M. di Bernardo, A. Nordmark, and G. Olivar, "Discontinuity-induced bifurcations of equilibria in piecewise-smooth and impacting dynamical systems," *Physica D*, vol. 237, no. 1, pp. 119–136, 2008.

[15] R. Muñoz, *Design and implementation of a COD control system of a prototype UASB reactor for treating leachates [M.S. thesis]*, National University of Colombia, 2006, (Spanish).

Hindawi Publishing Corporation
Mathematical Problems in Engineering
Volume 2013, Article ID 471429, 14 pages
http://dx.doi.org/10.1155/2013/471429

Review Article

Effect of Land Use and Climate Change on Runoff in the Dongjiang Basin of South China

Yanhu He,[1,2] Kairong Lin,[1,2] and Xiaohong Chen[1,2]

[1] *Center for Water Resources and Environment, Sun Yat-Sen University, Guangzhou 510275, China*
[2] *Key Laboratory of Water Cycle and Water Security in Southern China of Guangdong Higher Education Institutes, Guangzhou 510275, China*

Correspondence should be addressed to Xiaohong Chen; eescxh@mail.sysu.edu.cn

Received 15 February 2013; Revised 15 May 2013; Accepted 1 June 2013

Academic Editor: Yongping Li

Variability and availability of water resources under changing environment in a regional scale have been hot topics in recent years, due to the vulnerability of water resources associated with social and economic development. In this paper, four subbasins in the Dongjiang basin with a significant land use change were selected as case study. Runoffs of the four subbasins were simulated using the SCS monthly model to identify the quantitative impacts of land use and climate change. The results showed that (1), in the Dongjiang basin, temperature increased significantly, evaporation and sunlight decreased strongly, while precipitation showed a nonsignificant increase; (2) since the 1980s, land uses in the Dongjiang basin have experienced a significant change with a prominent increase in urban areas, a moderate increase in farmlands, and a great decrease in forest areas; (3) the SCS monthly model performed well in the four subbasins giving that the more significant land use change in each subbasin, the more runoff change correspondingly; (4) overall, runoff change was contributed half and half by climate change and human activities, respectively, in all the subbasins, in which about 20%~30% change was contributed by land use change.

1. Introduction

Environment Change (including land use change and climate change) and its impacts on water resources have always been the hot issues in recent years. The direct or indirect impacts on the hydrological regime brought by land use and climate change both have contributed to some water problems, such as water shortage, flooding, and water logging to different extent. Some researches have been conducted to study the impacts of land use and climate change on water resources in different basins [1–5]. Particularly in the humid region of south China, six hydrological models were used to simulate the hydrological impact of some climate change scenarios, and response strategies for water supply and flood control due to climate change were analyzed in the Dongjiang basin by Jiang et al. [6]. South China has identified an increasing trend of extreme rainfall events, and the correlation between such events and flood events was studied by Fu et al. [7]. Climate change makes flooding more frequent in some regions [8, 9]. Additionally, land use change also has notable impact on the hydrological cycle [10–12]. Overall, hydrological process and the variability and availability of water resources would change a lot due to land use change and climate change.

As the biggest developing country in the world, China has experienced an explosive economic growth over a couple of decades, which results in the prominent land use change. This change can alter evaporation patterns and potentially affect water resources in a region. The impacts of climate change on water resources and agriculture in China were analyzed by Piao et al. [13], and the results indicated that agriculture relying on the resultant increase in glacier runoff, especially in western China, would face a challenge, although its climate trends remained moderate compared to natural variability [13]. Even worse was the more frequent occurrence of drought and flood extremes largely due to climate change in different parts of China [14]. Some researches have focused on the variability of runoff in the Dongjiang basin under the impacts of climate change and human activities, especially land use change in recent decades [15]. Definitely, there is an increasingly serious challenge in the availability of water

resources, and its exploitation and management will be more or less affected.

As to a basin, climate change and human activities both contribute to the hydrological cycle, and this finding has been supported by many studies [16–19]. Many studies have been carried out to distinguish the roles of land use and climate change on water resources. The approach to the calculation for the runoff change due to precipitation and potential evaporation was proposed [20–22]. Based on which, the separated impacts of human activities and climate change on natural runoff change in the Poyang basin from 1992 to 2000 were analyzed quantitatively by Ye et al. [23]. In recent years, much attention has been paid to analyze the separated quantitative effects of land use and climate change, and some progress has been made, although further research still needs to be carried out. A simple approach to distinguish land-use and climate-change effects on water resources was developed with a coupled water-energy budget analysis in US Midwest area by Tomer and Schilling [11]. Combined impacts of land cover and climate changes on hydrological processes of the Kejie watershed in the eastern Himalayas were assessed with a SWAT model, which revealed that land-cover change had more effects than those of climate change in the short and middle terms [24]. Furthermore, in many river basins of China, many studies have been conducted to assess the impacts of climate change and human activities on the runoff variation. As to Tarim River, the impact of human activities had increased the runoff with a ratio of 41%~75% for different ages [25], and similar research can be found in the Wuding River [26]. In addition, some relative studies also took place in the Heihe catchment, Chaobai River, and Mian River basin [27–29], which came to a conclusion that climate change and human activities have the separated impacts on the runoff change varying from place to place. There is no exception for the Dongjiang basin [30]. However, few researches have been conducted to identify the quantitative effects of human activities and climate change on runoff in the study area. Moreover, most of the previous studies focused on a large scale basin and had no cases for comparison, which tends to limit our understanding of the impacts of climate change and human activities on water resources in the study area. The quantitative effect of land use change on runoff of the basin has not been revealed yet. Therefore, it is desirable to separate the impacts of climate change and human activities, specifically the land use change, on water resources under a changing environment in the study area.

Hydrological models have been widely used to study many practical and pressing issues that arise during planning, design, operation, and management of water resources systems [31, 32] and also to quantify the impacts of land use and climate change on the hydrological cycle. For example, a conceptual rainfall-runoff model was applied to the Rhine basin for the purpose of modeling the effect of land use change on the runoff. The results suggested that increased urbanization led to an increase in the lower peak runoff, compared to a considerable reduction of both the peak runoff and the total runoff volume resulted from intensified forestation [33]. Besides, the hydrological model considering other elements such as biogeochemistry was applied to reveal how land use change affects hydrological regimes at the watershed scale [34]. According to the available climate and hydrological data and the hydrological characteristics of the basin studied, many conceptual or distributed hydrological models were introduced to analyze the hydrological response under land use and climate change [35–38]. Trend analysis of climate variables is necessary to detect the variability of climate variables, such as temperature and precipitation [39, 40], which provides supports for study of the impacts on the hydrological cycle of land use change and climate change. Overall, hydrological model combined with statistic methods has been a prevalent and useful tool to clarify such an interesting phenomenon for a long time.

The Dongjiang River, which lies in south China, is an important fresh water source of the Pearl River Delta (one of the most developed areas in China). Specifically, it supplies 70% fresh water for Hong Kong. However, water shortage and water pollution in the Dongjiang basin appear to be more and more serious in recent years, due to the fast and persistent economic development and urbanization. Land use in this region has changed prominently since 1980s and contributed to hydrological response in the Dongjiang basin. Meanwhile, climate change under the global warming also plays an important role in the variation of hydrological processes. The combined effects of land use and climate changes lead to a series of conflicts between water use and water supply. In this paper, four sub-basins, the Shuntian, Lantang, Jiuzhou, and Yuecheng, within the Dongjiang basin are selected for study (Figure 1). Major climate variables were taken to trend analysis by using the Mann-Kendall test method, and runoffs in two different periods (natural and human activity periods) were simulated with the SCS monthly model for each basin. The aims of this study are to explore the temporal and spatial characteristics of land use change and climate variables in each sub-basin, to study the possible causes of the change, more specifically, to identify the roles played by land use change and climate change, as well as other human activities, on the runoff change, respectively. A comparison between the independent effect of land use and climate change in the four sub-basins will be conducted.

2. Basic Knowledge and Data

2.1. Study Area. The Dongjiang River (Figure 1) springs from Jiangxi Province and flows into the Pearl River estuary from northeast to southwest, which forms the Dongjiang basin. The Dongjiang basin is located between 113°52′ and 115°52′ E in longitude and 22°38′ and 25°14′ N in latitude. This basin has a drainage area of 35,340 km^2, about 90% of which is in Guangdong Province. The mainstream of the basin is about 562 km long with an average slope of about 0.039% [30].

The Dongjiang basin has a subtropical climate with a mean annual temperature of 21°C. The annual rainfall over the basin varies between 1500 mm in the dry season from October to March and 2400 mm in the wet or monsoon season from April to September. The basin has some different soil types and the dominated type is alluvial, which is centered largely in the central and southern part of the basin.

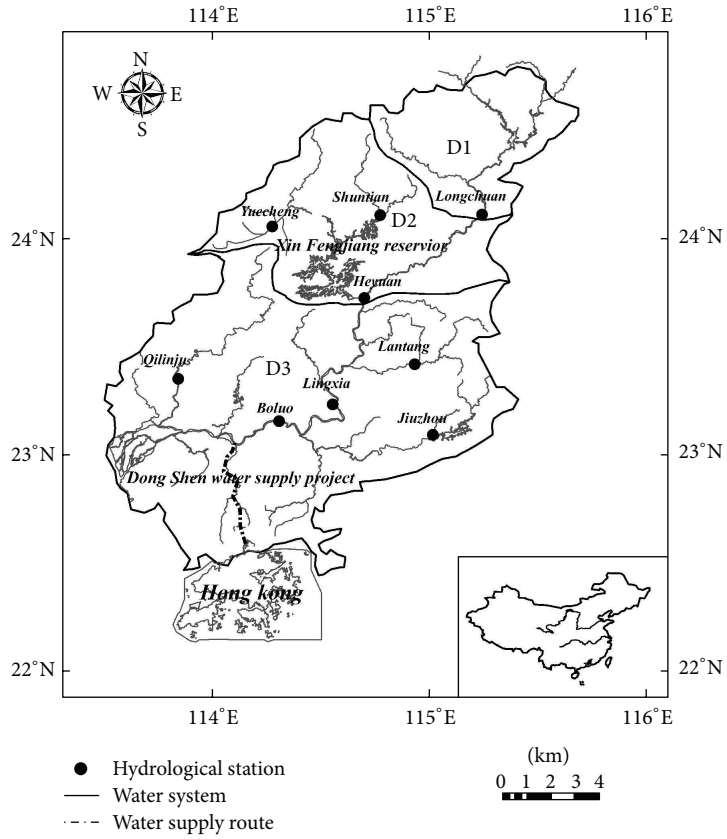

Figure 1: The sketch map of the Dongjiang Basin.

The major land use type of this area is forest, although the urban area has extended year by year with the fast pace of urbanization since the 1980s. Locations of the four sub-basins are shown in Figure 1.

2.2. Development of Economy and Society. The Dongjiang basin has experienced a fast development of economy and society over the recent 30 years. Population and GDP (gross domestic product) of the three regions (Huizhou, Heyuan, and Dongguan) within the basin from 1980 were analyzed. Detailed information can be seen in Figure 4.

Population and economy in the three regions have kept a rapid and persistent development due to China's reform and opening policy. Refering to Figure 4, population of each region has been expanding rapidly since 1980. In which, population of Huizhou had increased from 1.92 million in 1980 to 3.6 million in 2006, with the average growth rate of 1.08%. The GDP of each region also increased rapidly, especially Dongguan, whose GDP increased from 8 billion Chinese Yuan in 1980 to 262.7 billion Chinese Yuan in 2006 with the average growth rate of 14.34%. There is no doubt that the growth of population and the development of economy depend largely on land resources. Therefore, we can infer that land use has changed greatly for decades in accordance with the social and economic development in the study area.

2.3. Data. The climatic data used in the study, including time series of annual average precipitation, evaporation, and temperature from 1956 to 2008 of the 21 meteorological stations in the Dongjiang basin, was provided by the Guangdong Meteorological Bureau. The monthly runoff time series for 4 hydrological stations (Shuntian, Lantang, Jiuzhou, and Yuecheng) from 1970 to 2008 were acquired from Hydrological Bureau of Guangdong Province. The daily precipitation, evaporation, and runoff time series of the main rainfall and hydrological stations in the Dongjiang basin from 1970 to 1978 were extracted from Water Conservancy and Electric Power Bureau of Guangdong Province.

Two multitemporal satellite sensor images, Landsat Thematic Mapper (TM) imagery of the 1980s and 2000s, were downloaded from Global Land Cover Facility. Based on the images, two periods (1980s and 2000s) of land use and vegetation cover maps of the Dongjiang basin (Figure 2) were gained with the ArcGIS spatial analysis technique. A digital elevation model (DEM) with a spatial resolution of 30 m and soil type data with a spatial resolution of 90 m (Figure 3) of the Dongjiang basin were downloaded from China Soil Scientific Database (CSSD) and CGIAR-CSI, respectively.

3. Methodologies

3.1. Mann-Kendall Test for Time-Series Trend. Developed by Mann and later improved by Kendall [41, 42], highly

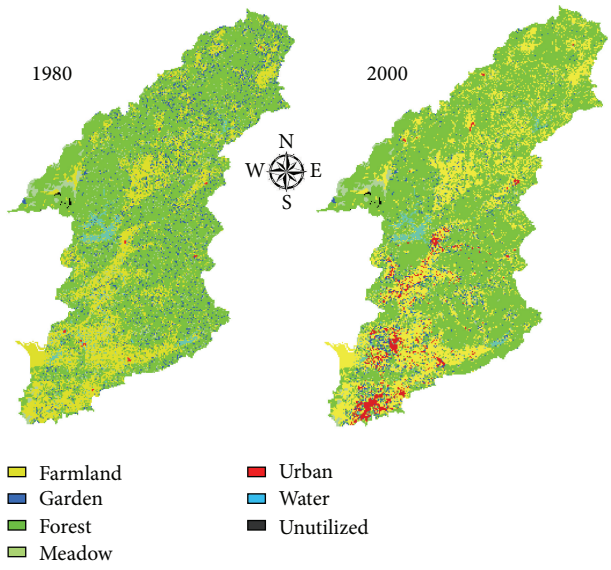

Figure 2: Land uses of two periods (1980 and 2000) in the Dongjiang basin.

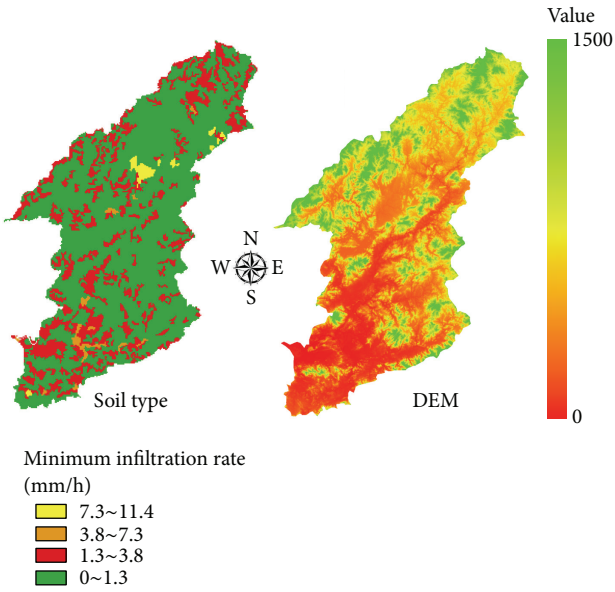

Figure 3: Soil type and DEM of the Dongjiang basin.

recommended for general use by the World Meteorological Organization [43], the Mann-Kendall test was widely used to detect time-series trends in hydrological and climatic data in many researches. The Mann-Kendall test has some advantages including its simplicity, ability to deal with nonnormal and missing data distributions, and robustness to the effects of outliers and gross data errors [44–46].

Firstly, the Mann-Kendall test defined a variable S as:

$$S = \sum_{k=1}^{n-1} \sum_{j=k+1}^{n} \operatorname{sgn}\left(x_i - x_j\right). \tag{1}$$

Then the presence of a statistically significant trend is evaluated using the Z value:

$$Z = \begin{cases} \dfrac{S-1}{\sqrt{\operatorname{Var}(S)}}, & S > 0, \\ 0, & S = 0, \\ \dfrac{S+1}{\sqrt{\operatorname{Var}(S)}}, & S < 0. \end{cases} \tag{2}$$

Besides, the standard normal cumulative distribution function F_n under the significance level α is given by $F_n(Z_\alpha/2) = \alpha/2$. If $|Z| > Z_\alpha/2$, the hypothesis of H_1 for a two-sided test can be accepted. Positive value Z indicates an upward trend while negative value a downward trend. More descriptions of this method can be found in many researches [47–49]. In this paper, trend analysis of climatic variables and runoff in the Dongjiang basin were conducted with the Mann-Kendall test based on over 50 years of climatic and hydrological data.

In addition, mutation detections of the climatic data were also conducted by the Mann-Kendall mutation analysis test method; a statistic variable of this method is

$$S_K = \sum_{i=1}^{k} r_i, \quad k = 2, 3, \ldots, n,$$
$$r_i = \begin{cases} +1, & x_i > x_j, \\ 0, & x_i \le x_j, \end{cases} \quad j = 1, 2, \ldots, i, \tag{3}$$

where S_K is the counts for the x series when x_i is greater than x_j.

UF_K is the standard normal distribution and can be calculated based on the x series:

$$UF_K = \frac{\left[S_K - E\left(S_K\right)\right]}{\sqrt{\operatorname{var}\left(S_K\right)}}, \quad k = 1, 2 \ldots, n, \tag{4}$$

where UF_1=0, $E(S_K)$ and var(S_K) are the expected value and variance of S_K which can be calculated on condition that the x series is mutually independent with the same continuous distribution:

$$E\left(S_K\right) = \frac{n(n+1)}{4},$$
$$\operatorname{var}\left(S_K\right) = \frac{n(n-1)(2n+5)}{72}. \tag{5}$$

3.2. SCS Rainfall-Runoff Model. Developed by the Soil Conservation Service of U.S. Department of Agriculture (USDA) early in 1954, the SCS model is widely used in the USA and many other countries [50, 51]. Several advantages of this model are as follows: (1) the characteristics of the land cover such as soil, slope, vegetation and land use in a basin can be considered with the SCS model; the possible change on the rainfall-runoff relationship can be preliminarily estimated according to the change of land use, and (2) it has the advantages of simplicity in structure and convenience in use with very low dependence on data.

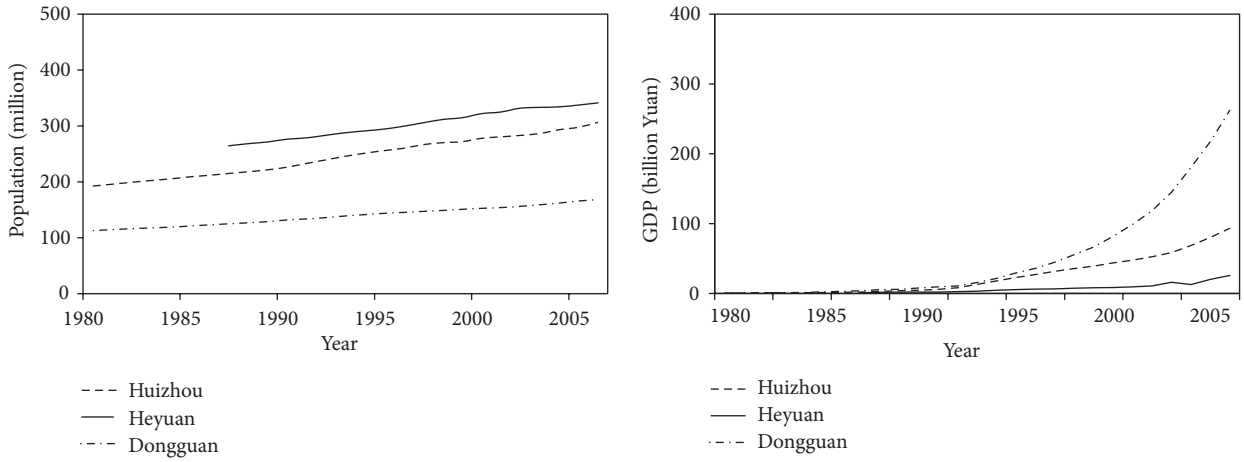

Figure 4: Sketch map of economic and social development in the Dongjiang basin.

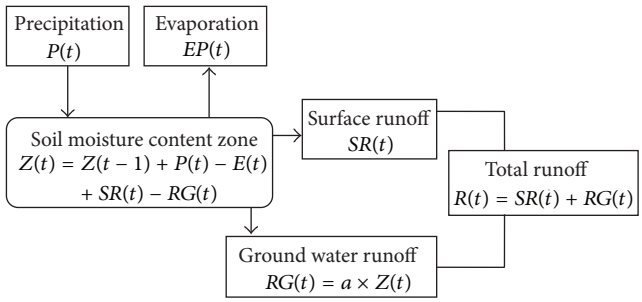

Figure 5: A schematic diagram of the water balance in a basin.

The runoff yield for the SCS model is

$$R = \begin{cases} \dfrac{(P - I_a)^2}{P + S - I_a}, & P \geq I_a, \\ 0, & P < I_a, \end{cases} \tag{6}$$

where R is the runoff, P is the precipitation, I_a is the initial loss, and S is the present probable maximum retention in the basin which is the top limit of the later loss.

Initial loss I_a can be calculated by an empirical correlation with S:

$$I_a = \alpha S, \tag{7}$$

where α is the coefficient of the initial losses which is related to the initial soil water content of the basin.

To eliminate the large variation scope of the S value, there is an empirical relation for CN (a non dimensional parameter) and S:

$$S = \frac{25400}{CN} - 254. \tag{8}$$

The curve number CN is a key and comprehensive parameter within SCS model. CN describes the watershed features before a rain and is affected by AMC (antecedent moisture condition), slope, vegetation, soil type, and land use condition with a value of 0~100. AMC can be divided into 3 classes: *AMC* I-arid condition, AMC II-normal condition, and *AMC* III-moist condition. The specific basis for the classification and the estimation of the CN value can be found in related references [52].

Input by the observed monthly precipitation and evaporation, the SCS model yields the monthly runoff. A key issue here is to calculate the actual evaporation by using the SCS monthly model. Based on the research results from the two-parameter monthly water balance model [53], the monthly actual evaporation can be calculated by

$$E(t) = C \times EP(t) \times \tanh\left(\frac{P(t)}{EP(t)}\right), \tag{9}$$

where $E(t)$ is the actual monthly evaporation, $EP(t)$ is the observed evaporation from the evaporating dish, $P(t)$ is the monthly precipitation, and C is one of the parameters in the model (nondimensional).

The total discharge consists of two parts: the surface flow ($SR(t)$) and the baseflow ($RG(t)$). $SR(t)$ can be gained by (6), while $RG(t)$ can be calculated with

$$RG(t) = a \times Z(t), \tag{10}$$

where a is the coefficient of the groundwater flow and $Z(t)$ is the soil moisture content which can be calculated by

$$Z(t) = Z(t-1) + P(t) - E(t) + SR(t) - RG(t). \tag{11}$$

A schematic diagram for the water balance in a basin is shown in Figure 5. The SCS model is used to simulate the monthly runoff process in this study. There are two parameters, C and α, in the model.

3.3. Approach to Distinguish the Respective Impact of Land Use and Climate Change to Water Resources. The total runoff change can be obtained by the difference between the observed runoffs in two different periods, respectively, that is, the intensive human activities period and the low human activities period (natural condition). It is assumed that the

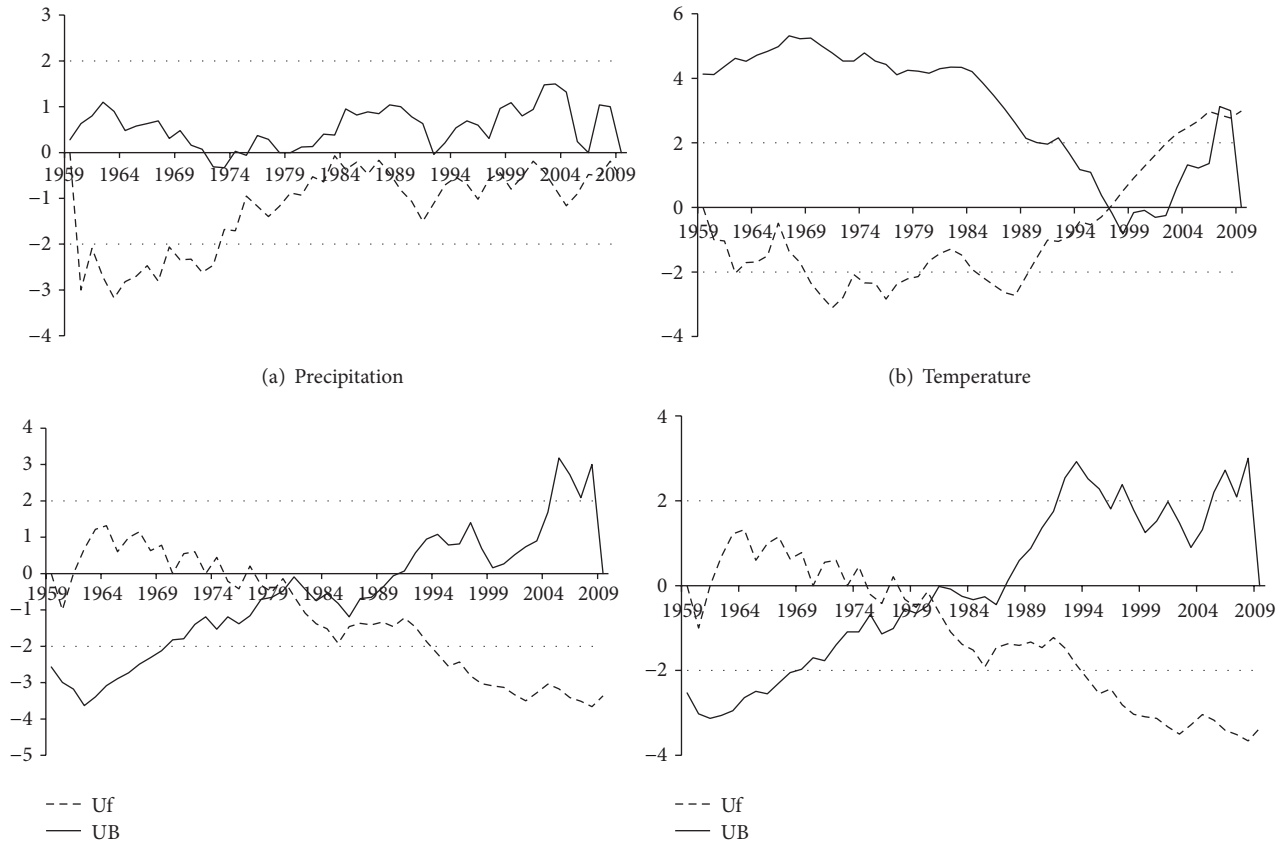

Figure 6: Mann-Kendall test trend of four meteorological elements in the Dongjing basin.

runoff change in the low human activities period is affected only by climate change.

Therefore, the impacts of climate change, land use change, and other human activities on runoff change can be separated according to the following calculations:

$$\begin{aligned}
\Delta R_L &= R_{H2} - R_{H1},\\
\Delta R_C &= R_B - R_{H1},\\
\Delta R_0 &= \Delta R_T - \Delta R_C - \Delta R_L,\\
\Delta &= \left|\Delta R_0\right| + \left|\Delta R_C\right| + \left|\Delta R_L\right|,\\
\mu L &= \frac{\left|\Delta R_L\right|}{\Delta} \times 100\%,\\
\mu C &= \frac{\left|\Delta R_C\right|}{\Delta} \times 100\%,\\
\mu R_0 &= \frac{\left|\Delta R_0\right|}{\Delta} \times 100\%,
\end{aligned} \tag{12}$$

where ΔR_L is the runoff change due to land use change, from time period of phase I to phase II; R_{H2} and R_{H1} are the simulated runoffs corresponding to the land uses of phase II and phase I, respectively, and both of them can be calculated with the SCS monthly model; ΔR_C is the runoff change caused by climate change; R_B is the natural runoff of phase I; ΔR_T is the total runoff change; ΔR_0 is the runoff change due to other human activities except for land use change; μL, μC, and μR_0 are the percentages for the roles played by land use change, climate change, and other human activities, respectively.

4. Results and Discussion

4.1. Time-Series Analysis. The variation trends of the climatic variables over 50 years in the study basin were analyzed with the linear regression and Mann-Kendall trend test method. Table 1 listed the detailed results obtained by the Mann-Kendall trend test method. Figure 6 demonstrated the results for mutation analysis with the Mann-Kendall trend test and the linear regression method, respectively.

It can be seen from Table 1 that each climatic variable showed different degree of change in the Dongjiang basin during the past 50 years (1959–2008), according to its statistics by the Mann-Kendall trend test method. Precipitation showed a nonsignificant increasing trend ($M = 0.22$) at 99% confidence level, which is largely due to local atmospheric circulation and topography. Temperature in the same period showed a significant increasing trend ($M = 3.34$). While sunlight showed a significant decreasing trend. Meanwhile, very fast urbanization caused quick increase of impervious

Table 1: M-K trend analysis for meteorological elements in the Dongjiang basin (1958–2009).

Statistics	Meteorological elements				
	Precipitation (mm)	Temperature (°C)	Evaporation (mm)	Humidity (g/m^3)	Sunlight (h)
$\overline{C}$	1852.92	21.30	1572.4	78.1	1813
C_v	0.16	0.02	0.05	0.03	0.09
C_s	0.13	0.56	0.50	−0.94	0.45
M	0.22	3.34	−2.94	−2.97	−4.18

area in the study basin in the last 50 years. These all contributed to a decreasing trend of evaporation. Temperature showed an increasing trend with a distinct mutation taking place around 1997, and sunlight and evaporation both had an abrupt change in 1982. Overall, the change of climatic variables in the Dongjiang basin during the past 50 years was significant.

It can be found from the C_v value of each climatic variable that there was a significant internal variation for precipitation but not for temperature. It can be illustrated by both the rainfall pattern and the atmospheric circulation in the study area: Dongjiang basin is located in the southern humid region in China and deeply affected by the monsoon circulation with the rainfall patterns of frontal rain and convectional rain. Therefore, the internal variation of precipitation is significant.

To clarify the relations among each climatic variable and the runoff, the correlation coefficients and relevancies were analyzed. According to the spatial differences of land cover and climatic variables, the Dongjiang basin was divided into three parts: the upper part centered with Longchuan, marked D1; the middle part centered with Heyuan, marked D2; and the whole basin centered with Boluo, marked D3. Tables 2 and 3 listed the correlation coefficients and relevancies, respectively. It can be seen from Table 2 that precipitation was positively related to runoff, and their correlation coefficient was the largest, which revealed that runoff in the Dongjiang basin depended mainly on precipitation. In contrast, temperature, sunlight, and evaporation were negatively related to runoff. Among the three parts of the basin, the correlation coefficient of precipitation and runoff in D2 was the least. The reason was that there located the biggest reservoir, the Xinfengjiang Reservoir (Figure 1) in D2. In addition, more than 20 middle and small sized reservoirs and hydraulic projects were constructed in the same period, which made a more significant change of land cover as compared to D1 and D3. Actually, runoff in D2 is mainly controlled by regulation of the reservoir, so precipitation was less correlation with runoff in D2. Table 3 showed that the relevancy between precipitation and runoff was the largest, indicating that precipitation was the major driver for runoff change in the whole study basin, which is similar to the results of correlation analysis.

4.2. Land Use Change Analysis. It has been found that the urban land and farmland increased in the study area [54]. Based on the raster graphics for land use of two periods (1980 and 2000), temporal and spatial variations of land use change in the Dongjiang basin were analyzed with the ArcGIS spatial analysis technique. Figure 2 showed the maps of land use in 1980 and 2000, respectively. Table 4 depicted the detailed information of the land use change in the form of a comparison.

It can be seen from Figure 2 that the dominant land uses in the study area, in 1980, were mainly forest (widely distributed in the whole basin) and farmland (mainly distributed in the upper basin), accounting for 64.56% and 22.33%, respectively. while garden, meadow, and water took a little part with the percentage of 5.94%, 4.71%, and 2.28%, respectively. Urban land mainly distributed in the downstream basin, and the unutilized land took the least percentage in the Dongjiang basin. The area of two types of land use, urban land and farmland, increased from 1980, along with the decrease of garden (2.65%), meadow (1.23%), water (0.49%), and forest (2.38%) in 2000, while the dominant land use was still forest in 2000. In all, since 1980s, the land use in the Dongjiang basin has been characterized with a prominent increase in urban land, a little increase in farmland, and great decrease in forest area, while little change in water area and unutilized land. This land use change due to fast social and economic development had a significant impact on the hydrological response and then contributed to the variability of water resources in the region.

4.3. Runoff Simulation and Runoff Change Analysis

4.3.1. The Value of CN. CN (curve number) can reflect the capacity of runoff yield for the land cover with a continuous spatial distribution. The CN isocline represents the runoff yield capacities in the study basin.

Based on land use maps of two periods (1980 and 2000) and soil type data of the Dongjiang basin, CN distribution maps (see Figure 7) of 3 AMC (antecedent moisture condition) scenarios in the same periods were obtained with spatial interpolation. Figure 8 showed the CN distribution maps for AMC II of the four sub-basins in the two periods.

4.3.2. Model Calibration and Validation. The SCS monthly model was calibrated in the period of 1970–1976 with climatic data and then validated in the period of 1977-1978 by manual calibration method with the acceptable set of parameters after CN value analysis. To measure the performance of the model, we chose Nash-Sutcliffe coefficient of efficiency (NSE) criterion [55] and relative error (RE) as objective function.

Table 2: The correlation coefficient of each meteorological element to runoff in the Dongjiang basin.

Basin units	Basin scope	Gauge stations	Temperature	Precipitation	Evaporation	Sunlight	Humidity
D1	Upper	Longchuan	−0.10	0.80	−0.4	−0.35	0.27
D2	Midstream	Heyuan	−0.23	0.69	−0.28	−0.39	0.35
D	The whole Basin	Boluo	−0.08	0.88	−0.54	−0.57	0.26

Table 3: The relevancies between each meteorological element and runoff in the Dongjiang basin.

Basin units	Basin scope	Gauge stations	Temperature	Precipitation	Evaporation	Sunlight	Humidity
D1	Upper	Longchuan	0.4884	0.5503	0.4688	0.449	0.4702
		Rank	2	1	4	5	3
D2	Midstream	Heyuan	0.4857	0.5389	0.4659	0.4313	0.4861
		Rank	3	1	4	5	2
D	The whole basin	Boluo	0.525	0.5968	0.4883	0.4495	0.5239
		Rank	2	1	4	5	3

Table 4: Comparison of land use in the Dongjiang basin during two different periods.

Land use	The year 1980		The year 2000		Δ_{area} (km^2)	Ratio (%)
	Area (km^2)	Ratio (%)	Area (km^2)	Ratio (%)		
Farmland	6083.49	22.33	7272.73	26.69	1189.24	4.36
Garden	1619.14	5.94	896.70	3.29	−722.44	−2.65
Forest	17586.88	64.56	16939.87	62.18	−647.01	−2.38
Meadow	1282.74	4.71	947.14	3.48	−335.60	−1.23
Built-up	30.02	0.12	682.25	2.5	652.23	2.38
Waters	619.99	2.28	480.12	1.79	−139.87	−0.49
Unutilized land	17.38	0.06	20.80	0.07	3.42	0.01

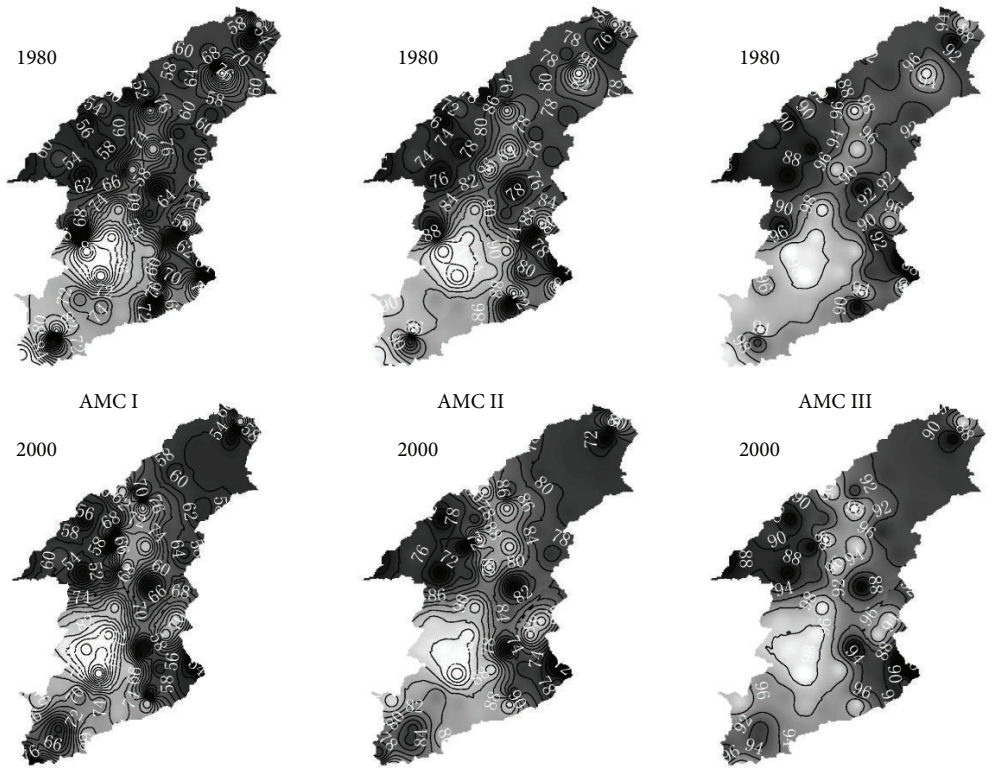

Figure 7: Comparison of CN distribution under 3 AMC scenarios in the Dongjiang basin of two periods (1980 and 2000).

Table 5: Calibration and validation of the SCS monthly model.

Sub-basins	Runoff coefficient	Calibration			NSE/%	RE/%	Evaluation		
		Data length/years	a	c			Data length/years	NSE/%	RE/%
Shuntian	0.596	7	0.699	0.858	81.6	1.0	2	92.5	−9.7
Yuecheng	0.658	7	0.592	0.604	84.0	0.9	2	86.0	11.1
Lantang	0.515	7	0.601	0.832	83.0	1.6	2	94.0	−1.8
Jiuzhou	0.571	7	0.674	0.821	82.3	−0.5	2	79.3	20.9

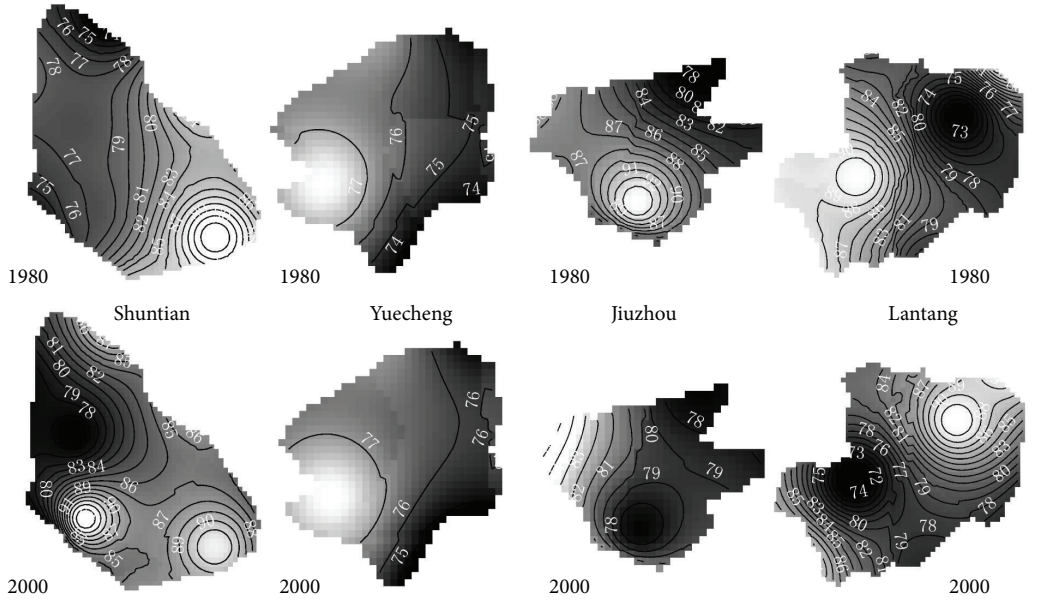

Figure 8: Comparison of the CN distribution under AMC II scenario for the four sub-basins in the Dongjiang basin of two periods (1980 and 2000).

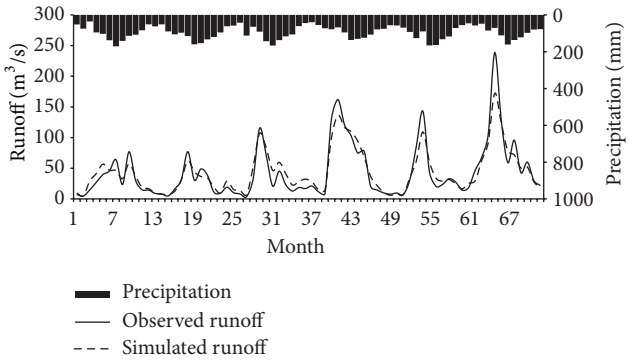

Figure 9: Comparison of simulated and observed runoffs in the calibration period (1970–1976) in the Shuntian subbasin.

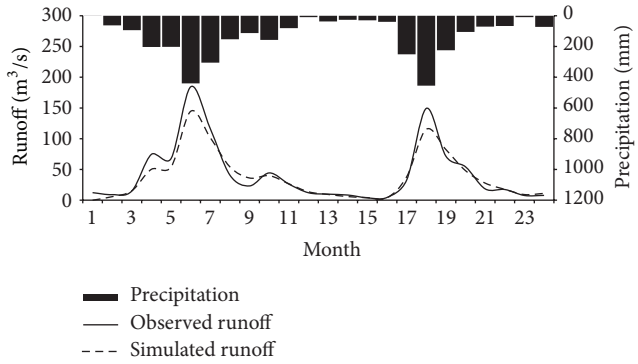

Figure 10: Comparison of simulated and observed runoffs in the validation period (1977–1978) in the Shuntian sub-basin.

The results of simulation were listed in Table 5. The comparisons between simulated and observed runoffs of the calibration and validation periods in Shuntian sub-basin were illustrated in Figures 9 and 10, respectively. The simulated results by the SCS monthly model were comparable with the observations in the four sub-basins. Nash-Sutcliffe coefficients were above 0.8, and RE was within the pale of 0.02 for those all four sub-basins in the calibration period. It can be inferred from Figures 9 and 10 that the simulated hydrograph matched well with the observed one, and the peak flows were coincided in both the calibration and validation periods. Overall, model performance was acceptable within the study domain, and reliable to be extended to reconstruct the natural runoff.

4.3.3. Runoff Simulation in Human Activity Period. Based on the CN value of land use in the first phase (before 1980)

Table 6: Monthly runoff changes of natural and human activity periods in the four sub-basins (10^8 m^3).

Sub-basin	Natural period R_N	R_{HR}	ΔR_T	Human activity period					
				Land use change		Climate change		Other human activities	
				ΔR_L	μL (%)	ΔR_C	μC (%)	ΔR_0	μR_0 (%)
Shuntian	1.12	1.16	0.04	0.08	24.11	−0.15	44.60	0.11	31.29
Yuecheng	0.55	0.53	−0.01	0.03	19.54	−0.08	54.74	0.04	25.72
Lantang	0.73	0.77	0.03	0.05	29.94	−0.07	40.51	0.05	29.55
Jiuzhou	0.34	0.34	−0.01	0.02	25.50	−0.05	53.22	0.02	21.27

and climatic data in the second phase (precipitation and evaporation, from 1980 to 2000) in the four sub-basins, the natural monthly runoff I and its process in the human activity period were simulated by using the SCS monthly model. And the monthly runoff II was obtained under the land use change condition (with the CN value of land use in 2000 as its input) by the same method. The difference between the simulated runoffs in the two phases was the runoff change due to land use change.

The simulated monthly runoff change due to land use change from 1980 to 2000 for each sub-basin was shown in Figure 11. It can be found that the runoff change varied from sub-basin to sub-basin, and the changes in Yuecheng sub-basin and Jiuzhou sub-basin were less than those of in Shuntian and Lantang, which was relevant to the variation scope of the CN value in the basins.

4.3.4. The Quantitative Effect due to Climate and Land Use Changes. The analysis of quantitative impacts on runoff due to human activities particularly land use and climate changes was carried out in the four sub-basins. The runoff change due to land use change was obtained from the simulated runoff by the SCS model in the two periods (human activity and natural periods). The quantitative impacts of climate change and human activities were identified by the method presented in (12), and the results were shown in Table 6.

It can be seen from Table 6 that, take Shuntian sub-basin, for instance, as compared to natural period, the runoff in human activity period increased by 4×10^6 m^3. The 24.11% increase of runoff was contributed by the land use change. On the contrary, climate change contributed the 44.6% decrease to runoff, which was superior to that of land use change. A meaningful clue has been found for explaining such a result: as two most important factors of the runoff change, precipitation showed an insignificant increasing trend, which was different from that of temperature (significant increasing trend), and the compound effects led to the reduction of the total runoff. Other factors including natural and human aspects accounted for 31.29% to the runoff change. Overall, all the driving factors can make the runoff change to a different level among which the role played by climate change took nearly the half for each sub-basin. This was in accordance with the result of identifying the quantitative effect of land use and climate change on runoff in the high flow period in the Dongjiang basin [30].

The impact of land use change on the total runoff change in Lantang sub-basin was the highest (29.94%) among the four sub-basins, while the impact ratios of climate change and other human activities were 40.51% and 29.55%, respectively. In summary, human activities contributed 59.49% to runoff change, which revealed that human activities were the major driver for runoff change.

It was obvious that climate change with increased precipitation and decreased evaporation caused the increase of runoff in the study area. Furthermore, changes of inner-annual distribution precipitation also affected the runoff change. Seven pairs of simulated runoff under nearly equal amount of precipitation were shown in Table 7. It can be found from Table 7 that the greater the percentage of precipitation in flood season, the greater the simulated runoff in Shuntian sub-basin, except for 1985 and 1987. It was also implied that precipitation was the major driver for runoff change in Shuntian sub-basin.

To analyze the impact of land use change, we divided annual precipitation into four classes as under 1500 mm, 1500–1800 mm, 1800–2000 mm, and above 2000 mm in the four sub-basins. The total runoff change due to land use change in each class was shown in Figure 12. It can be found that under larger precipitation, the runoff (to be flattened) of flood season was less as compared with that of drought season and the whole year in the four sub-basins. This was attributed to land cover conversion due to construction of reservoirs, which stored much water in flood season for flood prevention and water use. In addition, runoff yield changed to be much quick and more sensitive to precipitation, along with the land cover conversion from forest to urban areas or other vegetation types. The impact of land use change on runoff was more distinctive when the precipitation was larger.

Finally, it can be concluded that the runoff change was affected by many factors, and the contribution ratio of each factor was different. Climate change and human activities (especially the land use change) were the two dominant drivers which contributed about 40%~50% each to the runoff change. Particularly the land use change, whose impact on the runoff change in flood season under large precipitation, should not be neglected. The role played by climate change and human activities including land use change should be considered, respectively, in the analysis of variability and availability of water resources, and then reasonable measures and policies should be taken.

5. Conclusions

Based on land use maps of two time periods in the Dongjiang basin, this study identified the quantitative effects of land use and climate change on the runoff, which revealed some

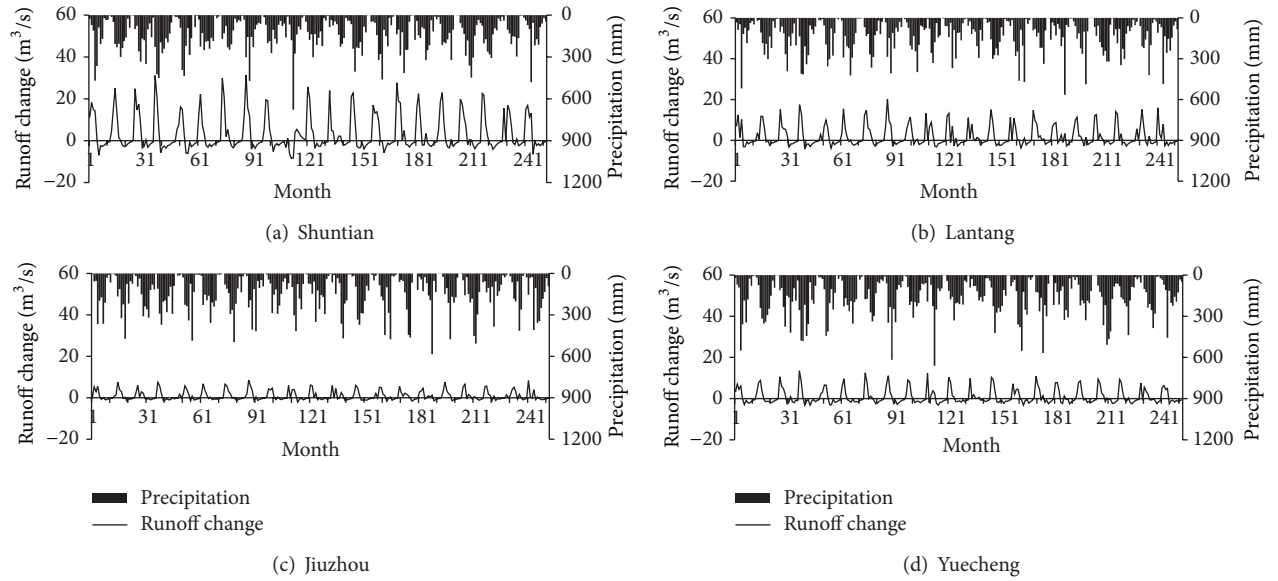

Figure 11: Processes of the simulated monthly runoffs change in the four sub-basins due to land use change from 1980 to 2000.

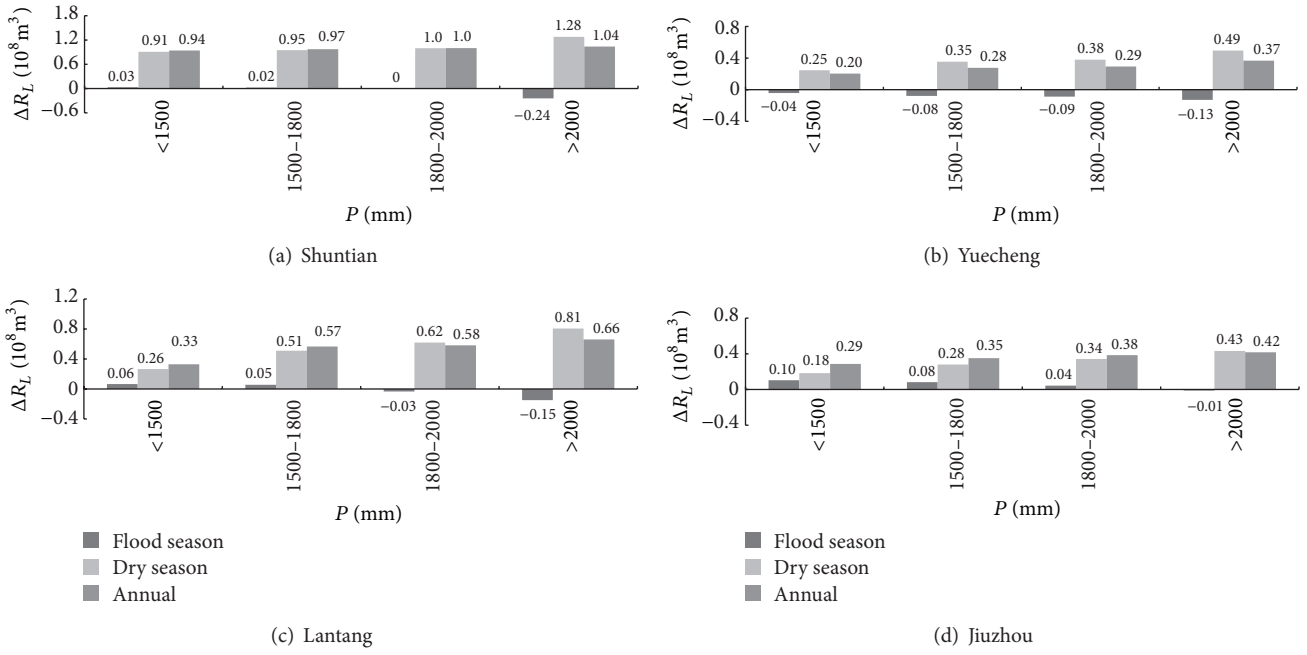

Figure 12: Average annual runoff change due to land use change under different precipitation classes in the four sub-basins.

interesting results with the application of the SCS monthly model.

(1) The climate experienced significant changes in the basin over the past 50 years, and the changes were detected using the Mann-Kendall test method with the results of nonsignificant increase in precipitation, significant increase in temperature while decrease in evaporation and sunlight.

(2) Land use has experienced a significant change since the 1980s in the Dongjiang basin with the characteristic of spatial distribution for the CN value under three AMC scenarios in two periods. The average value of CN increased and the CN value varied in each sub-basin due to different land use patterns. In particular, expansion of urban area in the south part of the study area (downstream) and deforestation in the whole area provided contributory factors that affected hydrological processes and subsequently increased runoff.

(3) The SCS monthly model performed well in the four sub-basins of the Dongjiang basin, and the results showed that the runoff change in each sub-basin during two time periods was different. The runoff change in Yuecheng sub-basin was less than that of Shuntian sub-basin and Lantang sub-basin, which was in good correlation to the variation

Table 7: Simulated runoff yielded by similar amount of precipitations in the three sub-basins.

Subbasins	Year	Precipitation (mm)			Simulated runoff (10^8 m^3)
		Annual	Flood season	Percentage of flood season (%)	
Shuntian	2004	1274	1108.10	86.57	7.56
	1999	1279	1107.50	87.00	8.41
	2002	1421	1079.61	76.00	8.12
	2003	1425	1256.16	88.17	9.80
	1985*	1639	1217.40	74.27	11.83
	1987*	1643	1185.57	72.14	13.15
	1982	1811	1396.43	77.11	13.04
	1984	1813	1592.17	87.83	14.70
Lantang	1986	1628	1259.60	77.39	7.96
	1998	1631	1148.10	70.39	8.77
Jiuzhou	1981	1754	1427.00	81.35	4.00
	1982	1752	1398.10	79.79	3.48
	1984	1577	1498.50	95.02	3.87
	1989	1575	1316.70	83.61	3.51

Annual precipitation for Yuecheng subbasin varies greatly all the years as compared with other sub-basins, and no similar amount of precipitations can be found in different years. The impact of inner-annual distribution of precipitation on the variation of runoff in Yuecheng subbasin was neglected.

scope of the CN value. The more land use changed, the greater the CN value changed, which resulted in the greater variation of the runoff under the same climatic condition.

(4) The separated quantitative effect of land use and climate change on the runoff showed that climate change and human activities (including land use) contributed half and half, respectively, to runoff change. While land use change independently contributed 20%~30% to the total runoff change. Moreover, the effect of land use on runoff change was in different level under different amounts of precipitation. The effect of climate change on runoff change had a different inner-annual distribution even under a same amount of annual precipitation.

Further research is required to acquire the regional future climate scenarios coupled with the hydrological model of a basin scale under GCMs (general circulation models) with the downscaling technique, so as to further quantify the relations between runoff and climatic variables. In addition, the space-time distribution of floods and droughts resulted from the runoff change should also be studied to provide scientific framework for basin-scale water resources management.

Acknowledgments

The research is financially supported by the National Natural Science Foundation of China (Grant no. 51210013), the Public Welfare Project of Ministry of Water Resources (Grant no. 201301071-02, 201301002-02), the project from Guangdong Science and Technology Department (Grant no. 2010B050300010), the project from Guangdong Water Resources Department (Grant no. 2009-39), Key Project of Chinese National Programs for Fundamental Research and Development (973 program) (Grant no. 2013CB036406, 2010CB951102), and the Pearl-River-New-Star of Science and Technology supported by Guangzhou City (Grant no. 2011J2200051).

References

[1] A. Bronstert, D. Niehoff, and G. Brger, "Effects of climate and land-use change on storm runoff generation: present knowledge and modelling capabilities," *Hydrological Processes*, vol. 16, no. 2, pp. 509–529, 2002.

[2] D. Legesse, C. Vallet-Coulomb, and F. Gasse, "Hydrological response of a catchment to climate and land use changes in Tropical Africa: case study south central Ethiopia," *Journal of Hydrology*, vol. 275, no. 1-2, pp. 67–85, 2003.

[3] B. Zimmermann, H. Elsenbeer, and J. M. De Moraes, "The influence of land-use changes on soil hydraulic properties: implications for runoff generation," *Forest Ecology and Management*, vol. 222, no. 1–3, pp. 29–38, 2006.

[4] D. Mao and K. A. Cherkauer, "Impacts of land-use change on hydrologic responses in the Great Lakes region," *Journal of Hydrology*, vol. 374, no. 1-2, pp. 71–82, 2009.

[5] N. A. Adnan and P. M. Atkinson, "Exploring the impact of climate and land use changes on streamflow trends in a monsoon catchment," *International Journal of Climatology*, vol. 31, no. 6, pp. 815–831, 2011.

[6] T. Jiang, Y. D. Chen, C.-Y. Xu, X. Chen, X. Chen, and V. P. Singh, "Comparison of hydrological impacts of climate change simulated by six hydrological models in the Dongjiang Basin, South China," *Journal of Hydrology*, vol. 336, no. 3-4, pp. 316–333, 2007.

[7] G. B. Fu, J. J. Yu, X. B. Yu et al., "Temporal variation of extreme rainfall events in China, 1961–2009," *Journal of Hydrology*, vol. 487, pp. 48–59, 2013.

[8] G. A. Meehl, F. Zwiers, J. Evans, T. Knutson, L. Mearns, and P. Whetton, "Trends in extreme weather and climate events: issues related to modeling extremes in projections of future climate

change," *Bulletin of the American Meteorological Society*, vol. 81, no. 3, pp. 427–436, 2000.

[9] S. Wang, S. Kang, L. Zhang, and F. Li, "Modelling hydrological response to different land-use and climate change scenarios in the Zamu River basin of northwest China," *Hydrological Processes*, vol. 22, no. 14, pp. 2502–2510, 2008.

[10] M. Verbunt, M. Groot Zwaaftink, and J. Gurtz, "The hydrologic impact of land cover changes and hydropower stations in the Alpine Rhine basin," *Ecological Modelling*, vol. 187, no. 1, pp. 71–84, 2005.

[11] M. D. Tomer and K. E. Schilling, "A simple approach to distinguish land-use and climate-change effects on watershed hydrology," *Journal of Hydrology*, vol. 376, no. 1-2, pp. 24–33, 2009.

[12] E.-S. Chung, K. Park, and K. S. Lee, "The relative impacts of climate change and urbanization on the hydrological response of a Korean urban watershed," *Hydrological Processes*, vol. 25, no. 4, pp. 544–560, 2011.

[13] S. Piao, P. Ciais, Y. Huang et al., "The impacts of climate change on water resources and agriculture in China," *Nature*, vol. 467, no. 7311, pp. 43–51, 2010.

[14] P. Zhai, X. Zhang, H. Wan, and X. Pan, "Trends in total precipitation and frequency of daily precipitation extremes over China," *Journal of Climate*, vol. 18, no. 7, pp. 1096–1108, 2005.

[15] Y. Q. Chen, Q. Zhang, X. H. Chen, and P. Wang, "Multi-scale variability of runoff changes in the Pearl River basin, China," *Quaternary International*, vol. 226, pp. 44–53, 2010.

[16] C. O. Wilson and Q. Weng, "Simulating the impacts of future land use and climate changes on surface water quality in the Des Plaines River watershed, Chicago Metropolitan Statistical Area, Illinois," *Science of the Total Environment*, vol. 409, no. 20, pp. 4387–4405, 2011.

[17] L. Cuo, T. K. Beyene, N. Voisin et al., "Effects of mid-twenty-first century climate and land cover change on the hydrology of the Puget Sound basin, Washington," *Hydrological Processes*, vol. 25, no. 11, pp. 1729–1753, 2011.

[18] J. I. López-Moreno, S. M. Vicente-Serrano, E. Moran-Tejeda, J. Zabalza, J. Lorenzo-Lacruz, and J. M. García-Ruiz, "Impact of climate evolution and land use changes on water yield in the ebro basin," *Hydrology and Earth System Sciences*, vol. 15, no. 1, pp. 311–322, 2011.

[19] L. M. Mango, A. M. Melesse, M. E. McClain, D. Gann, and S. G. Setegn, "Land use and climate change impacts on the hydrology of the upper Mara River Basin, Kenya: results of a modeling study to support better resource management," *Hydrology and Earth System Sciences*, vol. 15, no. 7, pp. 2245–2258, 2011.

[20] J. C. I. Dooge, M. Bruen, and B. Parmentier, "A simple model for estimating the sensitivity of runoff to long-term changes in precipitation without a change in vegetation," *Advances in Water Resources*, vol. 23, no. 2, pp. 153–163, 1999.

[21] R. D. Koster and M. J. Suarez, "A simple framework for examining the interannual variability of land surface moisture fluxes," *Journal of Climate*, vol. 12, no. 7, pp. 1911–1917, 1999.

[22] P. C. D. Milly and K. A. Dunne, "Macro-scale water fluxes: water and energy supply control of their inter-annual variability," *Water Resources Research*, vol. 38, p. 1206, 2002.

[23] X. C. Ye, Q. Zhang, and J. Liu, "Impact of climate change and human activities on runoff of Poyang Lake Catchment," *Journal of Glaciology and Geocryology*, vol. 31, no. 5, pp. 835–842, 2009 (Chinese).

[24] X. Ma, J. Xu, and M. van Noordwijk, "Sensitivity of streamflow from a Himalayan catchment to plausible changes in land cover and climate," *Hydrological Processes*, vol. 24, no. 11, pp. 1379–1390, 2010.

[25] X. Hao, Y. Chen, C. Xu, and W. Li, "Impacts of climate change and human activities on the surface runoff in the Tarim River Basin over the last fifty years," *Water Resources Management*, vol. 22, no. 9, pp. 1159–1171, 2008.

[26] J. Wang, Y. Hong, J. Gourley, P. Adhikari, L. Li, and F. Su, "Quantitative assessment of climate change and human impacts on long-term hydrologic response: a case study in a sub-basin of the Yellow River, China," *International Journal of Climatology*, vol. 30, no. 14, pp. 2130–2137, 2010.

[27] Z. Li, W.-Z. Liu, X.-C. Zhang, and F.-L. Zheng, "Impacts of land use change and climate variability on hydrology in an agricultural catchment on the Loess Plateau of China," *Journal of Hydrology*, vol. 377, no. 1-2, pp. 35–42, 2009.

[28] G. Wang, J. Xia, and J. Che, "Quantification of effects of climate variations and human activities on runoff by a monthly water balance model: a case study of the Chaobai River basin in northern China," *Water Resources Research*, vol. 45, no. 7, Article ID W00A11, 2009.

[29] J. Fan, F. Tian, Y. Yang, S. Han, and G. Qiu, "Quantifying the magnitude of the impact of climate change and human activity on runoff decline in Mian River Basin, China," *Water Science and Technology*, vol. 62, no. 4, pp. 783–791, 2010.

[30] D. Liu, X. Chen, Y. Lian, and Z. Lou, "Impacts of climate change and human activities on surface runoff in the Dongjiang River basin of China," *Hydrological Processes*, vol. 24, no. 11, pp. 1487–1495, 2010.

[31] K. Lin, S. Guo, W. Zhang, and P. Liu, "A new baseflow separation method based on analytical solutions of the Horton infiltration capacity curve," *Hydrological Processes*, vol. 21, no. 13, pp. 1719–1736, 2007.

[32] K. Lin, Q. Zhang, and X. Chen, "An evaluation of impacts of DEM resolution and parameter correlation on TOPMODEL modeling uncertainty," *Journal of Hydrology*, vol. 394, no. 3-4, pp. 370–383, 2010.

[33] Y. Hundecha and A. Bárdossy, "Modeling of the effect of land use changes on the runoff generation of a river basin through parameter regionalization of a watershed model," *Journal of Hydrology*, vol. 292, no. 1–4, pp. 281–295, 2004.

[34] K. Y. Li, M. T. Coe, N. Ramankutty, and R. D. Jong, "Modeling the hydrological impact of land-use change in West Africa," *Journal of Hydrology*, vol. 337, no. 3-4, pp. 258–268, 2007.

[35] G. Parkin, G. O'Donnell, J. Ewen, J. C. Bathurst, P. E. O'Connell, and J. Lavabre, "Validation of catchment models for predicting land-use and climate change impacts. 2. Case study for a Mediterranean catchment," *Journal of Hydrology*, vol. 175, no. 1–4, pp. 595–613, 1996.

[36] J. K. Lørup, J. C. Refsgaard, and D. Mazvimavi, "Assessing the effect of land use change on catchment runoff by combined use of statistical tests and hydrological modelling: case studies from Zimbabwe," *Journal of Hydrology*, vol. 205, no. 3-4, pp. 147–163, 1998.

[37] D. Niehoff, U. Fritsch, and A. Bronstert, "Land-use impacts on storm-runoff generation: scenarios of land-use change and simulation of hydrological response in a meso-scale catchment in SW-Germany," *Journal of Hydrology*, vol. 267, no. 1-2, pp. 80–93, 2002.

[38] B. Troy, C. Sarron, J. M. Fritsch, and D. Rollin, "Assessment of the impacts of land use changes on the hydrological regime of a

small rural catchment in South Africa," *Physics and Chemistry of the Earth*, vol. 32, no. 15–18, pp. 984–994, 2007.

[39] H. Chen, S. Guo, C.-Y. Xu, and V. P. Singh, "Historical temporal trends of hydro-climatic variables and runoff response to climate variability and their relevance in water resource management in the Hanjiang basin," *Journal of Hydrology*, vol. 344, no. 3-4, pp. 171–184, 2007.

[40] D. H. Burn, "Climatic influences on streamflow timing in the headwaters of the Mackenzie River Basin," *Journal of Hydrology*, vol. 352, no. 1-2, pp. 225–238, 2008.

[41] H. B. Mann, "Nonparametric tests against trend," *Econometrica*, vol. 13, no. 7, pp. 245–259, 1945.

[42] M. G. Kendall, *Rank Correlation Methods*, Griffin, London, UK, 1975.

[43] J. M. Mitchell, B. Dzerdzeevskii, H. Flohn et al., "Climate change," WMO Technical Note 79, World Meteorological Organization, 1966.

[44] E. Kahya and S. Kalayci, "Trend analysis of streamflow in Turkey," *Journal of Hydrology*, vol. 289, no. 1–4, pp. 128–144, 2004.

[45] Z. X. Xu, K. Takeuchi, H. Ishidaira, and J. Y. Li, "Long-term trend analysis for precipitation in Asian Pacific FRIEND river basins," *Hydrological Processes*, vol. 19, no. 18, pp. 3517–3532, 2005.

[46] R. Modarres and V. de Paulo Rodrigues da Silva, "Rainfall trends in arid and semi-arid regions of Iran," *Journal of Arid Environments*, vol. 70, no. 2, pp. 344–355, 2007.

[47] F.-W. Gerstengarbe and P. C. Werner, "Estimation of the beginning and end of recurrent events within a climate regime," *Climate Research*, vol. 11, no. 2, pp. 97–107, 1999.

[48] T. Jiang and Q. Zhang, "Climatic changes driving on floods in the Yangtze Delta, China during 1000–2002," *European Journal of Geography, Cybergeo*, vol. 296, pp. 1–21, 2004.

[49] M. Ç. Karabörk, "Trends in drought patterns of Turkey," *Journal of Environmental Engineering and Science*, vol. 6, no. 1, pp. 45–52, 2007.

[50] D. Ramakrishnan, A. Bandyopadhyay, and K. N. Kusuma, "SCS-CN and GIS-based approach for identifying potential water harvesting sites in the Kali Watershed, Mahi River Basin, India," *Journal of Earth System Science*, vol. 118, no. 4, pp. 355–368, 2009.

[51] R. K. Sahu, S. K. Mishra, and T. I. Eldho, "Comparative evaluation of SCS-CN-inspired models in applications to classified datasets," *Agricultural Water Management*, vol. 97, no. 5, pp. 749–756, 2010.

[52] D. G. Durbude, M. K. Jain, and S. K. Mishra, "Long-term hydrologic simulation using SCS-CN-based improved soil moisture accounting procedure," *Hydrological Processes*, vol. 25, no. 4, pp. 561–579, 2011.

[53] L. H. Xiong and S. L. Guo, *Distributed Hydrological Model*, China Water Power Press, 2004.

[54] X. H. Chen and Z. L. Wang, "Land use change and its impact on water resources in east river basin, south China," *Journal of Beijing Normal University*, vol. 46, no. 3, pp. 311–316, 2010 (Chinese).

[55] J. E. Nash and J. V. Sutcliffe, "River flow forecasting through conceptual models part I—a discussion of principles," *Journal of Hydrology*, vol. 10, no. 3, pp. 282–290, 1970.

Hindawi Publishing Corporation
Mathematical Problems in Engineering
Volume 2013, Article ID 104591, 10 pages
http://dx.doi.org/10.1155/2013/104591

Research Article

Numerical Study on Initial Field of Pollution in the Bohai Sea with an Adjoint Method

Chunhui Wang,[1,2] Xiaoyan Li,[1,3] and Xianqing Lv[1]

[1] *Laboratory of Physical Oceanography, Ocean University of China, Qingdao 266100, China*
[2] *Key Laboratory of Marine Spill Oil Identification and Damage Assessment Technology, The Organization of North China Sea Monitoring Center, Qingdao 266033, China*
[3] *Institute of Oceanology, Chinese Academy of Science, Qingdao 266071, China*

Correspondence should be addressed to Xianqing Lv; xqinglv@ouc.edu.cn

Received 24 January 2013; Revised 6 May 2013; Accepted 27 May 2013

Academic Editor: Bing Chen

Based on the simulation of a marine ecosystem dynamical model in the Bohai Sea, routine monitoring data are assimilated to study the initial field of pollution by using the adjoint method. In order to reduce variables that need to be optimized and make the simulation results more reasonable, an independent grid is selected every four grids both in longitude and latitude, and only the pollutant concentrations of these independent grids needed to be optimized while the other grids were calculated by interpolation method. Based on this method, the stability and reliability of this model were proved by a set of twin experiments. Therefore, this model could be applied in real experiment to simulate the initial field of the total nitrogen (totalN) in May, 2009. Moreover, the distribution of totalN in any time step could be calculated by this model, and the monthly mean distribution in May in the Bohai Sea could be obtained.

1. Introduction

The Bohai Sea is the only inland sea in China with a maritime area being $7.7 \times 10^4\,\mathrm{km}^2$. Its mean depth is 18 m, and the deepest point is located in the west of the Lao Tie Shan channel. Because the runoff of the Yellow River, the Haihe River and the Liao River are all discharged into the Bohai Sea; the organic pollutants are tremendous. Unfortunately, water exchange of the Bohai Sea is very weak and its physical self-cleaning capacity is poor due to its special geographical position. The Bohai Sea is surrounded by land on three sides, and it is only connected with the Yellow Sea through the Bohai strait on the east side. Therefore, it is hard to recover if the Bohai Sea is polluted. A mount of industrial effluent, living sewage, and aquaculture waste water are released into the Bohai Sea with rapid development of the economy along the Bohai Sea, which can cause accumulation of nutrient substances, such as nitrogen and phosphorus. The accumulation of nutrient substance brings a series of ecoenvironmental degradation, including red tide, decrease of seawater oxygen content, decline of biodiversity, and decrease in fish catch. In order to protect and recover the ecoenvironment of the Bohai Sea and to coordinate and improve coastal economy, an accurate simulation of the time-varying pollutant distribution is needed. Only in this way can we achieve rational utilization of marine resources and sustainable development of economy.

Recently, more and more numerical models (e.g., Chen et al. [1], Duan and Nanda [2], Lee and Seo [3], Liu et al. [4], Gupta et al. [5], Periáñez [6, 7], Rajar et al. [8], Rajar and Cetina [9]) for simulating pollutant dispersion have been actually developed since they can be used for decision making after releases of contaminants into the marine environment (Periáñez [10]). Gupta et al. [5] applied a two-dimensional numerical model considering organized wastewater discharges to determine the wastewater assimilative capacity of Thane creek. They found that on the basis of monitoring and simulation, the water quality had been deteriorated significantly due to limited flushing capacity. The volumetric load in the creek needed to be

restricted because projected wastewater flows and loads for 2015 were above the assimilative capacity of the creek. Huang et al. [11] investigated the distribution characteristics of heavier or lighter pollutants released at different cross-sectional positions of a wide river with a well-tested three-dimensional numerical model, and their findings assisted in cost-effective countermeasures to be taken for accidental or planned pollutant releases into a wide river. All the three major Siberian rivers, including Ob, Yenisei, and Lena, flow northward into Arctic, and they are supposed to be important sources for various contaminants, so Harms et al. [12] applied a three-dimensional coupled ice-ocean-models of different horizontal resolution to simulate the dispersion of water from these rivers. The model study confirmed that contaminant transport through sediment-laden sea ice offers a short and effective pathway for pollutant transport from Siberian River to the Barents and Nordic Seas. Different methodologies for coupling hydrodynamic submodels with mass transport submodels into integrated water quality models are described in a companion paper (Rajar et al. [8]). The conclusion is that the choice of the methodology depends on the space and time scales, on the prevalent forcing factors and on the nature of the contaminant.

The initial condition has dramatic influence on the simulated results when we use model both in meteorology and oceanography. But in most cases, we do not know the initial field in advance. Therefore, it is important to simulate the initial field accurately. For example, the pollutant distribution characteristics are very different if either the pollutant density or the release location is changed when pollutants are released into a river (Huang et al. [11]). A suite of experimental results of Pe ng and Xie [13] show that although forecast errors due to deficiencies in model physics or numerics cannot always be effectively corrected through improving initial conditions alone, the four-dimensional variational data assimilation algorithm based on Princeton Ocean Model (POM) leads to effective convergence between the forecasts and the "observations" by finding an "optimal" initial condition for the storm surge forecasting. Allen et al. [14] found the combination of source location, source strength, and surface wind direction that best matched the dispersion model output to the receptor data by using genetic algorithm (GA) and demonstrated that the GA was capable of computing the correct solution as long as the magnitude of the noise did not exceed that of the receptor data.

In order to obtain the initial condition or the average distribution of pollutant concentration in a certain period, the traditional way is to use all the observations within this period by interpolation method, such as Cressman and Kriging. However, this method only takes the spatial information of the observations into consideration but ignores the time information, which may lead to a big difference between the simulation results and the actual situation. Adjoint method minimizes a predetermined cost function which defines differences between model-derived quantities and measured quantities by using the existing observations to the maximum extent. Adjoint method is an effective variational assimilation technique based on mathematics strictly. It takes ocean model equations, initial conditions, and boundary conditions as the constraint conditions and combines variational principle and the theory of optimal control. With the accessible oceanic elements, some inaccessible oceanic elements can be obtained by optimizing initial field and/or parameters (Sasaki [15]; Lu and Zhang [16]).

Adjoint method was widely used in both meteorology and oceanography. Zhang et al. [17] applied this method to study the similarities and the differences between the Ekman (linear) and the Quadratic (nonlinear) bottom friction parameterizations for a two-dimensional tidal model. The simulation results indicated that the nonlinear Quadratic parameterization is more accurate than the linear Ekman parameterization if the traditional constant boundary friction coefficient is used. However, when the spatially varying boundary friction coefficients were used, the differences between the Ekman and the Quadratic approaches diminished. In the study of Fan and Lv [18], SeaWiFS chlorophyll-a data were assimilated into a simple NPZD model by the adjoint method in a climatological physical environment provided by FOAM. The results showed that the values of the selected sensitive parameters were spatially variable and the application of spatial parameterizations could improve the assimilation results significantly. Many researches (Yu and O'Brien [19], Lawson et al. [20], Zhao et al. [21], Zhao and Lu [22], Qi et al. [23]) have proved the validity and rationality of the adjoint method. Therefore, in this paper, we apply this method to simulate the distribution of totalN in any time step, and the monthly mean distribution in May in the Bohai Sea can be obtained.

The contents of this paper are organized as follows. Section 2 describes the ecosystem model and the database. Section 3 illustrates the adjoint method and independent grids briefly. Section 4 describes the twin experiment to validate the model's capability of inversing pollutant initial field and finds the optimal strategy of setting independent grids. Based on twin experiments, practical experiment is performed in Section 5 in order to obtain the initial field of totalN in the Bohai Sea in May. The conclusions of our work are presented in Section 6.

2. Model and Data

2.1. Model Equations. Based on hydrodynamic model, the transporting diffusion process of pollution can be written as follows:

$$\frac{\partial C}{\partial t} + u\frac{\partial C}{\partial x} + v\frac{\partial C}{\partial y} + w\frac{\partial C}{\partial z} = \frac{\partial}{\partial x}\left(A_H\frac{\partial C}{\partial x}\right) + \frac{\partial}{\partial y}\left(A_H\frac{\partial C}{\partial y}\right) + \frac{\partial}{\partial z}\left(K_H\frac{\partial C}{\partial z}\right) - rC, \quad (1)$$

where A_H and K_H represent horizontal and vertical eddy diffusivities, respectively, C is the concentration of pollution, and r is the degradation coefficient of pollution. When the pollution is conservative substance, $r = 0$; otherwise, $r \neq 0$. In this paper, we treat the pollution as conservative substance, so $r = 0$; the finite-difference form can be seen in Appendix A.

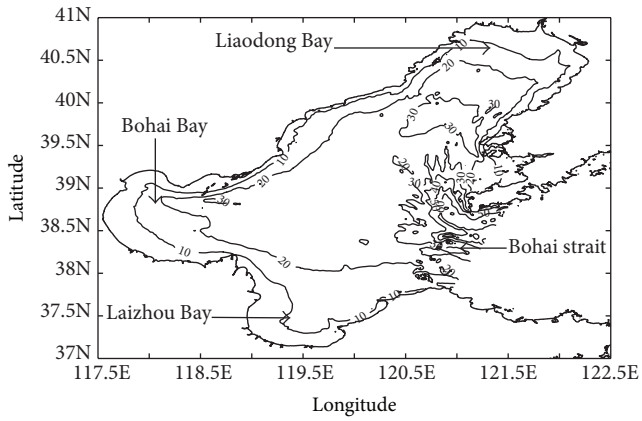

Figure 1: Location and morphology of the Bohai Sea. Values of the bathymetric isolines are in meters.

The three-dimensional Regional Ocean Model System (ROMS) is used to calculate the ambient physical velocities and temperature in the Bohai Sea (37°N~41°N, 122.5°E~127.5°E, Figure 1), and the horizontal resolution is 4 second in both latitude and longitude. The thickness of each layer from top to bottom is 10 m, 10 m, 10 m, 20 m, 25 m, and 25 m, respectively, and the integral time step is 6 hours.

Monthly mean horizontal currents in May in the Bohai Sea obtained by ROMS in 5 m depth, 15 m depth, and 25 m depth are shown in Figures 2(a), 2(b), and 2(c), respectively. On the whole, mean flow velocity decreases gradually from surface to bottom in the Bohai Sea. There is a clockwise vortex in the central Bohai Sea, and an anticlockwise vortex can be seen in the east part of Liaodong Bay. The circulation in Laizhou Bay is very weak, and there is a clockwise vortex in the mouth. Meanwhile, water flows out of Bohai Sea through north of Bohai Strait and into Bohai Sea through south of Bohai Strait.

2.2. Observations and Model-Generated Observations. The distribution of the conventional monitoring stations is depicted in Figure 3. We can see that most of the stations are located in the Bohai strait and the coastal areas while only a few of them are located in the central Bohai Sea. The observations are needed in practical experiments and some model-generated observations are needed in the twin experiments. We can choose some model-generated observations through the following methods: first, an initial pollutant distribution (initial field) in the Bohai Sea is assigned. Then, the forward model is run for 30 days, so the pollutant distribution at every time step can be obtained. As the sampling locations of the conventional monitoring stations have been known from Figure 3, we can pick up model-generated observations according to the following method: the sampling locations of the model-generated observations are the same as the conventional monitoring stations. The total number of the conventional monitoring stations is 121. Since the total calculating step is also 121, we prescribe that the number of model-generated stations are in one-to-one correspondence with the sampling time for the sake of simplicity. The observation numbers of each station depend on the depth of water. If the water depth is within three layers, the pollutant concentration of every layer is chosen as model-generated observations; otherwise, only the pollutant concentration of upper three layers is chosen as model-generated observations.

If a guess initial field of pollution is given, the initial field of the pollution can be optimized by using the observations (practical experiment) or the model-generated observations (twin experiment) through the adjoint method.

3. Method

3.1. Adjoint Assimilation Method. Adjoint assimilation method treats all the practical problems as minimum problems. It takes model equations, initial conditions, and boundary conditions as constraint conditions and minimizes a predetermined cost function which defines differences between model-derived quantities and measured quantities. The flowchart in Figure 4 summarizes the steps that make up the adjoint method.

Step 1. an initial distribution of pollution is given empirically (guess distribution);

Step 2. perform the simulation by running the forward model, and the simulation results are obtained;

Step 3. Calculate the cost function which defines the misfit between simulation results and observations. The cost function is defined by

$$J = \frac{1}{2} \sum K_C \left(C_{i,j,k} - \overline{C}_{i,j,k} \right)^2, \tag{2}$$

where $C_{i,j,k}$ represents the simulation result, $\overline{C}_{i,j,k}$ is the observation, the index triplet (i, j, k) is a pointer to certain grid cell, and K_C is the weight of the observation, which is defined as follows:

$$K_C = \begin{cases} 1, & \text{if the observations are available} \\ 0, & \text{otherwise;} \end{cases} \tag{3}$$

Step 4. the adjoint of the model (Appendix B) is run backward in time;

Step 5. calculate the gradient of the cost function with respect to initial field;

Step 6. update the initial pollutant distribution closer to the minimum of the cost function;

Step 7. return to Step 1; repeat the iteration with the updated pollutant distribution;

Step 8. end this procedure after a specific number of iterations or the cost function J is small enough to meet the criteria $J < \varepsilon$ (ε is a small real number, such as 0.01), and the optimized initial field of pollution is obtained. In this paper, we choose the former for easiness to compare the simulation results in twin experiment 1.

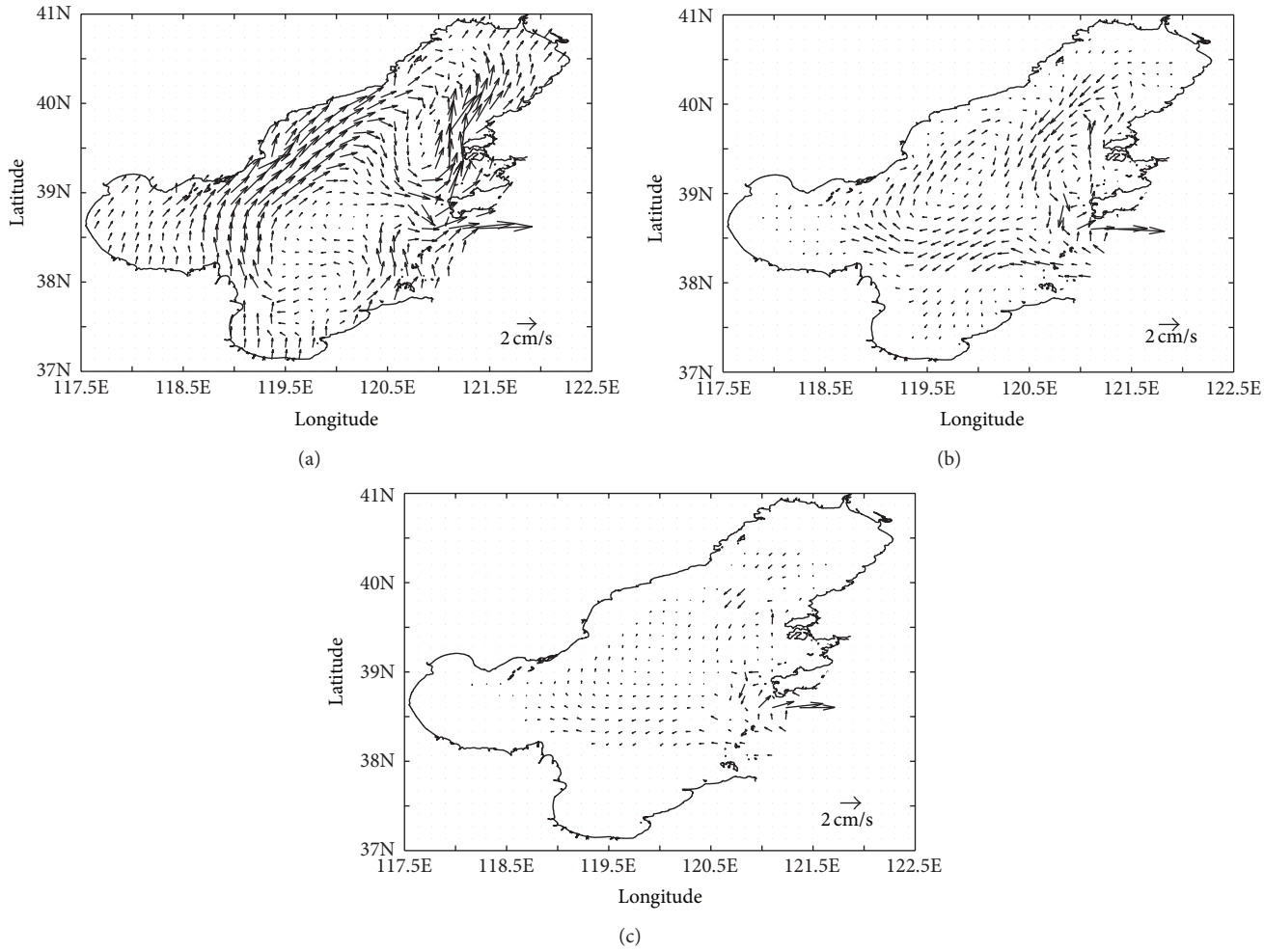

Figure 2: Monthly mean horizontal currents in May in the Bohai Sea in (a) 5 m depth, (b) 15 m depth, and (c) 25 m depth.

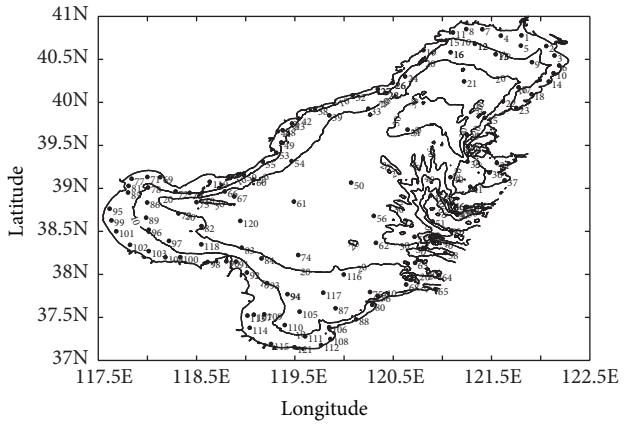

Figure 3: The regular monitoring stations in the Bohai Sea.

3.2. Independent Grids. If the pollutant concentration of each grid is optimized independently, then there are too many variables to constraint, and the pollutant distribution is not continuous, which is not reasonable. So, we can reduce variables that need to be optimized and guarantee that the simulation result coincides with the law of physics by using independent grids. Several grids are selected as independent grids and only pollutant concentrations of these independent grids need to be optimized while those of other grids are calculated by Cressman method [18]. Since cost function declines in the inverse direction of its gradient, the gradient is used to determine the direction to optimize the pollutant concentration. In this paper, the distributions of independent grids in longitude are the same as in latitude.

4. Numerical Experiments and Result Analysis

4.1. Twin Experiment 1: The Strategy of Independent Grids. The simulated results are affected by the number of independent grids, so we will discuss this factor in twin experiment 1. The experiment is designed as follows. Assume that the initial distribution of pollutant concentration shows a parabolic surface with upward convex, which means it is high in the centre and low in the surroundings. The independent grids are selected every 2 to 9 common grids. The influence radius is 1.2 times of the distance between adjacent independent

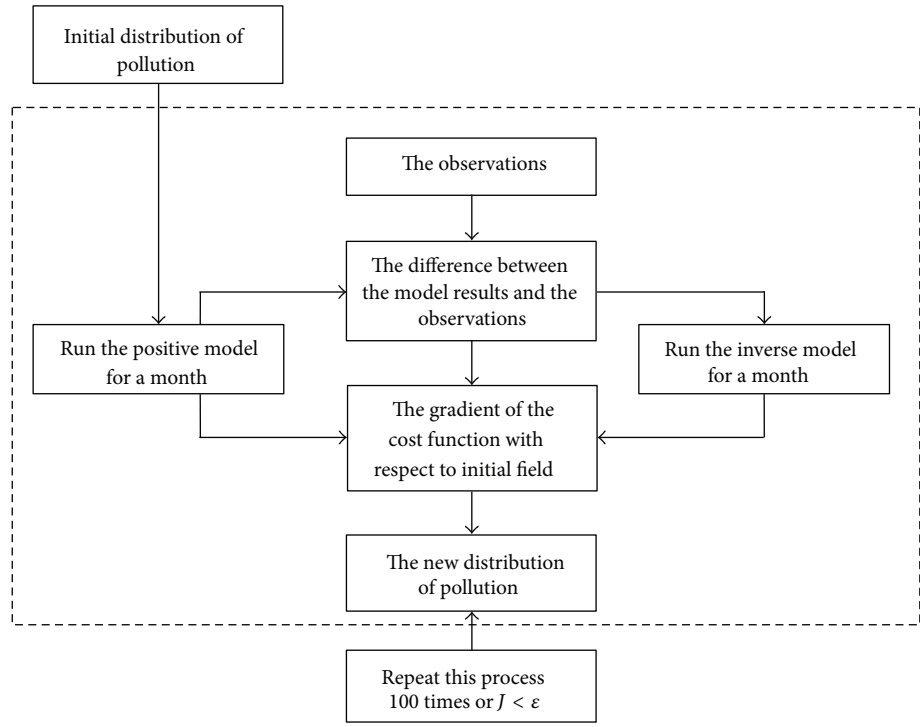

Figure 4: Flowchart of the adjoint assimilation method.

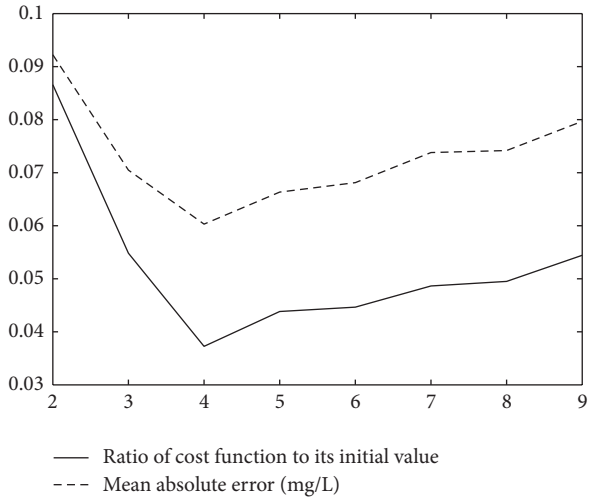

Figure 5: Relationship between inversion results and number of independent grid.

grids, and the number of iterations is set to 100 mainly based on the following considerations: (1) the misfit between "observations" and the simulated results is very small and approximately constant when it declines to a certain value after 100 iterations; (2) the cost functions are almost no longer falling after 100 iterations; and (3) the calculation amount is acceptable for the 100 iterations. The results are given in Figure 5.

In Figure 5, X-axis represents that there is one independent grid every 2 to 9 common grids. The solid line shows the ratio of cost function to its initial value while the dotted line indicates mean absolute error (MAE) of the model-generated observations. It shows that when independent grids get fewer, both the cost function and the MAE of the model-generated observations get smaller at first but larger after 1.2°. This means that choosing an independent grid every four grids is the best choice. Therefore, in the following experiments, we select an independent grid every four grids both in longitude and latitude.

4.2. Twin Experiment 2: The Pollutant Concentration Shows a Parabolic Surface

4.2.1. Parabolic Surface with Upward Convex. Assume that the initial distribution of pollutant concentration shows a parabolic surface with upward convex, which means it is high in the centre and low in the surroundings, and the pollutant concentration at any grid can be calculated by

$$C(i,j) = \left((\mathrm{lon}(i) - 120.0)^2 + (\mathrm{lat}(j) - 39.0)^2\right) \times 0.2 + 0.05, \tag{4}$$

where $\mathrm{lon}(i)$ and $\mathrm{lat}(j)$ indicate the longitude and latitude of grid (i, j), respectively. Equation (4) shows that the pollutant concentration varies from 0.05 to 2.10.

We guess that the initial pollutant concentration at any grid is 0.05 mg/L, and the number of iterations is the same as twin experiment 1.

As we can see from Figures 6 and 7, the cost function can reduce to 3.7 percent of its initial value. Table 1

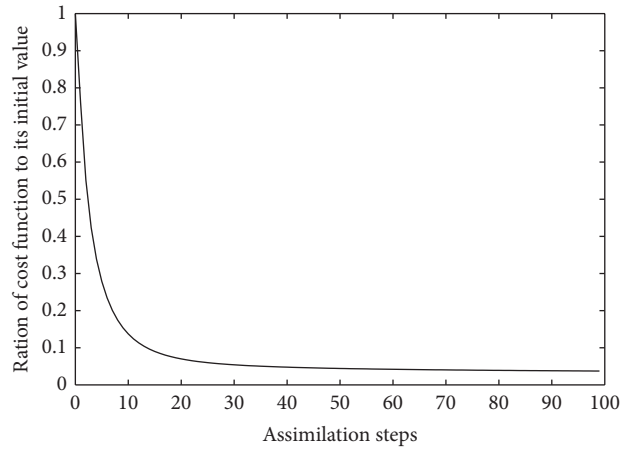

Figure 6: Ratio of cost function to its initial value versus assimilation step.

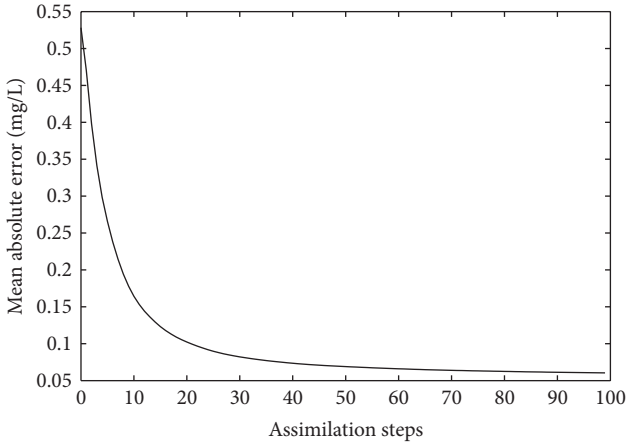

Figure 7: Mean absolute error versus assimilation step.

shows that the MAE of the model-generated observations declines from 0.53 mg/L to 0.06 mg/L, which decreases by 88.7 percent, and Table 2 shows that the mean relative error (MAE) also declined obviously after adjoint assimilation. The results indicate that through adjoint assimilation, the model-generated observations have been effectively used, and the given distribution can be inverted successfully. The given distribution and inversion results can be seen in Figures 8 and 9. The inversion results of the central Bohai Sea and the Laizhou Bay are very satisfactory while those of the transition zones between the central Bohai Sea and the three bays are a little worse. The inversion results are basically the same as the prescribed distribution.

4.2.2. Parabolic Surface with Downward Convex. Assume that the initial distribution of pollutant concentration shows a parabolic surface with downward convex, which means it

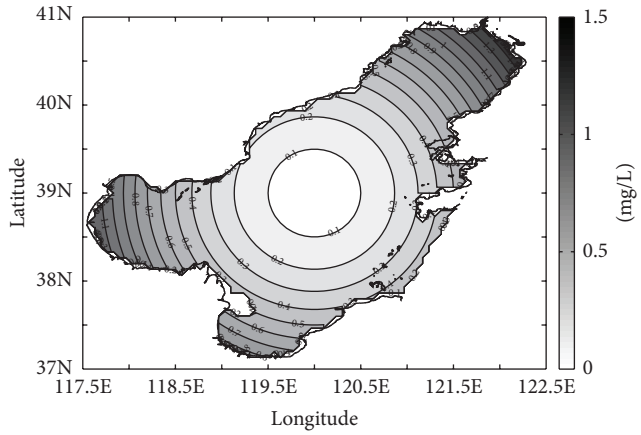

Figure 8: Prescribed initial distribution of pollutant concentration.

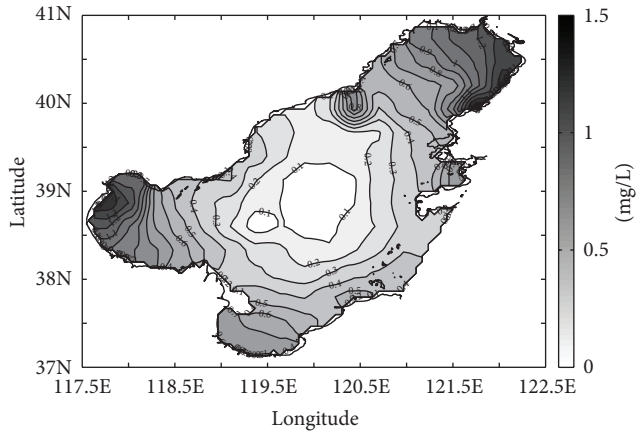

Figure 9: Inversion results of initial distribution of pollutant concentration.

is low in the centre and high in the surroundings, and the pollutant concentration at any grid can be calculated by

$$C(i,j) = -\left((\text{lon}(i) - 120.0)^2 + (\text{lat}(j) - 39.0)^2\right) \times 0.2 + 2.10. \quad (5)$$

Repeat the process of Section 4.2.1. The cost function can reduce to 8.3 percent of its initial value, and the MAE of the model-generated observations declines from 1.5 mg/L to 0.2 mg/L, indicating that the model is stable and valid. No matter which convex is given, the initial distribution can be inverted successfully.

4.3. Twin Experiment 3: The Pollutant Concentration Shows a Conical Surface. Assume that the initial pollutant concentration shows a conical surface with upward convex, and the pollutant concentration at any grid can be calculated by

$$C(i,j) = \sqrt{0.41 \times \left((\text{lon}(i) - 120.0)^2 + (\text{lat}(j) - 39.0)^2\right)} + 0.05. \quad (6)$$

Table 1: The change of cost function and MAE after reversion.

Type of pollutant distribution	Cost function	Initial value of MAE (mg/L)	Initial value of MAE (mg/L)	Reduction ration of MAE (%)
Parabolic surface				
Up direction	3.7×10^{-2}	0.53	0.06	88.7
Down direction	8.3×10^{-2}	1.52	0.20	86.9
Conical surface				
Up direction	4.4×10^{-2}	0.98	0.11	92.5
Down direction	9.1×10^{-2}	1.07	0.15	92.1

Table 2: The change of cost function and MRE after reversion.

Type of pollutant distribution	Initial value of MRE (%)	Final value of MRE (%)	Reduction ration of MRE (%)
Parabolic surface			
Up direction	86.3	12.8	85.2
Down direction	96.7	12.2	87.4
Conical surface			
Up direction	93.9	12.7	86.5
Down direction	95.1	12.3	87.1

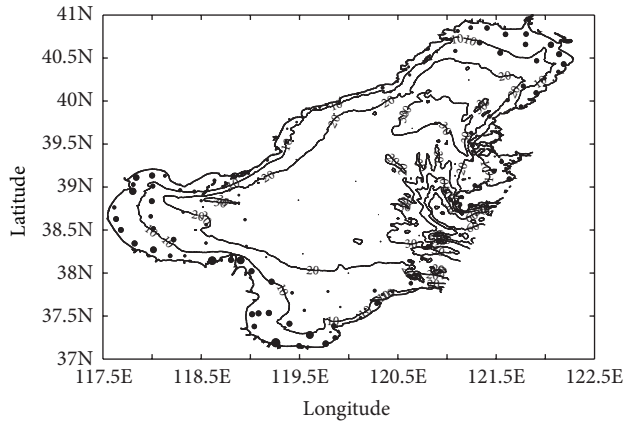

Figure 10: Distribution of totalN monitoring station in use in May, 2009.

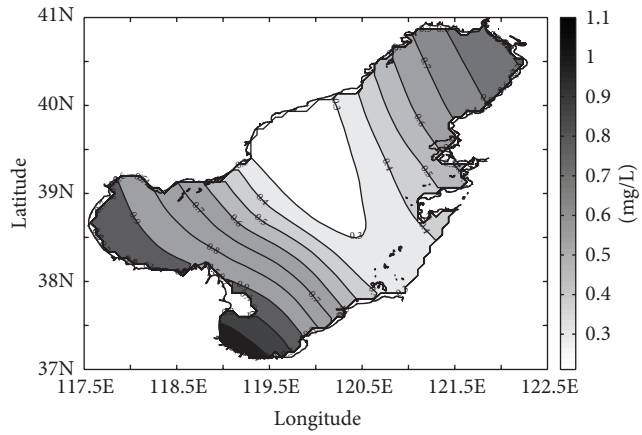

Figure 11: Monthly mean distribution of totalN in May in the Bohai Sea calculated by the Cressman method.

Assume that the initial pollutant concentration shows a conical surface with downward convex and the pollutant concentration at any grid can be calculated by

$$C(i, j) = -\sqrt{0.41 \times \left((\text{lon}(i) - 120.0)^2 + (\text{lat}(j) - 39.0)^2\right)} + 2.10. \quad (7)$$

Twin experiments can also be evaluated by the absolute and the relative difference between the prescribed and the inversion results.

In these circumstances, the initial pollutant concentration also varies from 0.05 to 2.10. Repeat the process of twin experiment 2, and the results are similar to those of twin experiment 2. The detailed information is presented in Table 1. These results once again verify the stability and validation of this model, indicating that the coupled model can be used in practical experiment. In other words, the initial field of the Bohai Sea can be inverted through adjoint method by using the regular monitoring observations.

5. Practical Experiment and Result Analysis

The distribution of totalN monitoring stations in May, 2009 is shown in Figure 10. The larger the dot is, the greater the observation it represents. According to the traditional method, the monthly mean distribution of totalN in surface layer is always obtained by interpolation method, such as Cressman and Kriging. The monthly mean distribution of totalN in surface layer calculated by Cressman method is depicted in Figure 11. When we make use of the coupled model mentioned in this paper, not only the initial totalN distribution in May, but also the distribution in any time step can be obtained. And then, we can get the monthly mean distribution of totalN in surface layer, which is depicted in Figure 12.

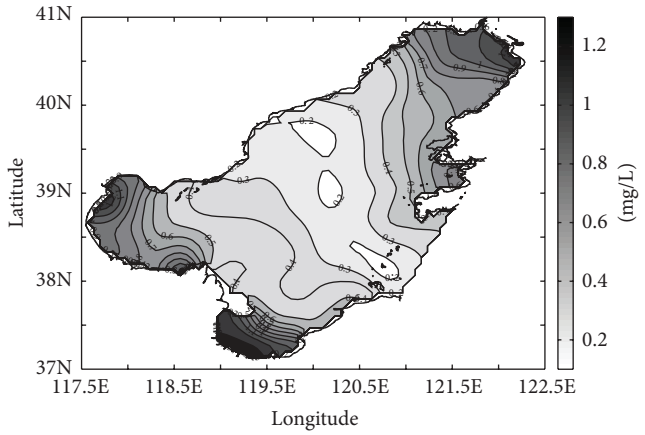

Figure 12: Monthly mean distribution of totalN in May in the Bohai Sea obtained by the adjoint method.

In the Bohai strait and the central Bohai Sea, the distribution of totalN calculated by the Cressman method is similar to the result obtained by the adjoint method. However, the latter is higher in the Laizhou Bay and lower in the Liaodong Bay than the former. The reason may be that the sampling time of each routine monitor station is not the same, and the observation cannot always reflect the mean value in a month. Moreover, the Cressman method only takes the spatial information of the stations into consideration and ignores the time information.

The average concentration of totalN in surface layer in the Bohai Sea is 0.49 mg/L by using the Cressman method while it is only 0.41 mg/L by using the adjoint method. The former is almost twenty percent greater than the latter. The reason is probably that most of routine monitoring stations are located in the Bohai strait and the coastal areas while only a few of those located in the central Bohai Sea. In the meantime, the observations in the Bohai strait and the coastal areas are of relativly high values while the observations in the central Bohai Sea are of relative low values. When we calculate the pollutant concentration between high-value observations and low-value observations by using the Cressman method, there may be more high-value observations involved in the calculation. Therefore, it will lead to a larger pollutant concentration than the real value in most areas. Moreover, although the interpolation results can guarantee the continuity of the totalN distribution, the totalN concentration at any grid cannot be larger or smaller than the observations we already have.

The adjoint method can make use of the observations to a maximum extent. By using this method, not only the values and locations of the observations, but also the sampling time is taken into consideration. The distribution characteristics of totalN in the Bohai Sea in May are depicted in Figure 12. The concentration of totalN is lowest in the central Bohai Sea and Bohai strait. In fact, the concentration is almost zero in these areas, and the highest concentration is no more than 0.5 mg/L. The totalN concentrations of three bays are higher than the central Bohai Sea, among them the concentration of Bohai Bay is the lowest, while Liaodong Bay takes the second place, and the concentration of most areas is less than 1.0 mg/L. The totalN concentration of the Laizhou is the highest. It is more than 1.0 mg in half of areas, and it even reaches 1.4 mg/L in some areas.

6. Conclusion

Recently, more and more numerical models for simulating pollutant dispersion have been actually developed since they can be used for decision-making purposes after releases of contaminants into the marine environment (Periáñez [10]). Regardless of which numerical model we employ, the initial field of pollution has dramatic influence on the simulated results. Therefore, in order to simulate the dispersion process of the pollution accurately, we need not only a good pollutant model and reasonable model parameters, but also an accurate initial distribution of pollution. Although some researchers have tried to inverse the pollutant location and strength, this is the first time to inverse the initial distribution of pollution as far as we know.

Based on the simulation of a marine ecosystem dynamical model in the Bohai Sea, routine monitoring data were assimilated to study the initial field of pollution in this paper. Firstly, in order to reduce variables that need to be optimized and make the simulation results more reasonable, an independent grid is selected every four grids both in longitude and latitude, and only the pollutant concentrations of these independent grids needed to be optimized while the other grids were calculated by interpolation method. Based on this method, the stability and reliability of this model were proved by a set of twin experiments. Therefore, this model could be applied in real experiment to simulate the initial field of the totalN in May, 2009. Furthermore, the distribution of totalN in any time step could be calculated by this model, and the monthly mean distribution in May in the Bohai Sea could be obtained. Compared with the Cressman method, the adjoint method can make use of the existing observations to the maximum extent. Not only the values and locations of the observations, but also the sampling time are taken into consideration by using this method. Therefore, it can reduce the misfit between inversion results and observations significantly and make the simulated results closer to reality. This method can also be used to simulate the distribution of other pollutions, such as total phosphorus, chemical oxygen demand, and petroleum hydrocarbon. So, it could most probably be used in solving environmental problems in the future.

Appendices

A. Finite-Difference Form of Equation (1)

Consider the following:

$$\frac{\left(C_{i,j,k}^{l+1} - C_{i,j,k}^{l}\right)}{\Delta t} - \left[\frac{K_H\left(C_{i,j,k+1}^{l+1} - C_{i,j,k}^{l+1}\right)}{\Delta z_{k+1/2} \cdot \Delta z_{k+1}} - \frac{K_H\left(C_{i,j,k}^{l+1} - C_{i,j,k-1}^{l+1}\right)}{\Delta z_{k+1/2} \cdot \Delta z_{k}}\right]$$

$$= -\frac{u^l_{i,j,k}\left(C^l_{i+1,j,k} - C^l_{i-1,j,k}\right)}{2\Delta x_j} - \frac{v^l_{i,j,k}\left(C^l_{i,j+1,k} - C^l_{i,j-1,k}\right)}{2\Delta y}$$
$$- \frac{w^l_{i,j,k}\left(C^l_{i,j,k+1} - C^l_{i,j,k-1}\right)}{2\Delta z_k}$$
$$+ \left[\frac{A_H\left(C^l_{i+1,j,k} - C^l_{i,j,k}\right)}{\Delta x_{j+1/2}\cdot\Delta x_{j+1}} - \frac{A_H\left(C^l_{i,j,k} - C^l_{i-1,j,k}\right)}{\Delta x_{j+1/2}\cdot\Delta x_j}\right]$$
$$+ \left[\frac{A_H\Delta t\cdot\left(C^l_{i,j+1,k} - C^l_{i,j,k}\right)}{(\Delta y)^2} - \frac{A_H\Delta t\cdot\left(C^l_{i,j,k} - C^l_{i,j-1,k}\right)}{(\Delta y)^2}\right], \tag{A.1}$$

where u and v are horizontal velocities and w is vertical velocity.

B. Adjoint Equation

Consider the following:

$$-\frac{\partial C^*}{\partial t} - \frac{\partial}{\partial z}\left(K_H\frac{\partial C^*}{\partial z}\right)$$
$$= \frac{\partial}{\partial x}\left(uC^*\right) + \frac{\partial}{\partial y}\left(vC^*\right) + \frac{\partial}{\partial z}\left(wC^*\right)$$
$$+\frac{\partial}{\partial x}\left(A_H\frac{\partial C^*}{\partial x}\right) + \frac{\partial}{\partial y}\left(A_H\frac{\partial C^*}{\partial y}\right) - K_C\left(C - \overline{C}\right), \tag{B.1}$$

where $\overline{C}$, C represent observation and corresponding simulating result, respectively. C^* is the adjoint operator of C. The finite-difference form of adjoint equation is as follows:

$$\frac{\left(C^{*l-1}_{i,j,k} - C^{*l}_{i,j,k}\right)}{\Delta t}$$
$$- \left[\frac{K_H\left(C^{*l-1}_{i,j,k+1} - C^{*l-1}_{i,j,k}\right)}{\Delta zz_k\cdot\Delta z_{k+1}} - \frac{K_H\left(C^{*l-1}_{i,j,k} - C^{*l-1}_{i,j,k-1}\right)}{\Delta zz_k\cdot\Delta z_k}\right]$$
$$= \frac{\left(u^l_{i+1,j,k}C^{*l}_{i+1,j,k} - u^l_{i-1,j,k}C^{*l}_{i-1,j,k}\right)}{2\Delta x_j}$$
$$+ \frac{\left(v^l_{i,j+1,k}C^{*l}_{i,j+1,k} - v^l_{i,j-1,k}C^{*l}_{i,j-1,k}\right)}{2\Delta y}$$
$$+ \frac{\left(w^l_{i,j,k+1}C^{*l}_{i,j,k+1} - w^l_{i,j,k-1}C^{*l}_{i,j,k-1}\right)}{2\Delta z_k}$$
$$+ \left[\frac{A_H\left(C^{*l}_{i+1,j,k} - C^{*l}_{i,j,k}\right)}{\Delta x_{j+1/2}\cdot\Delta x_{j+1}} - \frac{A_H\left(C^{*l}_{i,j,k} - C^{*l}_{i-1,j,k}\right)}{\Delta x_{j+1/2}\cdot\Delta x_j}\right]$$
$$+ \left[\frac{A_H\left(C^{*l}_{i,j+1,k} - C^{*l}_{i,j,k}\right)}{(\Delta y)^2} - \frac{A_H\left(C^{*l}_{i,j,k} - C^{*l}_{i,j-1,k}\right)}{(\Delta y)^2}\right]$$
$$- K_C\left(C^l_{i,j,k} - \overline{C^l_{i,j,k}}\right). \tag{B.2}$$

Acknowledgments

The authors acknowledge the support of the Major State Basic Research Development Program of China through Grant 2013CB956500, the National Natural Science Foundation of China through Grants 41076006 and 41206001, the Natural Science Foundation of Jiangsu Province of China through Grant BK2012315, and the Fundamental Research Funds for the Central Universities Grants 201261006 and 201262007.

References

[1] Q. Chen, K. Tan, C. Zhu, and R. Li, "Development and application of a two-dimensional water quality model for the Daqinghe River Mouth of the Dianchi Lake," *Journal of Environmental Sciences*, vol. 21, no. 3, pp. 313–318, 2009.

[2] J. G. Duan and S. K. Nanda, "Two-dimensional depth-averaged model simulation of suspended sediment concentration distribution in a groyne field," *Journal of Hydrology*, vol. 327, no. 3-4, pp. 426–437, 2006.

[3] M. E. Lee and I. W. Seo, "Analysis of pollutant transport in the Han River with tidal current using a 2D finite element model," *Journal of Hydro-Environment Research*, vol. 1, no. 1, pp. 30–42, 2007.

[4] X.-B. LIU, W.-Q. PENG, G.-J. HE, J.-L. LIU, and Y.-C. WANG, "A Coupled Model of Hydrodynamics and Water Quality for Yuqiao Reservoir in Haihe River Basin," *Journal of Hydrodynamics*, vol. 20, no. 5, pp. 574–582, 2008.

[5] I. Gupta, S. Dhage, A. A. Chandorkar, and A. Srivastav, "Numerical modeling for Thane creek," *Environmental Modelling and Software*, vol. 19, no. 6, pp. 571–579, 2004.

[6] R. Periáñez, "GISPART: a numerical model to simulate the dispersion of contaminants in the Strait of Gibraltar," *Environmental Modelling and Software*, vol. 20, no. 6, pp. 797–802, 2005.

[7] R. Periáñez, "Modelling the transport of suspended particulate matter by the Rhone River plume (France). Implications for pollutant dispersion," *Environmental Pollution*, vol. 133, no. 2, pp. 351–364, 2005.

[8] R. Rajar, M. Cetina, and A. Sirca, "Hydrodynamic and water quality modelling: case studies," *Ecological Modelling*, vol. 101, no. 2-3, pp. 209–228, 1997.

[9] R. Rajar and M. Cetina, "Hydrodynamic and water quality modelling: an experience," *Ecological Modelling*, vol. 101, no. 2-3, pp. 195–207, 1997.

[10] R. Periáñez, "A particle-tracking model for simulating pollutant dispersion in the Strait of Gibraltar," *Marine Pollution Bulletin*, vol. 49, no. 7-8, pp. 613–623, 2004.

[11] H. Huang, G. Chen, and Q.-F. Zhang, "The distribution characteristics of pollutants released at different cross-sectional positions of a river," *Environmental Pollution*, vol. 158, no. 5, pp. 1327–1333, 2010.

[12] I. H. Harms, M. J. Karcher, and D. Dethleff, "Modelling Siberian river runoff—implications for contaminant transport in the Arctic Ocean," *Journal of Marine Systems*, vol. 27, no. 1–3, pp. 95–115, 2000.

[13] S.-Q. Peng and L. Xie, "Effect of determining initial conditions by four-dimensional variational data assimilation on storm surge forecasting," *Ocean Modelling*, vol. 14, no. 1-2, pp. 1–18, 2006.

[14] C. T. Allen, G. S. Young, and S. E. Haupt, "Improving pollutant source characterization by better estimating wind direction with a genetic algorithm," *Atmospheric Environment*, vol. 41, no. 11, pp. 2283–2289, 2007.

[15] Y. Sasaki, "Some basic formalisms in numerical variational analysis," *Monthly Weather Review*, vol. 98, pp. 875–883, 1970.

[16] X. Lu and J. Zhang, "Numerical study on spatially varying bottom friction coefficient of a 2D tidal model with adjoint method," *Continental Shelf Research*, vol. 26, no. 16, pp. 1905–1923, 2006.

[17] J. Zhang, X. Lu, P. Wang, and Y. P. Wang, "Study on linear and nonlinear bottom friction parameterizations for regional tidal models using data assimilation," *Continental Shelf Research*, vol. 31, no. 6, pp. 555–573, 2011.

[18] W. Fan and X. Lv, "Data assimilation in a simple marine ecosystem model based on spatial biological parameterizations," *Ecological Modelling*, vol. 220, no. 17, pp. 1997–2008, 2009.

[19] L. S. Yu and J. J. O'Brien, "On the initial condion in parameter estimation," *Journal of Physical Oceanography*, vol. 22, pp. 1361–1364, 1992.

[20] L. M. Lawson, Y. H. Spitz, E. E. Hofmann, and R. B. Long, "A data assimilation technique applied to a predator-prey model," *Bulletin of Mathematical Biology*, vol. 57, no. 4, pp. 593–617, 1995.

[21] Q. Zhao, X. Hu, X. Lü, X. Xiong, and B. Yang, "Study on the transport of COD in the sea area around Maidao off Qingdao coast using data assimilation," *Journal of Ocean University of China*, vol. 6, no. 4, pp. 339–344, 2007.

[22] Q. Zhao and X. Lu, "Parameter estimation in a three-dimensional marine ecosystem model using the adjoint technique," *Journal of Marine Systems*, vol. 74, no. 1-2, pp. 443–452, 2008.

[23] P. Qi, C. Wang, X. Li, and X. Lv, "Numerical study on spatially varying control parameters of a marine ecosystem dynamical model with adjoint method," *Acta Oceanologica Sinica*, vol. 30, no. 1, pp. 7–14, 2011.

Hindawi Publishing Corporation
Mathematical Problems in Engineering
Volume 2013, Article ID 327374, 8 pages
http://dx.doi.org/10.1155/2013/327374

Research Article

Modified Palmer Drought Severity Index Based on Distributed Hydrological Simulation

Denghua Yan,[1] Xiaoliang Shi,[1,2] Zhiyong Yang,[1] Ying Li,[2] Kai Zhao,[2] and Yong Yuan[1,3]

[1] *Department of Water Resources, State Key Laboratory of Simulation and Regulation of Water Cycle in River Basin, China Institute of Water Resources and Hydropower Research, Beijing 100038, China*
[2] *Northeast Institute of Geography and Agroecology, Chinese Academy of Sciences, Changchun 130102, China*
[3] *College of Soil and Water Conservation, Beijing Forestry University, Beijing 100083, China*

Correspondence should be addressed to Xiaoliang Shi; shixiaoliang0305@gmail.com

Received 5 February 2013; Accepted 27 May 2013

Academic Editor: Yongping Li

Drought monitoring at large scale is essential for fighting against drought. Aiming at the limitation of acquiring long-time serial soil moisture and actual evapotranspiration for Palmer drought severity index (PDSI), the paper modified the PDSI based on distributed hydrological model on subbasin level in Luanhe river basin, North China. The water balance was simulated using the Soil and Water Assessment Tool (SWAT). Calibration and validation results showed good agreement between simulated and measured discharges, and the SWAT model can be used to predict hydrological processes in the study area. Then the simulation results of main hydrologic components were used to establish PDSI. The verification of the drought indices showed that the modified PDSI based on SWAT model and Palmer drought severity index could better describe the characteristics of regional drought evolution in the Luanhe river basin. High drought frequency areas were mainly distributed in the grassland regions of upstream located in the eastern part of Inner Mongolia plateau, and the drought area had a significant upward trend form 1973 to 2010. Compared with the traditional Palmer drought severity index, the modified PDSI could reflect the spatial heterogeneity of regional drought and improve the physical mechanism of PDSI. The drought monitoring method can provide technical support for comprehensive understanding of drought and effective preventing and relieving of drought disasters.

1. Introduction

Drought is a major natural hazard that can have devastating impacts on regional agriculture, water resources, and the environment, with farreaching impacts in an increasingly globalized world [1]. Besides, droughts are the world's costliest natural disasters, causing an average $6–$8 billion in global damages annually and affecting more people than any other form of natural disasters [2].

It is important to assess and monitor drought due to the consequences and pervasiveness of drought, and various drought indices had been derived to encapsulate drought severity on a regional basis and provide information for decision maker in recent decades [3]. Based on the considerable disagreement that exists about the definition of drought, the drought indices can be sorted as precipitation indices, soil moisture indices, water budget indices, and hydrological and various aridity indices [4]. The commonly used drought indices include standardized precipitation index (SPI) [5], Palmer drought severity index (PDSI) [6], and surface water supply index (SWSI), vegetation condition index [7, 8]. Heim [9] gave a comprehensive review of 20th century drought indices used in the United States.

Palmer Drought Severity Index (PDSI) is perhaps the most widely used regional drought index for monitoring droughts [10–12]. PDSI was developed by Palmer [13] to simulate moisture content of the soil month by month and to compare its monthly anomalies at regions having different climate and seasons [4]. Although referred to as an index of meteorological drought, the PDSI is based on meteorological and soil moisture content, it takes into account precipitation, evapotranspiration, and soil moisture conditions [10], and the PDSI can be used to determine the beginning, ending, and severity of the drought period; it has been normalized so as

to allow comparisons across space and time. However, the PDSI is traditionally calculated by using a two-layer bucket-type model to obtain data on water balance components. This model does not consider the effects of factors such as the spatial heterogeneity of soil, vegetation cover, and topography on watershed hydrological processes. Moreover, in present relative researches, the calculation of PDSI was mainly based on the records of meteorological stations at point scale, have the limitation of acquiring long-time serial soil moisture and actual evapotranspiration at large scale, and cannot clearly reflect the regional difference of drought. Besides, the PDSI uses a simplified model of potential evaporation that responds only to changes in temperature and thus responds incorrectly to global warming in recent decades [14].

Distribution hydrological model is increasingly being used to simulate hydrological processes involved in hydrological cycle [15]. These models can provide some key hydrologic components of long-time serial and large spatial extent (soil moisture, evapotranspiration, surface runoff, etc.) for the calculation of PDSI. As such, the accuracy of PDSI value could potentially be improved by using distribution hydrological model rather than the traditional two-layer bucket-type model for hydrological accounting.

For better reflecting the spatial heterogeneity of regional drought, the feasibility that integrates the distribution hydrological model and PDSI for monitoring drought at large scale was verified. To achieve this, the paper calibrated and validated the Soil and Water Assessment Tool (SWAT) in the Luanhe river basin located in North China, where there is a drought-prone area. Then the Palmer drought model was modified based on the simulation results of hydrological processes, and the spatial and temporal variation of regional drought was analyzed. The evaluation results based on modified PDSI may provide some scientific support for decision makers when formulating drought management policies to alleviate the adverse effects of drought.

2. Materials and Methods

2.1. Study Area. Luanhe river is the second largest river that separately flows into sea in North China. It originates from the northern foot of the Bayanguertu Mountain, near the border between Hebei province and Inner Mongolia autonomous region, and finally flows into Bohai Sea (Figure 1). The total length of the river is about 888 km, and main tributaries have Shandianhe river, Xingzhouhe river, Yixunhe river, Wuliehe river, Laoniuhe river, Liuhe river, Puhe river, Sahe river, and Qinglonghe river.

Luanhe river basin is located in the north-eastern part of North China plain, and has a drainage area of 44,750 km^2 with elevations ranging from 2 to 2229 m (the average elevation is 911 m). The basin is characterized by a typical temperate continental climate, with mean annual precipitation ranging from 400 mm to 700 mm with 67–76% falling in June through September, and the mean annual temperature ranges from 5 to 12°C. The multiannual natural runoff of Luanhe river basin is 46.94×10^8 m^3. The main land use types of the study area are forest (37.76%), pasture (31.45%), and agricultural lands (24.09%). The predominant soil types of the study area are brown and cinnamon soils.

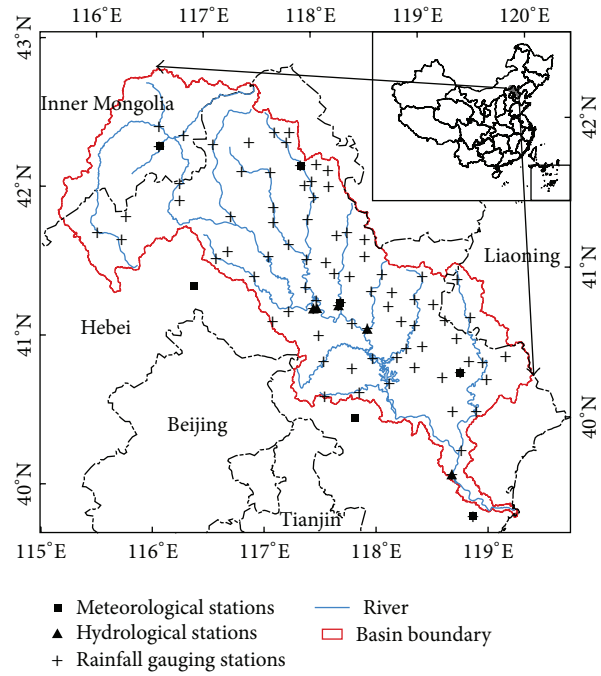

Figure 1: Location of Luanhe river basin with hydrological and meteorological stations.

2.2. The Establishment of SWAT Model

2.2.1. SWAT Description. The soil and Water Assessment Tool (SWAT) model is a watershed-scale, physically based, continuous-time, and distributed-parameter hydrological model that operates on a daily time step and is developed to predict the impact of land management practices on hydrologic and water quality response of complex watersheds with varying soils, land use, and management conditions [16]. It has several advantages, such as multiple functions, a modular design, and only a few parameters need to be optimized compared with many other hydrological models [17], so SWAT model was selected in the study.

In SWAT, a watershed is first divided into a number of subbasins according to the terrain and river channels and then further subdivided into multiple hydrologic response units (HRUs) consisting of unique combinations of land use, soils, and topography in each basin. An HRU is a fundamental spatial unit upon which SWAT simulates the water balance [16]. The runoff, sediment, and nutrient loadings from each HRU are calculated separately and then aggregated at the subbasin level and routed to the associated reach and to the basin outlet through the channel network.

The model provides two methods for estimating surface runoff: one is the curve number method developed by the Soil Conservation Service (SCS) of the United States Department of Agriculture and the other is the Green-Ampt method. In most cases, the curve number method is better than the Green-Ampt method [18]. For potential evapotranspiration

estimation, three methods are available in SWAT, that is, Penman-Monteith, Priestley-Taylor, and Hargreaves methods. Water flow is routed through the channel network using the variable storage method or the Muskingum method [19]. A detailed description of the model can be found form the model's public domain at http://swat.tamu.edu/.

2.2.2. Model Input. The SWAT model requires meteorological data input and three GIS data layers, namely, digital elevation model (DEM), land use, and soil. The SRTM DEM with a spatial resolution of 90 m was provided by International Scientific Data Service Platform, Computer Network Information Center, and Chinese Academy of Sciences (http://datamirror.csdb.cn).

Land use map for 1985 and 2000 was obtained from the Data Center for Resources and Environmental Sciences (RESDC), Chinese Academy of Sciences, and land use properties were directly from the SWAT model database.

Soil map at a scale of 1 : 1000000 was provided by Environmental and Ecological Science Data Center for West China, National Natural Science Foundation of China. (http://westdc.westgis.ac.cn). Soil physical properties (soil particle composition, saturated hydraulic conductivity, and bulk density, etc.) were mainly collected from China soil database (http://www.soil.csdb.cn) and a soil correlation system combined with the soil water characteristics software of SPAW (soil-plant-air-water) [20], which was developed by Washington State University, USA.

SWAT requires daily values of meteorological data as an input. These data are precipitation, maximum and minimum temperature, solar radiation, relative humidity, and wind speed. In the study, daily maximum and minimum air temperature, wind speed, and relative humidity for seven meteorological stations located within and around the watershed during 1970–2010 were collected from the National Meteorological Center of China (Figure 1). The daily solar radiations were estimated with the model based on the sunshine hours and geological information [21]. Due to short time series of daily precipitation records of 83 gauging stations (1972–1988) in the study area, the paper interpolated the daily precipitation of gauging stations with inverse distance weighted method from 1989 to 2010 based on precipitation data of seven meteorological stations.

The monthly natural discharge values were collected from five hydrological stations at the catchment outlet for the period of 1973 to 2000, which used to calibrate and validate the model spatially. The description of these stations and their catchments was list in Table 1.

2.2.3. Model Setup. Luanhe river basin was divided into 174 subbasins and further into 1327 HRUs when 1985 land use map was used and 1471 HRUs when 2000 land use map was used. The SCS curve number method was used for calculating surface runoff volume. The Penman-Monteith method and variable storage method were used to estimate the potential evapotranspiration and flow routing, respectively.

2.2.4. Model Calibration and Validation. Model calibration is an important component of hydrological modeling. In this study, owing to data limitation, the data for period 1973 to 1988 were used for calibration and 1989 to 2000 were used for validation of the model at the five catchment outlets. The 1985 land use map was used for calibration period and 2000 land use map was used for validation period. Period 1970–1972 and period 1987-1988 were used as "warm-up" periods for calibration and validation. The warm-up period allows the model to get the hydrological cycle fully operational.

Table 1: Hydrological stations used for SWAT calibration and validation.

Hydrological station	River	Catchment area (km^2)	Area percent (%)
Hanjiaying	Yixunhe river	6736.26	14.78
Chengde	Wuliehe river	2502.21	5.49
Xiabancheng	Laoniuhe river	1679.61	3.69
Sandaohezi	Luanhe river	18560.07	40.74
Luanxian	Luanhe river	44939.82	98.63

The performance of the model for simulating discharge can be quantified by the coefficient of determination (R^2), Nash-Sutcliffe efficiency (E_{NS}) [22], and relative error (RE) between the observations and the final best simulation, which were defined as follows:

$$R^2 = \frac{\left[\sum_{i=1}^{n}\left(Q_{\mathrm{sim}_i} - \overline{Q_{\mathrm{sim}}}\right)\left(Q_{\mathrm{obs}_i} - \overline{Q_{\mathrm{obs}}}\right)\right]^2}{\sum_{i=1}^{n}\left(Q_{\mathrm{obs}_i} - \overline{Q_{\mathrm{obs}}}\right)^2 \sum_{i=1}^{n}\left(Q_{\mathrm{sim}_i} - \overline{Q_{\mathrm{sim}}}\right)^2},$$

$$E_{\mathrm{NS}} = 1 - \frac{\sum_{i=1}^{n}\left(Q_{\mathrm{sim}_i} - Q_{\mathrm{obs}_i}\right)^2}{\sum_{i=1}^{n}\left(Q_{\mathrm{obs}_i} - \overline{Q_{\mathrm{obs}}}\right)^2}, \tag{1}$$

$$\mathrm{RE} = \left(\frac{\overline{Q_{\mathrm{sim}}} - \overline{Q_{\mathrm{obs}}}}{\overline{Q_{\mathrm{obs}}}}\right) \times 100,$$

where n is the number of discharge values, Q_{sim_i} and Q_{obs_i} are the simulated and measured values of discharge, respectively, and $\overline{Q_{\mathrm{sim}}}$ and $\overline{Q_{\mathrm{obs}}}$ are average of simulated and observed discharge over the simulation period, respectively.

The coefficient of determination (R^2) is the percent of the variation that can be explained by the regression equation, and the value of R^2 can range from 0 to 1, with higher value indicating a better model performance. The value of E_{NS} can range from $-\infty$ to 1, with higher values indicating a better overall fit and 1 indicating a perfect fit. A general acceptable criteria for E_{NS} is set to be greater than 0.5 for monthly data. RE of less than or equal to 15% is considered satisfactory during model calibration and validation [23].

2.3. The Modified Palmer Drought Severity Index. Palmer drought severity index (PDSI) was developed by W. C. Palmer in 1965, which incorporated antecedent precipitation, moisture supply, and moisture demand into a hydrologic accounting system [13]. The index that intended to be of reasonable comparable local significance both in space and time has been extensively used as a measure of drought for

both agricultural and water resources management. Basic concepts and steps for the computation of PDSI are as follows.

2.3.1. Moisture Anomaly Index. The PDSI is based on the water balance equation, and the difference d_i between the actual precipitation P_i and CAFEC (Climatically Appropriate For Existing Conditions) precipitation $\widehat{P}$ is an indicator of water deficiency or surplus in month i, which is defined as

$$\begin{aligned} d_i &= P_i - \widehat{P}_i, \\ \widehat{P}_i &= \alpha \mathrm{PE}_i + \beta \mathrm{PR}_i + \gamma \mathrm{PRO}_i + \delta \mathrm{PL}_i, \end{aligned} \tag{2}$$

PE_i is potential evapotranspiration; PR_i is potential recharge that indicates the amount of moisture required to bring the soil to its water holding capacity; PRO_i is potential runoff, which is defined as the difference between potential precipitation and potential recharge; and PL_i is potential loss defined as the amount of moisture that could be lost from the soil by evapotranspiration during a zero precipitation period [4]. The climatic coefficients α, β, γ, δ are means for each month averaged over the base period. For example,

$$\alpha = \frac{\overline{\mathrm{ET}}}{\overline{\mathrm{PE}}}, \tag{3}$$

where ET is the actual evapotranspiration and the overbar denotes the long term monthly from 1973 to 2010 in the study. In a similar way, β is the ratio of mean actual recharge R divided by mean potential recharge PR. γ is the ratio of mean actual runoff RO divided by mean potential runoff PRO, and δ is the ratio of mean actual loss L divided by mean potential loss PL.

A two-layer bucket-type model was applied to carry out the previous hydrological accounting in the traditional PDSI computation method. However, the two-layer bucket-type model just does not consider the impacts of the spatial heterogeneity of soil, vegetation, and topographical factors on the hydrological processes in a watershed. In the study, four subbasins that correspond to meteorological stations located within the study area were selected for initially establishing Palmer drought model, and the monthly PE, ET, and RO of selected subbasins were taken directly from simulated results of calibrated SWAT model, and the other parameters can be computed based on the simulated results of soil moisture for each month i, which were defined as follows [24]:

$$\begin{aligned} R_i &= \max\left(0, \left(\mathrm{SW}_i - \mathrm{SW}_{i-1}\right)\right), \\ \mathrm{PR}_i &= \mathrm{AWC} - \mathrm{SW}_{i-1}, \\ \mathrm{PRO}_i &= \mathrm{AWC} - \mathrm{PR}_i = \mathrm{SW}_{i-1}, \\ L_i &= \max\left(0, \left(\mathrm{SW}_{i-1} - \mathrm{SW}_i\right)\right), \\ \mathrm{PL}_i &= \min\left(\mathrm{PE}_i, \mathrm{SW}_{i-1}\right), \end{aligned} \tag{4}$$

where SW_{i-1} is the total soil moisture at the beginning of month and the SW_i is the total soil moisture at the ending of month. AWC is available moisture capacity. According to the Harmonized World Soil Database (HWSD), the study sets the AWC to 150 mm.

On that basis, the difference d_i was converted into indices of moisture anomaly z_i, which was defined as

$$z_i = \kappa^* \times d_i, \tag{5}$$

where κ^* is the climatic characteristic that can be estimated as

$$\kappa^* = \frac{\left(\overline{\mathrm{PE}} + \overline{R}\right)}{\left(\overline{P} + \overline{L}\right)}. \tag{6}$$

2.3.2. Drought Severity. The z-index time series were analyzed to develop criteria for the beginning and ending of drought periods and an empirical formula for determining drought severity. The index was given by the equation

$$X_i = 0.89 X_{i-1} + \frac{z_i}{55.71}, \tag{7}$$

where X_i is the PDSI for the ith month and X_{i-1} is previous month's PDSI. The equation indicates that PDSI of a given month strongly depends on its value in the previous months and on the moisture anomaly of the actual month.

The previous equation is one of the fundamental formulas for calculating drought indices, and its establishment was just based on four subbasins. However, when the method was subsequently applied to other regions of the study area with rather different types of climate, some of the results might be peculiar and unrealistic. Therefore, in order to make the established drought mode (7) that has good spatial comparability, there is a need to adjust the monthly k^* values and z,

$$z_i = K \times d_i, \tag{8}$$

$$K = \frac{438.91}{\sum_1^{12} DK'} K', \tag{9}$$

$$K' = 1.2459 \lg\left[\frac{\left(\overline{\mathrm{PE}} + \overline{R} + \overline{\mathrm{RO}}\right) / \left(\overline{P} + \overline{L}\right)}{\overline{D}}\right] + 3.3684. \tag{10}$$

$\overline{D}$ is the mean of the absolute values of d.

Equations (7) and (8) were final expression of modified PDSI in Luanhe river basin based on the SWAT model and the original Palmer drought severity index.

3. Results and Discussion

3.1. Verification of SWAT Model. The calibration and validation were completed using the monthly discharge records at multisites from 1973 through 2000, and the results were presented in Table 2. The values of R^2 and E_{NS} were greater than 0.8 for the calibration period except the upper Luanhe river at the Sandaohezi station, which indicated close relationship between simulated monthly discharges with observed values. The model slightly overestimated the monthly discharge at the Sandaohezi and Luanxian station located in the main

Table 2: Evaluation of the simulation results of monthly discharge.

	Calibration (1973–1988)			Validation (1989–2000)		
	R^2	E_{NS}	RE	R^2	E_{NS}	RE
Hanjiaying	0.89	0.89	−3.30%	0.73	0.66	−1.09%
Chengde	0.86	0.85	−1.34%	0.71	0.71	−7.32%
Xiabancheng	0.87	0.87	−5.82%	0.68	0.62	−2.75%
Sandaohezi	0.78	0.72	1.05%	0.71	0.62	−12.01%
Luanxian	0.93	0.93	3.40%	0.92	0.91	−2.59%

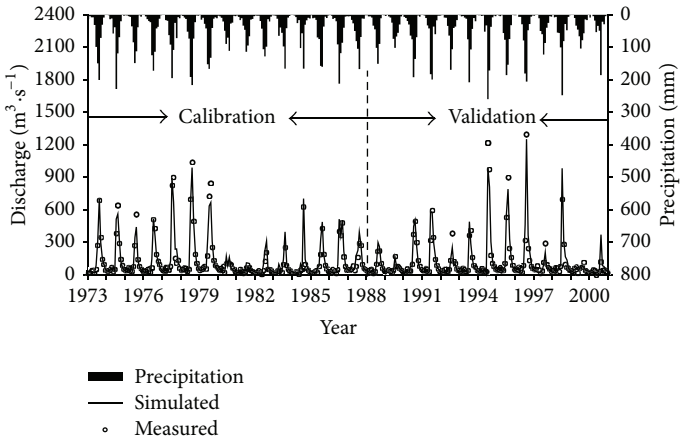

Figure 2: Comparison of the simulation and measured monthly hydrograph at Luanxian.

stream and underestimated the monthly discharge at other hydrological stations of three main tributaries, but the relative errors were less than 5%.

Because there were no precipitation records of gauging stations after 1988, the study used the interpolated data based on precipitation records of meteorological stations from 1989 to 2010. Therefore, the spatial heterogeneity of precipitation cannot be well reflected in some years, which led to the monthly discharges being underestimated at each hydrological station, and the value of R^2 and E_{NS} had decreased for validation period. Even so, the indicators basically can meet the requirements of accuracy. These results showed that the calibrated model can describe the hydrological processes, implying that SWAT model was applicable to the Luanhe river basin. The result after calibration and validation at Luanxian station was shown in Figure 2.

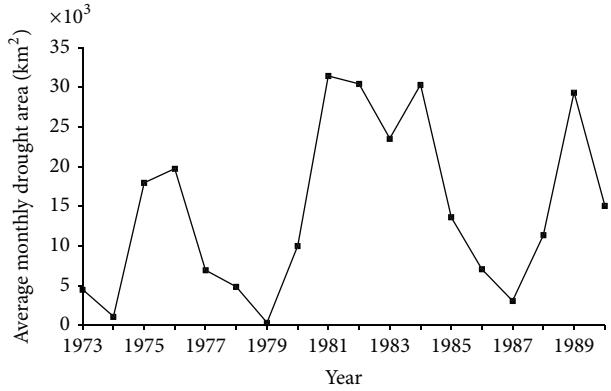

Figure 3: Average monthly drought area from 1973 to 1990 in Luanhe river basin.

3.2. The Verification of Modified Palmer Drought Severity Index. On the basis of the previous drought model, the values of monthly PDSI for each subbasin were calculated from 1973 to 2010. In order to verify the rationality of the model, the documented real drought [25] and drought area based on modified PDSI in the study were compared (Figure 3).

According to the documented records, during the period of 1973–1990, typical severe and extreme drought occurred in 1975, 1980–1984, and 1989. From Figure 3, it can be seen that the average monthly drought area of documented drought years based on modified PDSI was significantly larger than other years, especially drought area made up 69.06% of the basin in 1981, which was consistent with the documented drought. The value of drought indices based on the SWAT hydrological model and Palmer drought severity index can better describe the characteristics of regional drought evolution in the Luanhe river basin.

The drought evaluation results based on modified PDSI indicated that drought occurred in 1976, but there were no historical records. The reason of the disagreement was that historical records focus on the drought disaster, but the drought indices were mainly intended to evaluate drought from a water balance viewpoint [26]. Thus, there exist many other factors affecting the change from drought to disaster,

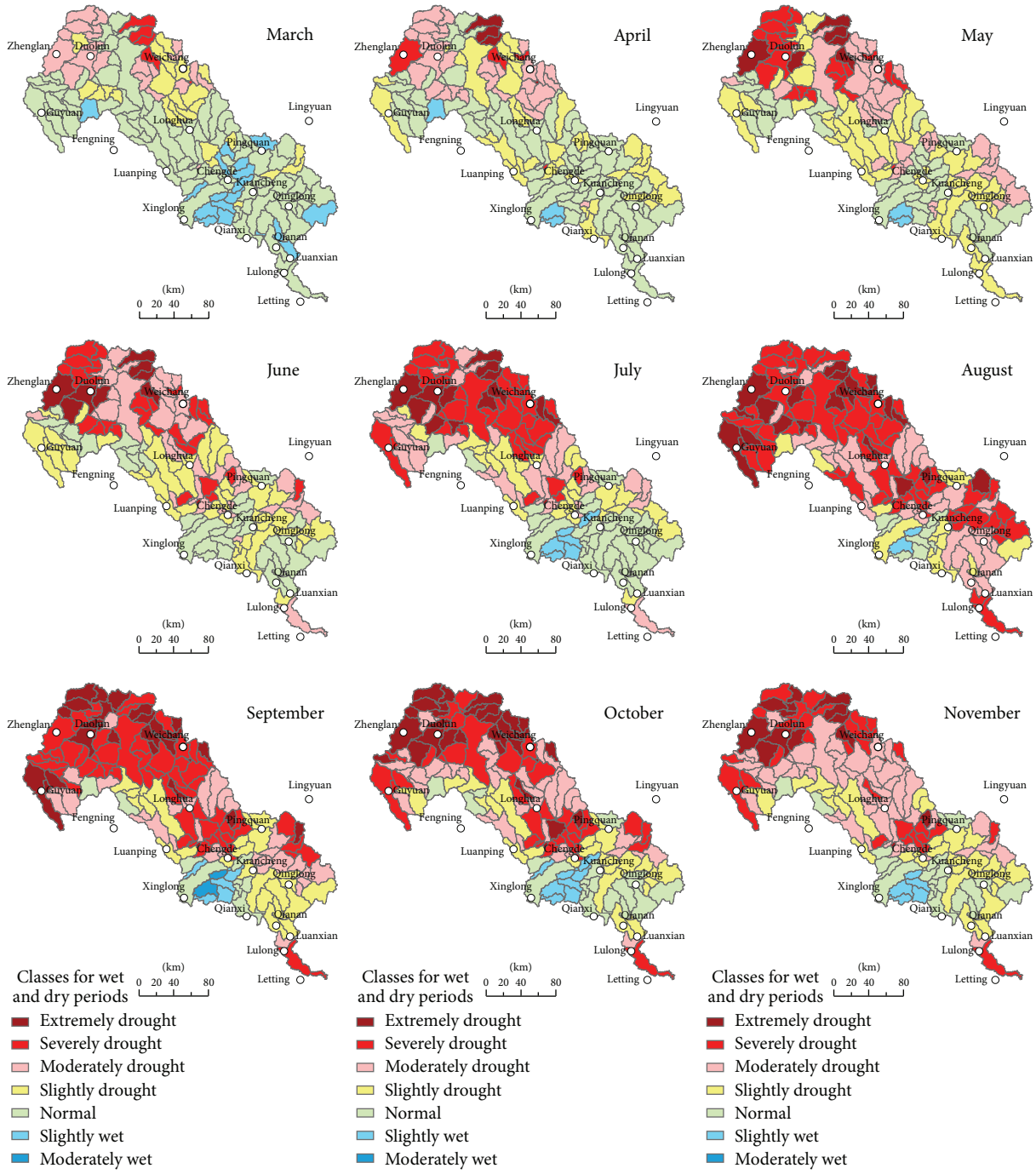

Figure 4: The distributed map of drought grades in 1989 based on modified PDSI.

that is, irrigation, which may lead to the little differences between documented and evaluated drought.

The drought distribution using modified PDSI was further verified in 1989 (Figure 4). It can be seen that the signs of drought came into being with the arrival of March, and it was distributed mainly in the northern Weichang county in the upper reach of Luanhe river basin. But after that, the drought area has gradually extended and the drought lasted until November. Overall, the spatial distribution of drought evaluation was consistent with documented real drought.

3.3. Spatial-Temporal Characteristics of Drought in Luanhe River Basin

3.3.1. Spatial Distribution Characteristics of Drought. Drought frequency representing how often drought occurs was calculated through dividing the number of months at which drought occurs by total months. The distribution map of drought frequency in Luanhe river basin was represented in Figure 5, which showed a high degree of spatial heterogeneity on subbasin level. High drought frequency areas

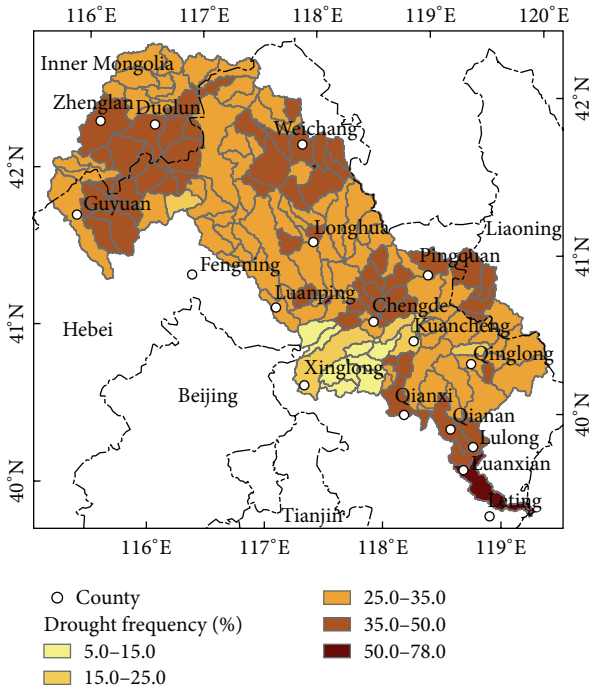

FIGURE 5: Distribution map of drought frequency based on modified PDSI.

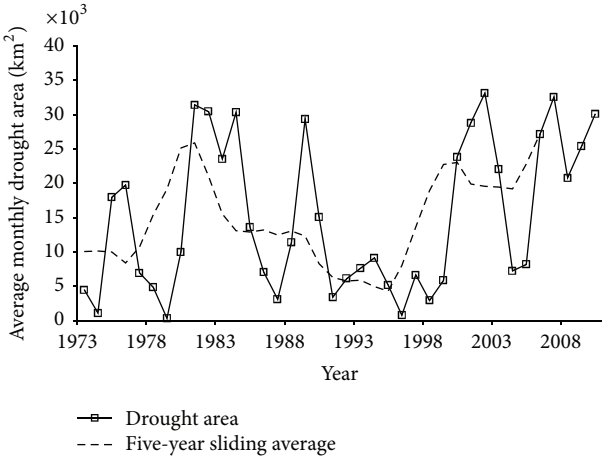

FIGURE 6: Annual variation of average monthly drought area from 1973 to 2010.

were mainly distributed in the grassland regions of upstream located in the eastern part of Inner Mongolia plateau, including Duolun and Guyuan county, the northern Weichang, Chengde and Pingquan county of middle reaches, and Qianxi, Qianan and Lulong county of downstream. The drought frequency was higher than 35% in these areas. And in relative terms, the drought less occurs in the area of southern Luanping to Xinglong county, where drought frequency was less than 20%.

Due to the limitation of data, the irrigation is not considered in the established SWAT model in the south of Luanxian county, downstream of Luanhe river, and the monthly natural streamflow; namely adding the social and economic water used including the water storage of the reservoirs, industrial and agricultural water used to measure runoff was used for model calibration and validation, which can eliminate the impact of human activities. Therefore, the evaluation results of drought frequency based on modified PDSI showed that these regions had the highest frequency. However, in practice, there are many large-scale irrigation areas in these regions where the frequency of drought that actually happened was not high. Thus, the evaluation results had not considered the effect of human activity on drought, that there was a need to further improve the established drought model.

3.3.2. Temporal Variation of Drought. The temporal variation of drought was analyzed with average monthly drought area from 1973 to 2010 (Figure 6), which showed that the drought had obviously interannual and interdecadal fluctuation in Luanhe river basin, and the average drought area was 14954.69 km^2. From 1970s to the late 1980s, the drought exhibited a significant upward trend. Compared with 1973 to 1990, the drought degree of 1990 to 2000 decreased. But the drought area increased rapidly again after 2000. Overall, the drought had a significant upward trend.

The break point of drought area was detected in 1985 and 2006 with Mann-Kendall's test. Because of increased precipitation, the drought showed an alleviating trend from 1985 to 2005 in the Luanhe river basin. However, with the decreasing of precipitation and the effect of human activities, the drought had intensified after 2006.

4. Conclusions

The SWAT model was applied to modify the Palmer drought severity index (PDSI) in Luanhe river basin. Calibration results of the SWAT model show that the good agreement between the measured and simulated monthly discharges. But due to the interpolation quality of precipitation data, the monthly discharges were underestimated and the value of R^2 and E_{NS} had decreased for validation period. Even so, the indicators basically can also meet the requirements of accuracy. It showed the calibrated model can be used to describe the hydrological processes in the study area. Then the simulation results of hydrological components were used for the calculation procedure of the PDSI on subbasin level. The method was applied to drought evaluation in Luanhe river basin, North China, and good results were obtained.

Many studies have analyzed drought trend with PDSI. Dai [6] compared and evaluated four forms of PDSI using available climate data from 1850 to 2008. Zhai et al. [27] analyzed the time series of the average annual PDSI and SPI calculated for 483 meteorological stations for 10 large regions covering the territory of China. Compared with the previous researches, the modified PDSI based on SWAT model not only can describe the spatial difference of regional drought, but also could improve the physical mechanism of PDSI and extend the scale from point to subbasin because the two-soil layer for calculating water balance was replaced by the distributed hydrological model.

The work should be considered as an attempt to monitor drought that integrated the Palmer drought severity index and SWAT model. However, there exist some limitations in the study. Due to insufficient irrigational data availability, the model could not represent the effect of human activity on drought. Besides, it is difficult to acquire the measure value of some internal state variables, so the model calibration was based on a comparison between simulated and measured discharges. In the next phase of this research, it is of major importance to take into account irrigation, and multivariable calibration and validation approach should be used to produce more realistic input parameters for the SWAT model and improve the evaluation accuracy of drought.

Acknowledgments

The paper was supported by the National Basic Research Program of China (no. 2010CB951102), the National Key Technology R&D Program of China during the 12th Five-year Plan Period (no. 2012BAC19B03), and the Foundation for Innovative Research Groups of the National Natural Science Foundation of China (no. 51021066).

References

[1] T. Sternberg, "Regional drought has a global impact," *Nature*, vol. 472, no. 7342, p. 169, 2011.

[2] L. Vasiliades and A. Loukas, "Hydrological response to meteorological drought using the Palmer drought indices in Thessaly, Greece," *Desalination*, vol. 237, no. 1–3, pp. 3–21, 2009.

[3] S. M. Quiring and T. N. Papakryiakou, "An evaluation of agricultural drought indices for the Canadian prairies," *Agricultural and Forest Meteorology*, vol. 118, no. 1-2, pp. 49–62, 2003.

[4] I. J. Szép, J. Mika, and Z. Dunkel, "Palmer drought severity index as soil moisture indicator: physical interpretation, statistical behaviour and relation to global climate," *Physics and Chemistry of the Earth*, vol. 30, no. 1–3, pp. 231–243, 2005.

[5] L. Vasiliades, A. Loukas, and N. Liberis, "A water balance derived drought index for Pinios river basin, Greece," *Water Resources Management*, vol. 25, no. 4, pp. 1087–1101, 2011.

[6] A. Dai, "Characteristics and trends in various forms of the Palmer Drought Severity Index during 1900–2008," *Journal of Geophysical Research D*, vol. 116, no. 12, Article ID D12115, 2011.

[7] T. Gebrehiwot, A. van der Veen, and B. Maathuis, "Spatial and temporal assessment of drought in the Northern highlands of Ethiopia," *International Journal of Applied Earth Observation and Geoinformation*, vol. 13, no. 3, pp. 309–321, 2011.

[8] A. K. Mishra and V. P. Singh, "A review of drought concepts," *Journal of Hydrology*, vol. 391, no. 1-2, pp. 202–216, 2010.

[9] R. R. Heim Jr., "A review of twentieth-century drought indices used in the United States," *Bulletin of the American Meteorological Society*, vol. 83, no. 8, pp. 1149–1165, 2002.

[10] W. M. Alley, "The Palmer Drought Severity Index: limitations and assumptions," *Journal of Climate & Applied Meteorology*, vol. 23, no. 7, pp. 1100–1109, 1984.

[11] Q. S. Hu and G. D. Willson, "Effects of temperature anomalies on the Palmer drought severity index in the central United States," *International Journal of Climatology*, vol. 20, pp. 1899–11911, 2000.

[12] E. Liang, X. Shao, H. Liu, and D. Eckstein, "Tree-ring based PDSI reconstruction since AD 1842 in the Ortindag Sand Land, east Inner Mongolia," *Chinese Science Bulletin*, vol. 52, no. 19, pp. 2715–2721, 2007.

[13] W. C. Palmer, "Meteorological drought," Research Paper 45, US Weather Bureau, Washington, DC, USA, 1965.

[14] J. Sheffield, E. F. Wood, and M. L. Roderick, "Little change in global drought over the past 60 years," *Nature*, vol. 491, no. 7424, pp. 435–438, 2012.

[15] Z. X. Xu, J. P. Pang, C. M. Liu, and J. Y. Li, "Assessment of runoff and sediment yield in the miyun reservoir catchment by using SWAT model," *Hydrological Processes*, vol. 23, no. 25, pp. 3619–3630, 2009.

[16] J. G. Arnold, R. Srinivasan, R. S. Muttiah, and J. R. Williams, "Large area hydrologic modeling and assessment—part I: model development," *Journal of the American Water Resources Association*, vol. 34, no. 1, pp. 73–89, 1998.

[17] S. Wang, S. Kang, L. Zhang, and F. Li, "Modelling hydrological response to different land-use and climate change scenarios in the Zamu River basin of northwest China," *Hydrological Processes*, vol. 22, no. 14, pp. 2502–2510, 2008.

[18] K. M. Loague and R. A. Freeze, "A comparison of rainfall-runoff modeling techniques on small upland catchments," *Water Resources Research*, vol. 21, no. 2, pp. 229–248, 1985.

[19] S. L. Neitsch, J. G. Arnold, J. R. Kiniry, and J. R. Williams, *Soil and Water Assessment Tool, Theoretical Documentation (Version 2005)*, Grassland, Soil and Water Research Laboratory, Agricultural Research Service & Blackland Research Center, Texas Agricultural Experiment Station, Temple, Tex, USA, 2005.

[20] K. E. Saxton, W. J. Rawls, J. S. Romberger, and R. I. Papendick, "Estimating generalized soil-water characteristics from texture," *Soil Science Society of America Journal*, vol. 50, no. 4, pp. 1031–1036, 1986.

[21] C. L. Tong, W. J. Zhang, and Y. Tang, "Estimation of daily solar radiation in China," *Chinese Journal of Agrometeorology*, vol. 26, no. 3, pp. 165–169, 2005 (Chinese).

[22] J. E. Nash and J. V. Sutcliffe, "River flow forecasting through conceptual models—part I: a discussion of principles," *Journal of Hydrology*, vol. 10, no. 3, pp. 282–290, 1970.

[23] S. Kumar and V. Merwade, "Impact of watershed subdivision and soil data resolution on swat model calibration and parameter uncertainty," *Journal of the American Water Resources Association*, vol. 45, no. 5, pp. 1179–1196, 2009.

[24] J.-J. Xu and D.-W. Yang, "New model for drought estimation and prediction based on distributed hydrological simulation," *Journal of Hydraulic Engineering*, vol. 41, no. 6, pp. 739–747, 2010 (Chinese).

[25] Water Resources Department of Hebei Province, *Floods and Droughts of Hebei Province*, China Water & Power Press, Beijing, China, 1997.

[26] N. B. Guttman, "Comparing the palmer drought index and the standardized precipitation index," *Journal of the American Water Resources Association*, vol. 34, no. 1, pp. 113–121, 1998.

[27] J. Zhai, B. Su, V. Krysanova, T. Vetter, C. Gao, and T. Jiang, "Spatial variation and trends in PDSI and SPI indices and their relation to streamflow in 10 large regions of china," *Journal of Climate*, vol. 23, no. 3, pp. 649–663, 2010.

Hindawi Publishing Corporation
Mathematical Problems in Engineering
Volume 2013, Article ID 976591, 9 pages
http://dx.doi.org/10.1155/2013/976591

Research Article

Detecting Abrupt Change of Streamflow at Lintong Station of Wei River

Jingjing Fan,[1] Qiang Huang,[1] Jianxia Chang,[1] Dongyong Sun,[2] and Shen Cui[1]

[1] *Xi'an University of Technology, Xi'an 710048, China*
[2] *Chang'an University, Xi'an 710054, China*

Correspondence should be addressed to Qiang Huang; wresh@mail.xaut.edu.cn

Received 19 February 2013; Accepted 7 April 2013

Academic Editor: Yongping Li

According to abrupt diagnosis of runoff, two methods, that is, moving approximate entropy and moving permutation entropy, are used to analyse the abrupt year of the daily river runoff from 1961 to 2006 at Lintong station of Wei River in Loess Plateau. The runoff series are divided into 4 stages. With the analysis of hydrological characters of different stages, we find that there are abrupt changes at the three years 1972, 1983, and 2002. The result shows that moving approximate entropy and moving permutation entropy methods are useful tools for abrupt diagnosis of runoff. The attribution of abrupt change at the Lintong runoff series is primarily due to the reduced precipitation, increased water conservancy project, increased water consumption of industry and agriculture, significantly decreased groundwater table, and increased evaporation.

1. Introduction

Runoff is an important hydrological variable in the hydrological cycle. Climate change and human activities have the potential to cause significant changes in runoff behavior, and it is likely that one of the most serious consequences of global warming will be an increased frequency of extreme hydrological events due to changes in runoff patterns [1–3]. This trend is illustrated by the ongoing intensification of various hydrological components of the water cycle [4–6]. A detailed understanding of hydrological series and the factors that affect them is essential for the sustainable exploitation and use of water resources, disaster prevention, and the effective management of water conservation projects. Two types of change can be discerned in hydrological time series: continuous change and abrupt change. In a continuous change the parameter of interest varies smoothly, whereas an abrupt change involves a sudden jump from one value to a much greater or lower value. Methods for the identification and analysis of nonlinear (i.e., discontinuous) variation have been developed by researchers examining meteorological variation. These techniques have had a substantial impact on modern climatology [7], resulting in a much greater emphasis being placed on complexity, interactions between different components of the climate system, and nonlinear factors than was once the case. The identification of abrupt changes requires careful statistical analysis and is highly sensitive to both the time scale over which an event takes place and the length of the analyzed data series.

After the introduction of nonlinear methods, many scholars came to realize that climatic variation is driven by both internal and external forcing mechanisms, resulting in the development of dynamic techniques for the analysis of climate change. For example, a recent study on five temperature series gathered from meteorological stations within the Yangtze Delta used the concept of conditional entropy to test the commonality of the series' underlying dynamics [8]. Similarly, GIS data were used in conjunction with information entropy analysis to analyze the spatial and temporal variation in precipitation around the Chaobai River basin [9]. Pincus and coworkers developed the concept of approximate entropy as a tool for analyzing time series and studying system complexity [10]. This approach has been applied to identify abrupt climate change events and mutations in the series' structural dynamics [11]. Weiping et al. used approximate entropy analysis to investigate the spatial

and temporal variation in climate data. Their studies demonstrated that approximate entropy analysis is an effective tool for highlighting structural changes in a system's dynamics [12]. Hou Wei and colleagues introduced the concept of permutation entropy and used it to analyze the variation in temperature data series for Northern China. By applying empirical mode decomposition to their results, they were able to demonstrate a close relationship between abrupt temperature changes and sunspot activity [13]. In this work, we used a similar approach to analyze the variation in runoff series for the Wei River basin.

2. Methodology

2.1. The Moving Approximate Entropy Test for Identifying Abrupt Changes. Some significant abrupt diagnosis methods of the basic concepts of probability and correlation analyses that are applicable in hydrologic engineering [14] are based on the linear theory and work with the system characteristics such as mean value and trend analysis. In physical sciences entropy relates macroscopic and microscopic aspects of nature and determines the behaviour of macroscopic systems in equilibrium [15]. Since the development of the entropy theory by Shannon in the late 1940s and the principle of maximum entropy (POME) by Jaynes in the late 1950s, there has been a proliferation of applications of entropy in a wide spectrum of hydrology [16, 17]. Approximate entropy was used as a diagnostic and it showed that *ApEn* had good computational efficiency and high robustness in characterizing the severity of structural defect [18]. Permutation entropy is useful in the presence of dynamical or observational noise [19]. These two methods are based on entropy theory, and they diagnose the abrupt point with the inside structure of the time series by using system control equation.

Approximate entropy (*ApEn*) analysis is a method for evaluating dynamic variation in data series that is based on entropy theory. It is conceptually straightforward and can be calculated quickly. Moreover, it is not highly sensitive to noise in the analyzed data set and can reliably provide an overview of the studied system's properties. This section describes how the approach was adapted to analyze dynamic structural variation in runoff time series. The moving approximate entropy (M-ApEn) is a nonnegative scalar that is used to represent the complexity of a time series; the greater its value, the greater the complexity of the data set. For any time series of the form $\{u(i);\ i = 1, 2, \ldots, n\}$ together with an initial dimensionality of m and a tolerance threshold r, the approximate entropy can be computed as follows.

(1) Construct a set of m-dimensional vectors:

$$X(i) = [u(i), u(i+1), \ldots, u(i+m-1)], \quad (i = 1, 2, \ldots, n-m+1). \tag{1}$$

(2) Calculate the Euclidean distance between the vectors $X(i)$ and $X(j)$:

$$d[X(i), X(j)] = \max\left[\left|X(i+k) - X(j+k)\right|\right], \quad (k = 0, 1, 2, \ldots, m-1). \tag{2}$$

(3) Determine the number of values of $i = 1, 2, \ldots, n-m+1$ for which $d[X(i), X(j)]$ is less than r; this number is denoted by $C_i^m(r)$;

$$C_i^m(r) = \text{number}\left\{d\left[X(i), X(j)\right] \le r\right\} / (N-m+1). \tag{3}$$

(4) Compute the average value of the logarithm of $C_i^m(r)$ for all values of i; the resulting term is denoted by ϕ^m:

$$\phi^m(r) = \frac{1}{N-m+1} \sum_{i=1}^{N-m+1} \ln C_i^m(r). \tag{4}$$

(5) Increase m by 1 and repeat steps (1) to (4).

(6) By performing steps (1) to (5) iteratively, one obtains the approximate entropy time series:

$$ApEn(m, r) = \phi^m(r) - \phi^{m+1}(r). \tag{5}$$

Steps (1) to (6) reconstruct the m-dimensional sequence based on the degree of similarity between two points in terms of their values and position within the vector. Increases in the value of m indicate an increased likelihood that there has been a shift to a new mean approximate entropy; the greater the increase, the greater the likelihood that there is a corresponding abrupt change in the underlying data set, and hence the greater its complexity. Differences in the *ApEn* value at different points in time can thus be used to keep the ability of self-similar state and divide the period covered by a data set into separate phases separated by abrupt transitions. The quantity computed in step (4) is the approximate entropy and is used in conjunction with values of m and r that can be obtained from the literature to compute the moving *ApEn*. In this work, the following values were selected for the moving approximate entropy analysis parameters: $m = 2$, $r = 0.1 - 0.2\sigma$, $L = 365$ days, and $M = 365$ days. The σ value was taken to be the standard deviation of the original sequence, $u(i)$.

2.2. The Moving Permutation Entropy Test for Detecting Abrupt Changes. Permutation entropy is a metric that is based on entropy theory and can be used to characterize dynamic variation. In this work, a moving average of the permutation entropy was computed, to give a quantity that was termed the moving permutation entropy (M-PE) and was used to analyze the dynamic structural variation in the Lintong runoff series. The permutation entropy provides a measure of the complexity of a dataset and is computed using the following algorithm.

Given a one-dimensional hydrological time series $\{x(i),\ i = 1, 2, \ldots, n\}$, for any $x(i)$, phase space reconstruction will produce a one-dimensional vector:

$$X(i) = [x(i), x(i+\tau), \ldots, x(i+(m-1)\tau)]. \tag{6}$$

Here, m and τ represent the embedding dimension and the delay time, respectively.

If the mth reconstruction components of $X(i)$, that is, $[x(i), x(i+\tau), \ldots, x(i+(m-1)\tau]$ are sorted in order of size, one obtains the following:

$$\left[x\left(i+\left(k_1-1\right)\right) \le x\left(i+\left(k_2-1\right)\tau\right) \le \cdots \le x\left(i+\left(k_p-1\right)\tau\right],$$
$$1 \le k \le n-m+1. \tag{7}$$

In the sorting process, if $x(i+(k_{i1}-1)\tau = x(i+(k_{i2}-1)\tau)$, any vector $X(i)$ can be used to generate a sequence of the following form by means of K sorting:

$$B(t) = \left[k_1, k_2, \ldots, k_t\right], \quad 1 \le t \le n-m+1. \tag{8}$$

For each group, there are a total of $m!$ Different permutation of the symbol sequence $[k_1, k_2, \ldots, k_m]$, and $B(t) = [k_1, k_2, \ldots, k_m]$ denotes one of these sequences. Probability analysis can be used to associate each sequence with a set of probabilities for the $n-m+1$ group: $P_1, P_2, \ldots, P_l$.

According to Shannon, information entropy can be calculated for such a set of probabilities, $P_1, P_2, \ldots, P_{m-p+1}$, as follows:

$$H_p(m) = -\sum_{i=1}^{l} P_i \ln P_i. \tag{9}$$

Theoretically, when $P_i = 1/m!$, $H_P(m)$ reaches a maximum of $\ln(m!)$. In practice, $H_P(m)$ is usually normalized against $\ln(n-m+1)$:

$$0 \le H_p = \frac{H_P(m)}{\ln(m!)} \le 1. \tag{10}$$

HP is the PE value, and its size reflects the degree of randomness in the studied time series. The lower the value of HP, the more regular (i.e., the less complex) the sequence. Conversely, the greater the HP value, the more random (i.e., complex) the sequence.

At present, there is no established method for selecting an appropriate subsequence length (n) or embedding dimension (m). The influence of the subsequence length and the m value on the outcome of the analysis has been discussed at length in the literature [19, 20]. It is known that if an excessively low subsequence length is used, the identification of abrupt changes in the time series becomes unreliable, and the reconfigurable vector containing too little information will make the PE algorithm invalid. Based on the literature results [13], the following values for these crucial parameters were adopted in the analyses presented below: a subsequence of length (n) of 5 years, a sliding step length L of 1 day, and an embedding dimensionality (m) of 5.

3. Study Area

The Wei River is the largest tributary of the Yellow River. Its origin is in Niaoshu Hill in Weiyuan County of Gansu province. The Wei River basin covers parts of the Gansu, Ningxia, and Shaanxi provinces, and it joins the Yellow River in Tongguan County of Shaanxi province (Figure 1). The basin's catchment area is 134800 km^2, and the river runs for 818 km. Its upper reaches, which account for around 70% of its total length, are primarily located in hilly Loess regions, at elevations of 2400 to 1200 m. The lower 10% of its length lies in river valleys at elevations of 1700 m–900 m. The midreaches of the Wei River lie in the northern Loess Plateau of northern Shaanxi province, at elevations of 2000–900 m, and the river plays a central role in Loess deposition. It joins the Yellow River on the alluvial plains of the Guanzhong basin, whose eastern regions have an elevation of 700 m–800 m that falls to 500–320 m on moving westwards. The Qin mountain range, which has many peaks above 2000 m, is located to the south of the Wei River basin. The river's basin covers both arid and humid regions, with most of the precipitation falling in the north; the mountainous regions and the valleys receive comparatively little rainfall. The majority of the area's precipitation occurs in July and August, with December and January being the driest months of the year. The period between July and October typically accounts for around 60% of the area's total annual precipitation. The basin has a continental monsoon climate, with the total rainfall and temperature gradually decreasing on moving from the southeast to the northwest. The average annual evaporation from wet surfaces in the basin is 660 mm–1600 mm; the rate of evaporation is lowest in December and highest in June or July. The period between July and October accounts for 46%–58% of the region's total annual evaporation. The Wei River basin has many tributaries, most of which join the river on its south bank. However, the larger tributaries generally join the main river through the north bank, producing a fan-shaped basin. The basin has 14 tributaries and a catchment area of more than 100,000 km^2. Most of the tributaries on the north bank originate in the Loess Hills and the Loess Plateau. They are generally longer than the southern tributaries, flow over shallower slopes, and have greater sediment loads. The tributaries on the south bank originate in the Qin mountains. They tend to be short and fast flowing, with steep slopes, high runoff volumes, and comparatively low sediment concentrations. The Lintong station is located in the river's downstream region and covers a drainage area of 97,300 km^2, which corresponds to 88.8% of the river's total drainage area (excluding the Beiluohe basin).

4. Data

Daily streamflow data acquired at the Lintong hydrological station (34°26′N, 109°12′E) during the period from 1961 to 2006 were obtained from the Bureau of Hydrology and Water Resources of Shaanxi province. The first measurements in the data series were acquired in January 1961. Lintong station is located downstream of the Wei River with drainage area of 97299 km^2. The locations of the hydrological stations in the Wei River Basin are shown in Figure 2. As seen from Figure 3, annual runoff stays at an almost constant level after some sudden upward jumps are recorded. The maximum annual runoff corresponding to differences is 158.21 billion m^3. The minimum and maximum were recorded as 19.61 billion m^3

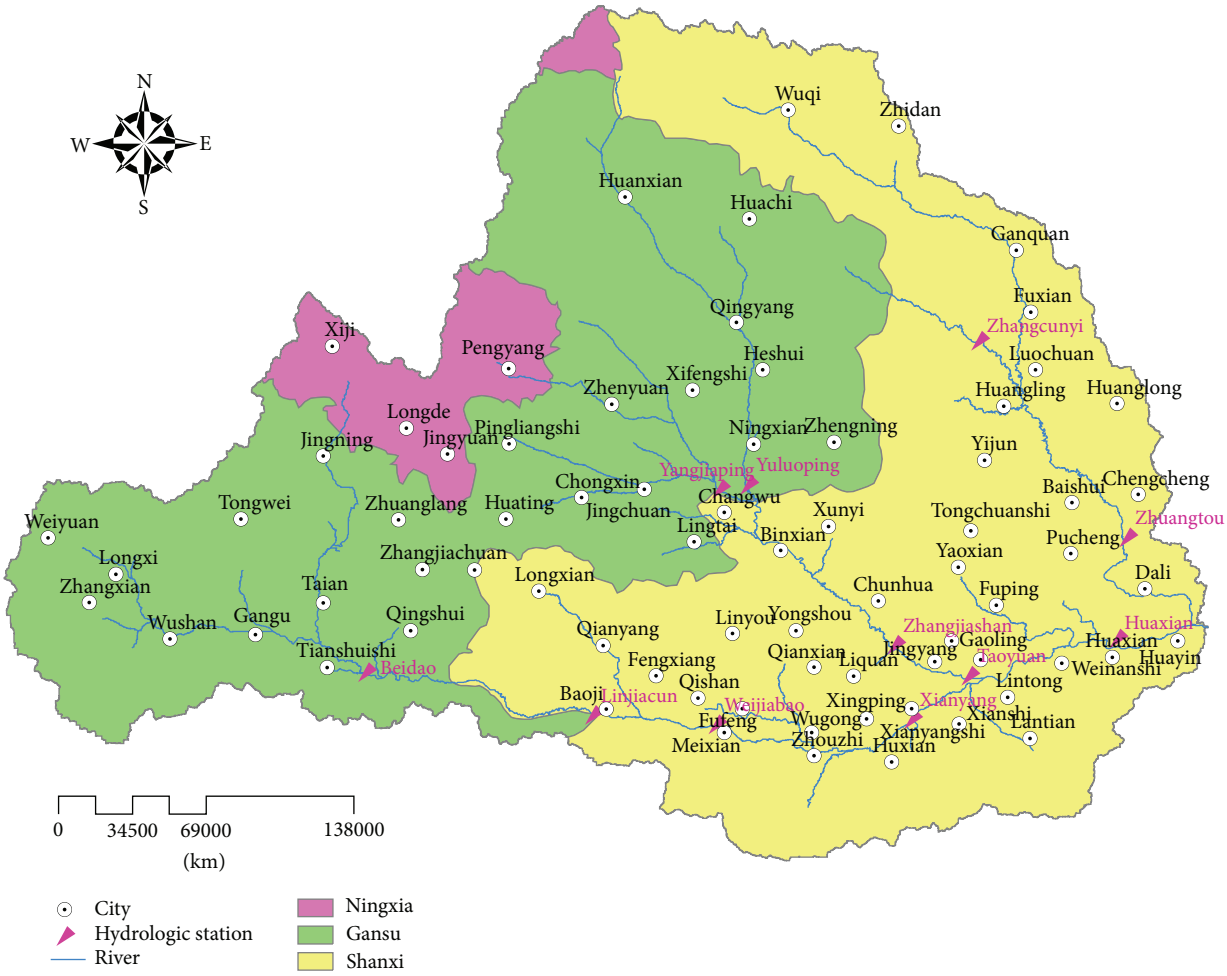

Figure 1: Map of the Wei River basin.

and 1.82 billion m^3. During observation period mean runoff is 6.59 billion m^3.

The hydrological variables considered in this work were the mean annual flow, the mean monthly flow, the maximum annual flow, the minimum annual flow, the timing of hydrologic events, maximum, and minimum flows on a daily, 3-day, 7-day, 30-day, and 90-day basis. These variables were selected because they are widely used in comparing flows and engineering applications. Variables associated with minimum flow were evaluated over four separate periods, that is, 1961–1971, 1972–1982, 1983–2001, and 2002–2006.

5. Analysis and Result

5.1. Results of the Moving Approximate Entropy Test. The M-ApEn method was used to detect abrupt changes in the Lintong station daily runoff time series. In this analysis, the value of m was chosen to be 2, the allowed deviation (r) was = 0.15σ, the moving step length L was 365 d, and the subsequence length M was also 365 d. Time points at which the difference between the *ApEn* value and the moving average *ApEn* was greater than 20% of the moving average were characterized as change points; that is, points at which an abrupt change had occurred. The calculated *ApEn* values for the Lintong Station daily runoff time series are shown in Figure 4. The *ApEn* value changes are clearly shown in Figure 1. The results show the four stages of abrupt change; appeared in 1972, 1983, and 2002.

(1) The first change point occurs in 1972, at which the difference between the *ApEn* value and the moving average is 22.9% of the moving average.

(2) The second change point occurs in 1983, at which the difference between the *ApEn* value and the moving average is 24.2% of the moving average.

(3) The third change point occurs in 2002, at which the difference between the *ApEn* value and the moving average is 34.1% of the moving average.

5.2. Results of the Moving Permutation Entropy Test. The M-PE method was used to analyze the daily runoff time series for the Lintong Station and to identify abrupt changes in the daily runoff volume. The parameter values used in the analysis were as follows: m = 5, lag time = 1 d, L = 1 d, and M = 5 a.

Figure 2: The locations of the hydrological monitoring stations in the Wei River basin.

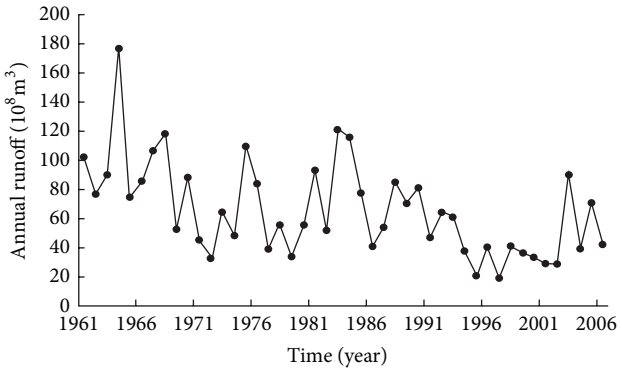

Figure 3: The annual daily runoff of Lintong station in the Wei River basin.

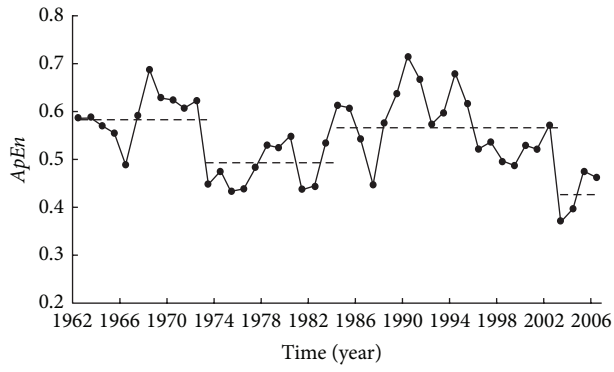

Figure 4: Calculated *ApEn* values based on the daily runoff series for the Lintong station in the Wei River.

The results obtained are shown in Figure 5. Inspection of this figure clearly shows that abrupt changes in the PE value occur in the early nineteen seventies and at the beginning of the twenty-first century.

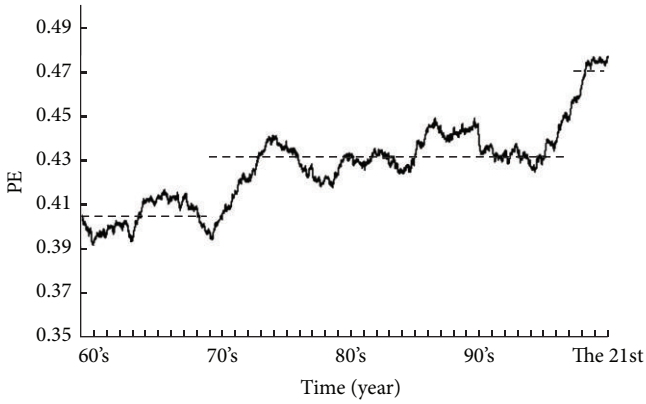

Figure 5: Calculated PE values based on the daily runoff for the Lintong station in the Wei River basin.

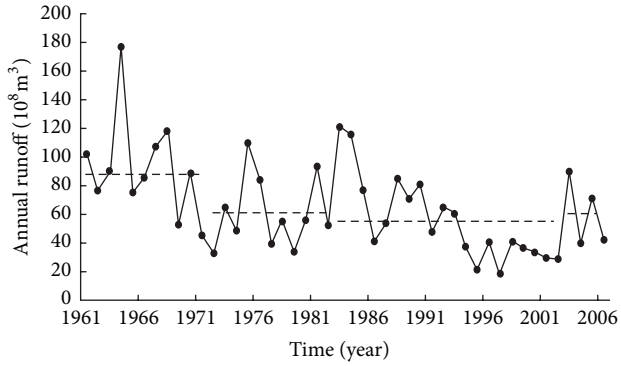

Figure 6: The annual daily runoff volume measured at the Lintong station in the Wei River basin.

The points of abrupt change in daily runoff volume identified using the M-ApEn method are 1972, 1983, and 2002. Using the M-PE method, abrupt changes were detected in the early 1970s and at the beginning of the 21st century. Considering the results of two methods, the abrupt changes are 1972, 1983, and 2002.

6. Discussion and Conclusions

6.1. Results of Hydrological Characteristics. Based on the results obtained in the M-ApEn and M-PE analyses, the runoff time series can be divided into four separate periods: 1961–1971, 1972–1982, 1983–2001, and 2002–2006.

For each of these periods, the values of selected hydrological variables measured at the Lintong Station were compared to those in the preceding period in an attempt to determine whether the abrupt changes detected by analyzing the daily runoff volume were associated with changes in other hydrological properties. The following noteworthy changes were identified.

(1) The mean annual runoff volume during the second period was 6.071 billion m^3, compared to 8.74 billion m^3 during the first period, representing a decrease of 31%. The mean annual runoff in the third period was 5.515 billion m^3, which represents a decrease of 9% relative to the second period. The mean annual runoff in the fourth period was 6.057 billion m^3, which corresponds to an increase of 10% relative to the third period. Overall, the most pronounced change in the mean annual runoff volume occurred between 1961–1971 and 1972–1982, corresponding to the abrupt change identified in 1972 in the M-ApEn analysis and in the early 1970s in the M-PE analysis. The results of the annual daily runoff volume measured at the Lintong station in the Wei River basin are shown in Figure 6.

(2) During the first period (1961–1971), the total runoff volumes in all months other than August were lower than those in the same months during the second period (1972–1982). For the months of March, April, May, and June, the total runoff volumes during the second period were less than half those measured during the first period. The monthly runoff volumes for the third period were generally greater than those for the second period. This was especially true in June, for which the mean runoff volume during the third period was 162% of that for the second period. The June runoff volume increased again during the fourth period, when it was 111% greater than that for the third period. The results of total monthly runoff volumes measured at the Lintong station in the Wei River basin are shown in Table 1.

(3) The maximum and minimum runoff volumes during the second period were generally lower than those during the first period; while max1 increased very slightly, the other maximum and minimum values fell by between 3% and 66%. There were very substantial changes between the second and third periods: the maximum values for the third period were all slightly lower than those for the second, whereas the minimum runoff volumes were all substantially greater. All of the maximum and minimum runoff volumes measured during the fourth period were greater than the corresponding values for the third period; the greatest change occurred for Min3, which increased by 44%. The results of minimum and maximum runoff volumes calculated over periods of 1, 3, 7, 30, and 90 days for the Lintong station in the Wei River basin are shown in Table 2.

6.2. Attribution of Abrupt Changes. The variation of runoff series is primarily due to climate change (reductions in precipitation) and increases in human activity. The present study shows that the precipitation changes are strongly impacted with the climate [15]; the climate strongly controlled the runoff conditions, and human activities (as water conservancy and water and soil conservation) are closely related to the runoff [21].

6.2.1. Reduced Precipitation. Inspection of Table 3 clearly shows that, compared with the 1970s, the average annual

Table 1: Total monthly runoff volumes measured at the Lintong station in the Wei River basin.

Month	First stage /(10^8 m^3)	Second stage /(10^8 m^3)	Mean difference /(10^8 m^3)	Rate of migration	Third stage /(10^8 m^3)	Mean difference (10^8 m^3)	Rate of migration	Fourth stage /(10^8 m^3)	Mean difference /(10^8 m^3)	Rate of migration
January	2.31	1.24	−1.07	−46%	1.44	0.2	16%	1.95	0.51	35%
February	2.33	1.36	−0.97	−42%	1.52	0.16	12%	1.94	0.42	28%
March	3.96	1.73	−2.23	−56%	2.36	0.63	36%	2.38	0.02	1%
April	7.24	2.92	−4.32	−60%	3.51	0.59	20%	2.67	−0.84	−24%
May	10.19	4.19	−6	−59%	4.95	0.76	18%	3.76	−1.19	−24%
June	4.63	1.98	−2.65	−57%	5.19	3.21	162%	11	5.77	111%
July	11.06	8.4	−2.66	−24%	8.7	0.3	4%	6.83	−1.87	−21%
August	7.69	9.67	1.98	26%	8.1	−1.57	−16%	12.2	4.11	51%
September	17.11	13.94	−3.17	−19%	8.02	−5.92	−42%	11.4	3.42	43%
October	14.51	9.34	−5.17	−36%	7.33	−2.01	−22%	12.5	5.16	70%
November	7.55	4.32	−3.23	−43%	3.81	−0.51	−12%	4	0.19	5%
December	3.77	1.68	−2.09	−55%	1.7	0.02	1%	2.59	0.89	52%

Table 2: Minimum and maximum runoff volumes calculated over periods of 1, 3, 7, 30, and 90 days for the Lintong station in the Wei River basin.

Value	First stage /(10^8 m^3)	Second stage /(10^8 m^3)	Mean difference /(10^8 m^3)	Rate of migration	Third stage /(10^8 m^3)	Mean difference (10^8 m^3)	Rate of migration	Fourth stage /(10^8 m^3)	Mean difference /(10^8 m^3)	Rate of migration
max1	3120.00	3148.09	28.09	1%	2091.37	−1056.72	−34%	2272.40	181.03	9%
max3	6828.09	6597.00	−231.09	−3%	4566.26	−2030.74	−31%	5175.60	609.34	13%
max7	10865.64	11735.64	870.00	8%	7263.49	−4472.15	−38%	8448.60	1185.11	16%
max30	26433.18	25706.53	−726.65	−3%	17245.20	−8461.33	−33%	18460.14	1214.94	7%
max90	52345.23	44413.50	−7931.73	−15%	34207.21	−10206.29	−23%	35926.12	1718.91	5%
min1	23.10	7.98	−15.12	−65%	20.67	12.69	159%	29.36	8.69	42%
min3	74.73	26.02	−48.71	−65%	65.14	39.12	150%	93.78	28.64	44%
min7	221.61	74.32	−147.29	−66%	170.53	96.21	129%	241.06	70.53	41%
min30	1578.29	703.96	−874.33	−55%	1102.14	398.19	57%	1472.88	370.74	34%
min90	8949.95	4311.14	−4638.81	−52%	5602.16	1291.02	30%	5665.44	63.28	1%

precipitation is all reduced in every stages. The mean annual precipitation volume during the 1972~1982 period was 340.75 mm, compared to 359.95 mm during the 1960~1971 period, representing a decrease of 5%. The mean annual precipitation in the 1983~2001 period was 31.79 mm, which represents a decrease of 9% relative to the first period. The mean annual precipitation in the 1983~2001 period was 10.57 mm, which represents a decrease of 3% relative to the first period.

For 1960~1971, 1972~1982, and 1983~2001 periods. The mean annual precipitation volumes were all decreased compared to those in the preceding period. The rate of the decrease from 1983 to 2001 was 3.70% which is smaller than before, and the rate of 2002~2006 represents an increase of 6.47% relative to 1983–2001. Hence, the precipitation variation is one of the most important factors for runoff change.

6.2.2. Increased Water Conservancy. A large number of water conservancy projects have been built in the early 1970s, such as Yangmaowan Reservoir (1970, with a total storage capacity of 120 million m^3), Shihmen Reservoir (1970, with a total storage capacity of 120 million m^3), Lin Gao Reservoir (1971, with a total capacity of 0.33 million m^3) and some irrigation districts as Hengshui River irrigation (effective irrigation area of 9407 hm^2), Baojixia irrigation (effective irrigation area of 188,553 hm^2), Wool Bay irrigation district (effective irrigation area of 16,000 hm^2), of Lin Gao Irrigation (effective irrigation area of 5733). The mean annual runoff in 1972–1982 was 6.07 billion m^3, which represents a decrease of 2.67 billion m^3 relative to 1960–1971 period. The human activities are significantly impacting factor on runoff.

A large number of water conservancy projects were built in the early 1980s, some reservoirs as Shitou River Reservoir (1981, with a total capacity of 147 million m^3), Taoqupo reservoir (1980, with a total capacity of 0.57 million m^3) and some irrigation districts as Dongfanghong irrigation (effective irrigation area of 55800 hm^2). The mean annual runoff in 1983–2001 was 5.51 billion m^3, which represents a decrease of 0.56 billion m^3 relative to 1972–1983 period.

Table 3: The annual precipitation volume measured at the Lintong station in the Wei River basin.

Period	Mean/(mm)	Compared to the first period		Compared to the preceding period	
		Mean difference/(mm)	Rate of migration	Mean difference/(mm)	Rate of migration
1960–1971	359.95				
1972–1982	340.75	−19.20	−5.33%	−19.20	−5.33%
1983–2001	328.16	−31.79	−8.83%	−12.59	−3.70%
2002–2005	349.38	−10.57	−2.94%	21.22	6.47%

The cumulative effects of human activities after 1990s, such as industrial and agricultural water consumption, soil and water conservation water consumption and evaporation continue to increase, Groundwater level and the water consumption of the national economy were significantly decreased. The mean annual runoff in 2002–2006 was 6.06 billion m^3, which represents an increase of 0.54 billion m^3 relative to 1983–2001 period.

6.3. Conclusion. Two methods for the identification of abrupt changes in time series—moving approximate entropy analysis and moving permutation entropy analysis—were used to study the variation of 46-year daily runoff series at the Lintong station in the Wei River basin. Both analyses indicated that abrupt changes occurred in the early 1970s (1972) and at the start of the 21st century (2002); in addition, the moving approximate entropy analysis revealed a third abrupt change that is estimated to have occurred in 1983. These so-called change points were used to separate the 46-year period covered by the runoff volume data set into four separate periods, and the mean values of selected hydrological variables within these periods were compared to evaluate the impact of these abrupt changes. Notable differences between the periods were identified in terms of the total annual runoff, total monthly runoff volumes, and the maximum and minimum runoff volumes over selected periods of time. The changes associated with the transition between the first and second periods in 1972 were especially pronounced. Overall, the observed changes in the selected hydrological variables are consistent with the abrupt changes identified using the two new analytical methods, which suggests that both of the new methods are useful for analyzing runoff series and identifying points of abrupt change. The attribution of abrupt change at the Lintong runoff series is primarily due to the reduced precipitation, increased human activities, increased water consumption of industry and agriculture, significantly decreased groundwater table, and increased evaporation.

Acknowledgments

Natural Science Foundation of China (no. 51190093, 51179148, 51179149), National Key Basic Research 973 of China (no. 2012CB417003), Governmental public industry research special funds for projects (no. 201101043), and Program for New Century Excellent Talents in University. Constructive comments from reviewers are gratefully acknowledged.

References

[1] A. M. Fowler and K. J. Hennessy, "Potential impacts of global warming on the frequency and magnitude of heavy precipitation," *Natural Hazards*, vol. 11, no. 3, pp. 283–303, 1995.

[2] IPCC, "Intergovernmental Panel on Climate Change," 2007.

[3] F. J. Wentz, L. Ricciardulli, K. Hilburn, and C. Mears, "How much more rain will global warming bring?" *Science*, vol. 317, no. 5835, pp. 233–235, 2007.

[4] K. E. Trenberth, "Conceptual framework for changes of extremes of the hydrological cycle with climate change," *Climatic Change*, vol. 42, no. 1, pp. 327–339, 1999.

[5] D. R. Easterling, G. A. Meehl, C. Parmesan, S. A. Changnon, T. R. Karl, and L. O. Mearns, "Climate extremes: observations, modeling, and impacts," *Science*, vol. 289, no. 5487, pp. 2068–2074, 2000.

[6] T. G. Huntington, "Evidence for intensification of the global water cycle: review and synthesis," *Journal of Hydrology*, vol. 319, no. 1–4, pp. 83–95, 2006.

[7] W. Fengying, *Modern Technology of Statistics, Diagnosis and Forecast for Climate*, China Meteorological Press, Beijing, China, 1999.

[8] W. Hou, G. Feng, W. Dong, and J. Li, "Technique for distinguishing dynamical species in the temperature time series of north China," *Acta Physica Sinica*, vol. 55, no. 5, pp. 2663–2668, 2006 (Chinese).

[9] G. H. Huang, C. P. Ou, and J. Xia, "Study of watershed hydrological spatio-temporal variability analysis based on information entropy," *Journal of Dalian University of Technology*, vol. 46, no. z1, pp. 168–173, 2006 (Chinese).

[10] S. M. Pincus, "Approximate entropy as a measure of system complexity," *Proceedings of the National Academy of Sciences of the United States of America*, vol. 88, no. 6, pp. 2297–2301, 1991.

[11] Q. Wang and Z. Zhang, "The research of detecting abrupt climate change with approximate entropy," *Acta Physica Sinica*, vol. 57, no. 3, pp. 1976–1983, 2008 (Chinese).

[12] W. He, Q. Wu, W. Zhang, Q. Wang, and Y. Zhang, "Comparison of characteristics of moving detrended fluctuation analysis with that of approximate entropy method in detecting abrupt dynamic change," *Acta Physica Sinica*, vol. 58, no. 4, pp. 2862–2871, 2009 (Chinese).

[13] W. Hou, G. L. Feng, W. J. Dong, and J. P. Li, "Technique for distinguishing dynamical species in the temperature time series of north China," *Acta Physica Sinica*, vol. 55, no. 5, pp. 2663–2668, 2006 (Chinese).

[14] L. R. Beard, *Statistical Methods in Hydrology*, DTIC Document, 1962.

[15] V. P. Singh, "The use of entropy in hydrology and water resources," *Hydrological Processes*, vol. 11, no. 6, pp. 587–626, 1997.

[16] N. B. Harmancioglu, V. P. Singh, and N. Alpaslan, "Versatile uses of the entropy concept in water resources," in *Entropy and Energy Dissipation in Water Resources*, V. P. Singh and M. Fiorentino, Eds., pp. 91–117, Kluwer Academic, Dordrecht, 1992.

[17] D. Koutsoyiannis, "Uncertainty, entropy, scaling and hydrological statistics. 1. Marginal distributional properties of hydrological processes and state scaling/Incertitude, entropie, effet d'échelle et propriétés stochastiques hydrologiques. 1. Propriétés distributionnelles marginales des processus hydrologiques et échelle d'état," *Hydrological Sciences Journal*, vol. 50, no. 3, 2005.

[18] R. Yan and R. X. Gao, "Approximate entropy as a diagnostic tool for machine health monitoring," *Mechanical Systems and Signal Processing*, vol. 21, no. 2, pp. 824–839, 2007.

[19] C. Bandt, G. Keller, and B. Pompe, "Entropy of interval maps via permutations," *Nonlinearity*, vol. 15, no. 5, pp. 1595–1602, 2002.

[20] Y. Cao, W. W. Tung, J. B. Gao, V. A. Protopopescu, and L. M. Hively, "Detecting dynamical changes in time series using the permutation entropy," *Physical Review E*, vol. 70, no. 4, part 2, Article ID 046217, 7 pages, 2004.

[21] L. J. Li, L. Zhang, H. Wang et al., "Assessing the impact of climate variability and human activities on streamflow from the Wuding River basin in China," *Hydrological Processes*, vol. 21, no. 25, pp. 3485–3491, 2007.

Hindawi Publishing Corporation
Mathematical Problems in Engineering
Volume 2013, Article ID 780354, 15 pages
http://dx.doi.org/10.1155/2013/780354

Research Article

RSW-MCFP: A Resource-Oriented Solid Waste Management System for a Mixed Rural-Urban Area through Monte Carlo Simulation-Based Fuzzy Programming

P. Li,[1] H. J. Wu,[1] and B. Chen[1,2]

[1] *Northern Region Persistent Organic Pollution Control (NRPOP) Laboratory, Faculty of Engineering and Applied Science, Memorial University of Newfoundland, St. John's, NL, Canada A1B 3X5*
[2] *Key Laboratory of Regional Energy and Environmental Systems Optimization, Ministry of Education, Resources and Environmental Research Academy, North China Electric Power University, Beijing 102206, China*

Correspondence should be addressed to B. Chen; bchen@mun.ca

Received 19 February 2013; Accepted 14 April 2013

Academic Editor: Guohe Huang

The growth of global population and economy continually increases the waste volumes and consequently creates challenges to handle and dispose solid wastes. It becomes more challenging in mixed rural-urban areas (i.e., areas of mixed land use for rural and urban purposes) where both agricultural waste (e.g., manure) and municipal solid waste are generated. The efficiency and confidence of decisions in current management practices significantly rely on the accurate information and subjective judgments, which are usually compromised by uncertainties. This study proposed a resource-oriented solid waste management system for mixed rural-urban areas. The system is featured by a novel Monte Carlo simulation-based fuzzy programming approach. The developed system was tested by a real-world case with consideration of various resource-oriented treatment technologies and the associated uncertainties. The modeling results indicated that the community-based bio-coal and household-based CH_4 facilities were necessary and would become predominant in the waste management system. The 95% confidence intervals of waste loadings to the CH_4 and bio-coal facilities were 387, 450 and 178, 215 tonne/day (mixed flow), respectively. In general, the developed system has high capability in supporting solid waste management for mixed rural-urban areas in a cost-efficient and sustainable manner under uncertainty.

1. Introduction

Solid waste is causing significant environmental problems in urban and suburban areas and consequently leading to numerous adverse health and environmental impacts around the world [1]. The concerns in handling and disposing solid waste are growing with the continuous increases of waste generation in the world, which is closely correlated with the growth of population and the economy [2]. Due to the rising waste generation rates and the lack of available space in landfills, urban communities and even some rural areas are facing some critical challenges in developing effective solid waste management systems particularly and partly due to the existence of various uncertainties in the system [3, 4]. These uncertainties may arise from a variety of possible sectors including waste generation rates, disposal capacity, treatment costs, and their interactions, as well as other general uncertainty sources such as incomplete information, measurement and sampling errors, subjective judgement, assumptions and approximation, and dynamics of environmental conditions [5–8]. These uncertainties affect the relative optimization and decision making processes, leading to significant complexities and compromising the confidence and efficiency of decisions [4, 9–11].

To address challenges from uncertainties, a number of optimization methods have been developed to handle different types of uncertainties in solid waste management in the past decades. Among these methods fuzzy programming and stochastic programming are widely reported in the literature [4, 8, 12–19]. Fuzzy techniques can be used to express the possibilistic uncertainties where vagueness of parameters is

characterized by membership functions [16, 20, 21]; stochastic techniques are able to handle the probabilistic uncertainties where the probability distributions can be used to represent random variability of parameters [22–24]. Nevertheless, both techniques have their own drawbacks: membership functions may lead to a loss of information when inappropriate subjective judgments have been made and/or when some parameters can be better represented by stochastic variables, while defining of probability distribution can be affected by the limited amount of data [20, 21, 25]. Furthermore, possibilistic and probabilistic uncertainties can frequently coexist in environmental systems such as municipal solid waste (MSW) management systems. It is necessary to develop integrated fuzzy and stochastic techniques to handle such cases, and one attempt has previously been made [26]. However, some difficulties have been reported in finding effective linkages between these two techniques and in appropriately interpreting optimized results from their outputs. For example, fuzzification and defuzzification are challenging when the stochastic distributions are involved. Thus, possibilistic and probabilistic uncertainties are usually treated separately [2, 20, 21, 27, 28].

Recently, some approaches have been developed to simultaneously deal with possibility and probability [4, 29, 30]. However, these approaches treat probabilistic uncertainties based on limited, discrete probability distributions and are unable to simultaneously handle continuous probability and subjective information [2, 21]. In practice, system variables usually include both subjective and objective information (or dual uncertainties) [2, 31]; therefore, the incorporation of fuzzy set theory and Monte Carlo simulation becomes necessary and valuable [21, 32, 33]. Monte Carlo simulation can address continuous probabilistic uncertainties by using probability density functions (PDFs) [34–36]. Therefore, the integration of fuzzy programming approaches with Monte Carlo simulation can be promising in addressing the limitations of treating possibilistic and continuous probabilistic uncertainties. However, challenges still remain in finding optimal solutions to the new coupled problem of the fuzzy programming and Monte Carlo simulation.

Furthermore, it is significantly difficult to design a successful solid waste management system due to complexities and uncertainties, especially in mixed rural-urban areas. These areas face a special challenge in treating and disposing agricultural residues and livestock manure, which may have much higher loadings than the common MSW stream. At the same time, manure can also be a potential valuable resource through resource-oriented recovery techniques (such as composting, CH_4 generation, and bio-coal generation). Unlike traditional solid waste management systems which treat the solid waste as burden, the resource-oriented solid waste management system treats it as potential resources or materials that can be used for reproduction. Under this perspective, the solid waste management system can be sustainably run by profit driven sectors rather than difficultly maintained by cost controlling from some administrative departments, and therefore can be easily controlled by the market [2, 8]. Therefore, resource-oriented solid waste management is a promising and potentially a preferred solution in the future. The resource-oriented concept is especially important for mixed rural-urban areas where livestock breeding exists. It can minimize environmental impacts with maximizing the economic benefits for mixed rural-urban areas and increase the motivation of application by different sectors (e.g., government and industry) [2, 37]. Although there are some attempts in applying resource-oriented waste management methods for industrial solid waste, studies targeting agricultural and municipal solid waste in mixed rural-urban areas are still insufficient [2, 38].

The Monte Carlo simulation-based fuzzy programming (MCFP) model is a new mathematical approach which has been recently developed [2]. However, the previous study only applied a simplified hypothetical case without further testing, particularly by real-world problems. In this study, the MCFP model is further defined with a resource-oriented solid waste management concept, to form a resource-oriented solid waste management system supported by Monte Carlo simulation-based fuzzy programming (RSW-MCFP) system for better supporting solid waste management in mixed rural-urban areas when possibilistic and continuous probabilistic uncertainties coexist in real-world applications. Another key objective of this new method is to reduce the amount of solid waste by recovering materials and energy from solid waste. In short, the objectives of this study are (1) to develop a resource-oriented solid waste management system for a mixed rural-urban area supported by a Monte Carlo simulation-based fuzzy programming (RSW-MCFP) and (2) to conduct feasibility and efficiency tests as well as a trade-off analysis through a real-world case study of solid waste management in the town of Shuangcheng in Northeast China. This approach is expected to efficiently handle various uncertainties in a complex system with fewer additional constraints and provide a powerful tool to generate a set of feasible decision alternatives for local decision makers to improve the efficiency and confidence in managing solid waste in mixed rural-urban areas.

2. Methodology

In the MCFP approach, a Monte Carlo simulation approach is introduced to handle the probabilistic uncertainties (continuous and discrete) [2]. By assigning random values to the uncertain parameters, the probabilistically uncertain information becomes deterministic one in a single loop of Monte Carlo simulation. Consequently, the original problem with dual uncertainties (coexistence of possibilistic and continually probabilistic uncertainties) becomes a fuzzy problem. Subsequently, a fuzzy programming approach based on the fuzzy-stochastic-interval linear programming (FSILP) method [10] is introduced to handle the possibilistic uncertainties, converting the fuzzy problem into a conventional linear problem.

In the FSILP approach, the Nguyen's method is used to convert the fuzzy and/or fuzzy stochastic linear programming problems into the conventional linear programs (LPs), by measuring the attainment values of fuzzy numbers and/or fuzzy random variables, as well as the superiority and inferiority between triangular fuzzy numbers/triangular fuzzy

stochastic variables [39]. An attainment value is a degree of attainment of the fuzzy goal. It is considered to be a concept similar to a degree of satisfaction of the fuzzy decision when the fuzzy constraint is replaced by the fuzzy expected payoff. It can also be interpreted as a possibility of attainment of the fuzzy goal. The FSILP approach is advanced from the Nguyen method [39] in different situations of relations in demand (left-hand-side, LHS) and resource (right-hand-side, RHS) as well as the introduction of interval programming. Although the FSILP approach is capable of handling the coexistence of uncertainties, its efficiency will decrease when the number of discrete probabilities increases. In addition, when the probabilistic uncertainty is described as a continuous distribution, integration is required in numerically processing the optimization, leading to difficulties. Furthermore, some of the distributions may not be integrable, making the optimization unachievable.

Monte Carlo simulation is a class of computation intensive algorithms based on randomization. These methods can provide near equivalent results to deterministic algorithms, making it a complement to the theoretical derivations. Monte Carlo simulation is especially suitable for problems with multiple probability distributions, while handling these distributions becomes complicated if using numerical methods. Due to incomplete or insufficient information from the literature and historical data as well as the subjective judgement, many input parameters are difficult to characterize by utilizing probability distributions for numerical applications. In many cases, the obtained probability distribution may be still uncertain where each data point contains a degree of belief, leading to dual uncertainties of possibility and continuous probability [29]. Consequently, in order to effectively tackle such dual uncertainties, fuzzy programming and Monte Carlo simulation need to be combined. However, the fuzzification and defuzzification processes in the conventional fuzzy programming are still difficult in such integration.

The FSILP approach can easily convert a fuzzy problem into a crisp deterministic problem without conventional fuzzification and defuzzification processes, which makes it significantly easier in coupling with the Monte Carlo simulation. The random values of the parameters are firstly assigned in each Monte Carlo simulation trial according to the probability distributions of parameters. Therefore, the parameters with probabilistic uncertainties become deterministic in a single loop of Monte Carlo simulation, leaving possibilistic uncertainties in the problem and leading to a fuzzy problem. Such fuzzy problem is then solved by the fuzzy programming from the FSILP approach. Finally, a group of solutions can be collected to present the most frequent occurrences of results under the different kinds of uncertainties in parameters.

Consider a fuzzy stochastic linear problem as follows:

$$\min \quad f = CX \tag{1a}$$

$$\text{s.t.} \quad \sum_{j=1}^{n} \left(\widetilde{A}_{ij}\right)_w X_j \le \left(\widetilde{B}_i\right)_w, \quad i = 1, \ldots, m \tag{1b}$$

$$X_j \ge 0, \quad w \in \Omega, \tag{1c}$$

where $C \in \{R\}^{1\times n}$ is the matrix of coefficients in the objective function and $(\widetilde{A}_{ij})_w \in \{R\}^{m\times n}$, $(\widetilde{B}_i)_w \in \{R\}^{m\times 1}$ are matrices of constraint coefficients with fuzzy random variables defined on a probability space (Ω, F, P). Assume that all fuzzy numbers are in a form of $\widetilde{t} = (t, \delta^-, \delta^+)$, where δ^- and $\delta^+$are the lower and upper spreads of the membership function as follows:

$$X_i = \left\{\widetilde{t};\ \widetilde{t} = \left(t, \delta^-, \delta^+\right), \delta^-, \delta^+ \ge 0\right\}, \tag{2}$$

$$\mu_{\widetilde{t}}\left(X_i\right) = \begin{cases} \max\left(0, 1 - \dfrac{t-y}{\delta^-}\right), & \text{if } y \le t \\ 1, & \text{if } a = 0,\ b = 0,\ t = y \\ \max\left(0, 1 - \dfrac{y-t}{\delta^+}\right), & \text{if } y \le t \\ 0, & \text{otherwise.} \end{cases} \tag{3}$$

According to the Monte Carlo simulation, deterministic values for parameters will be assigned to all the random variables in each trial (the lth trial) out of N trials based on the distributions of the parameters. Therefore, for the lth trial,the Problem (1a)–(1c) can be converted to a fuzzy problem as follows:

$$\min \quad f = CX \tag{4a}$$

$$\text{s.t.} \quad \sum_{j=1}^{n} \left(\widetilde{A}_{ij}\right)_l X_j \le \left(\widetilde{B}_i\right)_l, \quad i = 1, \ldots, m,\ l = 1, \ldots, N \tag{4b}$$

$$X_j \ge 0, \tag{4c}$$

where $(\widetilde{A}_{ij})_l \in \{R\}^{m\times n}$, $(\widetilde{B}_i)_l \in \{R\}^{m\times 1}$ are the matrices of constraint coefficients with fuzzy variables defined on a series of fuzzy membership functions with the assigned random variables in the lth trial.

According to the fuzzy programming from the FSILP approach, the fuzzy terms in the Problem (4a)–(4c) can be converted as follows [10]:

$$\min \quad f = CX + \sum_{i=1}^{u} \lambda_i^1 - \sum_{k=1}^{v} \lambda_k^2 \tag{5a}$$

$$\text{s.t.} \quad \frac{1}{2}\left(\sum_{j=1}^{n}\left(\left(\widetilde{A}_{ij}^1\right)_w X_j + \delta_{x_j}^+ X_j\right) + \delta_{B_i^1}^- + S_i - \left(\widetilde{B}_i^1\right)_w\right) = \lambda_i^1, \quad i = 1, \ldots, u \tag{5b}$$

$$\frac{1}{2}\left(\sum_{j=1}^{n}\left(\left(\widetilde{A}_{kj}^2\right)_w X_j - \delta_{x_j}^- X_j\right) - \delta_{B_k^2}^+ - \left(\widetilde{B}_k^2\right)_w\right) = \lambda_k^2, \quad k = 1, \ldots, v \tag{5c}$$

$$\lambda_i^1 \le \frac{1}{2}\left(\sum_{j=1}^{n}\delta_{x_j}^{+}X_j + \delta_{B_i^1}^{-}\right) \tag{5d}$$

$$\lambda_k^2 \le \frac{1}{2}\left(\sum_{j=1}^{n}\delta_{x_j}^{-}X_j + \delta_{B_k^2}^{+}\right) \tag{5e}$$

$$X_j, \delta_{x_j}^{-}, \delta_{x_j}^{+}, \delta_{B_i^1}^{-}, \delta_{B_k^1}^{+}, \lambda_i^1, \lambda_k^2, p_i^1, p_k^2, S_i \ge 0, \quad w \in \Omega, \tag{5f}$$

where $\lambda_i^1 \in \{R\}^{u\times 1}$ and $\lambda_k^2 \in \{R\}^{v\times 1}$ are matrices of control decision variables corresponding to the degree (membership grade) to which X solution fulfils the fuzzy constraints; $\widetilde{A}_{ij}^1 \in \{A\}^{u\times n}$ and $\widetilde{A}_{kj}^2 \in \{A\}^{v\times n}$ are matrices of positive and negative coefficients in the constraint, respectively; $\widetilde{B}_i^1 \in \{R\}^{u\times 1}$ and $\widetilde{B}_k^2 \in \{R\}^{v\times 1}$ are matrices of positive and negative RHS; and $S_i \in \{R\}^{m\times 1}$ is the matrix of the slack variables. Furthermore, the constraints of $\lambda_i^1 \le (1/2)(\sum_{j=1}^{n}\delta_{x_j}^{+}X_j + \delta_{B_i^1}^{-})$ and $\lambda_k^2 \le (1/2)(\sum_{j=1}^{n}\delta_{x_j}^{-}X_j + \delta_{B_k^2}^{+})$ are added because λ represents the attainment of the memberships of LHS and RHS which is also equivalent to the overlap of these two memberships on one side spread.

After N trials are finished, the sets of results can be obtained as follows:

$$f_{l,\text{opt}} = \left\{f\left(X_{jl,\text{opt}}\right); X_{jl,\text{opt}} \ge 0\right\}, \quad l = 1,\ldots,M; \quad j = 1,\ldots,Z, \tag{6}$$

where M is the number of the feasible solutions after N trials of the Monte Carlo simulation, and Z is the number of decision variables.

Assume that there is no uncertainty existing in the coefficients of the objective function (C); the final solution can be stated as follows [2]:

$$E\left(f_{\text{opt}}\right) = \left\{f\left(E\left(X_{j,\text{opt}}\right)\right); E\left(X_{j,\text{opt}}\right) \ge 0\right\}, \quad l = 1,\ldots,M. \tag{7}$$

The full details about the MCFP approach as well as the solution algorithms can be found in [2].

3. The MSW-MCFP System

3.1. System Analysis for the Solid Waste Management in the Town of Shuangcheng. The city of Shuangcheng is a county-level city under the administration of Harbin, the capital city of Heilongjiang Province in Northeast China. The city has 2,200 km^2 of cropland and is ranked as one of the top five crop production bases in China. The livestock and dairy sectors are rapidly developing and becoming dominant industries in the city.

There are more than 290,000 cows on dairy farms in the city, making it an important location for dairy livestock breeding in China. However, the fast growth of livestock has not been accompanied with appropriate regulations, management practices, and treatments/disposal of manure and wastewater from dairy farms. Consequently, most of the livestock manure, is dumped at various locations surrounding the villages, occupying large land areas, releasing bad odour, and even burying and blocking roads. Properly managing rural waste, especially livestock manure has been identified as a top priority by the local governments, the agrofood industry, and the public.

This study targets the town of Shuangcheng, which is the administrative and economic centre of the city of Shuangcheng and also a mixed rural-urban area. According to the historical census of the town, the information about household, population, natural growth rate, and cattle stocks from 2000 to 2007 is collected [40]. The number of households ranges from 65,053 to 76,561, and the mean value is 69,859 with standard deviation of 4,382. The population ranges from 181270 to 183206, and the mean value is 181,838 with standard deviation of 599. The natural growth rate ranges from 1.33‰ to 6.54‰, and the mean value is 4.84 with standard deviation of 1.81. The number of cattle ranges from 12,689 to 22,636, and the mean value is 17,959 with standard deviation of 3,613. It is estimated that the ratio of population between the urban and rural areas in the town is 2 : 1 [40]. Correspondingly, based on the assumption that the future growth rate of population remains the same level as the period from 2000 to 2007, the distributions for the population and cattle number within the planning period (2011–2015) can be determined (Figure 1).

It is reported that the generation rate of MSW in the rural area is 0.55 to 0.65 kg per capita per day, and which in the urban area is 1.1 to 1.3 kg per capita per day [41, 42]. Furthermore, the generation rate of manure from cattle is 5 to 15 kg per cattle per day [41, 42]. By involving possibility uncertainty, the membership functions for the loading of MSW and cattle manure are shown in Figure 2. For the sake of simplicity, symmetric triangular fuzzy numbers are used.

3.2. Development of a Resource-Oriented Solid Waste Management System. According to the system analysis (e.g., parameters and their functions as well as interactions among them) of the current situation of solid waste management, a system framework for resource-oriented solid waste management is proposed for the town of Shuangcheng (Figure 3). Over the 5-year planning period (2011–2015), the existing landfill and composting facilities will be available to meet the requirement of MSW treatment and disposal. Detailed operational and economic information has been collected in Tables 1 and 2 [40], including capacities, operation and maintenance costs, residue rates, revenues, and transportation costs of the proposed facilities (i.e., community-based bio-coal production and composting, household-based CH_4 generation and composting). Finally, a penalty rate of \$500/tonne waste is assigned for dumping solid waste in nondesignated areas.

Currently, the most critical and challenging problem in the mixed rural-urban area of the town of Shuangcheng is how to deal with a huge amount of livestock manure (especially cow dung). In the proposed system, manure can be utilized for the methane generating, composting and bio-coal manufacturing. After this, only a small residual is left and can

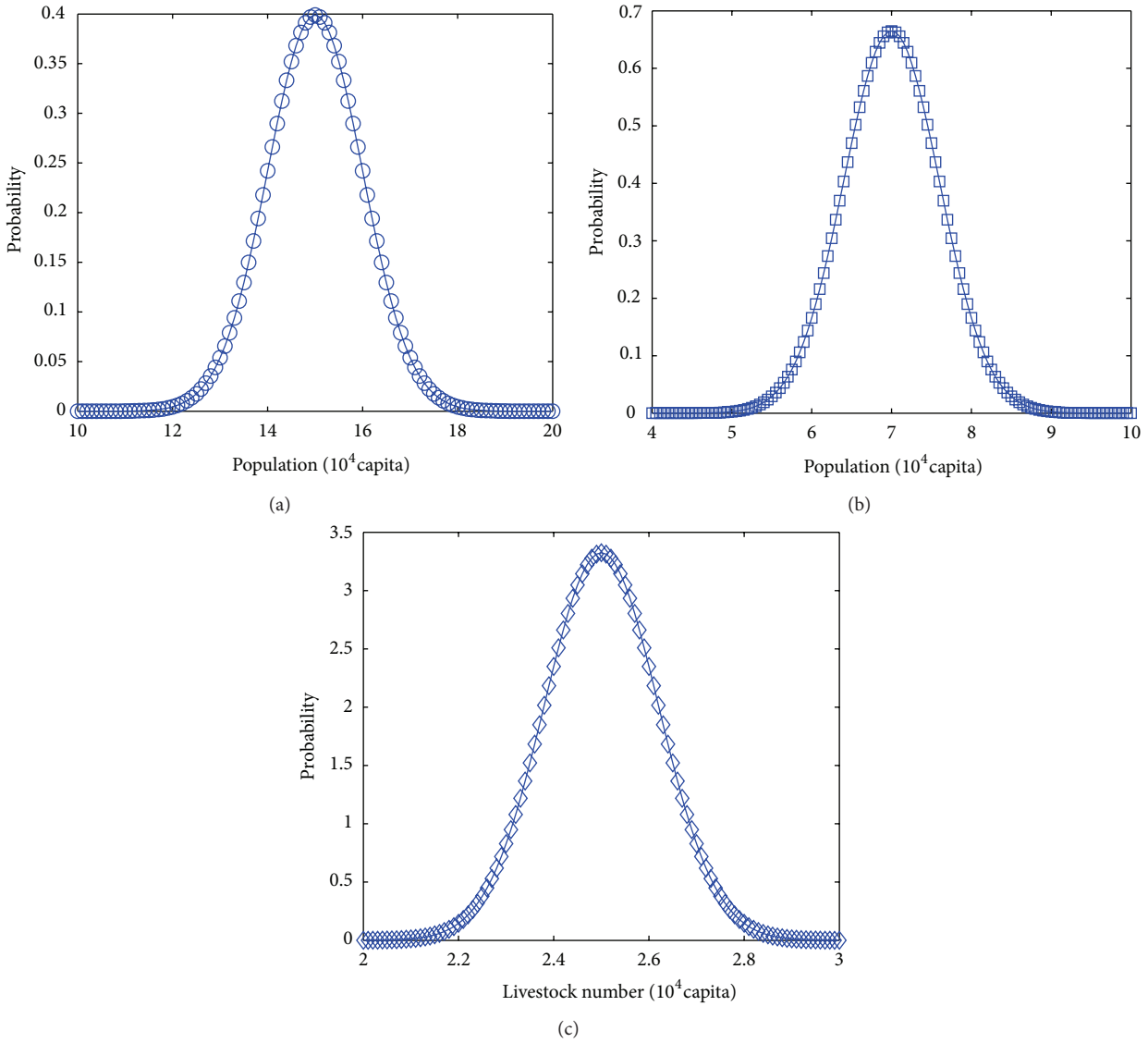

Figure 1: Probability distributions of the annual population from the (a) urban and (b) rural areas as well as (c) the number of livestock in the town of Shuangcheng from 2011 to 2015.

be used as fertilizer for farming, leading to substantial reduction of solid waste in the system. Furthermore, individual farmers can be driven by market incentives and form small firms to collect waste and send them to the waste treatment facilities such as composting plants and bio-coal generating plants. As a result, the farmers can get direct benefits from selling or collecting cattle manure; meanwhile, the treatment plants can generate profits by selling products or service (e.g., compost, bio-coal, and CH_4).

An assumption is placed that the demands of the corresponding products or services in the market are much higher than the production from the system. After the collectors transfer the dung to enterprises, products such as the organic fertilizer, methane, and bio-coal can be sold back to farmers. Since the costs of these products are postulated to be less than the chemical fertilizers or coal and electricity, the farmers may save their money by utilizing these recycled products and therefore increase their incomes.

3.3. Development of an MCFP Approach to Support Solid Waste Management. According to the proposed resource-oriented solid waste management system and the collected information, the corresponding optimization model can be developed as follows:

$$\begin{aligned}\text{minimize} \quad f = {} & \sum_{i=1}^{2}\sum_{j=1}^{5}\left(\mathrm{OP}_j + \mathrm{TR}_{ij}\right)x_{ij} \\ & + \sum_{j=1}^{5}\left(\mathrm{OP}_j + \mathrm{TR}_{2j}\right)y_j \\ & + \sum_{i=1}^{2}\sum_{j=2}^{5}\left(\mathrm{OP}_1 + \mathrm{TRL}_j\right)\mathrm{RM}_j x_{ij} \\ & + \sum_{j=2}^{5}\left(\mathrm{OP}_1 + \mathrm{TRL}_j\right)\mathrm{RC}_j y_j\end{aligned}$$

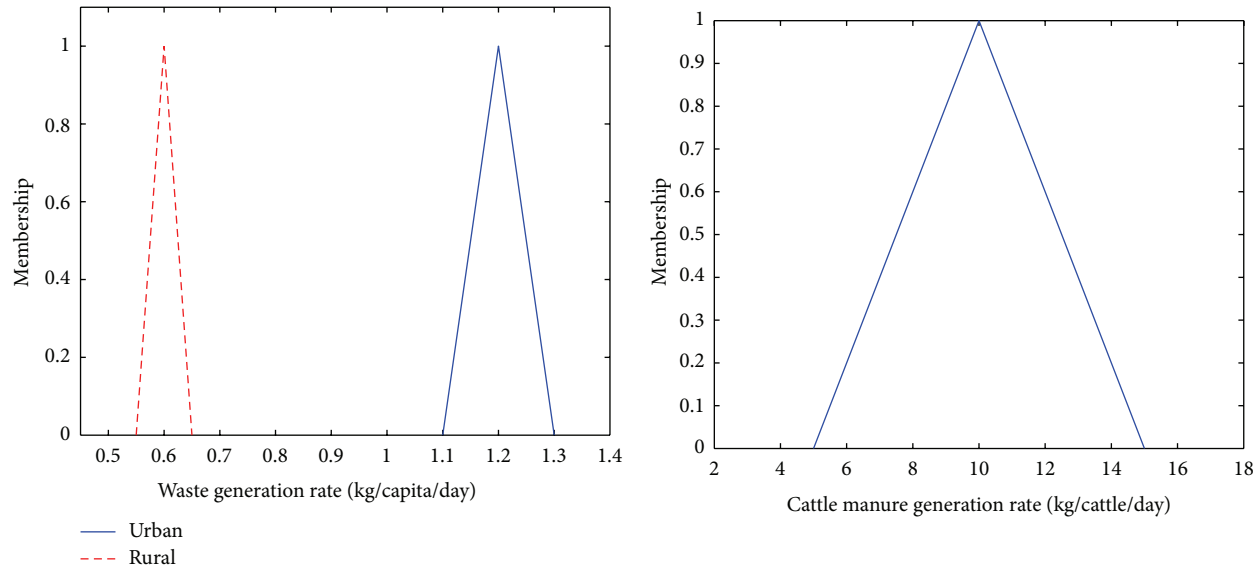

Figure 2: Fuzzy membership functions of (a) the MSW loadings from the urban and rural areas and (b) the cattle manure in the town of Shuangcheng from 2011 to 2015.

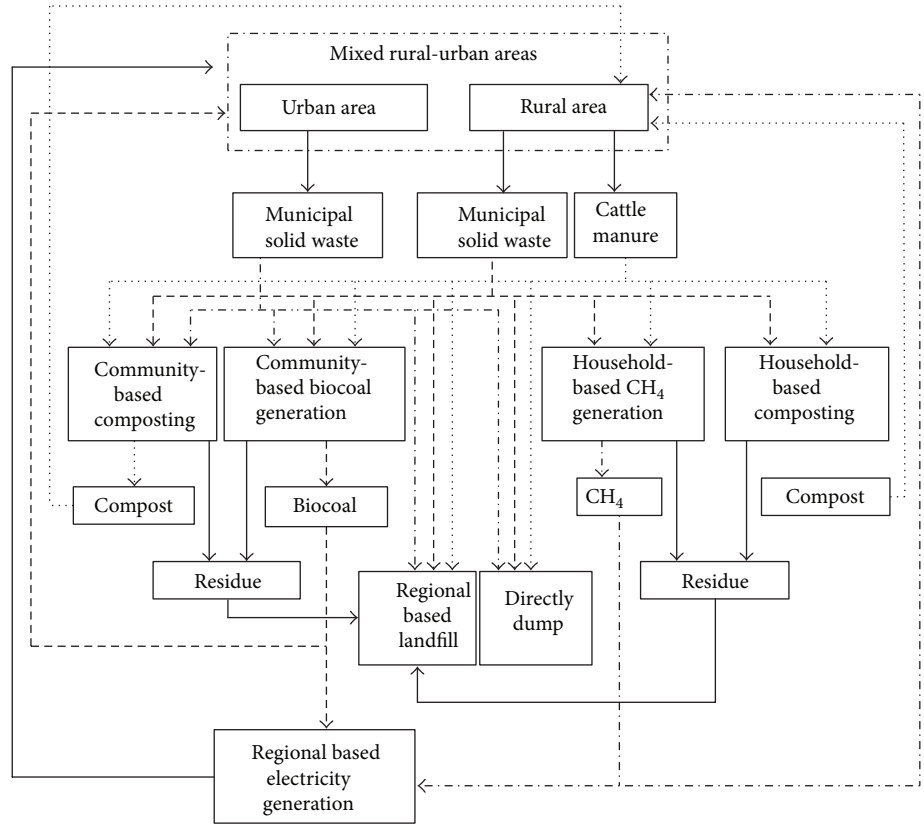

Figure 3: A resource-oriented solid waste management system for the mixed rural-urban area of Shuangcheng.

Table 1: The operational and economic information for the existing and proposed facilities in the town of Shuangcheng.

Facility	j	Capacity (tonne/day)	Running cost ($/tonne)	Residue from MSW	Residue from cattle manure	Revenue ($/tonne)	Transportation cost to landfill ($/tonne)
Regional based landfill	1	16438	50	\	\	0	\
Community-based biocoal generation	2	600	2000	0.3	0	2400	30
Community-based composting	3	600	100	0.4	0.2	400	30
Household-based composting	4	150	80	0.4	0.2	400	60
Household-based CH_4 generation	5	150	80	0.5	0.3	500	60
Directly dump	6	\	500	0	0	0	0

j is the index for the facilities used in the approach.

Table 2: The transportation cost from waste collecting areas to facilities.

Area	Facility	ij	Transportation cost ($/tonne)
Urban	Regional based landfill	11	60
Urban	Community-based bio-coal generation	12	60
Urban	Community-based composting	13	60
Urban	Household-based composting	14	80
Urban	Household-based CH_4 generation	15	80
Urban	Directly dump	16	0
Rural	Regional based landfill	21	60
Rural	Community-based bio-coal generation	22	30
Rural	Community-based composting	23	30
Rural	Household-based composting	24	0
Rural	Household-based CH_4 generation	25	0
Rural	Directly dump	26	0

Note: i is index for the areas and j is index for the facilities used in the approach.

$$+ \sum_{i=1}^{2} x_{i6} P + y_6 P - \sum_{i=1}^{2} \sum_{j=2}^{5} \mathrm{RE}_j x_{ij} - \sum_{j=2}^{5} \mathrm{RE}_j y_j \tag{8a}$$

subject to

$$\sum_{j=1}^{5} x_{ij} \geq \mathrm{MG}_i, \quad \forall i = 1, 2 \tag{8b}$$

$$\sum_{j=1}^{5} y_j \geq \mathrm{CG} \tag{8c}$$

$$\sum_{i=1}^{2} x_{ij} + y_j \leq b_j \mathrm{CP}_j, \quad \forall j = 2, \ldots, 6 \tag{8d}$$

$$\sum_{i=1}^{2} x_{i1} + \sum_{i=1}^{2} \sum_{j=2}^{5} \mathrm{RM}_j x_{ij} + \sum_{j=2}^{5} \mathrm{RC}_j y_j \leq \mathrm{CP}_1 \tag{8e}$$

$$x_{ij}, y_j \geq 0 \tag{8f}$$

$$b_j = 0 \text{ or } 1, \tag{8g}$$

where

f=the net system cost, $/d;

i = the index of area, $i = 1$ for urban area and $i = 2$ for rural area;

j = the index of facility, $j = 1, 2, \ldots, 6$;

x_{ij} = the municipal solid waste loading from area i to facility j, tonne/day;

y_j = the cattle manure loading from area i to facility j, tonne/day;

b_j = the binary variable for determining whether the facility j will be required in the planning period: "1" indicates that the facility will be required to install, and "0" indicates that the facility is not necessary;

OP_i = the operating cost of facility i, $/tonne;

TR_{ij} = the transportation cost from area i to facility j, $/tonne;

RM_j = the residue rate from facility j by treating municipal solid waste;

RC_j = the residue rate from facility j by treating cattle manure;

P = the penalty for the direct dump of waste or cattle manure, \$/tonne;

MG_i = the municipal solid waste generation rate in area i, tonne/day;

CG = the cattle manure generation rate in the town of Shuangcheng, tonne/day;

CP_i = the loading capacity of facility j, tonne/day;

TRL_j = the transportation cost from facility j to the landfill, \$/tonne;

RE_j = the revenue generated by facility j by treating the waste, \$/tonne.

According to the measurement of generation rates of MSW and manure from cattle as well as the population of cattle (Figures 1 and 2), it can be determined that the dual uncertainties of possibility and continuous probability exist in waste generation. Therefore, according to the algorithm of MCFP, especially (5a)–(5f), the original model (Problem (8a)–(8g)) can be converted as follows:

$$\begin{aligned}\text{minimize}\quad f = {} & \sum_{i=1}^{2}\sum_{j=1}^{5}\left(\mathrm{OP}_j + \mathrm{TR}_{ij}\right)x_{ij} \\ & + \sum_{j=1}^{5}\left(\mathrm{OP}_j + \mathrm{TR}_{2j}\right)y_j \\ & + \sum_{i=1}^{2}\sum_{j=2}^{5}\left(\mathrm{OP}_1 + \mathrm{TRL}_j\right)\mathrm{RM}_j x_{ij} \\ & + \sum_{j=2}^{5}\left(\mathrm{OP}_1 + \mathrm{TRL}_j\right)\mathrm{RC}_j y_j \\ & + \sum_{i=1}^{2}x_{i6}P + y_6 P \\ & - \sum_{i=1}^{2}\sum_{j=2}^{5}\mathrm{RE}_j x_{ij} - \sum_{j=2}^{5}\mathrm{RE}_j y_j + \sum_{i=1}^{2}\lambda_i^1 + \lambda^1\end{aligned} \tag{9a}$$

subject to

$$\sum_{j=1}^{5} x_{ij} - \delta_i^{\mathrm{MG}} - \mathrm{MG}_i = \lambda_i^1, \quad \forall i = 1, 2 \tag{9b}$$

$$\sum_{j=1}^{5} y_j - \delta_i^{\mathrm{CG}} - \mathrm{CG} = \lambda^2 \tag{9c}$$

$$\sum_{i=1}^{2} x_{ij} + y_j \le b_j \mathrm{CP}_j, \quad \forall j = 2, \ldots, 6 \tag{9d}$$

$$\sum_{i=1}^{2} x_{i1} + \sum_{i=1}^{2}\sum_{j=2}^{5}\mathrm{RM}_j x_{ij} + \sum_{j=2}^{5}\mathrm{RC}_j y_j \le \mathrm{CP}_1 \tag{9e}$$

$$\lambda_i^1 \le \delta_i^{\mathrm{MG}}, \quad \forall i = 1, 2 \tag{9f}$$

$$\lambda^2 \le \delta^{\mathrm{CG}} \tag{9g}$$

$$x_{ij}, y_j \ge 0 \tag{9h}$$

$$b_j = 0 \text{ or } 1, \tag{9i}$$

where δ_i^{MG} are the spreads of membership function of the MSW generation rates in Figure 2(a), which are $\delta_1^{\mathrm{MG}} = 0.1$ kg/capita/day for the urban area based on the fuzzy membership function $t_1^{\mathrm{MG}} = (1.2, 0.1, 0.1)$ kg/capita/day, and $\delta_2^{\mathrm{MG}} = 0.05$ kg/capita/day for the rural areas based on the fuzzy membership function $t_2^{\mathrm{MG}} = (0.5, 0.05, 0.05)$ kg/capita/day. δ^{CG} is the spread of membership function of the manure generation rates from cattle in Figure 2(b), which is $\delta^{\mathrm{CG}} = 5$ kg/cattle/day based on the fuzzy membership function $t^{\mathrm{CG}} = (10, 5, 5)$ kg/cattle/day.

The collected data were applied normality test by using statistical tools (i.e., Minitab), and results showed that P values are greater than 0.9. Therefore, the assumption has been made that the population and the number of cattle follow normal distributions. The population in the urban area is assumed normally distributed according to Figure 1(a),with a distribution function of $N \sim (15, 1)$. While the population in the rural areas is also normally distributed according to Figure 1(b), with a distribution function of $N \sim (7, 0.6)$. The number of cattle is also normally distributed according to Figure 1(c), with a distribution function of $N \sim (2.5, 0.12)$. According to the distribution of parameters and the solution algorithm of MCFP, the final optimization model for solid waste management in the town of Shuangcheng can be solved by programming software (i.e., MATLAB with LINDO API).

4. Results and Discussion

The modeling results indicate that all MSWS from both urban and rural areas as well as the cattle manure initially flow to two facilities: the community-based bio-coal and the household-based CH_4 facilities, and then the residues from these two facilities flow to the landfill for final disposal (Figure 4). The mean values and 95% confidence interval of the MSW flows from the urban area to the bio-coal facility are 195.1 tonne/day and "175.17, 215.63" tonne/day, respectively. The mean values and 95% confidence interval of the MSW flows from the rural area to the CH_4 facility are 45.24 tonne/day and "39.98, 51.15" tonne/day, respectively. The mean values and 95% confidence interval of the cattle manure flows to the bio-coal facility are 270.66 tonne/day and "250.22, 291.84" tonne/day, respectively. The mean values and 95% confidence interval of the cattle manure flows to the CH_4 facility are 104.76 tonne/day and "97.71, 110.99" tonne/day, respectively. The installations of the other proposed facilities are not suggested in the planning period. The mean values and 95% confidence interval of the optimal system cost are \$−218,866/day and

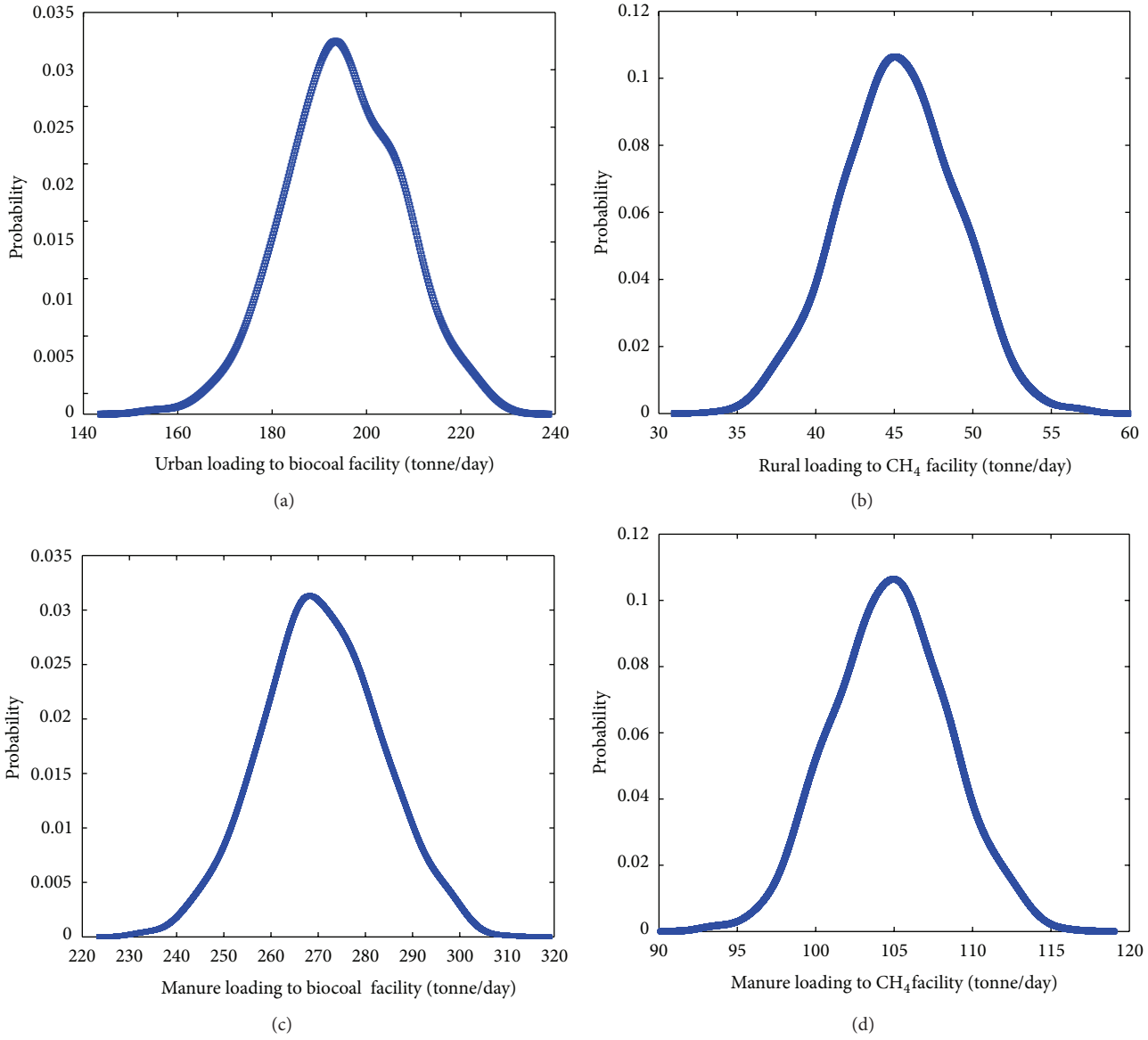

Figure 4: The probability distributions of (a) the MSW loading from the urban area and (c) the cattle manure loading to the community-based biocoal facility as well as (b) the MSW loading from the rural area and (d) the cattle manure loading to the household-based CH_4 facility.

"$−229,150, −209,010" day. In other words, the mean value and 95% confidence interval of the optimal system benefits are around $\$218.87 * 10^3$/day and $\$209.01, 229.15 * 10^3$/day, respectively (Figure 5).

Since waste and cattle manure are innovatively treated in the proposed management system as a type of recycled resource, the landfill becomes the last choice for waste flow even though the running cost is the lowest. The revenue from selling the products (e.g., bio-coal and methane gas) can cover the costs of operating and maintaining the facilities such as the transportation cost for the wastes from the households to the facilities, the residues from the facilities to the landfill, and the running cost of treating the residues in the landfill, leading to net benefits to the system. This demonstrates the feasibility and sustainability of the proposed system and the potential benefits to the local community and environment.

The optimization results also indicate different loadings of the waste generated from urban and rural areas. The MSW preferentially flows to the community-based bio-coal facility and then flows to the household-based CH_4 facility. For cattle manure, both the household-based CH_4 facility and the community-based bio-coal facility become destinations because the net profits of these two facilities are higher than the composting facilities. Although the household-based CH_4 facility is more profitable than the community-based bio-coal facility, the relatively high transportation cost restricts the MSW loading from the urban area to the

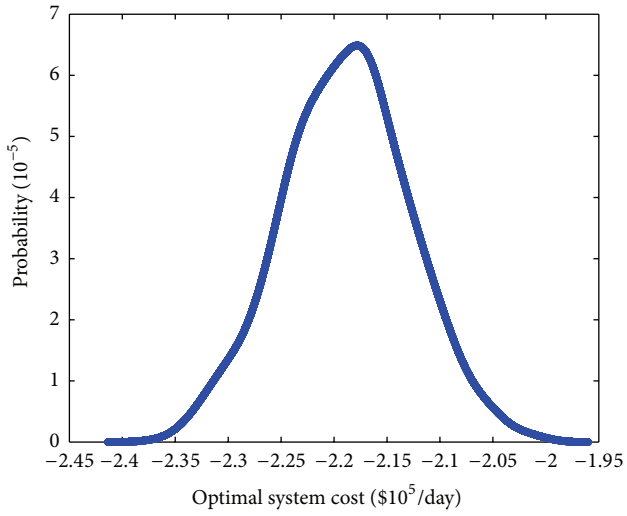

Figure 5: The probability distribution of the optimal system cost.

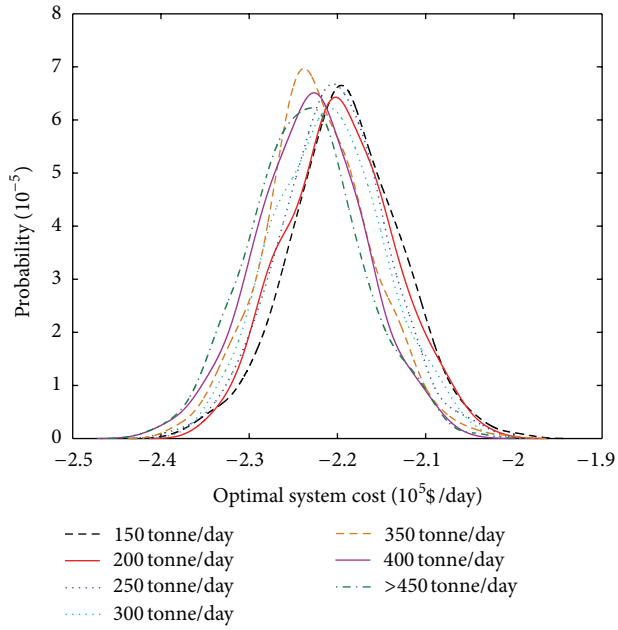

Figure 6: Probability distributions of optimal system cost with the changing capacity of the household-based CH_4 facility.

CH_4 facility. In contrast, due to zero transportation cost for waste and cattle manure loading to on-site CH_4 facility, this facility becomes dominant in the rural area. Similar costs are observed from the household-based composting facility and the community-based bio-coal facility with consideration of both running and transportation costs. However, there is no residue from the community-based bio-coal facility, while about 20% of residue from the household-based composting facility, eventually leading to additional costs in transferring and operating the residue from the composting facility to the landfill. Therefore, some portions of cattle manure are optimally loaded to the community-based bio-coal facility.

Based on the above results, it is recommended either to increase the capacity of household-based CH_4 facility to digest all the waste and cattle manure from the rural area and locate the community-based bio-coal facility closer to the town of Shuangcheng or to keep the current capacity of the household-based CH_4 facility and locate the community-based bio-coal facility between the urban and rural areas. However, because the household-based CH_4 facility is easier and more economical to install and operate (many households in the town of Shuangcheng already have CH_4 pits installed), it is more profitable to increase the capacity of the household-based CH_4 facility.

In order to further minimize the system cost or maximize the system net profit, series of MCFP optimization processes have been applied by changing the capacity of household-based CH_4 facility from 150 to 600 tonne/day with increments of 50 tonne/day. The results (Figures 6 to 11) indicate that the optimal system cost keeps decreasing when the capacity of household-based CH_4 facility increases from 150 to 450 tonne/day. When the capacity of CH_4 facility is 450 tonne/day, the system cost becomes the lowest ($\$-2.23 * 10^5$/day). After this optimal point, the system cost increases again, which is because capacity of the facility is overdesigned and extra maintenance and operational cost will be required (Figure 9).

The loading of cattle manure to the community-based bio-coal facility keeps decreasing; meanwhile, the loading to the household-based CH_4 facility keeps increasing due to its growing capacity. If the capacity of the household-based CH_4 facility is equal or higher than 450 tonne/day, all the waste from the rural area will be treated to produce CH_4 as the renewable energy source (Figures 9 and 11).

Because the community-based bio-coal facility is dominant in the urban waste flow, the capacity change of household-based CH_4 facility does not affect the MSW loading from the urban area to the community-based bio-coal facility (Figures 7(a) and 10(a)). In contrast, the household-based CH_4 facility is dominant in the rural waste (both municipal solid waste from the rural area and the cattle manure) flow. Because the capacity of the CH_4 facility is always higher than the total loading of the rural MSW which has the highest priory in flowing to the facility, the rural MSW loading to this facility does not have notable changes with the capacity change of the facility (Figures 7(b) and 10(b)).

Compared with the loading of cattle manure to the community-based bio-coal facility, the loading to the household-based CH_4 facility is dominant. When the capacity of the household-based CH_4 facility is limited for all the loadings of MSW and the cattle manure from the rural area, the extra cattle manure will hypothetically flow to the community-based bio-coal facility. Therefore, with the increasing capacity of the household-based CH_4 facility, the loading of cattle manure to the community-based bio-coal facility keeps decreasing and the loading to the household-based CH_4 facility keeps increasing. In addition, when the capacity of the household-based CH_4 facility is equal or higher than 450 tonnes/day, all the wastes from the rural area (MSW and cattle manure) will be delivered to this facility (Figures 8 and 11).

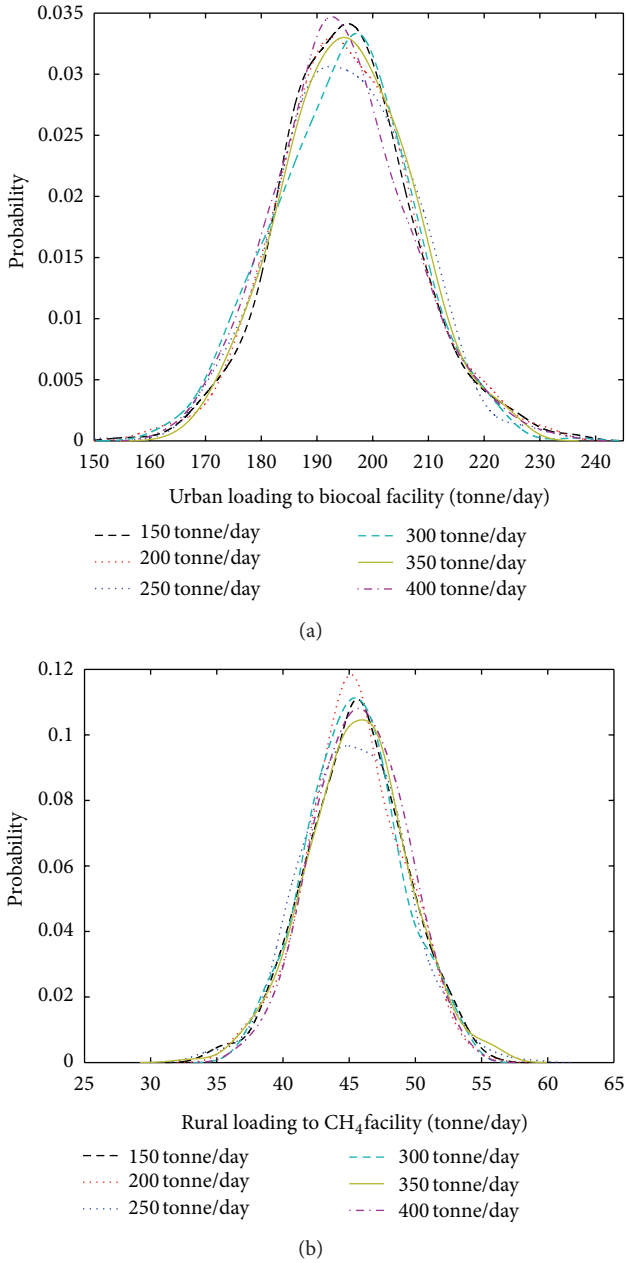

Figure 7: Probability distributions of optimal MSW loadings (a) from the urban area to the community-based bio-coal facility and (b) from the rural area to the household-based CH_4 facility with the changing capacity of household-based CH_4 facility.

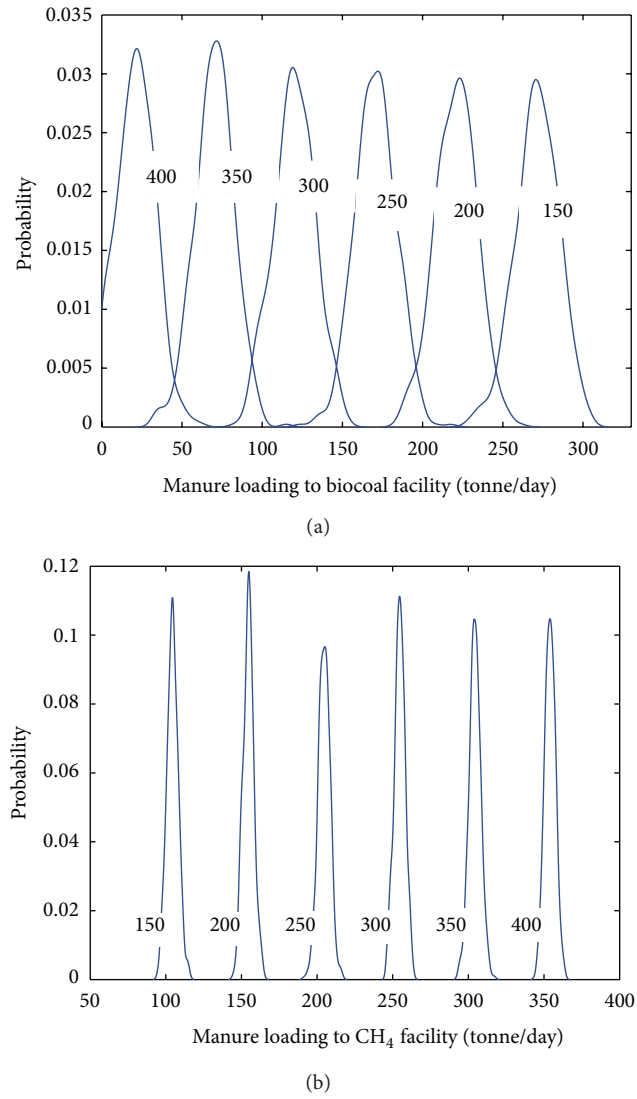

Figure 8: Probability distributions of optimal cattle manure loadings to (a) the community-based bio-coal facility and (b) the household-based CH_4 facility with the changing capacity of the household-based CH_4 facility.

In the case study, 1,000 trials were applied for the Monte Carlo simulation, and optimization results were obtained from 935 trials. The high ratio of optimization results achievement demonstrates a high feasibility of the model setting with the coverage of corresponding uncertainties. In the case that the model is infeasible (e.g., some constraints in the model conflict with the others), no solution can be obtained for the optimization. This situation is very common in many traditional optimization models (e.g., traditional fuzzy programming) considering multiple features in complex systems (e.g., the system in the case study of this paper). With the consideration of the full range of uncertain conditions, the proposed approach can obtain as many optimal solutions as possible under various conditions with uncertainty and complexity, making it more advantage from the traditional models. It is also worthwhile noting that the solutions can provide three types of decision to support decision makers at different levels to regulate, design, manage, and operate the solid waste management system. Firstly, the optimal distributions of the system investment or cost (Figure 5) with the corresponding waste and cattle manure flows (Figure 4) can provide a complete and clear image to local authorities. This can help legislate or amend related policies and regulations and further develop sound strategies for the resource oriented solid waste management in a mixed rural-urban area. Secondly, the ranges of most

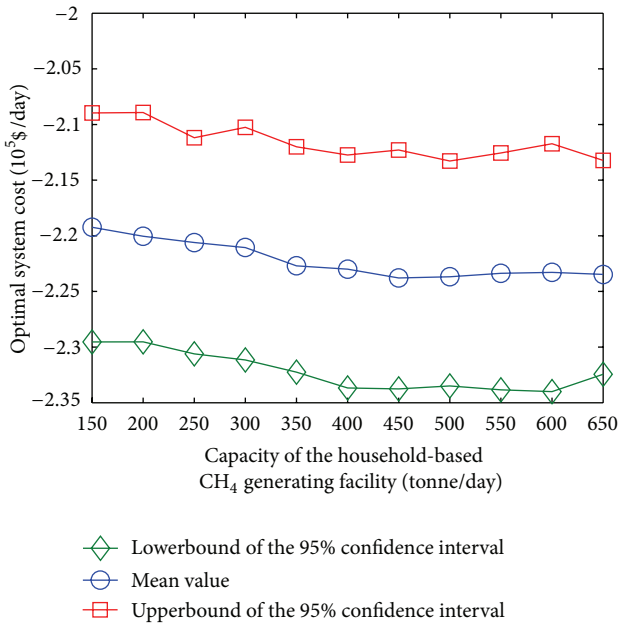

FIGURE 9: Changes of optimal system cost with the changing capacity of the household-based CH_4 facility.

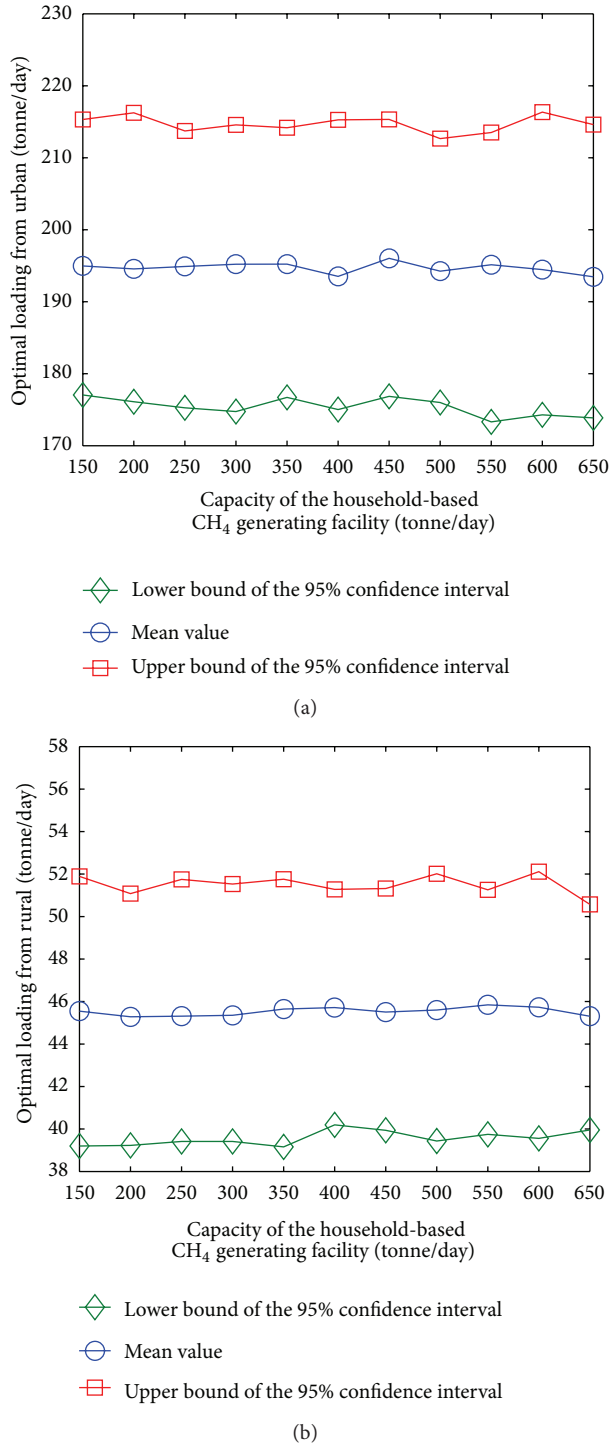

FIGURE 10: Changes of optimal MSW loading (a) from the urban area to the community-based bio-coal facility and (b) from the rural area to the household-based CH_4 facility with the changing capacity of household-based CH_4 facility.

frequent occurrences (the 95% confidence intervals) can assist facility managers to flexibly and effectively develop the production/treatment schedules for different facilities. Thirdly, the expected values of the optimal system cost with corresponding settings (the average loadings) can be used by facility operators (including individual farmers and their groups) to optimize their productions/profits regarding the solid waste management.

5. Conclusions

This study developed a resource-oriented solid waste management system for a mixed rural-urban area. The system was featured by a resource-oriented management framework and a Monte Carlo simulation-based fuzzy programming (RSW-MCFP). The resource-oriented solid waste management concept was adopted for formation and enhancement of the household and community stewardships and further supported by the optimization of energy, resources, capital, and waste flows under uncertainties. The cooperative stewardship was well reflected through resource-oriented waste treatment and cyclic economy development, leading to the independence and sustainability of the management system and local economy. The system could emphasize stewardship over the life span of solid waste including generation, collection, reusing, recycling, recovery, treatment, and final disposal. Therefore, based on the assumption that the optimum solution path is always followed in the real-world application, the system could help optimize the total internal waste flow and utilization recycling to achieve maximum economic and environmental benefits in a mixed rural-urban area.

The adopted Monte Carlo simulation-based fuzzy programming (MCFP) approach determined the waste flow to the waste treatment and disposal facilities and supported the decision-making process in determining the optimal management strategy under uncertainties. This approach could efficiently convert fuzzy problems to deterministic ones and achieve the optimal solutions with fewer additional

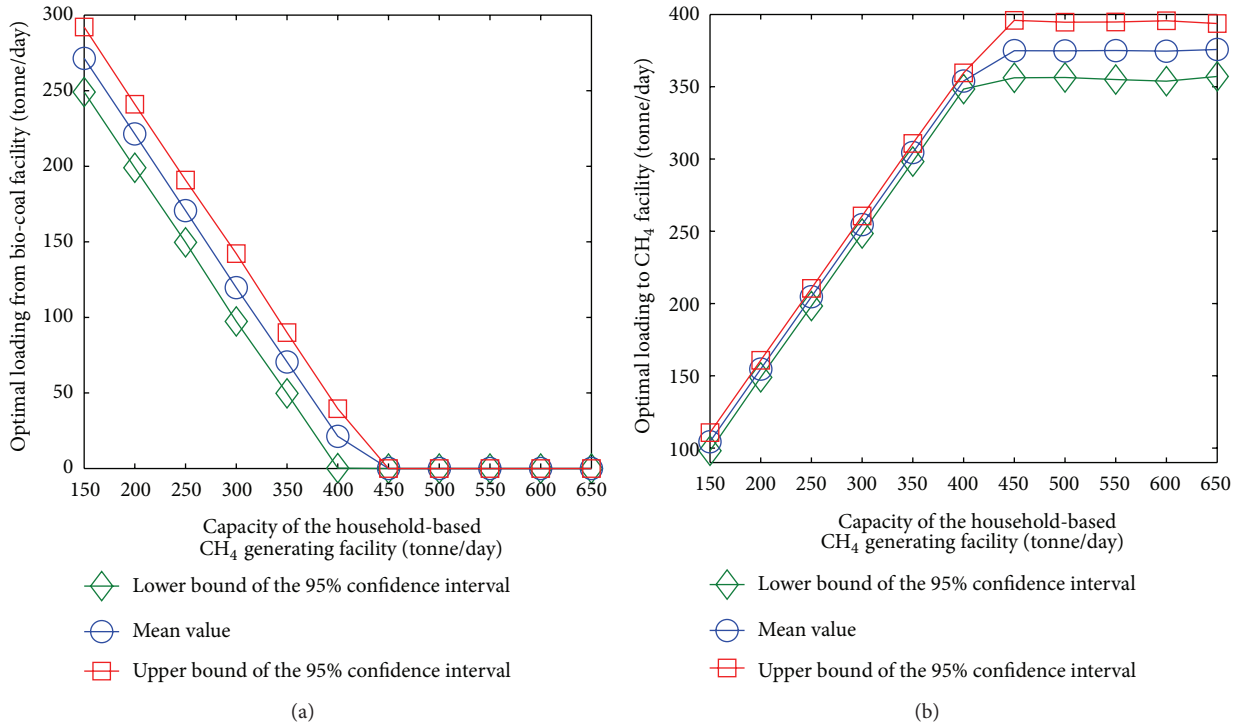

FIGURE 11: Changes of optimal cattle manure loadings to (a) the community-based bio-coal facility and (b) the household-based CH_4 facility with the changing capacity of the household-based CH_4 facility.

constraints, leading to significant reductions in system complexity and computational efforts. These advantages could help fuzzy programming easily and efficiently integrate with Monte Carlo simulation. Consequently, the MCFP approach could effectively tackle the coexistence of uncertainties in forms of fuzzy sets and continuous probability distributions.

The developed RSW-MCFP system was tested by a real-world application of solid waste management in the town of Shuangcheng, Northeast China. The modeling results indicated that the community-based bio-coal facility and the household-based CH_4 facility would be predominant in the management system and recommended increasing the capacity of the household-based CH_4 facility to digest all the municipal solid waste from the rural area and cattle manure in the mixed rural-urban area. The results also suggested locating the community-based bio-coal facility close to the urban area. In addition, the developed system could provide three levels of the optimal results to help decision makers effectively manage the system facilities. The first level included the entire distributions of objective functions and decision variables, which could provide decision support to general policy makers (e.g., regulating and consulting organizations) for long-term policy making and trade-off, risk, and reliability analyses of the system. The second level included the ranges of most frequent occurrences, which could help project or system managers design and plan the production in a medium arrangement. The third level indicated the expected values of the optimal results, which could directly provide decision alternatives to the system operators for short-term operation (e.g., adjusting the facility to minimize system cost).

The based assumption of the case study in this stage is that the resource or money flow was only driven by the profit, which may not occur in reality. Future study will focus on analyzing and reflecting the complex relations in the market in the developed system. In addition, the purpose of this case study is to provide decision support for the future planning of solid waste system. Most of the facilities in the proposed system are yet to be installed, making the results difficult to be analysed by solid evidence. The collection of detailed information regarding the proposed facilities will further conduct to make the approach more applicable in real-world decision making. Future studies are also expected to closely investigate the interactions and collective effects under different system conditions, providing optimal alternatives in managing key elements for a robust and sustainable development of solid waste industries.

Conflict of Interests

The authors of this manuscript do not have any direct financial relation with the commercial identities mentioned in the paper (i.e., Minitab, MATLAB, and LINDO API) that might lead to a conflict of interest.

Acknowledgments

The study was supported by the National Natural Science Foundation of China (51179070), Natural Science and Engineering Research Council of Canada, and United Nations Development Programme (UNDP) as well as the China International Center for Economic and Technical Exchanges (CICETE) of the Ministry of Commerce of China.

References

[1] A. Singh, "Municipal solid waste management in Jaipur: current status and way forward," Rajasthan State Pollution Control Board 4, Institutional Area, Jhalana Doongri, Jaipur, India, 2010.

[2] B. Chen, P. Li, and H. J. Wu, "MCFP: a Monte Carlo simulation based fuzzy programming approach for municipal solid waste management under dual uncertainties of possibility and continuous probability," *Engineering Optimization*. In press.

[3] G. H. Huang and N. B. Chang, "The perspectives of environmental informatics and systems analysis," *Journal of Environmental Informatics*, vol. 1, no. 1, pp. 1–7, 2003.

[4] S. Wang, G. H. Huang, and B. T. Yang, "An interval-valued fuzzy-stochastic programming approach and its application to municipal solid waste management," *Environmental Modelling and Software*, vol. 29, no. 1, pp. 34–36, 2011.

[5] G. H. Huang, B. W. Baetz, and G. G. Patry, "A grey fuzzy linear programming approach for municipal solid waste management planning under uncertainty," *Civil Engineering and Environmental Systems*, vol. 10, no. 2, pp. 123–146, 1993.

[6] B. Chen, H. Guo, G. Huang, Y. Yin, and B. Zhang, "IFMEP: an interval fuzzy multiobjective environmental planning model for urban systems," *Civil Engineering and Environmental Systems*, vol. 25, no. 2, pp. 99–125, 2008.

[7] Y. Gunalay, J. S. Yeomans, and G. H. Huang, "Modeling to generate alternative policies in highly uncertain environments: an application to municipal solid waste management planning," *Journal of Environmental Informatics*, vol. 19, no. 2, pp. 58–69, 2012.

[8] P. Li, B. Chen, B. Y. Zhang, and L. Jing, "A new agro-industrial waste management model for supporting rural co-operative stewardship and sustainable development," in *Proceeding of the 3rd International Scientific Conference on Industrial and Hazardous Waste Management*, Chania, Greece, 2012.

[9] Y. P. Li, G. H. Huang, Y. F. Huang, and H. D. Zhou, "A multistage fuzzy-stochastic programming model for supporting sustainable water-resources allocation and management," *Environmental Modelling and Software*, vol. 24, no. 7, pp. 786–797, 2009.

[10] P. Li and B. Chen, "FSILP: fuzzy-stochastic-interval linear programming for supporting municipal solid waste management," *Journal of Environmental Management*, vol. 92, no. 4, pp. 1198–1209, 2011.

[11] Z. S. Li, H. Z. Fu, and X. Y. Qu, "Estimating municipal solid waste generation by different activities and various resident groups: a case study of Beijing," *Science of the Total Environment*, vol. 409, no. 20, pp. 4406–4414, 2011.

[12] J. Ramik and M. Vlach, "Fuzzy mathematical programming: a unified approach based on fuzzy relations," *Fuzzy Optimization and Decision Making*, vol. 1, no. 4, pp. 335–346, 2002.

[13] Y. P. Cai, G. H. Huang, X. H. Nie, Y. P. Li, and Q. Tan, "Municipal solid waste management under uncertainty: a mixed interval parameter fuzzy-stochastic robust programming approach," *Environmental Engineering Science*, vol. 24, no. 3, pp. 338–352, 2007.

[14] Z. F. Liu, G. H. Huang, R. F. Liao, and L. He, "DIPIP: dual interval probabilistic integer programming for solid waste management," *Journal of Environmental Informatics*, vol. 14, no. 1, pp. 66–73, 2009.

[15] G. H. Lin, X. Chen, and M. Fukushima, "Solving stochastic mathematical programs with equilibrium constraints via approximation and smoothing implicit programming with penalization," *Mathematical Programming*, vol. 116, no. 1-2, pp. 343–368, 2009.

[16] Y. Xu, G. H. Huang, X. S. Qin, and Y. Huang, "SRFILP: a stochastic robust fuzzy interval linear programming model for municipal solid waste management under uncertainty," *Journal of Environmental Informatics*, vol. 14, no. 2, pp. 74–82, 2009.

[17] S. Galelli and R. Soncini-Sessa, "Combining metamodelling and stochastic dynamic programming for the design of reservoir release policies," *Environmental Modelling and Software*, vol. 25, no. 2, pp. 209–222, 2010.

[18] P. Guo, G. H. Huang, H. Zhu, and X. L. Wang, "A two-stage programming approach for water resources management under randomness and fuzziness," *Environmental Modelling and Software*, vol. 25, no. 12, pp. 1573–1581, 2010.

[19] Y. P. Li, G. H. Huang, and W. Sun, "Management of uncertain information for environmental systems using a multistage fuzzy-stochastic programming modle with soft constraints," *Journal of Environmental Informatics*, vol. 18, no. 1, pp. 28–37, 2011.

[20] X. S. Qin and G. H. Huang, "Characterizing uncertainties associated with contaminant transport modeling through a coupled fuzzy-stochastic approach," *Water, Air, and Soil Pollution*, vol. 197, no. 1–4, pp. 331–348, 2009.

[21] A. L. Yang, G. H. Huang, and X. S. Qin, "An integrated simulation-assessment approach for evaluating health risks of groundwater contamination under multiple uncertainties," *Water Resources Management*, vol. 24, no. 13, pp. 3349–3369, 2010.

[22] A. N. Blair, B. M. Ayyub, and W. J. Bender, "Fuzzy stochastic risk-based decision analysis with the mobile offshore base as a case study," *Marine Structures*, vol. 14, no. 1-2, pp. 69–88, 2001.

[23] P. Seuntjens, "Field-scale cadmium transport in a heterogeneous layered soil," *Water, Air, and Soil Pollution*, vol. 140, no. 1–4, pp. 401–423, 2002.

[24] C. Baudrit, D. Guyonnet, and D. Dubois, "Joint propagation of variability and imprecision in assessing the risk of groundwater contamination," *Journal of Contaminant Hydrology*, vol. 93, no. 1–4, pp. 72–84, 2007.

[25] J. B. Li, G. H. Huang, G. Zeng, I. Maqsood, and Y. Huang, "An integrated fuzzy-stochastic modeling approach for risk assessment of groundwater contamination," *Journal of Environmental Management*, vol. 82, no. 2, pp. 173–188, 2007.

[26] G. H. Cheng, G. H. Huang, Y. P. Li, M. F. Cao, and Y. R. Fan, "Planning of municipal solid waste management systems under dual uncertainties: a hybrid interval stochastic programming approach," *Stochastic Environmental Research and Risk Assessment*, vol. 23, no. 6, pp. 707–720, 2009.

[27] L. Liu, S. Y. Cheng, and H. C. Guo, "A simulation-assessment modeling approach for analyzing environmental risks of groundwater contamination at waste landfill sites," *Human and Ecological Risk Assessment*, vol. 10, no. 2, pp. 373–388, 2004.

[28] J. B. Li, L. Liu, G. H. Huang, and G. Zeng, "A fuzzy-set approach for addressing uncertainties in risk assessment of hydrocarbon-contaminated site," *Water, Air, and Soil Pollution*, vol. 171, no. 1–4, pp. 5–18, 2006.

[29] Y. P. Li and G. H. Huang, "Dual-interval fuzzy stochastic programming method for long-term planning of municipal solid waste management," *Journal of Computing in Civil Engineering*, vol. 24, no. 2, pp. 188–202, 2010.

[30] Y. P. Li, G. H. Huang, and S. L. Nie, "A mathematical model for identifying an optimal waste management policy under

uncertainty," *Applied Mathematical Modelling*, vol. 36, no. 6, pp. 2658–2673, 2012.

[31] T. Li, P. Li, B. Chen, M. Hu, and X. Zhang, "A simulation-based inexact two-stage chance constraint quadratic programming for sustainable water quality management under dual uncertainties," *Journal of Water Resources Planning and Management*, 2012.

[32] D. Guyonnet, B. Bourgine, D. Dubois, H. Fargier, B. Côme, and J. P. Chilès, "Hybrid approach for addressing uncertainty in risk assessments," *Journal of Environmental Engineering*, vol. 129, no. 1, pp. 68–78, 2003.

[33] M. Goldstein, "Subjective Bayesian analysis: principles and practice," *Bayesian Analysis*, vol. 1, no. 3, pp. 403–420, 2006.

[34] R. A. Freeze, H. Massmann, L. Smith, T. Sperling, and B. James, "Hydrogeological decision analysis: 1. A framework," *Ground Water*, vol. 28, no. 5, pp. 738–766, 1990.

[35] D. Vose, *Quantitative Risk Analysis: A Guide to Monte Carlo Simulation Modelling*, John Wiley & Sons, Hoboken, NJ, USA, 1996.

[36] P. H. Garthwaite, J. B. Kadane, and A. O'Hagan, "Statistical methods for eliciting probability distributions," *Journal of the American Statistical Association*, vol. 100, no. 470, pp. 680–701, 2005.

[37] I. Baud, S. Grafakos, M. Hordijk, and J. Post, "Quality of life and alliances in solid waste management. Contributions to Urban sustainable development," *Cities*, vol. 18, no. 1, pp. 3–12, 2001.

[38] M. N. U. Mia, *Product stewardship and stakeholder participation in solid waste management: a New Zealand study [M.S. thesis]*, Department of Social Science, Auckland University of Technology, 2011.

[39] N. V. Hop, "Fuzzy stochastic goal programming problems," *European Journal of Operational Research*, vol. 176, no. 1, pp. 77–86, 2007.

[40] Statistic Bureau of the City of Shuangcheng, *Statistics of Society and Economy of the City of Shuangcheng from 2000 to 2007*, Statistic Bureau of the City of Shuangcheng, Heilongjiang, China, 2010.

[41] Environmental Monitoring Station of the City of Shuangcheng, *Environmental Quality Outline of ShuangCheng—2008*, Environmental Monitoring Station of the City of Shuangcheng, Heilongjiang, China, 2009.

[42] Environmental Monitoring Station of the City of Shuangcheng, *Environmental Quality Outline of ShuangCheng—2009*, Environmental Monitoring Station of the City of Shuangcheng, Heilongjiang, China, 2010.

Hindawi Publishing Corporation
Mathematical Problems in Engineering
Volume 2013, Article ID 291930, 11 pages
http://dx.doi.org/10.1155/2013/291930

Research Article

A Sustainability-Oriented Multiobjective Optimization Model for Siting and Sizing Distributed Generation Plants in Distribution Systems

Guang Chen,[1] Bin Chen,[2] Pan Dai,[1] and Hao Zhou[1]

[1] *College of Electrical Engineering, Zhejiang University, Hangzhou 310027, China*
[2] *School of Environment, Beijing Normal University, Beijing 100875, China*

Correspondence should be addressed to Hao Zhou; zhouhao_ee@zju.edu.cn

Received 10 February 2013; Accepted 10 May 2013

Academic Editor: Bing Chen

This paper proposes a sustainability-oriented multiobjective optimization model for siting and sizing DG plants in distribution systems. Life cycle exergy (LCE) is used as a unified indicator of the entire system's environmental sustainability, and it is optimized as an objective function in the model. Other two objective functions include economic cost and expected power loss. Chance constraints are used to control the operation risks caused by the uncertain power loads and renewable energies. A semilinearized simulation method is proposed and combined with the Latin hypercube sampling (LHS) method to improve the efficiency of probabilistic load flow (PLF) analysis which is repeatedly performed to verify the chance constraints. A numerical study based on the modified IEEE 33-node system is performed to verify the proposed method. Numerical results show that the proposed semilinearized simulation method reduces about 93.3% of the calculation time of PLF analysis and guarantees satisfying accuracy. The results also indicate that benefits for environmental sustainability of using DG plants can be effectively reflected by the proposed model which helps the planner to make rational decision towards sustainable development of the distribution system.

1. Introduction

Distributed generation (DG) is developing fast all over the world in recent years due to its promising potential to reduce the portion of fossil energy consumption in electric power generation and mitigate power losses and harmful emissions [1, 2]. For the distribution system, DG plants can provide valuable reserve capacities and improve the flexibility of system operation [3–5]. However, if not properly planned, integrating DG plants may also cause some negative impacts, especially when they are driven by renewable energies such as wind and solar power, since these renewable energies are generally unstable and intermittent [6]. Additional difficulties in reactive power compensation, load flow control, fault protection, and power quality regulation are other possible negative impacts [7].

The performance of the DG plants in a distribution system is greatly impacted by the arrangement, that is, the sites and sizes, of the plants in the system [1, 8]. Thus, it is necessary to optimize the arrangement in the planning stage since it is much more difficult to modify the arrangement thereafter. Such optimization process is also called siting and sizing of DG plants [9]. Presently, several approaches have been proposed for siting and sizing DG plants in distribution systems, and brief reviews can be found in [1, 10]. The present optimization approaches can be categorized into analytical methods [11–13], metaheuristic methods [14, 15], artificial intelligent methods [16–19], and others [20, 21]. The technical and economic issues, for example, power losses, node voltages, line capacities, and economic costs, are mainly concerned in previous studies. Comparatively, the environmental sustainability, including various environmental effects such as harmful emissions and natural resource depletion of using DG plants in a distribution system is not fully evaluated. Most studies tend to presume the effectiveness and equivalence of different DG plants in environment protection

and to maximize the installed capacities considering some technical and economic constraints. However, the environmental impacts of different DG plants may vary considerably due to the differences in primary energy sources, production techniques, and utilization efficiencies of the generators. Thus, it is necessary and urgent to properly evaluate the environmental effects in the siting and sizing process to obtain better sustainability. Life cycle assessment (LCA) is generally regarded as an excellent measure to evaluate environmental effects of an energy system during its life cycle [22], but it lacks a mechanism to comprehensively measure various types of environmental factors. The weighting aggregation and the so-called neoclassical economic theory are two typical options for compensation, but there are some drawbacks of these methods, such as subjectivity, incompleteness, and overoptimism [23]. Exergy analysis is another option that takes exergy as a general indicator to evaluate the various factors and has the potential to overcome the above drawbacks [22]. Moreover, its unique capability of identifying the irreversibilities of energy systems by the second law of thermodynamics makes exergy an excellent indicator to measure the system's long-term sustainability [24, 25]. Several studies have combined exergy analysis with LCA to analyze or optimize the designs of energy systems [22, 26–28], forming the so-called exergetic LCA (ELCA). In this paper, the ELCA method is used to build a unified quantitative indicator of environmental sustainability for installing and utilizing DG plants in a distribution system, and then the siting and sizing problem is modeled as a multiobjective chance-constrained integer optimization problem. Thus, the proposed optimization model not only minimizes the economic cost and power loss but also optimizes environmental sustainability.

Another key problem in the optimization process is how to efficiently reflect the performance of the distribution system considering the unstable outputs of renewable energies, load levels, and other uncertain factors [7]. Presently, probabilistic load flow (PLF) analysis is widely used due to its capability of reflecting static system security [1, 7, 10, 18, 19]. Improving the efficiency of PLF analysis is of great significance since it is performed repeatedly for every candidate solution to determine its feasibility and fitness in the optimization process. Studies have proposed several methods for PLF analysis, such as cumulant-based series expansion methods (including Gram-Charlier expansion, Edgeworth expansion, and Cornish-Fisher expansion) [29], point estimate method [30], and sampling-based simulation methods (e.g., Monte Carlo sampling (MCS) [29, 30], Latin hypercube sampling (LHS) [31], etc.). In general, the sampling-based simulation methods are more accurate and reliable than the cumulant-based series expansion methods and the point estimate method but need much more calculation time [29–31]. Compared with MCS which samples randomly, LHS uses a more complicated sampling mechanism to obtain semirandom or deterministic samples and thus improves efficiency while guaranteeing accuracy [31–33]. To further improve the efficiency of LHS-based PLF analysis, a semilinearized simulation method is proposed to combine with it in this paper. In the proposed method, the time-consuming iteration process for nodal voltage calculation is avoided by using linearized load flow equation. Satisfying accuracy and reliability is guaranteed by retaining the nonlinearity of power flow calculation and the framework of LHS-based PLF analysis.

The rest of this paper is organized as follows: the models and methods are described in Section 2; Section 3 gives a numerical case study based on the modified IEEE (Institute of Electrical and Electronics Engineers) 33-node system; Section 4 concludes.

2. Methodology

2.1. Exergetic Life Cycle Assessment. ELCA evaluates all the exergies consumed within the life cycle of a system. As shown in (1), the life-cycle exergy (LCE) of a DG plant can be calculated as the sum of the cumulative exergy consumption (CEC) and the emission abatement exergy (AbatE). Here, CEC is defined as the sum of the exergies of all the consumed resources and reflects resource depletion [22]. AbatE is defined as the cumulative equivalent exergy caused by primary resource consumption to remove or separate the wasted emissions by an implemented or proposed treatment process and reflects the environmental effect of emissions [23, 34, 35]. Thus, the environmental sustainability of using a DG plant can be reflected by LCE [22–24, 27]:

$$\mathrm{LCE} = \mathrm{CEC} + \mathrm{AbatE}. \tag{1}$$

For convenience, the life cycle of a DG plant can be divided into 3 phases, that is, construction phase, operation phase, and disposal/recycle phase. Then, CEC and AbatE can be calculated as

$$\begin{aligned} \mathrm{CEC} &= \mathrm{CEC}_{\mathrm{Con}} + \mathrm{CEC}_{\mathrm{Opr}} + \mathrm{CEC}_{\mathrm{Dis}}, \\ \mathrm{AbatE} &= \mathrm{AbatE}_{\mathrm{Con}} + \mathrm{AbatE}_{\mathrm{Opr}} + \mathrm{AbatE}_{\mathrm{Dis}}, \end{aligned} \tag{2}$$

where Con, Opr, and Dis represent the construction, operation, and disposal/recycle phases, respectively.

In the construction phase, the cumulative exergy consumption ($\mathrm{CEC}_{\mathrm{Con}}$) is mainly caused by the consumption of fuels and the inputs of nonfuel materials (e.g. iron ore, limestone, sand, etc.) needed for constructing the DG plant. The exergies of fuels and non-fuel materials can be calculated by multiplying the consumed/input amounts with corresponding exergy content factors, that is,

$$\mathrm{CEC}_{\mathrm{Con}} = C_{\mathrm{DG}} \cdot \left(\sum_i \alpha_i q_i a_{\mathrm{Con},i} + \sum_j x_j b_{\mathrm{Con},j} \right), \tag{3}$$

$$\mathrm{AbatE}_{\mathrm{Con}} = C_{\mathrm{DG}} \sum_k \beta_k e_{\mathrm{Con},k}, \tag{4}$$

where C_{DG} is the installed capacity of the DG plant; α_i is the ratio between exergy and energy content for fuel i which can be collected from relevant studies; q_i is the energy content of per unit of fuel i; $a_{\mathrm{Con},i}$ is the amount of fuel j consumed to construct per capacity of the DG plant; x_j is the chemical exergy content of the non-fuel material j; $b_{\mathrm{Con},j}$ is the mass of the non-fuel material j needed for per capacity of the DG

plant; $e_{\mathrm{Con},k}$ is the emission amounts of pollutant k in the construction stage and the operation stage, respectively; β_k is the abatement exergy factor of pollutant k.

For the operation phase, the input of non-fuel materials is negligible, and thus the cumulative exergy consumption is mainly caused by fuel consumption which is proportional to power generation, shown as (5). For the DG plants that solely use renewable energies, the $\mathrm{CEC}_{\mathrm{Opr}}$ can be neglected. Similarly, the emission abatement exergy of fuel-driven DG can be calculated by multiplying the amounts of different emissions and abatement exergy factors as shown in (6) and that of the renewable energy-driven DG is neglected,

$$\mathrm{CEC}_{\mathrm{Opr}} = C_{\mathrm{DG}} H_{\mathrm{DG}} T_{\mathrm{DG}} \sum_i \frac{\alpha_i q_i a_{\mathrm{Opr},i}}{\eta_{\mathrm{Opr},i}}, \tag{5}$$

$$\mathrm{AbatE}_{\mathrm{Opr}} = C_{\mathrm{DG}} H_{\mathrm{DG}} T_{\mathrm{DG}} \sum_k \beta_k e_{\mathrm{Opr},k}, \tag{6}$$

where H_{DG} and T_{DG} are the annual utilization hours (AUH) and the operation expectancy of the DG plant, respectively; $a_{\mathrm{Opr},i}$ is the cumulative mass of fuel j consumed to generate per unit of electric power; $\eta_{\mathrm{Opr},i}$ is the overall efficiency of production and delivery for fuel i. $e_{\mathrm{Opr},k}$ is the emission amount of pollutant k in the construction stage and the operation stage, respectively.

The cumulative exergy consumption and emission abatement exergy in the disposal/recycle phase consist of exergy consumption for unit disposal and exergy saving for unit recycle. In general, these exergies can be calculated proportionally to the exergies in the construction phase, shown as follows:

$$\begin{aligned} \mathrm{CEC}_{\mathrm{Dis}} &= -\lambda_{\mathrm{CEC}} \mathrm{CEC}_{\mathrm{Con}}, \\ \mathrm{AbatE}_{\mathrm{Dis}} &= -\lambda_{\mathrm{Abat}} \mathrm{AbatE}_{\mathrm{Con}}, \end{aligned} \tag{7}$$

where λ_{CEC} and λ_{Abat} represent the exergy saving ratios with respect to $\mathrm{CEC}_{\mathrm{Con}}$ and $\mathrm{AbatE}_{\mathrm{Con}}$, respectively.

2.2. Optimization Model. The optimization variables of the siting and sizing problem are the locations of the DG plants in the studied distribution network and their installed capacities. The location variables can be expressed with integer numbers. Usually a DG unit is produced with a standard capacity, and thus the capacity variables of a DG plant can be expressed as integers that represent the number of installed DG units. Based on such arguments, the siting and sizing problem is modeled as a multi-objective integer programming problem in this paper. The objectives include minimizing the economic cost, life-cycle exergy consumption, and power losses.

2.2.1. Objective Functions. The multi-objective function can be written as

$$\mathrm{Min}\, F = \{F_1, F_2, F_3\}, \tag{8}$$

where F_1 represents the life-cycle economic cost of utilizing DG plants; F_2 represents the life-cycle exergy of using DG plants; F_3 represents the expected power loss considering the uncertainties of power loads and DG outputs.

The life-cycle economic cost of utilizing DG plants can be calculated as

$$F_1 = \sum_i \sum_j \left(C_{\mathrm{Con},ij} + C_{\mathrm{Opr},ij} + C_{\mathrm{Dis},ij} \right), \tag{9}$$

where $C_{\mathrm{Con},ij}$, $C_{\mathrm{Opr},ij}$ and $C_{\mathrm{Dis},ij}$, are economic costs spent on construction, operation, and disposal/recycle to use jth type of DG at node i which can be calculated as

$$\begin{aligned} C_{\mathrm{Con},ij} &= c_{\mathrm{Con},j} C_{\mathrm{DG},ij}, \\ C_{\mathrm{Opr},ij} &= \xi_{\mathrm{CPV},j} c_{\mathrm{Opr},j} C_{\mathrm{DG},ij} H_{\mathrm{DG},j}, \\ C_{\mathrm{Dis},i} &= -\zeta^{T_{\mathrm{DG},j}+1} d_{\mathrm{Cost},j} C_{\mathrm{Con},ij}, \end{aligned} \tag{10}$$

where $c_{\mathrm{Con},j}$ is the economic cost for constructing per capacity of jth-type DG; $c_{\mathrm{Opr},j}$ is the economic cost for generating per unit of electricity by jth-type DG; $d_{\mathrm{Cost},j}$ is the recycle coefficient for jth-type DG; coefficients $\xi_{\mathrm{CPV},j}$ and ζ can be calculated as (11), in which f and δ stand for the inflation rate and discount rate, respectively. Generally, due to the intermittency of renewable energies, both the operation costs and power generation of DG plants that solely use renewable energies are much less than those of the DG plants which have the same capacities but use fuels:

$$\begin{aligned} \xi_{\mathrm{CPV},j} &= \frac{\zeta - \zeta^{T_{\mathrm{DG},j}+1}}{1-\zeta}, \\ \zeta &= \frac{1+f}{1+\delta}. \end{aligned} \tag{11}$$

The objective function of minimizing life-cycle exergy can be written as

$$F_2 = \sum_i \sum_j \left(\mathrm{LCE}_{\mathrm{DG},ij} - E_{No\mathrm{DG},ij} \right), \tag{12}$$

where $\mathrm{LCE}_{\mathrm{DG},ij}$ is the life-cycle exergy used by the DG plant of jth type at node i; $E_{No\mathrm{DG},ij}$ stands for the expected exergy consumption to provide the same amount of DG-generated energies (electricity, heat, refrigeration, etc.) by alternative sources if DG plant ij is not installed.

$E_{No\mathrm{DG},ij}$ can be calculated as

$$E_{No\mathrm{DG},ij} = C_{\mathrm{DG},ij} H_{\mathrm{DG},j} \sum_{t=1}^{T_{\mathrm{DG},j}} \left(\gamma_{E,t} + \sum_k \upsilon_{jk} \gamma_{k,t} \right), \tag{13}$$

where $\gamma_{E,t}$ represents the exergy needed for providing per unit of electric power in tth year by alternative sources; υ_{jk} is the amount of by-product k when generating per unit of electric power; $\gamma_{k,t}$ stands for the exergy needed for providing per unit of by-product k in tth year by alternative sources.

The objective function of minimizing expected power loss as

$$F_3 = E\{E_{\mathrm{Loss}}\}, \tag{14}$$

where E_{Loss} stands for the power loss and $E\{E_{\mathrm{Loss}}\}$ represents the mean value of E_{Loss}.

2.2.2. Constraints. The total capacity of installed DG plants should be no higher than a given cap for the sake of safety and reliability of power supply, that is,

$$\sum_i \sum_j C_{\mathrm{DG},ij} \le C_{\mathrm{DG}}^{\max}. \tag{15}$$

Other main constraints include the nodal voltage magnitude limitations and the branch capacity limitations. In real operation, these limitations can be violated for short terms under some operating conditions. Considering the uncertainties of renewable energy sources and power loads, chance constraints are generally used to guarantee the practicability of the solution shown as follows:

$$\begin{aligned} \Pr\left\{V_i^{\min} < V_i < V_i^{\max}\right\} &\ge \eta_V, \\ \Pr\left\{\left|S_{i,j}\right| < S_{i,j}^{\max}\right\} &\ge \eta_S, \end{aligned} \tag{16}$$

where $S_{i,j}$ stands for the apparent power flow in the branch from node i to node k; $V_i^{\min}$, $V_i^{\max}$, and $S_{i,j}^{\max}$ are limitation values; η_V and η_S are required confidence parameters.

For each operation condition, the load flow equations need to be obeyed, that is,

$$\begin{aligned} P_i &= V_i \sum_{j\in i} V_j \left[G_{ij}\cos\left(\theta_i - \theta_j\right) + B_{ij}\sin\left(\theta_i - \theta_j\right)\right], \\ Q_i &= V_i \sum_{j\in i} V_j \left[G_{ij}\sin\left(\theta_i - \theta_j\right) - B_{ij}\cos\left(\theta_i - \theta_j\right)\right], \end{aligned} \tag{17}$$

where $j \in i$ represents the set of every node j which is directly connected with node i by a branch in the distribution network, including node i itself; P_i and Q_i stand for the active and reactive powers injected into node i; V_i and θ_i stand for the voltage magnitude and angle of node i; G_{ij} and B_{ij} represent the real and imaginary parts of admittance between node i and j.

2.3. Treatment of Uncertainties

2.3.1. Models of Uncertain Variables

Wind Turbine Output. Generally, the stochastic behaviors of the wind speed v in a wind farm can be described by the Weibull distribution whose probability density function (PDF) can be written as [37]

$$f_v(v) = \frac{k}{c^k} v^{k-1} \exp\left[-\left(\frac{v}{c}\right)^k\right], \tag{18}$$

where k and c are shape factor and scale factor of the wind speed PDF at the wind farm.

Ignoring minor nonlinearities, a turbine's power output can be calculated with a given wind speed v:

$$P_w = \begin{cases} 0 & v < v_I \text{ or } v > v_O \\ P_{wR}\dfrac{v - v_I}{v_R - v_I} & v_I \le v \le v_R \\ P_{wR} & v_R < v \le v_O, \end{cases} \tag{19}$$

where v_I, v_O and v_R are cut-in, cut-out, and rated wind speeds for the wind turbine; P_{wR} is the turbine's rated output.

PV Output. Ignoring the minor factors, the output of a PV unit can be characterized as a function of solar irradiance and PV cell temperature [29, 36]:

$$P_s = \frac{r}{r_{\max}}\left(1 - \kappa \cdot \Delta T\right) P_{s,\max}, \tag{20}$$

where r and $r_{\max}$ stand for the solar irradiance and its maximum value; $P_{s,\max}$ represents the maximum output at the rated cell temperature; ΔT is the deviation of the PV cell's temperature from the rated one; κ is a coefficient.

In the daytime, the PDF of solar irradiance can be characterized by Beta distribution [18, 29] which can be written as

$$f_r(r) = \frac{\Gamma\left(\alpha_r + \beta_r\right)}{\Gamma\left(\alpha_r\right)\Gamma\left(\beta_r\right)}\left(\frac{r}{r_{\max}}\right)^{\alpha_r - 1}\left(1 - \frac{r}{r_{\max}}\right)^{\beta_r - 1}, \tag{21}$$

where α_r and β_r are distribution coefficients.

The PV cell temperature is determined by the ambient temperature and prevailing wind speed. The deviation of the PV cell's temperature can be described by normal distribution [29], that is,

$$\Delta T \sim N\left(0, \sigma_{\Delta T}^2\right). \tag{22}$$

Power Load. Generally, the uncertainty of the power load at a node can be described with normal distribution while the power factor can be regarded as a constant for simplicity [7, 38]. Therefore,

$$P_{L,i} \sim N\left(\mu_{L,i}, \sigma_{L,i}^2\right), \tag{23}$$

where $P_{L,i}$ represents the active power load at node i; $\mu_{L,i}$ and $\sigma_{L,i}^2$ are the mean value and variance of $P_{L,i}$.

LHS-Based Semilinearized Probabilistic Load Flow Analysis. The typical procedure of LHS-based probabilistic load flow analysis can be found in [31], which consists of 3 steps: sampling, simulating, and accounting. In the sampling step, a required number of sample arrays of the uncertain variables are generated according to the variables' probability density functions (see Section 2.3.1). Correlations of variables can be taken into account by Nataf transformation [31]. Each sample array represents a possible operating point and is used to evaluate the corresponding node voltages and power flows by solving (17) in the simulating step. Accounting on simulation results is then performed to obtain the statistical properties of certain variables, such as the probabilities in (16) and the expected power loss in (14).

For simplicity, the load flow equation, that is, (17), can be expressed by (24) in which vector $\mathbf{Y}$ expresses the injected powers and vector $\mathbf{X}$ stands for the nodal voltages. Then, the power flows in branches can be expressed as a function of $\mathbf{X}$. Given an initial operating point $\mathbf{Y}_0$, the corresponding $\mathbf{X}_0$ and $\mathbf{S}_0$ can be calculated. However, since time-consuming

iterations are needed due to the complexity and nonlinearity of (24), that is, (17), calculating $\mathbf{X}_0$ needs much more time than calculating $\mathbf{S}_0$ by (25), and this makes the simulating step requires much more time than the other 2 steps in PLF analysis:

$$\mathbf{Y} = g(\mathbf{X}), \tag{24}$$

$$\mathbf{S} = h(\mathbf{X}). \tag{25}$$

Expanding (24) at $\mathbf{Y}_0$ according to Taylor series and omitting the terms higher than the second order will yield

$$\mathbf{X} = \mathbf{X}_0 + \Delta\mathbf{X} = \mathbf{X}_0 + \mathbf{M}_0\Delta\mathbf{Y}, \tag{26}$$

where vector $\Delta\mathbf{Y}$ expresses the changes of $\mathbf{Y}$ from $\mathbf{Y}_0$; vector $\Delta\mathbf{X}$ stands for the changes of $\mathbf{X}$; $\mathbf{M}_0 = \mathbf{J}_0^{-1}$, and $\mathbf{J}_0$ is the final Jacobian matrix at the initial operating point $\mathbf{Y}_0$. Equation (26) is also called "linearized load flow equation."

Similarly, (25) can be linearized as

$$\mathbf{S} = \mathbf{S}_0 + \Delta\mathbf{S} = \mathbf{S}_0 + \mathbf{T}_0\Delta\mathbf{Y}, \tag{27}$$

where $\mathbf{T}_0 = \mathbf{L}_0\mathbf{M}_0$ and $\mathbf{L}_0 = (\partial h(\mathbf{X}))/\partial\mathbf{X}|_{\mathbf{X}=\mathbf{X}_0}$.

Apparently, load flow simulation based on (26) and (27) will need much less calculating time than based on (24) and (25), and this is the theoretical fundament of cumulant-based series expansion methods for PLF analysis [29]. However, simulations show that (26) generates quite accurate results even with large values of $\Delta\mathbf{Y}$; while, on the contrary, (27) can not always produce accurate results since it needs two times linearization from $\Delta\mathbf{Y}$ to $\Delta\mathbf{X}$. Nevertheless, (26) can be utilized to improve the calculation efficiency of the simulating step in LHS-based PLF analysis following a semi-linearized simulation method as below.

Step 1. Select the operating condition when all the uncertain variables are fixed at their mean values as the initial operating point $\mathbf{Y}_0$. Substitute $\mathbf{Y}_0$ into (24) and solve the corresponding load flow equations to get the initial nodal voltage vector $\mathbf{X}_0$ and the Jacobian matrix $\mathbf{J}_0$.

Step 2. Set $i = 1$, and calculate $\Delta\mathbf{Y}_i = \mathbf{Y}_i - \mathbf{Y}_0$, where $\mathbf{Y}_i$ is the ith sample array generated by LHS method in the sampling step.

Step 3. Substitute $\Delta\mathbf{Y}_i$ into (26) and calculate $\mathbf{X}_i$.

Step 4. Substitute $\mathbf{X}_i$ into (25) to calculate $\mathbf{S}_i$.

Step 5. Set $i = i + 1$, repeat Step 2 to Step 5 until all the sample arrays are evaluated.

Thus, the semi-linearized simulation method avoids the time-consuming iterations in calculating the nodal voltages for different operating condition samples and guarantees the accuracy by keeping the nonlinearity of (25). Meanwhile, by using LHS-based PLF analysis framework, the inaccuracy and instability of cumulant-based series expansion are avoided in the PLF analysis.

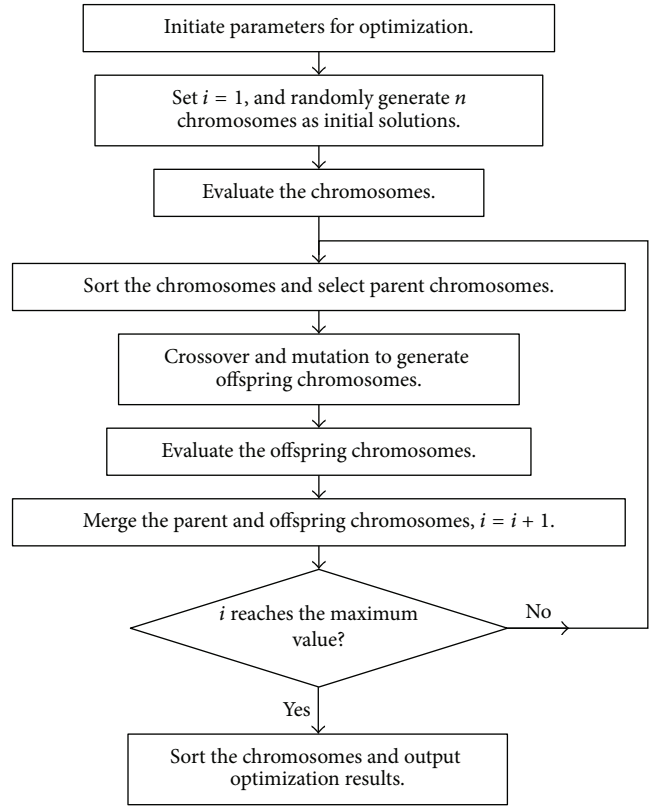

Figure 1: Brief framework of the NSGA-II algorithm in this paper.

2.4. Solving Approach and Methodology Framework. To solve the proposed multi-objective optimization model, the nondominated sorting genetic algorithm II (NSGA-II) [39] is used in this paper. NSGA-II greatly improves the performances of NSGA by introducing elitism and diversity-preserving mechanism algorithms and assures better convergence without losing solution diversity [40]. It should be noted that, instead of giving one optimal solution, NSGA and NSGA-II generate a set of nondominated solutions, that is, Pareto-optimal front, for multi-objective optimization problems according to the Pareto optimality principle [41]. Each solution actually represents the optimal solution under a different tradeoff relationship of the objectives. This enables the planner to see different possible solutions and helps the planner to choose a final solution based on certain tradeoff criteria according to a specific situation after comparing possible alternatives. The brief framework of the optimization algorithm used in this paper is shown in Figure 1, where the step of evaluating chromosomes consists of several substeps shown in Figure 2.

Each chromosome in the algorithm represents a candidate solution for the optimization problem and is coded with integer genes as shown in Figure 3, where each pane represents a gene in the chromosome. The position of the gene indicates the candidate site and type of a DG plant, and the value of the gene stands for the number of installed units.

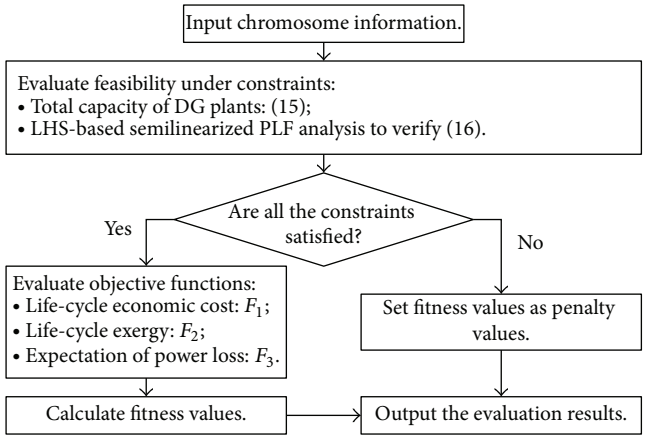

Figure 2: Substeps in the step of evaluating chromosomes.

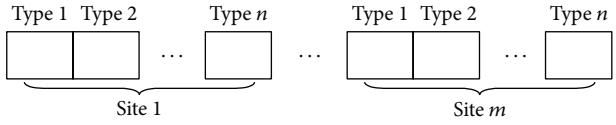

Figure 3: Coding scheme of the genes in a chromosome.

3. Case Study

3.1. System Data. The system under study is the typical IEEE (Institute of Electrical and Electronics Engineers) 33-node system as shown in Figure 4. The network parameters are available from [42, 43]. Candidate DG units include wind turbines (WT), photovoltaic units (PV), and micronatural gas turbines (MNGT). Possible sites and sizes of DG plants are listed in Table 1, in which each integer number of a DG plant represent the feasible maximum number of installed DG units. Each DG unit is assumed to have a rated power output of 20 kW. DG units of the same type have the same technical parameters regardless of the different sites. The cut-in, rated, and cut-out wind speeds for wind turbines are 4 m/s, 14 m/s, and 20 m/s, respectively. MNGT units are used as combined heat and power generators, which produce 1 kWh useful heat as a by-product when generating 1 kWh electricity. For simplicity, the statistical characteristics of wind speeds, solar irradiances, and PV cell temperatures are assumed to be, respectively, the same for different sites considering the short distances between them, which are listed in Table 2. For the power loads, the mean values are the constant values in [42], and the standard deviations are set as 5% of the corresponding mean values. Randomly generated positive definite matrices are used as the correlation matrices of uncertain variables [31]. The exergy consumption and economic cost parameter are collected from [27, 44] and listed in Table 3. The exergy cost for supplying 1 kWh electricity and 1 kWh heat by alternative sources are 19, 162 kJ and 10, 123 kJ, respectively, regardless of possible changes in the future. Both the required confidences for nodal voltage and branch apparent power flow (η_V and η_S) are 95%. The inflation rate and discount rate are 3% and 5.35%, respectively.

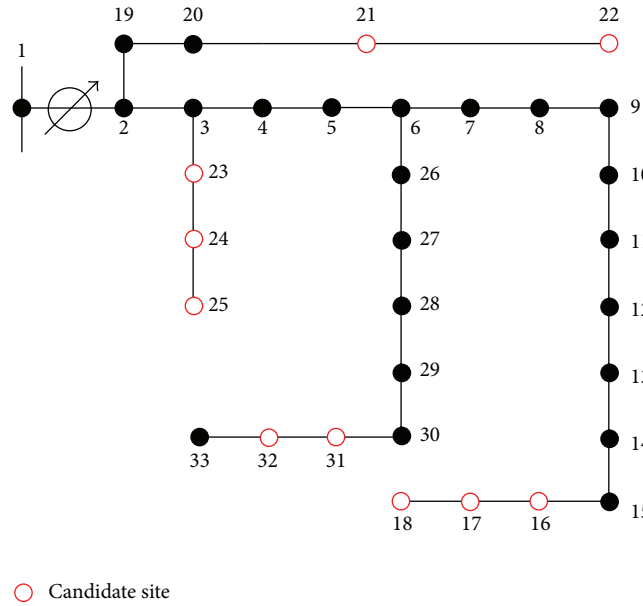

Figure 4: Structure of IEEE 33-node test system and candidate DG sites.

Table 1: Candidate sites and sizes of DG plants.

Node	16	17	18	21	22	23	24	25	31	32	Total
WT	4	4	4	3	3	3	4	3	4	4	36
PV	4	4	4	3	4	3	4	3	3	3	35
MNGT	2	2	2	0	3	2	2	3	2	0	18

Table 2: Parameters of wind speed, solar irradiance, and PV cell temperature [7, 29, 36].

k	c	α_r	β_r	κ	$\sigma_{\Delta T}$
2	6.5	5.5	1.8	0.0035	5

The optimization problem contains 28 integer variables, and the maximum number of uncertain variables in PLF reaches 52. The population of chromosomes in NSGA-II is set as 200 and the maximum generation of evolution as 100, which are large enough to guarantee the convergence of the algorithm.

3.2. Results and Discussions. To verify the proposed semi-linearized simulation method, probabilistic load flow analyses of 100 randomly-generated solutions are carried out first. Figures 5(a) and 5(b) show the comparison of the results calculated by the proposed method and the original LHS-based PLF method, where $\Pr\{S_{i,j}\}$ represents the overload probability of the branch from node i to node j, that is, $\Pr\{S_{i,j}\} = 1 - \Pr\{|S_{i,j}| < S_{i,j}^{\max}\}$. For simplicity, only the results of the branch from node 14 to node 15 and the branch from node 30 to node 31 are pictured since results of other branches are quite similar. It can be seen that the proposed method generates results very close to the original method. The largest difference is about 0.0035 which can be neglected

Table 3: Cost and operation parameters of DG units.

	c_{Con} (\$/kW)	c_{Opr} (\$/kWh)	d_{Cost}	T_{DG} (yr)	H_{DG} (h)	CEC (GJ)	AbatE (GJ)	E_{NoDG} (GJ)
WT	1,800	0.05	0.05	25	2,100	118.3	50.8	20,120.1
PV	2,000	0.03	0.05	30	1,650	406.5	189.2	18,970.4
MNGT	850	0.04	0.05	30	6,000	33,348.7	9,701.2	105,426.7

in analyses. Figure 5(c) shows the difference in calculation time of the two methods. In average, the proposed method uses about 0.072 s to perform a PLF analysis while the original method needs 0.941 s. That is to say, the proposed method can save about 92.3% of the calculation time for PLF analysis. These results demonstrate the accuracy and efficiency of the proposed LHS-based semi-linearized PLF analysis method.

Figure 6 shows the final Pareto-optimal front of the proposed optimization model. The optimization results indicate that as the economic cost of DG plants increases, that is, as the installed capacity of DG plants grows, the cost of exergy and expected power loss become lower. Since it costs more exergy to supply electricity and heat by other alternative sources than by DG plants, the exergy cost of installing DG plants is negative. The absolute value of exergy represents the saved exergy and indicates the benefit for maintaining the sustainability of using the DG plants in this case. If entirely converted by the equivalent exergy contents, 1 PJ of the saved exergy means a reduction of 45, 126.4 tons of coal consumption or 170, 648.5 tons of CO_2 emission. The maximum exergy that can be saved reaches 2.33 PJ, and the economic cost for this is 10.33 million US dollars. Before integrating DG plants, the expected power loss of the system reaches 202.9 kW. As the installed capacity of DG increases, the expected power loss can be reduced down to 133.5 kW, saving about 34.2%. Thus, it can be concluded that integrating DG plants properly into the distribution system can efficiently improve the system's sustainability and reduce the power loss.

Figures 6(b) and 6(c) show the changes in tradeoff relationships of the 3 objective functions in the Pareto-optimal front. Since the exergy saving of installing a certain DG unit is constant, the tradeoff relationship between the economic cost and saved exergy is close to linear relation. That is to say, if the planner wants to save a certain amount of exergy, a certain amount of economic cost is needed. Comparatively, the tradeoff relationship between the economic cost and the power loss is nonlinear. As the economic cost increases, the reduction in power loss caused by adding per unit of economic cost gets smaller. This indicates that adding more DG plants to reduce power loss is not so effective when there are already plenty of them.

The Pareto-optimal front of the proposed optimization model provides useful information for the system planner to set a desirable arrangement for the DG plants. It is convenient to choose one of the Pareto-optimal solutions as the final decision if the planner is satisfied with the corresponding tradeoff relationship according to a specific situation. Although usually not all of the Pareto-optimal solutions are provided in optimization, the distribution of these solutions helps the planner to investigate the possible range of the costs and benefits of the solutions, and thus the planner can determine the optimal tradeoff among the different objectives and at the same time set rational expectations for them. For example, if investment budget is limited, the planner may prefer solutions with lower economic costs but at the same time he or she has to accept the smaller benefits for improving environmental sustainability and reducing power loss.

Figure 7 shows the contributions and the variation tendencies of the three types of DG plants in the total DG capacity, economic cost, and saved exergy as the total economic cost increases in the Pareto-optimal front. All the installed capacities of WT, PV, and MNGT tend to increase when the total economic cost increases. The installed capacity of MNGT is always smaller than those of WT and PV but has a larger increase rate. The average installed capacities of WT, PV, and MNGT are 309.0 kW, 546.7 kW and 20 kW respectively when the total economic cost is lower than 5 million US dollars, which reach 644.7 kW, 675.0 kW and 250.9 kW, respectively, when the total economic cost is higher than 7 million US dollars. This indicates that MNGT is not the prior choice compared with WT, and PV when the economic cost is limited. Although an MNGT unit can bring 2.1~2.3 fold more exergy saving than WT unit, and PV unit, the much higher economic cost, which is 3.7~4.9 fold higher, prevents its application. The same amount of exergy saving caused by installing MNGT a unit can be obtained by installing more WT or PV units with lower cost if the constraints can be satisfied. However, as a reliable and stable power source, the MNGT units can be used to suppress the negative impacts of WT and PV units on the distribution system, and this is why the MNGT units can not be replaced by other DG units in the solutions of Pareto-optimal front.

Since the system is already close to its upper limit of power distribution due to the small capacities of branches, the uncertainties of power loads bring great overload risks. The assumption of tight correlations between the power loads at different nodes further increases the overload risks as the power loads tend to vary unanimously. Figure 6 shows the overload probabilities of distribution branches before and after the DG plants are installed. The applied siting and sizing plan of DG plants in Figure 6 is the minimum economic cost plan, whose details are shown in Table 4. This plan costs 1.60 million US dollars, −0.47 PJ of exergy and 174.1 kW of expected power loss. The overload probabilities of branches are obviously reduced by integrating DG plants as shown in Figure 8. Additionally, simulations show that more expensive plans generally perform better in reducing the overload risks than this plan.

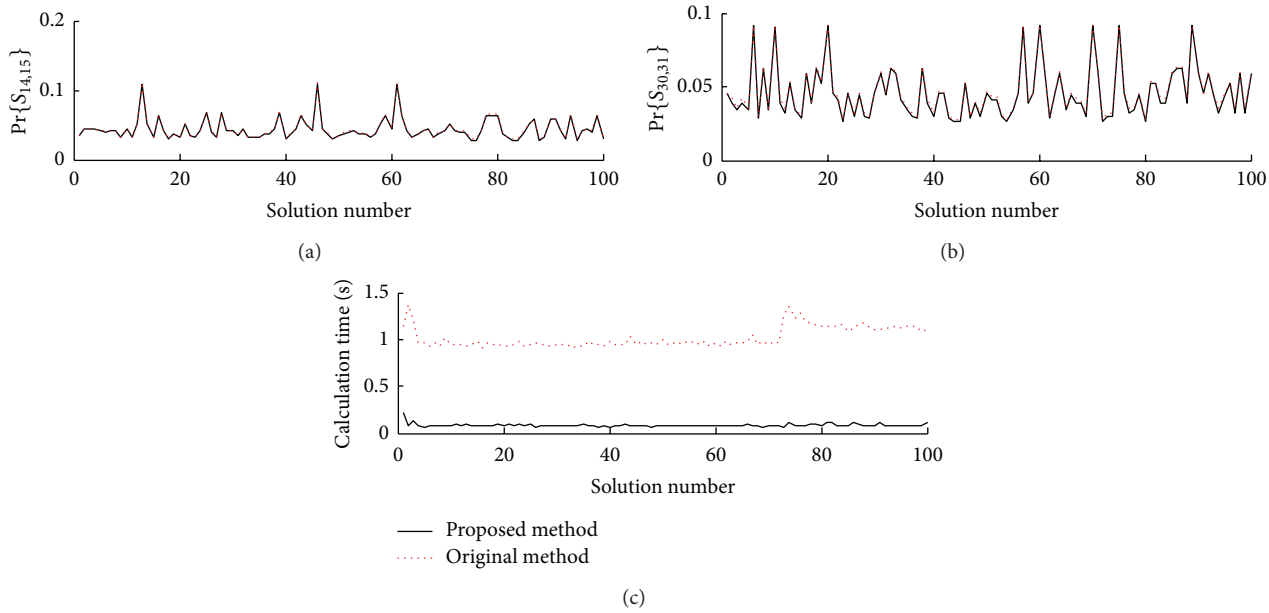

Figure 5: Comparison of the results from the proposed method and the original method.

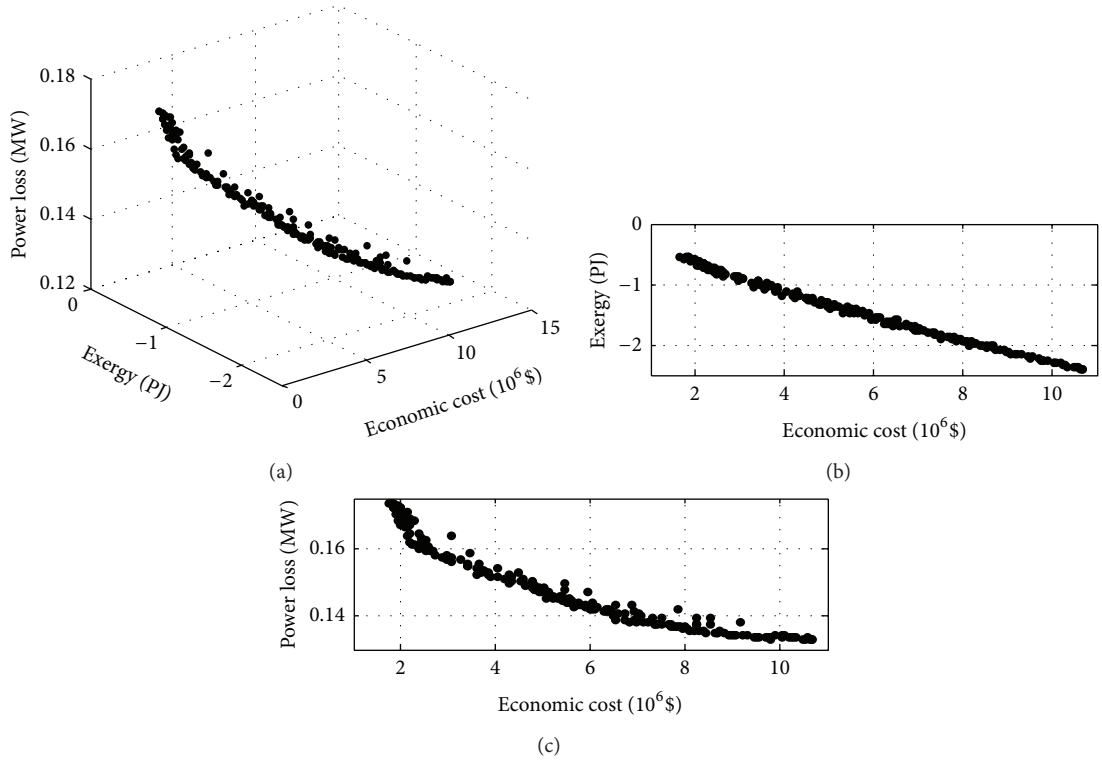

Figure 6: Pareto-optimal front of the optimization result. (a) The 3-dimensional distribution of the Pareto-optimal front. (b) The cost-exergy distribution of the Pareto-optimal front. (c) The cost-loss distribution of the Pareto-optimal front.

4. Conclusion

In this paper, a sustainability-oriented multi-objective optimization model for siting and sizing DG plants in distribution systems is proposed. In the model, life cycle exergy is used as a unified indicator of all the impacts on environmental sustainability of integrating DG plants, and it is optimized in the model to obtain better environmental sustainability. Exergetic life cycle analysis methodology is used to evaluate the life cycle exergy of the planned system. To control the risks

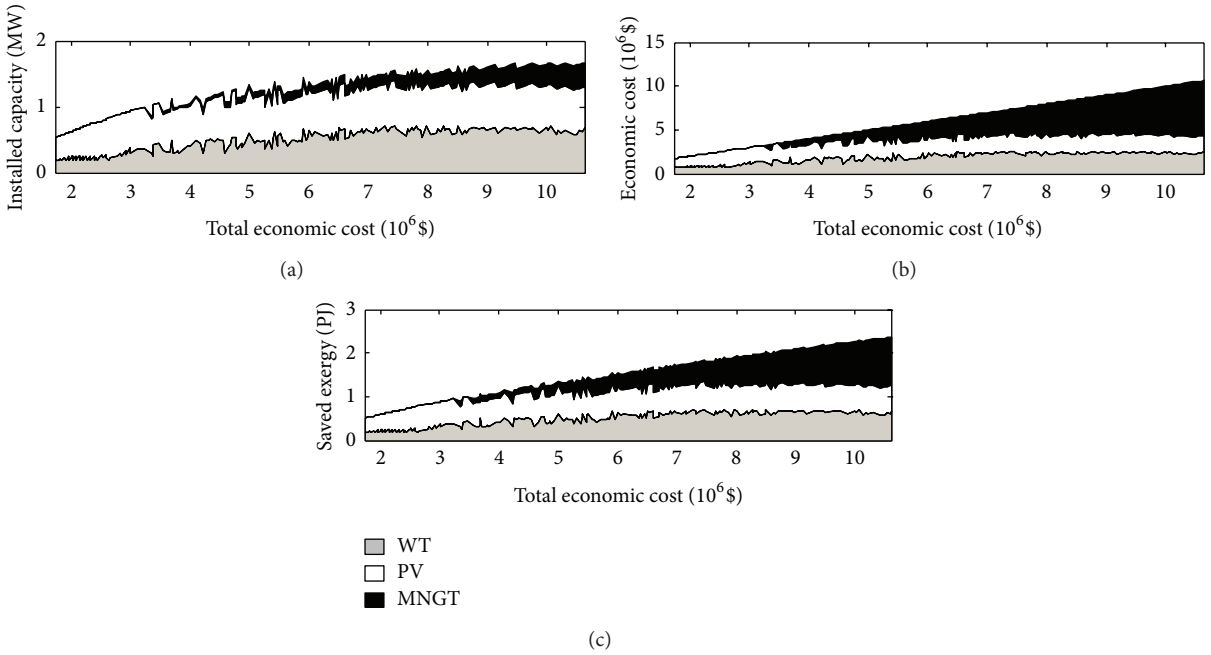

Figure 7: Contributions of WT, PV, and MNGT to the total DG capacity, economic cost, and saved exergy.

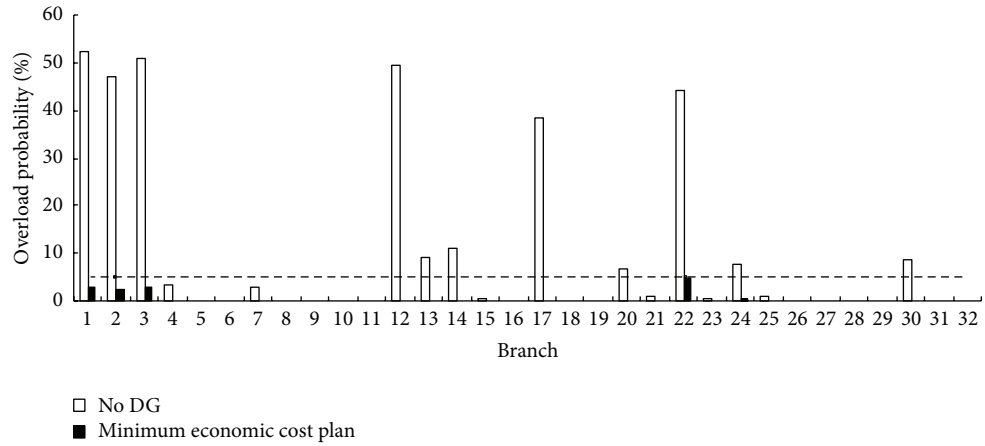

Figure 8: Overload probabilities of distribution branches. The dash line represents the overload probability of 5%.

brought by the unstable DG outputs and power loads, chance constraints are used in the optimization model. Additionally, a semi-linearized simulation method is proposed to improve the efficiency of probabilistic load flow analysis based on Latin hypercube sampling.

A case study based on modified IEEE 33-node system is carried out to demonstrate the proposed model and method. Numerical results show that the semi-linearized simulation method greatly improves the calculation efficiency of probabilistic load flow analysis, and the accuracy loss is little. The proposed optimization model generates a series of possible solutions known as the Pareto-optimal front and provides useful information for the system planner to set a desirable arrangement for the DG plants. The Pareto-optimal solutions in the case study indicate that with proper arrangement DG plants can produce considerable benefits for maintaining environmental sustainability, reducing power losses, and controlling operation risks. Wind turbines and photovoltaic units are prior choices compared to the micronatural gas turbines when the total economic cost is limited under a low level in this case study. More integration of micro natural gas turbines is beneficial for maintaining environmental sustainability and reducing power losses but obviously increases the economic cost.

How to finally determine the sites and sizes of the DG plants according to the Pareto-optimal solutions is another important problem that needs methods for multicriteria decision making. Further study on this problem should be carried out in the future. Additionally, some modifications can be made based on the proposed model for studies such as

Table 4: Installed units of the minimum economic cost solution.

Node	16	17	18	21	22	23	24	25	31	32
WT	1	1	0	0	0	1	2	1	1	1
PV	4	3	2	0	1	0	2	2	0	3
MNGT	0	0	0	0	0	0	0	0	0	0

optimization of reactive power compensation capacities and integration of electric vehicle charging stations.

Acknowledgments

This study was supported by the Key Program of National Natural Science Foundation (nos. 50939001, 41271543) and the Program for New Century Excellent Talents in University (NCET-09-0226).

References

[1] W.-S. Tan, M. Y. Hassan, M. S. Majid, and H. A. Rahman, "Optimal distributed renewable generation planning: a review of different approaches," *Renewable and Sustainable Energy Reviews*, vol. 18, pp. 626–645, 2013.

[2] T. Ackermann, G. Andersson, and L. Söder, "Distributed generation: a definition," *Electric Power Systems Research*, vol. 57, no. 3, pp. 195–204, 2001.

[3] G. Pepermans, J. Driesen, D. Haeseldonckx, R. Belmans, and W. D'haeseleer, "Distributed generation: definition, benefits and issues," *Energy Policy*, vol. 33, no. 6, pp. 787–798, 2005.

[4] A. Barina, L. F. Pozzattia, L. N. Canhaa, R. Q. Machadob, A. R. Abaidea, and G. Arend, "Multi-objective analysis of impacts of distributed generation placement on the operational characteristics of networks for distribution system planning," *International Journal of Electrical Power & Energy Systems*, vol. 32, no. 10, pp. 1157–1164, 2010.

[5] H. Falaghi, C. Singh, M.-R. Haghifam, and M. Ramezani, "DG integrated multistage distribution system expansion planning," *International Journal of Electrical Power and Energy Systems*, vol. 33, no. 8, pp. 1489–1497, 2011.

[6] O. M. Toledo, D. Oliveira Filho, and A. S. A. C. Diniz, "Distributed photovoltaic generation and energy storage systems: a review," *Renewable and Sustainable Energy Reviews*, vol. 14, no. 1, pp. 506–511, 2010.

[7] Z. Liu, F. Wen, and G. Ledwich, "Optimal siting and sizing of distributed generators in distribution systems considering uncertainties," *IEEE Transactions on Power Delivery*, vol. 26, no. 4, pp. 2541–2551, 2011.

[8] F. Rotaru, G. Chicco, G. Grigoras, and G. Cartina, "Two-stage distributed generation optimal sizing with clustering-based node selection," *International Journal of Electrical Power and Energy Systems*, 2012.

[9] Sh. Abdi and K. Afshar, "Application of IPSO-Monte Carlo for optimal distributed generation allocation and sizing," *International Journal of Electrical Power & Energy Systems*, vol. 44, no. 1, pp. 786–797, 2013.

[10] R. Viral and D. K. Khatod, "Optimal planning of distributed generation systems in distribution system: a review," *Renewable and Sustainable Energy Reviews*, vol. 16, no. 7, pp. 5146–5165, 2012.

[11] H. L. Willis, "Analytical methods and rules of thumb for modeling DG-distribution interaction," in *Proceedings of the Power Engineering Society Summer Meeting*, vol. 3, pp. 1643–1644, July 2000.

[12] C. Wang and M. H. Nehrir, "Analytical approaches for optimal placement of distributed generation sources in power systems," *IEEE Transactions on Power Systems*, vol. 19, no. 4, pp. 2068–2076, 2004.

[13] T. Gözel and M. H. Hocaoglu, "An analytical method for the sizing and siting of distributed generators in radial systems," *Electric Power Systems Research*, vol. 79, no. 6, pp. 912–918, 2009.

[14] M. E. H. Golshan and S. A. Arefifar, "Optimal allocation of distributed generation and reactive sources considering tap positions of voltage regulators as control variables," *European Transactions on Electrical Power*, vol. 17, no. 3, pp. 219–239, 2007.

[15] A. M. El-Zonkoly, "Optimal placement of multi-distributed generation units including different load models using particle swarm optimisation," *IET Generation, Transmission and Distribution*, vol. 5, no. 7, pp. 760–771, 2011.

[16] A. A. Abou El-Ela, S. M. Allam, and M. M. Shatla, "Maximal optimal benefits of distributed generation using genetic algorithms," *Electric Power Systems Research*, vol. 80, no. 7, pp. 869–877, 2010.

[17] L. D. Arya, A. Koshti, and S. C. Choube, "Distributed generation planning using differential evolution accounting voltage stability consideration," *International Journal of Electrical Power and Energy Systems*, vol. 42, no. 1, pp. 196–207, 2012.

[18] D. K. Khatod, V. Pant, and J. Sharma, "Evolutionary programming based optimal placement of renewable distributed generators," *IEEE Transactions on Power Systems*, vol. 28, no. 2, pp. 683–695, 2013.

[19] F. Ugranli and E. Karatepe, "Multiple-distributed generation planning under load uncertainty and different penetration levels," *International Journal of Electrical Power & Energy Systems*, vol. 46, pp. 132–144, 2013.

[20] W. El-Khattam, Y. G. Hegazy, and M. M. A. Salama, "An integrated distributed generation optimization model for distribution system planning," *IEEE Transactions on Power Systems*, vol. 20, no. 2, pp. 1158–1165, 2005.

[21] D. Singh, D. Singh, and K. S. Verma, "Multiobjective optimization for DG planning with load models," *IEEE Transactions on Power Systems*, vol. 24, no. 1, pp. 427–436, 2009.

[22] W. Wang, R. Zmeureanu, and H. Rivard, "Applying multi-objective genetic algorithms in green building design optimization," *Building and Environment*, vol. 40, no. 11, pp. 1512–1525, 2005.

[23] E. Sciubba, "Beyond thermoeconomics? The concept of extended exergy accounting and its application to the analysis and design of thermal systems," *Exergy, An International Journal*, vol. 1, no. 2, pp. 68–84, 2001.

[24] M. A. Rosen, I. Dincer, and M. Kanoglu, "Role of exergy in increasing efficiency and sustainability and reducing environmental impact," *Energy Policy*, vol. 36, no. 1, pp. 128–137, 2008.

[25] N. Lior, "Thoughts about future power generation systems and the role of exergy analysis in their development," *Energy Conversion and Management*, vol. 43, no. 9-12, pp. 1187–1198, 2002.

[26] C. Koroneos and M. Tsarouhis, "Exergy analysis and life cycle assessment of solar heating and cooling systems in the building environment," *Journal of Cleaner Production*, vol. 32, pp. 52–60, 2012.

[27] H. R. Becerra-Lopez and P. Golding, "Dynamic exergy analysis for capacity expansion of regional power-generation systems: case study of far West Texas," *Energy*, vol. 32, no. 11, pp. 2167–2186, 2007.

[28] J. Portha, S. Louret, M. Pons, and J. Jaubert, "Estimation of the environmental impact of a petrochemical process using coupled LCA and exergy analysis," *Resources, Conservation and Recycling*, vol. 54, no. 5, pp. 291–298, 2010.

[29] M. Fan, V. Vittal, G. T. Heydt, and R. Ayyanar, "Probabilistic power flow studies for transmission systems with photovoltaic generation using cumulants," *IEEE Transactions on Power Systems*, vol. 27, no. 4, pp. 2251–2261, 2012.

[30] C. Su, "Probabilistic load-flow computation using point estimate method," *IEEE Transactions on Power Systems*, vol. 20, no. 4, pp. 1843–1851, 2005.

[31] Y. Chen, J. Wen, and S. Cheng, "Probabilistic load flow method based on Nataf transformation and Latin hypercube sampling," *IEEE Transactions on Sustainable Energy*, vol. 4, no. 2, pp. 294–301, 2013.

[32] M. D. McKay, R. J. Beckman, and W. J. Conover, "A comparison of three methods for selecting values of input variables in the analysis of output from a computer code," *Technometrics*, vol. 21, no. 2, pp. 239–245, 1979.

[33] J. C. Helton and F. J. Davis, "Latin hypercube sampling and the propagation of uncertainty in analyses of complex systems," *Reliability Engineering and System Safety*, vol. 81, no. 1, pp. 23–69, 2003.

[34] M. J. Moran, *Availability Analysis: A Guide to Efficient Energy Use*, Prentice-Hall, Englewood Cliffs, NJ, USA, 1982.

[35] J. Dai, B. Fath, and B. Chen, "Constructing a network of the social-economic consumption system of China using extended exergy analysis," *Renewable and Sustainable Energy Reviews*, vol. 16, no. 7, pp. 4796–4808, 2012.

[36] D. L. King, W. E. Boyson, and J. A. Kratochvil, *Photovoltaic Array Performance Model*, Sandia National Laboratories, Albuquerque, NM, USA, 2004.

[37] J. Hetzer, D. C. Yu, and K. Bhattarai, "An economic dispatch model incorporating wind power," *IEEE Transactions on Energy Conversion*, vol. 23, no. 2, pp. 603–611, 2008.

[38] E. Handschin, F. Neise, H. Neumann, and R. Schultz, "Optimal operation of dispersed generation under uncertainty using mathematical programming," *International Journal of Electrical Power and Energy Systems*, vol. 28, no. 9, pp. 618–626, 2006.

[39] K. Deb, A. Pratap, S. Agarwal, and T. Meyarivan, "A fast and elitist multiobjective genetic algorithm: NSGA-II," *IEEE Transactions on Evolutionary Computation*, vol. 6, no. 2, pp. 182–197, 2002.

[40] D. F. Pires, C. H. Antunes, and A. G. Martins, "NSGA-II with local search for a multi-objective reactive power compensation problem," *International Journal of Electrical Power & Energy Systems*, vol. 43, no. 1, pp. 313–324, 2012.

[41] N. Srinivas and K. Deb, "Muiltiobjective optimization using nondominated sorting in genetic algorithms," *Evolutionary Computation*, vol. 2, no. 3, pp. 221–248, 1994.

[42] M. E. Baran and F. F. Wu, "Network reconfiguration in distribution systems for loss reduction and load balancing," *IEEE Transactions on Power Delivery*, vol. v, pp. 1401–1407, 1992.

[43] V. Kumar, R. H. C. Kumar, I. Gupta, and H. O. Gupta, "DG Integrated approach for service restoration under cold load pickup," *IEEE Transactions on Power Delivery*, vol. 25, no. 1, pp. 398–406, 2010.

[44] Z. Liu, F. Wen, Y. Xue, J. Xin, and G. Ledwich, "Optimal siting and sizing of distributed generators considering plug-in electric vehicles," *Automation of Electric Power Systems*, vol. 35, no. 18, pp. 11–16, 2011.

Hindawi Publishing Corporation
Mathematical Problems in Engineering
Volume 2013, Article ID 527461, 10 pages
http://dx.doi.org/10.1155/2013/527461

Research Article

Hydrological Design of Nonstationary Flood Extremes and Durations in Wujiang River, South China: Changing Properties, Causes, and Impacts

Xiaohong Chen,[1,2] Lijuan Zhang,[1,2] C.-Y. Xu,[3,4] Jiaming Zhang,[1,2] and Changqing Ye[1,2]

[1] *Department of Water Resources and Environment, Sun Yat-sen University, Guangzhou 510275, China*
[2] *Key Laboratory of Water Cycle and Water Security in Southern China of Guangdong High Education Institute, Sun Yat-sen University, Guangzhou 510275, China*
[3] *Department of Earth Sciences, Uppsala University, 752 36 Uppsala, Sweden*
[4] *Department of Geosciences, University of Oslo, 0316 Oslo, Norway*

Correspondence should be addressed to Changqing Ye; yechangqing2001@hotmail.com

Received 12 February 2013; Accepted 7 May 2013

Academic Editor: Guohe Huang

The flood-duration-frequency (QDF) analysis is performed using annual maximum streamflow series of 1–10 day durations observed at Pingshi and Lishi stations in southern China. The trends and change point of annual maximum flood flow and flood duration are also investigated by statistical tests. The results indicate that (1) the annual maximum flood flow only has a marginally increasing trend, whereas the flood duration exhibits a significant decreasing trend at the 0.10 significant level. The change point for the annual maximum flood flow series was found in 1991 and after which the mean maximum flood flow increased by 45.26%. (2) The period after 1991 is characterized by frequent and shorter duration floods due to increased rainstorm. However, land use change in the basin was found intensifying the increased tendency of annual maximum flow after 1991. And (3) under nonstationary environmental conditions, alternative definitions of return period should be adapted. The impacts on curve fitting of flood series showed an overall change of upper tail from "gentle" to "steep," and the design flood magnitude became larger. Therefore, a nonstationary frequency analysis taking account of change point in the data series is highly recommended for future studies.

1. Introduction

Inadequate understanding of the probabilistic behaviour of extreme flows when designing a hydraulic structure may have significant economical impacts on the design values of hydraulic projects [1–5]. Indeed, flood severity can best be characterized by its magnitude and duration. Thus, both of these characteristics need to be studied together. Moreover, the stationarity assumption has long been compromised by human disturbances in river basins, especially for the floods' volume and duration. The accuracy of design flood will be affected if the parameter change is not considered for flood frequency analysis. Designed by the existing engineering hydrologic analysis method, basin development and utilization project, flood control, antidrought projects, and operation dispatches will face the risk of distortion in design frequency caused by the ever-changing environment.

When refer to floods' volume and duration, two different approaches can be utilised: the peak-volume analysis and the QDF analysis [1]. It is important to mention that in the peak-volume analysis approach the determination of the flood event's starting and ending dates contains a part of subjectivity [1]. QDF models are extensions of standard flood frequency models, which summarize the frequency of flood events for different flood probabilities and durations by one compound formula [6]. There have been numerous studies

in the past on QDF approach, a few of which are discussed below. The work on QDF was initiated almost four decades ago [7]. In the 1990 s, Sherwood [8] and Balocki and Burges [9], among others, laid out the basis of the present form of the QDF model. Javelle et al. [1] successfully used converging approach to the QDF modeling based on the assumption of the convergence of different flood distributions for small return periods in Canada. This approach has been successfully applied in many areas around the world. such as Martinique, France, Burkina Faso, and Romania [6, 10–12].

Nevertheless, recent studies on stationarity of hydrologic records conducted in different parts of the world have identified significant changes in the statistical parameters of the analyzed records [6]. Many studies in meteorology and hydrology still do not attempt to detect the variability in this parameter. In fact, the effect of changes in variability in the detection of usual trends in average flood is only poorly understood [13]. After the nonstationarity of flood series is generated, the statistical properties of data samples (such as mean and standard deviation) and distribution curves change over time, and the uncertainties of exceedance probability and the corresponding design flow will also change [14]. A summary of non-stationary flood frequency analysis methods is provided in Kailaq [15]. Aiming at studying the nonstationarity of hydrologic statistical characteristics in the changing environment, the non-stationary series based on time-varying statistical parameters can be established. A frequency analysis model of non-stationary extreme value series was proposed by Strupczewski et al. [14], which embedded the trend component into the distribution of first- and second-order moments (time-varying moments, TVM); that is, the trends of mean and variance of statistical parameters were considered. The distribution function of the model is described through first and second moments, and thus the design flow can be obtained considering changes in time. TVM approach has been successfully applied in many areas around the world. Based on the same principle of TVM model, Vogel et al. [16] showed that the flood magnitude in many regions of the USA had an increasing trend, and floods with return periods of 100 years might become more common in some basins. Villarini [17] found that the design flow of 100-year flood calculated on a basis of traditional frequency analysis method changes over time. The study conducted by Strupczewski et al. [14] in analyzing the non-stationary hydrologic extreme value series showed that the function relationship can be established between the design flow x_P, design level P, and time t as $x_P = F(p, t)$. Therefore, under a certain design level P, the design flow x_P changes over time t.

The QDF models cited above reveal that changing environmental conditions call for further studies that can take into account the non-stationary character of hydrologic records and that can deal with time-dependent parameters of flood frequency distributions [6]. There are only a few studies focusing on QDF models applicable to non-stationary conditions in the recent hydrologic literature. Cunderlik and Ouarda [6] defined the key concepts of a non-stationary approach to regional QDF modelling from a hydrologically homogeneous region in Quebec. The approach refers to the TVM model proposed by Strupczewski et al. [14], based on the assumption of nonstationarity of the first two moments of the series. The case study results demonstrate that ignoring statistically significant nonstationarity of hydrologic records can seriously bias flood quantiles estimated for the near future.

Indeed, the nonstationarity of a flood series is not only defined by the variation of trend, but also by sudden changes. The TVM non-stationary model is only suitable for non-stationary flood series which have trend of variation [14]. While several books and articles in scientific journals use non-stationary QDF models for probability distributions with variation of trend, less study has been published in the hydrologic literature about non-stationary QDF analysis for sudden changes. This is a difficult task due to the problems in selecting the best non-stationary processing approach from the candidate flood frequency analysis methods available in the literature.

Due to the changes in meteorological variables (such as rainfall and evaporation) and human activities (such as land cover changes) in the Wujiang River basin, the runoff generation conditions and statistical properties of flood series samples (such as mean and standard deviation) have changed and shown the nonstationarity of the series prior and posterior to the change point. The aim of this research is to develop a statistical model that provides a more complete description of a basin's flood regime that can be used to (1) explore the changing characteristics and impact mechanism of design value for non-stationary hydrologic extreme flow with abrupt jumping change point and (2) investigate possible causes behind changes of hydrological extremes. The study gives an implication of the impact of climate/landuse change on flood occurrences and magnitudes. The findings from this study will benefit hazard mitigation under the influences of changing climate and intensifying human activities in the Wujiang basin and other basins in the world.

2. Methodology

2.1. Flood Frequency Distribution. Many probability distributions (PDs) have been considered, in different situations, for the probabilistic modeling of extreme events, including the Pearson type III (P3), log-Pearson III (LP3), two-parameter lognormal (LN2), three-parameter lognormal (LN3), Gumbel (extreme value type I, EV1), Weibull (extreme value type III), general extreme value (GEV), and generalized logistic distribution, (GLO). Rao and Hamed [18] and Reiss and Thomas [19] provide details of these probability density functions. Two of them are light-tailed distributions (P3, Weibull), four of them are mixed-tailed distributions (GEV, Gumbel, LN3, and LN2), and the other two are heavy-tailed distributions (GLO and LP3). These distributions have been selected because they are all currently in use in various regions.

2.2. Nonstationarity of Flood Series Detection. Cumulative curve method is often used to evaluate details on temporal variability of hydrological time series. Cumulative curve method was first proposed by Hurst [20] and used to reveal

the changes of reservoir capacity in Nile River. In this study, the Cumulative Sum of Departures of Modulus Coefficient (CSDMC) was used to detect the phase change characteristics of annual maximum flood flow. CSDMC method can be expressed by the following equations [21]:

$$R_i = \frac{Q_i}{\overline{Q}}, \quad (i = 1, 2, 3, \ldots, N),$$
$$K_p = \sum_{i=1}^{p} (R_i - 1), \quad (p = 1, 2, 3, \ldots, N), \tag{1}$$

where i indicates the sequence value of time series in N year, K_p indicates CSDMC cumulative moment balance value in $1 \sim p$ year, Q_i is the annual maximum peak flow, and $\overline{Q}$ indicates the multiyear mean annual maximum flood flow values. The period of K_p with a downward trend (negative slope) indicates the time of lower value than average annual maximum flood flow; on the contrary, the period of K_p with an upward trend (positive slope) indicates the time of higher value than average annual maximum flood flow [21].

Cumulative sum (CUSUM) charts are used for abrupt change point detection in climate series. Each significant change in the direction of CUSUM indicates a sudden fluctuation of mean. CUSUM chart with a relatively straight route indicates basically no changes in flow mean in this period.

2.3. QDF Model. The aim of the QDF modelling is to provide a continuous formulation of flood quantiles, $Q(d, T)$, as a function of probability, T, and duration, d [6]. An instantaneous streamflow time series can be used to characterise each observed flood by its instantaneous peak flow, $Q(t)$, and by the values of mean streamflows for given durations, $Q_d(t)$, using a moving average technique. The method is based on a moving average with a window length d over the time series $Q(t)$. From the series $Q_d(t)$, annual maximum values, $Q_d^{\max}(t)$, can be extracted as

$$Q_d^{\max}(t) = \max_{t^- \le t \le t^+} \{Q_d(t)\}, \tag{2}$$

where t^- and t^+ are the first and last days of the tth water year or calendar year. A set of $Q_d^{\max}(t)$ series, derived for different durations d, is then used to relate flood quantiles to the return period and flood duration [6].

Javelle et al. [1] defined a stationary at-site QDF model based on the following two assumptions. The first is the flood distributions which are self-affine along a horizontal line of equation. The second is that for a given return period the evolution of the quantile $Q(d, T)$ as a function of d can be described by a hyperbolic form. In these conditions the QDF model can be written as follows:

$$Q(d, T) = \frac{Q_0(d = 0, T)}{1 + d/\Delta}, \tag{3}$$

where $Q_0(d = 0, T)$ is the distribution corresponding to instantaneous peak discharges, d is the duration of flood, and Δ is a parameter describing the shape of the hyperbolic form, which can be related to flood dynamics [1]. A large value of Δ often indicates a slow flood while a small value of Δ implies flash floods. Consequently parameter Δ can be considered as a characteristic flood duration for the basin.

Equation (3) reveals that each distribution $Q(d, T)$ multiplied by $1 + d/\Delta$ is equal to the $Q_0(d = 0, \mathrm{T})$ distribution. This property can be used to estimate parameter Δ. The annual maximum streamflow series $Q_d^{\max}(t)$ is first scaled:

$$q_d^{\max}(t) = Q_d^{\max}(t) \left[1 + \frac{d}{\delta}\right]. \tag{4}$$

The characteristic duration $\Delta(t)$ at a time t is selected as the optimum value δ^{opt} that minimizes the dispersion ε of the experimental time-scaled values, $q_d^{\max}(t)$,

$$\Delta = \delta^{\mathrm{opt}},$$
$$\varepsilon = \min \left\{ \frac{1}{N} \frac{1}{D} \sum_{i=1}^{N} \sum_{j=1}^{D} \left[\frac{q_{d_j}^{\max}(i) - \overline{q}_d(i)}{\overline{q}_d(i)} \right]^2 \right\}, \tag{5}$$

where $\overline{q}_d(t)$ is the mean scaled value calculated for D durations d_j and N is the record length. Parameters of the distribution $Q_0(d = 0, T)$ are estimated by fitting a distribution function to the series $\overline{q}_d(t)$ [6].

3. Study Area and Data

Wujiang River is one of the branches of the Pearl River in South China, with the latitude ranging from 24°46′ to 25°41′N and the longitude ranging from 112°23′ to 113°36′E (Figure 1). The climate is dominated by the southwest and southeast Asia monsoons in summer, leading to comparatively high humidity and uneven distribution of precipitation through the season.

The main gauging stations, named Pingshi and Lishi, and the recorded lengths of the data are given in Table 1. The observed flood discharge series at each station is visually investigated to see if there are apparent trends or jumps. Statistical tests including the Mann-Kendall (M-K) test for trend are conducted [22, 23], from which it can be seen that there is no statistically significant trend for annual maximum daily discharges. The autocorrelation coefficient and randomness test indicate that hydrological sequences satisfy independent assumption. The precipitation time series data used in this study are collected from National Meteorological Information Center in China (Table 1).

4. Results

4.1. Nonstationarity of Flood Series Detection. It was found that annual maximum flood flow of short durations (1–5 days) exhibited stronger positive slopes and those of long durations (>5 days) exhibited moderately positive slopes. The annual maximum flood flow of Pingshi and Lishi stations showed a change process as "steady decline to significant rise" (Figure 2). The deluge events frequently occurred after 1990, basically concentrated in the last 20 years of the time series. CSDMC test was used to identify change point

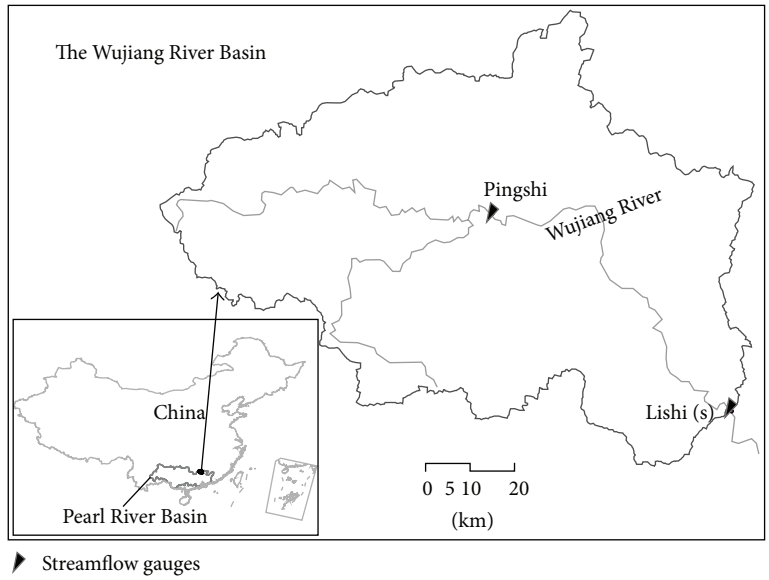

Figure 1: Location of the Wujiang River, the hydrological stations within the Wujiang River basin.

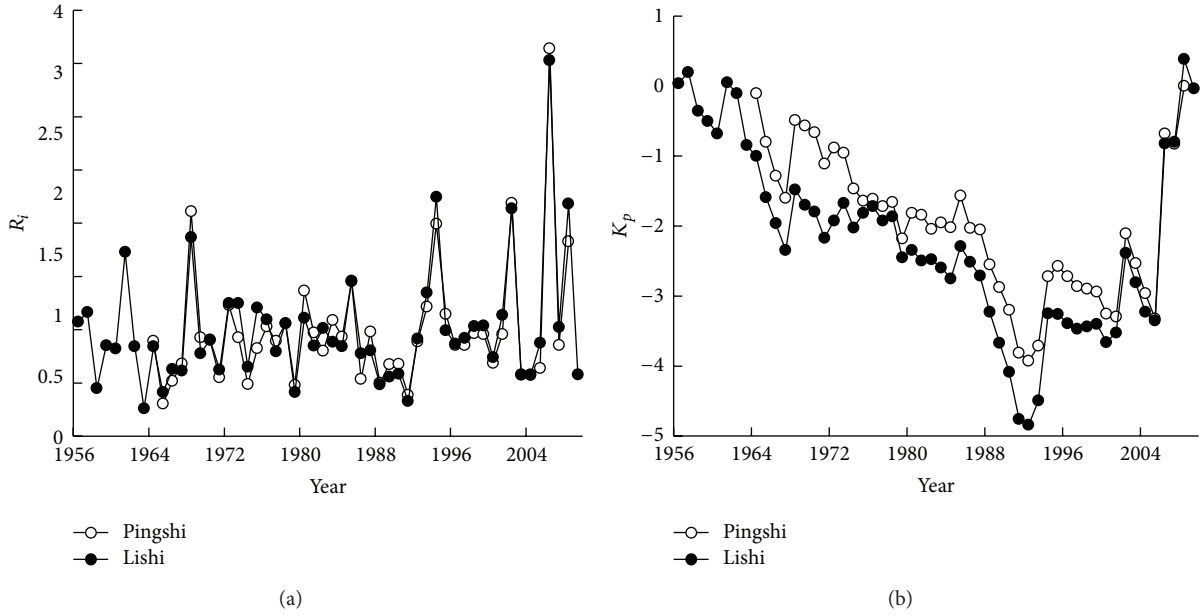

Figure 2: Change process (a) and Cumulative Sum of Departures of Modulus Coefficient test (b) of annual maximum flood flow series in Wujiang River.

and nonstationarity of series [15]. As shown in Figure 2, the change point appeared in 1991. Specifically, the annual maximum flood flow had a significant upward trend from 1991 to 2009.

4.2. Selection of Probability Distribution Function. Akaike information criterion (AIC) was taken as the discrimination criterion of the optimal model [24]. As viewed from the AIC fitting test values of different distribution curves, GLO model in Wujiang River is the best fitting model (Table 2). Parameter estimations for all the 8 distributions by maximum likelihood estimation (MLE) are given in Table 3. It showed that big floods happened more frequently after 1991, making steeper shape in the left side of the empirical flood distribution. Heavy-tailed GLO owns greater flexibility in terms of description of probability behaviours with great hydrological extremes. The GLO probability distribution function which fits the flood series well will be adopted as the best choice in describing the statistical properties of the flood series.

4.3. Designed Flood Flow Corresponding to Different Return Periods. For illustrative purposes, the flood flow series at the

Table 1: Detailed information on the stream flow gauging stations and rainfall stations.

Station	Location		Area (km^2)	Flow period	Reservoir capacity (10^8 m^3)	Rainfall stations	Rainfall period
Pingshi	113°05′E	25°28′N	3567	1964.1.1–2008.12.31	<1	Sanxi, Lechang, Lishi	1955.1.1–2009.12.31
Lishi	113°53′E	24°88′N	6976	1956.1.1–2009.12.31	3.38		

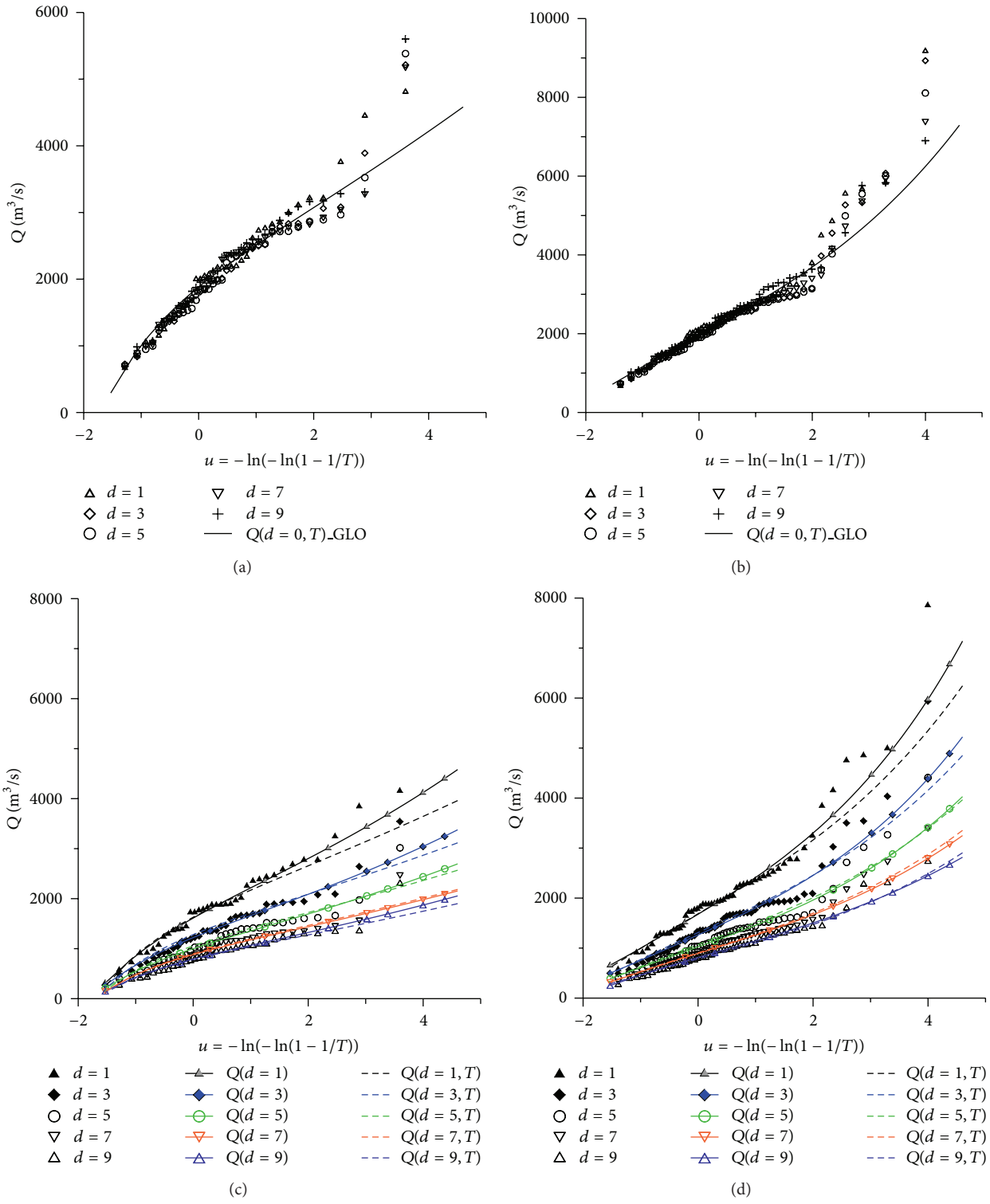

Figure 3: QDF growth curves at Lishi station in 1956–1991 (left) and in 1956–2009 (right).

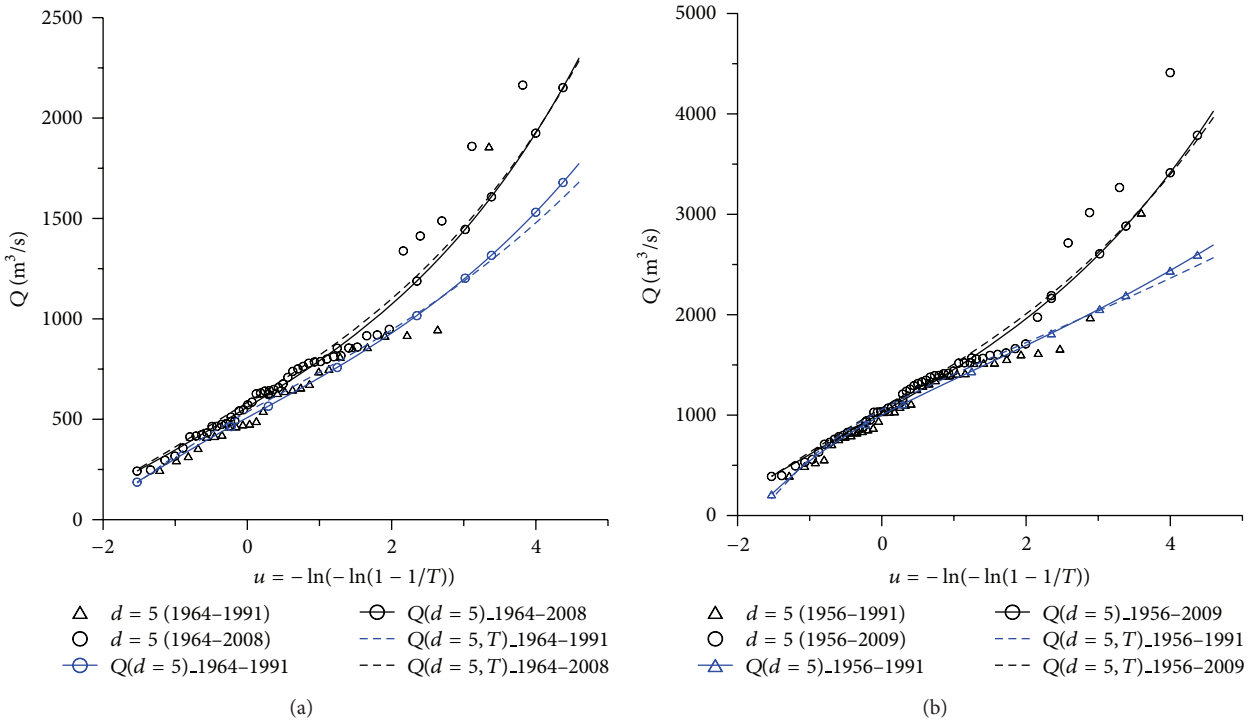

FIGURE 4: QDF growth curves for duration $d = 5$ days, $Q_T(d = 5)$, at Pingshi station (a) and Lishi station (b).

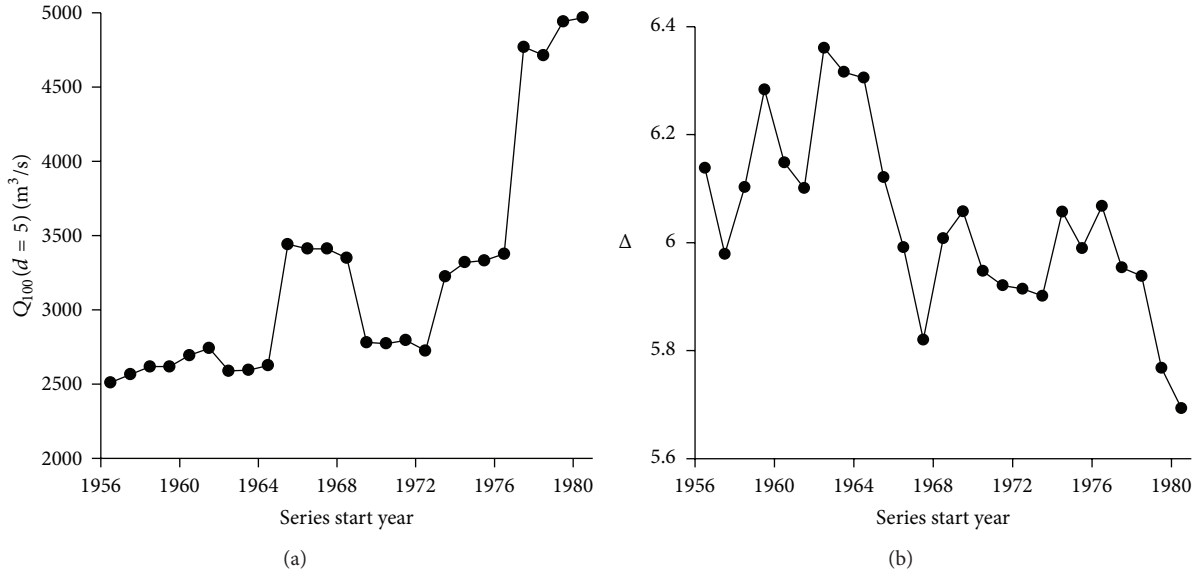

FIGURE 5: Change process of 100-year flood quantiles for duration $d = 5$ days, $Q_{100}(d = 5)$ (a) and parameter Δ (b) at Lishi station.

TABLE 2: AIC fitting test values of 8 distributions for flood frequency analysis in Wujiang River.

Station	P3	GLO	GEV	Weibull	GUM	LN3	LN2	LP3
Pingshi	716.96	**696.38**	697.57	702.07	701.27	730.21	697.06	697.77
Lishi	917.61	**913.32**	915.40	920.24	916.25	924.79	913.52	915.36

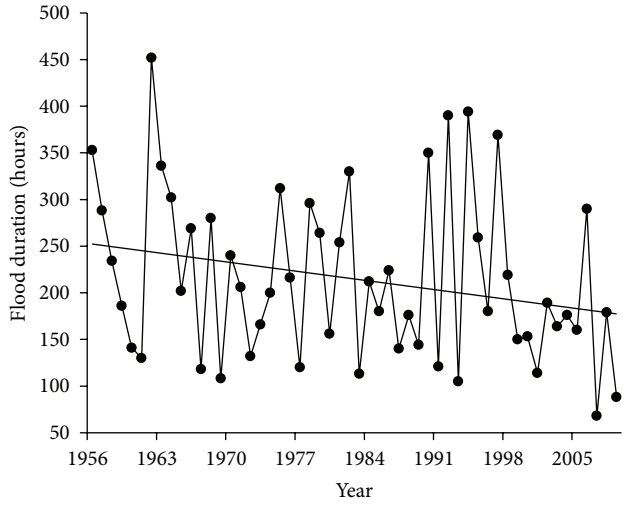

Figure 6: Original flood duration series at Lishi station in Wujiang River basin.

Table 3: Parameter estimation of optimal distribution model in Wujiang River (MLE).

Station	Flow period	PD	Parameters		
			Scale	Shape	Location
Pingshi	1964 ~ 2008	GLO	286.412	−0.346	1085.513
Lishi	1956 ~ 2009	GLO	512.532	−0.303	1940.168

Lishi station is used to demonstrate the study procedure and the results (Figure 3). In the first step, the first 36 years of the data (1956–1991) of the total observation period (1956–2009) were analyzed. In the second step of the analysis, the procedure was repeated using the data from the whole 54-year-long observation period 1956–2009. The results from both periods were then compared (Figure 3).

Figure 4 compares the QDF growth curves estimated for different time horizon by means of the stationary QDF methods for the 5-day duration, $Q_T(d = 5)$, at Pingshi and Lishi stations. The change characters of optimal linear frequency distribution at the Pingshi and Lishi stations before and after change point of flood flow are compared. The impacts on the fitted curve of flood series showed an overall upper tail from "gentle" to "steep," meaning that the design flood magnitude will become larger.

It can be seen from Table 4 that $Q_T(d = 5)$ values correspond to different return periods before and after the change point. For the same $Q_T(d = 5)$ value, the return periods at the Pingshi and Lishi stations come to be decreasing after the environment changed. Return periods of these stream flow events are about 25 years and could be more than 100 years before the change point, showing tremendous influences of changing environment on flood changes. After changes in the hydrological regime, the flood return period estimated before the change is often unable to well describe the flood frequency characteristics after environmental changes.

4.4. The Changes of Flood Duration Parameter Impact to the Designed Flood Flow. To further understand the flood frequency characteristics, the moving samples of finite length (30 years) were analysed, and it can be observed that variance and low-frequency quantiles, particularly of short-duration flood, are generally an increasing function of time. Taking Lishi station as a case study, the change process of $Q_{100}(d = 5)$ values corresponding to return periods of 100 years and parameters of QDF model was obtained (Figure 5). For the same design level P, the design value significantly altered over time. In this case, the TVM non-stationary model cannot catch the jumping of point for non-stationary flood series resulting in the distortion risk in design frequency.

On the contrary the parameter Δ shows a significant decreasing trend (Figure 5). Other parameters of the QDF model have demonstrated similar behavior with significant alterations over time. The impacts of parameters on distribution curve showed an overall performance as upper tail from "gentle" to "steep" (Figure 3), and the design flood magnitude will become larger. Generally, the original flood duration of Lishi Station in Wujiang River has a decreasing trend at the 10% significant level during the period from 1956 to 2009 (Figure 6). The trend of original flood duration is identical with the change process of parameter Δ using moving samples of finite length (30-year). Therefore, the change of flood duration is the main factor leading to the change of design flow by QDF model.

5. Discussions

It would be more important to investigate possible causes behind changes of hydrological extremes after 1990s, which can be attributed to the impact of climate change and human activities.

5.1. Relationship between Flood Flow and Precipitation. As the rainfall is the primary source of stream flow, we investigated the possible relationship between annual maximum stream flow and corresponding basin rainfall. After 1990s, the total precipitation amount and frequency of rainstorms in the Wujiang River basin are in evidently increasing tendency (Figure 7). On the contrary, the duration of precipitation is in slightly decreasing tendency, indicating that after 1990s, both the amount and intensity of precipitation are in evidently increasing tendency (Figure 7). The 1990s are characterized by highly frequent floods due to increased rainstorm in this time interval. Therefore, spatiotemporal distribution of precipitation changes and rainstorm is still the major cause behind the occurrence of flood events in the region.

5.2. Relationship between Flood Flow and Human Influences. To a certain extent, changes in annual runoff coefficient reflect human influences on the relationship of rainfall and runoff in the basin. CSDMC test was used to identify nonstationarity and change point of annual runoff coefficient in the Wujiang River. The change point of annual runoff coefficient is found in 1991. To better understand the possible relationship between the annual maximum flood flow and land cover, we also collected the land cover information during

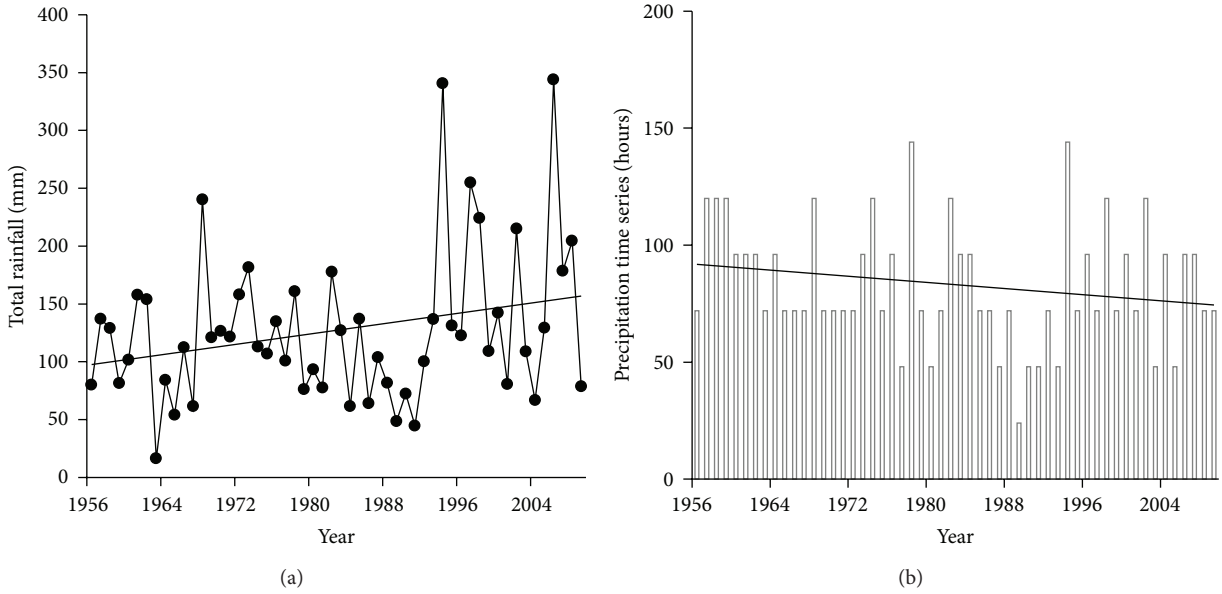

Figure 7: Change process of the corresponding basin rainfall of flood flow (a) and rainfall durations (b) in Wujiang River.

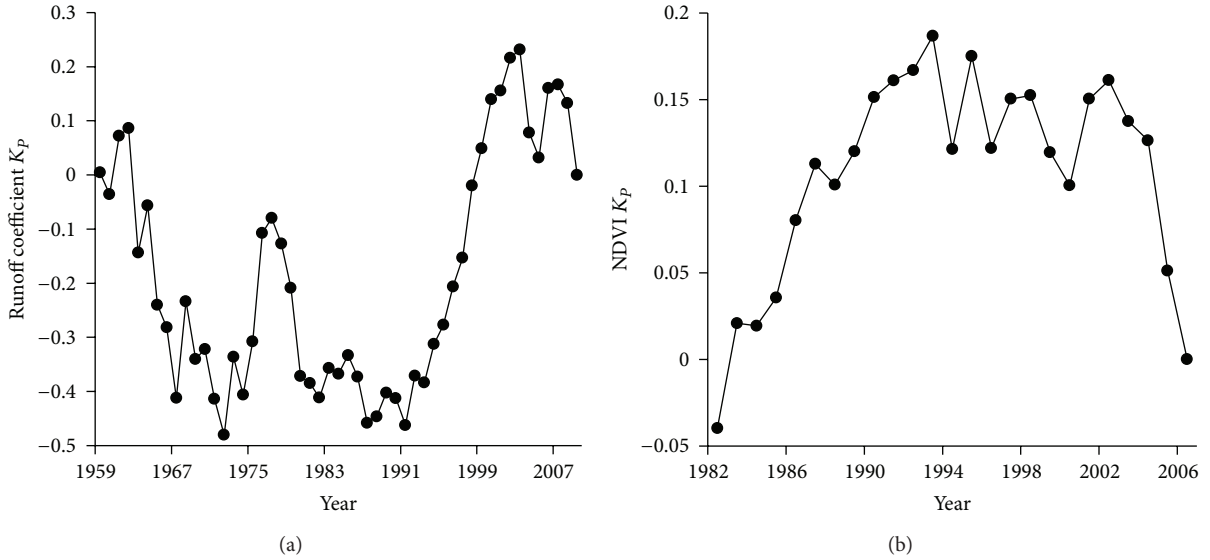

Figure 8: Cumulative Sum of Departures of Modulus Coefficient test of annual runoff coefficient (a) and NDVI (b) series in Wujiang River.

1981–2006 (Normalized Difference Vegetation Index: NDVI) (Figure 8). NDVI reflects the overall information for the ground vegetation. The data are from Global Inventory Modeling and Mapping Studies [25]. Note that the ground vegetation has a decreasing trend and with a change point in 1991 (see Figure 8), causing more quick flow and therefore strengthening flood events. So, land use change can be attributed as another reason affecting extreme hydrological events.

With the aim to explore impacts of water conservancy regulation on hydrological extremes, detailed information about water conservancy was collected. There are few reservoirs in the Wujiang River basin, and majority of which are mainly for agricultural irrigation, rather than for flood control. Furthermore, most water reservoirs were built along the tributaries, which greatly limits the flood control function of the water reservoirs. Thus, the flood control effects of the water reservoirs are not evident in general sense in this catchment. In the study conducted by Miller et al. [26] for 17 river basins in the UK, it is shown that the lakes have had a considerable impact on estimates of flood frequency and associated uncertainty.

Increasing meteorological extremes and enhancing precipitation intensity due to altered hydrological cycle may have

Table 4: Designed maximum flood flow $Q(d = 5)$ (m^3/s) and related return periods before and after environment change in Wujiang River.

Station	Distribution	Length of series	$T = 5$	$T = 10$	$T = 25$	$T = 50$	$T = 70$	$T = 100$
Pingshi	GLO	1964 ~ 1991	836.75	1001.95	1241.19	1447.35	1557.19	1681.49
		1964 ~ 2008	951.67	1180.43	1541.16	1877.61	2065.86	2286.11
Lishi	GLO	1956 ~ 1991	1566.15	1800.44	2100.47	2330.89	2445.16	2568.42
		1956 ~ 2009	1746.75	2147.87	2759.51	3312.53	3616.06	3966.57

the potential to intensify the flood events across the Wujiang River basin. Thus, flood control should be enhanced by construction of water reservoirs to reduce the risk of flooding.

6. Conclusions

In this study, extremes events are analysed based on the daily streamflow and peak flood dataset at Pingshi and Lishi hydrological stations using QDF model. Results indicate that GLO distribution is the right choice in the description of probability behaviours of extremes events in the Wujiang River basin. Besides, trends and change point of annual maximum flood flow and flood duration are investigated by statistical testing methods including the M-K test and the CSDMC technique.

From the trend analysis, it was found that the annual maximum flood flow only had marginally increasing trend, whereas the flood duration exhibited a decreasing trend at the 10% significant level. The change point for the annual maximum flood flow series was found in year 1991, and after which the mean maximum flood flow increased by 45.26%.

The 1990s are characterized by more frequent floods due to increased rainstorm in this time interval. Vegetation reduction in the basin magnified the increasing tendency of annual maximum flow for the period.

Due to the change of hydrologic regimes the flood return period estimated from data series before the change point does not apply properly to the period after the change point. The impacts on curve fitting of flood series showed an overall performance as upper tail from "gentle" to "steep," and the design flood magnitude will become larger. Therefore, nonstationary frequency analysis for the series with sudden change point is highly recommended for future studies.

Higher probability of floods will lead to serious challenges for flood control. More efforts should be paid to enhance human mitigation to floods in the Wujiang River basin.

Acknowledgments

The research is financially supported by the National Natural Science Foundation of China (Grants nos. 51210013, 50839005, and 51190091), the Public Welfare Project of Ministry of Water Resources (Grants nos. 201201094, 201301002-02), and the project from Guangdong Science and Technology Department (Grant no. 2010B050300010), the project from Guangdong Water Resources Department (Grant no. 2009-39). A collaborative contribution by the CSIRO Computation and Simulation Sciences Transformational Capability Platform is also acknowledged.

References

[1] P. Javelle, T. B. M. J. Ouarda, M. Lang, B. Bobée, G. Galéa, and J. M. Grésillon, "Development of regional flood-duration-frequency curves based on the index-flood method," *Journal of Hydrology*, vol. 258, no. 1–4, pp. 249–259, 2002.

[2] L. Brandimarte and G. Di Baldassarre, "Uncertainty in design flood profiles derived by hydraulic modelling," *Hydrology Research*, vol. 43, no. 6, pp. 753–761, 2012.

[3] D. Faulkner, C. Keef, and J. Martin, "Setting design inflows to hydrodynamic flood models using a dependence model," *Hydrology Research*, vol. 43, no. 5, pp. 663–674, 2012.

[4] A. I. Vornetti and R. S. Seoane, "Derived flood frequency distribution and sensitivity analysis to variations in model parameters," *Hydrology Research*, vol. 43, no. 3, pp. 249–261, 2012.

[5] A. Reihan, J. Kriauciuniene, D. Meilutyte-Barauskiene, and T. Kolcova, "Temporal variation of spring flood in rivers of the Baltic States," *Hydrology Research*, vol. 43, no. 4, pp. 301–314, 2012.

[6] J. M. Cunderlik and T. B. M. J. Ouarda, "Regional flood-duration-frequency modeling in the changing environment," *Journal of Hydrology*, vol. 318, no. 1–4, pp. 276–291, 2006.

[7] NERC, "Estimation of flood volumes over different durations," in *Flood Studies Report*, vol. 1, chapter 5, pp. 243–264, 1975.

[8] J. M. Sherwood, "Estimation of volume-duration-frequency relations of ungauged small urban streams in Ohio," *Water Resources Bulletin*, vol. 30, no. 2, pp. 261–269, 1994.

[9] J. B. Balocki and S. J. Burges, "Relationships between n-day flood volumes for infrequent large floods," *Journal of Water Resources Planning & Management*, vol. 120, no. 6, pp. 794–818, 1994.

[10] M. Meunier, "Regional flow-duration-frequency model for the tropical island of Martinique," *Journal of Hydrology*, vol. 247, no. 1-2, pp. 31–53, 2001.

[11] L. Mar, P. Gineste, M. Hamattan, A. Tounkara, L. Tapsoba, and P. Javelle, "Flood-duration-frequency modeling applied to big catchments in Burkina Faso," in *Proceedings of the 4th FRIEND International Conference*, Cape Town, South Africa, March 2002.

[12] R. Mic, G. Galee a, and P. Javelle, "Floods regionalization of the Cris catchments: application of the converging QDF modeling concept to the Pearson III law," in *Proceedings of the Conference of the Danube countries*, Bucharest, Romania, September 2002.

[13] J. J. M. Delgado, H. Apel, and B. Merz, "Flood trends and variability in the Mekong river," *Hydrology and Earth System Sciences*, vol. 14, pp. 407–418, 2010.

[14] W. G. Strupczewski, V. P. Singh, and W. Feluch, "Non-stationary approach to at-site flood frequency modelling I. Maximum likelihood estimation," *Journal of Hydrology*, vol. 248, no. 1–4, pp. 123–142, 2001.

[15] M. N. Khaliq, T. B. M. J. Ouarda, J. C. Ondo, P. Gachon, and B. Bobée, "Frequency analysis of a sequence of dependent and/or non-stationary hydro-meteorological observations: a review," *Journal of Hydrology*, vol. 329, no. 3-4, pp. 534–552, 2006.

[16] R. M. Vogel, C. Yaindl, and M. Walter, "Nonstationarity: flood magnification and recurrence reduction factors in the united states," *Journal of the American Water Resources Association*, vol. 47, no. 3, pp. 464–474, 2011.

[17] G. Villarini, J. A. Smith, F. Serinaldi, J. Bales, P. D. Bates, and W. F. Krajewski, "Flood frequency analysis for nonstationary annual peak records in an urban drainage basin," *Advances in Water Resources*, vol. 32, no. 8, pp. 1255–1266, 2009.

[18] A. R. Rao and K. H. Hamed, *Flood Frequency Analysis.*, CRC Press, Boca Raton, Fla, USA, 2000.

[19] R. D. Reiss and M. Thomas, *Statistical Analysis of Extreme Values: With Applications to Insurance, Finance, Hydrology and Other Fields*, Birkäuser, Boston, Mass, USA, 2001.

[20] H. Hurst, "Long term storage capacity of reservoirs," *Transactions of the American Society of Civil Engineers*, vol. 116, pp. 770–799, 1951.

[21] C. A. McGilchrist and K. D. Woodyer, "Note on a distribution-free CUSUM technique," *Technometrics*, vol. 17, no. 3, pp. 321–325, 1975.

[22] M. G. Kendall, *Rank Correlation Methods*, Griffin, London, UK, 1975.

[23] H. B. Mann, "Nonparametric tests against trend," *Econometrica*, vol. 13, pp. 245–259, 1945.

[24] H. Akaike, "A new look at the statistical model identification," *IEEE Transactions on Automatic Control*, vol. 19, no. 6, pp. 716–722, 1974.

[25] C. J. Tucker, J. E. Pinzon, M. E. Brown et al., "An extended AVHRR 8-km NDVI data set compatible with MODIS and SPOT vegetation NDVI data," *International Journal of Remote Sensing*, vol. 26, no. 20, pp. 4485–5598, 2005.

[26] J. D. Miller, T. R. Kjeldsen, J. Hannaford, and D. G. Morris, "A hydrological assessment of the November 2009 floods in Cumbria, UK," *Hydrology Research*, vol. 44, no. 1, pp. 180–197, 2013.

Hindawi Publishing Corporation
Mathematical Problems in Engineering
Volume 2013, Article ID 724632, 7 pages
http://dx.doi.org/10.1155/2013/724632

Research Article

Uncertainty Assessment of Hydrological Frequency Analysis Using Bootstrap Method

Yi-Ming Hu,[1,2] Zhong-Min Liang,[1,2] Bin-Quan Li,[1,2] and Zhong-Bo Yu[1,2,3]

[1] *State Key Laboratory of Hydrology-Water Resources and Hydraulic Engineering, Hohai University, Nanjing 210098, China*
[2] *College of Hydrology and Water Resources, Hohai University, Nanjing 210098, China*
[3] *Department of Geoscience, University of Nevada Las Vegas, Las Vegas, NV 89154, USA*

Correspondence should be addressed to Zhong-Min Liang; zmliang@hhu.edu.cn

Received 29 December 2012; Accepted 8 May 2013

Academic Editor: Yongping Li

The hydrological frequency analysis (HFA) is the foundation for the hydraulic engineering design and water resources management. Hydrological extreme observations or samples are the basis for HFA; the representativeness of a sample series to the population distribution is extremely important for the estimation reliability of the hydrological design value or quantile. However, for most of hydrological extreme data obtained in practical application, the size of the samples is usually small, for example, in China about 40~50 years. Generally, samples with small size cannot completely display the statistical properties of the population distribution, thus leading to uncertainties in the estimation of hydrological design values. In this paper, a new method based on bootstrap is put forward to analyze the impact of sampling uncertainty on the design value. By bootstrap resampling technique, a large number of bootstrap samples are constructed from the original flood extreme observations; the corresponding design value or quantile is estimated for each bootstrap sample, so that the sampling distribution of design value is constructed; based on the sampling distribution, the uncertainty of quantile estimation can be quantified. Compared with the conventional approach, this method provides not only the point estimation of a design value but also quantitative evaluation on uncertainties of the estimation.

1. Introduction

Estimations of flood frequency and magnitude are required for hydraulic engineering design, water resources planning, and management, for example, [1]. They involve the sampling of a sample series, the selection of a population distribution represented usually by a probability density function (pdf) where the samples are coming from, and the estimation of parameters of the pdf. The occurrences of various sources of errors in the above-mentioned procedure result in the existence of uncertainties in the final estimation of the hydrological design value. Among these errors, the sampling error, that is, an error due to the fact that the short of sample length is always taken as the main contribution to the significance of estimation uncertainties.

During the past several decades, studies on uncertainty analysis of the estimation for hydrological design value mainly have focused on the selection of the type of a pdf and the estimation of parameters of the pdf. The conventional method of moment (MOM) was once a widely used approach for parameter estimation, but Wallis et al. [2] and Kirby [3] showed that MOM bears high bias and is subjected to algebraic bounds, which indicated that MOM may bring extra uncertainties to quantile estimations. In order to improve the accuracy of parameter estimation and reduce uncertainties on quantile estimates, various parameter estimation approaches have been developed such as maximum Likelihood estimators (ML), probability-weighted moment [4], and linear-moment method (L-M) [5]; the regional frequency analysis method, which combines the information of single site and hydrological similar neighboring sites to decrease the uncertainty of hydrological design values at single site, also have been applied [6, 7]. In the view of assessing the uncertainty of the hydrological frequency analysis, Wood and

Rodriguez-Iturbe [8, 9] analyzed the impact of parameter uncertainties on the uncertainty of the design value based on Bayes method. Later, they proposed a theoretical framework for the uncertainty assessment of design values by coupling uncertainties from both the selection of a population distribution and the estimation of distribution parameters. However, due to the limitation of computation technique, they only analyzed the uncertainties of the design values based on a few simple probability distributions, such as normal distribution and lognormal distribution. Merz and Thieken [10] analyzed natural and epistemic uncertainties in flood frequency analysis, and they found that the former cannot be reduced, but the latter can be reduced by more knowledge. Reis and Stedinger [11] applied a fully Bayesian approach to provide an accurate description of flood risk and parameter uncertainties for flood quantiles. Ribatet et al. [12] developed a regional Bayesian POT model to reduce the estimation uncertainty considering the fact that the size of the sample is small. Lee and Kim [13] employed the Bayesian Markov Chain Monte Carlo (MCMC) method and the maximum likelihood estimation (MLE) to assess uncertainties of low-flow frequency analysis. Zhongmin et al. [14, 15] applied the Bayesian theory to separately analyze the impact of parameters uncertainty and both frequency model and parameters uncertainties on the uncertainties of estimation of design value or quantile.

However, studies on the impact of the sample representativeness on the uncertainty of design value estimation have been seldom reported. In this paper, considering the fact that the small size sample cannot perfectly reflect the statistical properties of the population distribution and it may cause uncertainties on design value estimation, we proposed a new approach based on bootstrap technique to analyze the impact of sampling uncertainty on the design value. The bootstrap method has been widely used for uncertainty analysis in hydrology. For example, Zucchuni and Adamson [16] applied the bootstrap method to estimate the confidence intervals of the design storms from exceedance series. Overeem et al. [17] applied the bootstrap method to analyze the uncertainty of rainfall depth-duration-frequency (DDF) curves and obtained 95% confidence bands of the DDF curves. They utilized the bootstrap-based artificial neural networks to investigate the uncertainty of flood forecasting.

In this paper, by bootstrap technique, resampling from the original flood extreme observations, a large number of bootstrap samples are constructed, on which the corresponding design value or quantile is estimated for each bootstrap sample, and then the distribution of estimation of the design value with some probabilities can be obtained. This method obtains the sampling distributions of design values; therefore, it can afford not only the point estimation as a conventional method does but also the quantitative evaluation on uncertainty of hydrological frequency analysis. As an example, annual precipitation series in the Kunming municipal area, China was applied to validate the proposed approach in this paper.

Throughout the following sections of this paper, the bootstrap method will be described first, and then the method considering the impact of the sample representativeness on the uncertainty of design value estimation will be outlined in Section 3. Then, Section 4 presents an example and result analysis. Finally, Section 5 presents concluding remarks.

2. Description of Bootstrap Method

The bootstrap method, a resampling technique, was introduced and named by Efron [18, 19]. The idea behind bootstrap is that sample values are the best guide to the underlying true distribution even when the information about the true distribution is lacking. It does not need the assumption of the true distribution and only depends on the obtained sample values. N groups of bootstrap samples can be generated by resampling from the original sample repeatedly. Then, based on these bootstrap samples, N estimations of the statistical parameter (mean, variance, etc.) can be derived. Finally, the distribution of the parameter is then approximated by N estimated values.

Resampling from the original sample is the essence of the bootstrap method. Assuming that $X = (x_1, x_2, \ldots, x_n)$ is an original sample; based on the sample, the empirical distribution F_n can be described as follows:

$$F_n = \begin{cases} 0, & x < x_{(1)}, \\ \dfrac{k}{n}, & x_{(k)} \le x < x_{(k+1)}, \\ 1, & x \ge x_{(k)}. \end{cases} \tag{1}$$

By resampling from the distribution F_n, the same size sample $X^* = (x_1^*, x_2^*, \ldots, x_n^*)$ can be obtained. Based on the bootstrap sample X^*, an estimation θ^* of parameter θ of the distribution function can be calculated.

Repeating the bootstrap sampling for N times, N groups of bootstrap samples can be obtained, $X^{*(j)} = (x_1^{*(j)}, x_2^{*(j)}, \ldots, x_n^{*(j)})$, $j = 1, 2, \ldots, N$, and N estimations of parameter θ can be derived, $\theta^{*(j)}$, $j = 1, 2, \ldots, N$.

Taking the $\theta^{*(j)}$, $j = 1, 2, \ldots, N$ as the sample of the unknown parameter θ, we can obtain the distribution of parameter θ. Based on the distribution, point estimation or interval estimation of parameter θ can be derived.

3. Considering the Impact of Sample Representativeness on Design Value Uncertainty

In the procedure of hydrological frequency analysis, numbers of extreme events or sample sizes are usually not large enough, so that estimations of hydrological design values based on the limited sample information inevitably come into being uncertainties. How to assess the uncertainties is a key issue because they are relevant to the safety of hydraulic engineering works. In this section, bootstrap method is applied to resample from the original sample to derive the distribution of estimation of design value corresponding to some nonexceedance probabilities, and based on the distribution, the impact of sampling uncertainty on hydrological frequency analysis results can be assessed.

In China, Person-type three probability distributions (*P*-III) are widely used for hydrological frequency analysis. A *P*-III function contains three parameters, that is, mean value E_x, coefficient of deviation C_v, and coefficient of skew C_s. Assuming that $X = (x_1, x_2, \ldots, x_n)$ is a hydrological extreme sample series, E_x, C_v, C_s represent the three population parameters and x_p the design value or quantile of the population distribution corresponding to a nonexceedance probability p; $\widehat{E}_x^{(j)}$, $\widehat{C}_v^{(j)}$, $\widehat{C}_s^{(j)}$ denote the estimations of E_x, C_v, C_s, respectively, by the jth resampled series, and $\widehat{x}_p$ is the estimation of x_p. The bootstrap procedure for assessing the impact of a sample on the uncertainty of quantile estimation can be described as follows.

(1) Resampling from the original sample $X = (x_1, x_2, \ldots, x_n)$ for N time, N groups of bootstrap samples $X^{*(j)} = (x_1^{*(j)}, x_2^{*(j)}, \ldots, x_n^{*(j)})$, $j = 1, 2, \ldots, N$ can be obtained.

(2) Using the linear-moment method (L-M) to estimate parameters E_x, C_v, C_s, gaining N estimations $\widehat{E}_x^{(j)}$, $\widehat{C}_v^{(j)}$, $\widehat{C}_s^{(j)}$, $j = 1, 2, \ldots, N$.

(3) Based on the N groups of $\widehat{E}_x^{(j)}$, $\widehat{C}_v^{(j)}$, $\widehat{C}_s^{(j)}$, $j = 1, 2, \ldots, N$, the N estimations of design value or quantile $\widehat{x}_p^{(j)}$, $j = 1, 2, \ldots, N$ can be acquired.

(4) Taking the $\widehat{x}_p^{(j)}$, $j = 1, 2, \ldots, N$ as the sampling series of x_p, we can obtain the sampling distribution of x_p, on which point estimation or interval estimation of x_p can be derived.

4. Case Study

4.1. Study Region and Data. The annual precipitation series from 1951 to 2010 in Kunming municipal area was applied to validate the proposed method in this paper. Kunming, capital of Yunnan province, is located in the middle of the Yunnan-Guizhou Plateau in southwest China, with a latitude of 24.23~26.22 N and a longitude of 102.10~103.40 E. The city area is about 21473 km^2. It belongs to the subtropical monsoon climate, mild and humid, with four distinct seasons. In the history, its highest and lowest extreme temperatures are 31.2°C and −7.8°C, with annual average temperature about 15°C. Annual precipitation distribution is uneven; that is, precipitation in the rainy season from May to October accounts for about 85% of the 1000 mm average annual precipitation, while precipitation in the dry season from November to April accounts for only about 15%.

4.2. Precipitation Series Analysis. Considering the fact that frequency analysis is based on the assumption that the hydrological time series is stationary, statistically independent and identically distributed (iid), trend test and change-point detection for the annual precipitation series of Kunming city are necessary. The annual precipitation time series was presented in Figure 1. From Figure 1, the linear regression trend of precipitation time series has not been detected, which shows that the series is stationary.

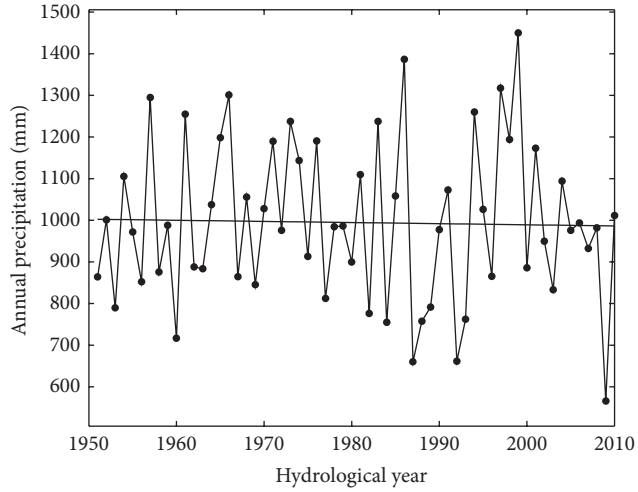

Figure 1: Temporal trend of annual precipitation in Kunming municipal area from 1951 to 2010: the straight line is the trend line of the observation series.

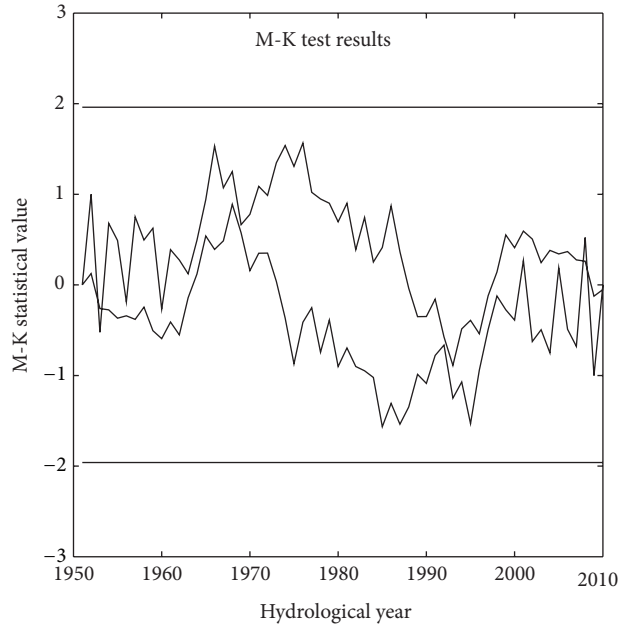

Figure 2: Trend detection by Mann-Kendall test for the annual precipitation time series of Kunming, China: the straight lines represent the boundary condition of the M-K test with the significance level $\alpha = 0.05$, and the related threshold values are ±1.96. The sample M-K statistical value is between −1.96 and 1.96, which implies that the annual precipitation series does not have a mutation trend.

In order to further analyze the mutation trend, the Mann-Kendall (M-K) nonparametric test method, widely used for trend test and change-point detection, was applied [20, 21]. The M-K test results were shown in Figure 2. In the M-K test, the significance level $\alpha = 0.05$, and the threshold values of the statistical test of Mann-Kendall are ±1.96. Figure 2 shows that the sample M-K statistical value is between −1.96 and 1.96. It implies that the annual precipitation series does not

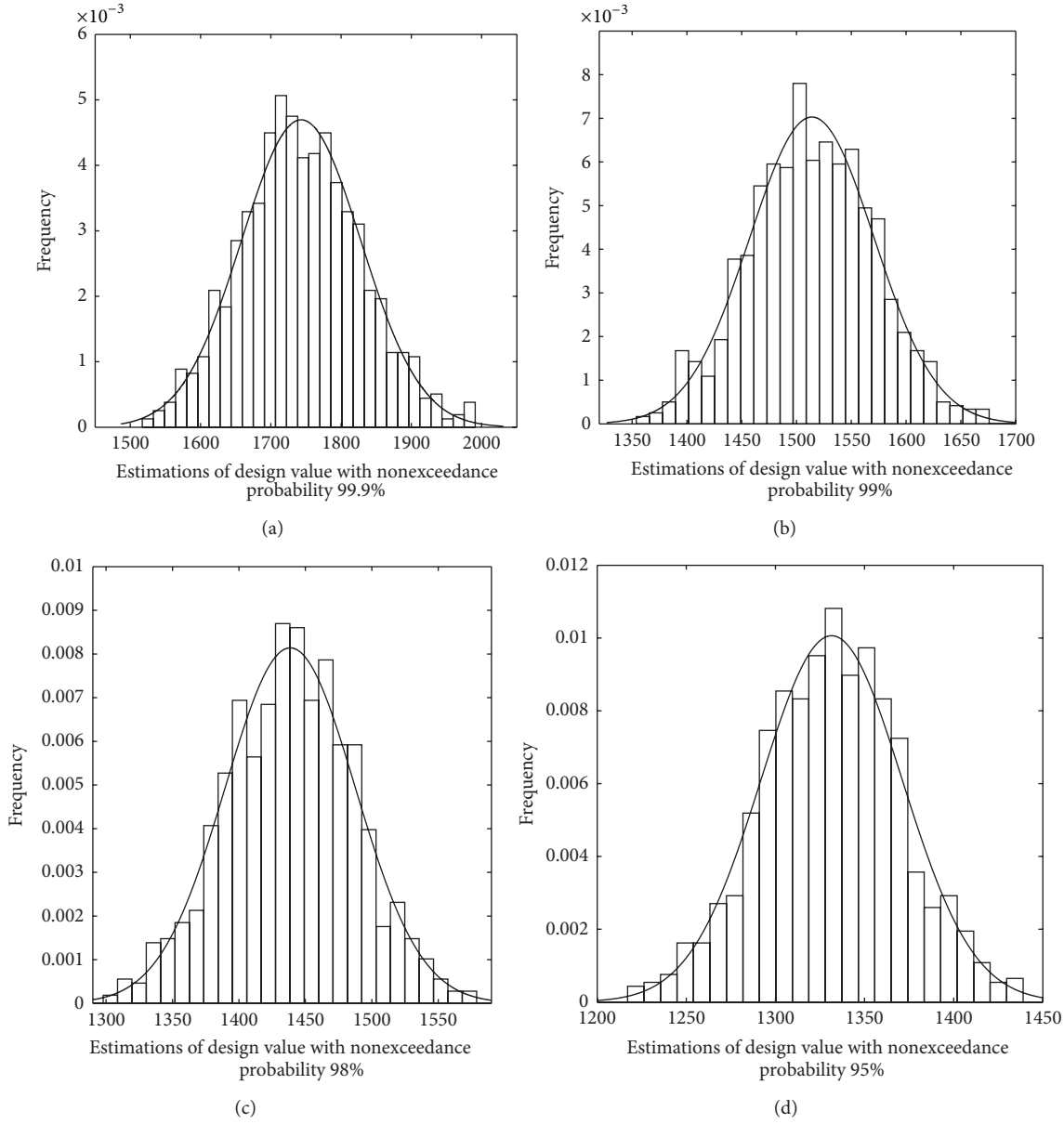

Figure 3: Frequency histogram of estimations of the design value x_p with nonexceedance probabilities 99.9%, 99%, 98%, and 95%. The curve is normal density function.

have a mutation trend. The analyses above indicate that the precipitation time series can be taken as a stationary and iid sample.

4.3. Design Value Estimation Considering Sample Uncertainty. According to Section 3, by resampling from the annual precipitation series, N groups of bootstrap samples can be obtained. Considering the fact that the lower limit of a Pearson-III distribution is a negative number when the value C_s/C_v is less than 2.0; in the process of resampling, those bootstrap samples whose value C_s/C_v is equal or greater than 2.0 were selected, and the total sets are $N = 1000$. L-M method was applied for estimations of the parameters E_x, C_s, C_v, and N estimations $\widehat{E}_x^{(j)}$, $\widehat{C}_v^{(j)}$, $\widehat{C}_s^{(j)}$, $j = 1, 2, \ldots, N$ can be obtained. In combination with the Pearson-III distribution, N estimates $\widehat{x}_p^{(j)}$, $j = 1, 2, \ldots, N$ of the design value x_p corresponding to nonexceedance probability P can be calculated. By the N estimations $\widehat{x}_p^{(j)}$, $j = 1, 2, \ldots, N$, the distribution of x_p can be approximated. Figure 3 presented the frequency histograms of the design values x_p with P = 99.9%, 99%, 98%, and 95%. Intuitively from these figures, a normal distribution may match well with the frequency histograms.

Normal probability plot was used to test whether the sampling distribution of x_p matches with a normal distribution. Figures 3 and 4 demonstrate, respectively, the fitting of a normal frequency curve to the empirical frequency data of $\widehat{x}_p^{(j)}$, $j = 1, 2, \ldots, N$, it is shown that plots uniformly distribute

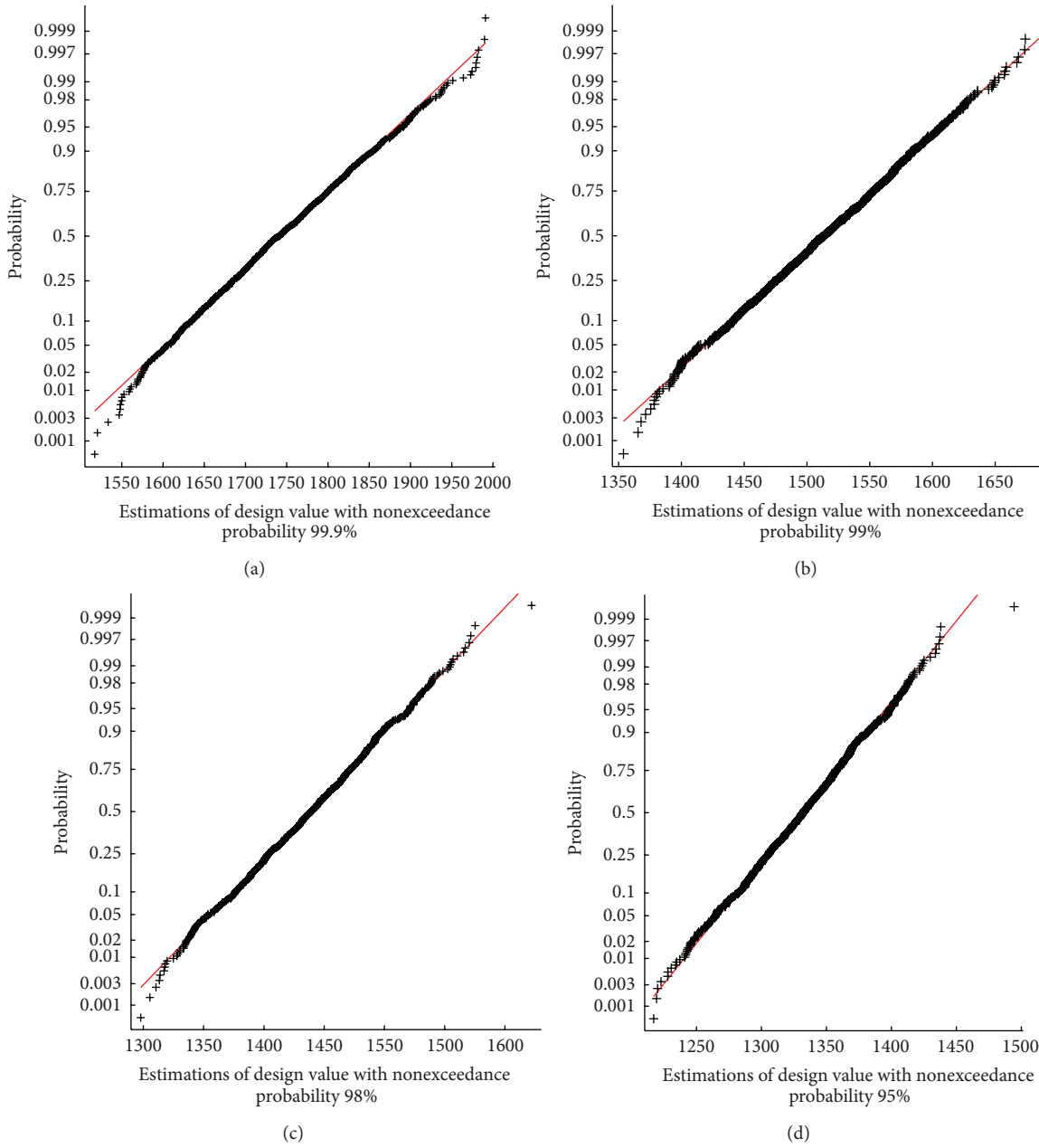

FIGURE 4: Normal probability plot of estimations of the design value x_p with nonexceedance probabilities 99.9%, 99%, 98%, and 95%: the symbol "+" is normal probability plot reflecting the relationship of the estimation of design value and the related normal quantile; the straight line is the fitted line of the normal probability plots; from Figure 4, it can be seen that plots uniformly distribute in the vicinity of the straight line, which means that the sampling distribution of design value x_p can be approximated by a normal probability distribution.

in the vicinity of the normal frequency line. Therefore, the sampling distribution of design value x_p can be approximated by a normal probability distribution. Similarly, sampling distributions of x_p with any nonexceedance probability p can be estimated.

Upon attaining the sampling distribution of x_p, hydrological frequency analysis based on the sampling distributions can be conducted as illustrated by Figure 5. Different from the conventional hydrological frequency analysis that provides only a point or a unique estimation of x_p, the method proposed in this study provides the sampling distribution of x_p. That is to say, for a specific unknown population x_p, there exists its infinite estimates, $\widehat{x}_p$, and these estimates form the sampling distribution of x_p. It is this distribution that provided the entire information about x_p; accordingly, the estimation or inference on x_p should rely on this distribution. For example, the expectation value of the sampling distribution Ex_p can replace the point estimation of any conventional

Table 1: Estimation of design value x_p.

Nonexceedance Probability p (%)	Bootstrap method					Curve-fitting method
	Sampling distribution of x_p	Ex_p (mm)	$CI_{90\%}$	CIL	SD	Point estimation (mm)
99.9	$X_{99.9\%} \sim N(1748,89)$	1748	[1601,1895]	294	89	1704
99	$X_{99\%} \sim N(1517,59)$	1517	[1420,1615]	195	59	1497
98	$X_{98\%} \sim N(1441,51)$	1441	[1357,1525]	168	51	1427
95	$X_{95\%} \sim N(1333,41)$	1333	[1265,1401]	136	41	1328

Notation: Ex_p is the expectation of the sampling distribution of x_p, and SD is its standard deviation; $CI_{90\%}$ is the 90% confidence intervals, and $CIL_{90\%}$ is its length.

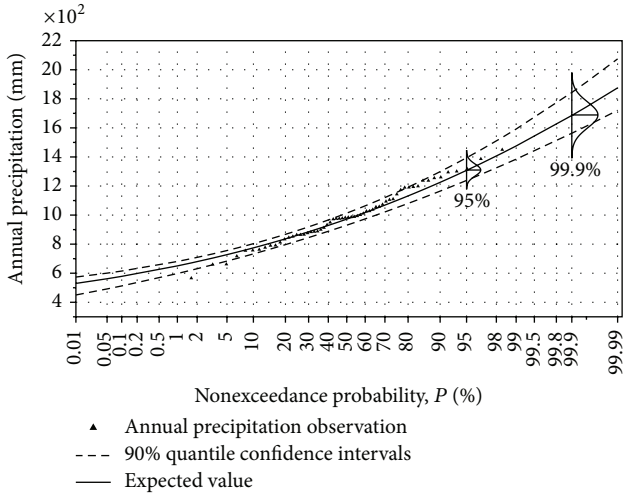

Figure 5: Estimation of x_p by bootstrap method for annual precipitation in Kunming municipal area: the first small figure denoted that 95% is the distribution of estimations of the design value with the nonexceedance 95%; the second small figure denoted that 99.9% is the distribution of estimations of the design value with the nonexceedance 99.9%.

method, while the confidence interval can be used to evaluate the uncertainties of hydrological frequency analysis with the given original samples.

The characteristics of the sampling distribution of the design value x_p for the 4 specific nonexceedance probabilities are summarized in Table 1, including the expectation Ex_p, standard deviation SD, and 90% confidence intervals $CI_{90\%}$ and its length $CIL_{90\%}$. For comparison, the corresponding point estimations of x_p from a conventional approach, namely, curve-fitting method, are also included. The curve-fitting method is a widely applied procedure in China for hydrological frequency analysis. From Table 1, it seems that there is no big gap between the expectation value Ex_p of sampling distribution and the point estimation of curve-fitting method for the four cases of nonexceedance probabilities. However, compared to the curve-fitting approach, the bootstrap method affords more information about the estimation. For example, with the increase of design standard or nonexceedance probability, the value of SD and $CIL_{90\%}$ is getting larger, ranging from 41 to 89 and from 136 to 294, respectively, which implies that the uncertainty of the estimation of design value with the rare probability will be much larger, so that it is necessary to provide quantitative uncertainty assessment for the estimation of the design value.

5. Summary and Conclusion

The sample size of hydrological extreme events in practical application is usually not large enough to guarantee that a reliable estimation is always obtained. Hence, for a given sample series, how to improve the estimation and evaluate quantitatively the uncertainty of the estimation is of use to the design of hydraulic engineering works. In this study, a new method based on bootstrap is put forward to analyze the impact of sampling uncertainty on the design value, which is not restricted to the probability models. Through resampling from the original sample series, the sampling distribution of the design value x_p or quantile is available, by which x_p could be estimated in a new manner. Compared to the conventional hydrological frequency analysis methods, such as the curve-fitting method, the proposed bootstrap-based method can provide not only the point estimation of x_p as the curve-fitting does but also afford more abundant information about the estimation; the uncertainties of the estimation on x_p could also be assessed by either the standard deviation SD of the sampling distribution or the confidence interval CI derived from the sampling distribution.

As an example, annual precipitation data in Kunming municipal area were used to validate the proposed method in this paper. As illustrated by Figure 5, the sampling distribution of x_p for any nonexceedance probability p was estimated by resampling, on which the expectation values of the sampling distribution can be used as the conventional point estimation, while the confidence interval can be the indicator to evaluate uncertainties of the estimation. Comparisons between the bootstrap and curve-fitting approaches (see Table 1) for 4 specific cases of P = 99.9%, 99%, 98%, and 95% indicate that, notwithstanding, there is almost no gap between point estimations of curve fitting and expectation values of bootstrap-based approach; the other features of the sampling distribution, such as the SD and $CI_{90\%}$ and its length $CIL_{90\%}$, provide the designers with extra information to assess the reliability of the design values to be adopted.

As we all know, uncertainties of estimation on design value x_p originate unreliabilities from the sample, the statistical model, and the parameter; this study addressed only the impact of sampling on the estimation uncertainties of x_p.

Although the bootstrap-based method was performed to *P*-III probability distribution, the procedure is capable of being applied to any other probability models. In this paper, due to the restriction of resampling condition, that is, considering the fact that the lower limit of a Pearson-III distribution is a negative number when the value C_s/C_v is less than 2.0, in the process of resampling, those bootstrap samples whose value C_s/C_v is equal or greater than 2.0 were selected, and the conclusions may not be applicable for other probability models because they do not have this restriction.

Acknowledgments

This study was supported by the Major Program of the National Natural Science Foundation of China (Grant no. 51190095), the National Basic Research Program of China (also called 973 Program, Grant no. 2010CB951102), and the National Natural Science Foundation of China (Grant no. 51079039 and 51179046). The authors wish to thank the referee, whose suggestions help them to improve the paper.

References

[1] J. R. Stedinger, R. M. Vogel, and E. Foufula-Georgiou, "Frequency analysis of extreme events," in *Handbook of Hydrology*, R. Maidment, Ed., chapter 18, pp. 18. 1–18. 66, McGraw-Hill, New York, NY, USA, 1992.

[2] J. R. Wallis, N. C. Matalas, N. C. Matas, and J. R. Slack, "Just a moment!," *Water Resources Research*, vol. 10, pp. 211–219, 1974.

[3] W. Kirby, "Algebraic boundedness of sample statistics," *Water Resources Research*, vol. 10, no. 2, pp. 220–222, 1974.

[4] J. A. Greenwood, J. M. Landwehr, N. C. Matalas, and J. R. Wallis, "Probability weighted moments: definition and relation to parameters of several distributions expressable in inverse form," *Water Resources Research*, vol. 15, no. 5, pp. 1049–1054, 1979.

[5] J. R. M. Hosking, "L-moments: analysis and estimation of distributions using linear combinations of order statistics," *Journal of the Royal Statistical Society B*, vol. 52, no. 1, pp. 105–124, 1990.

[6] J. R. M. Hosking and J. R. Wallis, *Regional Frequency Analysis: An Approach Based on L-Moments*, Cambridge University Press, New York, NY, USA, 1997.

[7] G. Kuczera, "Combining site-specific and regional information: an empirical Bayes approach," *Water Resources Research*, vol. 18, no. 2, pp. 306–314, 1982.

[8] E. F. Wood and I. Rodriguez-Iturbe, "Bayesian inference and decision making for extreme hydrological events," *Water Resources Research*, vol. 11, no. 4, pp. 533–554, 1975.

[9] E. F. Wood and I. Rodriguez-Iturbe, "A Bayesian approach to analyzing uncertainty among flood frequency models," *Water Resources Research*, vol. 11, no. 6, pp. 839–843, 1975.

[10] B. Merz and A. H. Thieken, "Separating natural and epistemic uncertainty in flood frequency analysis," *Journal of Hydrology*, vol. 309, no. 1–4, pp. 114–132, 2005.

[11] D. S. Reis Jr. and J. R. Stedinger, "Bayesian MCMC flood frequency analysis with historical information," *Journal of Hydrology*, vol. 313, no. 1-2, pp. 97–116, 2005.

[12] M. Ribatet, E. Sauquet, J.-M. Grésillon, and T. B. M. J. Ouarda, "A regional Bayesian POT model for flood frequency analysis," *Stochastic Environmental Research and Risk Assessment (SERRA)*, vol. 21, no. 4, pp. 327–339, 2007.

[13] K. S. Lee and S. U. Kim, "Identification of uncertainty in low flow frequency analysis using Bayesian MCMC method," *Hydrological Processes*, vol. 22, no. 12, pp. 1949–1964, 2008.

[14] L. Zhongmin, L. Binquan, Y. Zhongbo et al., "Application of Bayesian approach to hydrological frequency analysis," *Science China Technological Sciences*, vol. 54, no. 5, pp. 1183–1192, 2011.

[15] L. Zhongmin, C. Wenjun, and L. Binquan, "Bayesian flood frequency analysis in the light of model and parameter uncertainties," *Stochastic Environmental Research and Risk Assessment*, vol. 26, pp. 721–730, 2012.

[16] W. Zucchuni and P. T. Adamson, "Bootstrap confidence intervals for design storms from exceedance series," *Hydrologicat Sciences*, vol. 34, no. 6, pp. 719–721, 1989.

[17] A. Overeem, A. Buishand, and I. Holleman, "Rainfall depth-duration-frequency curves and their uncertainties," *Journal of Hydrology*, vol. 348, no. 1-2, pp. 124–134, 2008.

[18] B. Efron, "Bootstrap methods: another look at the jackknife," *The Annals of Statistics*, vol. 7, no. 1, pp. 1–26, 1979.

[19] B. Efron, "Computers and the theory of statistics: thinking the unthinkable," *SIAM Review*, vol. 21, no. 4, pp. 460–480, 1979.

[20] K. H. Hamed, "Trend detection in hydrologic data: the Mann-Kendall trend test under the scaling hypothesis," *Journal of Hydrology*, vol. 349, no. 3-4, pp. 350–363, 2008.

[21] M. Gocic and S. Trajkovic, "Analysis of changes in meteorological variables using Mann-Kendall and Sen's slope estimator statistical tests in Serbia," *Global and Planetary Change*, vol. 100, pp. 172–182, 2013.

Hindawi Publishing Corporation
Mathematical Problems in Engineering
Volume 2013, Article ID 701923, 9 pages
http://dx.doi.org/10.1155/2013/701923

Research Article

Generalized Likelihood Uncertainty Estimation Method in Uncertainty Analysis of Numerical Eutrophication Models: Take BLOOM as an Example

Zhijie Li,[1] Qiuwen Chen,[1,2] Qiang Xu,[1] and Koen Blanckaert[1]

[1] *RCEES, Chinese Academy of Science, Beijing 100085, China*
[2] *China Three Gorges University, Yichang 443002, China*

Correspondence should be addressed to Qiuwen Chen; qchen@rcees.ac.cn

Received 17 February 2013; Accepted 7 May 2013

Academic Editor: Yongping Li

Uncertainty analysis is of great importance to assess and quantify a model's reliability, which can improve decision making based on model results. Eutrophication and algal bloom are nowadays serious problems occurring on a worldwide scale. Numerical models offer an effective way to algal bloom prediction and management. Due to the complex processes of aquatic ecosystem, such numerical models usually contain a large number of parameters, which may lead to important uncertainty in the model results. This research investigates the applicability of generalized likelihood uncertainty estimation (GLUE) to analyze the uncertainty of numerical eutrophication models that have a large number of intercorrelated parameters. The 3-dimensional primary production model BLOOM, which has been broadly used in algal bloom simulations for both fresh and coastal waters, is used.

1. Introduction

Eutrophication and algal bloom are serious problems occurring on a worldwide scale, which deteriorate the water qualities in many aspects, including oxygen depletion, bad smell, and production of scums and toxins. Accurate and reliable predictions of algal blooms are essential for early warning and risk mitigating. Numerical eutrophication models offer an effective way to algal blooms prediction and management. There exist several well-developed eutrophication models, such as CE-QUAL-ICM [1, 2], EUTRO5 [3–5], BLOOM [6–10], CAEDYM [11, 12], and Pamolare [13, 14]. The choice of the most appropriate model may depend on the specific research objectives and data availability.

Due to the complexity of algal bloom processes, these numerical models usually have a large number of parameters, which inevitably brings uncertainty to model results. Modeling practice typically includes model development, calibration, validation, and application, while uncertainty analysis is often neglected. Uncertainty analysis is essential in the assessment and quantification of the reliability of models. Prior to the use of model results, information about model accuracy and confidence levels should be provided to guarantee that results are in accordance with measurements [15] and that the model is appropriate for its prospective application [16]. There are three major sources of uncertainty in modeling systems: parameter estimation, input data, and model structure [17–21]. Understanding and evaluating these various sources of uncertainty in eutrophication models are of importance for algal bloom management and aquatic ecosystem restoration.

Several methods for parameter uncertainty analysis are available, for example, probability theory method, Monte Carlo analysis, Bayesian method, and generalized likelihood uncertainty estimation (GLUE) method. Probability theory method employs probability theory of moments of linear combinations of random variables to define means and variances of random functions. It is straightforward for simple linear models, while it does not apply to nonlinear systems [22]. The Monte Carlo analysis computes output statistics by repeating simulations with randomly sampled input variables complying with probability density functions. It is easily

implemented and generally applicable, but the results gained from Monte Carlo analysis are not in an analytical form and the joint distributions of correlated variables are often unknown or difficult to derive. [18, 20, 23]. Bayesian methods quantify uncertainty by calculating probabilistic predictions. Determining the prior probability distribution of model parameters is the key step in Bayesian methods [24]. GLUE is a statistical method for simultaneously calibrating the input parameters and estimating the uncertainty of predictive models [25]. GLUE is based on the concept of equifinality, which means that different sets of input parameter may result in equally good and acceptable model outputs for a chosen model [26]. It searches for parameter sets that would give reliable simulations for a range of model inputs instead of searching for an optimum parameter set that would give the best simulation results [27]. Furthermore, model performance in GLUE is mainly dependent on parameter sets rather than individual parameters, whence interaction between parameters is implicitly accounted for.

Beven and Freer [28] pointed out that in complex dynamic models that contain a large number of highly intercorrelated parameters, many different combinations of parameters can give equivalently accurate predictions. In consideration of equivalence of parameter sets, the GLUE method is particularly appropriate for the uncertainty assessment of numerical eutrophication models, which are an example of complex dynamic models with highly intercorrelated parameters [28–30].

The GLUE method has already been adopted for uncertainty assessments in a variety of environmental modeling applications, including rainfall-runoff models [25, 31, 32], soil carbon models of forest ecosystems [33], agricultural nonpoint source (NPS) pollution models [34], groundwater flow models [35], urban stormwater quality models [36, 37], crop growth models [38], and wheat canopy models [39]. The popularity of the GLUE method can be attributed to its simplicity and wide applicability, especially when dealing with nonlinear and nonmonotonic ecological dynamic models.

The objectives of this paper are to make use of the broadly used eutrophication and algal bloom model BLOOM [6, 7], in order to investigate the applicability of the GLUE method to analyze and quantify the uncertainty in numerical eutrophication models that have a large number of intercorrelated parameters and to provide a reference for method selection when conducting uncertainty analysis for similar types of models.

2. Materials and Methodology

2.1. Study Area. The Meiliang Bay (31°27′N/120°10′E), which locates at the north of Taihu Lake in China (Figure 1), is chosen as the study area. Taihu Lake has high level of eutrophication, and algal blooms that cause enormous damage to drinking water safety, tourisms, and fish farming frequently break out in summer and autumn.

The Meiliang Bay has a length of 16.6 km from south to north, a width of 10 km from east to west, and an average depth of 1.95 m. There are two main rivers: the Zhihu Gang that flows into Taihu Lake and the Liangxi River that flows out

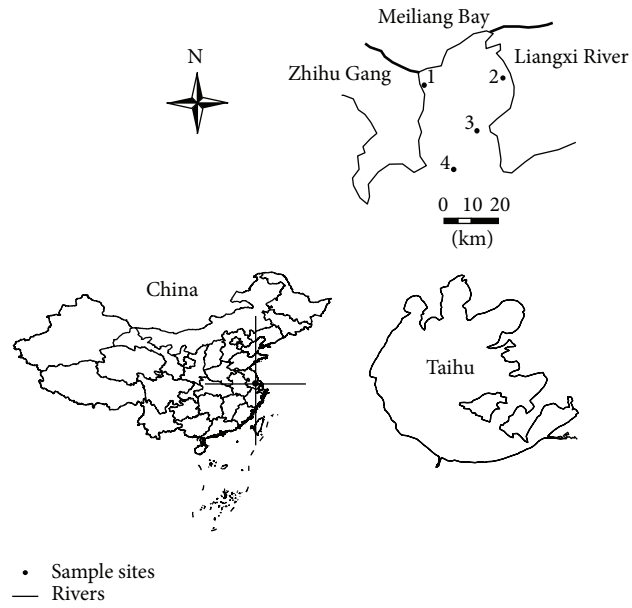

Figure 1: Location of the Taihu Lake and the Meiliang Bay (31°27′N/120°10′E).

of the lake. The exchange of substance between Meiliang Bay and the main body of Taihu Lake is taken into account in the study. The monthly observed data from four monitoring sites in the Meiliang Bay were collected during 2009 to 2011 for model calibration. These data include river discharge, water level, irradiance, temperature, concentrations of ammonia, nitrate, nitrite, phosphate, and biomass concentration of blue-green algae, green algae, and diatom.

In the composition of the algae blooms, blue-green algae is the dominant species and has the highest percentage of total biomass. Therefore it is selected to be the output variable of BLOOM on which the uncertainty analysis is performed.

2.2. BLOOM Model. BLOOM is a generic hydroenvironmental numerical model that can be applied to calculate primary production, chlorophyll-a concentration, and phytoplankton species composition [6–10]. Fifteen algae species can be modeled, including blue-green algae, green algae, and diatoms. Each algae species has up to three types, the N-type, P-type, and E-type, which correspond to nitrogen limiting conditions, phosphorus limiting conditions, and energy limiting conditions, respectively. Algae biomass in BLOOM mainly depends on primary production and transport.

The transport of dissolved or suspended matter in the water body is modeled by solving the advection-diffusion equation numerically:

$$\frac{\partial C}{\partial t} = D_x \frac{\partial^2 C}{\partial x^2} - v_x \frac{\partial C}{\partial x} + D_y \frac{\partial^2 C}{\partial y^2} - v_y \frac{\partial C}{\partial y} + S + fR(C,t), \tag{1}$$

where C: concentration (kg·m^{-3}); D_x, D_y: dispersion coefficient in x- and y-direction respectively (m^2·s^{-1}); S: source terms; $fR(C,t)$: reaction terms; t: time (s).

Primary production is mainly dependent on the specific rates of growth, mortality, and maintenance respiration, which are modulated according to the temperature:

$$kgp_i = \text{Proalg}_i^0 \times \text{TcPalg}_i^T,$$
$$kmrt_i = \text{Moralg}_i^0 \times \text{TcMalg}_i^T, \quad (2)$$
$$krsp_i = \text{Resalg}_i^0 \times \text{TcRalg}_i^T,$$

where kgp_i: potential specific growth rate of the fastest growing type of algae species (d^{-1}); Proalg_i^0: growth rate at 0°C (d^{-1}); TcPalg_i: temperature coefficient for growth (–); $kmrt_i$: specific mortality rate (d^{-1}); Moralg_i^0: mortality rate at 0°C (d^{-1}); TcMalg_i: temperature coefficient for mortality (–); $krsp_i$: specific maintenance respiration rate (d^{-1}); Resalg_i^0: maintenance respiration rate at 0°C (d^{-1}); TcRalg_i: temperature coefficient for respiration (–). More details of BLOOM can be found in Delft Hydraulics [6, 7].

2.3. Generalized Likelihood Uncertainty Estimation. The GLUE methodology [25] is based upon a large number of model runs performed with different sets of input parameter, sampled randomly from prior specified parameter distributions. The simulation result corresponding to each parameter set is evaluated by means of its likelihood value, which quantifies how well the model output conforms to the observed values. The higher the likelihood value, the better the correspondence between the model simulation and observations. Simulations with a likelihood value larger than a user-defined acceptability threshold will be retained to determine the uncertainty bounds of the model outputs [33, 40]. The major procedures for performing GLUE include determining the ranges and prior distributions of input parameters, generating random parameter sets, defining the generalized likelihood function, defining threshold value for behavioral parameter sets, and calculating the model output cumulative distribution function.

BLOOM contains hundreds of parameters. Ideally, all the parameters should be regarded stochastically and included in the uncertainty analysis. However, a more practical and typical manner to conduct uncertainty analysis is to focus on a few key parameters [25, 28, 41]. In eutrophication models, algal biomass is most closely related to the growth, mortality, and respiration processes, resulting in the selection of seven key parameters about blue-green algae according to (2). Table 1 summarizes the main characteristics of these seven parameters. The initial ranges of the parameters are obtained by model calibration and a uniform prior distribution reported in the literature [28] is considered for all parameters.

Latin Hypercube Sampling (LHS), which is a type of stratified Monte Carlo sampling, is employed in this study to generate random parameter sets from the prior parameter distributions. In total, 60,000 parameter combinations are generated for the model runs.

The GLUE method requires the definition of a likelihood function in order to quantify how well simulation results conform to observed data. The likelihood measure should increase monotonically with increasing conformity between simulation results and observations [25]. Various likelihood functions have been proposed and evaluated in the literature [35, 37, 38, 42]. Keesman and van Straten [43] defined the likelihood function based on the maximum absolute residual; Beven and Binley [25] defined the likelihood function based on the inverse error variance with a shape factor N; Romanowicz et al. [44] defined the likelihood function based on an autocorrelated Gaussian error model; Freer et al. [45] defined the likelihood function based on the Nash-Sutliffe efficiency criterion with shape factor N, as well as the exponential transformation of the error variance with shaping factor N; Wang et al. [41] defined the likelihood function based on minimum mean square error. In this study, the likelihood function $L(\theta_i \mid O)$ of the model run corresponding to the ith set of input parameters (θ_i) and observations O is defined based on the exponential transformation of the error variance σ_e^2 and the observation variance σ_0^2 with shape factor N [37, 45]:

$$L(\theta_i \mid O) = \exp\left(-N * \frac{\sigma_e^2}{\sigma_0^2}\right), \quad (3)$$

where $\sigma_e^2 = \sum (y_{\text{sim}} - y_{\text{obs}})^2$; $\sigma_o^2 = \sum (y_{\text{obs}} - \overline{y_{\text{obs}}})^2$; y_{sim} is the simulated blue-green algae biomass; y_{obs} is the observed blue-green algae biomass; $\overline{y_{\text{obs}}}$ is the average value of y_{obs}.

The sensitivity of the choice of the shape factor N will be analyzed and discussed. If the likelihood value of a simulation result is larger than a user-defined threshold, the model simulation is considered "behavioral" and retained for the subsequent analysis. Otherwise, the model simulation is considered "nonbehavioral," and removed from further analysis. There are two main methods for defining the threshold value for behavioral parameter sets: one is to allow a certain deviation from the highest likelihood value in the sample, and the other is to use a fixed percentage of the total number of simulations [46]. The latter is used in this study, and the acceptable sample rate (ASR) is defined as 60%. The sensitivity of the choice of the threshold in the form of the acceptable sample rate (ASR) will be analyzed and discussed.

The likelihood function is then normalized, such that the cumulative likelihood of all model runs equals 1:

$$L_w(\theta_i) = \frac{L(\theta_i \mid O)}{\sum_i L(\theta_i \mid O)}, \quad (4)$$

where $L_w(\theta_i)$ is the normalized likelihood for the$i$th set of input parameters (θ_i). The uncertainty analysis is performed by calculating the cumulative distribution function (CDF) of the normalized likelihood together with prediction quantiles.

The GLUE-derived 90% confidence intervals for the biomass of blue green are then obtained by reading 5% and 95% percentiles of the cumulative distribution functions.

3. Results

3.1. BLOOM Model Results. The calibration result for blue-green algae is shown in Figure 2, and the calibration

Table 1: Selected input parameters and their initial ranges.

Parameter	Category Equations (2)	Definition	Unit	Lower bound	Upper bound	Calibrated value
ProBlu_E^0	Proalg_i^0	Growth rate at 0°C for blue-green E-type	1/d	0.013	0.019	0.016
TcPBlu_E	TcPalg_i	Temperature coefficient for growth for blue-green E-type	—	1.040	1.100	1.08
TcPBlu_N	TcPalg_i	Temperature coefficient for growth for blue-green N-type	—	1.040	1.100	1.08
TcPBlu_P	TcPalg_i	Temperature coefficient for growth for blue-green P-type	—	1.040	1.100	1.08
MorBlu_ E^0	Moralg_i^0	Mortality rate at 0°C for blue-green E-type	1/d	0.028	0.042	0.035
TcMBlu_E	TcMalg_i	Temperature coefficient for mortality for blue-green E-type	—	1.000	1.020	1.01
TcRBlu_E	TcRalg_i	Temperature coefficient for maintenance respiration for blue-green E-type	—	1.040	1.100	1.072

Table 2: Statistical characteristics of observed data from 2009 to 2011.

Station	Mean (gC/m^3)	Standard deviation (gC/m^3)	Maximum (gC/m^3)	Minimum (gC/m^3)
1	1.023	1.504	6.744	0.015
2	1.144	2.073	9.885	0.002
3	1.135	1.369	5.037	0.004
4	1.179	1.564	5.534	0.010

parameters are summarized in the last column of Table 1. The statistical characteristics of the observed blue-green algae biomass are shown in Table 2. The mean values of the blue-green algae biomass for the four sample sites are similar. Therefore, in order to reduce the sampling uncertainties, the average of the four sampling sites has been retained as dependent variable in the present study.

The biomass of blue-green has a yearly cycle (Figure 2), with low values during spring, followed by a rapid increase towards peak values in summer or autumn. The growth periodicity of blue-green algae is mainly attributed to the periodic variation of temperature and algae dormancy. Taihu Lake experiences a subtropical monsoon climate, with four distinct seasons. The lowest temperature is about 2.8°C in average and appears in January, and the highest temperature is about 29.4°C in average and usually appears in August. The suitable temperature range for growth of blue-green algae is 25~35°C. As a result, the biomass of blue-green algae is low in spring. When temperature increases in summer, it is appropriate for blue-green algae breeding, leading to the sharp increase in biomass and the occurrence of the peak value around August.

The modes capture satisfactorily the observed evolution of the blue-green algae biomass, which indicates further analyses on model uncertainty are meaningful. The coefficient of determination (CoD), which is given by (5), is 0.85:

$$\text{CoD} = \frac{\sum_i \left(y_{si} - \overline{y_o}\right)^2}{\sum_i \left(y_{oi} - \overline{y_o}\right)^2}, \tag{5}$$

where y_{si}: the simulated biomass of blue-green algae at time step i; $\overline{y_o}$: the mean value of observed data; y_{oi}: the observed value of blue-green at time step i.

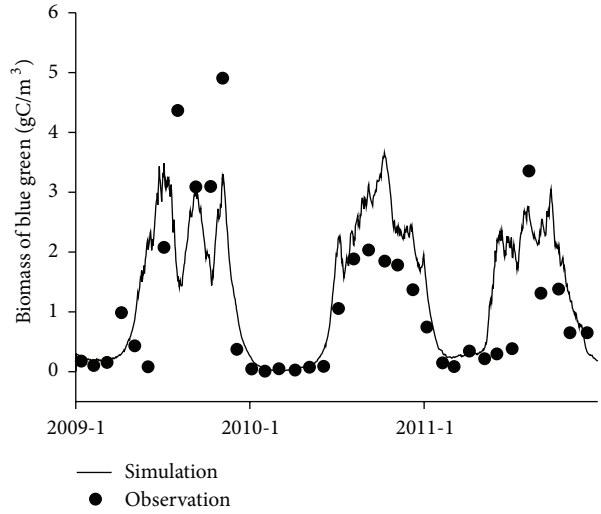

Figure 2: Modeled results and observations of blue-green algae.

3.2. Uncertainty Analysis Results. The confidence interval (CI) is obtained by calculating the cumulative distribution functions of model outputs based on the normalized likelihood (4) with $N = 1$ and ASR = 60%. Figure 3 presents the 90% confidence interval of blue-green algae biomass, which is estimated from the 5% and 95% quantiles of the cumulative distribution functions and the corresponding observations from January 2009 to December 2011. Table 3 summarizes the width of the 90% CI of each month and whether or not the observations are located within the 90% CI.

The 90% CI is narrow from January to May when the biomass of blue-green algae is low. The width of the 90% CI expands as the biomass of blue-green algae increases during summer and autumn. Among the total of 36 observations, 13 are located within the 90% CI of the simulations.

The subjective choice of the shape factor N in (1) considerably influences the GLUE results, whereas N is commonly taken as 1 [35]. Figure 4 displays the 90% CI when ASR = 60%, with shape factors N equal 50 and 100, respectively. The simulated 5% and 95% confidence quantiles and the weighted mean, as well as the corresponding observations of blue-green algae biomass, are shown.

Comparison of Figures 3 and 4 shows that the increase of shape factor N leads to a narrowing of the 90% CI. Figure 5

Table 3: Width of 90% confidence interval (CI) for each month and indication whether (Y) or not (N) the observations is located within the 90% CI band.

Year	Month	1	2	3	4	5	6	7	8	9	10	11	12
2009	90% CI (gC/m^3)	0.004	0.011	0.010	0.080	0.349	1.533	1.646	0.694	0.989	1.051	1.538	0.363
	within CI	N	Y	N	N	Y	N	Y	N	Y	N	N	N
2010	90% CI (gC/m^3)	0.093	0.029	0.009	0.013	0.038	0.147	1.078	1.362	1.567	0.768	1.199	1.272
	within CI	N	N	N	N	N	Y	Y	Y	Y	N	Y	Y
2011	90% CI (gC/m^3)	0.504	0.114	0.039	0.054	0.182	0.993	0.865	1.136	0.872	1.196	1.500	0.648
	within CI	Y	N	N	N	Y	N	N	N	N	N	N	Y

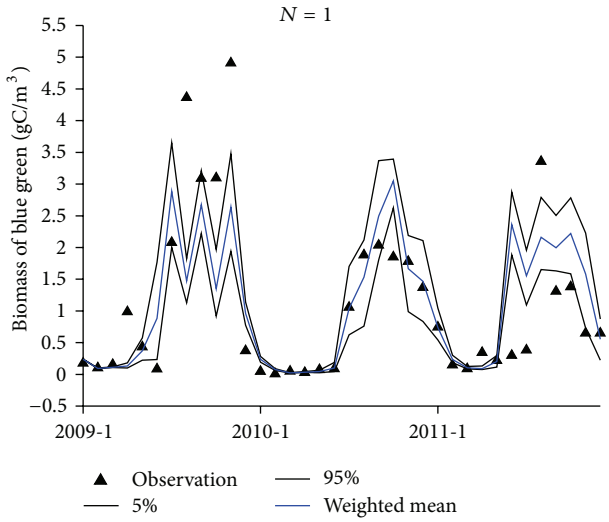

Figure 3: 5% and 95% confidence quantiles, and weigthed mean of simulated biomass of blue-green algae when ASR = 60% and N = 1, and corresponding observations from January 2009 to December 2011.

illustrates the effect of the shape factor N, which can be seen as a weight factor for the likelihood corresponding to each simulation. When $N = 1$, the magnitudes of the likelihood are similar for each simulation, and there is no clear division between acceptable and unacceptable simulations. As a result, the cumulative distribution functions increase gradually. With increasing N (e.g., $N = 50$), the high behavioral simulations have a higher weight, resulting in a larger gradient in the cumulative distribution function and a narrower CI. Theoretically, when $N = 0$, every simulation has equal likelihood, and the widest CI will be obtained. When $N \to \infty$, the single best simulation will have a normalized likelihood of 1, while all other simulations will get a likelihood of zero, resulting in the collapse of the 5% and 95% quantiles on a single line. This corresponds to the traditional calibration method that omits uncertainty analysis.

Previous studies have shown that the choice of threshold values for the likelihood measures is particularly important for the GLUE method [34, 36, 47]. In order to quantify the effect of threshold values on the uncertainty analyses, a series of acceptable sample rates (ASR) of 0.5%, 1%, 5%, 10%, 30%, 60%, 90%, 95%, 99% is investigated. In this study, average relative interval length (ARIL) and percentage of observations covered by the 90% confidence interval (P_{90CI}) are adopted as metrics for the analysis. These metrics are defined as follows:

$$\text{ARIL} = \frac{1}{n} \sum \frac{\text{Limit}_{\text{upper},t} - \text{Limit}_{\text{lower},t}}{B_{\text{obs},t}}, \quad (6)$$

where $\text{Limit}_{\text{upper},t}$ and $\text{Limit}_{\text{lower},t}$ are the upper and lower boundary values of the 90% confidence interval; n is the number of time steps; $B_{\text{obs},t}$ is the observed biomass of blue-green algae:

$$P_{90CI} = \frac{NQ_{\text{in}}}{N_{\text{obs}}} \times 100\%, \quad (7)$$

where NQ_{in} is the number of observations located within 90% CI; N_{obs} is the total number of observations.

Figures 6 and 7 present the influence of ASR on ARIL and P_{90CI} for $N = 1, 50, 100$. Figure 6 shows that, for all ASR values, ARIL has the highest value for $N = 1$ and decreases with increasing N, which confirms the results of Figure 4. For a given N value, ARIL increases with ASR. When ASR moves from 0.5% to 99%, the ARIL increases by 73.93%, 41.96% and 5.24% for $N = 1, 50, 100$, respectively. An increasing ASR, which corresponds to a lower threshold of the accepted likelihood, means that simulations with lower likelihood are considered "behavioral," which inevitably results in a larger ARIL.

From Figure 7, it is seen that P_{90CI} becomes larger as ASR increases for $N = 1$ and $N = 50$, while P_{90CI} keeps constant for $N = 100$. This is because the increase of ASR results in a larger ARIL, which logically leads to an increase in observations located within the 90% CI. When $N = 100$, the ARIL is low and P_{90CI} does not increase with ASR because the 90% CI does not widen.

The highest P_{90CI} is obtained for ASR close to 100% and $N = 1$. Its value of about 50% indicates that about half of the observed data remain outside the 90% CI for the greatest ASR. This can be attributed to other sources of uncertainty, such as the input parameters or the observations.

4. Discussion and Conclusion

The 90% confidence interval of the simulated results fails to enclose the peaks of the observed values in 2009 and 2011 (Figure 3). Such a feature is not unusual, and several reasons can lead to this result. Firstly, there are inherent uncertainties from inputs, boundaries, and model structure, which are not

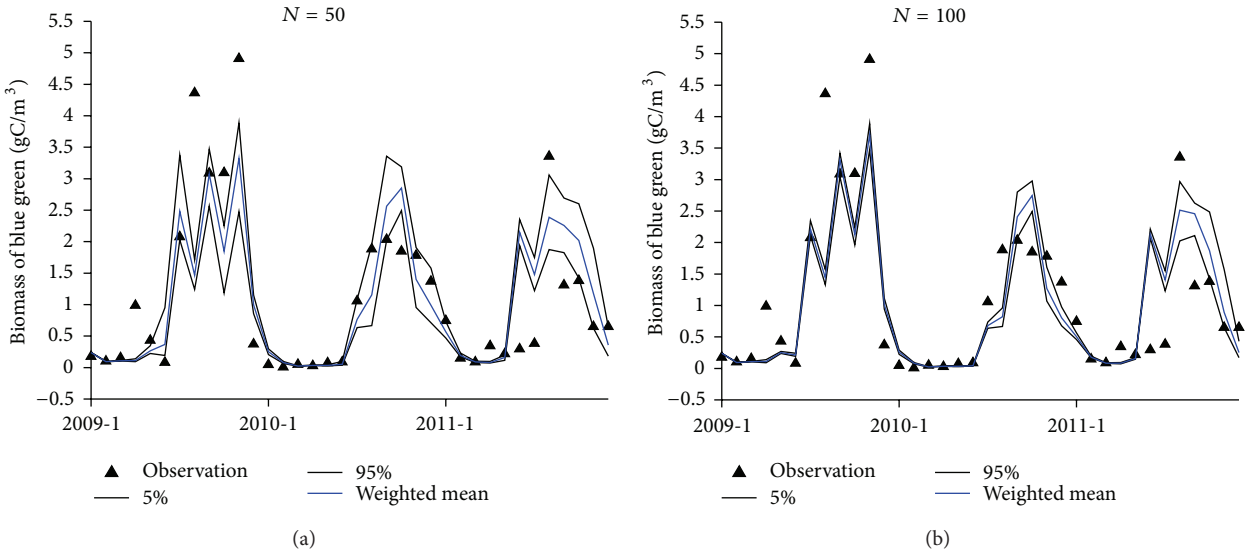

Figure 4: 5% and 95% confidence quantiles and weigthed mean of simulated biomass of blue-green algae when ASR = 60% and $N = 50$ (a) and 100 (b), and corresponding observations from January 2009 to December 2011.

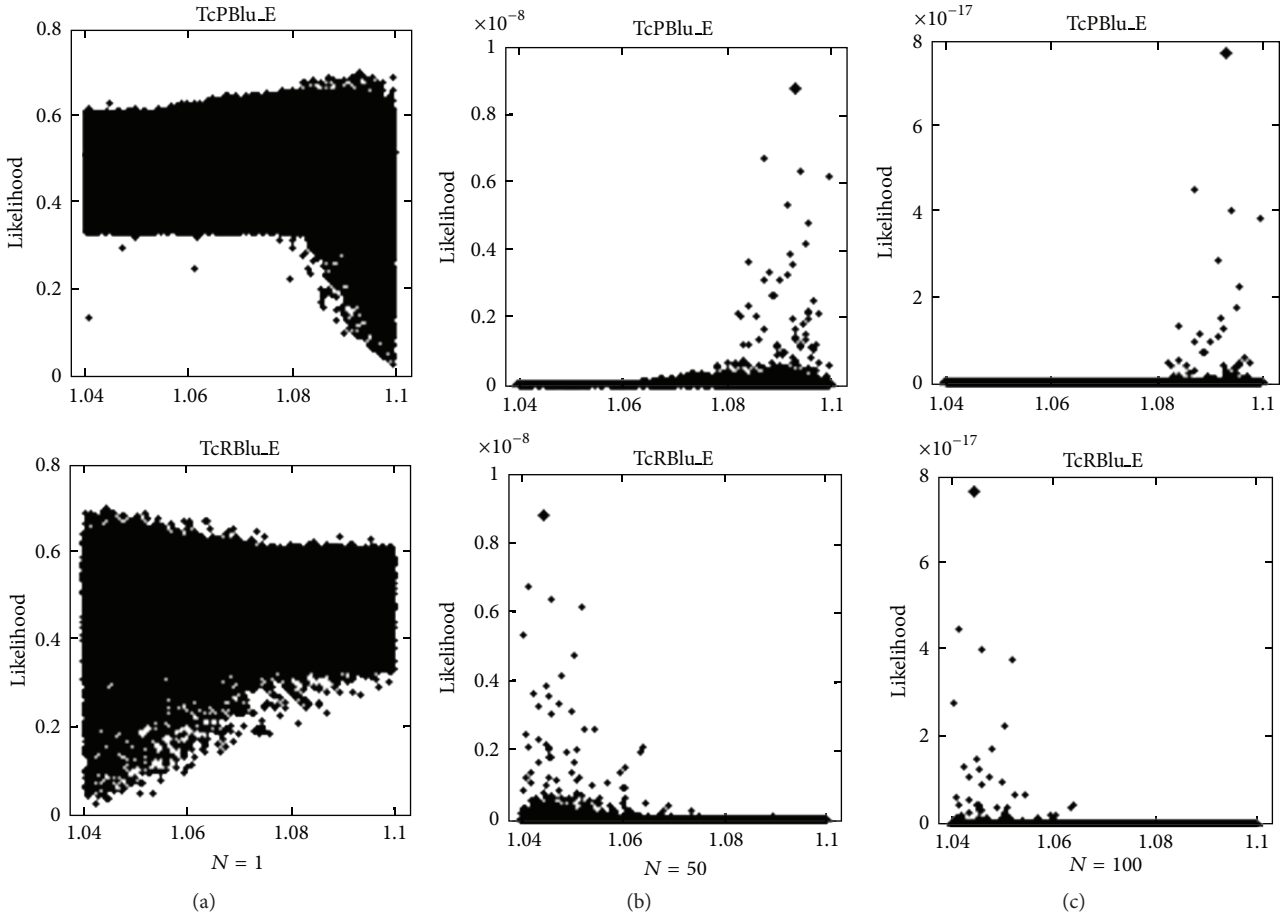

Figure 5: Dot plots of likelihood according to (4) when ASR = 100% and $N = 1$ (a), 50 (b), and 100 (c) for TcPBlu_E and TcRBlu_E (cf. Table 1).

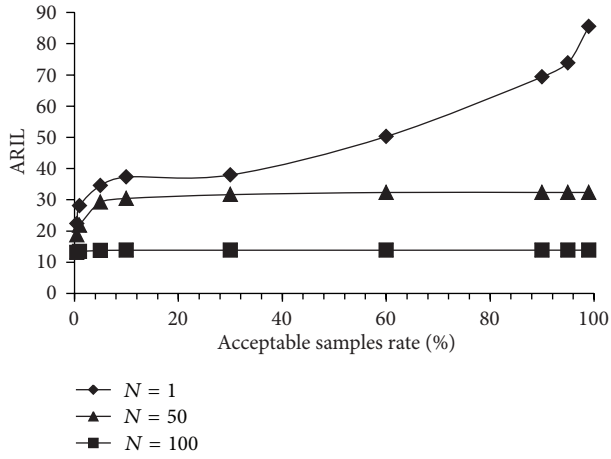

Figure 6: ARIL as function of ASR for N equals 1, 50, and 100.

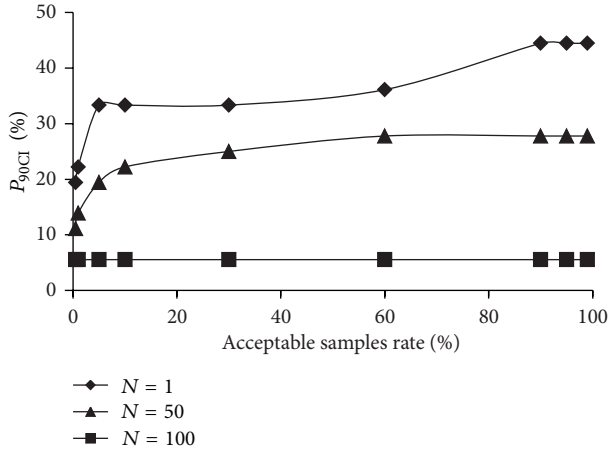

Figure 7: P_{90CI} as function of ASR for N equals 1, 50, and 100.

taken into account explicitly. Secondly, the observed values used for comparison are space averaged through arithmetic mean other than weighted mean, which could also introduce discrepancy. Finally, the original observations from the four stations contain measurement uncertainties. During summer and autumn when the algal blooms break out, the biomass of blue-green algae is high and shows pronounced daily temporal variations and spatial variations due to changes in irradiance, transport by flow and wind drifting. The measurements taken at a particular time and point cannot fully reflect these fine-scale spatial and temporal dynamics. The model calibrated in this study is, however, capable of simulating blue-green algae dynamics at large spatial (spatial averages) and temporal (seasonal) scales.

Ideally, accurate predictions require that the results are consistent with the observations, while the uncertainty spread of the results, quantified by the 90% CI, is as narrow as possible [46]. From Figures 6 and 7, it can be seen that while keeping ASR fixed, the 90% CI is narrowed by increasing the shape factor N at the expense of decreasing the percentage of observations that it covers (P_{90CI}). Similarly, while keeping N fixed, the 90% CI is narrowed by reducing ASR, but at the same time also P_{90CI} decreases. As a consequence, it is essential to optimally choose N and ASR in order to find the optimal compromise between the uncertainty spread and its coverage of observations.

As illustrated by the application to the BLOOM model for algal bloom, GLUE is an appropriate method for uncertainty analysis that can cope with equifinality between different parameter sets incurred by high level of model complexity. In conclusion, the study demonstrates that GLUE is an effective method for uncertainty analysis of complex dynamic ecosystem models, which provides a solid foundation for the use of the model predictions in decision making.

Acknowledgments

The authors are grateful for the financial support of the National Nature Science Foundation of China (50920105907), National Basic Research Program 973 (2010CB429004), "100 Talent Program of Chinese Academy of Sciences (A1049)," and the Chutian Scholarship (KJ2010B002). Koen Blanckaert was partially funded by the Chinese Academy of Sciences Visiting Professorship for Senior International Scientists (2011T2Z24).

References

[1] C. F. Cerco and T. Cole, "Three-dimensional eutrophication model of Chesapeake Bay," *Journal of Environmental Engineering*, vol. 119, no. 6, pp. 1006–1025, 1993.

[2] C. F. Cerco, D. Tillman, and J. D. Hagy, "Coupling and comparing a spatially- and temporally-detailed eutrophication model with an ecosystem network model: an initial application to Chesapeake Bay," *Environmental Modelling and Software*, vol. 25, no. 4, pp. 562–572, 2010.

[3] V. J. Bierman, S. C. Hinz, D. Zhu, W. J. Wiseman, N. N. Rabalais, and R. E. Turner, "A preliminary mass balance model of primary productivity and dissolved oxygen in the Mississippi River Plume/Inner Gulf Shelf Region," *Estuaries*, vol. 17, no. 4, pp. 886–899, 1994.

[4] W. S. Lung and C. E. Larson, "Water quality modeling of upper Mississippi River and Lake Pepin," *Journal of Environmental Engineering*, vol. 121, no. 10, pp. 691–699, 1995.

[5] P. Hernandez, R. B. Ambrose Jr., D. Prats, E. Ferrandis, and J. C. Asensi, "Modeling eutrophication kinetics in reservoir microcosms," *Water Research*, vol. 31, no. 10, pp. 2511–2519, 1997.

[6] Delft Hydraulics, *Technical Reference Manual Delft3D-WAQ*, WL, Delft Hydraulics, Delft, The Netherlands, 2005.

[7] Delft Hydraulics, *Delft3D-WAQ Users Manual*, WL, Delft Hydraulics, Delft, The Netherlands, 2009.

[8] F. J. Los and J. W. M. Wijsman, "Application of a validated primary production model (BLOOM) as a screening tool for marine, coastal and transitional waters," *Journal of Marine Systems*, vol. 64, no. 1–4, pp. 201–215, 2007.

[9] F. J. Los, M. T. Villars, and M. W. M. van der Tol, "A 3-dimensional primary production model (BLOOM/GEM) and its applications to the (southern) North Sea (coupled physical-chemical-ecological model)," *Journal of Marine Systems*, vol. 74, no. 1-2, pp. 259–294, 2008.

[10] K. Salacinska, G. Y. El Serafy, F. J. Los, and A. Blauw, "Sensitivity analysis of the two dimensional application of the generic ecological model (GEM) to algal bloom prediction in the North Sea," *Ecological Modelling*, vol. 221, no. 2, pp. 178–190, 2010.

[11] D. P. Hamilton and S. G. Schladow, "Prediction of water quality in lakes and reservoirs—part I: model description," *Ecological Modelling*, vol. 96, no. 1–3, pp. 91–110, 1997.

[12] D. Trolle, H. Skovgaard, and E. Jeppesen, "The water framework directive: setting the phosphorus loading target for a deep lake in Denmark using the 1D lake ecosystem model DYRESM-CAEDYM," *Ecological Modelling*, vol. 219, no. 1-2, pp. 138–152, 2008.

[13] S. E. Jrgensen, H. T. Tsuno, H. Mahler, and V. Santiago, "PAMOLARE Training Package, Planning and Management of Lakes and Reservoirs: Models for Eutrophication Management," UNEP DTIE IETC and ILEC, Shiga, Japan, 2003.

[14] Z. Gurkan, J. Zhang, and S. E. Jørgensen, "Development of a structurally dynamic model for forecasting the effects of restoration of Lake Fure, Denmark," *Ecological Modelling*, vol. 197, no. 1-2, pp. 89–102, 2006.

[15] N. Oreskes, K. Shrader-Frechette, and K. Belitz, "Verification, validation, and confirmation of numerical models in the earth sciences," *Science*, vol. 263, no. 5147, pp. 641–646, 1994.

[16] E. J. Rykiel, "Testing ecological models: the meaning of validation," *Ecological Modelling*, vol. 90, no. 3, pp. 229–244, 1996.

[17] M. B. Beck, "Water quality modeling: a review of the analysis of uncertainty," *Water Resources Research*, vol. 23, no. 8, pp. 1393–1442, 1987.

[18] R. W. Katz, "Techniques for estimating uncertainty in climate change scenarios and impact studies," *Climate Research*, vol. 20, no. 2, pp. 167–185, 2002.

[19] M. Radwan, P. Willems, and J. Berlamont, "Sensitivity and uncertainty analysis for river quality modeling," *Journal of Hydroinformatics*, vol. 6, no. 2, pp. 83–99, 2004.

[20] H. Li and J. Wu, "Uncertainty analysis in ecological studies," in *Scaling and Uncertainty Analysis in Ecology: Methods and Applications*, J. Wu, K. B. Jones, H. Li, and O. L. Loucks, Eds., pp. 45–66, Springer, Dordrecht, The Netherlands, 2006.

[21] K. E. Lindenschmidt, K. Fleischbein, and M. Baborowski, "Structural uncertainty in a river water quality modelling system," *Ecological Modeling*, vol. 204, no. 3-4, pp. 289–300, 2007.

[22] P. Wiwatanadate and H. G. Claycamp, "Exact propagation of uncertainties in multiplicative models," *Human and Ecological Risk Assessment*, vol. 6, no. 2, pp. 355–368, 2000.

[23] M. J. W. Jansen, "Prediction error through modelling concepts and uncertainty from basic data," *Nutrient Cycling in Agroecosystems*, vol. 50, no. 1–3, pp. 247–253, 1998.

[24] G. Freni and G. Mannina, "Bayesian approach for uncertainty quantification in water quality modelling: the influence of prior distribution," *Journal of Hydrology*, vol. 392, no. 1-2, pp. 31–39, 2010.

[25] K. Beven and A. Binley, "The future of distributed models: model calibration and uncertainty prediction," *Hydrological Processes*, vol. 6, no. 3, pp. 279–298, 1992.

[26] R. E. Brazier, K. J. Beven, J. Freer, and J. S. Rowan, "Equifinality and uncertainty in physically based soil erosion models: application of the GLUE methodology to WEPP—the water erosion prediction project—for sites in the UK and USA," *Earth Surface Processes and Landforms*, vol. 25, no. 8, pp. 825–845, 2000.

[27] A. Candela, L. V. Noto, and G. Aronica, "Influence of surface roughness in hydrological response of semiarid catchments," *Journal of Hydrology*, vol. 313, no. 3-4, pp. 119–131, 2005.

[28] K. Beven and J. Freer, "Equifinality, data assimilation, and uncertainty estimation in mechanistic modelling of complex environmental systems using the GLUE methodology," *Journal of Hydrology*, vol. 249, no. 1–4, pp. 11–29, 2001.

[29] J. Yang, P. Reichert, K. C. Abbaspour, J. Xia, and H. Yang, "Comparing uncertainty analysis techniques for a SWAT application to the Chaohe Basin in China," *Journal of Hydrology*, vol. 358, no. 1-2, pp. 1–23, 2008.

[30] R. F. Vázquez, K. Beven, and J. Feyen, "GLUE based assessment on the overall predictions of a MIKE SHE application," *Water Resources Management*, vol. 23, no. 7, pp. 1325–1349, 2009.

[31] R. Lamb, K. Beven, and S. Myrabø, "Use of spatially distributed water table observations to constrain uncertainty in a rainfall-runoff model," *Advances in Water Resources*, vol. 22, no. 4, pp. 305–317, 1998.

[32] H. T. Choi and K. Beven, "Multi-period and multi-criteria model conditioning to reduce prediction uncertainty in an application of TOPMODEL within the GLUE framework," *Journal of Hydrology*, vol. 332, no. 3-4, pp. 316–336, 2007.

[33] C. Ortiza, E. Karltuna, J. Stendahl, A. I. Gärdenäsa, and G. I. Ågren, "Modelling soil carbon development in Swedish coniferous forest soils—an uncertainty analysis of parameters and model estimates using the GLUE method," *Ecological Modelling*, vol. 222, no. 17, pp. 3020–3032, 2011.

[34] Y. Gong, Z. Shen, Q. Hong, R. Liu, and Q. Liao, "Parameter uncertainty analysis in watershed total phosphorus modeling using the GLUE methodology," *Agriculture, Ecosystems and Environment*, vol. 142, no. 3-4, pp. 246–24255, 2011.

[35] A. E. Hassan, H. M. Bekhit, and J. B. Chapman, "Uncertainty assessment of a stochastic groundwater flow model using GLUE analysis," *Journal of Hydrology*, vol. 362, no. 1-2, pp. 89–109, 2008.

[36] G. Freni, G. Mannina, and G. Viviani, "Uncertainty in urban stormwater quality modelling: the effect of acceptability threshold in the GLUE methodology," *Water Research*, vol. 42, no. 8-9, pp. 2061–2072, 2008.

[37] G. Freni, G. Mannina, and G. Viviani, "Uncertainty in urban stormwater quality modelling: the influence of likelihood measure formulation in the GLUE methodology," *Science of the Total Environment*, vol. 408, no. 1, pp. 138–145, 2009.

[38] J. He, J. W. Jones, W. D. Graham, and M. D. Dukes, "Influence of likelihood function choice for estimating crop model parameters using the generalized likelihood uncertainty estimation method," *Agricultural Systems*, vol. 103, no. 5, pp. 256–264, 2010.

[39] X. Mo and K. Beven, "Multi-objective parameter conditioning of a three-source wheat canopy model," *Agricultural and Forest Meteorology*, vol. 122, no. 1-2, pp. 39–63, 2004.

[40] P. Smith, K. J. Beven, and J. A. Tawn, "Informal likelihood measures in model assessment: theoretic development and investigation," *Advances in Water Resources*, vol. 31, no. 8, pp. 1087–1100, 2008.

[41] X. Wang, X. He, J. R. Williams, R. C. Izaurralde, and J. D. Atwood, "Sensitivity and uncertainty analyses of crop yields and soil organic carbon simulated with EPIC," *Transactions of the American Society of Agricultural Engineers*, vol. 48, no. 3, pp. 1041–1054, 2005.

[42] J. R. Stedinger, R. M. Vogel, S. U. Lee, and R. Batchelder, "Appraisal of the generalized likelihood uncertainty estimation

(GLUE) method," *Water Resources Research*, vol. 44, no. 12, Article ID W00B06, 2008.

[43] K. Keesman and G. van Straten, "Identification and prediction propagation of uncertainty in models with bounded noise," *International Journal of Control*, vol. 49, no. 6, pp. 2259–2269, 1989.

[44] R. Romanowicz, K. J. Beven, and J. Tawn, "Evaluation of predictive uncertainty in non-linear hydrological models using a Bayesian approach," in *Statistics for the Environment: Water Related Issues*, V. Barnett and K. F. Turkman, Eds., pp. 297–317, John Wiley & Sons, New York, NY, USA, 1994.

[45] J. Freer, K. Beven, and B. Ambroise, "Bayesian estimation of uncertainty in runoff prediction and the value of data: an application of the GLUE approach," *Water Resources Research*, vol. 32, no. 7, pp. 2161–2173, 1996.

[46] R. S. Blasone, J. A. Vrugt, H. Madsen, D. Rosbjerg, B. A. Robinson, and G. A. Zyvoloski, "Generalized likelihood uncertainty estimation (GLUE) using adaptive Markov Chain Monte Carlo sampling," *Advances in Water Resources*, vol. 31, no. 4, pp. 630–648, 2008.

[47] L. Li, J. Xia, C. Y. Xu, and V. P. Singh, "Evaluation of the subjective factors of the GLUE method and comparison with the formal Bayesian method in uncertainty assessment of hydrological models," *Journal of Hydrology*, vol. 390, no. 3-4, pp. 210–221, 2010.

Hindawi Publishing Corporation
Mathematical Problems in Engineering
Volume 2013, Article ID 528162, 9 pages
http://dx.doi.org/10.1155/2013/528162

Research Article

Guidance of Autonomous Amphibious Vehicles for Flood Rescue Support

Shankarachary Ragi,[1] ChingSeong Tan,[2] and Edwin K. P. Chong[1]

[1] *Department of Electrical and Computer Engineering, Colorado State University, Fort Collins, CO 80523-1373, USA*
[2] *Faculty of Engineering, Multimedia University, Malaysia*

Correspondence should be addressed to Shankarachary Ragi; shankar.ragi@colostate.edu

Received 14 February 2013; Revised 6 May 2013; Accepted 7 May 2013

Academic Editor: Yongping Li

We develop a path-planning algorithm to guide autonomous amphibious vehicles (AAVs) for flood rescue support missions. Specifically, we develop an algorithm to control multiple AAVs to reach/rescue multiple victims (also called targets) in a flood scenario in 2D, where the flood water flows across the scene and the targets move (drifted by the flood water) along the flood stream. A target is said to be rescued if an AAV lies within a circular region of a certain radius around the target. The goal is to control the AAVs such that each target gets rescued while optimizing a certain performance objective. The algorithm design is based on the theory of *partially observable Markov decision process* (POMDP). In practice, POMDP problems are hard to solve exactly, so we use an approximation method called *nominal belief-state optimization* (NBO). We compare the performance of the NBO approach with a greedy approach.

1. Introduction

Various guidance algorithms for autonomous amphibious vehicles (AAVs) are being designed and tested to fight today's global warming disasters such as flooding, typhoon, and hurricane [1–3]. With this motivation, we present a guidance framework to control multiple AAVs to rescue multiple victims (henceforth called targets) in a flood situation, where the flood water (interchangeably called river) flows along a valley as shown in Figure 1. A target is said to be rescued when an AAV is within the circular region of radius $d_{\text{dist-thresh}}$ on the 2D plane around the target. In general, AAVs are equipped with various advanced sensors such as polarized stereo vision, laser scanning, and SONAR [4–6]. The sensors onboard an AAV generate the (noisy) measurements corresponding to the targets and the river. Our goal is to design a path-planning algorithm that guides the AAVs so that every target gets rescued, while maximizing a performance measure (discussed later). The algorithm runs on a notional central fusion node, which collects the measurements from the sensors on-board each AAV, fuses them and updates the tracks on the targets and the river state (discussed later), computes the control commands for the AAVs, and sends the control commands back to the AAVs.

Guidance control methods [1, 7–9] for AAVs are normally based on a standard three-layered system architecture that requires human-machine interactions. We design the guidance algorithm based on the theory of *partially observable Markov decision process* (POMDP) [10, 11]. There are several other autonomous control methods in the literature for AAVs and underwater vehicles, for example, [12–14]. Our approach differs from these existing approaches in that we place the guidance problem in the context of POMDP, wherein this approach has a look-ahead property, which trades off short-term for long-term performance.

2. Problem Specification

The AAV guidance problem is specified as follows.

2.1. Targets. In this study, we assume that there are multiple mobile targets (flood victims) located in a river, being drifted down by the flood water, as shown in Figure 1.

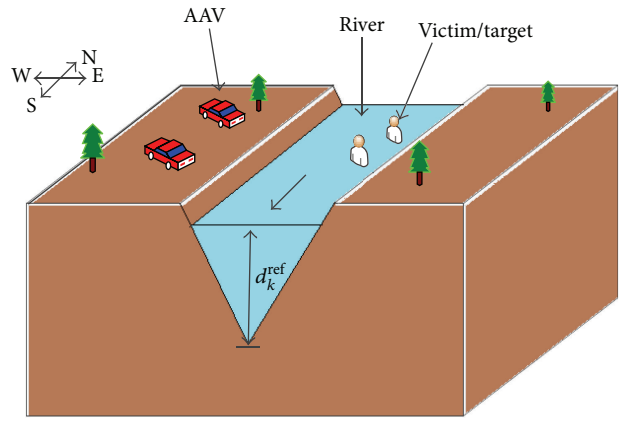

Figure 1: Flood scenario.

2.2. Autonomous Amphibious Vehicles (AAVs). There are multiple autonomous amphibious vehicles (AAVs) located on the shore, as shown in Figure 1. An AAV is controlled by the following kinematic controls: forward acceleration and steering angle. Each AAV is equipped with on-board sensors that generate measurements of targets and the river depth. In this problem, AAVs float when moving in the river. For the purpose of this study, we assume that the number of AAVs and the number of targets are the same.

2.3. Environmental Conditions. The elevation map of the region is known a priori. The landscape for this problem is shown in Figure 1, which shows a river flowing along a valley from the north toward the south. The state of the river includes the depth d_k^{ref} at a reference point on the map (lowest point in the landscape, e.g., some location at the bottom of the valley as shown in Figure 1).

2.4. River Model. Typically a river flows slowly near the coastlines (where the river is shallow) and flows quickly far from the coastlines (i.e., toward the center of the river where the river is deep). In this paper, we assume that the river flows from the north toward the south in a v-shaped channel as shown in Figure 1. We adopt the *logarithmic velocity profile* to model the velocity of the flow (see [15] for a detailed description). According to this model, the speed of the river, at the surface, at the location (p, q) at time k is given by

$$w_k(p,q) = C_1 \left[\log\left(d_k(p,q)\right) + C_2\right], \tag{1}$$

where $d_k(p,q)$ is the depth of the river at the location (p,q) at time k, and C_1 (a function of the viscosity and the density of flood water) and C_2 are constants (see [15] for more details).

2.5. Observations. The sensors onboard an AAV generate noisy observations of target locations and the depth of the river directly beneath the vehicle, that is, the sensors generate the observations of the depth of the river only when the AAV is in the river.

2.6. Objective. A target is said to be rescued if there is an AAV within a circular region of radius $d_{\text{dist-thresh}}$ around the target. The objective is to minimize the average rescue time, where the average is over the number of targets, and the rescue time of a target is defined as the time it takes to rescue the target.

3. Problem Formulation

We cast the AAV guidance problem into the framework of a *partially observable Markov decision process* (POMDP). A POMDP is a mathematical framework useful for solving resource control problems and enables us to exploit approximation methods for POMDPs to design our AAV guidance algorithm. A POMDP evolves in discrete time steps. We use k as the discrete-time index. To cast the AAV guidance problem into the POMDP framework, we need to define the following key components in terms of our guidance problem as follows.

3.1. States. Let x_k represent the state of the system at time k. The state of the system includes the state of the vehicles (AAVs) s_k, river state (depth of the river at a reference location) d_k^{ref}, target state χ_k, and track states $(\xi_k^{\text{riv}}, P_k^{\text{riv}}, \xi_k^{\text{targ}}, P_k^{\text{targ}})$, that is, $x_k = (s_k, d_k^{\text{ref}}, \chi_k, \xi_k^{\text{riv}}, P_k^{\text{riv}}, \xi_k^{\text{targ}}, P_k^{\text{targ}})$. The vehicle state s_k includes the locations and the velocities of the AAVs at time k. The river state d_k^{ref} is the depth of the river at the reference point at time k. The reference point is the lowest point in the elevation map, that is, some location at the bottom of the valley in the landscape, as shown in Figure 1. Here, we assume that the flow direction of the river is the same everywhere and is known a priori. The target state χ_k includes the locations and the velocities of the targets at time k. The track states represent the state of the tracking algorithm, where ξ_k^{riv} and P_k^{riv} are the mean and the variance, standard in Kalman filter equations, corresponding to the river state, and, similarly, ξ_k^{targ} is the mean vector and P_k^{targ} is the covariance matrix corresponding to the target state.

3.2. Observations and Observation Law. The vehicle and the track states are assumed to be fully observable. The river and the target states are only partially observable. The observation of the river state at an AAV is given by

$$z_k^{\text{riv}} = \begin{cases} d_k^{\text{ref}} + n_k^{\text{riv}} & \text{if AAV is in river,} \\ \text{no measurement} & \text{otherwise,} \end{cases} \tag{2}$$

where $n_k^{\text{riv}} \sim \mathcal{N}(0, R_k)$, and R_k is the measurement variance. The sensors at an AAV generate the measurement of the river state only when the AAV is in the river. In practice, the sensors on an AAV measure the depth of the river exactly below the AAV. We wrote the observation model (2) as if the sensors are generating the observations of the depth of the river at the reference point. The rationale behind this assumption is that we can always calculate the depth of the river at the reference point given the elevation map and the observed depth of

the river at a different location. The observation of the jth target at an AAV is given by

$$z_k^{\chi^j} = \begin{cases} H\chi_k^j + n_k^{\text{targ}} & \text{if there is line-of-sight,} \\ \text{no measurement} & \text{otherwise,} \end{cases} \quad (3)$$

where H is the target-state observation model, χ_k^j is the state of jth target, and $n_k^{\text{targ}} \sim \mathcal{N}(0, S_k)$, where S_k is the measurement covariance matrix. The line-of-sight between the target and the AAV is blocked sometimes, for example, whenever the target sinks in the water.

3.3. Actions. The actions include the controllable aspects of the system. In this problem, the actions include the decisions on the assignment of AAVs to targets, and kinematic control commands for AAVs. Let u_k be the action tuple at time k, which is given by $u_k = (g_k, a_k)$, where a_k represents kinematic control vectors (includes forward acceleration and steering angle for each AAV), and g_k is a vector, which represents the assignment of AAVs to targets, that is, $g_k(i) = j$ means that the ith AAV is assigned to the jth target. For the purpose of this study, the number of AAVs and the targets is the same. Each AAV is assigned to only one target, and each target gets assigned only one AAV, that is, g_k represents a one-to-one correspondence between the AAVs and the targets.

3.4. State-Transition Law. The state-transition law specifies the next-state distribution given the current state and the action. The transition function for the vehicle state is given by $s_{k+1} = \psi(s_k, a_k, \xi_k^{\text{riv}})$, where ψ (defined later) represents the AAV kinematic model, s_k is the vehicle state, a_k is the kinematic control vector (includes forward acceleration and steering angle), and ξ_k^{riv} is the estimated river state at time k. The river state evolves according to the following equation:

$$d_{k+1}^{\text{ref}} = d_k^{\text{ref}} + o_k, \quad o_k \sim \mathcal{N}\left(0, U_k^{\text{riv}}\right), \quad (4)$$

where U_k^{riv} is the process variance corresponding to the river state evolution. The target state evolves according to

$$\chi_{k+1} = F\chi_k + e_k, \quad e_k \sim \mathcal{N}\left(0, U_k^{\text{targ}}\right), \quad (5)$$

where F represents the target motion model, and U_k^{targ} is the process covariance matrix corresponding to the target state evolution. The track states evolve according to the Kalman filter equations given the observations from the sensors onboard the AAVs. When the observations are not available, the track states evolve according to the Kalman filter equations, where only the *prediction step* is performed and the *update step* is not performed.

3.5. Cost. The cost function represents the cost of performing an action at the current state. The cost function is given by

$$C(x_k, u_k) = \sum_{i=1}^{N} \mathbb{1}\left\{\mathrm{E}\left[\left\| s_{k+1}^{i,\text{pos}} - \xi_{k+1}^{g_k(i),\text{targ,pos}} \right\| \mid x_k, u_k\right] > d_{\text{dist-thresh}}\right\}, \quad (6)$$

where $s_{k+1}^{i,\text{pos}}$ represents the 2D position coordinates of ith AAV, $\xi_{k+1}^{j,\text{targ,pos}}$ represents the estimated 2D position coordinates of the jth target at time $k+1$, $\|\cdot\|$ is the Euclidean norm (everywhere in this paper), and $\mathbb{1}\{\cdot\}$ is the indicator function which equals 1 when the expected distance between the AAV and the target at time $k+1$ is greater than some threshold distance $d_{\text{dist-thresh}}$ and 0 otherwise.

3.6. Belief State. The belief state b_k is the posterior distribution of the state at time k. The vehicle and the track states are assumed to be fully observable, that is, the belief state corresponding to the vehicle state is given by $b_k^s(s) = \delta(s - s_k)$, where $\delta(\cdot)$ is the Kronecker delta function. Similarly, the belief states corresponding to the track states can be written in terms of the actual track states. The belief states corresponding to the river and the target are the posterior distributions of d_k^{ref} and χ_k, respectively, given the history of observations.

4. Objective and Optimal Policy

The goal is to find the action sequence $(u_0, u_1, \ldots, u_{H-1})$ such that the expected cumulative cost over a time horizon H is minimized. The expected cumulative cost is given by

$$J_H = \mathrm{E}\left[\sum_{k=0}^{H-1} C\left(x_k, u_k\right)\right]. \quad (7)$$

We can write the expected cumulative cost in terms of the belief states given the initial belief state b_0 (similar to the treatment in [10, 11]) as follows:

$$J_H\left(b_0\right) = \mathrm{E}\left[\sum_{k=0}^{H-1} c\left(b_k, u_k\right) \mid b_0\right], \quad (8)$$

where $c(b_k, u_k) = \int C(x, u_k) b_k(x) \mathrm{d}x$, and b_0 is the belief state at time $k = 0$. From Bellman's principle of optimality [16], the optimal objective function value is given by

$$J_H^*\left(b_0\right) = \min_u \left\{c\left(b_0, u\right) + \mathrm{E}\left[J_{H-1}^*\left(b_1\right) \mid b_0, u\right]\right\}, \quad (9)$$

where b_1 is the random next belief state, J_{H-1}^* is the optimal cumulative cost over the horizon $H-1, k = 1, 2, \ldots, H-1$, and $\mathrm{E}[\cdot \mid b_0, u]$ is the conditional expectation given the current belief state b_0 and the current action u at time $k = 0$. Let us define the Q value of taking action u given the current belief state b_0:

$$Q_H\left(b_0, u\right) = c\left(b_0, u\right) + \mathrm{E}\left[J_{H-1}^*\left(b_1\right) \mid b_0, u\right]. \quad (10)$$

The optimal policy (from Bellman's principle) at time $k = 0$ can be written as

$$\pi_0^*\left(b_0\right) = \arg\min_u Q_H\left(b_0, u\right). \quad (11)$$

In general, it is hard to obtain the Q value exactly. There are several approximation methods in the literature: heuristic expected-cost-to-go (ECTG) [17], parametric approximation

[18], policy rollout [19], hindsight optimization [20], and foresight optimization [21]. In this paper, we use one such approximation method called *nominal belief-state optimization* (NBO), which was introduced in [11] along with other approximations and techniques specific to guidance problems. The rationale behind choosing NBO method over other methods to solve POMDP is that it is relatively inexpensive in terms of computation time, that is, the computational requirements are not prohibitive unlike other approximation methods. The following subsection provides a brief description of the NBO method.

4.1. NBO Approximation Method. The computational requirements of obtaining the optimal assignments of AAVs to targets (g_k) over a long horizon are prohibitive. Also, we expect that the optimal assignment of AAVs to targets (g_k) over a long horizon does not change with time. For these reasons, in the NBO method, we keep the assignment of AAVs to targets fixed. In other words, in approximating the expected cost-to-go in (10), g_k remains fixed over the planning horizon H. Therefore, we drop the subscript k from g_k in the objective function used in the planning based on (10), that is, $g_k = g$ for all k. In the NBO approximation method, we use the following objective function, written in terms of belief states:

$$J_H(b_0) = \mathrm{E}\left[\sum_{k=0}^{H-1} c(b_k, a_k, g) \mid b_0\right], \tag{12}$$

where a_k represents the kinematic controls for the AAVs, and g is the assignment of AAVs to the targets.

The belief states corresponding to the river state and the target state are given by

$$\begin{aligned} b_k^{\mathrm{riv}}(d) &= \mathcal{N}\left(d - \xi_k^{\mathrm{riv}}, P_k^{\mathrm{riv}}\right), \\ b_k^{\mathrm{targ}}(\chi) &= \mathcal{N}\left(\chi - \xi_k^{\mathrm{targ}}, P_k^{\mathrm{targ}}\right), \end{aligned} \tag{13}$$

where $(\xi_k^{\mathrm{riv}}, P_k^{\mathrm{riv}}, \xi_k^{\mathrm{targ}}, P_k^{\mathrm{targ}})$ are the track states corresponding to the river and the target states, respectively, which evolve according to the Kalman filter equations. In the NBO method, we approximate the objective function as follows:

$$J_H(b_0) \approx \sum_{k=0}^{H-1} c\left(\widehat{b}_k, a_k, g\right), \tag{14}$$

where $\widehat{b}_1, \ldots, \widehat{b}_{H-1}$ is a *nominal* belief-state sequence, and the optimization is over an action sequence $g, a_0, \ldots, a_{H-1}$. We obtain the *nominal* belief states by evolving the current belief state with exactly zero-noise sequence over the horizon H (similar to the treatment in [10, 11]). Therefore, the objective function from the NBO method is given by

$$J_{\mathrm{NBO}}(b_0) = \sum_{k=0}^{H-1}\sum_{i=1}^{N} \mathbb{1}\left\{\left\|\widehat{s}_{k+1}^{i,\mathrm{pos}} - \widehat{\xi}_{k+1}^{g(i),\mathrm{targ,pos}}\right\| > d_{\text{dist-thresh}}\right\}, \tag{15}$$

where $\widehat{s}_{k+1}^{i,\mathrm{pos}}$ is the *nominal* position of the ith AAV (defined below), $\mathcal{N}(\widehat{\xi}_{k+1}^{j,\mathrm{targ}}, \widehat{P}_{k+1}^{j,\mathrm{targ}})$ is the *nominal* belief state of the jth target at time $k+1$, where $\widehat{\xi}_{k+1}^{j,\mathrm{targ,pos}}$ (component of $\widehat{\xi}_{k+1}^{j,\mathrm{targ}}$) represents the position estimate of the target. This *nominal* target belief state is obtained by evolving the track state component $\widehat{\xi}_k^{j,\mathrm{targ}}$ with exactly zero-noise sequence as follows:

$$\widehat{\xi}_{k+1}^{j,\mathrm{targ}} = F\widehat{\xi}_k^{j,\mathrm{targ}}. \tag{16}$$

The evolution of vehicle state depends on the river state estimate ξ_k^{riv}. In the NBO method, ξ_k^{riv} is replaced with $\widehat{\xi}_k^{\mathrm{riv}}$ in the AAV kinematic model $\psi(\cdot)$, where $(\widehat{\xi}_1^{\mathrm{riv}}, \ldots, \widehat{\xi}_H^{\mathrm{riv}})$ are the *nominal* track state components corresponding to the river state, and the obtained positions of the ith AAV $\widehat{s}_{k+1}^{i,\mathrm{pos}}$ are called *nominal positions*.

Here, we adopt an approach called "receding horizon control," according to which we optimize the action sequence for H time steps at the current time step, implement only the action corresponding to the current time step, and again optimize the action sequence for H time steps in the next time step. The length of the planning horizon H should be large enough for an AAV to receive a benefit by moving toward a target. Due to computational constraints, we cannot have an arbitrarily long horizon. Therefore, we truncate the length of the horizon to a few time steps (we set $H = 6$ in our simulations) and append the cost function with an appropriate expected cost-to-go (ECTG). The following is a distance-based ECTG:

$$J_H^{\text{dist-ECTG}} = \sum_{i=1}^{N} \left\|\widehat{s}_H^{i,\mathrm{pos}} - \widehat{\xi}_H^{g(i),\mathrm{targ,pos}}\right\|, \tag{17}$$

where $\widehat{s}_H^{i,\mathrm{pos}}$ is the *nominal* position of the ith AAV, and $\widehat{\xi}_H^{j,\mathrm{targ,pos}}$ is the estimated location of the jth target (from NBO approach) at time $k = H$. Therefore, the objective function from the NBO method is given by

$$J_{\mathrm{NBO}}(b_0) = \sum_{k=0}^{H-1}\sum_{i=1}^{N} \mathbb{1}\left\{\left\|\widehat{s}_{k+1}^{i,\mathrm{pos}} - \widehat{\xi}_{k+1}^{g(i),\mathrm{targ,pos}}\right\| > d_{\text{dist-thresh}}\right\} + J_H^{\text{dist-ECTG}}, \tag{18}$$

where $J_H^{\text{dist-ECTG}}$ is the distance-based ECTG.

4.2. AAV Kinematics. The kinematic equations of an AAV vary depending on whether the AAV is in the river or on the land. When the AAV is in the river, we take into account the speed of the river to write the kinematic equations. The steering and thrust generation of the vehicle are modeled based on the work done by the authors of [2, 22], which is designed using single drive system. The vehicle is front-wheel driven on land. When the AAV is in the river, it is propelled using the centrifugal pump from the front wheels. The following subsections describe the kinematics of AAV on the land and in the river.

4.2.1. Kinematics of AAVs on the Land. This subsection provides the definition of ψ, which was introduced in Section 3,

when the vehicle is on land. Let $s_k = (p_k, q_k, v_k, \theta_k)$ be the state of the vehicle at time k, where (p_k, q_k) represents the location of the vehicle on the 2D plane, v_k represents the speed of the vehicle along the heading direction, and θ_k represents the heading angle of the vehicle at time k. Let $a_k = (f_k, \phi_k)$ represent the action vector of the vehicle, where f_k represents the acceleration along the direction of the front wheels, and ϕ_k represents the steering angle of the front wheels. The (simplified) schematic of a basic four-wheeled vehicle is shown in Figure 2. The control variable f_k lies within the interval $[-f_{\text{land}}, f_{\text{land}}]$, where f_{land} (or $-f_{\text{land}}$) is the maximum acceleration (or deceleration), and the control variable ϕ_k lies within the interval $[-\delta_{\text{land}}, \delta_{\text{land}}]$, where δ_{land} is the maximum steering angle. The function ψ can be specified by a set of nonlinear kinematic equations, as shown below:

$$\begin{aligned} p_{k+1} &= p_k + v_k T \cos(\theta_k), \\ q_{k+1} &= q_k + v_k T \sin(\theta_k), \\ v_{k+1} &= v_k + \mathbf{f}_k T \cos(\phi_k), \\ \theta_{k+1} &= \theta_k - \frac{2\mathbf{f}_k T^2 L}{W^2 + L^2} \sin(\phi_k), \end{aligned} \tag{19}$$

where T is the length of the time step, W is the width of the vehicle, and L is the distance between the front axle and the rear axle. The derivation of the heading angle update (19) is as follows. When the front wheels of the vehicle are oriented at a particular angle ϕ_k with respect to the main axis of the vehicle (as shown in Figure 2), the heading direction of the vehicle at time $k+1$ is derived as follows:

$$\begin{aligned} \alpha &= \arctan\left(\frac{W}{L}\right), \\ \theta_{k+1} &= \theta_k + \frac{T^2}{\sqrt{L^2 + W^2}} \left(f_{k,1}^{\theta} - f_{k,2}^{\theta}\right) \\ &= \theta_k + \frac{f_k T^2}{\sqrt{L^2 + W^2}} \left[\sin(\alpha - \phi_k) - \sin(\alpha + \phi_k)\right] \\ &= \theta_k - \frac{2 f_k T^2}{\sqrt{L^2 + W^2}} \left[\cos(\alpha) \sin(\phi_k)\right] \\ &= \theta_k - \frac{2 f_k T^2 L}{W^2 + L^2} \sin(\phi_k). \end{aligned} \tag{20}$$

4.2.2. Kinematics of AAVs on the River. This subsection provides the definition of ψ, when the vehicle is in the river. The kinematic equations of the AAV motion are as follows:

$$\begin{aligned} p_{k+1} &= p_k + v_k T \cos(\theta_k) + \widehat{w}_k^x (p_k, q_k) T, \\ q_{k+1} &= q_k + v_k T \sin(\theta_k) + \widehat{w}_k^y (p_k, q_k) T, \end{aligned} \tag{21}$$

where $\widehat{w}_k^x(p_k, q_k)$ and $\widehat{w}_k^y(p_k, q_k)$ are the estimated speeds of the river at the location (p_k, q_k) in x and y directions, respectively, which are obtained from the river state estimate $\widehat{\xi}_k^{\text{riv}}$ and the river model presented in Section 2. The speed and the heading angle update equations remain the same as in the case of land. When in water (or river), the control variable f_k lies within the interval $[-f_{\text{water}}, f_{\text{water}}]$, where f_{water} is the maximum acceleration, and ϕ_k lies within the interval $[-\delta_{\text{water}}, \delta_{\text{water}}]$, where δ_{water} is the maximum steering angle. Typically, the values of f_{water} and δ_{water} are much smaller compared to that of f_{land} and δ_{land}.

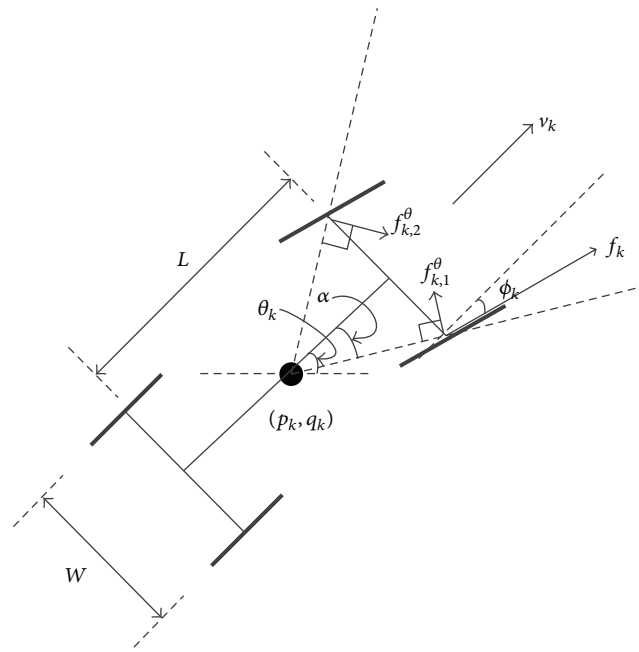

Figure 2: Free body diagram of an AAV.

5. Simulation

We implement the NBO method in MATLAB, and we use the command *fmincon* (MATLAB's optimization tool) to solve the optimization problem. For performance comparison, we also implement a greedy approach, where we optimize only the current kinematic control for the AAVs such that the following symmetric-distance-based cost is minimized:

$$\begin{aligned} J_{\text{Greedy}}(b_k) = &\sum_{i=1}^{N} \min_j \left\| \widehat{s}_{k+1}^{i,\text{pos}} - \widehat{\xi}_{k+1}^{j,\text{targ,pos}} \right\| \\ &+ \sum_{j=1}^{N} \min_i \left\| \widehat{s}_{k+1}^{i,\text{pos}} - \widehat{\xi}_{k+1}^{j,\text{targ,pos}} \right\|, \end{aligned} \tag{22}$$

where $\widehat{s}_{k+1}^{i,\text{pos}}$ and $\widehat{\xi}_{k+1}^{j,\text{targ,pos}}$ are the *nominal* positions (obtained by evolving the belief states with zero noise) of the ith AAV and the jth target at time $k+1$, respectively. Our simulation environment is two dimensional, that is, the AAVs, the river, and the targets move in 2D. According to the river model, the speed of the river stream w_k at a location (p, q) is given by $w_k(p, q) = C_1[\log(d_k(p, q)) + C_2]$, where $d_k(p, q)$ is the depth of the river at (p, q), and C_1 and C_2 are constants. Since the depth of the river is not fully observable, we estimate $d_k(p, q)$ as follows. The elevation map of the landscape is known

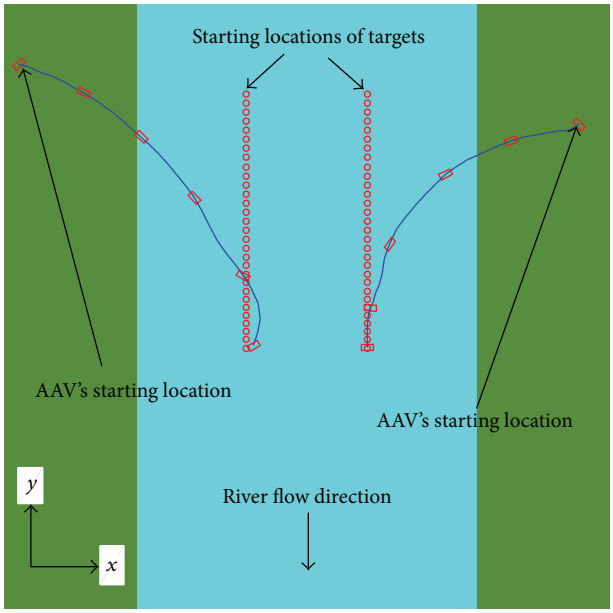

Figure 3: Simulation of Scenario I with NBO approach, *average rescue time* = 36 steps.

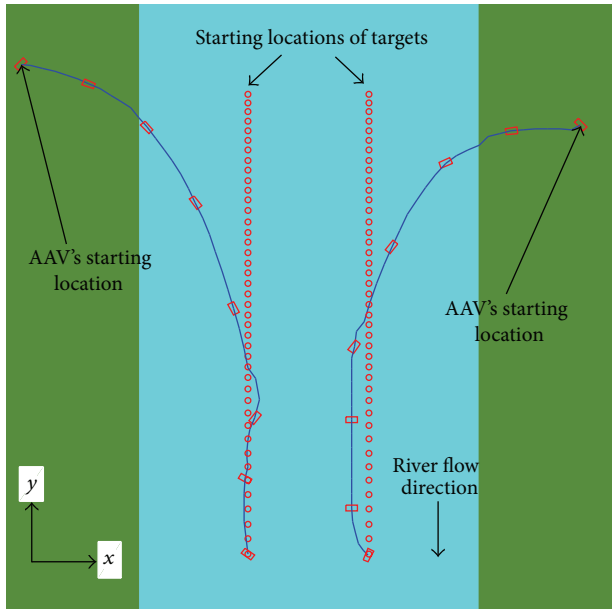

Figure 4: Simulation of Scenario I with greedy approach, *average rescue time* = 64 steps.

a priori, that is, if we know the depth of the river at a particular location, we can obtain the depth of the river at all locations. Therefore, we estimate the depth of the river at location (p, q), that is, $\widehat{d}_k(p, q)$ using the estimated depth of the river at the reference point $\widehat{d}_k^{\text{ref}}$ $(= \widehat{\xi}_k^{\text{riv}})$. Therefore, the estimated speed of the river at location (p, q) is given by $\widehat{w}_k(p, q) = C_1[\log(\widehat{d}_k(p, q)) + C_2]$. We set the length of the horizon H to 6 time steps, and the length of the times step T to 1 second. In the simulations, the flooded river flows along a valley in the landscape from the north toward the south as shown in Figure 1. Since the simulations are in 2D, the river flows toward the $-y$ direction, and the river speed in x direction (toward the east) is zero at every location. Therefore, the estimated speeds of the river at location (p, q) in x and y directions are given by $\widehat{w}_k^x(p, q) = 0$ and $\widehat{w}_k^y(p, q) = -C_1[\log(\widehat{d}_k(p, q)) + C_2]$. Here, we model the dynamics of the target motion by the *constant velocity model* (see [23] for the definition of the variables F and U_{targ} in (5)).

In the simulations, an AAV is represented by a rectangle, and the line connecting the rectangles represents the trajectory of the AAV. We define a performance metric called *average rescue time*—the average of the rescue times of each target (the rescue time of a target is the time elapsed after the start of the simulation until it is rescued). The POMDP cost function defined in Section 3 is reflective of this performance metric. We simulate three scenarios: Scenario I, Scenario II, and Scenario III. In Scenario I, there are two AAVs, each one located on the opposite banks of the river, and two targets are moving (being drifted by the moving water) in the river, as shown in Figure 3. Figure 3 shows a snapshot of the scenario at the end of the simulation with the NBO approach, where the *average rescue time* is 36 time steps. We also simulate

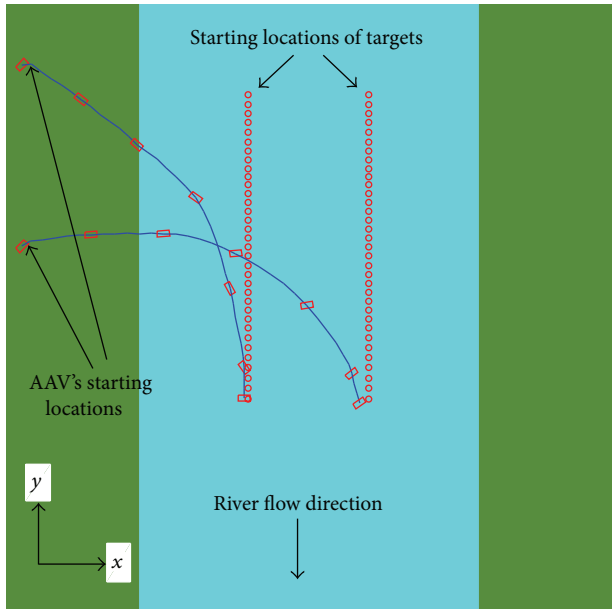

Figure 5: Simulation of Scenario II with NBO approach, *average rescue time* = 45 steps.

Scenario I with the greedy approach, as shown in Figure 4, where the *average rescue time* is 64 time steps. In Scenario II, there are two AAVs on the left bank of the river, and two targets are moving in the river. We simulate this scenario with both the NBO and the greedy approaches. Figure 5 shows the snapshot of the scenario with the NBO approach at the end of the simulation, where the *average rescue time* is 45 time

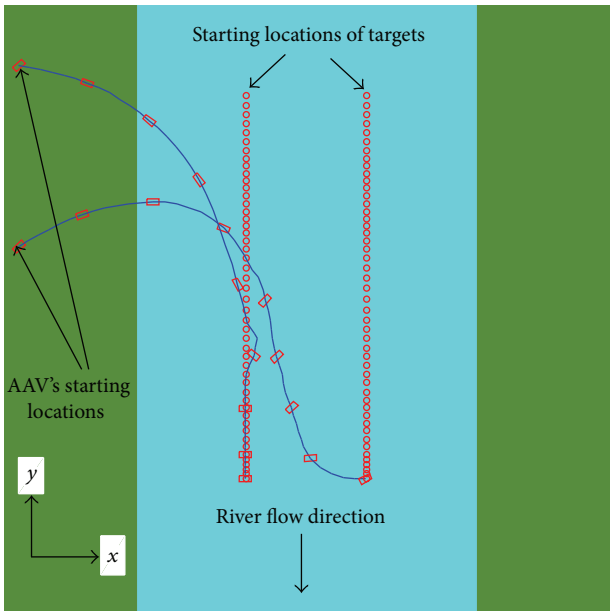

Figure 6: Simulation of Scenario II with the greedy approach, *average rescue time* = 62 steps.

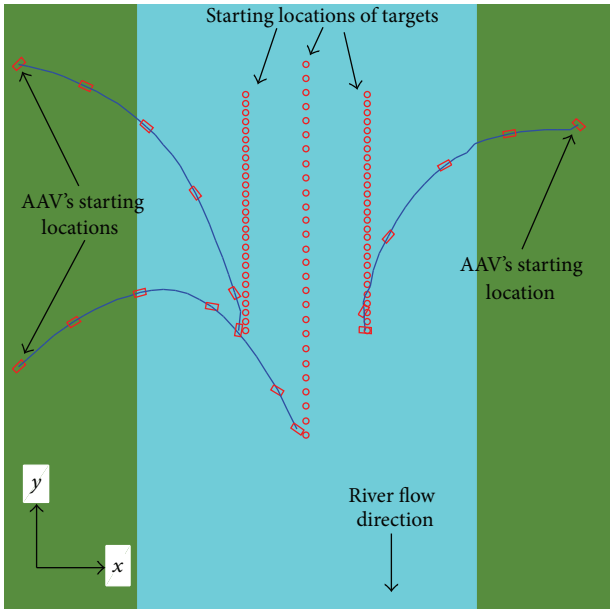

Figure 7: Simulation of Scenario III with NBO approach, *average rescue time* = 48 steps.

steps, and Figure 6 shows the simulation of the same scenario with the greedy approach, where the *average rescue time* is 62 time steps. In Scenario III, there are three AAVs (two on the left bank of the river and one on the right), and three targets are moving in the river. We simulate this scenario with both the NBO and the greedy approaches. Figure 7 shows the scenario with the NBO approach, where the *average rescue time* is 48 time steps, and Figure 8 shows the simulation of the same scenario with the greedy approach, where the

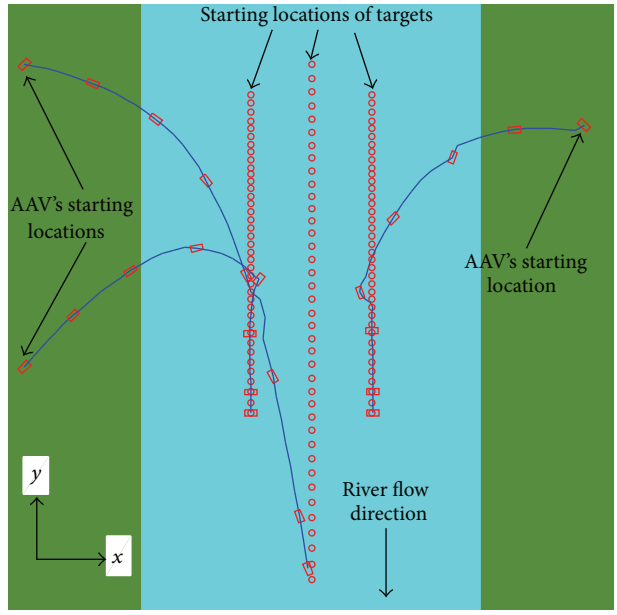

Figure 8: Simulation of Scenario III with the greedy approach, *average rescue time* = 76 steps.

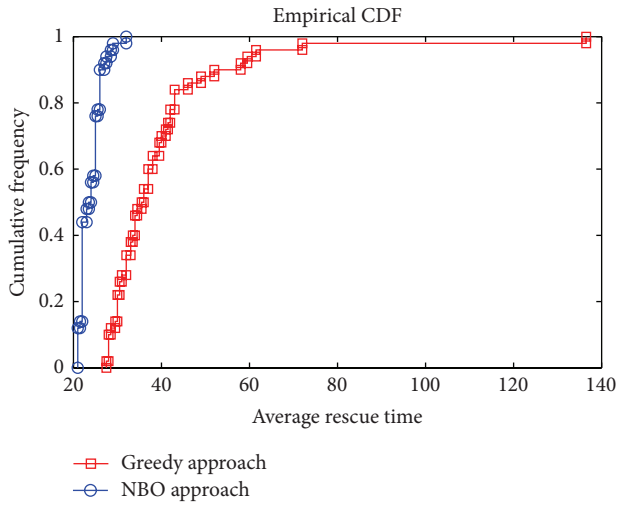

Figure 9: Performance comparison for Scenario I: NBO approach versus greedy approach.

average rescue time is 76 time steps. The simulation of these scenarios demonstrates that the NBO approach achieves a better coordination among the AAVs compared to the greedy approach while rescuing the targets, as evident from the *average rescue times*.

We compare the performance of the NBO approach with that of the greedy approach through Monte-Carlo simulations. We simulate the above scenarios with the NBO and the greedy approaches separately for 50 Monte-Carlo runs. In each scenario, we compute the *average rescue time* in every run for both the NBO and the greedy approaches. Figures 9, 10, and 11 show the plots of the cumulative

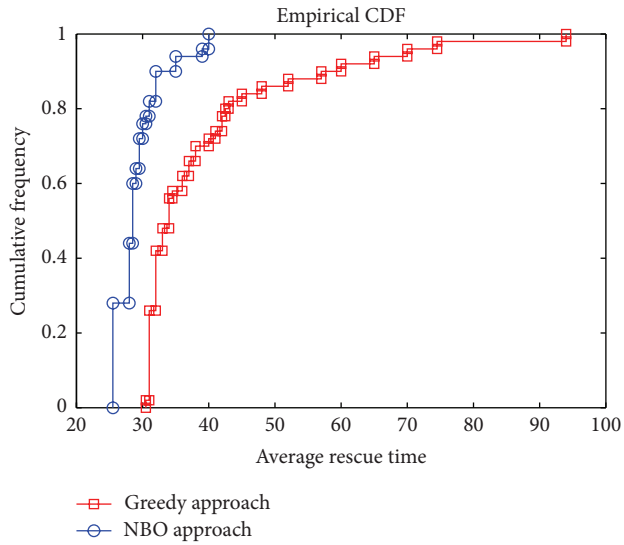

Figure 10: Performance comparison for Scenario II: NBO approach versus greedy approach.

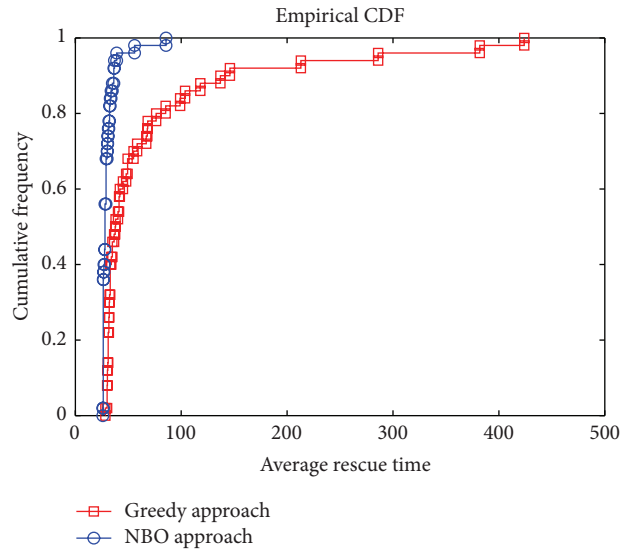

Figure 11: Performance comparison for Scenario III: NBO approach versus greedy approach.

frequencies of *average rescue times* for the NBO and the greedy approaches for Scenarios I, II, and III, respectively. Figures 9, 10, and 11 demonstrate that the NBO approach significantly outperforms the greedy approach.

The algorithm (NBO) runtime to compute the control commands for three AAVs (in Scenario III) in any time step in MATLAB is approximately 4 seconds on a lab computer (Intel Core i7-860 Quad-Core Processor with 8 MB Cache and 2.80 GHz speed). This runtime can be greatly reduced on a better processor and by further optimizing the code. Since the algorithm runtime is not prohibitive, it can be used in real time (i.e., for practical purposes).

6. Conclusions, Remarks, and Future Scope

We designed a guidance algorithm for autonomous amphibious vehicles (AAVs) to rescue moving targets in a 2D flood scenario, where the flood water flows across the scene, and the targets move in the flood water. We designed this algorithm based on the theory of *partially observable Markov decision process* (POMDP). Since a POMDP problem is intractable to solve exactly, we used an approximation method called *nominal belief-state optimization* (NBO). We simulated a few scenarios to demonstrate the coordination among the AAVs achieved by the NBO approach. We defined a performance metric called *average rescue time* to compare the performance of our approach with a greedy approach. Our results show that the NBO approach outperforms the greedy approach significantly. This was expected because unlike the greedy approach the NBO approach has a lookahead property, that is, the NBO approach trades off the short-term performance for the long-term performance. Although the greedy approach achieves coordination among the AAVs in that the AAVs eventually rescue all the targets, but the performance in terms of *average rescue time*, which is crucial in these kinds of rescue missions, is poor compared to our NBO approach. In our future work, we would like to develop methods to further improve our NBO approach (e.g., NBO with adaptive horizon). We would also like to extend our approach to a decentralized AAV guidance problem to rescue multiple targets. In this decentralized case, we will induce coordination among the AAVs to rescue multiple targets by appropriately optimizing the communication (at the network level) between the AAVs along with the kinematic controls for the AAVs.

Acknowledgments

This work was supported in part by the Fulbright Foundation. The authors would also like to acknowledge Colorado State University's support via the Libraries Open Access Research and Scholarship Fund (OARS).

References

[1] M. Frejek and S. Nokleby, "Design of a small-scale autonomous amphibious vehicle," in *Proceedings of IEEE Canadian Conference on Electrical and Computer Engineering (CCECE '08)*, pp. 781–786, Niagara Falls, Canada, May 2008.

[2] E. Papadopoulos and M. Misailidis, "On differential drive robot odometry with application to path planning," in *Proceedings of the European Control Conference*, pp. 5492–5499, Kos, Greece, July 2007.

[3] Y. Tee, Y. Tan, B. Teoh, E. Tan, and Z. Wong, "A compact design of zero-radius steering autonomous amphibious vehicle with direct differential directional drive—UTAR-AAV," in *Proceedings of IEEE International Conference on Robotics, Automation and Mechatronics (RAM '10)*, pp. 176–181, Singapore, June 2010.

[4] Q. P. Ha, T. H. Tran, S. Scheding, G. Dissanayake, and H. F. Durrant-Whyte, "Control issues of an autonomous vehicle," in *Proceedings of the 22nd International Symposium on Automation and Robotics in Construction (ISARC '05)*, Ferrara, Italy, September 2005.

[5] W. Masayoshi, "Research and development of electric vehicles for clean transportation," *Journal of Environmental Sciences*, vol. 21, no. 6, pp. 745–749, 2009.

[6] T. Brunl, *Embedded Robotics*, Springer, Berlin, Germany, 3rd edition, 2008.

[7] T. H. Tran, Q. P. Ha, R. Grover, and S. Scheding, "Modelling of an autonomous amphibious vehicle," in *Proceedings of the Australasian Conference on Robotics and Automation (ACRA '04)*, Canberra, Australia, December 2004.

[8] R. Manduchi, A. Castano, A. Talukder, and L. Matthies, "Obstacle detection and terrain classification for autonomous off-road navigation," *Autonomous Robots*, vol. 18, no. 1, pp. 81–102, 2005.

[9] S. Lacroix, A. Mallet, D. Bonnafous et al., "Autonomous rover navigation on unknown terrains: functions and integration," *International Journal of Robotics Research*, vol. 21, no. 10-11, pp. 917–942, 2002.

[10] S. Ragi and E. K. P. Chong, "Dynamic UAV path planning for multitargte tracking," in *Proceedings of the American Control Conference (ACC '12)*, pp. 3845–3850, Montreal, Canada, June 2012.

[11] S. A. Miller, Z. A. Harris, and E. K. P. Chong, "A POMDP framework for coordinated guidance of autonomous UAVs for multitarget tracking," *EURASIP Journal on Advances in Signal Processing*, vol. 2009, Article ID 724597, 17 pages, 2009.

[12] T. H. Tran, *Modelling and control of unmanned ground vehicles [Ph.D. thesis]*, 2007.

[13] S. A. Watson and P. N. Green, "Design considerations for micro-autonomous underwater vehicles (μAUVs)," in *Proceedings of the IEEE International Conference on Robotics, Automation and Mechatronics (RAM '10)*, pp. 429–434, Singapore, June 2010.

[14] S. A. Watson and P. N. Green, "Propulsion systems for micro-autonomous underwater vehicles (μAUVs)," in *Proceedings of IEEE International Conference on Robotics, Automation and Mechatronics (RAM '10)*, pp. 435–440, Singapore, June 2010.

[15] L. D. Landau, *Fluid Mechanics*, chapter IV, Pergamon Press, 2nd edition, 2000.

[16] R. Bellman, *Dynamic Programming*, Princeton University Press, Princeton, NJ, USA, 1957.

[17] C. Kreucher, A. O. Hero, K. Kastella, and D. Chang, "Efficient methods of non-myopic sensor management for multitarget tracking," in *Proceedings of the 43rd IEEE Conference on Decision and Control (CDC '04)*, pp. 722–727, Paradise Island, Bahamas, December 2004.

[18] D. P. Bertsekas and J. N. Tsitsiklis, *Neuro-Dynamic Programming*, Athena Scientific, Belmont, Mass, USA, 1996.

[19] D. P. Bertsekas and D. A. Castañon, "Rollout algorithms for stochastic scheduling problems," *Journal of Heuristics*, vol. 5, no. 1, pp. 89–108, 1999.

[20] E. K. P. Chong, R. L. Givan, and H. S. Chang, "A framework for simulation-based network control via hindsight optimization," in *Proceedings of the 39th IEEE Confernce on Decision and Control*, pp. 1433–1438, Sydney, Australia, December 2000.

[21] D. P. Bertsekas, *Dynamic Programming and Optimal Control*, vol. 2, Athena Scientific, Belmont, Mass, USA, 2007.

[22] Y. Tee, B. Teoh, D. E. B. Tan, Z. Wong, C. Tan, and Y. Tan, "Design considerations of autonomous amphibious vehicle (UTAR-AAV)," in *Proceedings of IEEE Conference on Sustainable Utilization and Development in Engineering and Technology (STUDENT '10)*, pp. 13–18, Petaling Jaya, Malaysia, November 2010.

[23] S. Blackman and R. Popoli, *Design and Analysis of Modern Tracking Systems*, Artech House, Boston, Mass, USA, 1999.

Hindawi Publishing Corporation
Mathematical Problems in Engineering
Volume 2013, Article ID 808565, 9 pages
http://dx.doi.org/10.1155/2013/808565

Research Article

Modelling Snowmelt Runoff under Climate Change Scenarios in an Ungauged Mountainous Watershed, Northwest China

Yonggang Ma,[1,2,3] Yue Huang,[1] Xi Chen,[1] Yongping Li,[4] and Anming Bao[1]

[1] *State Key Laboratory of Desert and Oasis Ecology, Xinjiang Institute of Ecology and Geography, Chinese Academy of Sciences, Urumqi 830011, China*
[2] *College of Resources and Environment Science, Xinjiang University, Urumqi 830046, China*
[3] *Xinjiang Remote Sensing Center, Urumqi 830011, China*
[4] *MOE Key Laboratory of Regional Energy Systems Optimization, Sino-Canada Resources and Environmental Research Academy, North China Electric Power University, Beijing 102206, China*

Correspondence should be addressed to Yue Huang; hy800821@163.com

Received 1 February 2013; Accepted 14 April 2013

Academic Editor: Songlin Nie

An integrated modeling system has been developed for analyzing the impact of climate change on snowmelt runoff in Kaidu Watershed, Northwest China. The system couples Hadley Centre Coupled Model version 3 (HadCM3) outputs with Snowmelt Runoff Model (SRM). The SRM was verified against observed discharge for outlet hydrological station of the watershed during the period from April to September in 2001 and generally performed well for Nash-Sutcliffe coefficient (EF) and water balance coefficient (RE). The EF is approximately over 0.8, and the water balance error is lower than ± 10%, indicating reasonable prediction accuracy. The Statistical Downscaling Model (SDSM) was used to downscale coarse outputs of HadCM3, and then the downscaled future climate data were used as inputs of the SRM. Four scenarios were considered for analyzing the climate change impact on snowmelt flow in the Kaidu Watershed. And the results indicated that watershed hydrology would alter under different climate change scenarios. The stream flow in spring is likely to increase with the increased mean temperature; the discharge and peck flow in summer decrease with the decreased precipitation under Scenarios 1 and 2. Moreover, the consideration of the change in cryosphere area would intensify the variability of stream flow under Scenarios 3 and 4. The modeling results provide useful decision support for water resources management.

1. Introduction

Northwest of China is a typical arid region, which is characterized by low and irregular rainfall, high temperature, and evaporation. A major proportion of flow in the rivers in this region is contributed by snow and glacier-fed river catchments located in the mountainous area [1]. Particularly in springs, the inflow coming from the snowmelt process is accounting for an average of approximately 70% of total annual river flow [2]. Snowmelt is the major source of many rivers and significantly contributes to the local populace and social-economic development. However, when snowmelt and storms combine, the area is also easily flooded [3, 4]. Therefore, it is essential to estimate the snowmelt runoff for these mountainous catchments and evaluate the impact of climate change on snowmelt runoff for water resources management of the arid area.

Hydrologic model is a useful tool for flood forecasting and water resources management [5]. Previously, different hydrological models with a snow component were used to simulate the daily stream flows in snow- and glacier-fed catchments [1, 6–9]. However, most of the hydrological models are not satisfactory for daily stream flow simulation and forecasting in the mountainous catchments, where the snowmelt is a major factor in the water cycle [10, 11]. Since most of these models are sensitive to the precipitation forcing, the precipitation data available from the high altitude catchments is not of very good quality [1, 12]. Lack of information for temporal and spatial rainfall variability has brought large uncertainty in snowmelt runoff forecasting [6, 13].

Snowmelt Runoff Model (SRM) [14] is one of the widely used models to simulate and forecast the daily stream flows in these types of mountainous catchments [1]. It is currently based on a simple degree-day method. The daily precipitation, air temperature, and snow cover area are the input data. In addition, a number of basin characteristics such as basin area, zone area, and the hypsometric (area elevation) curve are also needed. The daily water produced from the snowmelt and rainfall is superimposed on the calculated recession flow and transformed into daily discharge from the catchment [1]. The main advantage of the SRM is its weak sensibility to the precipitation inputs and more sensitive to the daily snow cover and temperature data. Due to the progress of satellite remote-sensing of the cryosphere, the SRM has been applied to larger and larger basins [15]. Previously, a number of researchers applied the SRM to simulate the snow melting runoff by using MODIS snow cover products as basic inputs [15–18]. Additionally, few researchers found that the SRM combined with MODIS snow cover and TRMM rainfall data significantly improves regional runoff modeling for the Himalayas [19]. In the Northwest of China, several studies focused on applying the SRM to simulate the snowmelt runoff processes [20–22]. Wang et al. [23] used the SRM, in which MODIS snow covered area products and meteorological stations data were used as input parameters, to simulate the snowmelt process in three watersheds in the upper reaches of Heihe River Basin. Zhang et al. [21] used the SRM for daily runoff forecast of Manasi Watershed, in which CMA T213 meteorological data for forecasting zonal temperature and precipitation of the watershed were used in snow melting runoff modeling. Zhang et al. [3] analyzed the influence of catchment characteristics on the parameters of the SRM and discussed the corresponding determination strategy to improve the accuracy of snowmelt simulation and forecast. Ma and Cheng [22] found a Nash-Sutcliffe coefficient value of 0.80 when simulating the stream flow in the Gongnaisi Watershed in the Western Tianshan Mountains by applying the SRM. The previous studies of applying the SRM to mountainous watershed of Northwest China and other regions of the world suggest that the model can efficiently be applied in the snow- and glacier-fed river basins to simulate and forecast the daily stream flows.

Most recently, the SRM has been applied to evaluate the effect of climate change on seasonal snow cover and runoff [10]. For example, Tahir et al. [1] integrated the SRM with MODIS remote-sensing snow cover products to simulate the daily runoff and to study the climate change impact on discharge in the Hunza River Basin. Immerzeel et al. [16] applied the SRM in the upper Indus Basin and reported that regional warming is affecting the hydrology process due to accelerated glacial melting during the simulation period. Liu et al. [24] simulated the relationship among air temperature, precipitation, and runoff when the temperature rises by 1°C in Dongkemadi River Basin, China; the result indicated that the rise of air temperature would speed up snowmelt, and the changes of precipitation state are the main reasons of the runoff increase from May to June; the rise of runoff from July to October is mainly caused by the melting of glacier.

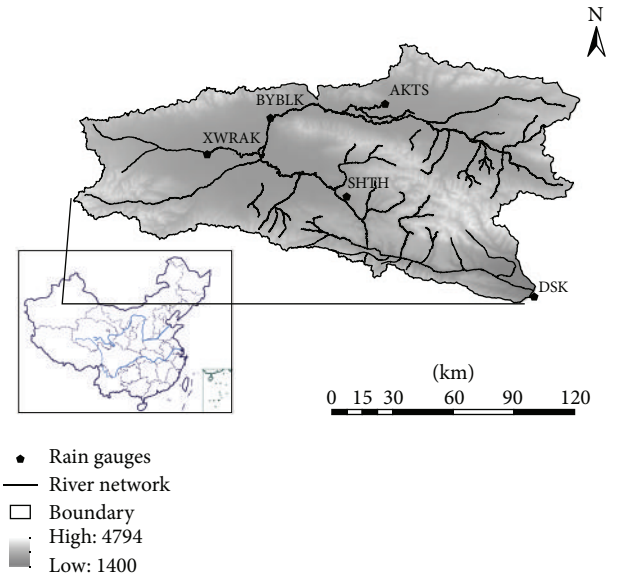

Figure 1: Study area of Kaidu Watershed (China's borders were downloaded from National Administration of Surveying, Mapping, and Geoinformation; number: GS(2008)1045).

However, the scenarios of future climate change in most pervious SRM simulations were simply defined by increasing or decreasing the temperature and precipitation forcing data. Few works focus on integrating climate change scenarios which based on the General Circulation Model (GCM) with the SRM in the snowmelt runoff modeling of mountainous catchment [25].

Therefore, the objective of this study is to develop an intergraded modeling system through coupling the GCM outputs with the SRM for analyzing the impact of future climate change on snowmelt flow and water resources in the Kaidu Watershed, Northwest China. In the study, the SRM model will be used to simulate the hydrological response on snow and glacier melting runoff; GCM data will be used for defining future climate change scenarios, used as inputs for simulating the climate impact on hydrology. The results obtained will be used for helping the planers to establish effective water exploitation and allocation policies and thus improve the local ecosystem sustainability and social-economic development.

2. Study Area

The Kaidu Watershed is located in the middle reach of the Tarim River and has an area of approximately 19.0×10^3 km^2. Figure 1 shows the outline of the catchment with the major river system, rain gauges, and DEM. There is no doubt that the discharge and flood events of Kaidu River not only represent destructive natural hazard in the mountainous, but also are the obvious complements for the lower reach of the Tarim River. The mean elevation of the watershed ranges from 2400 m to 2600 m above sea level in the basin, and from 4000 m to 5500 m in the mountain. The spatial and temporal distribution of precipitation is strongly heterogeneous. The

average rainfall is about 273 mm/year. More than 80% of the total annual precipitation falls from May to September, and less than 20% of the total falls from November to the following April. The Kaidu Watershed has an extreme cold climate with an average temperature of −4.16°C. Average pan evaporation is about 1157 mm/year. Snow melting is one of the most important sources in spring and summer.

There are two possible water release peaks per year. The snow on the lower mountains melts in spring, and glaciers in the high mountains melt in summer. Stream flow from May to October contributes more than 70% of the total flow. Peak flows at the DSK station reach around 400–700 m^3/s in August and September and drop to almost zero during the end of the dry season. The spring snowmelt water is also the main water source for the germination of the Bayanbulak pasture [3]. Therefore, it is deemed necessary to develop effective modeling system for analyzing the impact of climate change on snowmelt runoff and water resources in the study area [13, 26].

3. Methodology

3.1. Data Collection. Kaidu Watershed is a typical ungauged catchment in Northwest China, and conventional meteorological observations began in 1956. There are six gauge stations in the watershed, but only two stations have continuous long time records of the meteorological and hydrological elements. One is the Bayanbulak (BYBLK) station which records temperature and precipitation data, and the other is the Dashankou (DSK) station which provides temperature and runoff data (Figure 1). General meteorological data comprising air temperatures and daily precipitation were collected for the period of 1961–2001.

The input topography map was derived from the 90 m × 90 m digital elevation model (DEM). As the physical environment varies drastically with increasing altitudes, the basin with a great elevation range was divided into several zones to better describe the physical environment [1]. Former studies suggest that an interval less than 500 m is better for the elevation zones, while excessively small intervals would increase the modeling complexity. Thus, we divided the elevation zone with an interval of 425 m in this study (Figure 2).

The Moderate Resolution Imaging Spectroradiometer (MODIS) MOD10A2 products were used to generate snow cover inputs of the SRM. The MODIS/Terra Snow Cover 8-Day L3 Global 500 m Grid (MOD10A2) contains data fields for maximum snow cover extent over an 8-day repeated period and has a resolution of approximately 500 m completely covering the Kaidu Watershed [27]. When the percentage of cloud cover exceeded 20% on a specific date, the record was removed and then the average snow cover was estimated on this date by interpolating linearly between the previous and the next available cloud-free images [28]. The snow cover area was also calculated for the different altitudinal zones to use further for snowmelt-runoff modeling.

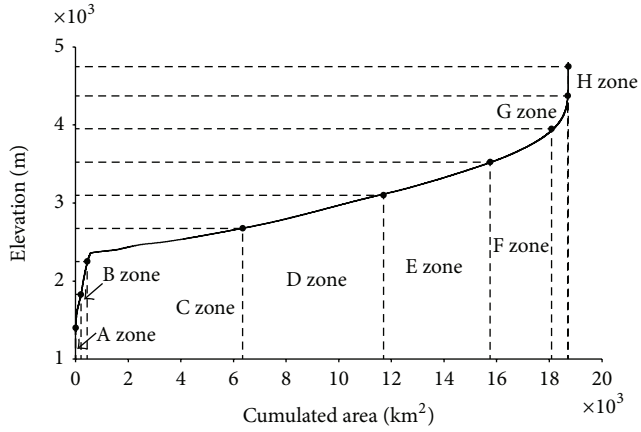

Figure 2: Area distributions of different elevation zones in the Kaidu Watershed.

3.2. Snowmelt-Runoff Model (SRM). SRM is a conceptual, deterministic, degree day hydrologic model used to simulate daily runoff resulting from snowmelt and rainfall in mountainous regions. SRM requires daily temperature, precipitation, and daily snow covered area values as input parameters. Stream flow is calculated according to the following equation [14]:

$$Q_{n+1} = \left[\mathrm{Csn} \cdot a_n \left(T_n + \Delta T_n\right) S_n + \mathrm{Crn} P_n\right] \cdot A \cdot \left(\frac{10000}{86400}\right) \cdot \left(1 - k_{n+1}\right) + Q_n \cdot k_{n+1}, \quad (1)$$

where Q_{n+1} (m^3/s) is the discharge at day $n + 1$; Csn (—) is the snow runoff coefficient; a_n is degree day factor on day n ($cm^\circ C^{-1} d^{-1}$); $T_n + \Delta T_n$ (°C) are the degree days; S_n (—) is the fractional snow cover; Crn (—) is the rainfall runoff factor; P_n (cm) is the rain on day n; A is total area (km^2); k_{n+1} is the discharge recession coefficient.

The SRM was used to simulate the daily discharges in the Kaidu River at outlet DSK station. It used the MODIS snow cover data as basic input. The model was run for snowmelt season in 2001 (April to September 2001) to simulate the daily discharges in the Kaidu Watershed. The SRM parametric values were estimated during the calibration of the model and extracted from the studies conducted previously on mountainous watersheds in Tianshan Mountains (e.g., [3, 22]).

The time series of discharge at DSK station available for 2001 was used for calibrating the SRM. The Nash-Sutcliffe coefficient (EF) and the water balance coefficient (RE) were used to evaluate the relationship between the observed and simulated daily discharges in the applications of the SRM. Consider

$$\text{Nash-Sutcliffe coefficient: } \mathrm{EF} = 1 - \frac{\sum_{i=1}^{n} \left(Q_{\mathrm{obs},i} - Q_{\mathrm{sim},i}\right)^2}{\sum_{i=1}^{n} \left(Q_{\mathrm{obs},i} - \overline{Q}_{\mathrm{obs}}\right)^2},$$

$$\text{Water balance coefficient: } \mathrm{RE} = 1 - \frac{\sum_{i=1}^{n} \left|Q_{\mathrm{obs},i} - Q_{\mathrm{sim},i}\right|}{\sum_{i=1}^{n} Q_{\mathrm{obs},i}}, \quad (2)$$

where $Q_{obs,i}$ is the observed discharge at time step i, $Q_{sim,i}$ is the simulated discharge at time step i, $\overline{Q}_{obs}$ is the mean observed discharge, and n is the total number of time steps. Note that the SRM estimations are optimal when EF and RE are close to 1.

3.3. Climate Change Impact Detection. Globe circulation model (GCM) accounts for dynamics of global circulation patterns and earth surface-atmosphere system, but their results are too coarse to be used for hydrologic processes [25]. In order to link output from GCM with basin-scale hydrologic models, a downscaling process is necessary. The Statistical Downscaling Model (SDSM) [29] was used to downscale the GCM outputs for the Kaidu Watershed. Daily precipitations as well as daily mean temperature data were chosen as predictand variables for the downscaling experiments.

The Bayanbulak (BYBLK) meteorological stations, which are inside this watershed, and with 50 years of precipitation and temperature records representing the current climate (1961–2000), were identified for the downscaling experiments. Observed daily data of large-scale predictor variables representing the current climate condition was derived from the NCEP reanalysis data set. Climate variables corresponding to the future climate change for the study area were extracted from the Hadley Centre Coupled Model version 3 (HadCM3) output under IPCC SRES A2 and B2 scenarios at a grid point which is closest to the BYBLK station. Data was extracted for three distinct periods named 2020s (covering a 30-year period between 2010 and 2039), 2050s (2040–2069), and 2080s (2070–2099).

The verified SRM would be used to simulate the impact of climate change on the Kaidu River runoff. The verified SRM would be used to simulate the impact of climate change on the Kaidu River runoff. Some researches indicate that the climate change had a significant impact on the hydrological process of the Kaidu Watershed during the past 50 years [3]. In mountainous region like the Kaidu Watershed, variation of river runoff is mainly influenced by two factors: (1) time and space distribution change of the precipitation, and (2) snow and glacier melting which is caused by rising temperatures [4, 6, 13]. Therefore, we defined the future climate change scenarios by using downscaled GCMs simulation data, and also considered the impact of rainfall, snow melting, and glacier melting on stream flows. Four scenarios were defined as follows.

(a) In Scenario 1, the change of cryosphere area was not considered, while the mean temperature and precipitation were changed based on the statistical downscaling results of HadCM3 outputs under SERS A2 scenario.

(b) In Scenario 2, the change of cryosphere area was not considered, while the mean temperature and precipitation area changed based on the statistical downscaling results of HadCM3 outputs under SERS B2 scenario.

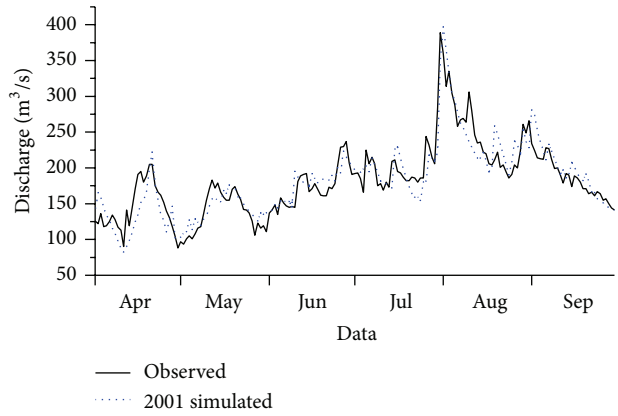

Figure 3: Simulation results of the SRM at DSK station in Kaidu Watershed.

(c) In Scenario 3, the mean temperature and precipitation were changed based on the statistical downscaling results of HadCM3 outputs under SERS A2 scenario; in addition, the cryosphere area was assumed to increase or decrease 20%.

(d) In Scenario 4, the mean temperature and precipitation were changed based on the statistical downscaling results of HadCM3 outputs under SERS B2 scenario; the cryosphere area was assumed to increase or decrease 50%.

4. Results Analysis

4.1. Results of SRM Simulation. Simulations were performed for the Kaidu Watershed, where the conventional meteorological data were available for the period of 2001. Parameters adjustment was carried out manually by using a trial-and-error procedure. Sensitivity analysis was conducted to investigate the effects of the model responses to its parameters and to identify those which should have further calibration [30]. The most sensitive parameters are snowmelt runoff coefficient (C_s), rainfall runoff coefficient (C_r), and degree-day factor (a). The values of the main parameters for SRM in the Kaidu Watershed are listed in Table 1.

Figure 3 shows the simulated and observed hydrographs for snow melting periods. There is a statistically significant relationship between the simulated and the observed data, and the simulated river flow captures the interannual variations well. The simulation results are encouraging with EF of 0.81 and RE of 0.91, respectively. Table 2 presents the statistics for model performance of the SRM during April to September in 2001. The best performance of the model is found in May, and the worst performance of the model is found in April with the lowest EF value of 0.32, and the lowest RE value of 0.84. In addition, several main parameters in the SRM model can be inputted by basin wide (BWM) or by zone (ZWM); simulation results of the stream flow under a different parameter input mode were also compared (Figure 4).

Table 1: Value of main parameters for the SRM.

Parameter	A zone	B zone	C zone	D zone	E zone	F zone	G zone	H zone
Lapse rate (°C/100 m)	0.55	0.55	0.55	0.55	0.65	0.65	0.65	0.65
T_{cric} (°C)	−0.5 (Apr, Sep) 0 (May–Aug)						−0.5	−0.5
DDF (cm °C^{-1} d^{-1})	0.3 (Apr, Sep) 0.45 (May–Jul) 0.55 (Aug)						0.6	
Lag time (h)	18							
C_s	0	0	0.1	0.1	0.15	0.15	0.2	0.2
C_r	0.35 (Apr, Sep) 0.40 (May–Jul) 0.45 (Aug)	0.30 (Apr, Sep) 0.35 (May–Jul) 0.40 (Aug)	0.30 (Apr, Sep) 0.35 (May–Jul) 0.40 (Aug)	0.30 (Apr, Sep) 0.35 (May–Aug)	0.25 (Apr, Sep) 0.30 (May–Jul) 0.35 (Aug)	0.25 (Apr, Sep) 0.30 (May–Aug)	0.25	0.25
RCA	1	1	1	1	1 (Apr 1th–15th) 0 (Apr 16th–Sep)	1 (Apr 1th–15th) 0 (Apr 15th–Sep)	0	0
X_c	0.98							
Y_c	0.02							

Table 2: Performance of the daily snowmelt runoff simulation.

	EF	RE
Snowmelt seasons	0.81	0.91
April	0.32	0.84
May	0.69	0.91
June	0.66	0.93
July	0.66	0.91
August	0.63	0.92
September	0.48	0.93

4.2. Downscaling Results of HadCM3 Outputs. Observed daily data of large-scale predictor variables representing the current climate condition (1961–2000) which are derived from the NCEP reanalysis data set were used to investigate the percentage of variance explained by each predictand-predictor pairs. The correlation between the predictor variables and each predictand is very low in case of daily precipitation compared to that of daily mean temperature. Moreover, the strength of individual predictors varies on a month by month basis. Therefore, the most appropriate combination of predictors has to be chosen by looking at the analysis output of all the twelve months. From the 40 years of data representing the current climate, the first 30 years (1961–1990) were considered for calibrating the regression models, while the remaining ten years of the data (1991–2000) were used to validate those models. Some of the SDSM setup parameters, such as event threshold, bias correction, and variance inflation, were adjusted during calibration to get the best statistical agreement between observed and simulated climate variables. Figure 5(a) shows the performance of the SDSM during the validation periods. The graphs show a comparison between the observed and simulated outputs for the cases of mean precipitation. Figure 5(b) illustrates the validation performance of the downscaling model for mean temperature, and the result shows satisfactory agreement between the observed data and the simulation outputs.

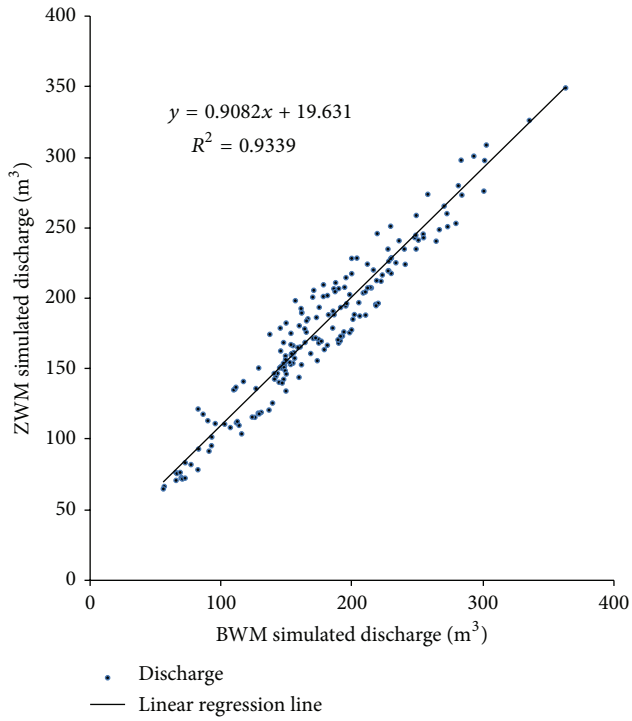

Figure 4: Comparation of the simulated discharges used parameter values by basin wide (BWM) and by zones (ZWM).

Figure 6(a) displays the average changes in precipitation under the A2 and B2 scenarios in 2020s to 2080s, and Figure 6(b) shows changes in mean temperature. The results indicate that the annual precipitation of the watershed in the future would exhibit a decreasing trend. Both A2 and B2 scenarios show a decreasing trend in monthly precipitation

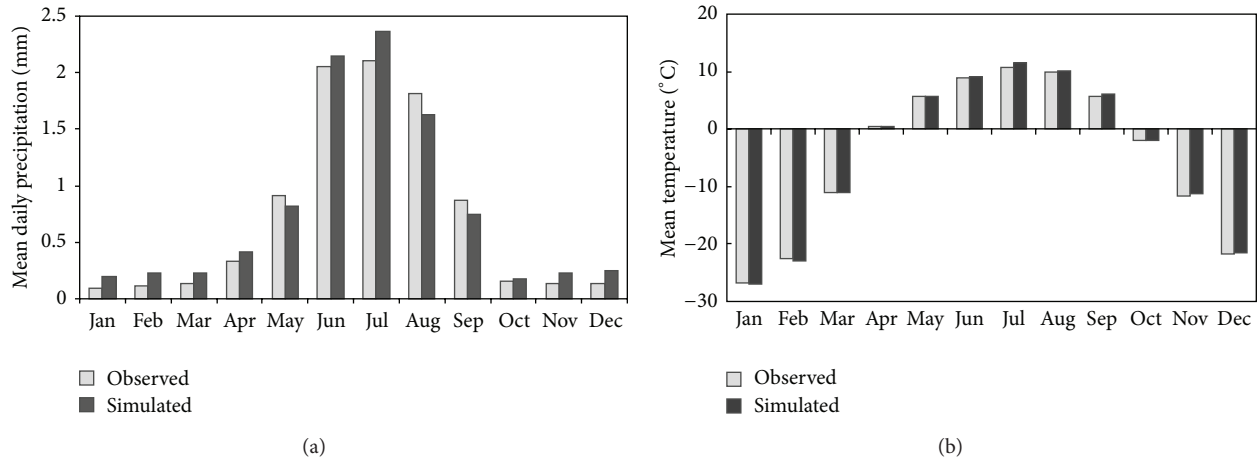

Figure 5: Validation results of SDSM downscaling of daily precipitation and daily mean temperature at BYBLK.

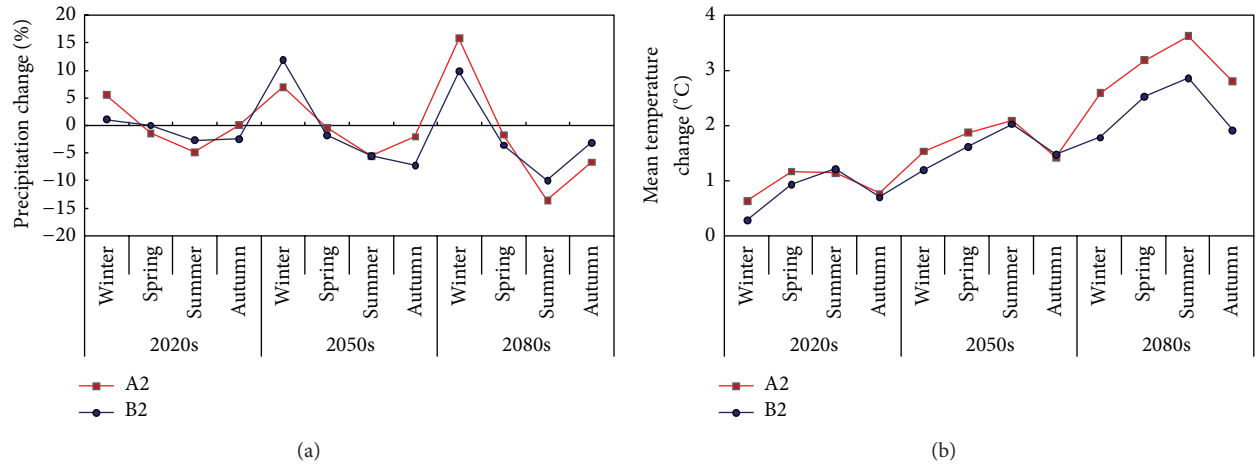

Figure 6: Changes in precipitation and temperature under IPCC SERS A2 and B2 scenarios from 2020s to 2080s.

during spring, summer, and autumn and show an increasing trend in winter. Contrarily, there is an obvious increasing trend for the future mean temperature, at a daily, monthly, seasonal, and yearly scale, respectively. The increase range under A2 scenario is larger than that in B2 scenario in the Kaidu Watershed.

4.3. Impact of Future Climate Change on Snowmelt Runoff. After verification on the present time (year of reference 2001), the SRM was used to study the impact of climate change on the Kaidu River runoff. The simulated discharge in 2001 was used as reference for the present climate. Four scenarios were considered in this study. Figure 7 shows the discharges simulated under Scenario 1 from 2020s to 2080s. In 2020s, the average precipitation was assumed to decrease 1.4% and 4.9% in spring and summer, respectively, while the mean temperatures of the watershed were assumed to increase 1.2°C in both spring and summer. In 2050s, the average precipitation was assumed to decrease 0.4% and 5.6% in spring and summer, respectively, while the mean temperatures of the catchment were assumed to increase 1.9°C and 2.1°C in spring and summer, respectively. And in 2080s, the average precipitation was assumed to decrease 1.8% and 13.6% in spring and summer, respectively, while the mean temperatures of the catchment were assumed to increase 3.2°C and 3.6°C in spring and summer, respectively. The results indicate that the stream flow in spring is likely to increase with the increased mean temperature; the stream flow in summer decreases with the decreased precipitation. The mean discharge during the snow melting seasons is decreased 5.9% in 2020s, while increased 1.0% and 11.8% in 2050s and 2080s, respectively. The spring peck flows under Scenario 1 are increased 16.5%, 21.1%, and 46.0% in 2020s, 2050s, and 2080s, respectively, while the summer peck flows are decreased 11.9%, 6.9%, and 0.5% in 2020s, 2050s, and 2080s, respectively.

Figure 8 shows the discharges simulated under Scenario 2 from 2020s to 2080s. In 2020s, the average precipitation was assumed to decrease 0.1% and 2.7% in spring and summer, respectively, while the mean temperatures of the catchment were assumed to increase 0.95°C and 1.23°C in spring and summer, respectively. In 2050s, the average precipitation was assumed to decrease 1.8% and 5.6% in spring and summer,

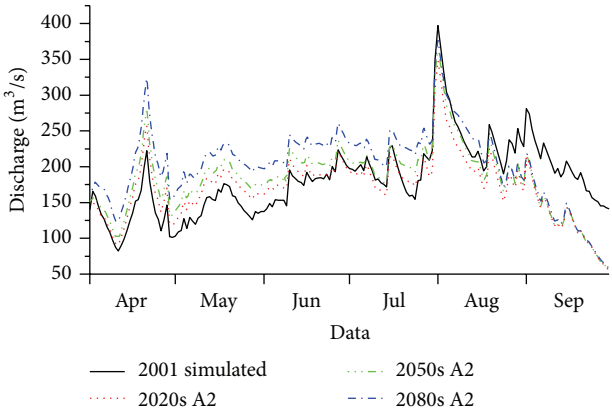

Figure 7: Simulated stream flows under Scenario 1 from 2020s to 2080s.

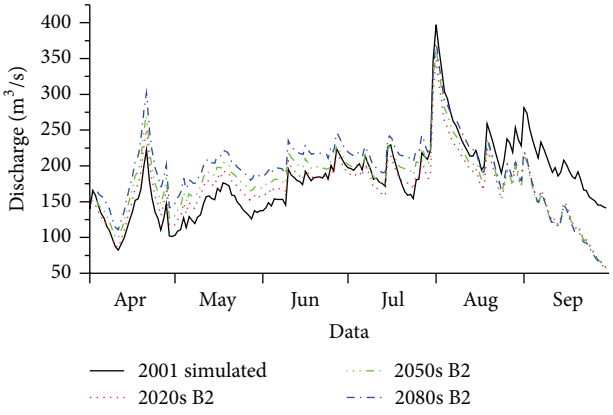

Figure 8: Simulated stream flows under Scenario 2 from 2020s to 2080.

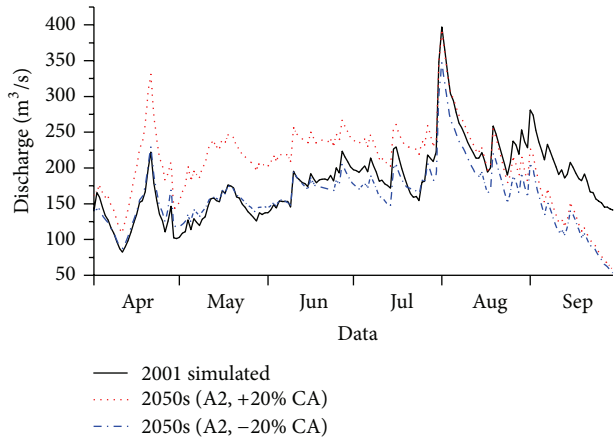

Figure 9: Simulated stream flows under Scenario 3 in 2050s.

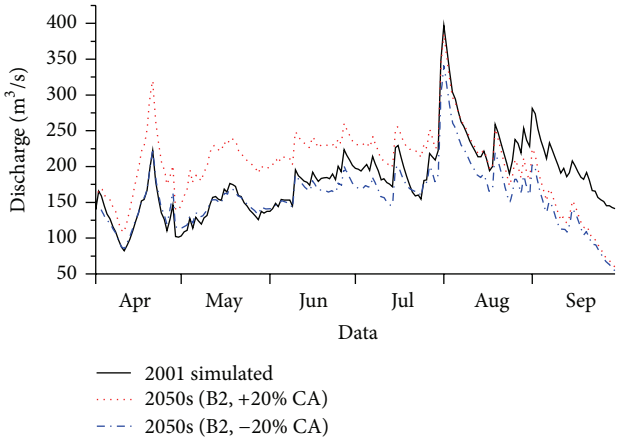

Figure 10: Simulated stream flows under Scenario 4 in 2050s.

respectively, while the mean temperatures of the catchment were assumed to increase 1.6°C and 2.0°C in spring and summer, respectively. And in 2080s, the average precipitation was assumed to decrease 3.6% and 9.9% in spring and summer, respectively, while the mean temperatures of the catchment were assumed to increase 2.6°C and 2.9°C in spring and summer, respectively. The results indicate that the variability of the simulated stream flow under Scenario 2 becomes less significant than Scenario 1. The mean discharge is decreased 6.8% and 1.2% in 2020s and 2050s, respectively; in 2080s, the mean discharge is increased 6.2%. The spring peck flows under Scenario 2 are increased 13.3%, 22.9%, and 36.4% in 2020s, 2050s, and 2080s, respectively, while the summer peck flows are decreased 12.4%, 8.1%, and 6.0% in 2020s, 2050s, and 2080s, respectively.

Figure 9 shows the discharges simulated under Scenario 3 in 2050s. The snow cover area was assumed to increase 20% as a result of increasing precipitation in winter; impact of a 20% decrease in snow cover area of watershed on the Kaidu River discharge was also studied. The results indicate that the spring and summer stream flow is likely to increase with increased snow cover area. A 20% snow cover increase forces the mean discharge during the snowmelt seasons to increase by 13.7% (i.e., 24.9 m^3/s). The mean discharge decreases by 11.6% if the snow cover area is assumed to decrease by 20%. The increase of snow cover area also results in an obvious increase of peck flow in spring, while the decrease of snow cover area would lead to a decreased peck flow in summer.

Figure 10 shows the discharges simulated under Scenario 4 in 2050s. The snow cover area was assumed to increase 50% or decrease 50% in the Kaidu Watershed. The results indicate that the change of simulated stream flow would intensify with increased or decreased 50% of snow cover area. A 50% snow cover increase results in a nearly 32.4% (i.e., 58.8 m^3/s) increase in mean discharge, and a 50% snow cover decrease would result in a 31.8% (i.e., 57.1 m^3/s) decrease in mean discharge during the snowmelt seasons.

5. Conclusions

In this study, an integrated modeling system has been developed for estimating the impact of climate change on snowmelt runoff in Kaidu Watershed, Northwest China. The modeling results obtained will provide useful decision support for water resources management and thus improve

the local ecosystem sustainability and social-economic development.

The SRM based on a degree day factor can efficiently simulate the daily discharge in the snow- and glacier-fed catchments of the Upper Tarim River Basin. The SRM's efficiency in mountainous catchments can be attributed to the use of the MOD10A2 remotely sensed snow cover data as input to the model. The simulated discharge is encouraging with EF value of 0.81. The HadCM3 outputs of present climate and future SRES A2 and B2 climate scenarios are presented in this paper. And the SDSM was used to bridge the scale gap between coarse GCM outputs and hydrological modeling at the basin scale. In the Kaidu Watershed, temperature shows an increase towards the end of the 21st century, while precipitation presents an increase trend in winter and a decrease trend in other seasons.

By inputting climate data into the SRM, impact of climate change on the hydrological process was estimated. The analysis of the climate change impact indicated that watershed hydrology would alter under different climate change scenarios. The stream flow in spring is likely to increase with the increased mean temperature; the discharge and peck flow in summer decrease with the decreased precipitation under Scenarios 1 and 2. And consideration of the change in cryosphere area would intensify the variability of stream flow. The increased snow cover area also results in the increasing of total flow and peck flow during spring and summer, while the mean discharge and peck flow would decrease if the snow cover area was assumed to decrease under Scenarios 3 and 4. The results of this research provide useful information to manage water resources for the region's future needs.

Acknowledgments

This research was supported by the "Western Light" Dr. Program of Chinese Academy of Science (XBBS201010); National Program of Key Basic Research Project (no. 2009CB825105); National Natural Science Foundation for Distinguished Young Scholar (51225904).

References

[1] A. A. Tahir, P. Chevallier, Y. Arnaud, and B. Ahmad, "Snow cover dynamics and hydrological regime of the Hunza River basin, Karakoram Range, Northern Pakistan," *Hydrology and Earth System Sciences*, vol. 15, no. 7, pp. 2275–2290, 2011.

[2] J. Wang, Y. P. Shen, A. X. Lu et al., "Impact of climate change on snowmelt runoff in the mountainous regions of northwest China," *Journal of Glaciology and Geocryology*, vol. 23, no. 1, pp. 28–33, 2001.

[3] Y. C. Zhang, B. L. Li, A. M. Bao, C. H. Zhou, X. Chen, and X. R. Zhang, "Study on snowmelt runoff simulation in the Kaidu River basin," *Science in China, Series D*, vol. 50, no. 1, pp. 26–35, 2007.

[4] Y. Huang, X. Chen, Y. P. Li, A. M. Bao, and Y. G. Ma, "A simulation-based two-stage interval-stochastic programming model for water resources management in Kaidu-Konqi watershed, China," *Journal of Arid Land*, vol. 4, no. 4, pp. 390–398, 2012.

[5] G. B. Sahoo, C. Ray, and E. H. de Carlo, "Calibration and validation of a physically distributed hydrological model, MIKE SHE, to predict streamflow at high frequency in a flashy mountainous Hawaii stream," *Journal of Hydrology*, vol. 327, no. 1-2, pp. 94–109, 2006.

[6] Y. Huang, X. Chen, Y. Li, P. Willems, and T. Liu, "Integrated modeling system for water resources management of Tarim River Basin," *Environmental Engineering Science*, vol. 27, no. 3, pp. 255–269, 2010.

[7] A. A. Şorman, A. Şensoy, A. E. Tekeli, A. Ü. Şorman, and Z. Akyürek, "Modelling and forecasting snowmelt runoff process using the HBV model in the eastern part of Turkey," *Hydrological Processes*, vol. 23, no. 7, pp. 1031–1040, 2009.

[8] A. Verdhen and T. Prasad, "Snowmelt Runoff simulation models and their suitability in Himalayan conditions," in *Snow and Glacier Hydrology*, IAHS Publication no. 218, Kathmandu, Nepal, 2001.

[9] WMO, *Intercomparison of Models of Snowmelt Runoff*, World Meteorological Organization, Geneva, Switzerland, 1986.

[10] J. Martinec, A. Rango, and R. Roberts, *Snowmelt Runoff Model (SRM) User's Manual*, 2007.

[11] Z. Liu and S. T. Y. Tong, "Using HSPF to model the hydrologic and water quality impacts of riparian land-use change in a small watershed," *Journal of Environmental Informatics*, vol. 17, no. 1, pp. 1–14, 2011.

[12] H. Zhao, J. Zhang, R. T. James, and J. Laing, "Application of MIKE SHE/MIKE 11 model to structural BMPs in S191 Basin, Florida," *Journal of Environmental Informatics*, vol. 19, no. 1, pp. 10–19, 2012.

[13] Y. Huang, X. Chen, Y. P. Li, G. H. Huang, and T. Liu, "A fuzzy-based simulation method for modelling hydrological processes under uncertainty," *Hydrological Processes*, vol. 24, no. 25, pp. 3718–3732, 2010.

[14] J. Martinec, "Snowmelt-Runoff Model for stream flow forecasts," *Nordic Hydrology*, vol. 6, no. 3, pp. 145–154, 1975.

[15] M. V. Georgievsky, "Application of the Snowmelt Runoff model in the Kuban river basin using MODIS satellite images," *Environmental Research Letters*, vol. 4, no. 4, Article ID 045017, pp. 1–5, 2009.

[16] W. W. Immerzeel, P. Droogers, S. M. de Jong, and M. F. P. Bierkens, "Large-scale monitoring of snow cover and runoff simulation in Himalayan river basins using remote sensing," *Remote Sensing of Environment*, vol. 113, no. 1, pp. 40–49, 2009.

[17] S. Lee, A. G. Klein, and T. M. Over, "A comparison of MODIS and NOHRSC snow-cover products for simulating streamflow using the Snowmelt Runoff Model," *Hydrological Processes*, vol. 19, no. 15, pp. 2951–2972, 2005.

[18] V. H. Prasad and P. S. Roy, "Estimation of snowmelt runoff in Beas Basin, India," *Geocarto International*, vol. 20, no. 2, pp. 41–47, 2005.

[19] B. Bookhagen and D. W. Burbank, "Toward a complete Himalayan hydrological budget: spatiotemporal distribution of snowmelt and rainfall and their impact on river discharge," *Journal of Geophysical Research F*, vol. 115, no. 3, Article ID F03019, 2010.

[20] T. Liu, P. Willems, X. W. Feng et al., "On the usefulness of remote sensing input data for spatially distributed hydrological modelling: case of the Tarim River basin in China," *Hydrological Processes*, vol. 26, no. 3, pp. 335–344, 2012.

[21] P. Zhang, J. Wang, and Y. Liu, "Application of SRM to flood forecast and forwarning of Manasi River Basin in Spring,"

Remote Sensing Technology and Application, vol. 24, no. 4, pp. 456–461, 2009.

[22] H. Ma and G. Cheng, "A test of Snowmelt Runoff Model (SRM) for the Gongnaisi River basin in the western Tianshan Mountains, China," *Chinese Science Bulletin*, vol. 48, no. 20, pp. 2253–2259, 2003.

[23] C. Wang, C. Y. Zhao, and Z. D. Feng, "Simulating snow process by using SRM in different watersheds in the upper reaches of Heihe river basin," *Journal of Lanzhou University (Natural Sciences)*, vol. 47, no. 3, pp. 1–8, 2011.

[24] J. Liu, J. Yang, R. Chen, and Y. Yang, "The simulation of snowmelt runoff model in the Dongkemadi River Basin, headwater of the Yangtze River," *Acta Geographica Sinica*, vol. 61, no. 11, pp. 1149–1159, 2006.

[25] M. Akhtar, N. Ahmad, and M. J. Booij, "Use of regional climate model simulations as input for hydrological models for the Hindukush-Karakorum-Himalaya region," *Hydrology and Earth System Sciences Discussions*, vol. 5, pp. 865–902, 2008.

[26] Y. P. Li and G. H. Huang, "Planning agricultural water resources system associated with fuzzy and random features," *Journal of the American Water Resources Association*, vol. 47, no. 4, pp. 841–860, 2011.

[27] D. Hall, G. Riggs, and V. Salomonson, *Updated Weekly MODIS/Terra Snow Cover 8-Day L3 Global 500 M Grid V005, [March 2000 to December 2009]*, National Snow and Ice Data Center. Digital Media, Boulder, Colo, USA, 2006.

[28] Q. K. Hassan, N. S. Sekhon, R. Magai, and P. McEachern, "Reconstruction of snow water equivalent and snow depth using remote sensing data," *Journal of Environmental Informatics*, vol. 20, no. 2, pp. 67–74, 2012.

[29] R. L. Wilby, C. W. Dawson, and E. M. Barrow, "SDSM—a decision support tool for the assessment of regional climate change impacts," *Environmental Modelling and Software*, vol. 17, no. 2, pp. 147–159, 2002.

[30] Y. P. Li and G. H. Huang, "Fuzzy-stochastic-based violation analysis method for planning water resources management systems with uncertain information," *Information Sciences*, vol. 179, no. 24, pp. 4261–4276, 2009.

Hindawi Publishing Corporation
Mathematical Problems in Engineering
Volume 2013, Article ID 942343, 12 pages
http://dx.doi.org/10.1155/2013/942343

Research Article

An Interval-Parameter Fuzzy Linear Programming with Stochastic Vertices Model for Water Resources Management under Uncertainty

Yan Han,[1,2] Yuefei Huang,[3] Shaofeng Jia,[1] and Jiahong Liu[2]

[1] *Institute of Geographic Sciences and Natural Resources Research, Chinese Academy of Sciences, Beijing 100101, China*
[2] *State Key Laboratory of Simulation and Regulation of Water Cycle in River Basin, China Institute of Water Resources and Hydropower Research, Beijing 100038, China*
[3] *State Key Laboratory of Hydroscience and Engineering, Tsinghua University, Beijing 100084, China*

Correspondence should be addressed to Yuefei Huang; yuefeihuang@tsinghua.edu.cn

Received 13 February 2013; Accepted 14 April 2013

Academic Editor: Yongping Li

An interval-parameter fuzzy linear programming with stochastic vertices (IFLPSV) method is developed for water resources management under uncertainty by coupling interval-parameter fuzzy linear programming (IFLP) with stochastic programming (SP). As an extension of existing interval parameter fuzzy linear programming, the developed IFLPSV approach has advantages in dealing with dual uncertainty optimization problems, which uncertainty presents as interval parameter with stochastic vertices in both of the objective functions and constraints. The developed IFLPSV method improves upon the IFLP method by allowing dual uncertainty parameters to be incorporated into the optimization processes. A hybrid intelligent algorithm based on genetic algorithm and artificial neural network is used to solve the developed model. The developed method is then applied to water resources allocation in Beijing city of China in 2020, where water resources shortage is a challenging issue. The results indicate that reasonable solutions have been obtained, which are helpful and useful for decision makers. Although the amount of water supply from Guanting and Miyun reservoirs is declining with rainfall reduction, water supply from the South-to-North Water Transfer project will have important impact on water supply structure of Beijing city, particularly in dry year and extraordinary dry year.

1. Introduction

Water shortage has become serious issue in process of urbanization as well as socioeconomic development gradually, especially in metropolis, where water resources are limited. Therefore, effective allocation of water resources to various users is important. There are many uncertain factors in practical management and decision making of complex water resources system, which might result in significant difficulties in optimizing water resources allocation. Conventional deterministic optimization methods have difficulties in reflecting these uncertainties [1]. Many researchers have tried to tackle these uncertain problems through fuzzy programming, interval programming, and stochastic programming [2–10]. In many real-world problems, several types of uncertainties may exist together in a complex system. Therefore, hybrid uncertainty methods have been desired for solving the problem with several types of uncertainties. Based on inexact chance-constrained programming (ICCP) method, Huang [11] proposed a hybrid inexact-stochastic water management model, which improves upon the existing inexact and stochastic programming approaches by allowing both distribution information in right hand and uncertainties in left hand or coefficients of objective. Hybrid uncertainties, including interval and stochastic distribution information in parameters and coefficients, can be directly communicated into the optimization process through representing the uncertain parameters or coefficients as fuzzy sets and random variables [3, 9, 10, 12–15]. In these hybrid uncertainty approaches, each coefficient or parameter has only one kind of uncertainty, and the stochastic distribution information is treated with the discrete way.

Due to the complexity of the real world, highly uncertain information may exist. Such boundaries of interval parameters of the optimization model are also uncertain. Nie et al. [16] proposed an interval parameter fuzzy-robust programming (IFRP) model through introducing the concept of fuzzy boundary interval. The parameters of the IFRP model were represented as interval numbers with fuzzy uncertain boundary, and the uncertainties were directly communicated into the optimization process and resulting solution. In this way, the robustness of the optimization process and solution can be enhanced. Considering the interval uncertain of boundaries of interval parameters, Liu and Huang [17] proposed a dual interval two-stage restricted-recourse programming (DITRP) method for flood-diversion planning. Liu et al. [18] established a dual-interval linear programming (DILP) model by introducing ILP approach into the existing interval-parameter linear programming framework. Some of coefficients and parameters in the DILP model were represented as interval-parameter with interval vertices. The DILP approach improved the ILP method by allowing dual uncertainties (presented as dual intervals) to be incorporated into the optimization process. For the fuzzy feature of boundaries of interval parameters, Li et al. [19] proposed a dual-interval vertex (DIV) method by incorporating the vertex method within an interval-parameter programming framework, and a fuzzy vertex analysis approach was proposed for solving the DIV model. The DIV approach can tackle uncertainties expressed as dual intervals that exist in both objective function and left-hand and right-hand sides of the constraints. However, these above methods hardly deal with the dual uncertainties including stochastic distribution attributes. Considering the stochastic attribute of boundaries of interval parameters in objective functions and constraints, Han et al. [20] proposed an interval linear programming with stochastic vertices (ILPSV) method to tackle dual uncertainties, which were presented as interval parameter with stochastic vertices problem. The fuzzy attribute of objective and constraints is not for concern in the ILPSV model. Therefore, one potential approach for better accounting for integrated uncertainties of parameters of model is to incorporate the stochastic distribution within a general fuzzy linear programming framework. This leads to an interval-parameter fuzzy linear programming with stochastic vertices method under dual uncertainty.

The objective of this paper is to propose an interval-parameter fuzzy linear programming model with stochastic vertices by coupling inexact fuzzy linear programming (IFLP) and stochastic vertices method. Highly uncertain information for the lower and upper bounds of interval parameters that exist in optimization model due to the complexity of the real world can be effectively handled through allowing the stochastic boundary of interval parameter to be incorporated into the optimization processes. In addition, the dual uncertainty concept (being stochastic boundaries of interval) is presented when the available information is highly uncertain for boundaries of interval parameter of objective functions and constraints. A hybrid intelligent algorithm based on Liu [21, 22] has been proposed for solving the developed model. The developed IFLPSV model is then applied to allocation of multisource water to multiple users in Beijing city of China in 2020, where water resources shortage is a challenging issue.

2. Methodology

2.1. Dual Uncertain Linear Programming Model. In many practical problems, the lower and upper bounds of some interval parameters in a water resources management system can rarely be acquired as deterministic. Instead, they can only be expressed by interval, fuzzy, or stochastic numbers. For a system with such dual uncertainty, an interval-parameter linear programming with stochastic vertices is generated as follows:

$$\max \quad \overline{\widetilde{f}} = \sum_{j=1}^{n} \left(\overline{c}_j + \overline{\widetilde{d}}_j \right) \overline{x}_j \tag{1a}$$

$$\text{Subject to} \quad \sum_{j=1}^{n} \overline{a}_{rj} \overline{x}_j \le \overline{b}_r, \quad (r = 1, 2, \ldots, s), \tag{1b}$$

$$\sum_{j=1}^{n} \overline{\widetilde{a}}_{tj} \overline{x}_j \le \overline{\widetilde{b}}_t, \quad (t = s+1, s+2, \ldots, m), \tag{1c}$$

$$\overline{x}_j \ge 0, \quad \forall j, \tag{1d}$$

where $\overline{c}_j$, $\overline{a}_{rj}$, and $\overline{b}_r$ are the intervals with deterministic lower and upper bounds, respectively; $\overline{\widetilde{a}}_{tj}$, $\overline{\widetilde{b}}_t$, and $\overline{\widetilde{d}}_j$ are the uncertain intervals with stochastic lower and upper vertices, respectively; j is the index of decision variables; n is the total number of decision variables; r is the index of single interval constraints; s is the number of single uncertain constraints; t is the index of dual uncertain constraints; and m is the total number of constraints. The models (1a), (1b), (1c), and (1d) can then be reformulated as follows:

$$\max \quad \overline{\widetilde{f}} = \sum_{j=1}^{n} \overline{c}_j \overline{x}_j + \sum_{j=1}^{n} \left[\overline{d}_j^L, \overline{d}_j^U \right] \overline{x}_j \tag{2a}$$

$$\text{Subject to} \quad \sum_{j=1}^{n} \overline{a}_{rj} \overline{x}_j \le \overline{b}_r, \quad (r = 1, 2, \ldots, s), \tag{2b}$$

$$\sum_{j=1}^{n} \left[\overline{a}_{tj}^L, \overline{a}_{tj}^U \right] \overline{x}_j \le \left[\overline{b}_t^L, \overline{b}_t^U \right], \quad (t = s+1, s+2, \ldots, m), \tag{2c}$$

$$\overline{x}_j \ge 0, \quad \forall j, \tag{2d}$$

where $\overline{a}_{tj}^L$ and $\overline{a}_{tj}^U$, $\overline{b}_t^L$, and $\overline{b}_t^U$, $\overline{d}_j^L$, and $\overline{d}_j^U$ are the stochastic lower and upper bounds of $\overline{\widetilde{a}}_{tj}$, $\overline{\widetilde{b}}_t$, and $\overline{\widetilde{d}}_j$ ($\overline{a}_{tj}^L \le \overline{a}_{tj}^U$, $\overline{b}_t^L \le \overline{b}_t^U$, and $\overline{d}_j^L \le \overline{d}_j^U$), respectively. The lower and upper bounds of interval number in ILP are certain as shown in Figure 1(a).

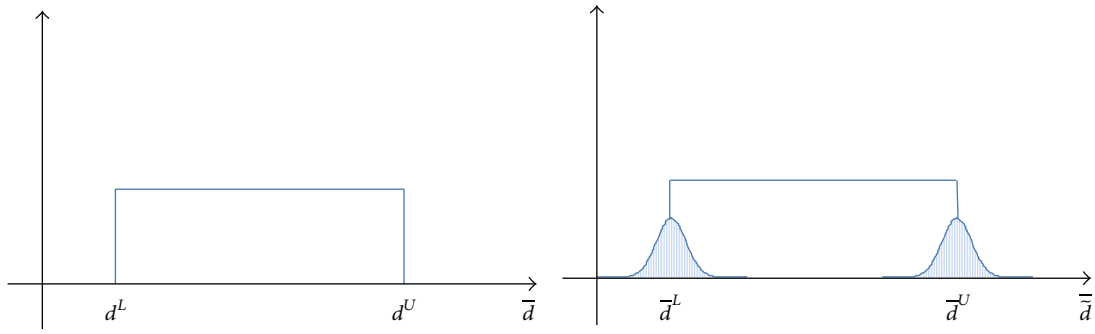

Figure 1: Interval number with certain and uncertain vertices.

The interval number of dual uncertainty linear programming is shown in Figure 1(b), and the vertices may possess a certain distribution function, such as formal distribution. The y-axis in Figure 1 does not represent any physical meaning since the figure is used to illustrate an interval number or an interval number with randomly distributed lower and upper bounds. The models (2a), (2b), (2c), and (2d) are an interval parameter linear programming with stochastic vertices, and it possesses the randomly distributed attribute of stochastic vertices and interval attribute of interval parameter; therefore, it is a dual uncertain optimization model. The traditional solution algorithm for interval-parameter linear programming (ILP) is not applicable to solve the models (2a), (2b), (2c) and (2d) due to stochastic variables existence.

Considering the fuzzy features of interval number of linear programming model under dual uncertainty, a potential approach for handling such complexities in the dual uncertain linear programming framework is to introduce IFLP technique into models (2a), (2b), (2c), and (2d). This leads to an interval-parameter fuzzy linear programming with stochastic vertices (IFLPSV) model as follows:

$$\max \quad \overline{\lambda} \tag{3a}$$

$$\begin{aligned}\text{subject to} \quad & \sum_{j=1}^{k_1}\left[c_j^L+\overline{d}_j^L\right]x_j^L+\sum_{j=k_1+1}^{n}\left[c_j^L+\overline{d}_j^L\right]x_j^U \\ & \geq \widetilde{f}_{\text{opt}}^L+\overline{\lambda}\left(\widetilde{f}_{\text{opt}}^U-\widetilde{f}_{\text{opt}}^L\right),\end{aligned} \tag{3b}$$

$$\begin{aligned}&\sum_{j=1}^{k_1}\left|a_{rj}\right|^U\text{Sign}\left(a_{rj}^U\right)x_j^L \\ &+\sum_{j=k_1+1}^{n}\left|a_{rj}\right|^L\text{Sign}\left(a_{rj}^L\right)x_j^U \\ &\leq b_r^U-\overline{\lambda}\left(b_r^U-b_r^L\right), \\ &(r=1,2,\ldots,s),\end{aligned} \tag{3c}$$

$$\begin{aligned}&\sum_{j=1}^{k_1}\left|\overline{a}_{tj}\right|^U\text{Sign}\left(\overline{a}_{tj}^U\right)x_j^L \\ &+\sum_{j=k_1+1}^{n}\left|\overline{a}_{tj}\right|^L\text{Sign}\left(\overline{a}_{tj}^L\right)x_j^U \\ &\leq \overline{b}_t^U-\overline{\lambda}\left(\overline{b}_t^U-\overline{b}_t^L\right), \\ &(t=s+1,s+2,\ldots,m),\end{aligned} \tag{3d}$$

$$x_j^L\geq 0, \quad (j=1,2,\ldots,k_1), \tag{3e}$$

$$x_j^U\geq 0, \quad (j=k_1+1,k_1+2,\ldots,n), \tag{3f}$$

where $\overline{\lambda}$ is the fuzzy membership grade, x_j^L $(j=1,2,\ldots,k_1)$ are variables with positive coefficients in the objective function, and x_j^U $(j=k_1+1,k_1+2,\ldots,n)$ are variables with negative coefficients in the objective function. $\widetilde{f}_{\text{opt}}^U$ and $\widetilde{f}_{\text{opt}}^L$ are upper and lower bounds of objective values from models (2a), (2b), (2c), and (2d).

2.2. Solving the IFLPSV. According to Huang et al. [23, 24], the above models (3a), (3b), (3c), (3d), (3e), and (3f) can be transformed into two submodels, which correspond to the upper and lower bounds of the desired objective function value. With a two-step interactive algorithm, one submodel corresponding to λ^U (lower bound of the membership grade) can be first formulated as

$$\max \quad \lambda^U \tag{4a}$$

$$\begin{aligned}\text{subject to} \quad & \sum_{j=1}^{k_1}\left[c_j^U+\overline{d}_j^U\right]x_j^U+\sum_{j=k_1+1}^{n}\left[c_j^U+\overline{d}_j^U\right]x_j^U \\ & \geq \widetilde{f}_{\text{opt}}^L+\lambda^U\left(\widetilde{f}_{\text{opt}}^U-\widetilde{f}_{\text{opt}}^L\right),\end{aligned} \tag{4b}$$

$$\sum_{j=1}^{k_1} \left|a_{rj}\right|^L \mathrm{Sign}\left(a_{rj}^L\right) x_j^U + \sum_{j=k_1+1}^{n} \left|a_{rj}\right|^U \mathrm{Sign}\left(a_{rj}^U\right) x_j^L \le b_r^U - \lambda^U\left(b_r^U - b_r^L\right), \quad (r = 1, 2, \ldots, s), \tag{4c}$$

$$\sum_{j=1}^{k_1} \left|\overline{a}_{tj}\right|^L \mathrm{Sign}\left(\overline{a}_{tj}^L\right) x_j^U + \sum_{j=k_1+1}^{n} \left|\overline{a}_{tj}\right|^U \mathrm{Sign}\left(\overline{a}_{tj}^U\right) x_j^L \le \overline{b}_t^U - \lambda^U\left(\overline{b}_t^U - \overline{b}_t^L\right), \quad (t = s+1, s+2, \ldots, m), \tag{4d}$$

$$x_j^U \ge 0, \quad (j = 1, 2, \ldots, k_1), \tag{4e}$$

$$x_j^L \ge 0, \quad (j = k_1 + 1, k_1 + 2, \ldots, n), \tag{4f}$$

$$0 \le \lambda^U \le 1. \tag{4g}$$

With the solutions of models (4a), (4b), (4c), (4d), (4e), (4f), and (4g), another submodel corresponding to λ^L (lower bound of the membership grade) can be formulated as

$$\max \quad \lambda^L \tag{5a}$$

$$\text{subject to} \quad \sum_{j=1}^{k_1} \left[c_j^L + \overline{d}_j^L\right] x_j^L + \sum_{j=k_1+1}^{n} \left[c_j^L + \overline{d}_j^L\right] x_j^L \ge \widetilde{f}_{\mathrm{opt}}^L + \lambda^L\left(\widetilde{f}_{\mathrm{opt}}^U - \widetilde{f}_{\mathrm{opt}}^L\right), \tag{5b}$$

$$\sum_{j=1}^{k_1} \left|a_{rj}\right|^U \mathrm{Sign}\left(a_{rj}^U\right) x_j^L + \sum_{j=k_1+1}^{n} \left|a_{rj}\right|^L \mathrm{Sign}\left(a_{rj}^L\right) x_j^U \le b_r^U - \lambda^U\left(b_r^U - b_r^L\right), \quad (r = 1, 2, \ldots, s), \tag{5c}$$

$$\sum_{j=1}^{k_1} \left|\overline{a}_{tj}\right|^U \mathrm{Sign}\left(\overline{a}_{tj}^U\right) x_j^L + \sum_{j=k_1+1}^{n} \left|\overline{a}_{tj}\right|^L \mathrm{Sign}\left(\overline{a}_{tj}^L\right) x_j^U \le \overline{b}_t^U - \lambda^U\left(\overline{b}_t^U - \overline{b}_t^L\right), \quad (t = s+1, s+2, \ldots, m), \tag{5d}$$

$$0 \le x_j^L \le x_{j\,\mathrm{opt}}^U, \quad (j = 1, 2, \ldots, k_1), \tag{5e}$$

$$x_j^U \ge x_{j\,\mathrm{opt}}^L, \quad (j = k_1 + 1, k_1 + 2, \ldots, n), \tag{5f}$$

$$0 \le \lambda^L \le \lambda_{\mathrm{opt}}^U, \tag{5g}$$

where $x_{j\,\mathrm{opt}}^U$ $(j = 1, 2, \ldots, k_1)$, $x_{j\,\mathrm{opt}}^L$ $(j = k_1 + 1, k_1 + 2, \ldots, n)$, and λ_{opt}^U are solutions of models (4a), (4b), (4c), (4d), (4e), (4f), and (4g). Due to the stochastic variables existence in the models (4a), (4b), (4c), (4d), (4e), (4f), (4g), (5a), (5b), (5c), (5d), (5e), (5f), and (5g), the traditional solving algorithms of ILP (Liu et al. [18]) and DIV (Li et al. [19]) methods are impracticable. The hybrid intelligent algorithm, which incorporates ANN and GA, can be used to deal with the stochastic variables in objective function, left-hand and right-hand sides of constraints. The stochastic variables of objective function and constraints need not to be initially set up, and they are automatically determined through many times iteration of the GA and ANN. Therefore, it is proposed as an intelligent algorithm. The procedure of solving the IFLPSV model by hybrid intelligent algorithm is shown in Figure 2.

3. Illustrative Example

The following illustrative example can be formulated to demonstrate the applicability of the proposed method:

$$\max \quad \overline{f} = \left[\xi_1, \xi_2\right] \overline{x}_1 - [5.5, 6.0]\, \overline{x}_2 \tag{6a}$$

$$\text{Subject to} \quad [8, 10]\, \overline{x}_1 - [12, 14]\, \overline{x}_2 \le \left[\eta_1, \eta_2\right], \tag{6b}$$

$$\left[\gamma_1, \gamma_2\right] \overline{x}_1 + [3, 4]\, \overline{x}_2 \le [6.0, 6.5], \tag{6c}$$

$$\overline{x}_1, \overline{x}_2 \ge 0, \tag{6d}$$

where, ξ_1, ξ_2, γ_1, γ_2, η_1, and η_2 are the stochastic variables with normal distributions of $N(26.5, 0.02)$, $N(29.5, 0.02)$, $N(2.4, 0.01)$, $N(2.8, 0.01)$, $N(3.8, 0.01)$, and $N(4.2, 0.01)$, respectively. According to two-step method, the models (6a), (6b), (6c), and (6d) can be converted into two sub-models. A running of the hybrid intelligent algorithm (200 iteration simulations, 500 data in ANN, and 50 generations in GA) was undertaken to solve the two sub-models. Through two-step method and hybrid artificial algorithm, the interval solutions of models (6a), (6b), (6c), and (6d) are $\overline{x}_1 = [1.3104, 1.6401]$, $\overline{x}_2 = [0.6376, 0.7748]$, and $\overline{f} = [29.5070, 45.0840]$ (as shown in Table 1, no units for all results since it is only an illustrative example).

Based on formulas (3a), (3b), (3c), (3d), (3e), and (3f) and Huang et al.'s [24], the models (6a), (6b), (6c), and (6d) can be converted to an IFLP problem as follows:

$$\max \quad \overline{\lambda} \tag{7a}$$

$$\text{Subject to} \quad \left[\xi_1, \xi_2\right] \overline{x}_1 - [5.5, 6.0]\, \overline{x}_2 \ge f_{\mathrm{opt1}}^L + \overline{\lambda}\left[f_{\mathrm{opt1}}^U - f_{\mathrm{opt1}}^L\right], \tag{7b}$$

$$[8, 10]\, \overline{x}_1 - [12, 14]\, \overline{x}_2 \le \eta_2 - \overline{\lambda}\left[\eta_2 - \eta_1\right], \tag{7c}$$

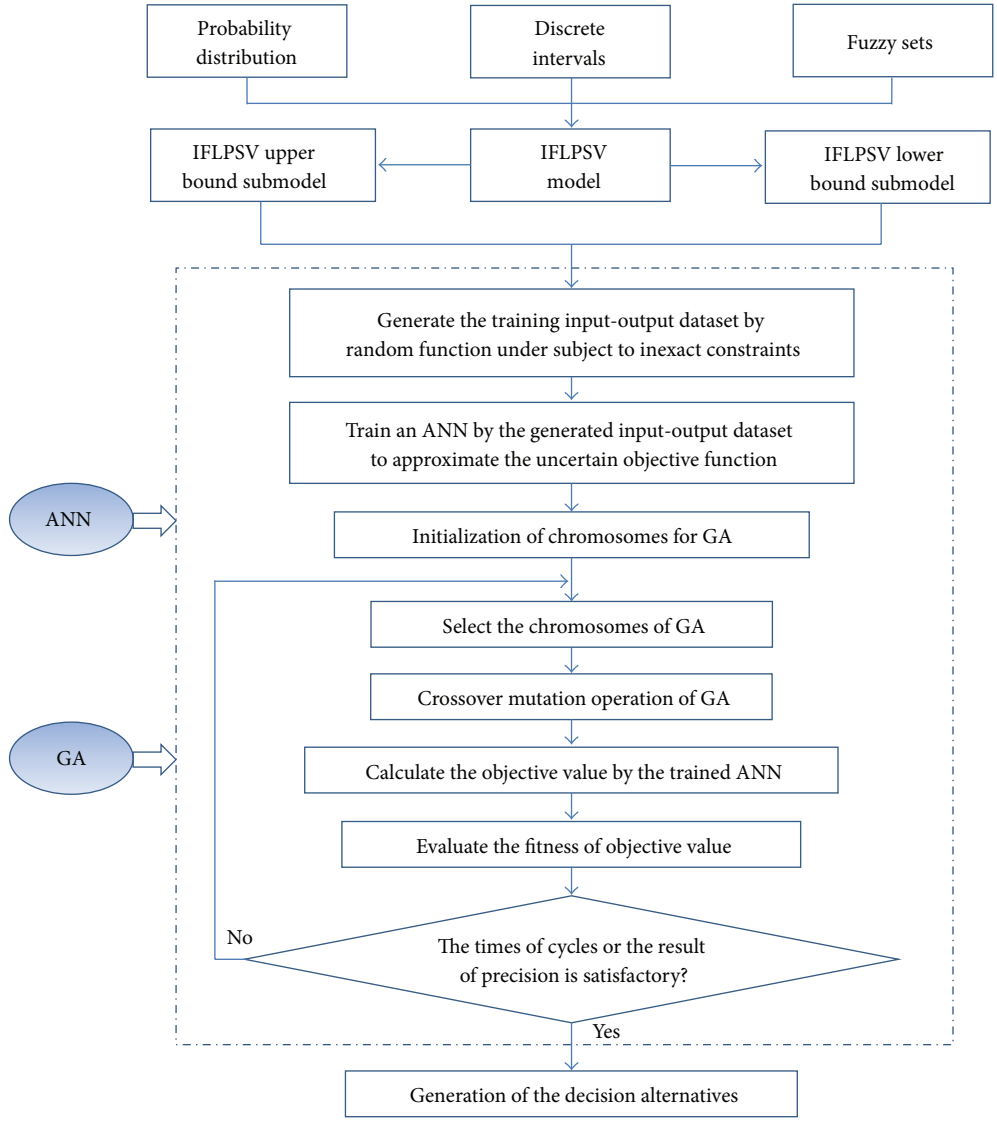

Figure 2: Flow chart of solving the IFLPSV model by hybrid intelligent algorithm.

Table 1: Comparison of results of ILP, DIV, ILPSV, and IFLPSV method.

Methods	ILP	DIV	ILPSV	IFLPSV
Objective value	[[29.438, 32.150], [42.172, 45.784]]	[[30.099, 31.455], [43.053, 44.895]]	[29.5070, 45.0840]	[30.9548, 42.6913]

$$[\gamma_1, \gamma_2]\,\overline{x}_1 + [3,4]\,\overline{x}_2 \le 6.5 - \overline{\lambda}\,[6.5 - 6.0]\,, \tag{7d}$$

$$0 \le \overline{\lambda} \le 1, \tag{7e}$$

where f^U_{opt1} and f^L_{opt1} are upper and lower bounds of objective value of models (6a), (6b), (6c), and (6d), $f^U_{\text{opt1}} = 45.0840$, and $f^L_{\text{opt1}} = 29.5070$. The above models (7a), (7b), (7c), (7d), and (7e) can be solved through a two-step method where a sub-model corresponding to λ^U is first formulated and solved. This is based on the fact that the λ^Ucorresponding to f^U and the system objective are to be maximized. In the second step, the other sub-model corresponding to λ^L can then be formulated supported by the solution of the first sub-model. The first sub-model can be formulated as follows:

$$\max \quad \lambda^U \tag{8a}$$

$$\text{Subject to} \quad -\xi_2 x_1^U + 5.5 x_2^L + 15.7928\lambda^U \le -29.2912, \tag{8b}$$

$$8x_1^U - 14x_2^L + (\eta_2 - \eta_1)\,\lambda^U \le \eta_2, \tag{8c}$$

$$\gamma_1 x_1^U + 4x_2^L + 0.5\lambda^U \le 6.5, \tag{8d}$$

$$0 \le \lambda^U \le 1. \tag{8e}$$

With the hybrid intelligent algorithm, the solutions of models (8a), (8b), (8c), (8d), and (8e) are $x_1^U = 1.5333$ and $x_2^L = 0.6014$, and the corresponding upper bound of membership grade value is $\lambda^U = 0.7539$ (as Figure 3).

Then the sub-model corresponding to λ^L can be formulated as follows:

$$\max \quad \lambda^L \tag{9a}$$

$$\text{Subject to} \quad -\xi_1 x_1^L + 6.0x_2^U + 15.7928\lambda^L \leq -29.2912, \tag{9b}$$

$$10x_1^L - 12x_2^U + (\eta_2 - \eta_1)\lambda^L \leq \eta_2, \tag{9c}$$

$$\gamma_2 x_1^L + 4x_2^U + 0.5\lambda^L \leq 6.5, \tag{9d}$$

$$x_1^L \leq x_{1\,\text{opt}}^U, \tag{9e}$$

$$x_2^U \geq x_{2\,\text{opt}}^L, \tag{9f}$$

$$0 \leq \lambda^L \leq \lambda_{\text{opt}}^U. \tag{9g}$$

The solutions of models (9a), (9b), (9c), (9d), (9e), (9f), and (9g) are $x_1^L = 1.4078$ and $x_2^U = 0.6080$, and corresponding lower bound of membership grade value is $\lambda^L = 0.2164$ (as Figure 4).

Therefore, the solutions of problem models (7a), (7b), (7c), (7d), and (7e) are $\overline{x}_1 = [1.4078, 1.5333]$ and $\overline{x}_2 = [0.6014, 0.6080]$, and interval objective value is $\overline{f} = [30.9548, 42.6913]$. In the work by Li et al. [19], dual uncertain parameters were interval values, and the DIV method was employed. The results of illustrative examples (6a), (6b), (6c), and (6d) by ILP, DIV, ILPSV, and IFLPSV method are shown in Table 1.

The ILP method can tackle uncertainties expressed as interval values with known lower and upper bounds, but the distribution functions of uncertain parameters are unknown. The result of objective value from ILP is [[29.438, 32.150], [42.172, 45.784]]. The solutions might compose fuzzy information due to the parameter's large boundary range. The DIV can tackle the uncertainties presented as interval parameter with fuzzy vertices by incorporating the vertex method within an interval parameter programming. The result of objective value from DIV is [[30.099, 31.455], [43.053, 44.895]]. Some feasible solutions might be missed by DIV method due to using the discrete vertex way, and the DIV method is unable to deal with the vertex presented as certain stochastic distribution function problem. The upper bound (42.6913) of objective value from IFLPSV is smaller than the interval [43.053, 44.895] of upper bound of DIV method. The reason is that normal distribution of upper and lower bounds of the interval parameter has more information than that of DIV model. The ILPSV method can tackle the interval-parameter linear programming with stochastic vertices. The result of objective value from IFLPSV is [30.9548, 42.6913]. The upper and lower bounds of the objective value from IFLPSV have less uncertainty than ILPSV since parameters with membership function have less uncertainty than those with interval numbers. Furthermore, the upper and lower bounds of the objective values from IFLPSV model all lie in the interval of the upper and lower bounds from ILP model. The reason is that coefficients of IFLPSV model with fuzzy membership function and stochastic vertices have less uncertainty degree than interval parameters of ILP with interval bounds. Therefore, the uncertainty degree of the solution from the IFLPSV is also less. The developed IFLPSV model is an integrated optimization model under dual uncertainty, which considers fuzzy, interval, and stochastic attributes of parameters and coefficients of optimization model.

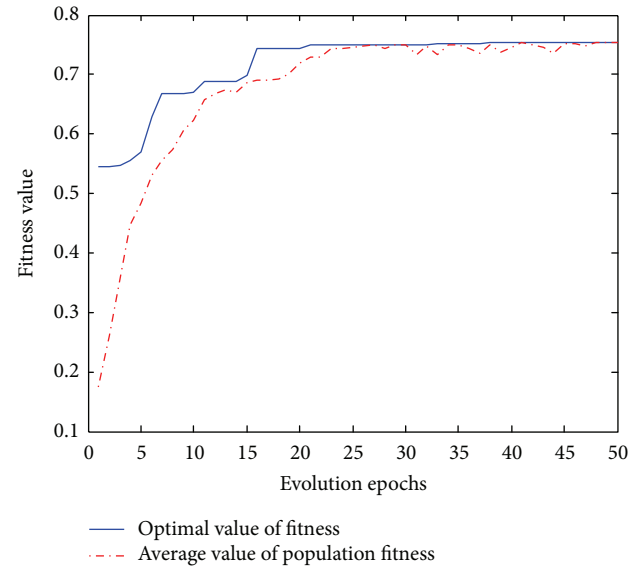

Figure 3: Evolution process of upper bound of membership function by genetic algorithm.

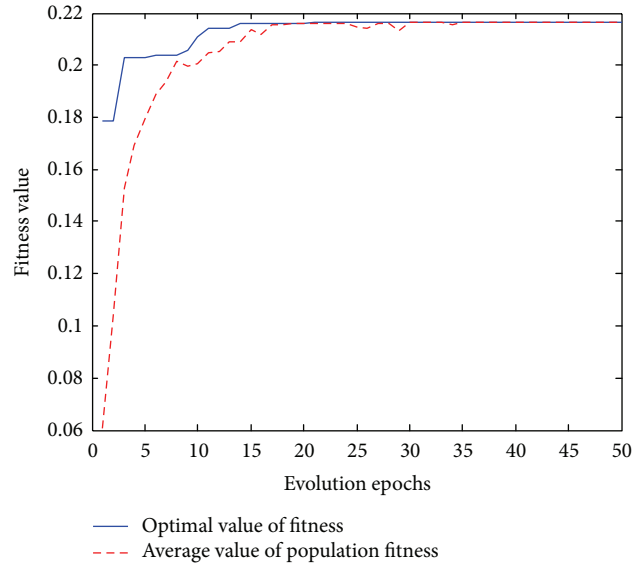

Figure 4: Evolution process of lower bound of membership function by genetic algorithm.

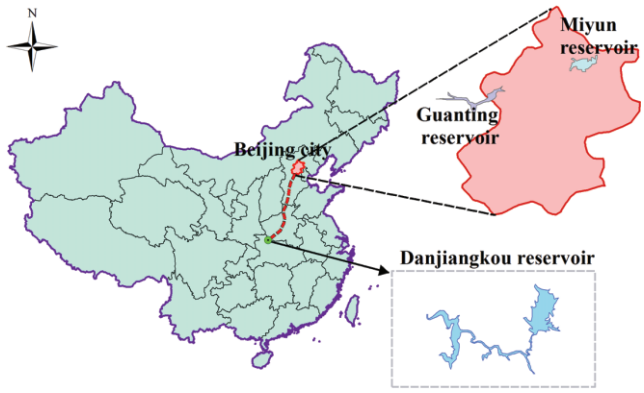

FIGURE 5: Location illustration of main water resources in the study area.

4. Application

4.1. Overview of the Study Area. Beijing city, the capital of China, is located in the northern part of the North China Plain as shown in Figure 5. The annual precipitation is about 590 mm in Beijing, with 85% of the annual precipitation falling during the period from July to September. The main surface water source is from Guanting reservoir and Miyun reservoir in Beijing city. The amount of exploitable water resources ranges from 3.0 to 4.12 billion m^3 per year. However, under changing climate and overexploitation of water resources, the total of exploitable water resources is 2.308 billion m^3 in 2010 [26], including surface water resources 0.722 billion m^3 and groundwater 1.586 billion m^3. The water consumption users include industry, agriculture, domestic, and environment in Beijing city. The amount of water consumption of Beijing city was 3.52 billion m^3 in 2010. Water shortage problem is severe, and there has appeared four times water crisis in urbanization process of Beijing city. The per capita water resource in Beijing city is less than 300 cubic meters, which is one-thirtieth of the world average. Beijing has become one of the most water-scarce megacities in the world. Water resource has become a key factor which limits urbanization process and socioeconomic development in Beijing city.

In order to meet water requirements of Northwest and North China, the South-to-North Water Diversion Projects have been developed early. The Middle Route of South-to-North Water Diversion Project will transfer water from the Danjiangkou Reservoir on the Hanjiang river, a tributary of the Yangtze river, to Beijing city through opening channel. The Middle Route Project will be completed in 2014. The total amount of transferred water to Beijing city ranges from 1.0 to 1.4 billion m^3 per year, which will be another important part of water resources for Beijing city in the future.

4.2. IFLPSV Optimization Model for Water Resources Allocation in Beijing City. Reasonable allocation of urban water resources is usually a multiobjective problem. In this study, the objective functions include net economic benefit maximization and greenbelt irrigation area maximization as shown in formulas (10a) and (10b). The objective functions are subject to ten kinds of constraints, including water delivery capacity limit from river or lake as formula (10c), Guanting reservoir water supply capacity limit as formula (10d), Miyun reservoir water supply capacity limit as formula (10e), groundwater supply capacity limit as formula (10f), reused water supply capacity limit as formula (10g), South-to-North Water Transfer supply capacity limit as formula (10h), the lowest requirement limit of domestic water consumption as formula (10i), the lowest requirement limit of industry water consumption as formula (10j), the lowest requirement limit of agriculture water consumption as formula (10k), the lowest requirement limit of greenbelt water irrigation as formula (10l), nonnegativity constraint is as formula (10m):

$$\overline{f}_1 = \sum_{i=1}^{m}\sum_{j=1}^{n} \overline{b}_{ij}\overline{x}_{ij}\,(\text{net benefit of economy}), \tag{10a}$$

$$\overline{f}_2 = \sum_{i=1}^{m} \frac{1}{\overline{p}}\overline{x}_i\,(\text{greenbelt irrigation area}), \tag{10b}$$

Subject to

$$\sum_{j=1}^{n} \overline{x}_j \le \overline{Q}_{\text{deliv}}\,(\text{water deliver capacity constraint from river or lake}), \tag{10c}$$

$$\sum_{j=1}^{n} \overline{x}_j \le \overline{Q}_{\text{reser1}}\,(\text{Guanting reservoir water supply capacity constraint}), \tag{10d}$$

$$\sum_{j=1}^{n} \overline{x}_j \le \overline{Q}_{\text{reser2}}\,(\text{Miyun reservoir water supply capacity constraint}), \tag{10e}$$

$$\sum_{j=1}^{n} \overline{x}_j \le \overline{Q}_{\text{ground}}\,(\text{groundwater supply capacity constraint}), \tag{10f}$$

$$\sum_{j=1}^{n} \overline{x}_j \le \overline{Q}_{\text{reuse}}\,(\text{reused water supply capacity constraint}), \tag{10g}$$

$$\sum_{j=1}^{n} \overline{x}_{ij} \le \overline{Q}_{\text{trans}}\,(\text{South-to-North Water Transfer supply capacity constraint}), \tag{10h}$$

$$\sum_{i=1}^{m} \overline{x}_i \geq \overline{Q}_{\text{domes}} \left(\text{the lowest requirement of domestic water consumption}\right), \tag{10i}$$

$$\sum_{i=1}^{m} \overline{x}_i \geq \overline{Q}_{\text{indus}} \left(\text{the lowest requirement of industry water consumption}\right), \tag{10j}$$

$$\sum_{i=1}^{m} \overline{x}_i \geq \overline{Q}_{\text{agri}} \left(\text{the lowest requirement of agriculture water consumption}\right), \tag{10k}$$

$$\sum_{i=1}^{m} \overline{x}_{ij} \geq \overline{Q}_{\text{env}} \left(\text{the lowest requirement of greenbelt water irrigation}\right), \tag{10l}$$

$$\overline{x}_{ij} \geq 0 \ \left(\text{non-negativity constraint}\right), \tag{10m}$$

where $\overline{f}_1$, $\overline{f}_2$ are the interval objective function of the net economic benefit maximization and greenbelt irrigation area maximization, respectively, $\overline{x}_{ij}$ ($i = 1, 2, 3, \ldots, m$; $j = 1, 2, 3, \ldots, n$) denotes the interval amount of water source i supply to j water user, $m = 6$ is the total number of water source (lift or deliver water from river and lake, Guanting reservoir, Miyun reservoir, groundwater, reused water, and South-to-North Water Transfer); $n = 4$ is the total number of water users (domestic, industry, agriculture and environment), $\overline{b}_{ij}$ is the benefit coefficient of the water source i supply to j user, which belongs an interval number, $\overline{p}$ is the interval coefficient of greenbelt irrigation water consumption per acre, $\overline{Q}_{\text{deliv}}$ is the maximization water deliver capacity from rivers and lakes, which is an interval number, $\overline{Q}_{\text{reser1}}$ is the water supply capacity of the Guanting reservoir, which is an interval number, $\overline{Q}_{\text{reser2}}$ is the water supply capacity of the Miyun reservoir, which is an interval number, $\overline{Q}_{\text{ground}}$ is the groundwater supply capacity, which is an interval number, $\overline{Q}_{\text{reuse}}$ is the reused water supply capacity, which is an interval range, $\overline{Q}_{\text{trans}}$ is the available water amount from the South-to-North Water Diversion Project, which is an interval number, $\overline{Q}_{\text{domes}}$ is the lowest amount of domestic water requirement, which belongs an interval range, the reused water for domestic is small, it is ignored, $\overline{Q}_{\text{indus}}$ is the lowest amount of industry water requirement, which is an interval number, $\overline{Q}_{\text{agri}}$ is the lowest amount of agriculture water requirement, depending on weather and rainfall. The value of agriculture water requirement is an interval number with normal distribution boundaries, $N(12.05 \times 10^8, 10000)$ m^3 and $N(12.01 \times 10^8, 10000)$ m^3 respectively; $\overline{Q}_{\text{env}}$ is the lowest amount of greenbelt irrigation water requirement, which is an interval number. In this study, the greenbelt irrigation water requirement includes river water supplement and urban roadway watering.

The developed model is a multiobjective optimization model, including two conflict objectives. In this study, the multiobjective weighted method is adopted to solve the multi-objective model. The two objective functions are transferred to a single objective function as follows:

$$F(X) = \sum_{i=1}^{m} w_i f_i(x), \tag{11}$$

where $m = 2$ and w_i is the weight coefficient of the i objective function $f_i(x)$, ($\sum_i^m w_i = 1$). In this study, $w_1 = w_2 = 0.5$, and it means that economic benefit and environment protection are considered to be of the same importance. Table 2 shows the coefficients and parameters in models (10a), (10b), (10c), (10d), (10e), (10f), (10g), (10h), (10i), (10j), (10k), (10l), and (10m).

The capacity of water source supply under different flow frequencies is shown in Table 3.

Scenario 1 denotes the normal flow year, in which frequency of flow is 50%. The total amount of water resource is [6.184, 6.285] billion cubic meters in scenario 1. The amount of available water from local rivers and lakes is $[1.38, 1.40] \times 10^8$ m^3. The available water from the Guanting and Miyun reservoirs is $[7.51, 7.55] \times 10^8$ m^3 and $[9.15, 9.20] \times 10^8$ m^3, respectively. The amount of water from the South-to-North Middle Rout Project is $[9.5, 10.0] \times 10^8$ m^3 in scenario 1. Scenario 2 denotes the dry year, in which frequency of flow is 75%. The total amount of water resource is [5.751, 5.851] billion cubic meters in scenario 2, which decline 0.434 billion cubic meters comparing with scenario 1. The amount of available water from local rivers and lakes is $[1.05, 1.08] \times 10^8$ m^3 in scenario 2, which declines to $[0.32, 0.33] \times 10^8$ m^3 compared with scenario 1. The water amounts from the Guanting and Miyun reservoirs are $[4.45, 4.49] \times 10^8$ m^3 and $[6.20, 6.24] \times 10^8$ m^3, respectively, in scenario 2, which corresponding declines to $[3.06, 3.06] \times 10^8$ m^3 and $[3.04, 3.05] \times 10^8$ m^3 compared with scenario 1. The amount of water from the South-to-North Middle Route Project is $[11.5, 12.0] \times 10^8$ m^3 in scenario 2, in which increase 0.2 billion cubic meters comparing with scenario 1. Scenario 3 denotes the extraordinary dry year, which frequency of flow is 90%. The total amount of water resource is [5.40, 5.50] billion cubic meters in scenario 3. The amount of available water from local rivers and lakes is $[0.70, 0.72] \times 10^8$ m^3 in scenario 3, in which declines to 0.68×10^8 m^3 compared with scenario 1. The amounts of water from the Guanting and Miyun reservoirs are only $[1.90, 1.94] \times 10^8$ m^3 and $[3.60, 3.64] \times 10^8$ m^3, respectively, in scenario 3, in which declines to 5.61×10^8 m^3 and $[5.55, 5.56] \times 10^8$ m^3 compared with scenario 1. The amount of water from South-to-North Middle Route Project is $[13.5, 14.0] \times 10^8$ m^3 in scenario 3, which increase 0.4 billion cubic meters compared with scenario 1. The amount of exploitable groundwater and reused water keep the same for all three scenarios.

4.3. Results and Discussion. Table 4 shows the results of water allocation to water users under three scenarios. The total amount of allocated water is [6184, 6285] million m^3 in

Table 2: Coefficients and parameters of model.

Water source	Benefit coefficients (RMB/m^3)			Greenbelt irrigation ration (m^3/acre)
	Domestic	Industry	Agriculture	environment
Deliver water from river or lake	[4.0, 4.5]	[455, 465]	[0.07, 0.08]	[1.5, 2.0]
Guanting reservoir	[4.0, 4.5]	[460, 470]	[0.06, 0.08]	[1.5, 2.0]
Miyun reservoir	[4.0, 4.5]	[460, 470]	[0.06, 0.08]	[1.5, 2.0]
Groundwater	[4.0, 4.5]	[460, 470]	[0.05, 0.07]	[1.5, 2.0]
Reused water	[0.0, 0.0]	[460, 470]	[0.00, 0.00]	[1.5, 2.0]
South-to-North Water Transfer	[4.0, 4.5]	[460, 470]	[0.06, 0.08]	[1.5, 2.0]

RMB: monetary symbol in China.

Table 3: Capacity of water source supply under three scenarios.

Flow frequency	Deliver water from rivers or lakes	Guanting reservoir	Miyun reservoir	Ground water	Reused water	South-to-North Water Transfer
Scenario 1 (50%)	[1.38, 1.40]	[7.51, 7.55]	[9.15, 9.20]	[26.3, 26.5]	[8.0, 8.2]	[9.5, 10.0]
Scenario 2 (75%)	[1.05, 1.08]	[4.45, 4.49]	[6.20, 6.24]	[26.3, 26.5]	[8.0, 8.2]	[11.5, 12.0]
Scenario 3 (90%)	[0.70, 0.72]	[1.90, 1.94]	[3.60, 3.64]	[26.3, 26.5]	[8.0, 8.2]	[13.5, 14.0]

Data source from [25].
(units 10^8 m^3).

Table 4: Results of water resources allocation among water users under three scenarios.

Scenario no.	Domestic	Industry	Agriculture	Environment	Total water consumption
Scenario 1 (50%)	[1634, 1634]	[2146, 2146]	[1205, 1220]	[1199, 1285]	[6184, 6285]
Scenario 2 (75%)	[1634, 1634]	[1712, 1712]	[1205, 1220]	[1200, 1285]	[5751, 5851]
Scenario 3 (90%)	[1632, 1634]	[1361, 1361]	[1205, 1220]	[1201, 1285]	[5400, 5500]

(units million m^3).

normal flow year (50%). The total amount of allocated water is [5751, 5851] million m^3 in dry year (75%), less [433, 434] million m^3 than that in scenario 1. The total amount of allocated water is only [5400, 5500] million m^3 in scenario 3, less [784, 785] million m^3 than that in scenario 1.

In Table 4 and Figure 6, the industry and domestic are main water utilization sectors in Beijing city. For example, in scenario 1, the amount of water allocation to industry is [2146, 2146] million cubic meters, which accounts for [34.1%, 34.7%] of total allocated water. The amount of allocated water to domestic is [1634, 1634] million cubic meters, which accounts for [26.0%, 26.4%] of total allocated water. In scenario 2, the amount of water allocation to industry is declined to [1712, 1712] million cubic meters, which accounts for [29.3%, 29.8%] of total allocated water. The amount of allocated water to domestic is [1634, 1634] million cubic meters, which accounts for [27.9%, 28.4%] of total allocated water. In scenario 3, the industrial water consumption is declined to [1361, 1361] million cubic meters, which only accounts for [24.7%, 25.2%] of total allocated water. The amount of allocated water to domestic is [1632, 1634] million cubic meters, which accounts for [29.7%, 30.2%] of total allocated water. Although the amount of domestic water consumption is almost not changed, its proportion is more than industrial in scenario 3. The proportion of domestic water consumption increases from [26.0%, 26.4%] in scenario 1 to [29.7%, 30.2%] in scenario 3. The results show that domestic has higher priority than industry on water consumption under water shortage situation. The amount of water consumption of agriculture and environment reach its least requirement in Beijing city. Therefore, the amounts of agricultural and environmental water consumption are almost the same under three scenarios. In the dry year or extraordinary dry year, the water crisis might be relieved by reducing industrial water consumption.

Figure 7 shows the allocation results of different water source supplies to different water users in Beijing city under three scenarios. Domestic water consumption of Beijing city is mainly from groundwater, reservoirs, and South-to-North Middle Route Project in 2020. Although the total amount of the domestic water consumption is the same under three scenarios, the amounts of water in Guanting and Miyun reservoirs (reservoir1 and reservoir 2 in Figure 2) for the domestic sector evidently decreased with rainfall reduction. Moreover, groundwater is the primary and reliable water source for the domestic sector. The allocated groundwater for domestic sector is raised from [738.2, 738.2] million m^3 in scenario 1 to [764.3, 764.3] million m^3 in scenario 2 and to [808.2, 808.2] million m^3 in scenario 3. Meanwhile, the water amount for the domestic sector from South-to-North Middle Route Project is raised from [325.7, 325.7] million m^3 in scenario 1 to [401.8, 401.8] million m^3 in scenario 2 and to [495.7, 495.7] million m^3 in scenario 3. The South-to-North Middle Route Project gradually becomes

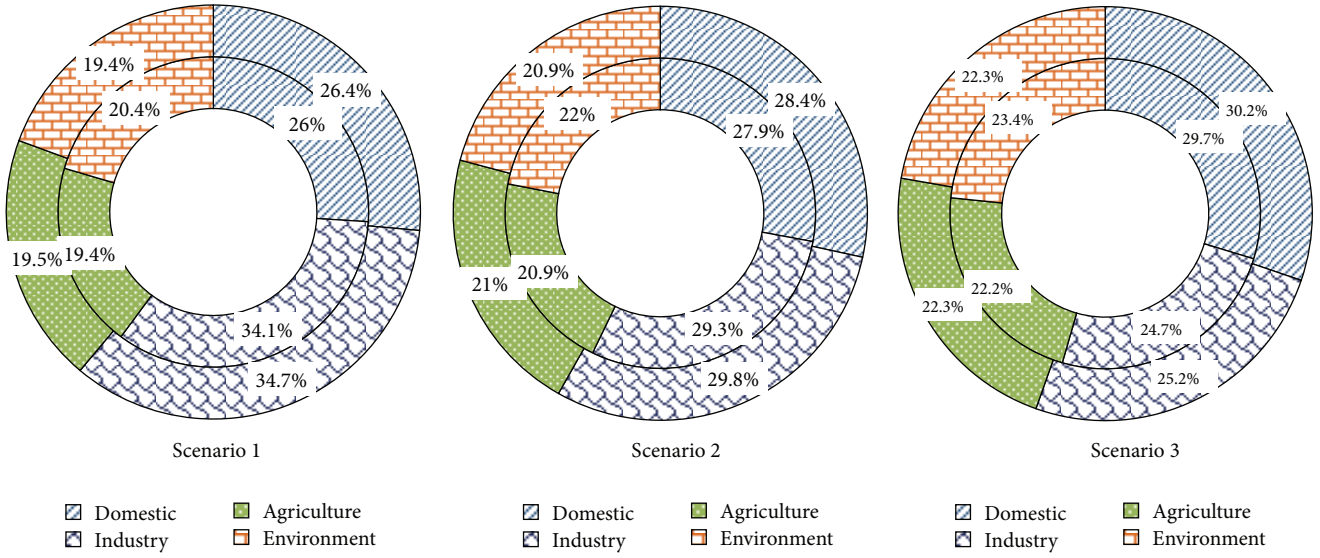

Figure 6: Rate of water resources allocation among water users under three scenarios.

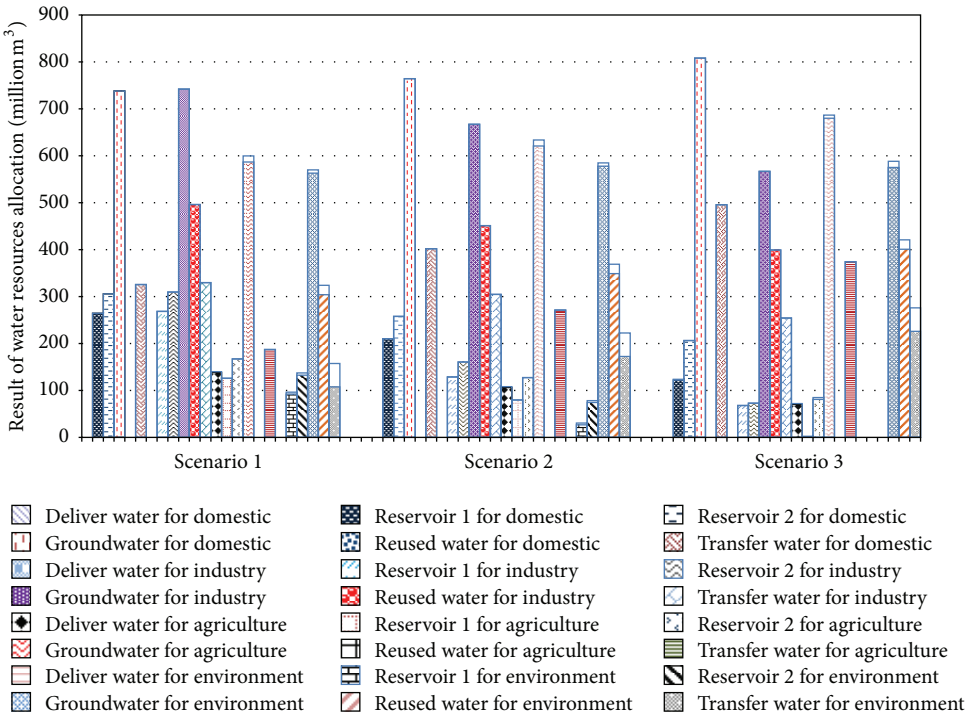

Figure 7: Result of water source supply among sectors under three scenarios.

the second water source for the domestic sector when water supply capacity of the Guanting and Miyun reservoirs decreases in dry and extraordinary dry year. Industry sector mainly uses groundwater, reused water, reservoirs water, and South-to-North Middle Route Project water. The allocated water amount from these water sources for industry are all declined with total available water reducing. For example, the groundwater for industry is significantly declined, from [742.2, 742.2] million m^3 in scenario 1 to [667.1, 667.1] billion m^3 in scenario 2 and to [566.8, 566.8] million m^3 in scenario 3. Although the total amount of reused water supply is same, the amount of reused water for industry is declined from [496.1, 496.1] million m^3 in scenario 1 to [451.1, 451.1] million m^3 in scenario 2 and to [399.2, 399.2] million m^3 in scenario 3. The agricultural water consumption is mainly from rivers and lakes, reservoirs, groundwater, and South-to-North Middle Route Project. Because the available water from rivers, lakes, and reservoirs is declined with

rainfall reduction in dry year and extraordinary dry year, the exploitation amount of groundwater and South-to-North Middle Route Project water is raised to compensate water shortage of the agriculture sector. The allocated groundwater for agriculture is raised from [586.7, 599.7] million m^3 in scenario 1 to [620.8, 633.8] million m^3 in scenario 2 and to [679.9, 686.7] million m^3 in scenario 3. The amount of South-to-North Middle Route Project water for agriculture is also raised from [187.2, 187.2] million m^3 in scenario 1 to [271.3, 271.3] million m^3 in scenario 2 and to [374.2, 374.2] million m^3 in scenario 3. The environment mainly uses reservoirs water, groundwater, reused water, and South-to-North Middle Route Project water. The water amount of Guanting and Miyun reservoirs for environment is declined with rainfall reduction. Contrarily, the groundwater, reused water, and transfer water for environment are all raised. For example, the reused water amount for environment is remarkably raised from [303.9, 323.9] million m^3 in scenario 1 to [348.9, 368.9] million m^3 in scenario 2 and to [400.8, 420.8] million m^3 in scenario 3. The results show that transfer water from South-to-North Middle Route Project has significant impact on water supply structure in Beijing city. It will mitigate the water shortage issue of social and economy development in Beijing city in some extent, particularly in dry year and extraordinary dry year.

5. Conclusion

An interval-parameter fuzzy linear programming with stochastic vertices (IFLPSV) has been developed for water resources allocation under dual uncertainty. The developed IFLPSV model improves upon the existing IFLP method by allowing the uncertain boundaries of interval parameter to be incorporated into the optimization processes. A hybrid intelligent algorithm based on genetic algorithm and artificial neural network was used to solve the developed model. The developed IFLPSV considers fuzzy, interval, and stochastic attributes of parameters and coefficients of objective functions and constraints. The application results indicated that it is effective for regional water resources allocation and planning under dual uncertainty. IFLPSV may provide more satisfactory solutions for an optimization problem under dual uncertainty. The developed IFLPSV model has been applied to multisource water allocation among multiple users in Beijing city in 2020, where water resources shortage is a challenging issue. The results indicate that transfering water from South-to-North Middle Route Project has an important impact on water supply structure in Beijing city, particularly in dry year and extraordinary dry year. The developed model and solution algorithm can be extended to other water resources system and environment management, where bounds of interval parameters or coefficients are dual uncertainty.

In this study, only two objectives including economic and greenbelt irrigation area maximization have been considered when carrying out water allocation in Beijing city. In the future, other objectives, such as social and environmental objective, might also be involved into water resources allocation in Beijing city. Moreover, interactive method for solving multi-objective optimization model is supposed to be incorporated into the methodology, so that the decision makers can make compromise among conflict objectives.

There are many uncertain factors in practical management and decision making of water resources system. The interval programming is an effective method to tackle uncertainties expressed as interval values with known lower and upper bounds. However, due to high complexity of water resources system, sometimes it is hard to determine the exact values of both the lower and upper bounds. They might be with characteristics of interval, fuzzy, or random. Therefore, in this paper, the dual uncertainties are defined as interval or fuzzy numbers with lower and upper bounds with interval, fuzzy, or random characteristics. Although the bounds of interval parameters might be randomly distributed, the elements within the interval are regarded as certain numbers. In future research, physical meaning of the stochastic attribute of upper and lower bounds of interval parameters is suggested to in-depth investigation. Further discussion should be undertaken to answer whats the difference between interval number with randomly distributed bounds when the elements within the interval are simply considered as certain numbers and interval parameter as simply a random parameter with its own distribution.

Acknowledgments

This research has been supported by the Open Research Fund of State Key Laboratory of Simulation and Regulation of Water Cycle in River Basin (China Institute of Water Resources and Hydropower Research). Grant no. IWHR-SKL-201214, and the National Natural Science Foundation of China (no. 91125018). The authors are grateful to the editor and the anonymous reviewers for their insightful and helpful comments and suggestions.

References

[1] Y. P. Li, G. H. Huang, G. Q. Wang, and Y. F. Huang, "FSWM: a hybrid fuzzy-stochastic water-management model for agricultural sustainability under uncertainty," *Agricultural Water Management*, vol. 96, no. 12, pp. 1807–1818, 2009.

[2] A. Abrishamchi, M. A. Marino, and A. Afshar, "Reservoir planning for irrigation district," *Journal of Water Resources Planning and Management*, vol. 117, no. 1, pp. 74–85, 1991.

[3] J. Kindler, "Rationalizing water requirements with aid of fuzzy allocation model," *Journal of Water Resources Planning & Management*, vol. 118, no. 3, pp. 308–323, 1992.

[4] J. M. Wagner, U. Shamir, and D. H. Marks, "Containing groundwater contamination: planning models using stochastic programming with recourse," *European Journal of Operational Research*, vol. 77, no. 1, pp. 1–26, 1994.

[5] O. Beaumont, "Solving interval linear systems with linear programming techniques," *Linear Algebra and Its Applications*, vol. 281, no. 1–3, pp. 293–309, 1998.

[6] P. G. Jairaj and S. Vedula, "Multi-reservoir system optimization using fuzzy mathematical programming," *Water Resources Management*, vol. 14, no. 6, pp. 457–472, 2000.

[7] J. Q. Ma, S. Y. Chen, and L. Qiu, "A multi-objective fuzzy optimization model for cropping structure and water resources and its method," *Agriculture Science & Technology*, vol. 5, no. 1, pp. 5–10, 2004.

[8] I. Maqsood, G. H. Huang, and J. S. Yeomans, "An interval-parameter fuzzy two-stage stochastic program for water resources management under uncertainty," *European Journal of Operational Research*, vol. 167, no. 1, pp. 208–225, 2005.

[9] Y. P. Li, G. H. Huang, and S. L. Nie, "An interval-parameter multi-stage stochastic programming model for water resources management under uncertainty," *Advances in Water Resources*, vol. 29, no. 5, pp. 776–789, 2006.

[10] Y. P. Li, G. H. Huang, Z. F. Yang, and S. L. Nie, "IFMP: interval-fuzzy multistage programming for water resources management under uncertainty," *Resources, Conservation and Recycling*, vol. 52, no. 5, pp. 800–812, 2008.

[11] G. H. Huang, "A hybrid inexact-stochastic water management model," *European Journal of Operational Research*, vol. 107, no. 1, pp. 137–158, 1998.

[12] G. H. Huang and D. P. Loucks, "An inexact two-stage stochastic programming model for water resources management under uncertainty," *Civil Engineering and Environmental Systems*, vol. 17, no. 2, pp. 95–118, 2000.

[13] Q. G. Lin, G. H. Huang, B. Bass, and X. S. Qin, "IFTEM: an interval-fuzzy two-stage stochastic optimization model for regional energy systems planning under uncertainty," *Energy Policy*, vol. 37, no. 3, pp. 868–878, 2009.

[14] H. W. Lu, G. H. Huang, G. M. Zeng, I. Maqsood, and L. He, "An inexact two-stage fuzzy-stochastic programming model for water resources management," *Water Resources Management*, vol. 22, no. 8, pp. 991–1016, 2008.

[15] H. W. Lu, G. H. Huang, and L. He, "A semi-infinite analysis-based inexact two-stage stochastic fuzzy linear programming approach for water resources management," *Engineering Optimization*, vol. 41, no. 1, pp. 73–85, 2009.

[16] X. H. Nie, G. H. Huang, Y. P. Li, and L. Liu, "IFRP: a hybrid interval-parameter fuzzy robust programming approach for waste management planning under uncertainty," *Journal of Environmental Management*, vol. 84, no. 1, pp. 1–11, 2007.

[17] Z. F. Liu and G. H. Huang, "Dual-interval two-stage optimization for flood management and risk analyses," *Water Resources Management*, vol. 23, no. 11, pp. 2141–2162, 2009.

[18] Z. F. Liu, G. H. Huang, X. H. Nie, and L. He, "Dual-interval linear programming model and its application to solid waste management planning," *Environmental Engineering Science*, vol. 26, no. 6, pp. 1033–1045, 2009.

[19] Y. P. Li, G. H. Huang, P. Guo, Z. F. Yang, and S. L. Nie, "A dual-interval vertex analysis method and its application to environmental decision making under uncertainty," *European Journal of Operational Research*, vol. 200, no. 2, pp. 536–550, 2010.

[20] Y. Han, Y. F. Huang, and G. Q. Wang, "Interval-parameter linear optimization model with stochastic vertices for land and water resources allocation under dual uncertainty," *Environmental Engineering Science*, vol. 28, no. 3, pp. 197–205, 2011.

[21] B. D. Liu, *Theory and Practice of Uncertain Programming*, Physica, Heidelberg, Germany, 2002.

[22] B. D. Liu, *Theory and Practice of Uncertain Programming*, Springer, Berlin, Germany, 3rd edition, 2009.

[23] G. H. Huang, B. W. Baetz, and G. G. Patry, "A grey linear programming approach for municipal solid waste management planning under uncertainty," *Civil Engineering Systems*, vol. 9, no. 4, pp. 319–335, 1992.

[24] G. H. Huang, B. W. Baetz, and G. G. Patry, "A grey fuzzy linear programming approach for municipal solid waste management planning under uncertainty," *Civil Engineering Systems*, vol. 10, no. 2, pp. 123–146, 1993.

[25] B.-Y. Wei and J. Wang, "Analysis of water resources supply and demand in the Beijing city," *South-to-North Water Transfers and Water Science & Technology*, vol. 7, no. 2, pp. 41–42, 2009 (Chinese).

[26] Beijing hydrology and water resources station, Beijing water resources Bulletin, Beijing water authority, 2010.

Hindawi Publishing Corporation
Mathematical Problems in Engineering
Volume 2013, Article ID 892321, 14 pages
http://dx.doi.org/10.1155/2013/892321

Research Article

Development of Optimal Water-Resources Management Strategies for Kaidu-Kongque Watershed under Multiple Uncertainties

Y. Zhou,[1] Y. P. Li,[1] G. H. Huang,[1] and Y. Huang[2]

[1] *MOE Key Laboratory of Regional Energy and Environmental Systems Optimization, Resources and Environmental Research Academy, North China Electric Power University, Beijing 102206, China*
[2] *State Key Laboratory of Desert and Oasis Ecology, Xinjiang Institute of Ecology and Geography, Chinese Academy of Sciences, Urumqi 830011, China*

Correspondence should be addressed to Y. P. Li; yongping.li33@gmail.com

Received 15 February 2013; Accepted 12 April 2013

Academic Editor: Xiaosheng Qin

In this study, an interval-stochastic fractile optimization (ISFO) model is advanced for developing optimal water-resources management strategies under multiple uncertainties. The ISFO model can not only handle uncertainties presented in terms of probability distributions and intervals with possibility distribution boundary, but also quantify subjective information (i.e., expected system benefit preference and risk-averse attitude) from different decision makers. The ISFO model is then applied to a real case of water-resources systems planning in Kaidu-kongque watershed, China, and a number of scenarios with different ecological water-allocation policies under varied p-necessity fractiles are analyzed. Results indicate that different policies for ecological water allocation can lead to varied water supplies, economic penalties, and system benefits. The solutions obtained can help decision makers identify optimized water-allocation alternatives, alleviate the water supply-demand conflict, and achieve socioeconomic and ecological sustainability, particularly when limited water resources are available for multiple competing users.

1. Introduction

The combined pressures from increasing water demands and limited water supplies have forced planners to contemplate comprehensive and efficient schemes for water resources management, especially in arid and semiarid regions [1, 2]. Nowadays, continuing economic growth and rapid population increase are likely to aggravate water-shortage problems that may lead to controversial and conflict-laden water-allocation issues among multiple competing interests (e.g., municipal, industrial, stockbreeding, forestry, ecological, and agricultural). Moreover, more and more arid inland watersheds suffer from ecological degradation and vegetation losses as a result of limited water resources, severe weather conditions, poor management practices, and failed policy instructions [3–5]. Consequently, the conflicts between environmental protection and economic development in arid and semiarid regions have been pressing challenges for decision makers. Efficient and equitable water-resources management is required for regional socioeconomic and environmental sustainability.

Previously, a large number of modeling approaches based on stochastic mathematical programming (SMP) were advanced for allocating and managing water resources in more effective and sustainable ways [6–14]. For example, Watkins Jr et al. [15] proposed a scenario-based multistage stochastic programming model for planning water supplies from highland lakes. By explicitly considering a number of inflow scenarios, the stochastic model could help determine a contract for water delivery in the coming year. Harrison [16] advanced a chance-constrained linear programming model to allocate available land and water resources optimally on seasonal basis so as to maximize the net annual return from the study area, where net irrigation water requirements of crops were considered as stochastic variable. Li et al. [17] proposed a multistage fuzzy-stochastic programming model for supporting water resources management under uncertainty, which could tackle uncertainties expressed as

fuzzy sets and probability distributions. Xu et al. [18] put forward an interval-parameter stochastic chance-constrained programming model for supporting multilayer urban water-supply system management under multiple uncertainties. Housh et al. [19] developed a limited multistage stochastic programming model for managing water-supply systems, where the number of decision variables at each stage remains constant, and thus the total number of decision variables increased only linearly as the number of scenarios and stages grew. Generally, SMP (i.e., multistage stochastic programming (MSP)) approach allows recourse actions to be undertaken in each stage based on updated information for realized system targets that take away the uncertainties, which could effectively reflect dynamic variations of multiple system components or conditions [20, 21]. Nevertheless, the main limitation of conventional SMP approach is that the probability distributions of uncertain parameters may not be available due to the inadequate information; even if these distributions were known, reflection of them in large-scale stochastic models could be extremely challenging [22].

Consequently, an attractive technique named fractile optimization (FO) approach can solve the above limitations, which is an effective solution algorithm of fuzzy possibilistic programming (FPP) and could enable the flexible estimation of results with high satisfaction degree [23–26]. FO approach represents the possible or necessity degree of event occurrence for imprecise data described by fuzzy possibility distributions which can be obtained rather easily from decision makers' perception owing to the ordinality of possibility [27]. Inuiguchi and Ramík [23] proposed the concept of fractile which ranges between 0 and 1 and expresses the decision makers' preferences (i.e., risk-averse attitudes) and necessity or possibility degree towards the objective function. Katagiri et al. [28] advanced an interactive fuzzy satisficing method for solving a fuzzy random multiobjective linear programming problem, while the developed method is based on fractile optimization model with possibility and necessity measures, and the uncertain objective function could be transformed into a deterministic one with high satisfaction degree. Zhang et al. [29] developed a robust fractile optimization model for water-quality management, where the fractile optimization approach could be beneficial for acquiring maximized agricultural income and decreasing the system violation risk. Although the FO approach could be effective for handling the ambiguous parameters in the objective function, it has difficulties in dealing with uncertainties presented as interval numbers and/or probability distributions in a nonfuzzy decision space [23].

Actually, in real-world water-resources management problems, uncertainties could influence desired decision makings and they may exist in the system components, their interactions and their economic implications, such as water availability, economic parameters, water allocations, subjective judgments, sustainability requirements, and policy regulations. Some uncertainties can be quantified as single uncertainties (i.e., discrete intervals, probabilities) while the others may be expressed as dual uncertainties (i.e., intervals with possibility distribution boundary). For instance, fluctuating stream inflows may be presented as random variables with known probabilities; also, the water-allocation targets are difficult to be promised as deterministic values when available water resources are uncertain, and they may be obtained as interval numbers. Meanwhile, water would be allocated to multiple users over a multiperiod planning horizon, while the uncertainties can result in dynamic water-allocation schemes and varied water shortages. Moreover, owing to the intrinsic fluctuations of cash flow, economic parameters are often estimated by experts with interval values, and, at the same time, their lower and upper bounds of these intervals may be provided as subjective judgments from a number of decision makers (i.e., expressed as possibility distributions). The conventional FO approach may become infeasible in handling such dual uncertainties presented in terms of intervals with possibility distribution boundary. One potential approach is to integrate interval-parameter programming (IPP), MSP, and FO approach to effectively address such single and dual uncertainties. IPP approach is conducive to tackling the uncertainties expressed as crisp interval values in objective function and constraints without probability distributions and membership functions [30, 31].

Therefore, the objective of this study aims to develop an interval-stochastic fractile optimization (ISFO) model for optimal water-resources management strategies under multiple uncertainties. The ISFO model can not only handle uncertainties presented in terms of probability distributions and intervals with possibility distribution boundary, but also quantify subjective information (i.e., expected system benefit preference and risk-averse attitude) from different decision makers. The ISFO model will be applied to a real case of water-resources systems planning in the Kaidu-kongque watershed, a region threatened by serious water shortages and extremely vulnerable ecological system, while the continued vegetation degradation and human-induced soil erosion lead to increasingly intensified conflict between ecological preservation and economic development in water resources utilization. The obtained results with various p-necessity fractiles will be beneficial for identifying optimized water-allocation alternatives, alleviating the water supply-demand conflict, and achieving socioeconomic and ecological sustainability, particularly when limited water resources are available for multiple competing users.

The paper will be organized as follows: Section 2 describes the development process of ISFO model, where multiple uncertainties are considered; Section 3 presents the application in Kaidu-kongque watershed through the developed model; Section 4 provides result analysis and discussion, where a number of solutions associated with robust reflection of multiple uncertainties in relation to water-resources allocation, water-management policy, benefit analysis and risk-averse level are analyzed; Section 5 draws some conclusions.

2. Model Development

The study problem under consideration is how to allocate water from upstream of river to multiple users to maximize expected system net benefit and achieve environmental sustainability over a multiperiod planning horizon. In case of insufficient water availability, competition for water exists

among different users. When the promised water is not delivered and the available water cannot meet the demands, the users will have to face a dilemma of either obtaining water from higher-priced schemes or curb the development plans, leading to incremental expenses or diminished benefits [32]. For instance, industries may have to decrease production levels, and farmlands may not be irrigated as planned. It is thus essential for allocating available water in more sustainable ways to reduce the related punishments. Being presented as random variables, the stream flows of the river may vary in various flow levels during different periods, which result in the dynamic water-allocation schemes. The associated decisions must be made at discrete points in discrete probability levels. In addition, owing to the intrinsic fluctuations of influence factors (e.g., cash flow and production price) and incomplete and imprecise datum, many coefficients and variables (i.e., water-allocation target, water availability, and economic parameter) are difficult for obtaining deterministic values and are thus expressed by interval numbers. Therefore, an interval-stochastic programming model can be formulated for study problem associated with multiple uncertainties:

$$\begin{aligned}\text{Max } f^{\pm} = {} & \sum_{i=1}^{I}\sum_{t=1}^{T} SY_{it}^{\pm}\cdot FT_{it}^{\pm} \\ & - \sum_{i=1}^{I}\sum_{t=1}^{T}\sum_{k=1}^{K_t} p_{tk} EP_{it}^{\pm}\cdot WD_{itk}^{\pm}\end{aligned} \tag{1a}$$

subject to

$$\sum_{i=1}^{I}\left(FT_{it}^{\pm} - WD_{itk}^{\pm}\right) \le WA_{th}^{\pm} + EW_{(t-1)k}^{\pm}, \quad \forall h,\ k = 1,2,\ldots,K_t;\ t = 1,2,\ldots,T, \tag{1b}$$

$$EW_{(t-1)k}^{\pm} = WA_{(t-1)h}^{\pm} - \sum_{i=1}^{I}\left(FT_{i(t-1)}^{\pm} - WD_{i(t-1)k}^{\pm}\right) + EW_{(t-2)k}^{\pm}, \quad \forall h,\ k = 1,2,\ldots,K_{t-1}, \tag{1c}$$

$$FT_{it\max} \ge FT_{it}^{\pm} \ge WD_{itk}^{\pm}, \quad \forall i,t,\ k = 1,2,\ldots,K_t, \tag{1d}$$

$$FT_{it}^{\pm} - WD_{itk}^{\pm} \ge MWR_{it}, \quad \forall t,\ k = 1,2,\ldots,K_t, \tag{1e}$$

$$FT_{it}^{\pm}, WD_{itk}^{\pm} \ge 0, \quad \forall i,t,\ k = 1,2,\ldots,K_t, \tag{1f}$$

where $f^{\pm}$ is the net system benefit over the planning horizon (\$); i is the water user, $i = 1,2,\ldots,I$; t is the planning time period, $t = 1,2,\ldots,T$; h is the available flow level ($h = 1,2,\ldots,H$), with $h = 1$ for the lowest flow and $h = H$ for the highest flow; K_t is the number of scenarios in period t and should be related to H_t, and the total number of scenarios is $K = \sum_{t=1}^{T} K_t = 1$; $WA_{th}^{\pm}$ is the water availability with probability level of p_{tk} for K_t scenario at each time stage (t) (10^6 m^3); $SY_{it}^{\pm}$ is the net benefits to user i per unit of water allocated during period t (\$/10^3 m^3); $EP_{it}^{\pm}$ is the reduction of net benefit to user i per unit of water not delivered during period t ($C_{it} > B_{it}$) (\$/10^3 m^3); p_{tk} is the probability of occurrence for scenario k in period t, with $p_{th} > 0$ and $\sum_{K=1}^{K_i} p_{tk} = 1$; $EW_{(t-1)k}^{\pm}$ is the surplus water in the reservoir when water is delivered in period $t-1$ under scenario k (10^6 m^3); $FT_{it\max}$ is the maximum allowable allocation amount for user i in period t (10^6 m^3); MWR_{it} is the minimum amount that should be allocated to user i in period t (10^6 m^3); $FT_{it}^{\pm}$ is the fixed water allocation target that is, promised to user i during period t (10^6 m^3); $WD_{itk}^{\pm}$ is the amount by which the water-allocation targets are not met when the seasonal flows are q_{th} (10^6 m^3).

Obviously, model ((1a), (1b), (1c), (1d), (1e), (1f)) can be effective for handling uncertainties presented as crisp interval values in objective function and constraints and random variables in the right-hand sides with known probability distributions. However, modeling parameters may be provided as subjective judgments from a number of stakeholders and decision makers (i.e., expressed as possibility distributions), which makes interval-stochastic programming model become infeasible [33]. Therefore, fractile optimization (FO) approach, based on the fuzzy possibilistic programming (FPP), can effectively solve uncertainties presented as possibility distributions, while its necessity is described as the treatment of an objective function [23–26, 34]. When uncertainties are expressed as possibility distributions in the ambiguous coefficients of objective function, a general FPP model can be formulated as follows [35–37]:

$$\text{Max } \underset{\sim}{f} = \underset{\sim}{C}X \tag{2a}$$

subject to

$$AX \le B, \tag{2b}$$

$$X \ge 0, \tag{2c}$$

where coefficient $\underset{\sim}{C}$ represents the fuzzy possibilistic variables restricted by fuzzy triangular numbers with possibility distribution. Generally, possibility distribution can be regarded as fuzzy membership function, and possibility degree can be considered as the membership value [38]. In virtue of the computational efficiency and simplicity in data acquisition, a symmetric triangular fuzzy number $\underset{\sim}{C}$ is considered, which can be determined by a center c^c and a spread w, and can be described as $\underset{\sim}{C} = (c^c, w)$ [34, 39]. Accordingly, the linear objective function of the model ((2a), (2b), (2c)) with ambiguous parameters (i.e., Equation (2a)) can be transformed as follows:

$$\text{Max } \underset{\sim}{f} = \left(c^c X, w\,|X|\right). \tag{3}$$

In the possibility theory, necessity measure is defined as follows [23, 34, 35]:

$$N_C(B) = \inf_r \max\left(1 - \mu_C(r), \mu_B(r)\right), \tag{4}$$

where μ_B is the membership function of the fuzzy set B; $N_C(B)$ denotes the certainty (or necessity) degree of the event

that fuzzy possibilistic variable $\underset{\sim}{C}$ restricted by the possibility distribution μ_C is in the fuzzy set B. Let $B = (-\infty, u]$ or $[u, +\infty)$, which is indicated as a crisp set of real numbers which is not greater (or not smaller) than u. Then, we obtain the following indices by necessity measure defined by (5) and (6) [23, 34]:

$$\mathrm{Nes}\left(\underset{\sim}{C} \le u\right) = N_C\left((-\infty, u]\right) = 1 - \sup\left\{\mu_C(r) \mid r > u\right\}, \tag{5}$$

$$\mathrm{Nes}\left(\underset{\sim}{C} \ge u\right) = N_C\left([u, +\infty)\right) = 1 - \sup\left\{\mu_C(r) \mid r < u\right\}. \tag{6}$$

Based on the definition of necessity measure mentioned above, the p-necessity fractile is defined as follows [33]:

$$\mathrm{Nes}\left(\underset{\sim}{f} \ge u\right) \ge p_{\mathrm{nes}}, \tag{7}$$

where u denotes the p-fractile value; $\underset{\sim}{f}$ means the fuzzy possibilistic variable (i.e., model (2a)) restricted by fuzzy numbers; the value of necessity measure (i.e., Nes $(\cdot)$) belongs to the interval $[0, 1]$. Given the appropriate level p_{nes} $[0, 1]$, the problem is transformed to maximize the p-fractile value under the condition that a necessity measure of the event that the objective function value is not lesser than p-fractile value u is greater than or equal to p_{nes}. The diverse p_{nes} levels express the decision makers' preferences toward the objective function value, which implies the certainty (necessity) degree of the objective function (also named p-necessity level). In real-world applications, the decision makers prefer that the objective function should be satisfied under a high certainty degree (high p-necessity level). Given the p-necessity level, the problem (i.e., model (2a), (2b), (2c)) can be transformed into the following linear necessity fractile optimization model with deterministic objective:

$$\mathrm{Max}\, u \tag{8a}$$

subject to

$$\mathrm{Nes}\left\{\left(c^c X, w\,|X|\right) \ge u\right\} \ge p_{\mathrm{nes}}. \tag{8b}$$

Based on the fractile optimization model (as illustrated in Figure 1), the problem is to maximize the p-necessity fractile of a possibilistic variable $\underset{\sim}{f}$, and model (5) corresponds to

$$\mathrm{Max}\left(c^c X - p_{\mathrm{nes}} w\,|X|\right). \tag{9}$$

In practical water resources systems planning, interval parameters (i.e., economic data) may fluctuate with their bounds being available as subjective preferences (i.e., expected system benefit standpoint and risk-averse attitude), which may be provided by possibility distributions. The concept of intervals with possibility distribution boundary is proposed in this study to represent the dual uncertainties in the system components. Consequently, FO approach is introduced into the above interval-stochastic programming framework to handle such dual uncertainties in the objective function. This leads to an interval-stochastic fractile optimization (ISFO) model as follows:

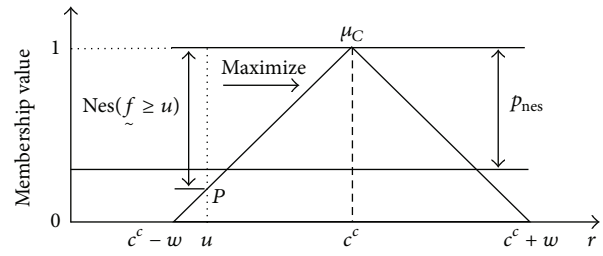

Figure 1: Fractile optimization model.

$$\mathrm{Max}\ \underset{\sim}{f}^{\pm} = \sum_{i=1}^{I}\sum_{t=1}^{T} \underset{\sim it}{SY}^{\pm} \cdot FT_{it}^{\pm} - \sum_{i=1}^{I}\sum_{t=1}^{T}\sum_{k=1}^{K_t} p_{tk}\, \underset{\sim it}{EP}^{\pm} \cdot WD_{itk}^{\pm} \tag{10a}$$

subject to

$$\sum_{i=1}^{I}\left(FT_{it}^{\pm} - WD_{itk}^{\pm}\right) \le WA_{th}^{\pm} + EW_{(t-1)k}^{\pm}, \quad \forall h,\ k = 1, 2, \ldots, K_t,\ t = 1, 2, \ldots, T, \tag{10b}$$

$$EW_{(t-1)k}^{\pm} = WA_{(t-1)h}^{\pm} - \sum_{i=1}^{I}\left(FT_{i(t-1)}^{\pm} - WD_{i(t-1)k}^{\pm}\right) + EW_{(t-2)k}^{\pm}, \quad \forall h,\ k = 1, 2, \ldots, K_{t-1}, \tag{10c}$$

$$FT_{it\,\max} \ge FT_{it}^{\pm} \ge WD_{itk}^{\pm}, \quad \forall i, t,\ k = 1, 2, \ldots, K_t, \tag{10d}$$

$$FT_{it}^{\pm} - WD_{itk}^{\pm} \ge MWR_{it}, \quad \forall t,\ k = 1, 2, \ldots, K_t, \tag{10e}$$

$$FT_{it}^{\pm}, WD_{itk}^{\pm} \ge 0, \quad \forall i, t,\ k = 1, 2, \ldots, K_t. \tag{10f}$$

For model (10a), (10b), (10c), (10d), (10e), (10f), in order to identify an optimized set of target values (i.e., $FT_t^{\pm}$), z_t are introduced to be decision variables into models (10a), (10b), (10c), (10d), (10e), and (10f). Let $FT_t^{\pm} = FT_t^{-} + \Delta FT_t \cdot z_t$, where $\Delta FT_t = FT_t^{+} - FT_t^{-}$ and $z_t \in [0, 1]$. Thus, when $FT_t^{\pm}$ reach their upper bounds (i.e., when $z_t = 1$), a relatively high objective function value will be gained in the case of satisfactory water demand; an associated high penalty may have to be paid when the promised water is not delivered. On the contrary, when $FT_t^{\pm}$ approach their lower bounds (i.e., when $z_t = 0$), a lower objective function value and related lower risk will be obtained. Accordingly, through introducing decision variables z_t, the ISFO model can be transformed into two deterministic submodels.

Submodels (11a), (11b), (11c), (11d), (11e), and (11f):

$$\begin{aligned}\text{Max } f^{+} = {} & \sum_{i=1}^{I}\sum_{t=1}^{T} SY_{it}^{c+}\left(FT_{it}^{-} + \Delta FT_{it}\cdot z_t\right) \\ & - \sum_{i=1}^{I}\sum_{t=1}^{T} p_{\text{nes}} w_{SY}\left|\left(FT_{it}^{-} + \Delta FT_{it}\cdot z_t\right)\right| \\ & - \sum_{i=1}^{I}\sum_{t=1}^{T}\sum_{k=1}^{K_t} p_{tk} EP_{it}^{c-} WD_{itk}^{-} \\ & + \sum_{i=1}^{I}\sum_{t=1}^{T}\sum_{k=1}^{K_t} p_{tk} p_{\text{nes}} w_{EP}\left|WD_{itk}^{-}\right|\end{aligned} \tag{11a}$$

subject to

$$\sum_{i=1}^{I}\left[\left(FT_{it}^{-} + \Delta FT_{it}\cdot z_t\right) - WD_{itk}^{-}\right] \le WA_{th}^{+} + EW_{(t-1)k}^{+}, \quad \forall h,\ k = 1,2,\ldots,K_t,\ t = 1,2,\ldots,T, \tag{11b}$$

$$EW_{(t-1)k}^{+} = WA_{(t-1)h}^{+} - \sum_{i=1}^{I}\left[\left(FT_{it}^{-} + \Delta FT_{it}\cdot z_t\right) - WD_{itk}^{-}\right] + EW_{(t-2)k}^{+}, \quad \forall h,\ k = 1,2,\ldots,K_{t-1}, \tag{11c}$$

$$FT_{it\max} \ge FT_{it}^{-} + \Delta FT_{it}\cdot z_t \ge WD_{itk}^{-}, \quad \forall i,t,\ k = 1,2,\ldots,K_t, \tag{11d}$$

$$\left(FT_{it}^{-} + \Delta FT_{it}\cdot z_t\right) - WD_{itk}^{-} \ge MWR_{it}, \quad \forall t,\ k = 1,2,\ldots,K_t, \tag{11e}$$

$$FT_{it}^{-} + \Delta FT_{it}\cdot z_t \ge 0, \quad WD_{itk}^{-} \ge 0, \quad \forall i,t,\ k = 1,2,\ldots,K_t. \tag{11f}$$

Submodels (12a), (12b), (12c), (12d), (12e), and (12f):

$$\begin{aligned}\text{Max } f^{-} = {} & \sum_{i=1}^{I}\sum_{t=1}^{T} SY_{it}^{c-}\left(FT_{it}^{-} + \Delta FT_{it}\cdot z_{t\,\text{opt}}\right) \\ & - \sum_{i=1}^{I}\sum_{t=1}^{T} p_{\text{nes}} w_{SY}\left|\left(FT_{it}^{-} + \Delta FT_{it}\cdot z_{t\,\text{opt}}\right)\right| \\ & - \sum_{i=1}^{I}\sum_{t=1}^{T}\sum_{k=1}^{K_t} p_{tk} EP_{it}^{c+} WD_{itk}^{+} \\ & + \sum_{i=1}^{I}\sum_{t=1}^{T}\sum_{k=1}^{K_t} p_{tk} p_{\text{nes}} w_{EP}\left|WD_{itk}^{+}\right|\end{aligned} \tag{12a}$$

subject to

$$\sum_{i=1}^{I}\left[\left(FT_{it}^{-} + \Delta FT_{it}\cdot z_{t\,\text{opt}}\right) - WD_{itk}^{+}\right] \le WA_{th}^{-} + EW_{(t-1)k}^{-}, \quad \forall h,\ k = 1,2,\ldots,K_t,\ t = 1,2,\ldots,T, \tag{12b}$$

$$EW_{(t-1)k}^{-} = WA_{(t-1)h}^{-} - \sum_{i=1}^{I}\left[\left(FT_{it}^{-} + \Delta FT_{it}\cdot z_{t\,\text{opt}}\right) - WD_{itk}^{+}\right] + EW_{(t-2)k}^{-}, \quad \forall h,\ k = 1,2,\ldots,K_{t-1}, \tag{12c}$$

$$FT_{it\max} \ge FT_{it}^{-} + \Delta FT_{it}\cdot z_{t\,\text{opt}} \ge WD_{itk}^{+}, \quad \forall i,t,\ k = 1,2,\ldots,K_t, \tag{12d}$$

$$\left(FT_{it}^{-} + \Delta FT_{it}\cdot z_{t\,\text{opt}}\right) - WD_{itk}^{+} \ge MWR_{it}, \quad \forall t,\ k = 1,2,\ldots,K_t, \tag{12e}$$

$$FT_{it}^{-} + \Delta FT_{it}\cdot z_{t\,\text{opt}} \ge 0, \quad WD_{itk}^{+} \ge 0, \quad \forall i,t,\ k = 1,2,\ldots,K_t. \tag{12f}$$

By solving above two submodels, the final solutions for ISFO model $f_{\text{opt}}^{\pm} = [f_{\text{opt}}^{-}, f_{\text{opt}}^{+}]$, $FT_{it\,\text{opt}}^{\pm} = FT_{it}^{-} + \Delta FT_{it}\cdot z_{t\,\text{opt}}$ and $WD_{itk\,\text{opt}}^{\pm} = [WD_{itk\,\text{opt}}^{-}, WD_{itk\,\text{opt}}^{+}]$ can be acquired. The actual water allocation would be the difference between the promised target values (i.e., $FT_{it\,\text{opt}}^{\pm}$) and the shortage values (i.e., $WD_{itk\,\text{opt}}^{\pm}$).

3. Case Study

Kaidu-Kongque watershed (within E85°20′–87°30′, N41°10′–42°30′), one of mainstreams of the Tarim River, is situated in the Bayangol Mongol autonomous prefecture in Xinjiang Uygur autonomous region of northwest China. As the upper reach of the watershed, Kaidu River originates from Saaer mountain of the middle Tianshan Mountains, passes through Yourdusi basin, enters Yanqi basin, flows into Bosten Lake, then is pumped into Kongque River at southwest of the lake, crosses Kezile mountain of the south Tianshan Mountains, and finally reaches Tarim basin. The watershed contains one city (i.e., Ku'erle city), five countries (i.e., Yanqi, Hejing, Heshuo, Bohu, and Weili), and ten production and construction corps, covering an area of approximately 31.40×10^3 km^2. A temperate continental arid climate characterizes the watershed. The annual average precipitation ranges from 47.3 mm to 75.0 mm and mainly concentrates in May and October, indicating uneven distribution of precipitation through the year. The annual average pan evaporation ranges from 1887 mm to 2777 mm. The watershed is mainly recharged by rainfall and alpine glacier-snow melt water, while the gross amount of water resources of the watershed is approximately 4.41×10^9 m^3. The water from upstream of Kaidu-kongque River is allocated to six users, including municipal, industrial, stockbreeding, forestry, agricultural, and ecological sectors (as shown in Figure 2). At the end of 2008, the total population of the watershed was 1.03 million, and the gross industrial output value reached RMB ¥ 8.37 billion. Besides, the largest alpine meadow of China, named Bayanbulak Grassland, is located in the watershed, with a total area of 23.00×10^3 km^2, which is beneficial for stockbreeding. Moreover, owing to suitable environmental conditions in the lower beach of Kaidu River,

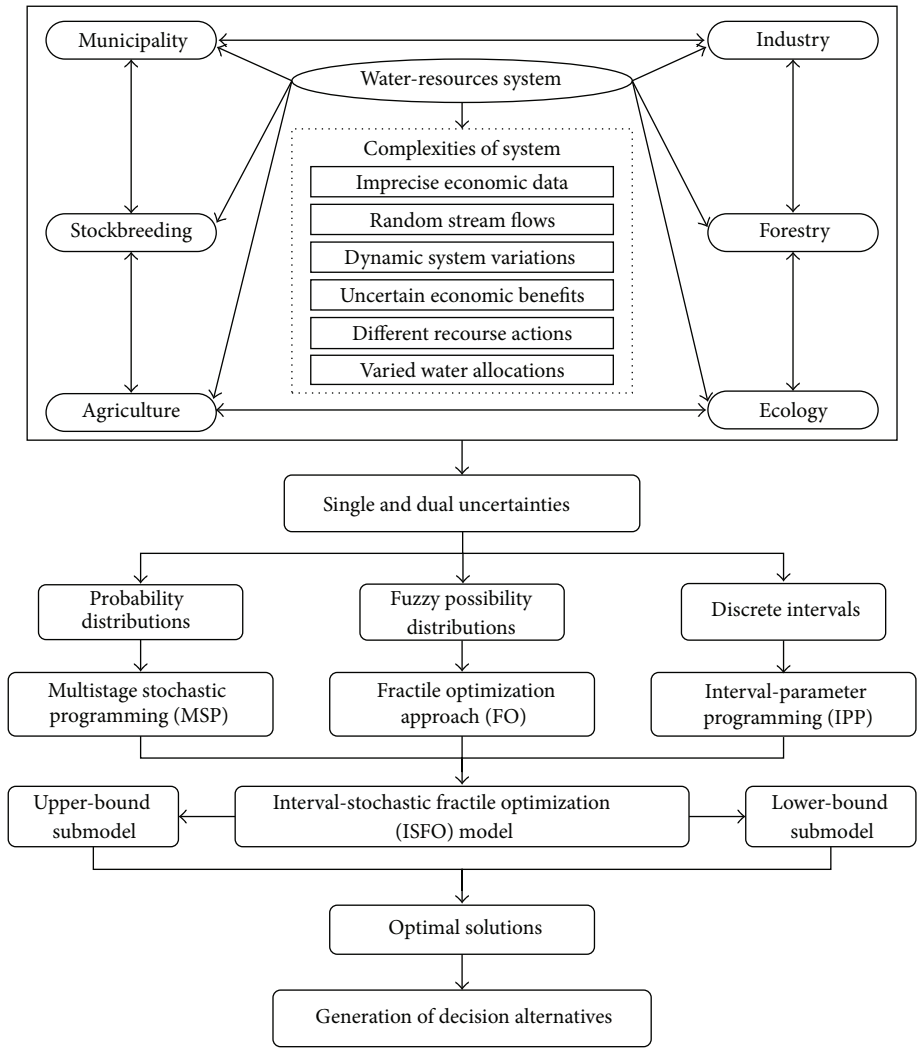

Figure 2: Diagram of planning water-resources system.

the Kaidu-kongque watershed has been a significant region for agricultural production, processing and exporting in Xinjiang province. At the same time, the ecosystems in this region are extremely vulnerable to disturbances and habitat degradation owing to severe water resource shortage [40]. Being in the middle reach of the Tarim River basin, the watershed is the supplement for ecosystem recovering of the lower reach of the Tarim River.

In recent years, with incremental population growth, rapid economic development and accelerating industrialization and urbanization processes, water demand of the watershed has been experienced a continuous and significant increment. Nevertheless, past practice experience and sustainable development strategies in water resources management have raised increasing concerns in irrational utilization and over exploitation of water resources. Kaidu-kongque watershed confronts with serious water shortages, while agricultural sector contributes to the largest water consumer. Owing to the severe weather conditions with characteristics of scarce rainfall, high temperature and high evaporation in the region, over 95 percent of the arable land in the watershed needs irrigation [41]. The statistics suggest that agricultural irrigation area of the watershed ran up to 391.62×10^3 m^2 in 2009, while agricultural water consumption came up to 2.40×10^9 m^3, accounting for the 96.31% of the total water consumption. Furthermore, the seasonal variation of stream flow leads to the water scarcity in spring and water surplus in summer which gives rise to water utilization conflicts in local agricultural production. Consequently, under the circumstance of excessive agricultural water consumption and unreasonable irrigation mode, the pressure on local water resources intensifies, resulting in tensions, conflicts among water users, and excessive pressure on ecological environment. Specifically, natural variability and intensive human activities (i.e., excessive water withdrawal and consumption in upper and middle reaches of the river) have led to a large decrease in streamflow, dried-up riverbed, and withered natural vegetations (i.e., populus euphratica and meadow) in the lower beaches of river, which further aggravate the ecological degradation. Such irrational water

utilization and over-exploitation problems intensify the water supply-demand conflict, accelerate the ecological environment destruction, threaten the sustainable development, and even have far-reaching impacts on watershed environment and human beings' lives. Unfortunately, in this region, there is a lack of effective plan for facilitating efficient, equitable and sustainable water resources management. Previous water-resources management in the watershed is mostly based on statistical analyses of historical data. Therefore, in order to recovery the ecological system in the lower reaches of the watershed, it is essential to develop an effective modeling technique for supporting water resources management under such conflicts.

As shown in Figure 2, the water resources system of the study area could be considered as an interrelated network connected by various system components. It is indicated that all kinds of complexities may exist in the study system, including imprecise economic data, random stream flows, dynamic system variables, uncertain economic benefits, various recourse actions, and varied water allocations. These components and their interactions must be systematically estimated in planning an integrated water resources management model within multiperiod. Specifically, due to spatial and temporal variations of precipitation, evapotranspiration and snow melting in the study system, the stream flow of Kaidu-kongque River presents a remarkable pattern of seasonal variation. Summer stream flow contributes to the greatest proportion, amounting to 45.0%, followed by spring stream flow (23.2%), fall stream flow (21.1%), and winter stream flow (10.7%). Accordingly, the fluctuating stream flows are expressed as with known probabilities, which may lead to varied water-allocation plans and various recourse actions. Moreover, several economic implications associated with economic fluctuations and subjective judgments could bring about uncertain system benefits and affect water-allocation decision makings. Imprecise economic data are highly uncertain and represented as intervals with possibility distribution boundary; this results in dual uncertainties in the objective function. In order to generate a desired compromise between the required environmental objective and maximized system benefit, how to effectively handle such single and dual uncertainties is regarded as a primary concern. Comprehensive optimization models are effective methods for allocating and managing water resources in more efficient and environmentally benign ways.

In real-world water-resources management problems, uncertainties are often associated with various in terms of information quality [42]. The random characteristic of stream flow and ambiguity in benefits and penalties parameters are all possible sources of uncertainties. The stream flow is expressed as a random variable; its probability distribution is obtained by statistical analysis when the collection data are enough. However, due to inadequate information or subjective judgment of decision makers, possibilistic distributions of economic parameters could be estimated through a number of questionnaires. Generally, random parameters are expressed as probability density functions (PDFs), while possibility distribution can be regarded as fuzzy membership function [43].

In this study, the time horizon under consideration is 3 years, which is divided into three planning periods. Modeling parameters are estimated based on the statistical yearbook of Bayangol Mongol Autonomous Prefecture and Xinjiang Uygur Autonomous Region or derived from published reports and papers [41, 44]. For example, water availability is presented as random variable, which is obtained through the 46-year statistical analyses with simulation results of annual stream flow of the Kaidu-kongque River; based on the previous simulation results, after determining the probability distribution (i.e., gamma distribution) of the simulated stream flow, its discretization values with different probability levels can be acquired [41]. Table 1 presents discrete intervals of stream flows and associated probability levels during three planning periods. Table 2 provides the promised water-allocation targets as well as maximum allowable allocations from municipal, industrial, stockbreeding, forestry, agricultural, and ecological sectors, which is on the basis of previous studies [41]. Shortages in water supply will occur if available water is less than water demands, such that the promised targets cannot be delivered (i.e., water shortage = promised target − available water). Under such circumstances, the actual water allocation will be the difference between the promised target and the probabilistic water shortage (i.e., actual water allocation = promised target − water shortage). Table 3 shows the relevant system benefits and penalties data, which are expressed by intervals with possibility distribution boundary. Specifically, the interval values of net benefit for each unit of water can be calculated by historical data through dividing the gross annual value of each water user by its annual water consumption, while the possibility distributions are estimated by the subjective judgments of 100 decision makers and stakeholders through 120 questionnaires. The economic penalties correspond to the acquisition of water from higher-priced alternatives and/or the negative consequences generated from the curbing of regional development plans when the promised water is not delivered [45]. Besides, a water-resources management policy based on minimum water requirement for ecological sector is considered through ISFO model, which complies with the policy on recovering the ecological system in the lower beaches of the river. Case 1 is based on the current water-resource allocation policies with p-necessity level of 0.90, while 100×10^6 m^3 of minimum water requirement for ecological sector is required to be satisfied (means the basic case); in Case 2, minimum water requirement for ecological sector is not considered in the ISFO model when p-necessity level =0.90.

4. Results and Discussion

4.1. Results under Basic Case. In this study, three stream flow levels (i.e., low, medium, and high) were considered in each period. Accordingly, a three-period (four-stage) scenario tree can be generated for each of water users, which resulted in 3 nodes (scenarios) in period 1 (stage 2), 9 nodes (scenarios) in period 2 (stage 3), and 27 nodes (scenarios) in period 3 (stage 4). The solutions obtained under basic case (e.g., Case 1) are presented in Figures 3–5. The results (i.e., objective function

Table 1: Stream flows and associated probabilities.

Flow level	$t = 1$		$t = 2$		$t = 3$	
	Probability	Stream flow (10^6 m^3)	Probability	Stream flow (10^6 m^3)	Probability	Stream flow (10^6 m^3)
Low (L)	0.304	[2459, 2989]	0.370	[2399, 3003]	0.174	[2602, 2901]
Medium (M)	0.455	[3002, 3721]	0.502	[3062, 3847]	0.490	[2917, 3626]
High (H)	0.241	[3752, 5708]	0.128	[4068, 5676]	0.336	[3700, 5500]

Table 2: Water resource allocations for each sector (unit: 10^6 m^3).

	Time period		
	$t = 1$	$t = 2$	$t = 3$
Water-resource allocation target			
Municipality	[69, 191]	[80, 200]	[90, 220]
Industry	[469, 803]	[550, 900]	[420, 800]
Stockbreeding	[41, 155]	[45, 170]	[50, 175]
Forestry	[407, 527]	[460, 588]	[480, 600]
Agriculture	[2335, 3113]	[2420, 3200]	[2480, 3350]
Ecology	[445, 1051]	[500, 1100]	[500, 1100]
Maximum allowable water allocation			
Municipality	200	200	200
Industry	900	900	900
Stockbreeding	200	200	200
Forestry	600	600	600
Agriculture	3500	3500	3500
Ecology	1200	1200	1200

value and decision variables) included the interval, probabilistic, and fuzzy possibilistic information, in which multiple uncertainties (i.e., probability distributions and intervals with possibility distribution boundary) can be facilitated to obtain multiple decision alternatives.

Figure 3 presents the optimized water-allocation targets for various users over the planning horizon under the basic case. The results indicate that the optimized water-allocation target for municipal sector would be 191×10^6, 200×10^6 and 200×10^6 m^3, which amount to their upper-bound targets in periods 1-2 and approaches the upper-bound target in period 3. Similarly, the optimized water-allocation targets for industrial, stockbreeding, and ecological sectors would also reach their upper-bounds. In comparison, the optimized water-allocation target for forestry sector would be in the range of its lower- and upper-bound targets for water resource allocations, amounting to 527×10^6, 586×10^6, and 480×10^6 m^3 during three periods; the optimized water-allocation target for agricultural sector would approach its lower-bound water-allocation target, reaching 2682×10^6, 2420×10^6, and 2480×10^6 m^3 over the planning horizon. This demonstrates that the planning allocation target for ecological sector would meet its water demand, while the planning allocation target for agricultural sector would not meet its essential demand, if a minimum amount of ecological water requirement was considered by the modeling formulation.

Shortages in water supply would occur if available stream flows could not satisfy the water-allocation targets, where the actual water-allocation plans of each user would be the difference between the optimized water-allocation target and the probabilistic water shortage. In case of insufficient water supply, the municipal sector should be the highest priority since it brings the highest benefits when water demand is satisfied, then to stockbreeding, industrial, agricultural, ecological, and forestry sectors. The solutions through ISFO model demonstrate that municipal, industrial and stockbreeding sectors would not be subject to any water deficit under all stream flows, while the water deficits would be occur for forestry, agricultural, and ecological sectors. This is attributed to the fact that the municipal, industrial and stockbreeding sectors bring relative high benefits when promised waters are delivered; meanwhile, they are subject to the high penalties the promised targets are not satisfied.

Figure 4 represents the water-allocation plans for agricultural sector over the planning horizon under the basic condition. By a three-period (four-stage) scenario tree, the solutions of water deficit could reflect the dynamic system variations. The maximum value of the deficit is associated with lower system benefit; contrarily, the minimum value of the deficit corresponds to higher system benefit. As shown in Figure 4, when stream flows are low in all of the three periods (i.e., under scenario LLL with a joint probability of 1.96%), the probabilistic water deficits for agricultural sector would be [947, 1477] $\times 10^6$ m^3 in period 1 (probability = 30.4%), [801, 1405] $\times 10^6$ m^3 in period 2 (probability = 11.2%), and [868, 1167] $\times 10^6$ m^3 in period 3 (probability = 1.96%), respectively. Accordingly, the optimized water allocated to agricultural sector would be [1205, 1735] $\times 10^6$ m^3 in period 1, [1015, 1619] $\times 10^6$ m^3 in period 2, and [1313, 1612] $\times 10^6$ m^3 in period 3, respectively; the total water-allocation amount to this user would be [3532, 4965] $\times 10^6$ m^3 under this scenario. The solutions for water deficits and water-allocation plans under other scenarios could be similarly analyzed based on the solutions represented in Figure 4.

Besides, the solutions imply that varied seasonal flows result in different water allocations to various users. For instance, when stream flows are high in all of the three periods, the optimized water allocation to forestry sector would, respectively, be [0, 527] $\times 10^6$ m^3 in period 1 (probability = 24.1%), [0, 586] $\times 10^6$ m^3 in period 2 (probability = 3.08%), and [0, 445] $\times 10^6$ m^3 in period 3 (probability = 1.04%), while the optimized water allocation to ecological sector would be [105, 1051] $\times 10^6$ m^3 in period 1, [378, 1100] $\times 10^6$ m^3 in period 2, and [114, 1090] $\times 10^6$ m^3 in period 3. When a

Table 3: Net benefits and penalties (unit: $/10^3 m^3).

	Time period		
	$t = 1$	$t = 2$	$t = 3$
	Net benefit when water demand is satisfied		
Municipality	[(6443, 7857, 9271), (8200, 10000, 11800)]	[(5664, 6907, 8150), (8120, 9903, 11686)]	[(5920, 7220, 8520), (8202, 10003, 11804)]
Industry	[(1693, 1820, 1947), (5965, 6414, 6863)]	[(1767, 1900, 2033), (5859, 6300, 6741)]	[(1830, 1968, 2106), (6511, 7001, 7491)]
Stockbreeding	[(3510, 3900, 4290), (5837, 6485, 7134)]	[(3510, 3900, 4290), (5651, 6279, 6907)]	[(3447, 3830, 4213), (5400, 6000, 6600)]
Forestry	[(254, 257, 260), (366, 371, 376)]	[(284, 288, 292), (402, 407, 412)]	[(267, 269, 272), (387, 392, 397)]
Agriculture	[(336, 341, 346), (448, 455, 462)]	[(362, 367, 373), (473, 480, 487)]	[(384, 390, 396), (547, 555, 563)]
Ecology	[(155, 157, 159), (424, 429, 434)]	[(168, 170, 172), (514, 520, 526)]	[(189, 191, 193), (523, 529, 535)]
	Penalty when promised water is not delivered		
Municipality	[(12142, 14285, 16428), (15785, 18571, 21357)]	[(11121, 13084, 15047), (16148, 18998, 21848)]	[(12266, 14430, 16595), (16405, 19300, 22195)]
Industry	[(3456, 3600, 3744), (10984, 11442, 11900)]	[(3360, 3500, 3640), (11520, 12000, 12480)]	[(3539, 3687, 3834), (12672, 13200, 13728)]
Stockbreeding	[(7307, 7857, 8407), (11957, 12857, 13757)]	[(6975, 7500, 8025), (10560, 11355, 12150)]	[(7068, 7600, 8132), (11102, 11938, 12774)]
Forestry	[(511, 515, 519), (736, 742, 748)]	[(526, 530, 534), (794, 800, 806)]	[(516, 520, 524), (774, 780, 786)]
Agriculture	[(636, 642, 648), (990, 1000, 1010)]	[(713, 720, 727), (1089, 1100, 1111)]	[(772, 780, 788), (1089, 1100, 1111)]
Ecology	[(283, 285, 287), (639, 643, 647)]	[(303, 305, 307), (995, 1002, 1009)]	[(323, 325, 327), (950, 956, 962)]

minimum water supply for ecological sector is satisfied, the total water-allocation amount to ecological user would be [597, 3251] $\times 10^6$ m^3 over the planning horizon. Such minimum water requirement for ecological sector could alleviate the conflict between ecological conservation and economic development, and develop regional ecological sustainability. In summary, among these water users, agricultural irrigation and ecological requirement would account for a substantial proportion of the total water resources. Several measures regarding water saving and increased water recycling rates would be promoted in the local agricultural production, especially in arid region (i.e., Kaidu-kongque watershed). The obtained solutions suggest that useful information regarding various activities and investments could be provided through the foreseen information that is needed to make decisions.

Figure 5 shows that the system benefits under different p-necessity levels through ISFO model under the basic case. The results demonstrate that different p-necessity levels result in varied system benefits, which could reflect expected system benefit preference and risk-averse attitude of decision makers. For example, the system benefit would be diminished from \$ [7.51, 27.64] $\times 10^9$ to \$ [7.45, 27.51] $\times 10^9$, \$ [7.38, 27.38] $\times 10^9$, \$ [7.32, 27.25] $\times 10^9$, \$ [7.25, 27.12] $\times 10^9$, \$ [7.18, 27.02] $\times 10^9$, \$ [7.15, 26.93] $\times 10^9$, \$ [7.13, 26.89] $\times 10^9$ and \$ [7.12, 26.87] $\times 10^9$, with incremental p-necessity levels from 0.70 to 0.75, 0.80, 0.85, 0.90, 0.95, 0.975, 0.99 and 1, respectively. If the decision makers prefer to obtain the maximized expected system benefit with high certainty (i.e., necessity), a higher p-necessity level would be determined, indicating conservative attitude towards the expected system benefit and decreased uncertainty for the imprecise objective. On the contrary, the lower p-necessity level and increased uncertainty for the imprecise objective would correspond to optimistic attitude on the expected system benefit. At the same time, the uncertain system benefits are presented in term of interval values. The lower bounds of solutions indicate an optimistic estimation of decision makers, while upper bounds show a conservative attitude. In summary, the decision variables with p-necessity levels and interval values are beneficial for justifying the decision schemes for associated activities and investments through incorporation of their implicit knowledge, evading the risk of water shortage, environment degradation, and system failure and thereby obtaining maximized system benefits.

4.2. Policy Analysis for Ecological Water Allocation. The study area is threatened by serious water shortages and extremely vulnerable ecological system, while ecological environment plays a significant role in the regional sustainable development. Policy analysis associated with different water resources management based on minimum water requirement for ecological sector is essential to make in-depth analysis. Table 4 presents the solutions of optimized water allocations for ecological sector under various policies and scenarios. The results demonstrate that diverse policies for allocating water resources would yield different water shortages and water-allocation patterns for the ecological sector. For instance, when a minimum amount for ecological water supply is not considered, ecological water supply would first be reduced. The amount of ecological water supply would be zero under Case 2, when stream flows are low and medium in all of the three periods. When the stream flows are high

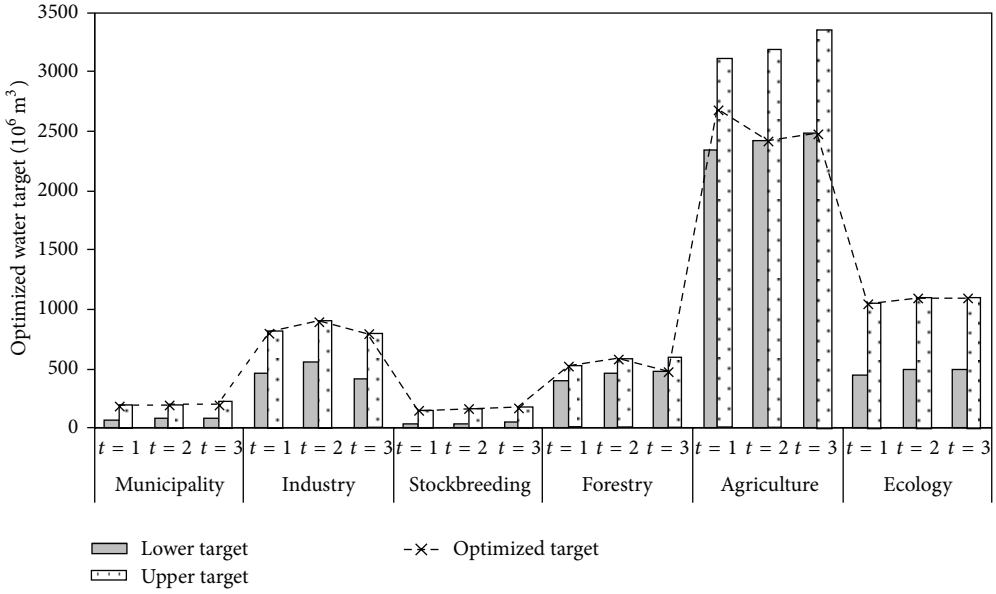

Figure 3: Optimized water-allocation targets for different users.

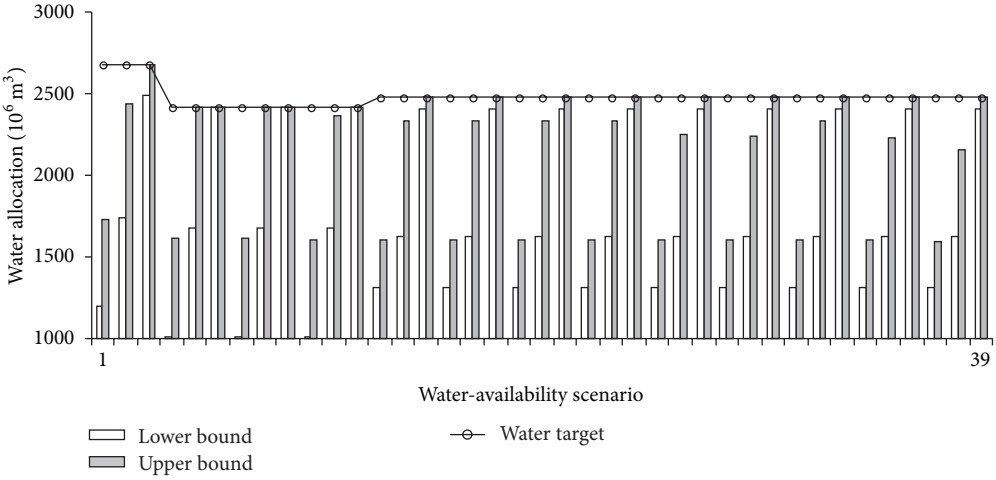

Figure 4: Water-allocation plans for agricultural sector.

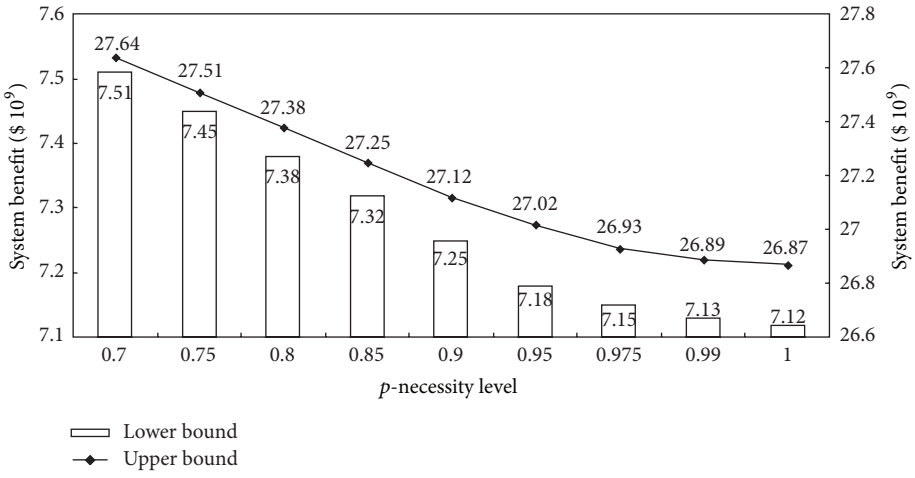

Figure 5: System benefits under different p-necessity levels.

Table 4: Results of ecological water allocation under different policies.

Flow level	Probability (%)	Period	Optimized water allocation (10^6 m^3)	
			Case 1	Case 2
L	30.4	1	105	0
M	45.5	1	[105, 113]	0
H	24.1	1	[105, 1051]	[0, 1051]
LL	11.24	2	114	0
LM	15.26	2	114	0
LH	3.89	2	[378, 1100]	[252, 1100]
ML	16.83	2	114	0
MM	22.84	2	[114, 135]	0
MH	5.82	2	[378, 1100]	[252, 1100]
HL	8.91	2	[114, 120]	0
HM	12.10	2	[114, 205]	0
HH	3.08	2	[378, 1100]	[252, 1100]
LLL	1.96	3	114	0
LLM	5.51	3	114	0
LLH	3.80	3	[114, 1065]	[45, 1065]
LML	2.66	3	114	0
LMM	7.48	3	114	0
LMH	5.13	3	[114, 1065]	[45, 1065]
LHL	0.68	3	114.4	0
LHM	1.91	3	114.4	0
LHH	1.31	3	[114, 1065]	[45, 1065]
MLL	2.93	3	114	0
MLM	8.25	3	114	0
MLH	5.66	3	[114, 1065]	[45, 1065]
MML	3.97	3	[114, 115]	0
MMM	11.19	3	[114, 197]	0
MMH	7.67	3	[114, 1065]	[45, 1065]
MHL	1.01	3	114	0
MHM	2.85	3	[114, 208]	0
MHH	1.96	3	[114, 1082]	[45, 1065]
HLL	1.56	3	114	0
HLM	4.37	3	114	0
HLH	3.00	3	[114, 1065]	[45, 1065]
HML	2.11	3	[114, 119]	0
HMM	5.93	3	[114, 217]	0
HMH	4.06	3	[114, 1085]	[45, 1065]
HHL	0.54	3	[114, 124]	0
HHM	1.51	3	[114, 220]	0
HHH	1.04	3	[114, 1090]	[45, 1065]

The symbols of L, M, and H indicate that the stream flows are low, medium, and high (i.e., LMH denotes that the stream flow are low in period 1, medium in period 2, and high in period 3).

in all of the three periods, the total water-allocation amount to ecological sector under Case 1 and Case 2 would be in the range of [580, 3241] $\times$ 10^6 and [297, 3216] $\times$ 10^6 m^3 over the planning horizon, respectively. In general, under Case 2, the water allocation to ecological sector would first be reduced in case of insufficient water (due to its lowest economic benefit); then, the water shortage would be passed to the agricultural sector. Under Case 1, some water would still be allocated to the ecological sector even under very disadvantageous conditions (i.e., very low inflow). Therefore, water-management policies associated with a minimum ecological water requirement is beneficial for minimizing unfair competition among multiple users and recovering the ecological system in the lower beaches of the river.

At the same time, the solutions of ecological water-allocation policies indicate that owing to benefit and penalty effects on the water-allocation patterns, interactions exist among water supplies for multiple competing users when water deficits occur. The results imply that when a water-management policy associated with a minimum ecological water requirement was undertaken, the amount of agricultural water allocation would be decreased, particularly under low and medium stream flow levels. Figure 6 shows the agricultural water allocations under Case 1 and Case 2. For example, when stream flows are medium in all of the three periods, the water allocation to agricultural sector would be [5053, 7110] $\times$ 10^6 m^3 under Case 1 and [5386, 7555] $\times$ 10^6 m^3 under Case 2, respectively. Besides, the agricultural water-allocation target would be in the range of [7235, 9663] $\times$ 10^6 m^3 over the planning horizon. This indicates that there would be a marked water shortage for agricultural sector when the minimum ecological water requirement was regulated. Moreover, the water-management policy associated with a minimum ecological water requirement would be helpful for altering traditional agricultural irrigation mode, increasing the water efficiency in the agricultural production and achieving optimal allocation of water resources utilization in arid and semiarid regions. For the municipal, industrial and stockbreeding sectors, the allotment would not be reduced. This is attributed to the fact that these users could bring higher benefits when water demands are satisfied and higher penalties when promised targets are not delivered. The municipal and industrial water play significant roles in living standard and economic development.

In addition, various water-management policies would result in different system benefits (when water was allocated to users). The system benefit under Case 2 would be \$ [7.29, 27.24] $\times$ 10^9, which is far larger than the Case 1 (\$ [7.25, 27.12] $\times$ 10^9). This indicates that ecological sector brings the lowest benefit to the region economic development. Decision makers would usually prefer to allocate the water resources to the users which could bring high benefits. However, the study area is facing increasingly serious water shortages, leading to continued vegetation degradation and human-induced soil erosion. The limited water resources should be allocated in more efficient and sustainable ways. Therefore, willingness to accept a low system benefit (and a low violation risk) could guarantee meeting the ecological water requirement, while a strong desire to obtain a high system benefit could lead to a high risk of ecological water shortage, vegetation loss, and environment degradation.

5. Conclusions

In this study, an interval-stochastic fractile optimization (ISFO) model has been proposed for developing optimal water-resources management strategies under multiple

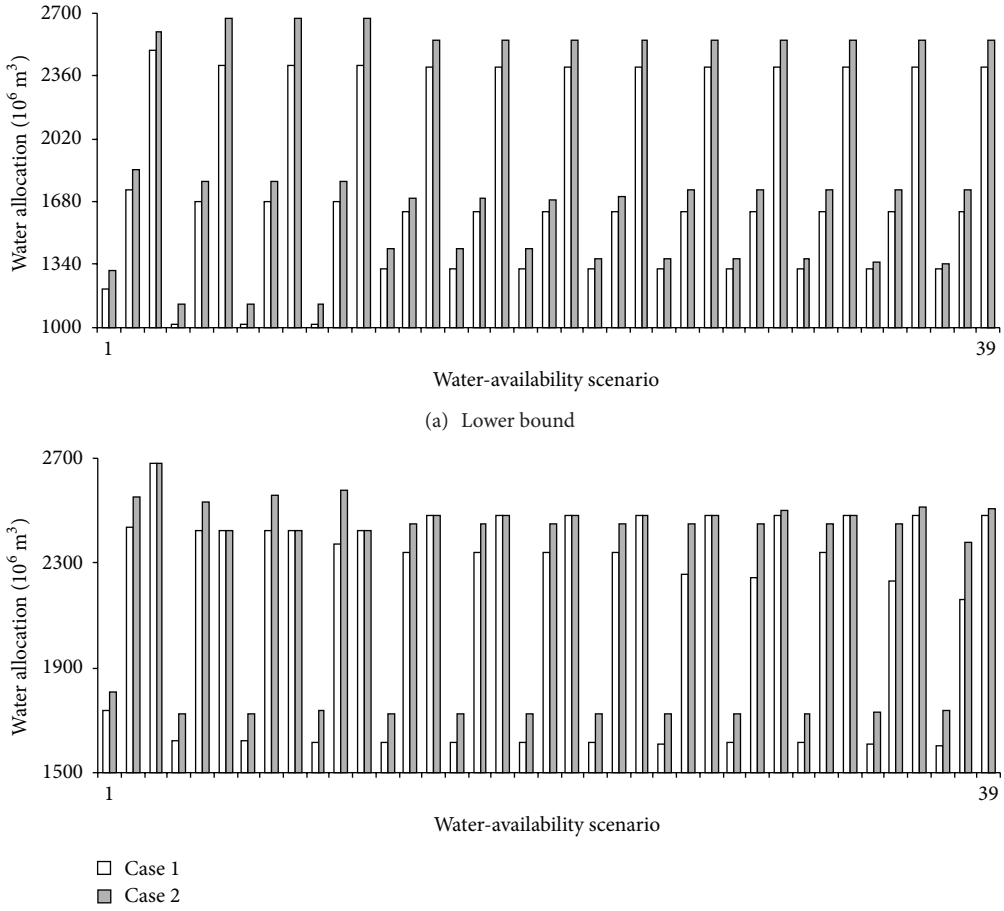

Figure 6: Agricultural water allocation under different policies.

uncertainties. The ISFO model can not only handle uncertainties presented in terms of probability distributions and intervals with possibility distribution boundary but also quantify subjective information (i.e., expected system benefit preference and risk-averse attitude) from different decision makers. It can be utilized for analyzing various policy scenarios associated with different levels of economic consequences when the promised targets are violated. The ISFO model is applied to a real case of water-resources systems planning in Kaidu-kongque watershed, China, and a number of scenarios with different ecological water-allocation policies under varied p-necessity fractiles are analyzed. Results indicate that different policies for ecological water allocation can lead to varied water supplies, economic penalties, and system benefits. The solutions obtained can help decision makers identify optimized water-allocation alternatives, alleviate the water supply-demand conflict, and achieve socioeconomic and ecological sustainability, particularly when limited water resources are available for multiple competing users.

The study is the first attempt to propose an ISFO model and apply it to water-resources systems planning in Kaidu-kongque watershed. Nevertheless, there are still several factors that need to be further considered in future research. Firstly, economic parameters are presented by fuzzy triangular numbers with possibility distribution. More sophisticated solution methods should be proposed to tackle imprecise parameters with nonlinear possibility distribution. Secondly, the dynamic system variations (i.e., nonsequential interactions) are reflected under a multistage context. Advanced methods would be desired to permit revised decisions in each stage based on sequentially realizations for uncertain events. Thirdly, the ISFO model is a single objective model subjected to a set of constraint. Multiobjective programming method should be considered for multicriterion decision analysis with multiple objectives. Therefore, future research needs to be conducted into incorporating powerful optimization techniques within the modeling framework to further enhance the capabilities of the ISFO model.

Acknowledgments

This research was supported by the National Natural Science Foundation for Distinguished Young Scholar (51225904), the Open Research Fund Program of State Key Laboratory of Hydroscience and Engineering (sklhse-2012-A-03), the National High-Tech R&D (863) Program (2012AA091103),

and the Program for Innovative Research Team in University (IRT1127). The authors are grateful to the editor and the anonymous reviewers for their insightful and helpful comments and suggestions.

References

[1] C. Bao and C. L. Fang, "Water resources constraint force on urbanization in water deficient regions: a case study of the Hexi Corridor, arid area of NW China," *Ecological Economics*, vol. 62, no. 3-4, pp. 508–517, 2007.

[2] E. Kondili, J. K. Kaldellis, and C. Papapostolou, "A novel systemic approach to water resources optimisation in areas with limited water resources," *Desalination*, vol. 250, no. 1, pp. 297–301, 2010.

[3] Y. Yang, Y. Chen, W. Li, M. Wang, and G. Sun, "Impacts of climatic change on river runoff in Northern Xinjiang of China over last fifty years," *Chinese Geographical Science*, vol. 20, no. 3, pp. 193–201, 2010.

[4] L. Jing and B. Chen, "Field investigation and hydrological modelling of a subarctic wetland-the Deer River watershed," *Journal of Environmental Informatics*, vol. 17, no. 1, pp. 36–45, 2011.

[5] L. Y. Su, P. Christensen, and J. L. Liu, "Comparative study of water resource management and policies for ecosystems in China and Denmark," *Journal of Environmental Informatics*, vol. 21, no. 1, pp. 72–83, 2013.

[6] I. Maqsood, G. H. Huang, and J. S. Yeomans, "An interval-parameter fuzzy two-stage stochastic program for water resources management under uncertainty," *European Journal of Operational Research*, vol. 167, no. 1, pp. 208–225, 2005.

[7] L. N. Sethi, S. N. Panda, and M. K. Nayak, "Optimal crop planning and water resources allocation in a coastal groundwater basin, Orissa, India," *Agricultural Water Management*, vol. 83, no. 3, pp. 209–220, 2006.

[8] M. Bravo and I. Gonzalez, "Applying stochastic goal programming: a case study on water use planning," *European Journal of Operational Research*, vol. 196, no. 3, pp. 1123–1129, 2009.

[9] X. H. Zhang, H. W. Zhang, B. Chen, H. C. Guo, G. Q. Chen, and B. A. Zhao, "An inexact-stochastic dual water supply programming model," *Communications in Nonlinear Science and Numerical Simulation*, vol. 14, no. 1, pp. 301–309, 2009.

[10] Y. P. Li and G. H. Huang, "Fuzzy-stochastic-based violation analysis method for planning water resources management systems with uncertain information," *Information Sciences*, vol. 179, no. 24, pp. 4261–4276, 2009.

[11] S. Galelli and R. Soncini-Sessa, "Combining metamodelling and stochastic dynamic programming for the design of reservoir release policies," *Environmental Modelling & Software*, vol. 25, no. 2, pp. 209–222, 2010.

[12] Y. P. Li, G. H. Huang, and S. L. Nie, "Optimization of regional economic and environmental systems under fuzzy and random uncertainties," *Journal of Environmental Management*, vol. 92, no. 8, pp. 2010–2020, 2011.

[13] Y. P. Li, G. H. Huang, S. L. Nie, and X. Chen, "A robust modeling approach for regional water management under multiple uncertainties," *Agricultural Water Management*, vol. 98, no. 10, pp. 1577–1588, 2011.

[14] A. A. Gaivoronski, G. M. Sechi, and P. Zuddas, "Balancing cost-risk in management optimization of water resource systems under uncertainty," *Physics and Chemistry of the Earth, Parts A/B/C*, vol. 42–44, pp. 98–107, 2012.

[15] D. W. Watkins Jr, D. C. McKinney, L. S. Lasdon, S. S. Nielsen, and Q. W. Martin, "A scenario-based stochastic programming model for water supplies from the highland lakes," *International Transactions in Operational Research*, vol. 7, pp. 211–230, 2000.

[16] K. W. Harrison, "Two-stage decision-making under uncertainty and stochasticity: Bayesian programming," *Advances in Water Resources*, vol. 30, no. 3, pp. 641–664, 2007.

[17] Y. P. Li, G. H. Huang, Y. F. Huang, and H. D. Zhou, "A multistage fuzzy-stochastic programming model for supporting sustainable water-resources allocation and management," *Environmental Modelling & Software*, vol. 24, no. 7, pp. 786–797, 2009.

[18] Y. Xu, G. H. Huang, and T. Y. Xu, "Inexact management modeling for urban water supply systems," *Journal of Environmental Informatics*, vol. 20, no. 1, pp. 34–43, 2012.

[19] M. Housh, A. Ostfeld, and U. Shamir, "Limited multi-stage stochastic programming for managing water supply systems," *Environmental Modelling & Software*, vol. 41, pp. 53–64, 2013.

[20] M. V. F. Pereira and L. M. V. G. Pinto, "Multi-stage stochastic optimization applied to energy planning," *Mathematical Programming*, vol. 52, no. 1–3, pp. 359–375, 1991.

[21] S. Ahmed, A. J. King, and G. Parija, "A multi-stage stochastic integer programming approach for capacity expansion under uncertainty," *Journal of Global Optimization*, vol. 26, no. 1, pp. 3–24, 2003.

[22] J. Dupačová, "Applications of stochastic programming: achievements and questions," *European Journal of Operational Research*, vol. 140, no. 2, pp. 281–290, 2002.

[23] M. Inuiguchi and J. Ramík, "Possibilistic linear programming: a brief review of fuzzy mathematical programming and a comparison with stochastic programming in portfolio selection problem," *Fuzzy Sets and Systems*, vol. 111, no. 1, pp. 3–28, 2000.

[24] M. Inuiguchi and T. Tanino, "Portfolio selection under independent possibilistic information," *Fuzzy Sets and Systems*, vol. 115, no. 1, pp. 83–92, 2000.

[25] N. Arbaiy and J. Watada, "Fractile optimization approach for possibilistic programming problem," in *Proceedings of the International Conference on Man-Machine Systems (ICoMMS '12)*, 2012.

[26] M. Inuiguchi, "Robust optimization by fuzzy linear programming," in *Managing Safety of Heterogeneous Systems*, vol. 658 of *Lecture Notes in Economics and Mathematical Systems*, pp. 219–239, Springer, 2012.

[27] M. Inuiguchi, "Fuzzy programming approaches to robust optimization," in *Proceedings of the 9th international conference on Modeling Decisions for Artificial Intelligence (MDAI '12)*, pp. 11–12, 2012.

[28] H. Katagiri, M. Sakawa, K. Kato, and S. Ohsaki, "An interactive fuzzy satisficing method based on the fractile optimization model using possibility and necessity measures for a fuzzy random multiobjective linear programming problem," *Electronics and Communications in Japan, Part III*, vol. 88, no. 5, pp. 20–28, 2005.

[29] X. Zhang, G. H. Huang, and X. Nie, "Robust stochastic fuzzy possibilistic programming for environmental decision making under uncertainty," *Science of the Total Environment*, vol. 408, no. 2, pp. 192–201, 2009.

[30] G. H. Huang and M. F. Cao, "Analysis of solution methods for interval linear programming," *Journal of Environmental Informatics*, vol. 17, no. 2, pp. 54–64, 2011.

[31] Y. R. Fan and G. H. Huang, "A robust two-step method for solving interval linear programming problems within an

environmental management context," *Journal of Environmental Informatics*, vol. 19, no. 1, pp. 1–9, 2012.

[32] Y. P. Li, G. H. Huang, and S. L. Nie, "Planning water resources management systems using a fuzzy-boundary interval-stochastic programming method," *Advances in Water Resources*, vol. 33, no. 9, pp. 1105–1117, 2010.

[33] Y. Zhou, Y. P. Li, G. H. Huang, and Y. Zhou, "A robust approach for planning electric power systems associated with environmental policy analysis," *Electric Power Systems Research*, vol. 95, pp. 99–111, 2013.

[34] D. Dubois and H. Prade, *Possibility Theory: An Approach to Computerized Processing of Uncertainty*, Plenum Press, New York, NY, USA, 1988.

[35] L. A. Zadeh, "Fuzzy sets as a basis for a theory of possibility," *Fuzzy Sets and Systems*, vol. 1, no. 1, pp. 3–28, 1978.

[36] H. Tanaka, P. Guo, and H. J. Zimmermann, "Possibility distributions of fuzzy decision variables obtained from possibilistic linear programming problems," *Fuzzy Sets and Systems*, vol. 113, no. 2, pp. 323–332, 2000.

[37] S. A. Torabi and E. Hassini, "An interactive possibilistic programming approach for multiple objective supply chain master planning," *Fuzzy Sets and Systems*, vol. 159, no. 2, pp. 193–214, 2008.

[38] Z. F. Liu, G. H. Huang, and N. Li, "A dynamic optimization approach for power generation planning under uncertainty," *Energy Sources, Part A*, vol. 30, no. 14-15, pp. 1413–1431, 2008.

[39] S. A. Torabi and E. Hassini, "An interactive possibilistic programming approach for multiple objective supply chain master planning," *Fuzzy Sets and Systems*, vol. 159, no. 2, pp. 193–214, 2008.

[40] H. L. Xu, M. Ye, and J. M. Li, "Changes in groundwater levels and the response of natural vegetation to transfer of water to the lower reaches of the Tarim River," *Journal of Environmental Sciences*, vol. 19, no. 10, pp. 1199–1207, 2007.

[41] Y. Huang, Y. P. Li, X. Chen, A. M. Bao, and Y. G. Ma, "A multistage simulation-based optimization model for water resources management in Tarim River Basin, China," *Stochastic Environmental Research and Risk Assessment*, vol. 27, no. 1, pp. 147–158, 2013.

[42] Y. P. Li, G. H. Huang, Z. F. Yang, and S. L. Nie, "IFMP: interval-fuzzy multistage programming for water resources management under uncertainty," *Resources, Conservation and Recycling*, vol. 52, no. 5, pp. 800–812, 2008.

[43] Y. P. Li, G. H. Huang, X. H. Nie, and S. L. Nie, "An inexact fuzzy-robust two-stage programming model for managing sulfur dioxide abatement under uncertainty," *Environmental Modeling and Assessment*, vol. 13, no. 1, pp. 77–91, 2008.

[44] Statistical Bureau of Bayangol Mongol Autonomous Prefecture, *Statistical Yearbook of Bayangol*, China Statistic Press, Beijing, China, 2000–2009.

[45] Y. P. Li, G. H. Huang, G. Q. Wang, and Y. F. Huang, "FSWM: a hybrid fuzzy-stochastic water-management model for agricultural sustainability under uncertainty," *Agricultural Water Management*, vol. 96, no. 12, pp. 1807–1818, 2009.

Hindawi Publishing Corporation
Mathematical Problems in Engineering
Volume 2013, Article ID 482095, 15 pages
http://dx.doi.org/10.1155/2013/482095

Research Article

An Inventory-Theory-Based Inexact Multistage Stochastic Programming Model for Water Resources Management

M. Q. Suo,[1] Y. P. Li,[1] G. H. Huang,[1] Y. R. Fan,[2] and Z. Li[2]

[1] *MOE Key Laboratory of Regional Energy Systems Optimization, Sino-Canada Energy and Environmental Research Academy, North China Electric Power University, Zhuxinzhuang, Beijing 102206, China*
[2] *Faculty of Engineering and Applied Science, University of Regina, Regina, SK, Canada S4S 0A2*

Correspondence should be addressed to Y. P. Li; yongping.li@iseis.org

Received 31 December 2012; Accepted 1 March 2013

Academic Editor: Xiaosheng Qin

An inventory-theory-based inexact multistage stochastic programming (IB-IMSP) method is developed for planning water resources systems under uncertainty. The IB-IMSP is based on inexact multistage stochastic programming and inventory theory. The IB-IMSP cannot only effectively handle system uncertainties represented as probability density functions and discrete intervals but also efficiently reflect dynamic features of system conditions under different flow levels within a multistage context. Moreover, it can provide reasonable transferring schemes (i.e., the amount and batch of transferring as well as the corresponding transferring period) associated with various flow scenarios for solving water shortage problems. The applicability of the proposed IB-IMSP is demonstrated by a case study of planning water resources management. The solutions obtained are helpful for decision makers in not only identifying different transferring schemes when the promised water is not met, but also making decisions of water allocation associated with different economic objectives.

1. Introduction

With speedy population growth, the constantly increasing demand for water in terms of both sufficient quantity and satisfied quality has forced a number of researchers to draw optimal water resources management policies [1–5]. However, water resources systems can be complex with uncertainties which may exist in technical, social, environmental, political, and financial factors. In addition, these complexities and uncertainties could be multiplied by not only the dynamic characteristics of the system, but also the related economic deficits if the targeted demand is not met. Furthermore, because of the temporal and spatial variations of the relationships between water demand and supply, the desired schemes for water allocation may also vary dynamically [6]. Correspondingly, insufficient water may be encountered particularly in the case of continuously low flow levels over a long period. Therefore, it is deemed necessary to develop effective optimization methods for supporting water resources management under such complexities.

Previously, numerous methods were developed for planning water resources management systems under various uncertainties [7–12]. Among them, two-stage stochastic programming (TSP) was an effective technique for problems where an analysis of policy scenarios was desired and the related coefficients are random with known probability distributions. The fundamental idea behind TSP is the concept of recourse, which is the ability to take corrective actions after a random event has taken place [13, 14]. In the past decades, TSP was developed and applied in water resources management under uncertainty [15–21]. However, TSP can only take recourse actions at the second stage to correct any infeasibility, and thus, it can hardly reflect the dynamic variations of system conditions, especially for multistage problems with a sequential structure. To address such a dynamic characteristic, a lot of multistage stochastic programming (MSP) methods were proposed as extensions of dynamic stochastic optimization approaches [13, 22–28]. MSP was improved upon the conventional TSP methods by permitting revised decisions in each time stage based on the information of sequentially realized uncertain events [29]. The uncertain information in an MSP was often modeled through a multilayer scenario tree. The primary advantage of

scenario-based stochastic programming was the flexibility it offered in modeling the decision process and defining the scenarios, particularly if the state dimension was high [22]. A few researchers applied the MSP to water resources management under uncertainty [24, 30–32]. For example, Li and Huang [31] developed a fuzzy-stochastic-based violation analysis approach for the planning of water resources management systems with uncertain information, based on a multistage fuzzy-stochastic integer programming model. Zhou et al. [32] developed a factorial multistage stochastic programming approach to obtain the desired water-allocation schemes and maximize the total net benefit under multiple uncertainties. Although the MSP was useful for dealing with probabilistic uncertainties within the optimization framework, its recourse action was to minimize penalties resulted from water shortages, not to provide a useful alternative to solve this problem positively. Actually, in the case of insufficiency, only penalties analysis is not enough, and more efforts are needed to solve the insufficiency corresponding to various penalties. Undoubtedly, transferring water from abundant regions would be a preferred choice for the water shortage problem. In this case, three questions should be answered by the managers: (a) how much is the amount of transferring water associated with different flow levels? (b) How much is the transferring batch corresponding to varied transferring amount each time? (c) How long is the transferring period between every two transferring actions? Fortunately, all these challenges can be well responded by the inventory theory. The aim of the inventory theory is to design schemes for managers to maximize system benefit/minimize system cost as well as guarantee the users' demand for materials.

In the past decades, a number of methods based on inventory theory were developed for solving the problems of materials' supply and demand [33–38]. For instance, Axsäter [39] considered a two-echelon distribution inventory system with a central warehouse and a number of retailers, where the system is controlled by continuous review installation stock policies with given batch quantities; Gupta et al. [40] proposed a discrete-time model for setting clearance prices for clearing retail inventories of fashion goods, where a heuristic procedure was developed to find near-optimal prices; Yadavalli et al. [41] considered a continuous review inventory system at a service facility, wherein an item demanded by a customer was issued to him/her only after performing service of random duration on the item; Arnold et al. [42] developed a deterministic optimal control approach optimizing the procurement and inventory policy of an enterprise that is processing a raw material when the purchasing price, holding cost, and the demand rate are fluctuating over time; Schmitt et al. [43] modeled a retailer whose supplier was subject to complete supply disruptions, where discrete event uncertainty and continuous sources of uncertainty were combined. Tsao and Lu [44] addressed an integrated facility location and inventory allocation problem through considering two types of transportation cost discounts: quantity discounts for inbound transportation cost and distance discounts for outbound transportation cost. However, most of the past inventory models were rarely developed and applied in water resources management. Although Suo et al. [21] proposed an inventory-theory-based two-stage stochastic programming model for solving water shortage problem, this model did not consider the dynamic variations of system conditions, particularly for sequential influences of different flow levels among multiple stages. In addition, multiple uncertainties existed in water resources management systems, such as the continuously changed water availabilities, various targeted water demand associated with timely policy scenarios, and fluctuant water benefit as well as related transferring cost. The conventional inexact optimization methods had difficulties in tackling such complexities.

Therefore, as an extension of the previous efforts, an inventory-theory-based inexact multistage stochastic programming model (IB-IMSP) will be developed for supporting water resources management planning. The IB-IMSP is an integrated method of inventory theory, inexact optimization, and multistage stochastic programming. It can tackle uncertainties represented as not only probability density functions but also discrete intervals as well as identify the system dynamics and decision processes under a series of scenarios. In addition, water transferring is exercised with recourse against any infeasibility, which allows exhaustive analyses of different policy scenarios with respect to varied levels of economic consequences if the targeted water allocations are infringed. Correspondingly, reasonable transferring schemes (the transferring amount, batch, and the corresponding transferring period) associated with various flow scenarios would be provided for decision makers for solving water shortage problem. A hypothetical case study of water resources management will then be provided to validate the applicability of the developed approach. The results obtained can help the managers gain insight into the water resources management with maximizing economic objectives and satisfying targeted water demands from users.

2. Methodology

2.1. Inexact Multistage Linear Programming. In many real-world problems, uncertainties can be denoted as random variables, and the related study systems are of dynamic feature. Thus, the relevant decisions must be made at each time stage under varying probability levels. Such a problem can be formulated as a scenario-based multistage stochastic programming (MSP) model with recourse as follows:

$$\max \quad f = \sum_{t=1}^{T} U_t X_t - \sum_{t=1}^{T} \sum_{h=1}^{h_t} p_{th} K_{th} Y_{th} \tag{1a}$$

$$\text{s.t.} \quad A_{rt} X_t \le B_{rt}, \quad r = 1, 2, \ldots, m_1;\ t = 1, 2, \ldots, T, \tag{1b}$$

$$A_{it} X_t + A'_{ith} Y_{th} \ge w_{ith}, \quad i = 1, 2, \ldots, m_2; \quad t = 1, 2, \ldots, T;\ h = 1, 2, \ldots, h_t, \tag{1c}$$

$$x_{jt} \ge 0, x_{jt} \in X_t, \quad j = 1, 2, \ldots, n_1;\ t = 1, 2, \ldots, T, \tag{1d}$$

$$y_{jth} \ge 0, y_{jth} \in Y_{th}, \quad j = 1, 2, \ldots, n_1; \quad t = 1, 2, \ldots, T;\ h = 1, 2, \ldots, h_t, \tag{1e}$$

where p_{th} is the probability of occurrence for scenario h in period t, with $p_{th} \geq 0$ and $\sum_{h=1}^{h_t} p_{th} = 1$. K_{th} are coefficients of recourse variables (Y_{th}) in the objective function; A'_{ith} are coefficients of Y_{th} in constraint i; w_{ith} is the random variable of constraint i, which is associated with probability levels q_{th}; h_t is the number of scenarios in period t, with the total being $H = \sum_{t=1}^{T} h_t$. In model (1a)–(1e), the decision variables are divided into two subsets: those that must be determined before the realizations of random variables are known (i.e., x_{jt}), and those (recourse variables) that can be determined after the realized random-variable values are available (i.e., y_{jth}).

Obviously, model (1a)–(1e) can only deal with uncertainties in the right-hand sides expressed as PDFs (probability density functions) when coefficients in A and U are deterministic. However, in real-world problems, the quality of information that can be obtained is often not good enough to be expressed as probabilistic distributions; in addition, even though these distributions are available, reflection of them in large-scale MSP models could be extremely challenging [45]. Correspondingly, interval parameters can be introduced into the multistage programming framework to identify uncertainties in parameters. This leads to an integrated inexact MSP (IMSP) model as follows:

$$\text{Max} \quad f^{\pm} = \sum_{t=1}^{T} U_t^{\pm} X_t^{\pm} - \sum_{t=1}^{T} \sum_{h=1}^{h_t} p_{th} K_{th}^{\pm} Y_{th}^{\pm} \tag{2a}$$

$$\text{s.t.} \quad A_{rt}^{\pm} X_t^{\pm} \leq B_{rt}^{\pm}, \quad r = 1, 2, \ldots, m_1; \quad t = 1, 2, \ldots, T, \tag{2b}$$

$$A_{it}^{\pm} X_t^{\pm} + A_{ith}^{\pm\prime} Y_{th}^{\pm} \geq w_{ith}^{\pm}, \quad i = 1, 2, \ldots, m_2; \quad t = 1, 2, \ldots, T; \; h = 1, 2, \ldots, h_t, \tag{2c}$$

$$x_{jt}^{\pm} \geq 0, \; x_{jt}^{\pm} \in X_t^{\pm}, \quad j = 1, 2, \ldots, n_1; \; t = 1, 2, \ldots, T, \tag{2d}$$

$$y_{jth}^{\pm} \geq 0, \; y_{jth}^{\pm} \in Y_{th}^{\pm}, \quad j = 1, 2, \ldots, n_1; \quad t = 1, 2, \ldots, T; \; h = 1, 2, \ldots, h_t, \tag{2e}$$

where $U_t^{\pm}$, $X_t^{\pm}$, $K_{th}^{\pm}$, $Y_{th}^{\pm}$, $A_{rt}^{\pm}$, $B_{rt}^{\pm}$, $A_{it}^{\pm}$, $A_{ith}^{\pm\prime}$, and $w_{ith}^{\pm}$ are interval parameters/variables. An interval is defined as a number with known upper and lower bounds but unknown distribution information [46]. Let U_t^- and U_t^+ be the lower and upper bounds of $U_t^{\pm}$, respectively. When $U_t^- = U_t^+$, $U_t^{\pm}$ becomes a deterministic number.

However, in water resources management system, with the shortage of water availability, water transferring from other abundant regions is considered as an adaptive measure to meet the water demands in arid regions. In this case, it is noticed that the reservoir storage capacity, available water transferring, and the related costs happened in the transferring process (e.g., communication cost, unit cost, and reservoir's protection cost) should be considered. In addition, transferring too much water cannot only make the cost of reservoir operation, insurance, and protection increase, but also can bring on a high risk for the reservoir's storage capacity; transferring too little water is not enough to satisfy the water demand, and can increase the transferring times. Hence, reasonable transferring batch size and period are needed to optimize the transferring process, which is actually an inventory problem. Therefore, it is necessary to introduce inventory theory into the water resources management system [21].

2.2. Inventory-Theory-Based Inexact Multistage Stochastic Programming. The aim of inventory theory is to ascertain rules that managers can use to minimize the cost (maximize the benefit) associated with balancing the materials' supply and demand for different users. Supposing that one material should be purchased or produced and its shortage is not allowed, the demand is D units per unit time. The relative costs include S (setup cost for ordering one batch ($)), C (unit cost for purchasing or producing each unit ($/unit)), and C_1 (holding cost per unit per unit of time held in inventory ($/month)). In detail, setup cost means all the costs for ordering one batch to replenish the storage, including the handling charge, communication expenses, and travelling expenses encountered in the ordering process; unit cost is the purchase or produce cost for one unit; holding cost represents all the costs associated with the storage of the inventory until it is used, including the cost of capital tied up, space, insurance, protection, and taxes attributed to storage. The objective is to determine when and how much to replenish inventory in order to minimize the sum of the produce or purchase costs per unit time [21]. Correspondingly, a basic EOQ model can be formulated as follows:

$$f(Q) = \frac{C_1 Q}{2} + \frac{SD}{Q} + CD, \tag{3a}$$

where Q is the purchasing or producing batch in the period of t; $C_1Q/2$ is the holding cost per period; SD/Q is the ordering cost per period; CD is the purchase or produce cost per period; $f(Q)$ is the total cost, which is a function of Q. By setting the first derivative of $f(Q)$ to zero (and noting that the second derivative is positive), the economic order quantity (batch) can be obtained as follows:

$$Q^* = \sqrt{\frac{2SD}{C_1}}. \tag{3b}$$

Accordingly, the purchasing or producing period $t$can be obtained by the following equation:

$$t = \frac{Q}{D}. \tag{3c}$$

In this case, the total cost $f(Q)$ would reach its minimum value. Model (3a)–(3c) is the actual economic order quantity (EOQ) model, which can effectively tackle the complexities of inventory theory issues associated with purchasing or producing batch and period. Actually, the similar inventory problems exist in water resources management system. For

example, the excessive transferring water could bring on risks for reservoir capacity and water waste. Too short a transferring period could increase the transferring cost and bring on inconvenience in management; too long a transferring period may not meet the water demand, and both of these could cause economic losses. Consequently, a comprehensive method including both the advantages of EOQ model and IMSP model is needed, which leads to an inventory-theory-based inexact multistage stochastic programming (IB-IMSP) model. Concretely, IB-IMSP can be formulated as follows:

$$\text{Max} \quad f^{\pm} = \sum_{t=1}^{T} U_t^{\pm} X_t^{\pm} - \sum_{t=1}^{T}\sum_{h=1}^{h_t} p_{th}\left(\frac{1}{2}C_{1t}^{\pm}Q_{th}^{\pm} + C_t^{\pm}D_{th}^{\pm} + \frac{S_t^{\pm}D_{th}^{\pm}}{Q_{th}^{\pm}}\right) \tag{4a}$$

$$\text{s.t.} \quad A_{rt}^{\pm}X_t^{\pm} \le B_{rt}^{\pm}, \quad r = 1,2,\ldots,m_1; \; t = 1,2,\ldots,T, \tag{4b}$$

$$A_{it}^{\pm}X_t^{\pm} + \left(A'_{ith}\right)^{\pm}D_{th}^{\pm} \ge w_{ith}^{\pm}, \quad i = 1,2,\ldots,m_2; \; t = 1,2,\ldots,T; \; h = 1,2,\ldots,h_t, \tag{4c}$$

$$x_{jt}^{\pm} \ge 0, \; x_{jt}^{\pm} \in X_t^{\pm}, \quad j = 1,2,\ldots,n_1; \; t = 1,2,\ldots,T, \tag{4d}$$

$$D_{th}^{\pm}, \quad t = 1,2,\ldots,T; \; h = 1,2,\ldots,h_t. \tag{4e}$$

According to (3b), the batch size can be replaced by a function of D. Therefore, model (4a)–(4e) can be transferred as follows:

$$\text{Max} \quad f^{\pm} = \sum_{t=1}^{T} U_t^{\pm} X_t^{\pm} - \sum_{t=1}^{T}\sum_{h=1}^{h_t} p_{th}\left(\frac{1}{2}C_{1t}^{\pm}\sqrt{\frac{2S_t^{\pm}D_{th}^{\pm}}{C_{1t}^{\pm}}} + C_t^{\pm}D_{th}^{\pm} + \sqrt{\frac{S_t^{\pm}D_{th}^{\pm}C_{1t}^{\pm}}{2}}\right) \tag{5a}$$

$$\text{s.t.} \quad A_{rt}^{\pm}X_t^{\pm} \le B_{rt}^{\pm}, \quad r = 1,2,\ldots,m_1; \; t = 1,2,\ldots,T, \tag{5b}$$

$$A_{it}^{\pm}X_t^{\pm} + \left(A'_{ith}\right)^{\pm}D_{th}^{\pm} \ge w_{ith}^{\pm}, \quad i = 1,2,\ldots,m_2; \; t = 1,2,\ldots,T; \; h = 1,2,\ldots,h_t, \tag{5c}$$

$$x_{jt}^{\pm} \ge 0, \; x_{jt}^{\pm} \in X_t^{\pm}, \quad j = 1,2,\ldots,n_1; \; t = 1,2,\ldots,T, \tag{5d}$$

$$D_{th}^{\pm}, \quad t = 1,2,\ldots,T; \; h = 1,2,\ldots,h_t, \tag{5e}$$

$$Q_{th}^{\pm} = \sqrt{\frac{2S_t^{\pm}D_{th}^{\pm}}{C_{1t}^{\pm}}}. \tag{5f}$$

In (5a), let $f^{\pm} = f_1^{\pm} - f_2^{\pm}$, in which $f_1^{\pm} = \sum_{t=1}^{T} U_t^{\pm}X_t^{\pm}$, and $f_2^{\pm} = \sum_{t=}^{T}\sum_{h=1}^{h_t} p_{th}(1/2C_{1t}^{\pm}\sqrt{2S_t^{\pm}D_{th}^{\pm}/C_{1t}^{\pm}} + C_t^{\pm}D_{th}^{\pm} + \sqrt{S_t^{\pm}D_{th}^{\pm}C_{1t}^{\pm}/2})$. Since $C_{1t}^{\pm}$, $S_t^{\pm}$, and $C_t^{\pm}$ are parameters about different costs and $D_{th}^{\pm}$ is variable about transferring water, all of them would be greater than zero. In addition, p_{th} is probability, and thus, it can be easily obtained that $f_2^{\pm} \ge 0$ and $f_2^{\pm}$ is an increasing function of $C_{1t}^{\pm}$, $S_t^{\pm}$, $C_t^{\pm}$, and $D_{th}^{\pm}$. In this case, $|f_2|^{-}\text{Sign}(f_2^{-}) = f_2^{-}$ and $|f_2|^{+}\text{Sign}(f_2^{+}) = f_2^{+}$. Accordingly, model (5a)–(5f) can be converted into two deterministic submodels based on a two-step interactive algorithm [47]. The submodel for f^{+} can be formulated in the first step when the system objective is to be maximized; the other submodel (corresponding to f^{-}) can then be formulated based on the solution of the first submodel. Therefore, the first submodel is

$$\text{Max} \quad f^{+} = \sum_{t=1}^{T}\left(\sum_{j=1}^{j_1} u_{jt}^{+}x_{jt}^{+} + \sum_{j=j_1+1}^{n_1} u_{jt}^{+}x_{jt}^{-}\right) - \sum_{t=1}^{T}\sum_{h=1}^{h_t} p_{th}\left(\frac{1}{2}C_{1t}^{-}\sqrt{\frac{2S_t^{-}D_{th}^{-}}{C_{1t}^{-}}} + C_t^{-}D_{th}^{-} + \sqrt{\frac{S_t^{-}D_{th}^{-}C_{1t}^{-}}{2}}\right) \tag{6a}$$

$$\text{s.t.} \quad \sum_{j=1}^{j_1}\left|a_{rjt}\right|^{-}\text{sign}\left(a_{rjt}^{-}\right)x_{jt}^{+} + \sum_{j=j_1+1}^{n_1}\left|a_{rjt}\right|^{+}\text{sign}\left(a_{rjt}^{+}\right)x_{jt}^{-} \le B_{rt}^{+}, \quad r = 1,2,\ldots,m_1; \; t = 1,2,\ldots,T, \tag{6b}$$

$$\sum_{j=1}^{j_1}\left|a_{ijt}\right|^{-}\text{sign}\left(a_{ijt}^{-}\right)x_{jt}^{+} + \sum_{j=j_1+1}^{n_1}\left|a_{ijt}\right|^{+}\text{sign}\left(a_{ijt}^{+}\right)x_{jt}^{-} + \left|A'_{ith}\right|^{+}\text{sign}\left(A'^{+}_{ith}\right)D_{th}^{-} \ge w_{ith}^{-}, \quad i = 1,2,\ldots,m_2; \; t = 1,2,\ldots,T; \; h = 1,2,\ldots,h_t, \tag{6c}$$

$$x_{jt}^{+} \ge 0, \quad j = 1,2,\ldots,j_1; \; t = 1,2,\ldots,T, \tag{6d}$$

$$x_{jt}^{-} \ge 0, \quad j = j_1+1, j_1+2,\ldots,n_1; \; t = 1,2,\ldots,T, \tag{6e}$$

$$D_{th}^{-}, \quad t = 1,2,\ldots,T; \; h = 1,2,\ldots,h_t, \tag{6f}$$

$$Q_{th}^{-} = \sqrt{\frac{2S_t^{-}D_{th}^{-}}{C_{1t}^{-}}}, \tag{6g}$$

where $x_{jt}^{\pm}$ $(j = 1,2,\ldots,j_1)$ are interval variables with positive coefficients in the objective function; $x_{jt}^{\pm}$ $(j = j_1+1, j_1+2,\ldots,n_1)$ are interval variables with negative coefficients. Solutions of $x_{jt\,\text{opt}}^{+}$ $(j = 1,2,\ldots,j_1)$, $x_{jt\,\text{opt}}^{-}$ $(j = j_1+1, j_1+$

$2, \ldots, n_1)$, $D^-_{th\,\mathrm{opt}}$, and $Q^-_{th\,\mathrm{opt}}$ can be obtained from submodel (6a)–(6g). Based on the above solutions, the second submodel for f^- can be formulated as follows:

$$\begin{aligned}\text{Max} \quad f^- = &\sum_{t=1}^{T}\left(\sum_{j=1}^{j_1} u^-_{jt}x^-_{jt} + \sum_{j=j_1+1}^{n_1} u^-_{jt}x^+_{jt}\right) \\ &- \sum_{t=1}^{T}\sum_{h=1}^{h_t} p_{th}\left(\frac{1}{2}C^+_{1t}\sqrt{\frac{2S^+_t D^+_{th}}{C^+_{1t}}}\right. \\ &\left. + C^+_t D^+_{th} + \sqrt{\frac{S^+_t D^+_{th} C^+_{1t}}{2}}\right) \end{aligned} \tag{7a}$$

$$\begin{aligned}\text{s.t.} \quad &\sum_{j=1}^{j_1}\left|a_{rjt}\right|^+ \operatorname{sign}\left(a^+_{rjt}\right)x^-_{jt} \\ &+ \sum_{j=j_1+1}^{n_1}\left|a_{rjt}\right|^- \operatorname{sign}\left(a^-_{rjt}\right)x^+_{jt} \le B^-_{rt}, \\ &r = 1, 2, \ldots, m_1;\ t = 1, 2, \ldots, T, \end{aligned} \tag{7b}$$

$$\begin{aligned}&\sum_{j=1}^{j_1}\left|a_{ijt}\right|^+ \operatorname{sign}\left(a^+_{ijt}\right)x^-_{jt} + \sum_{j=j_1+1}^{n_1}\left|a_{ijt}\right|^- \operatorname{sign}\left(a^-_{ijt}\right)x^+_{jt} \\ &+ \left|A'_{ith}\right|^- \operatorname{sign}\left(A'^-_{ith}\right)D^+_{th} \ge w^+_{ith}, \\ &i = 1, 2, \ldots, m_2;\ t = 1, 2, \ldots, T;\ h = 1, 2, \ldots, h_t, \end{aligned} \tag{7c}$$

$$0 \le x^-_{jt} \le x^+_{jt\,\mathrm{opt}}, \quad j = 1, 2, \ldots, j_1;\ t = 1, 2, \ldots, T, \tag{7d}$$

$$x^+_{jt} \ge x^-_{jt\,\mathrm{opt}}, j = j_1 + 1, j_1 + 2, \ldots, n_1;\ t = 1, 2, \ldots, T, \tag{7e}$$

$$D^-_{th} \le D^+_{th\,\mathrm{opt}}, \quad t = 1, 2, \ldots, T;\ h = 1, 2, \ldots, h_t, \tag{7f}$$

$$Q^+_{th} = \sqrt{\frac{2S^+_t D^+_{th}}{C^+_{1t}}}. \tag{7g}$$

Solutions of $x^-_{jt\,\mathrm{opt}}$ $(j = 1, 2, \ldots, j_1)$, $x^+_{jt\,\mathrm{opt}}$ $(j = j_1 + 1, j_1 + 2, \ldots, n_1)$, $D^+_{th\,\mathrm{opt}}$, and $Q^+_{th\,\mathrm{opt}}$ can be obtained by solving submodel (7a)–(7g). Then, the expected objective function value can be calculated as follows:

$$\begin{aligned}f^+_{\mathrm{opt}} = &\sum_{t=1}^{T}\left(\sum_{j=1}^{j_1} u^+_{jt}x^+_{jt} + \sum_{j=j_1+1}^{n_1} u^+_{jt}x^-_{jt}\right) \\ &- \sum_{t=1}^{T}\sum_{h=1}^{h_t} p_{th}\left(\frac{1}{2}C^-_{1t}\sqrt{\frac{2S^-_t D^-_{th}}{C^-_{1t}}}\right. \\ &\left. + C^-_t D^-_{th} + \sqrt{\frac{S^-_t D^-_{th} C^-_{1t}}{2}}\right), \end{aligned} \tag{8a}$$

$$\begin{aligned}f^-_{\mathrm{opt}} = &\sum_{t=1}^{T}\left(\sum_{j=1}^{j_1} u^-_{jt}x^-_{jt} + \sum_{j=j_1+1}^{n_1} u^-_{jt}x^+_{jt}\right) \\ &- \sum_{t=1}^{T}\sum_{h=1}^{h_t} p_{th}\left(\frac{1}{2}C^+_{1t}\sqrt{\frac{2S^+_t D^+_{th}}{C^+_{1t}}}\right. \\ &\left. + C^+_t D^+_{th} + \sqrt{\frac{S^+_t D^+_{th} C^+_{1t}}{2}}\right). \end{aligned} \tag{8b}$$

Consequently, through combining solutions of submodels (6a)–(6g) and (7a)–(7g), the solution for IB-IMSP model can be obtained as follows:

$$x^\pm_{jt\,\mathrm{opt}} = \left[x^-_{jt\,\mathrm{opt}}, x^+_{jt\,\mathrm{opt}}\right], \quad \forall j, t, \tag{8c}$$

$$D^\pm_{th\,\mathrm{opt}} = \left[D^-_{th\,\mathrm{opt}}, D^+_{th\,\mathrm{opt}}\right], \quad \forall t, h = 1, 2, \ldots, h_t, \tag{8d}$$

$$Q^\pm_{th\,\mathrm{opt}} = \left[Q^-_{th\,\mathrm{opt}}, Q^+_{th\,\mathrm{opt}}\right], \quad \forall t, h = 1, 2, \ldots, h_t, \tag{8e}$$

$$f^\pm_{\mathrm{opt}} = \left[f^-_{\mathrm{opt}}, f^+_{\mathrm{opt}}\right]. \tag{8f}$$

Figure 1 shows the framework of the IB-IMSP model, which is based on EOQ and IMSP techniques. The introduction of EOQ model makes the IB-IMSP can provide the transferring batch size and period, avoiding unnecessary waste of capital and time as well as solving water shortage problem. The application of IMSP enhances the IB-IMSP's capacities in handling the uncertainties and dynamic complexities. For example, the proposed IB-IMSP can tackle uncertainties expressed as random variables, interval parameters as well as their combinations. In addition, the IB-IMSP can identify dynamics of not only the uncertainties but also the related decisions. Therefore, the method can be used for generating decision alternatives and help decision makers to identify desired policies under different flow levels, and analyze all possible policy scenarios that are associated with different transferring schemes.

3. Application

The following water resources management problem will be used to demonstrate the applicability of the proposed IB-IMSP model. A manager is responsible for delivering water from an unregulated reservoir during three planning periods (with each one being five years) to three users: a municipality, an industrial concern, and an agricultural sector. All users want to know how much water they can expect over the three periods. If the promised water is delivered, a net benefit to the local economy will be generated for each unit of water allocated. However, if the promised water is not delivered, they will try to transfer water from other abundant water sources to ensure the local normal life and economic growth. Correspondingly, transferring water will be decided based on the available water resources and target demands from the three users. In addition, although transferring water can solve the water shortage problem, it will result in a reduced net system benefit from three main aspects: setup cost, unit cost,

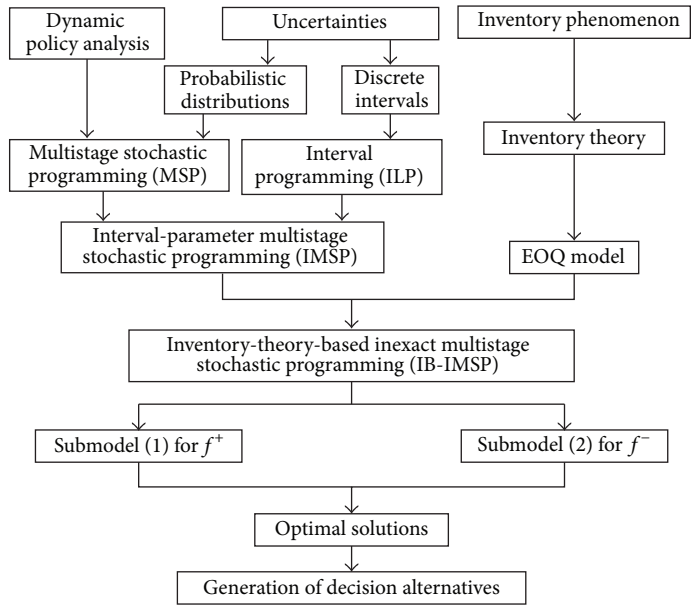

Figure 1: Framework of the IB-IMSP model.

Table 1: Stream flows in the three periods (supply).

Stream flow level	Probability	Stream flow (10^6 m^3)		
		$t = 1$	$t = 2$	$t = 3$
Low (L)	0.2	[4.2, 5.8]	[4.7, 6.5]	[4.3, 5.9]
Medium (M)	0.6	[8.0, 9.6]	[7.9, 8.9]	[8.3, 9.2]
High (H)	0.2	[12.3, 13.6]	[11.8, 13.9]	[12.6, 13.4]

Table 2: Water allocation targets for users.

	Time period		
	$t = 1$	$t = 2$	$t = 3$
Water allocation target (10^6 m^3):			
$W_{1t}^{\pm}$ (to municipal)	[4.1, 5.1]	[5.5, 6.4]	[6.4, 7.5]
$W_{2t}^{\pm}$ (to industrial)	6.2	[7.2, 8.3]	[7.8, 8.9]
$W_{3t}^{\pm}$ (to agricultural)	7.8	9.1	[8.7, 9.1]
Maximum allowable allocation (10^6 m^3):			
$W_{1t\ \max}^{\pm}$ (to municipal)	[4.1, 4.5]	[5.4, 6.0]	[5.4, 6.1]
$W_{2t\ \max}^{\pm}$ (to industrial)	[5.1, 5.5]	[6.8, 7.4]	[7.2, 9.4]
$W_{3t\ \max}^{\pm}$ (to agricultural)	[6.5, 8.3]	[7.0, 8.1]	[7.3, 8.1]

Table 3: Related economic data.

	Time period		
	$t = 1$	$t = 2$	$t = 3$
Net benefit when water demand is satisfied, $NB_{it}^{\pm}$ ($/m^3):			
Municipal ($i = 1$)	[90, 110]	[95, 115]	[100, 120]
Industrial ($i = 2$)	[45, 55]	[55, 70]	[65, 85]
Agricultural ($i = 3$)	[30, 35]	[35, 50]	[35, 50]
Costs when water is transferred:			
$C_{1t}^{\pm}$ (holding cost, $/m^3)	[18.0, 22.0]	[19.0, 23.0]	[20.0, 25.0]
$C_t^{\pm}$ (unit cost, $/m^3)	[1.2, 1.6]	[2.3, 3.0]	[3.4, 4.0]
$S_t^{\pm}$ (setup cost, $)	[6.5, 8.0]	[7.0, 9.0]	[7.5, 9.0]

and holding cost for water transferring. Tables 1 and 2 denote the available water resources from the local region and target demands. Table 3 provides the associated economic data. The objective is to maximize the expected value of the net benefits over the planning horizon.

Under this condition, random variables (available water supply) with probability p_{th} to construct three scenario trees for the planning horizon with a branching structure of 1-3-3-3 can be applied. Therefore, a three-period (four-stage) scenario tree can be generated for each of the three water users. All of the scenario trees have the same structure with one initial node at time 0 and three succeeding ones in period 1; each node in period 1 has three succeeding nodes in period 2, and so on for each node in period 3. These result in 27 nodes in period 3 (and thus 81 scenarios since here are three water users). Figure 2 shows the formulation of the scenario tree.

In this study, the random stream flow under each scenario may be expressed as discrete interval. Moreover, the relevant water allocation plan would be of dynamic feature, where the related decisions must be made at discrete points in time under multiple probability levels. In addition, different transferring water under each probability level will affect the system benefit. For example, if too much water is transferred per unit time, the holding cost will increase; conversely, if too little water is transferred per unit time, the transferring frequency and setup cost will increase. Therefore, to identify these uncertainties and dynamics, as well as solving the water

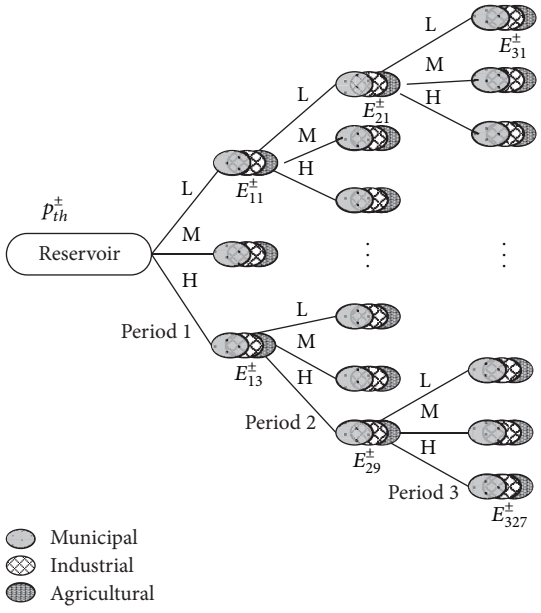

Figure 2: Formulation of scenario tree.

shortage problem, an IB-IMSP model can be formulated as follows:

$$\text{Max} \quad f^{\pm} = \sum_{i=1}^{I}\sum_{t=1}^{T} NB_{it}^{\pm} W_{it}^{\pm} - \sum_{t=1}^{T}\sum_{h=1}^{h_t} p_{th}\left(\frac{1}{2}C_{1t}^{\pm}\sqrt{\frac{2S_t^{\pm}D_{th}^{+}}{C_{1t}^{\pm}}} + C_t^{\pm}D_{th}^{\pm} + \sqrt{\frac{S_t^{\pm}D_{th}^{\pm}C_{1t}^{\pm}}{2}}\right) \tag{9a}$$

Subject to

(constraint of available water flow)

$$\sum_{i=1}^{I} W_{it}^{\pm} \le q_{th}^{\pm} + D_{th}^{\pm} + E_{(t-1)h}^{\pm}, \quad \forall t = 1,2,3;\ h = 1,2,\ldots,h_t \tag{9b}$$

$$q_{th}^{\pm} + D_{th}^{\pm} + E_{(t-1)h}^{\pm} \le \sum_{i=1}^{I} W_{it\,\max}^{\pm}, \quad \forall t = 1,2,3;\ h = 1,2,\ldots,h_t, \tag{9c}$$

(constraint of surplus water)

$$E_{th}^{\pm} = q_{tk}^{\pm} + D_{th}^{\pm} - \sum_{i=1}^{I} W_{it}^{\pm} + E_{(t-1)h}^{\pm},\ E_{0h}^{\pm} = 0, \quad \forall t = 1,2,3;\ h = 1,2,\ldots,h_t, \tag{9d}$$

(constraint of reservoir capacity)

$$q_{th}^{\pm} + E_{(t-1)h}^{\pm} + D_{th}^{\pm} - \sum_{i=1}^{I} W_{it}^{\pm} \le RC^{\pm}, \quad \forall t;\ h = 1,2,\ldots,h_t, \tag{9e}$$

(constraint of transferring water batch)

$$Q_{th}^{\pm} = \sqrt{\frac{2S_t^{\pm}D_{th}^{\pm}}{C_{1t}^{\pm}}}, \tag{9f}$$

(non-negative constraint)

$$D_{th}^{\pm} \ge 0, \quad \forall t;\ h = 1,2,\ldots,h_t, \tag{9g}$$

where

i = water user, $i = 1, 2, 3$,

t = planning time period, $t = 1, 2, 3$,

h = available flow level, $h = 1, 2, \ldots, h_t$,

p_{th} = probability level of available water during period t with $p_{th} > 0$ and $\sum_{h=1}^{h_t} p_{th} = 1$,

$q_{th}^{\pm}$ = random variable of total water availability during period t with probability level of p_{th} (m^3),

$f^{\pm}$ = net system benefit over the planning horizon (\$),

$C_t^{\pm}$ = unit cost for transferring water during period t (\$/m^3),

$C_{1t}^{\pm}$ = holding cost per unit per unit of time held in reservoir (\$/m^3),

$D_{th}^{\pm}$ = transferring water amount from other abundant water sources when the total water-allocation target is not met under the flow of $q_{th}^{\pm}$ (m^3),

$E_{(t-1)h}^{\pm}$ = surplus flow when water is delivered in period $t-1$ (m^3),

$E_{(t-2)h}^{\pm}$ = surplus flow when water is delivered in period $t-2$ (m^3),

$Q_{th}^{\pm}$ = transferring water batch when the flow is $q_{th}^{\pm}$ (m^3),

$S_t^{\pm}$ = setup cost for transferring one batch (\$),

$\mathrm{NB}_{it}^{\pm}$ = net benefit (i.e. revenue minus expense) to user i per unit of water allocated during period t (\$/m^3),

$RC^{\pm}$ = storage capacity of the reservoir (m^3),

$W_{it}^{\pm}$ = fixed allocation target for water that is promised to user i during period t (m^3),

$W_{it\,\max}^{\pm}$= maximum amount that should be allocated to user i during period t (m^3).

In model (9a)–(9g), $D_{th}^{\pm}$ are decision variables, which are affected by local flow levels. Random variables (available water supplies) under different probability levels (p_{th}) are used to construct the scenario tree. Correspondingly, the IB-IMSP model can identify nonanticipativity of the water

Table 4: Solution of the IB-IMSP model (period 1).

Water flow level	Probability	Optimized transferring water (10^6 m^3)	Optimized transferring batch (10^3 m^3)	Optimized transferring period (hour)
L	0.2	[13.30, 13.90]	[3.10, 3.18]	[9.88, 10.06]
M	0.6	[9.50, 10.10]	[2.62, 2.71]	[11.59, 11.91]
H	0.2	[5.50, 5.80]	[1.99, 2.05]	[15.30, 15.65]

Table 5: Solution of the IB-IMSP model (period 2).

Water flow level	Probability	Joint flow	Optimized transferring water (10^6 m^3)	Optimized transferring batch (10^3 m^3)	Optimized transferring period (hour)
L	0.04	L-L	[11.50, 12.90]	[2.91, 3.18]	[10.64, 10.94]
L	0.12	L-M	[9.10, 9.70]	[2.59, 2.76]	[12.27, 12.29]
L	0.04	L-H	[4.10, 5.80]	[1.74, 2.13]	[15.87, 18.31]
M	0.12	M-L	[7.70, 9.10]	[2.38, 2.67]	[12.67, 13.36]
M	0.36	M-M	[5.30, 5.90]	[1.98, 2.15]	[15.73, 16.11]
M	0.12	M-H	[0.30, 2.00]	[0.47, 1.25]	[27.02, 67.70]
H	0.04	H-L	[3.70, 4.80]	[[1.65, 1.94]	[17.44, 19.28]
H	0.12	H-M	[1.30, 1.60]	[0.98, 1.12]	[30.21, 32.52]
H	0.04	H-H	0	0	0

resources management system, where a decision must be made in each stage without the knowledge of the realizations of random variables in the future stages. Based on the method depicted in Section 2, the IB-IMSP model can be converted into two deterministic submodels. Interval solutions can then be obtained by solving the two submodels sequentially. The specific solution process can be summarized as follows.

Step 1. Formulate IB-IMSP model (9a)–(9g).

Step 2. Transform model (9a)–(9g) into two submodels, where the upper bound (f^+) is first solved because the objective is to maximize $f^\pm$.

Step 3. Solve the f^+ submodel and obtain solutions of $D^-_{th\,\mathrm{opt}}$, $Q^-_{th\,\mathrm{opt}}$, and f^+_{opt}.

Step 4. Formulate the objective function and relevant constraints of the f^- submodel.

Step 5. Solve the f^- submodel and obtain solutions of $D^+_{th\,\mathrm{opt}}$, $Q^+_{th\,\mathrm{opt}}$, and f^-_{opt}.

Step 6. Make the second programming using ILP based on the solution of $D^\pm_{th\,\mathrm{opt}}$, and obtain the actual allocation $W^\pm_{ith\,\mathrm{opt}}$.

Step 7. Integrate solutions of the two submodels and $W^\pm_{ith\,\mathrm{opt}}$, and the optimal results can be expressed as $D^\pm_{th\,\mathrm{opt}} = [D^-_{th\,\mathrm{opt}},\ D^+_{th\,\mathrm{opt}}]$, $Q^\pm_{th\,\mathrm{opt}} = [Q^-_{th\,\mathrm{opt}}, Q^+_{th\,\mathrm{opt}}]$, $W^\pm_{ith\,\mathrm{opt}} = [W^-_{ith\,\mathrm{opt}}, W^+_{ith\,\mathrm{opt}}]$, and $f^\pm_{\mathrm{opt}} = [f^-_{\mathrm{opt}}, f^+_{\mathrm{opt}}]$.

Step 8. Stop.

4. Results Analysis

Tables 4–6 denote the optimized transferring water schemes under different flow levels during the planning horizon. It is shown that the solutions for the objective function value and most of the nonzero decision variables are intervals. Commonly, solutions expressed as intervals indicate that the associated decisions should be sensitive to the uncertain modeling inputs. For instance, the interval solutions for $D^\pm_{th}$ under the given targets reveal potential system-condition variations caused by uncertain inputs of $NB^\pm_{it}$, $C^\pm_t$, $C^\pm_{1t}$, $S^\pm_t$, and $q^\pm_{th}$. The demands and shortages are associated to water availability. Shortages would happen if the available water resources cannot satisfy the users' demands. Under the condition of insufficient water, more water needs to be transferred from other abundant water sources to guarantee the local normal life and economic development.

Tables 4–6 show the solution of water transferring schemes obtained from the IB-IMSP model, including transferring amount, transferring batch, and transferring period. Different transferring water is associated with varied flow levels and the targeted water demands. If the manager is optimistic of water supply to users and thus promises an upper-bound water quantity, the shortages probability would be small, and thus less water should be transferred; conversely, if the manager has a conservative attitude towards water supply, more water should be transferred to meet the users' basic demands. The transferring batch means the quantity of transferring water in every transferring scheme, which is mainly influenced by the transferring amount. The transferring period represents a cycle length from one the transferring scheme to the next scheme, and equals to transferring batch divided by demand and then multiplied by each planning period.

Table 6: Solution of the IB-IMSP model (period 3).

Water flow level	Probability	Joint flow	Optimized transferring water (10^6 m^3)	Optimized transferring batch (10^3 m^3)	Optimized transferring period (hour)
L	0.008	L-L-L	[7.30, 9.70]	[2.40, 2.64]	[11.77, 13.85]
L	0.024	L-L-M	[4.00, 5.70]	[1.73, 2.02]	[15.35, 18.71]
L	0.008	L-L-H	[0, 1.40]	[0, 1.03]	[0, 30.98]
L	0.024	L-M-L	[4.90, 6.50]	[1.92, 2.16]	[14.38, 16.90]
L	0.072	L-M-M	[1.60, 2.50]	[1.10, 1.34]	[23.18, 29.58]
L	0.024	L-M-H	0	0	0
L	0.008	L-H-L	[0, 2.60]	[0, 1.37]	[0, 22.73]
L	0.024	L-H-M	0	0	0
L	0.008	L-H-H	0	0	0
M	0.024	M-L-L	[3.50, 5.90]	[1.62, 2.06]	[15.09, 20.00]
M	0.072	M-L-M	[0.20, 1.90]	[0.39, 1.17]	[26.59, 83.66]
M	0.024	M-L-H	0	0	0
M	0.072	M-M-L	[1.10, 2.70]	[0.91, 1.39]	[24.17, 27.89]
M	0.216	M-M-M	0	0	0
M	0.072	M-M-H	0	0	0
M	0.024	M-H-L	0	0	0
M	0.072	M-H-M	0	0	0
M	0.024	M-H-H	0	0	0
H	0.008	H-L-L	[0, 1.60]	[0, 1.07]	[0, 28.98]
H	0.024	H-L-M	0	0	0
H	0.008	H-L-H	0	0	0
H	0.024	H-M-L	0	0	0
H	0.072	H-M-M	0	0	0
H	0.024	H-M-H	0	0	0
H	0.008	H-H-L	0	0	0
H	0.024	H-H-M	0	0	0
H	0.008	H-H-H	0	0	0

Total expected value of net benefit ($\$10^9$): $f^{\pm}_{\text{opt}} = [3.53, 5.03]$.

Table 4 provides the optimized water transferring schemes under three different flow levels in the first period. For example, the solutions of $D^{\pm}_{11\,\text{opt}} = [13.30, 13.90] \times 10^6$ m^3 means much more water should be transferred under low flow level (probability = 20%), which leads to larger transferring batch ($Q^{\pm}_{11\,\text{opt}} = [3.10, 3.18] \times 10^3$ m^3). Correspondingly, the transferring period ([9.88, 10.06] hour) would be smaller, which is calculated by (3c) and means that the transferring frequency would become more frequent. When the flow level is medium (probability = 60%), the transferring water ($D^{\pm}_{12\,\text{opt}} = [9.50, 10.10] \times 10^6$ m^3) and transferring batch ($Q^{\pm}_{12\,\text{opt}} = [2.62, 2.71] \times 10^3$ m^3) are smaller than the solutions of low flow level, which are associated with a wide transferring period ([11.59, 11.91] hour). Under high flow level (probability = 20%), the related transferring water and transferring batch are the smallest, while the transferring period is the widest, being $[5.50, 5.80] \times 10^6$ m^3, $[1.99, 2.05] \times 10^3$ m^3, and [15.30, 15.65] hour, individually. This implies that the water shortage under high flow is the least serious compared with low and medium flow levels under the same demand condition.

Table 5 presents the optimized water transferring schemes under all possible scenarios in period 2. Under low-, medium-, high-flow levels in period 2 (following a low flow in period 1), the needing transferring water would be $[11.50, 12.90] \times 10^6$ m^3, $[9.10, 9.70] \times 10^6$ m^3, and $[4.10, 5.80] \times 10^6$ m^3, respectively (with probability levels of 4%, 12%, and 4%). Accordingly, the transferring batches would be $[2.91, 3.18] \times 10^3$ m^3, $[2.59, 2.76] \times 10^3$ m^3, and $[1.74, 2.13] \times 10^3$ m^3, individually, associated with the transferring periods being [10.64, 10.94] hour, [12.27, 12.29] hour, and [15.87, 18.31] hour. This transferring scheme demonstrates that although the water flow is high in period 2, water transferring is still needed since low flow is in period 1. On the contrast, the solutions of $D^{\pm}_{27\,\text{opt}} = [3.70, 4.80] \times 10^6$ m^3, $D^{\pm}_{28\,\text{opt}} = [1.30, 1.60] \times 10^6$ m^3,

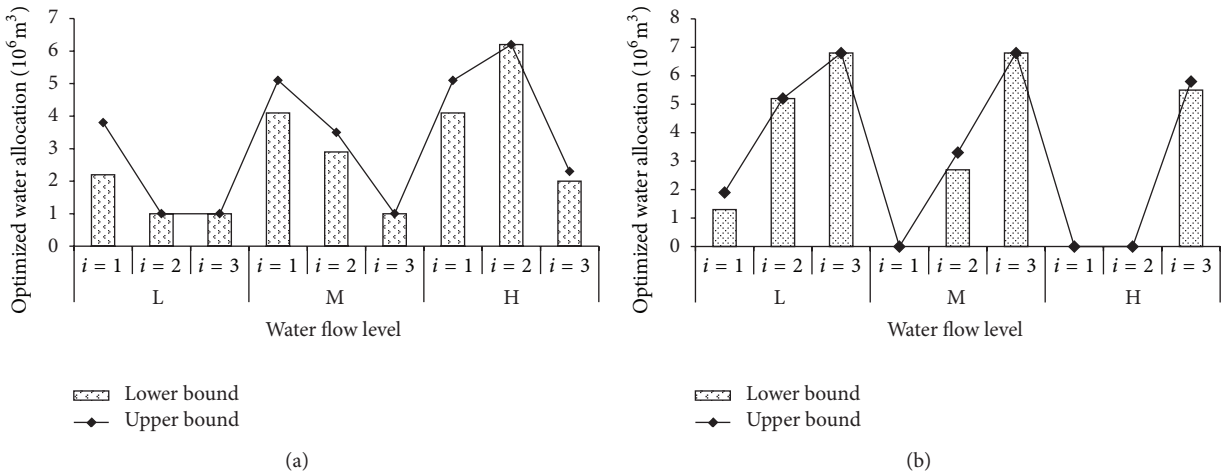

Figure 3: (a) Optimized water allocation from local water source in period 1. (b) Optimized water allocation from water transferring in period 1.

and $D^{\pm}_{29\,\mathrm{opt}} = 0$ imply that there would be less water shortages even without shortages during the second period if the water flow is high in the first period.

Table 6 shows the optimized water transferring alternatives under all possible scenarios in period 3. The solutions of $D^{\pm}_{31\,\mathrm{opt}} = [7.30, 9.70] \times 10^6$ m^3, $D^{\pm}_{32\,\mathrm{opt}} = [4.00, 5.70] \times 10^6$ m^3 and $D^{\pm}_{33\,\mathrm{opt}} = [0, 1.40] \times 10^6$ m^3 mean that, if the flows are low in the previous two periods, there would be $[7.30, 9.70] \times 10^6$ m^3, $[4.00, 5.70] \times 10^6$ m^3 and $[0, 1.40] \times 10^6$ m^3 of transferring water under low, medium and high water-flow scenarios, individually (probability = 0.8%, 24% and 0.8%), followed with the transferring batch being $[2.40, 2.64] \times 10^3$ m^3, $[1.73, 2.02] \times 10^3$ m^3 and $[0, 1.03] \times 10^3$ m^3, individually. If the flow is low in period 1 and high in period 2, then there would be $[0, 2.60] \times 10^6$ m^3, 0, and 0 of water transferring needed under low-, medium- and high-flow scenarios in period 3. The water shortage in period 3 would become less if there is some surplus in the reservoir due to the high-flow condition during period 2.

The solutions also indicate that under the worst-case scenario (probability = 0.8%) when the water flows are low during the entire planning period, the total of transferring water would be $[7.30, 9.70] \times 10^6$ m^3 associated with the total water demand from the three users being $[22.9, 25.5] \times 10^6$ m^3, implying a serious shortage in water supply. Therefore, the users need to transfer water from the other more expensive sources and ensure their demands. Under the best scenario (probability = 0.8%) when the water flows are high during the entire planning period, the total of transferring water would be 0, indicating that the water demands of the three users could generally be satisfied. Although the probability of the worst-case scenario is low (0.8%), the deficits due to the occurrence of such an extreme event are high. Consequently, an optimal policy that is formulated based on the analyses of not only the system benefits but also the related deficits would be desired.

Two extreme expected values of the net system benefit over the planning period are provided by the solution of the objective function ($f^{\pm}_{\mathrm{opt}} = \$\,[3.53, 5.03] \times 10^9$). With the actual value of every continuous variable changing within its lower and upper bounds, the desired system benefit would fluctuate accordingly between f^{-}_{opt} and f^{+}_{opt} with a range of dependability levels. Given varied water availability conditions and underlying probability distributions, the consequential plans of water transferring (and system benefit) would differ between their related solution intervals. A plan with lower system benefit might need more water transferring, while that of higher benefit would link to smaller transferring water under advantageous situations.

With water transferring, users' demands can be well satisfied under various water flow levels, and meanwhile water shortage risks can be avoided. Figures 3–6 show the optimized water allocations from the local water source and the transferring under different flow levels over the planning horizon (except the optimized water allocation from H-L-L to H-H-H in period 3). With only considering local water availability, the allotment to the agricultural sector would be first decreased, followed by that to industrial sector in the case of water insufficiency. The municipal use would be guaranteed because it brings the highest benefit when its water demand is met. In comparison, the industrial and agricultural uses match to lower benefits (see Table 3).

Figures 3(a) and 3(b) describe the optimized water allocations to three users from the local water source and the transferring under three flow levels in the first period, respectively. Under low flow, the solution of water allocation to municipal sector, industrial sector, and agricultural sector would be $[2.2, 3.8] \times 10^6$ m^3, 1×10^6 m^3, and 1×10^6 m^3 from local water source, which implies that encountering water shortage, the industrial sector and agricultural sector only obtain the minimum amount to guarantee their necessary uses while the municipal sector can gain more water (Figure 3(a)). Correspondingly, the water allocation from the transferring to agricultural sector would be the largest (6.8×10^6 m^3), followed by industrial sector (5.2×10^6 m^3) and municipal sector ($[1.3, 1.9] \times 10^6$ m^3), which are shown

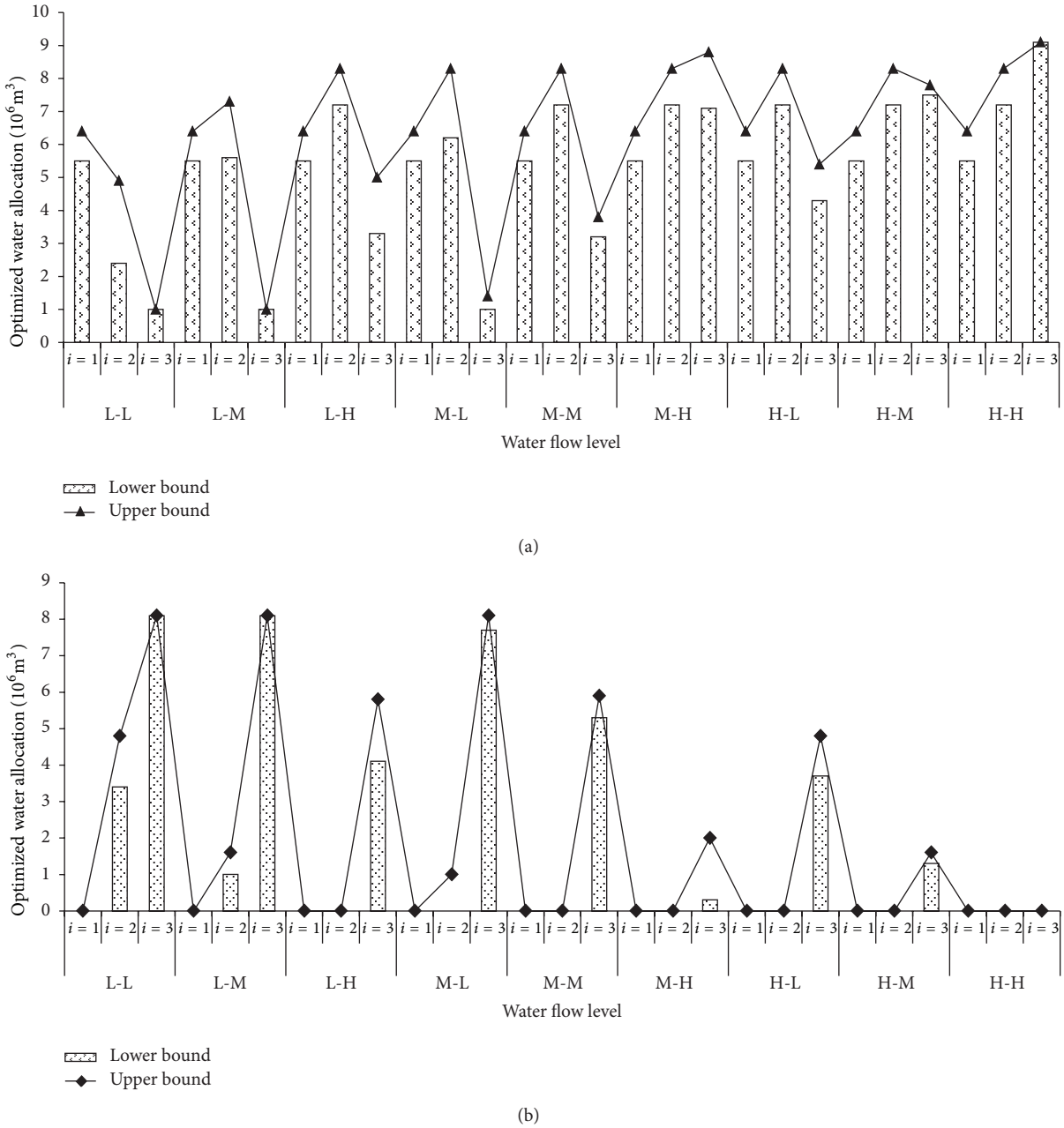

Figure 4: (a) Optimized water allocation from local water source in period 2. (b) Optimized water allocation from water transferring in period 2.

in Figure 3(b). Under high flow, both the targeted water demands from municipal and industrial users can be satisfied under the local water supply, while the agricultural sector still needs water transferring to reach its targeted demand.

Figures 4(a) and 4(b) present the optimized water allocations to all users from the local water source and the transferring under all possible flow scenarios in period 2, individually. Under low, medium, and high flow levels in period 2 (following a low flow in period 1), the solution of water allocation to agricultural sector would be 1.0×10^6 m^3, 1.0×10^6 m^3, and $[3.3, 5.0] \times 10^6$ m^3 from the local water supply, respectively (with probability levels of 4%, 12%, and 4%); correspondingly, it would be 8.1×10^6 m^3, 8.1×10^6 m^3, and $[4.1, 5.8] \times 10^6$ m^3 from transferring, individually. This allocation implies that although the water flow is high in period 2, the agricultural sector still cannot be satisfied by local water supply since low flow in period 1. In comparison, the water allocation of $[4.3, 5.4] \times 10^6$ m^3, $[7.5, 7.8] \times 10^6$ m^3, and 9.1×10^6 m^3 from local water supply, and $[3.7, 4.8] \times 10^6$ m^3, $[1.3, 1.6] \times 10^6$ m^3, and 0 from transferring to agricultural sector under the last three flow scenarios implies that less water transferring would be needed during the second period if the water flow is high in the first period.

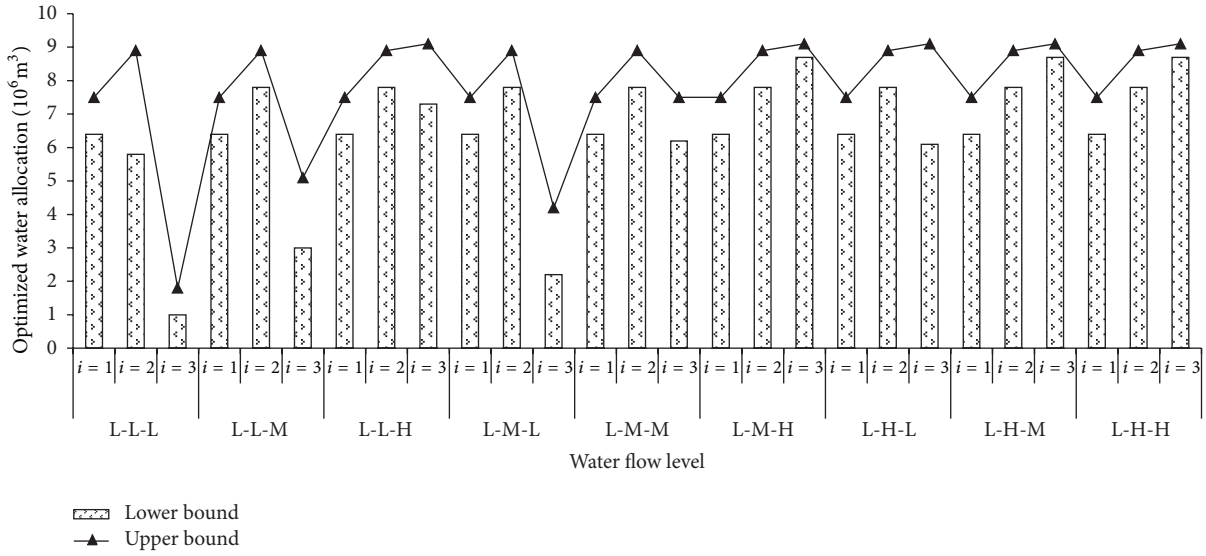

(a)

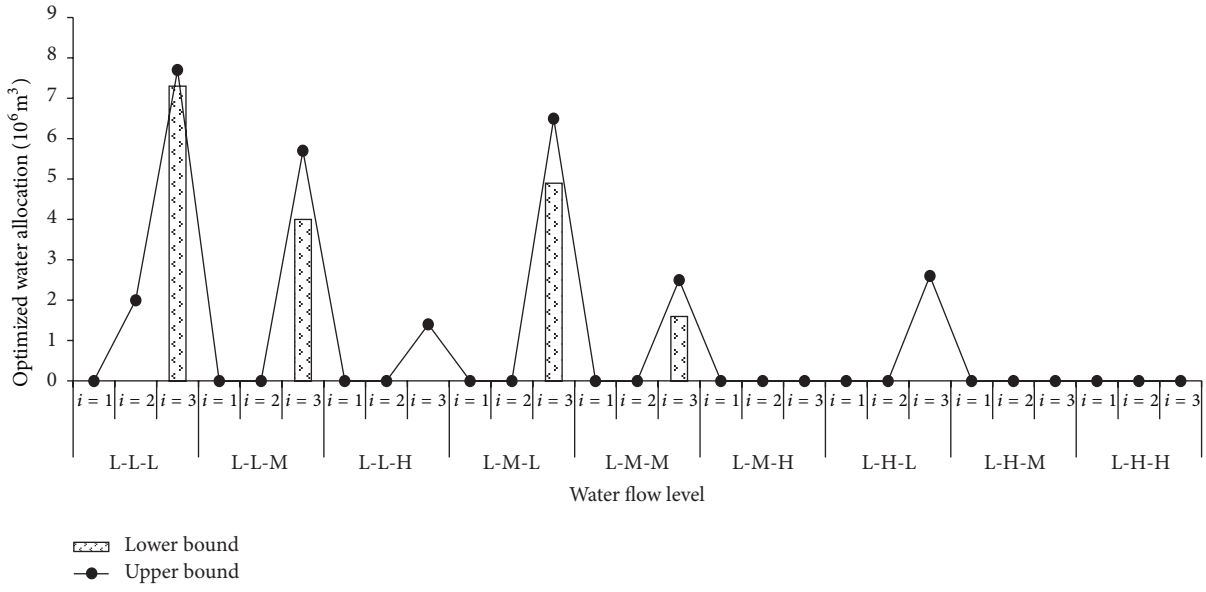

(b)

Figure 5: (a) Optimized water allocation from local water source (from L-L-L to L-H-H) in period 3. (b) Optimized water allocation from water transferring (from L-L-L to L-H-H) in period 3.

Figures 5(a), 5(b), 6(a), and 6(b) provide the optimized water allocations to the three users from local water source and the transferring under the flow scenarios from L-L-L to M-H-H in period 3, respectively. The water allocation to the agricultural sector from local water source ($[1.0, 1.8] \times 10^6$ m^3, $[3.0, 5.1] \times 10^6$ m^3, and $[7.3, 9.1] \times 10^6$ m^3) under the scenarios of low-low-low, low-low-medium, and low-low-high mean that if the flows are low in the previous two periods, there would be $[7.3, 7.7] \times 10^6$ m^3, $[4.0, 5.7] \times 10^6$ m^3, and $[0, 1.4] \times 10^6$ m^3 of transferring water under low, medium, and high water-flow scenarios, respectively (probability = 0.8%, 24%, and 0.8%). If the flow is low in period 1 and high in period 2, then the water allocation to agricultural sector would be $[6.1, 9.1] \times 10^6$ m^3, $[8.7, 9.1] \times 10^6$ m^3, and $[8.7, 9.1] \times 10^6$ m^3 from local water source, and $[0, 2.6] \times 10^6$ m^3, 0 and 0 from transferring under low-, medium-, and high-flow scenarios in period 3. The water transferring in period 3 would be less in the case of some surplus existing owing to the high-flow condition in period 2. Under the flow levels of H-L-L to H-H-H, the available water from local water source can basically satisfy the users' demands, and thus a little of water needs to be transferred, which can be seen in Table 3.

Based on the above analysis, it can be obtained that the IB-IMSP has three main advantages. Firstly, it can handle uncertainties existing in water flows by producing scenarios

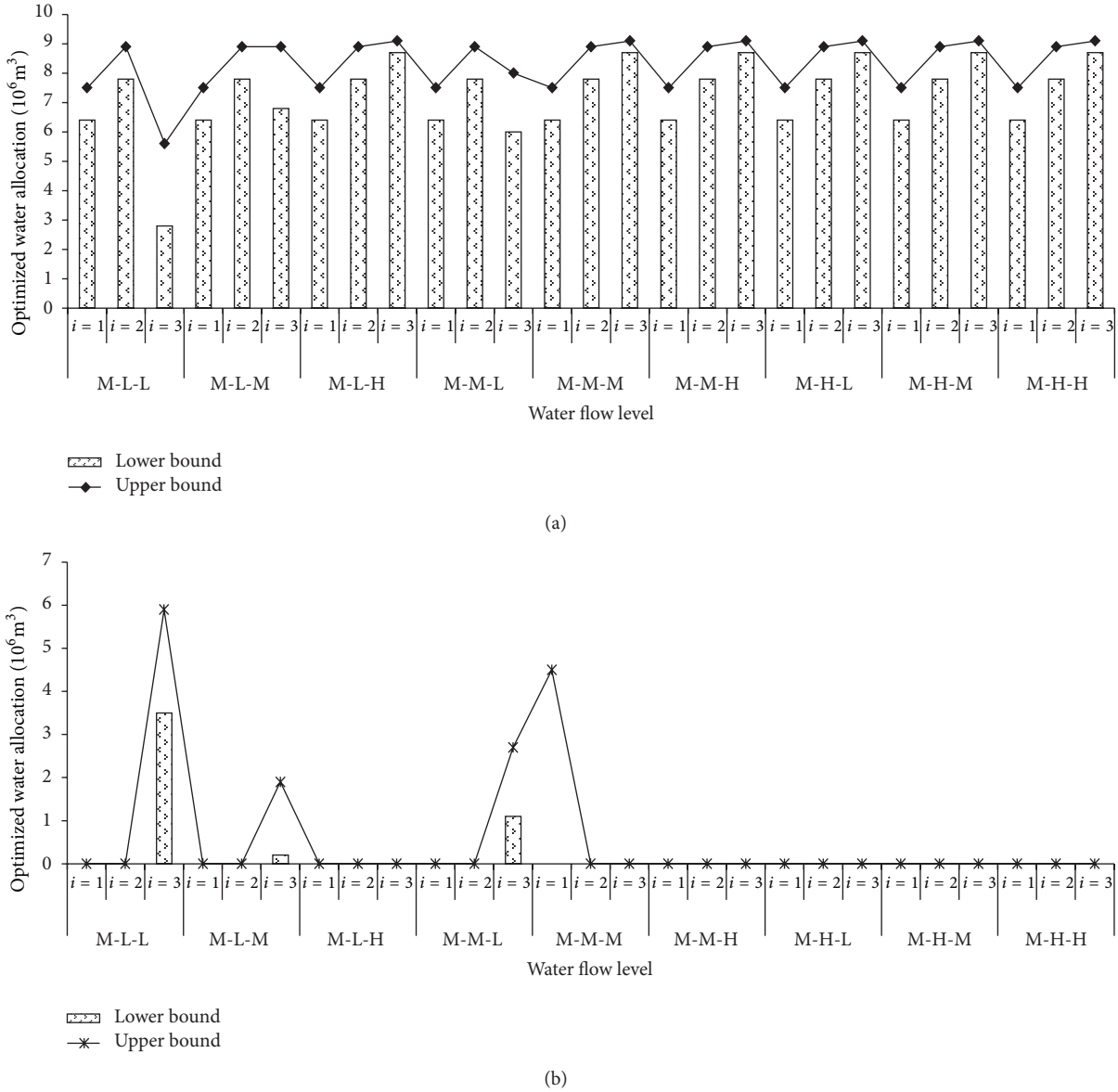

Figure 6: (a) Optimized water allocation from local water source (from M-L-L to M-H-H) in period 3. (b) Optimized water allocation from water transferring (from M-L-L to M-H-H) in period 3.

of its future events; these scenarios correspond to varied influences of different water allocations on the economic objectives. Secondly, the IB-IMSP can provide reasonable water transferring schemes (including transferring amount, transferring batch, and transferring period) with respect to all possible flow scenarios, as well as the optimized water allocations to all users from transferring. Thirdly, the IB-IMSP can efficiently identify the dynamics of not only the uncertainties but also the related decisions. With considering all scenarios, a decision can be ascertained at every stage in a real-time manner according to information about the definite realizations of the random variables along with previous decisions; this permits corrective actions to be carried dynamically for the predefined policies and can thus help reduce the deficit.

5. Conclusions

In this study, an inventory-theory-based inexact multistage stochastic programming (IB-IMSP) method has been developed for water resources decision making under uncertainty. This method advanced upon the existing inexact multistage stochastic programming by introducing inventory theory into the optimization framework. The developed IB-IMSP method can not only effectively handle uncertainties represented as probability density functions and discrete intervals, but also efficiently reflect dynamic features of the system conditions through transactions at discrete points in time during the planning horizon. In addition, it can provide reasonable transferring schemes (the transferring amount, batch, and the corresponding transferring period) associated with various flow scenarios for solving water shortage problems.

A hypothetical case study has been provided for demonstrating applicability of the developed method. The solutions obtained have then been analyzed for producing decision alternatives under different system conditions. The results provided the managers with optimal transferring schemes as well as optimized water allocation alternatives from local water availability and transferring to different users for various water shortage problems under all possible flow scenarios over the planning horizon. Therefore, the results can help the managers gain insight into the water resources management with maximizing economic objectives and satisfying targeted water demands from users. Although this study is the first attempt for planning water resources management by the proposal of an IB-IMSP method, the results indicate that this compound technique is effective and can be advanced to other environmental problems that include policy analysis. It can also be incorporated with other optimization techniques to improve their capacities in handling uncertainties presented in multiple forms.

Acknowledgments

This research was supported by the National Natural Science Foundation for Distinguished Young Scholar (51225904), the Natural Sciences Foundation of China (51190095), the Open Research Fund Program of State Key Laboratory of Hydroscience and Engineering (sklhse-2012-A-03), the National Basic Research Program of China (2013CB430406), and the Program for Changjiang Scholars and Innovative Research Team in University (IRT1127). The authors are grateful to the editors and the anonymous reviewers for their insightful comments and suggestions.

References

[1] S. A. Avlonitis, I. Poulios, N. Vlachakis et al., "Water resources management for the prefecture of Dodekanisa of Greece," *Desalination*, vol. 152, no. 1–3, pp. 41–50, 2003.

[2] H. G. Rees, M. G. R. Holmes, M. J. Fry, A. R. Young, D. G. Pitson, and S. R. Kansakar, "An integrated water resource management tool for the Himalayan region," *Environmental Modelling & Software*, vol. 21, no. 7, pp. 1001–1012, 2006.

[3] M. Zarghami and F. Szidarovszky, "Revising the OWA operator for multi criteria decision making problems under uncertainty," *European Journal of Operational Research*, vol. 198, no. 1, pp. 259–265, 2009.

[4] S. S. Liu, F. Konstantopoulou, P. Gikas, and L. G. Papageorgiou, "A mixed integer optimisation approach for integrated water resources management," *Computers & Chemical Engineering*, vol. 35, no. 5, pp. 858–875, 2011.

[5] Y. Zeng, Y. P. Cai, P. Jia, and H. K. Jee, "Development of a web-based decision support system for supporting integrated water resources management in Daegu city, South Korea," *Expert Systems with Applications*, vol. 39, no. 11, pp. 10091–10102, 2012.

[6] Y. P. Li, G. H. Huang, and S. L. Nie, "Optimization of regional economic and environmental systems under fuzzy and random uncertainties," *Journal of Environmental Management*, vol. 92, no. 8, pp. 2010–2020, 2011.

[7] I. Maqsood, G. H. Huang, and J. S. Yeomans, "An interval-parameter fuzzy two-stage stochastic program for water resources management under uncertainty," *European Journal of Operational Research*, vol. 167, no. 1, pp. 208–225, 2005.

[8] Y. P. Li and G. H. Huang, "Interval-parameter two-stage stochastic nonlinear programming for water resources management under uncertainty," *Water Resources Management*, vol. 22, no. 6, pp. 681–698, 2008.

[9] B. Chen, L. Jing, B. Y. Zhang, and S. Liu, "Wetland monitoring, characterization and modeling under changing climate in the Canadian subarctic," *Journal of Environmental Informatics*, vol. 18, no. 2, pp. 55–64, 2011.

[10] Z. Liu and S. T. Y. Tong, "Using HSPF to model the hydrologic and water quality impacts of riparian land-use change in a small watershed," *Journal of Environmental Informatics*, vol. 17, no. 1, pp. 1–14, 2011.

[11] S. Wang and G. H. Huang, "Interactive two-stage stochastic fuzzy programming for water resources management," *Journal of Environmental Management*, vol. 92, no. 8, pp. 1986–1995, 2011.

[12] Y. Xu, G. H. Huang, and T. Y. Xu, "Inexact management modeling for urban water supply systems," *Journal of Environmental Informatics*, vol. 20, no. 1, pp. 34–43, 2012.

[13] J. R. Birge and F. V. Louveaux, *Introduction to Stochastic Programming*, Springer, New York, NY, USA, 1997.

[14] Y. P. Li, G. H. Huang, X. H. Nie, and S. L. Nie, "An inexact fuzzy-robust two-stage programming model for managing sulfur dioxide abatement under uncertainty," *Environmental Modeling and Assessment*, vol. 13, no. 1, pp. 77–91, 2008.

[15] R. W. Ferrero, J. F. Rivera, and S. M. Shahidehpour, "A dynamic programming two-stage algorithm for long-term hydrothermal scheduling of multireservoir systems," *IEEE Transactions on Power Systems*, vol. 13, no. 4, pp. 1534–1540, 1998.

[16] G. H. Huang and D. P. Loucks, "An inexact two-stage stochastic programming model for water resources management under uncertainty," *Civil Engineering and Environmental Systems*, vol. 17, no. 2, pp. 95–118, 2000.

[17] S. Ahmed, M. Tawarmalani, and N. V. Sahinidis, "A finite branch-and-bound algorithm for two-stage stochastic integer programs," *Mathematical Programming*, vol. 100, no. 2, pp. 355–377, 2004.

[18] K. W. Harrison, "Two-stage decision-making under uncertainty and stochasticity: Bayesian Programming," *Advances in Water Resources*, vol. 30, no. 3, pp. 641–664, 2007.

[19] G. C. Li, G. H. Huang, C. Z. Wu, Y. P. Li, Y. M. Chen, and Q. Tan, "TISEM: a two-stage interval-stochastic evacuation management model," *Journal of Environmental Informatics*, vol. 12, no. 1, pp. 64–74, 2008.

[20] P. Guo and G. H. Huang, "Two-stage fuzzy chance-constrained programming—application to water resources management under dual uncertainties," *Stochastic Environmental Research and Risk Assessment*, vol. 23, no. 3, pp. 349–359, 2009.

[21] M. Q. Suo, Y. P. Li, and G. H. Huang, "An inventory-theory-based interval-parameter two-stage stochastic programming model for water resources management," *Engineering Optimization*, vol. 43, no. 9, pp. 999–1018, 2011.

[22] J. R. Birge, "Decomposition and partitioning methods for multistage stochastic linear programs," *Operations Research*, vol. 33, no. 5, pp. 989–1007, 1985.

[23] A. Ruszczyński, "Parallel decomposition of multistage stochastic programming problems," *Mathematical Programming*, vol. 58, no. 1–3, pp. 201–228, 1993.

[24] D. W. Watkins Jr., D. C. McKinney, L. S. Lasdon, S. S. Nielsen, and Q. W. Martin, "A scenario-based stochastic programming model for water supplies from the highland lakes," *International Transactions in Operational Research*, vol. 7, no. 3, pp. 211–230, 2000.

[25] S. Ahmed, A. J. King, and G. Parija, "A multistage stochastic integer programming approach for capacity expansion under uncertainty," *Journal of Global Optimization*, vol. 26, no. 1, pp. 3–24, 2003.

[26] J. Thénié and J. P. Vial, "Step decision rules for multistage stochastic programming: a heuristic approach," *Automatica*, vol. 44, no. 6, pp. 1569–1584, 2008.

[27] Y. P. Li, G. H. Huang, Y. F. Huang, and H. D. Zhou, "A multistage fuzzy-stochastic programming model for supporting sustainable water-resources allocation and management," *Environmental Modelling & Software*, vol. 24, no. 7, pp. 786–797, 2009.

[28] E. Körpeoğlu, H. Yaman, and M. S. Aktürk, "A multi-stage stochastic programming approach in master production scheduling," *European Journal of Operational Research*, vol. 213, no. 1, pp. 166–179, 2011.

[29] Y. P. Li, G. H. Huang, and S. L. Nie, "Planning water resources management systems using a fuzzy-boundary interval-stochastic programming method," *Advances in Water Resources*, vol. 33, no. 9, pp. 1105–1117, 2010.

[30] Y. P. Li, G. H. Huang, S. L. Nie, and L. Liu, "Inexact multistage stochastic integer programming for water resources management under uncertainty," *Journal of Environmental Management*, vol. 88, no. 1, pp. 93–107, 2008.

[31] Y. P. Li and G. H. Huang, "Fuzzy-stochastic-based violation analysis method for planning water resources management systems with uncertain information," *Information Sciences*, vol. 179, no. 24, pp. 4261–4276, 2009.

[32] Y. Zhou, G. H. Huang, and B. Yang, "Water resources management under multi-parameter interactions: a factorial multistage stochastic programming approach," *Omega*, vol. 41, no. 3, pp. 559–573, 2013.

[33] T. R. Willemain, C. N. Smart, and H. F. Schwarz, "A new approach to forecasting intermittent demand for service parts inventories," *International Journal of Forecasting*, vol. 20, no. 3, pp. 375–387, 2004.

[34] A. Kukreja and C. P. Schmidt, "A model for lumpy demand parts in a multi-location inventory system with transshipments," *Computers and Operations Research*, vol. 32, no. 8, pp. 2059–2075, 2005.

[35] E. Porras and R. Dekker, "An inventory control system for spare parts at a refinery: an empirical comparison of different re-order point methods," *European Journal of Operational Research*, vol. 184, no. 1, pp. 101–132, 2008.

[36] A. M. A. El Saadany and M. Y. Jaber, "A production/remanufacturing inventory model with price and quality dependant return rate," *Computers & Industrial Engineering*, vol. 58, no. 3, pp. 352–362, 2010.

[37] Y. R. Duan, G. P. Li, J. M. Tien, and J. Z. Huo, "Inventory models for perishable items with inventory level dependent demand rate," *Applied Mathematical Modelling*, vol. 36, no. 10, pp. 5015–5028, 2012.

[38] M. A. Ahmed, T. A. Al-Khamis, and L. Benkherouf, "Inventory models with ramp type demand rate, partial backlogging and general deterioration rate," *Applied Mathematics and Computation*, vol. 219, no. 9, pp. 4288–4307, 2013.

[39] S. Axsäter, "Approximate optimization of a two-level distribution inventory system," *International Journal of Production Economics*, vol. 81-82, pp. 545–553, 2003.

[40] D. Gupta, A. V. Hill, and T. Bouzdine-Chameeva, "A pricing model for clearing end-of-season retail inventory," *European Journal of Operational Research*, vol. 170, no. 2, pp. 518–540, 2006.

[41] V. S. S. Yadavalli, B. Sivakumar, and G. Arivarignan, "Inventory system with renewal demands at service facilities," *International Journal of Production Economics*, vol. 114, no. 1, pp. 252–264, 2008.

[42] J. Arnold, S. Minner, and B. Eidam, "Raw material procurement with fluctuating prices," *International Journal of Production Economics*, vol. 121, no. 2, pp. 353–364, 2009.

[43] A. J. Schmitt, L. V. Snyder, and Z.-J. Max Shen, "Inventory systems with stochastic demand and supply: properties and approximations," *European Journal of Operational Research*, vol. 206, no. 2, pp. 313–328, 2010.

[44] Y. C. Tsao and J. C. Lu, "A supply chain network design considering transportation cost discounts," *Transportation Research E*, vol. 48, no. 2, pp. 401–414, 2012.

[45] Y. P. Li, G. H. Huang, Z. F. Yang, and S. L. Nie, "IFMP: interval-fuzzy multistage programming for water resources management under uncertainty," *Resources, Conservation and Recycling*, vol. 52, no. 5, pp. 800–812, 2008.

[46] G. H. Huang and M. F. Cao, "Analysis of solution methods for interval linear programming," *Journal of Environmental Informatics*, vol. 17, no. 2, pp. 54–64, 2011.

[47] Y. R. Fan and G. H. Huang, "A robust two-step method for solving interval linear programming problems within an environmental management context," *Journal of Environmental Informatics*, vol. 19, no. 1, pp. 1–9, 2012.

Hindawi Publishing Corporation
Mathematical Problems in Engineering
Volume 2013, Article ID 456143, 7 pages
http://dx.doi.org/10.1155/2013/456143

Research Article

Experimental Study and Modeling of Fouling in Immersed Membrane Bioreactor Operating in Constant Pressure Filtration

Mostafa Hosseinzadeh, Mohammad Reza Mehrnia, and Navid Mostoufi

School of Chemical Engineering, College of Engineering, University of Tehran, P.O. Box 11155-4563, Tehran, Iran

Correspondence should be addressed to Mohammad Reza Mehrnia; mmehrnia@ut.ac.ir

Received 5 December 2012; Revised 3 April 2013; Accepted 12 April 2013

Academic Editor: Xiaosheng Qin

A new mathematical model is proposed based on filtration mechanisms for the prediction of fouling in airlift immersed membrane bioreactors (iMBRs). The cake formation on the membrane surface through constant pressure filtration process in the iMBR was explained by a proposed cake filtration mechanism which assumes that no particle enters the pores when forming the cake layer on the membrane surface. The cake porosity reduction due to diffusion of particles was described by an intermediate blocking mechanism. Experimental study of fouling was also performed in a lab-scale airlift flat-sheet iMBR operating at constant vacuum. The mixed liquor suspended solid (MLSS) concentration was changed within the range of 5000 to 15000 mg/L, while the superficial air velocity was varied between 32 and 128 $m^3/m^2/h$. The presented model includes two parameters, that is, ultimate filtration resistance and initial rate of cake formation. The effect of the MLSS concentration and superficial air velocity on the parameters of the proposed model was studied. The results obtained from the model demonstrated that the ultimate filtration resistance and the initial rate of cake formation are more sensitive to the aeration rate at lower superficial velocities. It was also shown that the ultimate filtration resistance has a linear relation with MLSS concentration. A good agreement exists between the results of the model and the experimental data. The proposed model also showed a better compatibility with the experimental data compared to other fouling models available in the literature.

1. Introduction

Membrane bioreactor (MBR) is a relatively new technology that is widely used for wastewater treatment [1–3]. An MBR has many advantages, including high removal rate of chemical oxygen demand (COD), high efficiency of the treatment, high concentration of biomass, reduced demanded area, and sludge production [4–8]. Fouling is a crucial problem in MBRs which takes place due to the accumulation of particles on the membrane surface. This phenomenon in the immersed membrane bioreactor (iMBR) occurs both internally (pore blocking) and externally (cake formation). Biomass concentration and aeration rate are two important parameters which affect fouling in iMBR systems. Although high concentration of biomass improves the treatment efficiency and reduces the space needed for the treatment process, it leads to a higher fouling rate. On the other hand, high aeration rate decreases the fouling and provides oxygen required by microorganisms. However, it accounts for more than 70% of the total energy consumption in wastewater treatment plants, especially in MBRs [8–13].

Modeling is essential in the design of processes and especially in predicting the performance of a system. Many researchers have offered several models to describe fouling phenomena in the MBR and considered different operating parameters in their model [14–16]. Lee et al. [17] proposed a simple model based on activated sludge models (ASMs) to predict the total hydraulic resistance in MBRs. However, their model cannot predict the fouling with enough accuracy in the iMBR, and specific experimental verification is necessary for general use of such model [6, 14, 18]. Moreover, it has some shortcomings due to the biological model used in their approach [19]. Therefore, other models such as fractal permeation, empirical hydrodynamic, and resistance in series were introduced by other researchers [20–22]. The fractal permeation model, presented by Meng et al. [20], has fewer

parameters and was indirectly validated for the prediction of cake permeability. However, this model does not show how operational parameters affect the filtration resistance [14].

Empirical hydrodynamic models are useful for illustrating hydrodynamic effects on the fouling process [21]. Nevertheless, such models may not be suitable for design and operational purposes [14]. Sectional resistance models are only able to capture general trends and are not appropriate for description of membrane fouling phenomena [14, 22]. Common filtration models divide the total hydraulic resistance, based on Hermia's theory, into cake formation, complete blocking, intermediate blocking, and standard blocking [23]. Cake filtration model is based on the fouling occurring by the deposition of suspended solids on the membrane surface. Pore blockage is divided into three parts: complete pore blockage, intermediate pore blockage, and standard pore blockage which correspond to the portion of particles blocking the pores completely, particles with specific probability to block a pore, and particles deposited inside the pores and reduced the diameter of pores, respectively. Drews et al. [24] studied these models and concluded that none of them can individually properly predict the fouling in an MBR. In addition, they developed the automated mechanism recognition (AMR) by the combination of these models in order to describe the fouling tendency.

In general, fouling is a very complex phenomenon which is affected by several biological and hydrodynamic factors [18, 25]. The mixed liquor suspended solid (MLSS) concentration is expected to be the efficient biochemical parameters on the membrane fouling [26] and the aeration as an operating parameter has a critical role in the formation of cake layer and its architecture [27]. In this study, the effect of MLSS concentration and aeration intensity on fouling in the iMBR was examined. The main objective of this study was to experimentally evaluate the membrane fouling in the iMBR and to theoretically develop a simple model for prediction of membrane fouling at constant pressure operation of iMBR.

2. Modeling

There exist mechanistic models which calculate filtration resistance in the iMBR ~~sMBR~~. However, they have not yet been used for process control. Therefore, it can be proposed to develop a new model based on the mechanism of fouling. In the filtration process, Darcy's law describes the relation between permeate flux (J) and resistance (R) through the following equation:

$$J = \frac{\Delta P}{\mu R}. \tag{1}$$

Hermia's theory describes the filtration process by [23]

$$-\frac{dJ}{dt} = k\left(J - J^*\right)J^{n-2}, \tag{2}$$

where J^* is considered to be the limit value of the permeate flux attained at the steady-state conditions [28]. In the constant pressure filtration process, the flux drastically reduces initially due to the rapid settling of suspended solids on the membrane surface, and a cake layer is formed. In this case, particles do not enter the membrane pores but form a biofilm layer on the membrane surface. The cake filtration model can be obtained by putting $n = 0$ and $J^* = 0$ in (2) [28]. Combining (1) and (2) results in the following equation for the cake filtration mechanism:

$$R\frac{dR}{dt} = k\left(\frac{\Delta P}{\mu}\right)^2, \tag{3}$$

where k is defined as follows when main process mechanism is cake filtration [29]:

$$k = \frac{\alpha\rho\phi}{F^2 R_m J_0\left(1 - m\phi\right)}, \tag{4}$$

in which F is an active opening surface of the filtration area and can change with time, while the specific resistance of filtration cake (α), filtrate density (ρ), shape factor of suspended solid (ϕ), and ratio of the mass of humid cake to dry cake (m) is constant.

The cake filtration model proposed by Hermia was derived for dead-end filtration condition [30], and it should be modified for cross-flow filtration systems such as iMBR. In iMBRs, the cake layer, formed on the surface of membrane, develops a dynamic biofilm layer. Its structure changes biologically due to underneath anoxic layer [31]. Also, the penetration of colloids and soluble extracellular polymeric substances (EPS) into the cake layer results in the reduction of the porosity of the biofilm [31, 32]. Thus, in cross-flow models, the constant k in (3) should be considered a variable through the filtration process in the iMBR. It can be suggested that a new biofilm layer forms the existing deposited biofilm. Thus, the opening pores on the membrane surface area (F) change through the filtration process in the iMBR. These changes can be described by the intermediate blocking mechanism. It seems that a new biofilm layer is formed on the existing deposited biofilm. In other words, suspended particles settle on the cellular structure and alter the porosity of the cake layer formed on the membrane surface, leading to a reduction in filtration flux [20]. Therefore, the active surface of filtration decreases linearly with time which is shown by [33]

$$\frac{F}{F_0} = 1 + C_1 t, \tag{5}$$

where F_0 is the area of the membrane surface before the contact of the activated sludge. Also, according to (1),

$$J_0 R_m = \frac{\Delta P}{\mu}. \tag{6}$$

Combining (3), (4), (5), and (6) results in

$$R\frac{dR}{dt} = \frac{\alpha\rho\phi\Delta P}{\mu F_0^2\left(1 - m\phi\right)\left(1 + C_1 t\right)^2}. \tag{7}$$

According to (7), if the system operates for a long time, variation of the fouling intensity becomes insignificant, and the permeate flow rate reaches a constant value.

Equation (7) can be rewritten as

$$\frac{1}{J^2} - \frac{1}{J_0^2} = \left(\frac{\mu R_\infty}{\Delta P}\right)^2 \left(\frac{t}{t + (R_\infty / r_R)}\right). \tag{8}$$

This equation has only two parameters, r_R and R_∞:

$$R_\infty = \sqrt{\frac{2\alpha\rho\phi R_m J_0}{C_1 F_0^2 (1 - m\phi)}},$$
$$r_R = \frac{\alpha\rho\phi J_0}{F_0^2 (1 - m\phi)}. \tag{9}$$

The parameter r_R is the initial rate of cake formation; that is,

$$\left.\frac{\partial R}{\partial t}\right|_{t=0} = r_R. \tag{10}$$

This value indicates the tendency of the system to form cake on the surface of membrane at the start of filtration. Also, R_∞ is the ultimate filtration resistance; that is,

$$\lim_{t \to \infty} R = R_\infty. \tag{11}$$

This parameter illustrates the resistance of the formed cake that the system would eventually reach due to membrane fouling.

3. Experiments

A flat sheet chlorinated polyethylene membrane (KUBOTA Membrane Europe Ltd., Porlock, UK) with an area of 0.11 m^2 and a mean pore size of 0.45 μm was used in the experiments. The biomass was from a municipal wastewater treatment plant in west of Tehran, Iran. The experiments were carried out in an airlift iMBR, the schematic of which is shown in Figure 1. The bioreactor was 55 cm high, 23 cm long, and 21 cm width in which the membrane was submerged. Two baffles were placed at both sides of the membrane with 4 cm distance. The driving force for filtration was created by vacuum. Fouling starts to form on the membrane surface when the flux and the permeability of the membrane begin to decrease at constant pressure filtration condition. The permeate flow rate was measured by a digital balance. MLSS and COD were measured according to standard methods [34].

In all experiments, the system was fed by a synthetic influent, glucose, ammonium nitrate, and potassium phosphate which are the sources of carbon, nitrogen, and phosphorus, respectively, with a ratio of 100/5/1 for COD/N/P. The COD of feed was 1000 mg/L. During the experiments, temperature, pH, volume of activated sludge in the bioreactor, and transmembrane pressure (TMP) were kept constant as 25°C, 7.5 ± 0.5, 20 L, and 20–40 kPa, respectively. The tests were carried out at four different aeration intensities (32, 64, 96, and 128 $m^3/m^2/hr$) and at four MLSS concentrations (5000, 8000, 12000, and 15000 mg/L). The mean hydraulic retention time (HRT) of the system was about 12 hours. The solids retention time (SRT) of the system was infinite. The activated sludge suspensions were acclimatized for two weeks with the same operating conditions of the iMBR. Each test run was performed for analysis of fouling mechanism after two weeks in order to reach the same biological steady state.

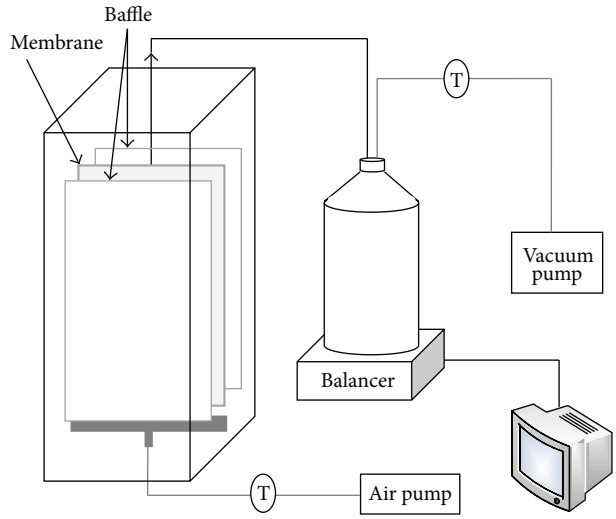

Figure 1: Schematics of the experimental setup.

4. Results and Discussion

At the initial steps of operation, the efficiency of removal of COD was 90 ± 2%. Then, this value increased and reached to more than 95% after 30 min of operation, followed by a plateau in the rest of the experiment. The steady-state COD removal efficiency of the iMBR was about 96%. When the cake layer was gradually formed on the membrane surface, the increase in the permeate flux and the decrease in the HRT occurred with the operation time. Therefore, the biomass had more time to remove COD and, consequently, enhanced the removal efficiency. Furthermore, the cake layer acted as a second biological barrier in removing COD. This is in agreement with previous reports which showed that the cake layer can affect COD removal in the iMBR [35].

Figure 2 illustrates application of Hermia's model (2) to different experimental conditions. By assumption that $J^* = 0$, the slop of the line of $\mathrm{Ln}(-dJ/dt)$ against $\mathrm{Ln}(J)$ is equal to 3-n which specifies the fouling mechanism. This figure shows that n is close to zero (from −0.0713 to 0.1289) at the initial steps of the processes in all experiments. Therefore, the cake filtration mechanism is the dominant mechanism at the startup of the processes. However, the governing mechanism changes during the operation. As indicated in (11), if the system operates for a long time, the variation of the fouling intensity becomes insignificant, and the permeate flow rate reaches a stable value. In all cases, the model was fitted to the experimental data of this work with a correlation coefficient of greater than 0.97. Calculated model parameters for all tests and the corresponding correlation coefficients are listed in Table 1.

In order to test the ability of the model to predict the fouling intensity, model parameters, R_∞ and r_R, were

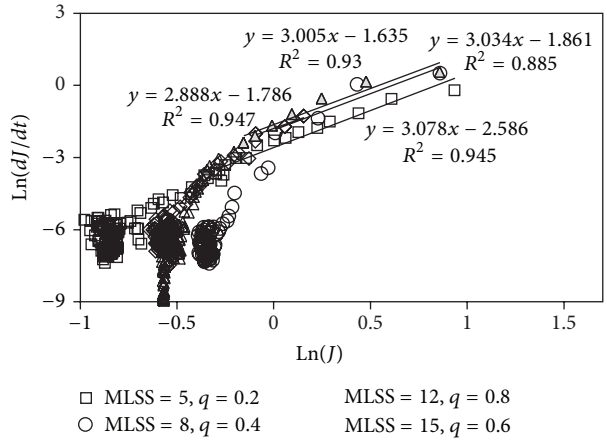

Figure 2: Experiments data agreements with Hermia's model (TMP = 40 kPa, MLSS = 5000 mg/L, and $q = 128\ m^3/m^2/hr$).

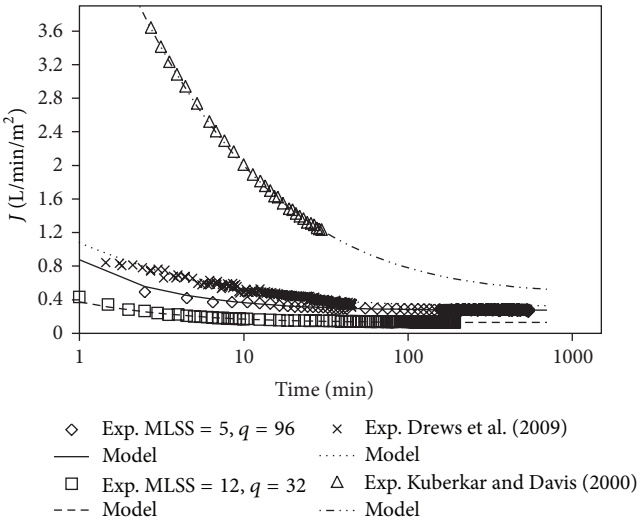

Figure 3: Experimental and predicted flux against time.

obtained based on the data from the first hour of the experiments. Then, these parameters were used for predicting the fouling in the rest of operation. Figure 3 shows the presented model prediction for the data of this research and other researchers for the iMBR operating at constant TMP using the flat sheet membrane [24, 36]. This figure demonstrates that the proposed model predicts the liquid flux through the membrane at long time as well as short time operation even though they had different operation conditions (such as MLSS, aeration intensity, HRT, and SRT). Therefore, this model can be used for the prediction of biofouling in flat-sheet iMBR systems operating at constant TMP.

Fouling models based on various mechanisms are shown in Table 2 [23, 24]. Figure 4 demonstrates a comparison between the performances of these models with the model developed in this work. As can be seen in this figure, previous models cannot predict the fouling in the iMBR properly since they are based on the theories that cannot explain the fouling in iMBRs. However, the model developed in this work is

Table 1: Model parameters at various MLSS concentration and superficial velocity, calculated based on the first hour of the fouling process.

Aeration intensity ($m^3/m^2/hr$)	MLSS concentration (mg/L)	5000	8000	12000	15000
32	R_∞ [10^{12}/m]	2.2227	2.4900	2.1968	2.5889
	r_R [10^{12}/m/min]	0.2286	0.5619	0.7409	0.8916
	R^2	0.9649	0.9677	0.9846	0.9668
64	R_∞ [10^{12}/m]	1.3363	1.5513	1.4839	1.6511
	r_R [10^{12}/m/min]	0.1862	0.4407	0.7267	0.8400
	R^2	0.9799	0.9816	0.9828	0.9838
96	R_∞ [10^{12}/m]	1.0365	1.2646	1.3161	1.4391
	r_R [10^{12}/m/min]	0.1577	0.3429	0.5790	0.9943
	R^2	0.9856	0.9872	0.9861	0.9844
128	R_∞ [10^{12}/m]	0.8218	1.0519	1.1765	1.3108
	r_R [10^{12}/m/min]	0.1359	0.3157	0.4478	0.6711
	R^2	0.9797	0.9855	0.981	0.9885

Table 2: Convectional models of fouling [23, 24].

No.	Theory	Equation	R^2
E1	Cake filtration	$\frac{Q_0}{Q} = 1 + \frac{aX}{\rho A R_m} V(t) - \frac{aQ_\infty}{AR_m}$	0.950
E2	Standard blocking	$\frac{t}{V(t)} = \frac{1}{Q_0} + \frac{\Delta P \sigma t}{\mu A Q_0 R_m}$	0.904
E3	Intermediate blocking	$\frac{1}{Q} = \frac{1}{Q_0} + \frac{\Delta P \sigma t}{\mu Q_0 R_m}$	0.781
E4	Complete blocking	$Q = Q_0 - \frac{\Delta P \sigma V(t)}{\mu R_m}$	0.769

in good agreement with the experimental data. The fitted parameters of the models, shown in Table 2, were calculated from the data of the first hour of the fouling process. The filtration resistance can be attributed to formation of cake on the membrane surface which is a function of permeate flux as well as time. This function can be described by cake filtration and intermediate blocking filtration mechanisms. The cake initially forms on the surface of the membrane and then reaches the steady-state condition. Initial formation of cake can be defined by r_R, and the steady-state condition can be represented by R_∞.

The constants of the model obtained from the first hours of the filtration can appropriately predict the membrane fouling intensity of flat-sheet iMBRs in the constant pressure processes. The proposed model has two constants, that is, initial rate of cake formation (r_R) and ultimate filtration resistance (R_∞), related to cake formation and standard blocking mechanisms, respectively. Since the MLSS concentration and the superficial gas velocity are accepted to be the two major operating parameters influencing the membrane fouling, the effect of MLSS concentration and superficial air velocity on the parameters of the proposed model was evaluated.

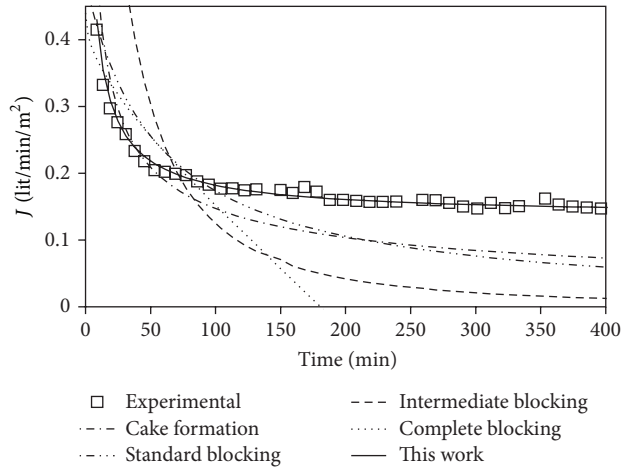

Figure 4: Comparison between convectional models of fouling with the model presented in this work (TMP = 40 kPa, MLSS = 12000 mg/L, and $q = 32\,m^3/m^2/hr$).

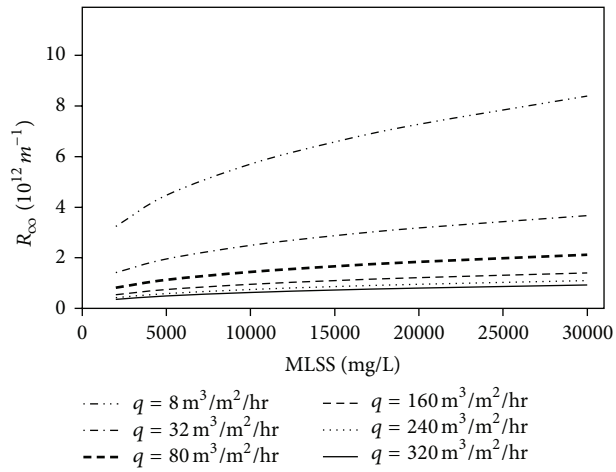

Figure 5: Ultimate filtration resistance as a function of MLSS concentration at various aeration intensities.

In order to generalize the proposed model, the parameters of the model, R_∞ and r_R, were correlated to MLSS concentration and superficial air velocity by the following power law functions:

$$R_\infty = 0.9429 \times 10^8 X^{1.5402} q^{-0.3872}, \quad (12)$$

$$r_R = 0.1250 \times 10^8 X^{0.3513} q^{-0.5970}, \quad (13)$$

for which correlation coefficients of 0.9615 and 0.9856, respectively, were obtained by using the linear least squares regression method.

Figure 5 illustrates the ultimate filtration resistance (R_∞) of the system as a function of MLSS concentration at various aeration intensities, calculated based on (12). This figure shows that the resistance increases by increasing the MLSS concentration. At low superficial air velocity, the resistance is highly sensitive to the superficial air velocity, while it is not sensitive to the aeration rate at high superficial air velocity. In

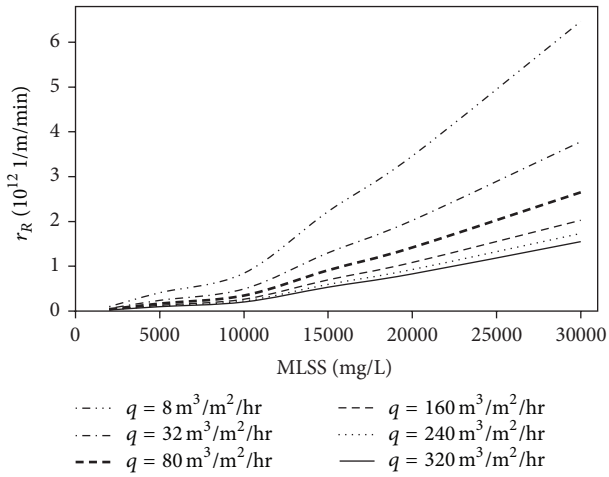

Figure 6: Initial rate of cake formation as a function of MLSS concentration at various aeration intensities.

fact, aeration removes deposited particles on the membrane surface and, consequently, prevents formation of cake. At a constant TMP, by increasing the superficial air velocity the process reaches an equilibrium condition at which increasing the superficial air velocity does not affect cake formation and filtration resistance. It is also observed in Figure 5 that the MLSS concentration has a negligible effect on the ultimate filtration resistance. In fact, when the cake on the surface of the membrane is formed completely, the process reaches the steady-state condition. At such a condition, the driving force (TMP) and resistance force (superficial air velocity) reach equilibrium so that by changing the MLSS concentration, the cake formed on the surface of the membrane does not change significantly. The value of R_∞ thus becomes important when the system operates at steady-state condition.

Initial rate of cake formation (r_R) corresponds to the tendency of fouling of the system. Figure 6 shows the effect of MLSS concentration on the initial rate of cake formation at various aeration intensities, calculated based on (13). As can be seen in this figure, the initial rate of cake formation increases rapidly by increasing the MLSS concentration. When the MLSS concentration is higher than 10000 mg/L, the initial rate of the increase of cake formation is more significant. This trend may be explained by the fact that the tendency of cake formation increases at high MLSS concentration. In fact, increasing the MLSS concentration increases the aggregation of suspended particles on the membrane surface, thereby causing an increase in the cake formation rate. The initial rate of cake formation decreases sharply by increasing the superficial air velocity at low aeration intensities, while this change is not sensitive to the aeration rate at high aeration intensities. In fact, increase in superficial air velocity causes increment of the shear stress due to higher cross flow rate of fluid on the membrane surface. Shear stress is not a linear function of superficial air velocity; thus, increasing the velocity at high aeration rate has low effect on the shear stress and cake formation. The value of r_R becomes

important when the system is to be operated in short periods with frequent washing of the surface of the membrane.

5. Conclusions

A new model is proposed for the prediction of fouling in the iMBR based on cake formation on the membrane surface through constant pressure filtration process in which the reduction of the cake porosity is explained by intermediate blocking mechanism. The presented model can be applied to the prediction of membrane fouling of flat-sheet iMBRs which operate at constant pressure condition. The model includes two main parameters, that is, the ultimate filtration resistance and the initial rate of cake formation. These parameters were determined by fitting the experimental data of flow rate obtained from the beginning stage of the operation of the iMBR to the model. The value of R_∞ indicates the ultimate fouling resistance and is important when the system is to be operated for a long time. The parameter r_R is the initial fouling rate and is important when the system operates at short time and/or the surface of the membrane is washed frequently. The proposed model is in good agreement with other experimental data reported in the literature. This model can predict the fouling properly. It was also shown that the new model performs considerably better in the iMBR than other conventional fouling models at constant filtration pressure. The effect of MLSS concentration and superficial air velocity on the model parameters was studied. It was shown that the sensitivity of ultimate filtration resistance and initial rate of cake formation to the aeration rate at lower superficial velocity is more than that at higher aeration rate. It was also observed that the ultimate filtration resistance has a linear relation with MLSS concentration. By increasing the MLSS concentration, the initial rate of cake formation increases which causes increasing in the tendency of fouling. Future studies are necessary to improve this model to evaluate the effect of other operational parameters such as biological polymeric substances, HRT, and SRT.

Symbols

A: Membrane surface area m^2
a: Specific cake resistance $1/m^2$
C_1: Model parameter 1/min
d_p: Particle diameter M
F: Active opening surface of the filtration area m^2
J: Flux L/min/m^2
k: Hermia's model parameter
m: Ration between the mass of humid cake and dry cake
n: Hermia's model parameter
Q: Flow rate L/min
q: Superficial velocity $m^3/m^2/hr$
R^2: Correlation coefficient
R: Filtration resistance 1/m
R_∞: Ultimate filtration resistance 1/m
R_m: Membrane resistance 1/m
r_R: Initial rate of cake formation 1/m/min
t: Time per min
V: Filtrated volume L
X: MLSS concentrations mg/L

Greek Letters

α: Specific resistance of filtration cake 1/m
σ: Blocked area per unit filtrate volume m^2/m^3
$\triangle P$: Trans-membrane pressure Pa
μ: Viscosity Pa·s
ϕ: Share of solid body in the filtrated suspension
ρ: Density of cake kg/m^3.

Acknowledgment

This work was supported by a grant from the Isfahan Water and Wastewater Company, Iran.

References

[1] W. Khongnakorn, C. Wisniewski, L. Pottier, and L. Vachoud, "Physical properties of activated sludge in a submerged membrane bioreactor and relation with membrane fouling," *Separation and Purification Technology*, vol. 55, no. 1, pp. 125–131, 2007.

[2] J. Schaller, A. Drews, and M. Kraume, "Analyses and modelling of filtration processes in MBR and test cells," *Desalination*, vol. 199, no. 1–3, pp. 507–508, 2006.

[3] A. Zarragoitia-González, S. Schetrite, M. Alliet, U. Jáuregui-Haza, and C. Albasi, "Modelling of submerged membrane bioreactor: conceptual study about link between activated slugde biokinetics, aeration and fouling process," *Journal of Membrane Science*, vol. 325, no. 2, pp. 612–624, 2008.

[4] G. di Bella, G. Mannina, and G. Viviani, "An integrated model for physical-biological wastewater organic removal in a submerged membrane bioreactor: model development and parameter estimation," *Journal of Membrane Science*, vol. 322, no. 1, pp. 1–12, 2008.

[5] S. Rosenberger, C. Laabs, B. Lesjean et al., "Impact of colloidal and soluble organic material on membrane performance in membrane bioreactors for municipal wastewater treatment," *Water Research*, vol. 40, no. 4, pp. 710–720, 2006.

[6] D. P. Saroj, G. Guglielmi, D. Chiarani, and G. Andreottola, "Sub-critical fouling behaviour modelling of membrane bioreactors for municipal wastewater treatment: the prediction of the time to reach critical operating condition," *Desalination*, vol. 231, no. 1–3, pp. 175–181, 2008.

[7] I. Martin, M. Pidou, A. Soares, S. Judd, and B. Jefferson, "Modelling the energy demands of aerobic and anaerobic membrane bioreactors for wastewater treatment," *Environmental Technology*, vol. 32, no. 9, pp. 921–932, 2011.

[8] C. C. Ho and A. L. Zydney, "Overview of fouling phenomena and modeling approaches for membrane bioreactors," *Separation Science and Technology*, vol. 41, no. 7, pp. 1231–1251, 2006.

[9] N. Ratkovich, C. C. V. Chan, P. R. Berube, and I. Nopens, "Experimental study and CFD modelling of a two-phase slug flow for an airlift tubular membrane," *Chemical Engineering Science*, vol. 64, no. 16, pp. 3576–3584, 2009.

[10] S. J. Judd, "A review of fouling of membrane bioreactors in sewage treatment," *Water Science and Technology*, vol. 49, no. 2, pp. 229–235, 2004.

[11] X.-M. Wang, X.-Y. Li, and X. Huang, "Membrane fouling in a submerged membrane bioreactor (SMBR): characterisation of

the sludge cake and its high filtration resistance," *Separation and Purification Technology*, vol. 52, no. 3, pp. 439–445, 2007.

[12] P. Cornel, M. Wagner, and S. Krause, "Investigation of oxygen transfer rates in full scale membrane bioreactors," *Water Science and Technology*, vol. 47, no. 11, pp. 313–319, 2003.

[13] H. Dhaouadi and B. Marrot, "Olive mill wastewater treatment in a membrane bioreactor: process stability and fouling aspects," *Environmental Technology*, vol. 31, no. 7, pp. 761–770, 2010.

[14] A. N. L. Ng and A. S. Kim, "A mini-review of modeling studies on membrane bioreactor (MBR) treatment for municipal wastewaters," *Desalination*, vol. 212, no. 1–3, pp. 261–281, 2007.

[15] M. Spérandio and M. C. Espinosa, "Modelling an aerobic submerged membrane bioreactor with ASM models on a large range of sludge retention time," *Desalination*, vol. 231, no. 1–3, pp. 82–90, 2008.

[16] A. Khalili-Garakani, M. R. Mehrnia, N. Mostoufi, and M. H. Sarrafzadeh, "Analyze and control fouling in an airlift membrane bioreactor: CFD simulation and experimental studies," *Process Biochemistry*, vol. 46, no. 5, pp. 1138–1145, 2011.

[17] Y. Lee, J. Cho, Y. Seo, J. W. Lee, and K.-H. Ahn, "Modeling of submerged membrane bioreactor process for wastewater treatment," *Desalination*, vol. 146, no. 1–3, pp. 451–457, 2002.

[18] T. Jiang, S. Myngheer, D. J. W. de Pauw et al., "Modelling the production and degradation of soluble microbial products (SMP) in membrane bioreactors (MBR)," *Water Research*, vol. 42, no. 20, pp. 4955–4964, 2008.

[19] G. Mannina, G. di Bella, and G. Viviani, "An integrated model for biological and physical process simulation in membrane bioreactors (MBRs)," *Journal of Membrane Science*, vol. 376, no. 1-2, pp. 56–69, 2011.

[20] F. Meng, H. Zhang, Y. Li, X. Zhang, and F. Yang, "Application of fractal permeation model to investigate membrane fouling in membrane bioreactor," *Journal of Membrane Science*, vol. 262, no. 1-2, pp. 107–116, 2005.

[21] R. Liu, X. Huang, Y. F. Sun, and Y. Qian, "Hydrodynamic effect on sludge accumulation over membrane surfaces in a submerged membrane bioreactor," *Process Biochemistry*, vol. 39, no. 2, pp. 157–163, 2003.

[22] X.-Y. Li and X.-M. Wang, "Modelling of membrane fouling in a submerged membrane bioreactor," *Journal of Membrane Science*, vol. 278, no. 1-2, pp. 151–161, 2006.

[23] J. Hermia, "Constant pressure blocking filtration laws application to power law non newtonian fluids," *Chemical Engineering Research and Design* , vol. 60, no. 3, pp. 183–187, 1982.

[24] A. Drews, H. Arellano-Garcia, J. Schöneberger, J. Schaller, G. Wozny, and M. Kraume, "Model-based recognition of fouling mechanisms in membrane bioreactors," *Desalination*, vol. 236, no. 1–3, pp. 224–233, 2009.

[25] J. Busch, A. Cruse, and W. Marquardt, "Modeling submerged hollow-fiber membrane filtration for wastewater treatment," *Journal of Membrane Science*, vol. 288, no. 1-2, pp. 94–111, 2007.

[26] D.-W. Gao, Y. Fu, Y. Tao, W.-M. Wu, R. An, and X.-X. Li, "Current research and development of controlling membrane fouling of MBR," *The African Journal of Biotechnology*, vol. 8, no. 13, pp. 2993–2998, 2009.

[27] Q. Wang, Z. Wang, Z. Wu, J. Ma, and Z. Jiang, "Insights into membrane fouling of submerged membrane bioreactors by characterizing different fouling layers formed on membrane surfaces," *Chemical Engineering Journal*, vol. 179, pp. 169–177.

[28] L. Giorno, L. Donato, S. Todisco, and E. Drioli, "Study of fouling phenomena in apple juice clarification by enzyme membrane reactor," *Separation Science and Technology*, vol. 33, no. 5, pp. 739–756, 1998.

[29] K. Konieczny and J. Rafa, "Modeling of the membrane filtration process of natural waters," *Polish Journal of Environmental Studies*, vol. 9, no. 1, pp. 57–63, 2000.

[30] S. Rosenberger, H. Evenblij, S. Te Poele, T. Wintgens, and C. Laabs, "The importance of liquid phase analyses to understand fouling in membrane assisted activated sludge processes—six case studies of different European research groups," *Journal of Membrane Science*, vol. 263, no. 1-2, pp. 113–126, 2005.

[31] S.-H. Hong, W.-N. Lee, H.-S. Oh et al., "The effects of intermittent aeration on the characteristics of bio-cake layers in a membrane bioreactor," *Environmental Science and Technology*, vol. 41, no. 17, pp. 6270–6276, 2007.

[32] I. Ivanovic and T. O. Leiknes, "The biofilm membrane bioreactor (BF-MBR)-a review," *Desalination and Water Treatment*, vol. 37, no. 1–3, pp. 288–295, 2012.

[33] B. Tansel, W. Y. Bao, and I. N. Tansel, "Characterization of fouling kinetics in ultrafiltration systems by resistances in series model," *Desalination*, vol. 129, no. 1, pp. 7–14, 2000.

[34] APHA, *Standard Methods for the Examination of Water and Wastewater*, American Public Health Association, Washington, DC, USA, 17th edition, 1989.

[35] S. Mafirad, M. R. Mehrnia, H. Azami, and M. H. Sarrafzadeh, "Effects of biofilm formation on membrane performance in submerged membrane bioreactors," *Biofouling*, vol. 27, no. 5, pp. 477–485, 2011.

[36] V. T. Kuberkar and R. H. Davis, "Modeling of fouling reduction by secondary membranes," *Journal of Membrane Science*, vol. 168, no. 1-2, pp. 243–258, 2000.

Hindawi Publishing Corporation
Mathematical Problems in Engineering
Volume 2013, Article ID 136453, 12 pages
http://dx.doi.org/10.1155/2013/136453

Research Article

Application of MM5-CAMx-PSAT Modeling Approach for Investigating Emission Source Contribution to Atmospheric SO_2 Pollution in Tangshan, Northern China

Li Li,[1,2] Shuiyuan Cheng,[1] Jianbing Li,[3] Jianlei Lang,[1] and Dongsheng Chen[1]

[1] *College of Environmental & Energy Engineering, Beijing University of Technology, Beijing 100124, China*
[2] *Beijing General Research Institute of Mining & Metallurgy, Beijing 100070, China*
[3] *Environmental Engineering Program, University of Northern British Columbia, Prince George, Canada V2N 4Z9*

Correspondence should be addressed to Shuiyuan Cheng; bjutpaper@gmail.com

Received 19 February 2013; Accepted 13 March 2013

Academic Editor: Guohe Huang

The MM5-CMAx-PSAT modeling approach was presented to identify the variation of emission contribution from each modeling grid to regional and urban air quality per unit emission rate change. The method was applied to a case study in Tangshan Municipality, a typical industrial region in northern China. The variation of emission contribution to the monthly atmospheric SO_2 concentrations in Tangshan from each modeling grid of 9×9 km per 1000 t/yr of emission rate change was simulated for four representative months in 2006. It was found that the northwestern part of Tangshan region had the maximum contribution variation ratio (i.e., greater than 0.36%) to regional air quality, while the lowest contribution variation ratio (i.e., less than 0.3%) occurred in the coastal areas. Principal component analysis (PCA), canonical correlation analysis (CCA), and Pearson correlation analysis indicated that there was an obvious negative correlation between the grid-based variation of emission contribution to regional air quality and planetary boundary layer height (PBLH) as well as wind speed, while terrain data presented insignificant impacts on emission contribution variation. The proposed method was also applied to analyze the variation of emission contribution to the urban air quality of Tangshan (i.e., a smaller scale).

1. Introduction

Air pollution is a serious environmental problem faced by many industrial cities in China as a consequence of many years' rapid economic expansion and insufficient environmental protection measures. It not only poses threats to human health, but also directly affects local economic development [1]. A variety of factors, such as emission sources, land surface characteristics, and meteorological conditions, could affect air pollution simulation. Thus, effective air quality management is usually a challenging task. To tackle such difficulties, it is of crucial importance to quantify the impacts of pollutant emission sources on the air quality of a planning region and understand the corresponding response of atmospheric pollutant concentration to perturbations in pollutant emission rate [2].

Previously, the method of wind rose based on wind speed and direction has been used for qualitatively investigating the impacts of emission sources on regional air quality [3]. Nowadays, computer modeling tools have been recognized as useful means to investigate such impacts [4]. Particularly, there has been a growing interest of applying advanced 3-D chemistry-transport models coupled with meteorological models for air quality studies, such as the Model-3 Community Multiscale Air Quality (Model-3/CMAQ) [5, 6], the Comprehensive Air quality Model with extensions

(CAMx) [7, 8], the PSU/NCAR mesoscale meteorological model MM5 [9], and the Weather Research and Forecast (WRF) model coupled with Chemistry (WRF-Chem) [10]. For example, Cheng et al. [11] used the coupled MM5-ARPS-CMAQ to examine contributions of various emission sources to ambient PM_{10} concentrations in Beijing, China; Titov et al. [12] applied a MM5-CAMx for predicting PM_{10} concentrations over the city of Christchurch in New Zealand during critical pollution episodes; Lee et al. [13] employed MM5-CAMx to simulate atmospheric pollutant transport and recirculation in the Santa Claria valley, USA; Shimadera et al. [14] applied MM5-CMAQ to estimate the contribution of transboundary transport of air pollutants from other Asian countries to Japan; Borrego et al. [15] applied MM5-CAMx to simulate surface concentrations of ozone and its precursors over the metropolitan area of Porto Alegre, Brazil, and identified the main emission sources of photochemical pollution.

In terms of examining the response of atmospheric pollutant concentration to perturbations in pollutant emission rate, a number of approaches have been proposed in the past years by using various models [4, 11, 16, 17]. Particularly, a technique named particulate matter source apportionment technology (PSAT) [18] has been implemented in CAMx to provide source apportionment for primary and secondary particulate matter (PM) species according to emission source categories and their geographic locations [19]. This technique is useful for identifying emission sources that significantly contribute to gaseous or PM pollution. For example, Wagstrom et al. [20] used PSAT to investigate the contribution of power plant SO_2 emissions to particulate sulfate concentrations in the Eastern United States, and the results illustrated that PSAT could provide a computationally efficient particulate matter apportionment algorithm to investigate pollutant transport and emission source contributions on regional scales; Koo et al. [21] compared two different methods of investigating relationships between PM concentrations and emission sources and found that PSAT was best at apportioning sulfate, nitrate, and ammonium to sources emitting SO_2, NO_x, and NH_3, respectively. In addition, there are some other methods to examine emission source apportionment [22–24], which used principal component analysis (PCA) and multilinear regression analysis (MLRA) to identify possible sources of particulate matter (PM) and to determine their contribution to air pollution.

In general, many of the previous source apportionment and emission contribution analysis works focused on examining relationship between the total emission amount of a source from a large-scale planning region and its air pollutant concentration [25]. In fact, for air pollution control strategy development, the more practical question is how pollutant concentrations would respond to emission changes within different small-scale areas of a large planning region [2]. The contribution of emission sources within different small-scale areas to regional and urban air quality could be quite different due to different land surface and meteorological conditions. Thus, it is of critical importance to identify the variation of atmospheric concentration to perturbations in emission rates of small-scale areas within a large planning region. The priority regulation of emissions with high contribution variation could result in significantly environmental and cost effectiveness. As an extension of our previous efforts, this study was focused on the establishment and application of the MM5-CAMx-PAST modeling approach for examining air quality variation due to perturbation in emission rates from small-scale areas within a large planning region, and it analyzed the possible affected factors. More accurate results can be obtained with the development of the advanced model simulation. The approach and results can provide sound decision making basis for effective air quality management. A case study for Tangshan, a typical industrial region in China, was presented to illustrate the proposed methodology. The MM5-CAMx was used to provide meteorological inputs and to simulate atmospheric SO_2 concentrations, and PSAT was applied to investigate the emission contribution variations. An air quality modeling domain with a spatial resolution of 9 by 9 km was adopted, and the regional and urban air quality variations due to SO_2 emission rate perturbation of 1000 t/yr within each modeling grid were simulated. Principal component analysis (PCA), canonical correlation analysis (CCA), and Pearson correlation analysis methods were then used to analyze the impacts of meteorological variables and terrain data on the emission source contribution variations.

2. Overview of the Study Area

Tangshan Municipality, located at about 300 km east of Beijing, is the biggest industrial center within Hebei province in northern China. It has a total population of 6.9 million in 2000 and a total area of 13,472 km^2 including 12 districts as shown in Figure 1. The municipality is situated on the alluvial plain formed by the diluvial sediments from the Yan Mountains in the north. Its mean sea level tends to decrease gradually from its northwest to southeast towards the Bohai Bay. It has a temperate continental climate influenced by wet monsoon, and there is an apparent distinction among four seasons, that is, windy and dry spring, hot and wet summer, mild and clear autumn, and cold and dry winter. The annual average temperature is 10–11.20°C, and annual average precipitation is about 600 mm. As one of the biggest industrial centers in northern China, Tangshan Municipality has experienced considerable changes through rapid industrialization and urbanization processes in the past decades. However, its growth has also been associated with a number of environmental concerns. Among them, the deteriorated air quality due to a combination of circumstances (i.e., increased energy consumption, population growth, increased industrial emissions, infrastructure construction/expansion, growth of passenger vehicles, and ineffective pollution control measures) posed significant challenges to the public, governments, and industries. Particularly, SO_2 pollution has been recognized as an important environmental issue.

3. Methodology

3.1. MM5-CAMx-PSAT Modeling. The fifth-generation NCAR/Penn State mesoscale meteorological model (MM5)

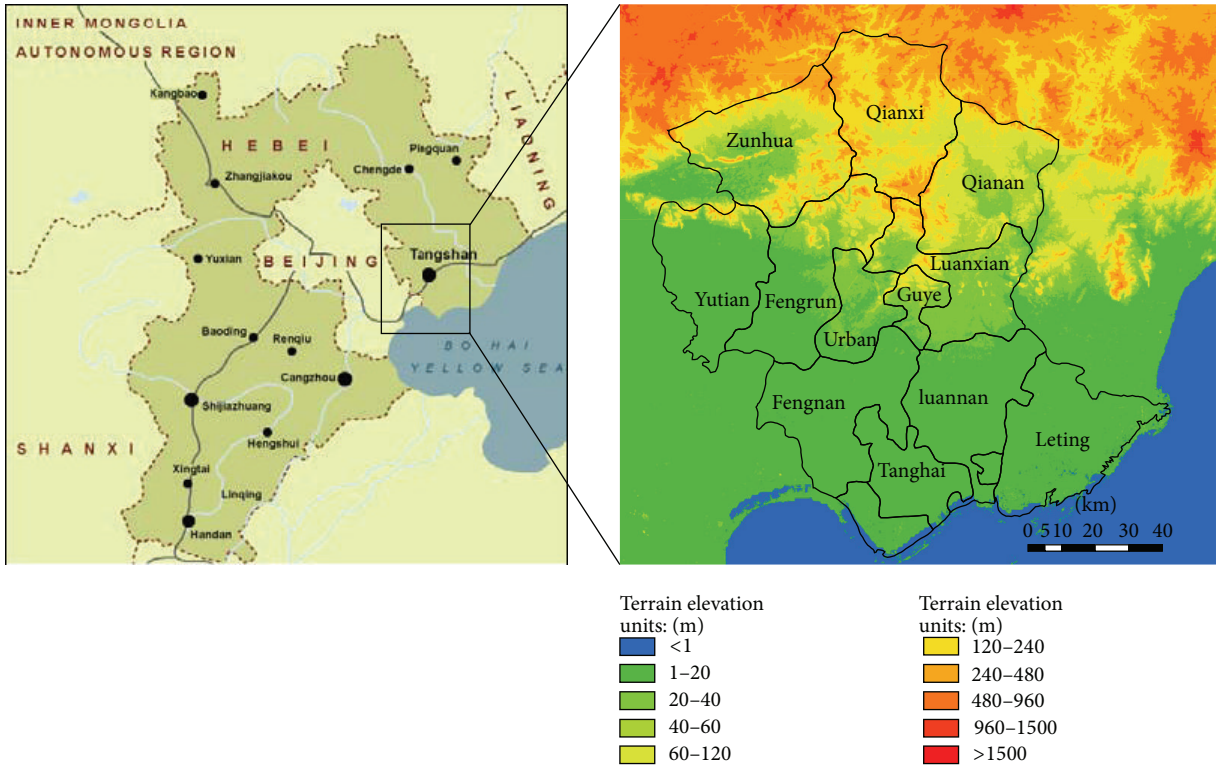

Figure 1: Tangshan Municipality and its surrounding cities.

is a limited-area, nonhydrostatic, terrain-following sigma-coordinate model designed to predict meso- and regional-scale atmospheric circulations [9]. It has been frequently used to provide meteorological inputs for many air quality modeling systems [26]. In this study, MM5 (version 3.7) model was applied and configured using two-level nested modeling domains (112–120°E, 37–43°N) as shown in Figure 2, where domain 1 has a spatial resolution of 27 km by 27 km and has been established with a dimension of 60 × 60 grid cells, and domain 2 has a spatial resolution of 9 by 9 km and has been established with a dimension of 94 × 82 grid cells. Twenty-four full σ levels extending from the ground surface to the top of modeling domain (i.e., 200 hpa) were applied. The 3-D first-guess meteorological fields for modeling were obtained from the Global Tropospheric Analyses datasets provided by the US National Center for Environmental Prediction (NCEP FNL data) and were available with six-hour resolution on a grid of 1°× 1°. The four-dimensional data assimilation (FDDA) was implemented using the meteorological observations from surface (eight times a day) and upper air (two times a day) monitoring stations of the Chinese Meteorological Information Comprehensive Analysis and Process System (MICAPS). The following physical parameters schemes in MM5 were selected, including (a) land-use scheme using five-layer LSM, (b) PBL scheme using medium-range forecasts (MRF), (c) cloud microphysics selecting mixed-phase, (d) cumulus parameterization schemes selecting Grell, and (e) radiation schemes selecting the highly accurate and efficient method (RRTM). The terrain and land-use data were obtained from USGS with a spatial resolution of 30 s.

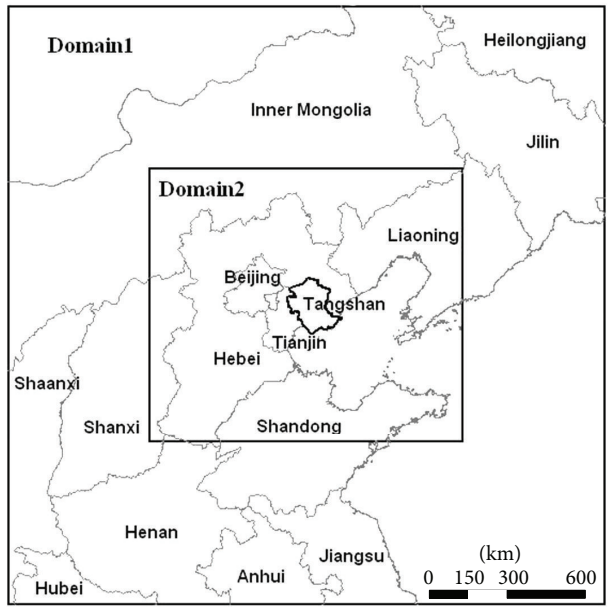

Figure 2: Two-level nested modeling domain for MM5.

The comprehensive air quality model CAMx version 5.1 was used in this study. It is an Eulerian photochemical dispersion model that allows for an integrated assessment of gaseous and particulate air pollutants over many scales ranging from suburban to continental. This model simulates emission, dispersion, chemical reaction, and removal of pollutants in the troposphere by solving the pollutant continuity equation for each chemical species. Its modeling input file formats are compatible with MM5 model. To study the regional emission contributions, the PSAT has been implemented in CAMx to provide SO_2 source apportionment among specific geographic regions and source categories [19]. For the simulation of air quality in Tangshan Municipality, CAMx was configured using one modeling domain which was the same as domain 2 of MM5 (Figure 2). Its physical parameters schemes were selected as follows: (a) two-way interactive grid nesting, (b) 12 vertical layers, (c) gas-phase chemistry using CB05 mechanism which includes 156 reactions formulations, and (d) aerosol chemistry using M4/ISORROPIA. In terms of air pollutant emission inventory, it was provided by Tangshan Environmental Protection Agency. The emission inventories of Tangshan's surrounding regions, including Hebei province, Shanxi province, Beijing, Tianjin, and Inner Mongolia, were obtained from the respective environmental protection administrations. The emission inventory of other regions was obtained from Zhang and Streets [27].

The MM5-CAMx was then used to simulate SO_2 concentrations in Tangshan for four representative months in 2006, including January, April, July, and October. Two scenarios were selected, including simulating the variation of emission contribution from emission rate perturbation in each modeling grid (9×9 km scale) to both regional and urban air quality, represented by the monthly average SO_2 concentration of the entire Tangshan region (i.e., large-scale receptor 1) and only its urban area (i.e., small-scale receptor 2) (Figure 3), respectively. The modeling procedures include (1) using MM5-CMAx to predict the temporal and spatial distributions of SO_2 concentrations within Tangshan Municipality based on its actual emissions in 2006 (i.e., base emission inventory), and the monthly average SO_2 concentrations within receptors 1 and 2 were then calculated based on the simulated hourly concentrations, respectively; (2) identifying the contribution variation of each modeling grid to the monthly average SO_2 concentrations through adding 1000 t/yr of SO_2 emission (i.e., an arbitrarily selected number) to each grid in addition to the base emission inventory, and the MM5-CMAx was used to predict the temporal and spatial distributions of SO_2 concentrations within Tangshan Municipality based on the new emission inventory (base emission inventory plus 1000 t/yr in a certain grid), and then the monthly average SO_2 concentrations within receptors 1 and 2 were calculated, respectively. The difference between the monthly average SO_2 concentrations calculated using base inventory and new inventory is regarded as the emission source contribution variation of that grid.

3.2. Multivariate Analysis. The multivariate analysis methods, including PCA and CCA, were used to analyze the impacts of meteorological variables and terrain data on the simulated variation of emission contribution to regional and urban air quality. PCA maximizes the correlation between the original total variance to form new variables that are mutually orthogonal, or uncorrelated. The CCA application was run to investigate possible relationship between these two data sets, especially to establish the maximum correlation among sets of variables. The objective of PCA was to obtain a small number of components that would explain most (i.e., typically above 60%) of the total variation [28]. In this study, the hourly data of six meteorological variables within MM5, including PBL height (PBLH), temperature at 2 m above ground (T2), wind speed at 10 m above ground (WS10), wind direction at 10 m above ground (WD), sea level pressure (PSLV), and relative humidity (RH), were selected to analyze the principal components of meteorological variables within four representative months in 2006. The objective of CCA was then to investigate possible relationship between the six selected meteorological variables as well as terrain data and the contribution variation of emission within each modeling grid [29].

4. Results and Discussions

4.1. Modeling Performance. The performance of the MM5-CAMx was evaluated using scatter plots [30]. The ground-based SO_2 observation results from three air quality monitoring stations located within Tangshan urban ("Urban" is showed in Figure 1) were averaged and were then compared with the predicted daily SO_2 concentration of the Tangshan urban area in the four selected months in 2006. Figure 4 displays the comparison results. The $y = x$ line on the scatter plots represents perfect agreement between the two data sets. A pair value above the $y = x$ line indicates a situation of overprediction, while the pair value below the line indicates underprediction. In general, Figure 4 shows that most of the scatter plots are adjacently distributed on both sides of $y = x$ line, which does highlight a consistent over- and underprediction for SO_2 concentration using the modeling system. Considering the inherent uncertain nature associated with meteorological parameters and air quality prediction, this fluctuation still indicates that the accuracy of model prediction is reasonable. In fact, the correlation coefficients between simulated and observed data were calculated as 0.781, 0.621, 0.690, and 0.801 for January, April, July, and October, respectively. Thus the performance of the coupled modeling system is satisfactory and acceptable [4].

4.2. Simulated SO_2 Concentration Distribution Using Base Emission Inventory. In the year of 2006, Tangshan Municipality had a total of 598 industrial establishments, including electrical, metallurgical, mining, chemical, construction materials, and textile industries. Spatial distributions and emission rates of SO_2 from these sources were investigated and shown in Figure 5(a). The hourly SO_2 concentrations in January 2006 in the entire Tangshan region were simulated using MM5-CAMx, and their corresponding monthly averages were then calculated. Figure 5(b) displays the simulated

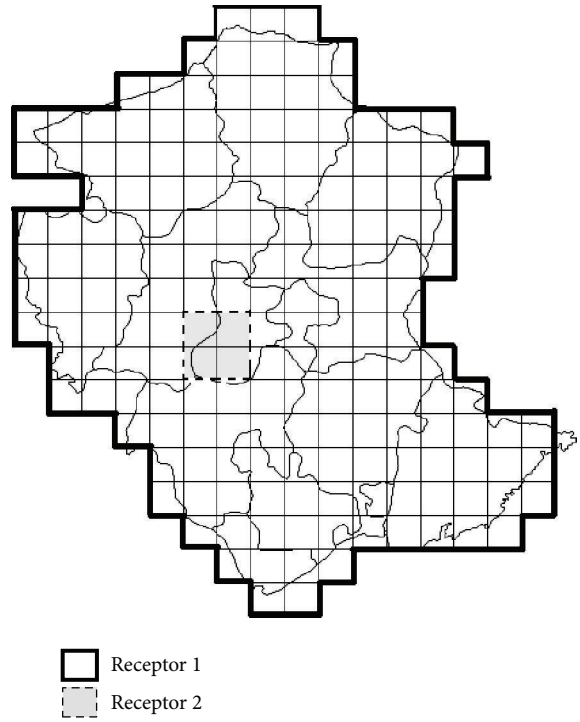

Figure 3: Schematic of modeling scenarios showing receptors 1 and 2.

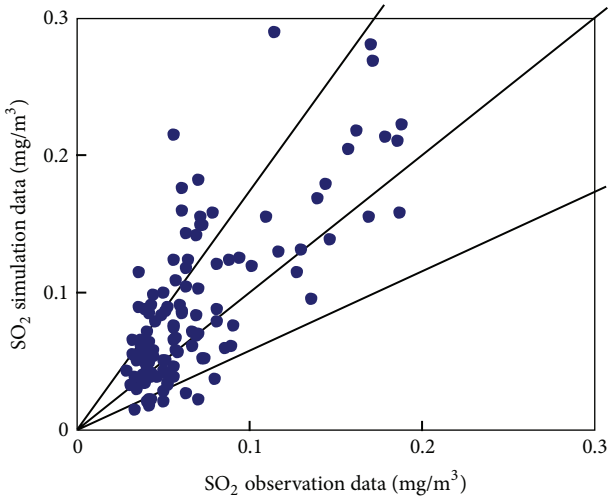

Figure 4: Comparison between observed and predicted SO_2 concentrations (daily average value of January, April, July, and October 2006).

SO_2 concentration in Tangshan region in January 2006, and it illustrates that SO_2 pollutions occurred in most areas of Tangshan region due to pollutant emissions and unfavorable meteorological conditions. In general, the air quality in Tangshan region was not satisfactory, and the municipal government and industries need to take actions to improve such situation. For cost-effective air quality management in Tangshan, the identification of the variation of emission source contribution to the regional and urban air quality due to emission perturbation in each small-scale emission area is of fundamental importance. Such information could provide sound basis for identifying emission areas requiring priority regulation.

4.3. Variation of Seasonal Emission Source Contribution to Regional Air Quality. The variation of emission contribution to the receptor 1 (shown in Figure 3) air quality due to SO_2 emission perturbation of 1000 t/yr of each modeling grid was calculated at first for the four representative months in 2006 using the MM5-CAMx-PSAT. Then, the corresponding monthly arithmetic averages were plotted using Geographic Information System (GIS) interpolation method. Figure 6 presents the spatial distribution of the variation of emission contribution to regional monthly SO_2 concentration in Tangshan. It is observed from Figure 6(a) that emissions in the junction of Yutian and Zunhua Counties had the maximum variation of emission contribution to air pollution in receptor 1, with more than 52 $\mu g/m^3$ of variation per 1000 t/yr of SO_2 emission per 9 × 9 km modeling grid in January, while emissions from the coastal areas of the southeast of Tangshan had the minimum variation of emission contribution (i.e., less than 35 $\mu g/m^3$ of variation per 1000 t/yr of SO_2 emission per modeling grid of 9 × 9 km). It can also be found that the grid-based variation of emission contribution to SO_2 pollution tended to gradually decrease from the northwest to southeast of Tangshan Municipality in January. In April, as shown in Figure 6(b), emissions from the southeast of Qianan County and the southern coastal areas of Tangshan displayed the maximum variations of contribution to SO_2 pollution in receptor 1, with more than 13.9 $\mu g/m^3$ of contribution variation per 1000 t/yr of SO_2 emission per grid. Meanwhile, emissions from the eastern area of Leting and northern part of Qianxi County showed minimum contribution variations. In terms of July, as shown in Figure 6(c), emissions from the coastal areas of Tangshan made the largest contribution variations (i.e., greater than 14.6 $\mu g/m^3$ of variation per 1000 t/yr of SO_2 emission per grid), while the spatial distribution of emission contribution variations showed several local high-value points, and the minimum contribution variation occurred in Qianxi County. It is shown in Figure 6(d) that the variation of emission contributions to the average SO_2 concentration in receptor 1 in October displayed a relatively even distribution, tending to gradually decrease from the high-value area of Yutian County (i.e., with contribution variation of greater than 26.0 $\mu g/m^3$) to the east and southeast of Tangshan. Consequently, the simulation results indicate that the largest variations of emission contribution to air pollution occurred in January, and the contribution variation distribution displayed an apparent seasonal difference. This is due to the fact that Tangshan has the temperate continental climate, and different meteorological conditions among four seasons would cause such seasonal differences.

4.4. Impacts of Meteorological Factors on Emission Source Contribution Variation. PCA was used to identify the principal

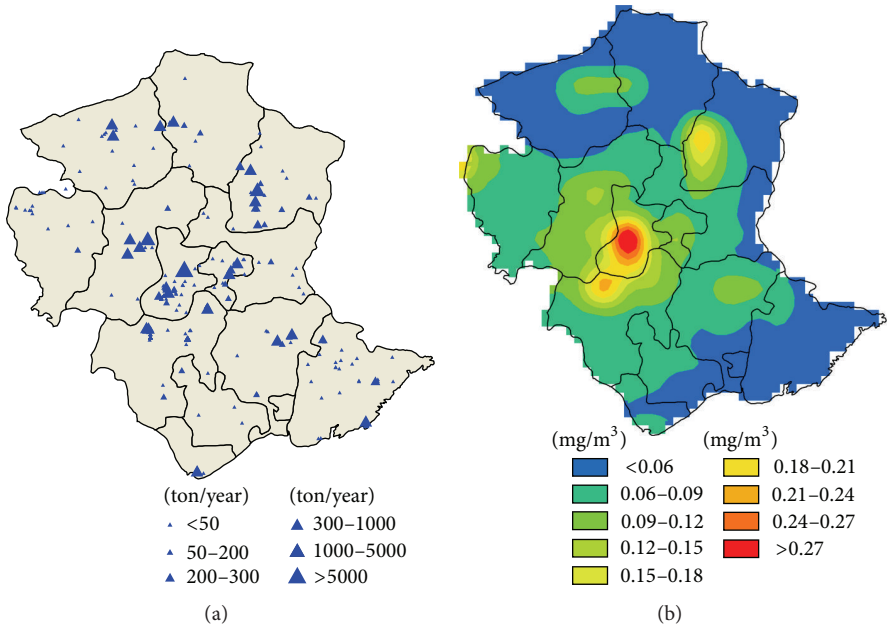

Figure 5: Annual emission rate of SO_2 and simulated monthly SO_2 concentration in January 2006: (a) emission rate; (b) concentration distribution.

components from six meteorological variables in Tangshan. Table 1 lists the PCA results for January, April, July, and October 2006, respectively, and the eigenvalues of PCA for the meteorological variables are also presented. It is found from Table 1 that examination of 30-day data for each modeling grid in January led to three principal components accounting for 81.8% of the total variance. Using the values of the respective principal component loadings presented in Table 1, there is a reasonable interpretation for these components. Only loadings with absolute values greater than 50% were selected for PC interpretation [31]. The first PC was PBL height (with component loadings of −0.503), and the second PCs showed that a main source of variation was wind speed (with component loadings of 0.529) and temperature (with component loadings of 0.598), while the third PC was wind direction (with component loadings of 0.801). Thus, the PCA results for January indicated low PBL height and prevalent northwest winds as well as inversion weather. These meteorological conditions could result in higher atmospheric stability in surface layer in Tangshan which then facilitated the accumulation of pollutants near the ground, leading to the highest variation of emission contributions to regional air quality from the modeling grids as compared to other months (Figure 6(a)). In terms of meteorological conditions in April, Table 1 illustrates that the first PCs were PBL height (with component loadings of 0.574) and relative humidity (with component loadings of −0.515). The second PCs were temperature (with component loadings of 0.715) and sea level pressure (with component loadings of −0.603), while the third PC was wind speed (with component loadings of 0.723). The PCA results for April indicate a dry spring with high PBLH, high temperature, low sea level pressure, and strong wind, and such meteorological conditions were conducive for dispersion of pollutants, leading to relatively low variation of emission contribution to regional air quality from modeling grids (Figure 6(b)). For meteorological conditions in July, the PCA results illustrate that the first PCs were PBL height (with component loadings of 0.603) and relative humidity (with component loadings of 0.549), and the second PC was wind direction (with component loadings of −0.698), while the third PC was wind speed (with component loadings of −0.832). The PCA results indicate a wet and rainy summer with high PBL height and prevalent southeast winds influenced by the maritime climate. Such meteorological conditions would help disperse and reduce pollutant concentrations, leading to minimum variation of emission contribution to regional air quality in July as compared to other months (Figure 6(c)). For October, the PCA results showed a mild and clear autumn, with first PCs being the temperature (with component loading of 0.52) and sea level pressure (with component loading of −0.576), the second PCs being PBLH (with component loading of 0.684) and wind speed (with component loading of 0.649), and the third PC being relative humidity (with component loading of −0.696). These values illustrate that the temperature in autumn was slightly higher than that in spring, wind was not stronger than that in spring, and the prevalently northwest wind was influenced by the invasion of cold air. Due to the impact of such meteorological conditions, the variation of emission contribution to regional air quality in October from modeling grids was between the minimum and maximum (Figure 6(d)).

Results of CCA between grid-based variation of emission contribution to regional air quality and meteorology-terrain data in Tangshan are presented in Table 2. In this study, there was only one canonical variable (CV). The correlations of

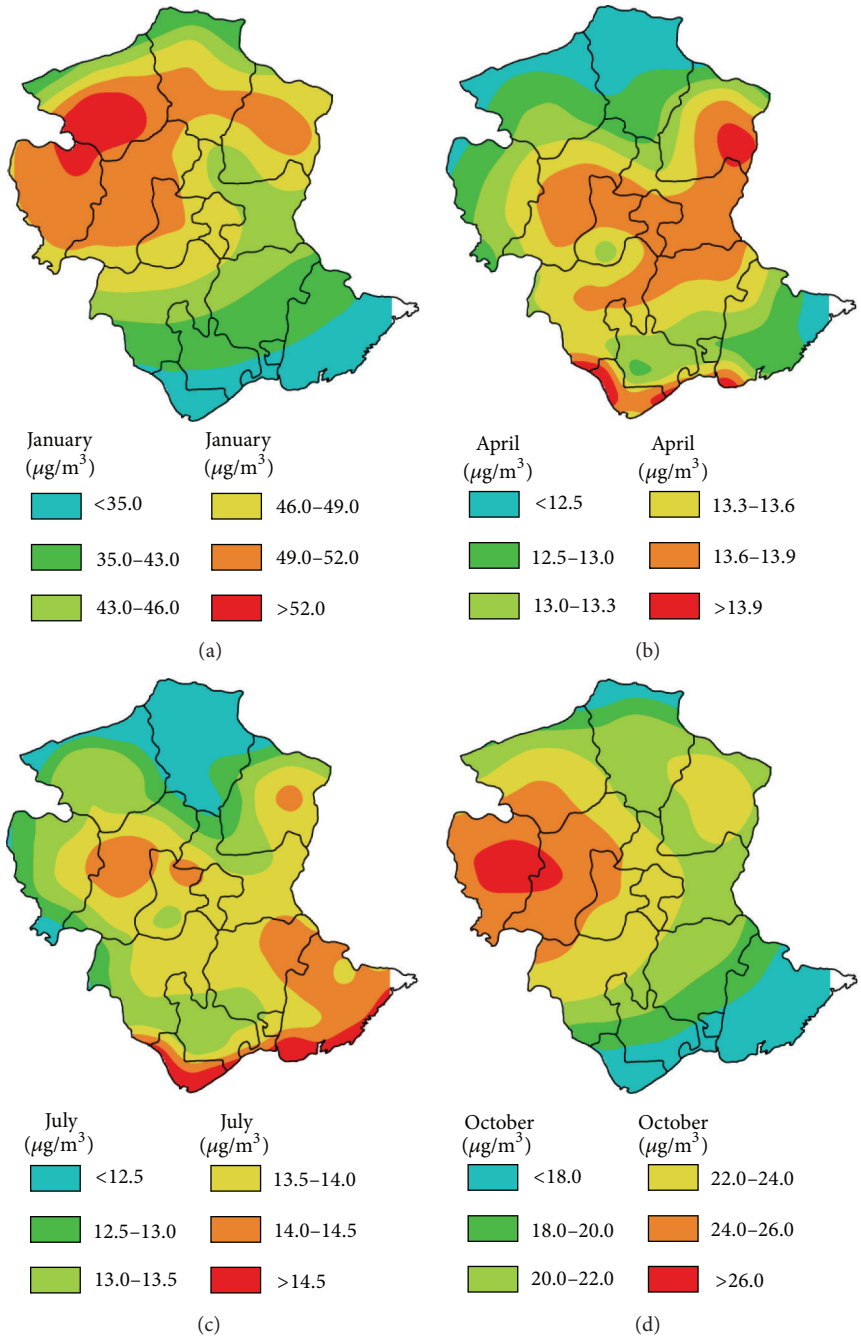

FIGURE 6: Simulated monthly average emission contribution response to regional average SO_2 concentration (i.e., receptor 1) due to SO_2 emission perturbation of 1000 t/yr.

CV1 were 0.781, 0.748, 0.725, and 0.807 for the four selected months, respectively, and all CCAs passed the statistical test of significance. According to the variable loading values shown in Table 2, the main meteorological variables were PBL height and wind speed in January which showed a negative correlation with grid-based variation of emission contribution to air quality in receptor 1. Pearson correlation analysis also gave the same results as CCA. Figure 7 presents the monthly average PBLH and WS10 in January, and the contours exhibit negative correlation with Figure 6(a). This indicates that high variation of emission contribution was related to low PBL height and low wind speed conditions. It is found from Table 2 that the variable loading values for April and October gave similar results for January. However, CCA and Pearson correlation analysis gave different results for July. The CCA results showed that relative humidity was associated

Table 1: PCA results for meteorological variables in four selected months in 2006.

PC	Eigenvalue	Proportion variance	Cumulative proportion	Variable	Principal component loadings			
					PC1	PC2	PC3	PC4
(a) January								
PC1	1.492	0.371	0.371	PBLH	−0.503	0.421	−0.209	0.000
PC2	1.279	0.273	0.644	T2m	0.326	0.598	0.000	−0.26
PC3	1.022	0.174	0.818	WS10	−0.411	0.529	−0.132	0.28
PC4	0.772	0.099	0.918	PSLV	−0.391	−0.405	−0.488	0.21
PC5	0.554	0.051	0.969	RH	0.479	0.147	−0.244	0.799
PC6	0.433	0.031	1.000	WD	−0.297	0.000	0.801	0.412
(b) April								
PC1	1.516	0.383	0.383	PBLH	0.574	0.207	−0.143	0.000
PC2	1.280	0.273	0.656	T2m	−0.106	0.715	−0.215	0.000
PC3	0.982	0.161	0.817	WS10	0.318	0.171	0.723	−0.56
PC4	0.813	0.110	0.927	PSLV	0.294	−0.603	−0.305	−0.23
PC5	0.523	0.046	0.973	RH	−0.515	−0.22	0.453	0.227
PC6	0.405	0.027	1.000	WD	0.455	0.000	0.336	0.758
(c) July								
PC1	1.435	0.343	0.343	PBLH	0.603	−0.242	0.000	−0.141
PC2	1.182	0.233	0.576	T2m	0.484	0.337	−0.207	−0.465
PC3	1.056	0.186	0.762	WS10	−0.137	−0.171	−0.832	−0.33
PC4	0.785	0.103	0.865	PSLV	−0.279	−0.497	0.404	−0.71
PC5	0.729	0.089	0.953	RH	0.549	0.255	−0.188	0.000
PC6	0.529	0.047	1.000	WD	0.000	−0.698	−0.257	0.381
(d) October								
PC1	1.535	0.392	0.392	PBLH	−0.134	0.684	−0.127	0.000
PC2	1.324	0.292	0.685	T2m	0.52	0.301	0.397	0.000
PC3	0.951	0.151	0.835	WS10	−0.226	0.649	−0.132	0.000
PC4	0.785	0.103	0.938	PSLV	−0.576	−0.138	−0.352	−0.13
PC5	0.498	0.041	0.979	RH	0.376	0.000	−0.696	0.607
PC6	0.351	0.021	1.000	WD	−0.433	0.000	0.448	0.781

with the second highest absolute loading value (i.e., −0.715) which indicated an obvious negative correlation between humidity and grid-based variation of emission contribution. However, the Pearson correlation value for RH was just −0.066. Since it is widely recognized that wet deposition has the function of removing pollutant, the results of CCA seemed more reasonable to find the relationship between more than two variables. The terrain data did not show obvious correlation with grid-based emission contribution variation through CCA and Pearson correlation analysis. This can be explained by the fact that most areas of Tangshan are flat although it is located in the alluvial plains of the Yanshan Mountains, with higher elevation in the northwestern part and lower elevation in the southeastern region.

4.5. Variation of Annual Emission Contribution to Regional Air Quality. The modeling results (Figure 6) indicated significant seasonal change of emission contribution variation for each modeling grid due to the impacts of many meteorological factors such as PBL height and wind speed. Thus, a parameter of emission contribution variation ratio was introduced in this study for investigating the variation of annual average emission contribution to regional air quality for the convenience of air quality management. The calculation of emission contribution variation ratio is as follows:

$$R_i = \frac{1}{4}\left|\sum \frac{C_{i,j}}{\sum_{i=1}^{n} C_{i,j}}\right|, \quad (1)$$

where $C_{i,j}$ is the variation of emission contribution to the monthly average SO_2 concentration of the receptor area in month j (i.e., January, April, July, and October) per 1000 t/yr of emission rate change in grid i ($\mu g/m^3$); R_i is the annual average emission contribution variation ratio of grid i due to 1000 t/yr of emission rate change; n is the total number of modeling grids. Figure 8(a) presents the annual emission contribution variation ratio of each grid to average SO_2 concentration in receptor 1 in 2006. It is found that the northwestern part of Tangshan such as the junction area of Yutian and Fengrun Counties had the maximum emission contribution variation ratio (i.e., greater than 0.36%) to the air quality of receptor 1, indicating that the regional air quality was more sensitive to the emissions from the northwestern part of Tangshan. The contribution variation ratio tended to decrease towards the north and southeast of Tangshan, while

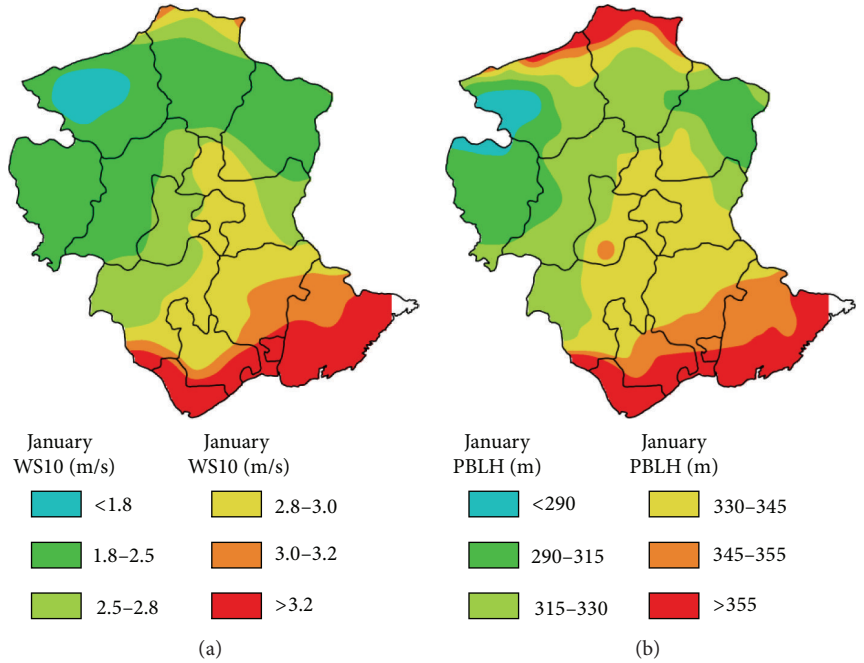

Figure 7: Monthly average wind speed at 10 m above ground (WS10) (a) and planetary boundary layer height (PBLH) (b) in January 2006.

Table 2: Results of CCA between grid-based variation of emission contribution to air quality in receptor 1 and meteorological/terrain data in Tangshan, 2006.

	(a) January			(b) April	
CV	Correlation	Pearson	CV	Correlation	Pearson
CV1	0.781	Correlation	CV1	0.748	Correlation
Variable	Loadings		Variable	Loadings	
Contribution	0.987	1.000	Contribution	0.987	1.000
PBLH	−0.439	−0.677	PBLH	−0.639	−0.483
T2m	−0.062	−0.163	T2m	−0.387	−0.188
WS10	−0.626	−0.746	WS10	−0.672	−0.588
TERRAIN	0.009	0.041	TERRAIN	−0.039	0.242
PSLV	0.061	−0.002	PSLV	−0.038	0.205
RH	−0.160	0.094	RH	−0.479	0.221
WD	−0.069	−0.150	WD	−0.011	−0.243
	(c) July			(d) October	
CV	Correlation	Pearson	CV	Correlation	Pearson
CV1	0.725	Correlation	CV1	0.807	Correlation
Variable	Loadings		Variable	Loadings	
Contribution	0.987	1.000	Contribution	0.987	1.000
PBLH	−0.989	−0.416	PBLH	−0.434	−0.724
T2m	−0.061	−0.167	T2m	−0.088	−0.113
WS10	−0.502	−0.347	WS10	−0.591	−0.729
TERRAIN	−0.005	0.346	TERRAIN	−0.003	0.045
PSLV	−0.050	0.029	PSLV	0.010	−0.001
RH	−0.715	−0.066	RH	−0.120	0.029
WD	0.091	−0.086	WD	0.010	−0.035

some local higher values occurred within Qianan County. The lowest emission contribution variation ratio (i.e., less than 0.3%) occurred in the coastal areas of Tangshan and the northern part of Qianxi County, implying that the regional air quality was less sensitive to the emissions from these areas. As a result, in order to improve regional air quality, the industries (Figure 5(a)) located within the more sensitive areas (i.e., northwestern part of Tangshan) should reduce their emissions or be relocated to the less sensitive areas such as the coastal area of Tangshan Municipality.

As described earlier, CCA indicated that a negative correlation existed between wind speed and grid-based emission contribution variation. This can be proved from another perspective. The data from three state-controlled weather stations located in Zunhua (northwestern area), Tangshan urban (center area), and Leting (southeastern area) (Figure 1) were used for meteorological factor analysis. The monthly average wind speed and calm frequency were previously identified as the main meteorological factors affecting air pollution [25] and thus were used for analysis in this study. Table 3 lists the average wind speed and calm frequency of the four representative months in 2006. Previous studies suggested that the greater the wind speed and the smaller the calm frequency, the more beneficial for pollutant dispersion. It can be observed from Table 3 that the ranking of monthly and yearly average wind speed from large to small is Leting, Tangshan urban, and Zunhua. This would indicate that the dispersion capability of pollutants gradually decreases from the coast (i.e., Leting) to inland area (i.e., Zunhua), leading to gradually increased emission contribution variation from the coastal area to inland area as shown in Figure 8(a). However, the order of calm frequency for the three selected areas does not hold the same as that of average wind speed. Although the calm frequency in Zunhua area was higher than that in other two areas in all seasons which was less conducive to the dispersion of pollutants, the calm frequencies in Tanghan urban area in April and July were significantly lower than those in Leting, which could give a good explanation for the local low emission contribution variation values shown in the center area of Tangshan in Figures 6(b) and 6(c). In addition, Figure 8(a) not only displays the annual average emission contribution variation ratios of the modeling grids to air quality in the entire Tangshan region, but also gives a visual representation of the dominant wind direction. It is found from Figure 8(a) that the east-west direction modeling grids had higher contribution variation ratios than north-south direction girds, implying that east-west was the dominant wind direction in Tangshan Municipality.

4.6. Variation of Annual Emission Contribution to Urban Air Quality. Air quality control within a smaller area than regional scale is usually important and more practical in urban environmental management. In this study, the urban area of Tangshan was selected as a control area (i.e., receptor 2), and the grid-based variation of emission contribution to the average air quality of receptor 2 was then simulated using MM5-CAMx-PSAT. Figure 8(b) shows the distribution of grid-based annual emission contribution variation ratio.

Table 3: Wind speed and calm wind frequency in Tangshan in 2006.

Area	Month	Wind speed (m/s)	Calm frequency (%)
Zunhua	January	1.49	5.71
	April	2.61	3.00
	July	1.66	4.12
	October	1.43	11.07
	Annual	1.80	6.01
Tangshan urban	January	1.91	1.22
	April	2.63	0.43
	July	1.91	0.82
	October	1.77	7.79
	Annual	2.06	2.59
Leting	January	2.09	3.67
	April	3.03	2.14
	July	2.08	1.23
	October	1.86	4.51
	Annual	2.27	2.90

It is found that the grids with largest contribution variation ratios were receptor 2 itself (with contribution variation ratio of greater than 10.0%), and the second were the grids mainly surrounding receptor 2. Figure 8(b) also reveals that emission contribution variation ratio had correlation with the distance between emission grids and the receptor area. The east-west modeling grids around receptor 2 had slightly higher emission contribution variation ratio than the north-south grids. This could be explained by the fact that east and west winds were the main wind directions in the study area as observed from the monitoring data in 2006. The contribution variation ratios of the remaining parts of Tangshan Municipality were very small, with minimum contribution variation ratios occurring in the coastal areas and northern parts of Tangshan (i.e., less than 0.2%). The results indicated that the receptor itself as emission grids had significant contribution to the urban air quality. The obtained emission contribution variation analysis results are of practical importance for air quality management. For example, to improve the urban air quality in Tangshan, the industries (Figure 5(a)) within the more sensitive areas (i.e., Tangshan urban, Fengrun, and Fengnan) should be relocated to the less sensitive areas (i.e., coastal area of Tangshan), and the new industrial projects with SO_2 emissions such as power plants should also be located within the less sensitive coastal areas.

5. Conclusions

A modeling grid-based emission contribution analysis approach was proposed to identify emission areas with higher response of regional and urban air quality change due to emission rate perturbation. This approach relied on a coupled MM5-CAMx where MM5 was used to provide meteorological inputs for the air quality model CAMx, while CAMx was used to predict air pollutant concentration distributions. The particulate matter source apportioning

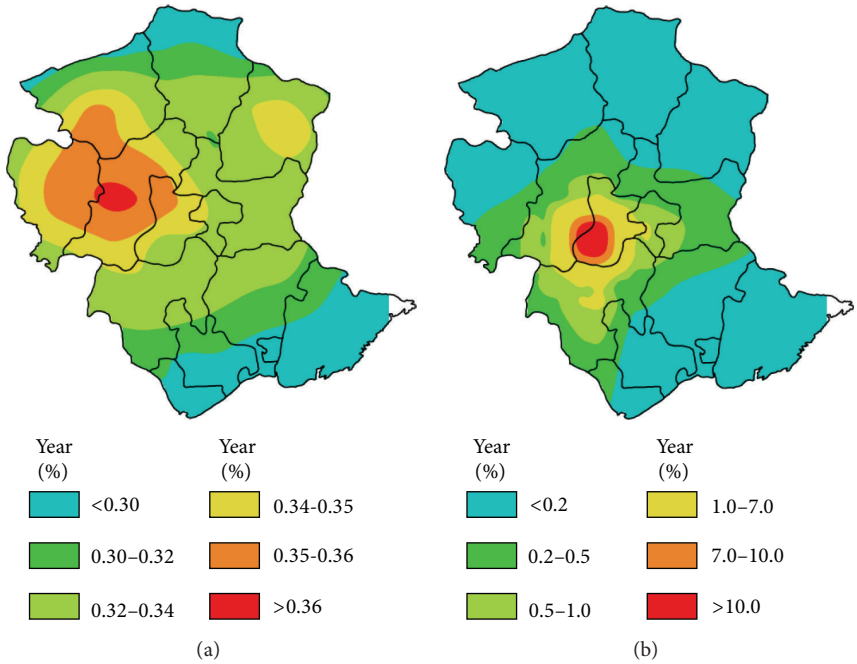

Figure 8: Distribution of annual average emission contribution variation ratio of modeling grids to air quality in (a) receptor 1 and (b) receptor 2.

technology (PSAT) within CAMx was used to calculate the variation of emission contribution to air quality from emission rate perturbation within each modeling grid. The method was applied to a case study in Tangshan Municipality in northern China. The MM5-CMAx was implemented to predict hourly SO_2 concentrations based on the base emission inventory of SO_2 in 2006 with modeling grid scale of 9×9 km, and the impact of emission perturbation in each modeling grid to atmospheric SO_2 concentrations was calculated by using PSAT technology through adding 1000 t/yr of SO_2 emission to the grid in addition to the base emission inventory. The variation of emission contribution to regional air quality from each modeling grid per 1000 t/yr of emission rate change was obtained for four representative months (January, April, July, and October) in 2006. PCA and CCA were conducted to examine the impacts of meteorological factors on the variation of emission source contribution, and the results indicated that there was an obvious negative correlation between emission contribution variation and planetary boundary layer height (PBLH) as well as wind speed. The analysis of the variation of emission contribution to annual regional SO_2 concentration (i.e., larger scale) indicated that the northwestern part of Tangshan was the most sensitive area with emission contribution variation ratio of more than 0.36%, while the southern coastal area had the lowest contribution variation ratio of less than 0.30%. The proposed method was also applied to analyze the variation of emission contribution to the SO_2 pollution in the urban area in Tangshan (i.e., at a smaller scale), and it was found that the largest contribution grids were the urban area itself (with contribution variation ratio of greater than 10.0%), and the minimum contribution variation ratios (i.e., less than 0.2%) occurred in the coastal areas and northern parts of Tangshan. Based on the modeling results, the emission sources within the areas with higher contribution variation ratios should be regulated with priority or relocated to other areas with lower contribution variation ratios such as the coastal areas in Tangshan. In summary, the proposed methodology can be applied to address many other regional and urban air pollution problems, and the results would provide sound scientific basis for effective air quality management.

Acknowledgments

This research was supported by the Natural Sciences Foundation of China (no. 51038001) and the Ministry of Environmental Protection Special Funds for Scientific Research on Public Causes (no. 201209003). The authors would like to thank Natural Science Foundation of Beijing (no. 8092004), Beijing NOVA Program of China (no. 2009B07), Innovation Team Project of Beijing Municipal Education Commission (PHR201007105), and the Cultivation Fund of the Key Scientific and Technical Innovation Project, Ministry of Education of China (708017), for supporting this work.

References

[1] D. S. Chen, S. Y. Cheng, L. Liu, T. Chen, and X. R. Guo, "An integrated MM5—CMAQ modeling approach for assessing trans-boundary PM_{10} contribution to the host city of 2008 Olympic summer games—Beijing, China," *Atmospheric Environment*, vol. 41, no. 6, pp. 1237–1250, 2007.

[2] D. S. Cohan, A. Hakami, Y. Hu, and A. G. Russell, "Nonlinear response of ozone to emissions: source apportionment and sensitivity analysis," *Environmental Science and Technology*, vol. 39, no. 17, pp. 6739–6748, 2005.

[3] F. Wang, D. S. Chen, S. Y. Cheng, and M. J. Li, "Impacts of air pollutant transport based on air trajectory clustering," *Research of Environmental Sciences*, vol. 22, no. 6, pp. 637–642, 2009 (Chinese).

[4] S. Cheng, D. Chen, J. Li, X. Guo, and H. Wang, "An ARPS-CMAQ modeling approach for assessing the atmospheric assimilative capacity of the Beijing metropolitan region," *Water, Air, and Soil Pollution*, vol. 181, no. 1–4, pp. 211–224, 2007.

[5] S. M. Lee, H. J. S. Fernando, and S. Grossman-Clarke, "MM5-SMOKE-CMAQ as a modeling tool for 8-h ozone regulatory enforcement: application to the state of Arizona," *Environmental Modeling and Assessment*, vol. 12, no. 1, pp. 63–74, 2007.

[6] Y. Zhou, S. Y. Cheng, L. Liu, and D. S. Chen, "A Coupled MM5-CMAQ modeling system for assessing effects of restriction measures on PM_{10} pollution in Olympic city of Beijing, China," *Journal of Environmental Informatics*, vol. 19, no. 2, pp. 120–127, 2012.

[7] E. Angelino, M. Bedogni, C. Carnevale et al., "PM_{10} chemical model simulations over Northern Italy in the framework of the citydelta exercise," *Environmental Modeling and Assessment*, vol. 13, no. 3, pp. 401–413, 2008.

[8] U. Nopmongcol, B. Koo, E. Tai et al., "Modeling Europe with CAMx for the air quality model evaluation international initiative (AQMEII)," *Atmospheric Environment*, vol. 53, no. 7, pp. 177–185, 2012.

[9] J. Dudhia, D. Gill, K. Manning, W. Wang, and C. Bruyere, *PSU/NCAR Mesoscale Modeling System Tutorial Class Notes and User's Guide: MM5 Modeling System Version 3*, National Center for Atmospheric Research, 2004.

[10] X. Tie, S. Madronich, G. Li et al., "Characterizations of chemical oxidants in Mexico City: a regional chemical dynamical model (WRF-Chem) study," *Atmospheric Environment*, vol. 41, no. 9, pp. 1989–2008, 2007.

[11] S. Cheng, D. Chen, J. Li, H. Wang, and X. Guo, "The assessment of emission-source contributions to air quality by using a coupled MM5-ARPS-CMAQ modeling system: a case study in the Beijing metropolitan region, China," *Environmental Modelling and Software*, vol. 22, no. 11, pp. 1601–1616, 2007.

[12] M. Titov, A. P. Sturman, and P. Zawar-Reza, "Application of MM5 and CAMx4 to local scale dispersion of particulate matter for the city of Christchurch, New Zealand," *Atmospheric Environment*, vol. 41, no. 2, pp. 327–338, 2007.

[13] S. M. Lee, M. Princevac, S. Mitsutomi, and J. Cassmassi, "MM5 simulations for air quality modeling: an application to a coastal area with complex terrain," *Atmospheric Environment*, vol. 43, no. 2, pp. 447–457, 2009.

[14] H. Shimadera, A. Kondo, A. Kaga, K. L. Shrestha, and Y. Inoue, "Contribution of transboundary air pollution to ionic concentrations in fog in the Kinki Region of Japan," *Atmospheric Environment*, vol. 43, no. 37, pp. 5894–5907, 2009.

[15] C. Borrego, A. Monteiro, J. Ferreira et al., "Modelling the photochemical pollution over the metropolitan area of Porto Alegre, Brazil," *Atmospheric Environment*, vol. 44, no. 3, pp. 370–380, 2010.

[16] D. G. Streets, J. S. Fu, C. J. Jang et al., "Air quality during the 2008 Beijing Olympic Games," *Atmospheric Environment*, vol. 41, no. 3, pp. 480–492, 2007.

[17] Y. Zhou, S. Y. Cheng, J. B. Li, J. L. Lang, L. Li, and D. S. Chen, "A new statistical modeling and optimization framework for establishing high-resolution PM_{10} emission inventory—II. Integrated air quality simulation and optimization for performance improvement," *Atmospheric Environment*, vol. 60, pp. 623–631, 2012.

[18] Q. Huang, S. Y. Cheng, J. B. Li, D. S. Chen, H. Y. Wang, and X. R. Guo, "Assessment of PM_{10} emission sources for priority regulation in urban air quality management using a new coupled MM5-CAMx-PSAT modeling approach," *Environmental Engineering Science*, vol. 29, no. 5, pp. 343–349, 2012.

[19] A. M. Dunker, G. Yarwood, J. P. Ortmann, and G. M. Wilson, "Comparison of source apportionment and source sensitivity of ozone in a three-dimensional air quality model," *Environmental Science and Technology*, vol. 36, no. 13, pp. 2953–2964, 2002.

[20] K. M. Wagstrom, S. N. Pandis, G. Yarwood, G. M. Wilson, and R. E. Morris, "Development and application of a computationally efficient particulate matter apportionment algorithm in a three-dimensional chemical transport model," *Atmospheric Environment*, vol. 42, no. 22, pp. 5650–5659, 2008.

[21] B. Koo, G. M. Wilson, R. E. Morris, A. M. Dunker, and G. Yarwood, "Comparison of source apportionment and sensitivity analysis in a particulate matter air quality model," *Environmental Science and Technology*, vol. 43, no. 17, pp. 6669–6675, 2009.

[22] S. M. Almeida, C. A. Pio, M. C. Freitas, M. A. Reis, and M. A. Trancoso, "Source apportionment of fine and coarse particulate matter in a sub-urban area at the Western European Coast," *Atmospheric Environment*, vol. 39, no. 17, pp. 3127–3138, 2005.

[23] S. S. Park and Y. J. Kim, "Source contributions to fine particulate matter in an urban atmosphere," *Chemosphere*, vol. 59, no. 2, pp. 217–226, 2005.

[24] A. Srivastava, S. Gupta, and V. K. Jain, "Source apportionment of total suspended particulate matter in coarse and fine size ranges over Delhi," *Aerosol and Air Quality Research*, vol. 8, no. 2, pp. 188–200, 2008.

[25] Z. H. Chen, S. Y. Cheng, J. B. Li, X. R. Guo, W. H. Wang, and D. S. Chen, "Relationship between atmospheric pollution processes and synoptic pressure patterns in northern China," *Atmospheric Environment*, vol. 42, no. 24, pp. 6078–6087, 2008.

[26] F. Wang, D. S. Chen, S. Y. Cheng, J. B. Li, M. J. Li, and Z. H. Ren, "Identification of regional atmospheric PM_{10} transport pathways using HYSPLIT, MM5-CMAQ and synoptic pressure pattern analysis," *Environmental Modelling and Software*, vol. 25, no. 8, pp. 927–934, 2010.

[27] Q. Zhang and D. G. Streets, "2006 Asia Emissions for INTEX-B," December 2009, http://www.cgrer.uiowa.edu/EMISSION_DATA_new/index_16.html.

[28] M. Viana, X. Querol, A. Alastuey, J. I. Gil, and M. Menéndez, "Identification of PM sources by principal component analysis (PCA) coupled with wind direction data," *Chemosphere*, vol. 65, no. 11, pp. 2411–2418, 2006.

[29] M. Statheropoulos, N. Vassiliadis, and A. Pappa, "Principal component and canonical correlation analysis for examining air pollution and meteorological data," *Atmospheric Environment*, vol. 32, no. 6, pp. 1087–1095, 1998.

[30] V. Isakov, A. Venkatram, J. S. Touma, D. Koračin, and T. L. Otte, "Evaluating the use of outputs from comprehensive meteorological models in air quality modeling applications," *Atmospheric Environment*, vol. 41, no. 8, pp. 1689–1705, 2007.

[31] S. A. Abdul-Wahab, C. S. Bakheit, and S. M. Al-Alawi, "Principal component and multiple regression analysis in modelling of ground-level ozone and factors affecting its concentrations," *Environmental Modelling and Software*, vol. 20, no. 10, pp. 1263–1271, 2005.

Hindawi Publishing Corporation
Mathematical Problems in Engineering
Volume 2013, Article ID 874805, 10 pages
http://dx.doi.org/10.1155/2013/874805

Research Article

A Hybrid Stochastic-Interval Analytic Hierarchy Process Approach for Prioritizing the Strategies of Reusing Treated Wastewater

Liang Jing,[1] Bing Chen,[1,2] Baiyu Zhang,[1] and Pu Li[1]

[1] *Northern Region Persistent Organic Pollution Control (NRPOP) Laboratory, Faculty of Engineering and Applied Science, Memorial University of Newfoundland, St. John's, NL, Canada A1B 3X5*
[2] *Key Laboratory of Regional Energy and Environmental Systems Optimization, Ministry of Education, Resources and Environmental Research Academy, North China Electric Power University, Beijing 102206, China*

Correspondence should be addressed to Bing Chen; bchen@mun.ca

Received 26 February 2013; Accepted 31 March 2013

Academic Editor: Guohe Huang

This paper proposes a hybrid stochastic-interval analytic hierarchy process (SIAHP) approach to address uncertainty in group decision making by integrating interval judgment, probabilistic distribution, lexicographic goal programming, and Monte Carlo simulation. A case study related to wastewater treatment plant (WWTP) effluent reuse was conducted to demonstrate the feasibility of the proposed approach. Four candidate alternatives including city moat landscaping, municipal reuse, industrial reuse, and agricultural irrigation were evaluated by five experts according to technical, economic, and environmental criteria. The results suggest that industrial reuse (0.18–0.3) is more preferred over municipal reuse (0.16–0.25) or agricultural irrigation (0.17–0.26) in most replications. The final score of city moat landscaping ranges from 0.11 to 0.31 which indicates a great divergence of expert opinions. It can be concluded that choosing industrial reuse seems to give the best overall account of technical, economic, and environmental concerns. The proposed SIAHP approach can aid group decision making by accommodating linguistic information and dealing with insufficient information or biased opinions.

1. Introduction

As a major factor influencing social and economic development, the global water shortage has been exacerbated due to population growth, urbanization, climate change, and industrialization [1–4]. The reuse of treated wastewater from wastewater treatment plants (WWTPs) has been gaining significant attention as a potential solution to cope up with the increasing water stress. Possible beneficial applications include, but are not limited to, toilet flushing, irrigation, groundwater recharge, fire protection, cooling water, landscaping, boiler feed water, and some working procedures of stocking, pulping, and paper making [5–7]. It is of importance that conventional WWTPs are commonly designed to remove suspended solids and bulk organics rather than pathogenic microorganisms. Therefore, treated wastewater may still contain significant levels of fecal coliforms and many other pollutants (e.g., heavy metals) that need to be removed prior to reuse. Friedler et al. highlighted that improper planning of wastewater reuse may expose people to hazardous pathogenic microorganisms, posing a serious threat to public health [6]. Kon and Watanabe argued that the promotion of reusing treated wastewater can be compromised by many factors such as the need for posttreatment, the concerns associated with water quality and functionality, and the economic efficiency [8]. Former works have shown that the selection of reuse schemes depends not only on their technical, economic, and environmental feasibility but also mainly on public support, in other words, the decision makers who represent the interests of society.

Decision makers usually use multicriteria decision making (MCDM) methods to aid the decision making process [9–15]. A widely used one is the analytic hierarchy process (AHP), a prominent tool for making decisions in situations

involving multiple objectives [12]. Many investigations have been undertaken in the past to apply the AHP to problems with high complexity and uncertainty, especially in the environmental sector [9, 16–20]. Despite its numerous applications, there are critiques in the literature about using inconvenient crisp values and not including uncertainty analysis. Rosenbloom reported that alternatives are not statistically distinguishable if their scores are too close [21]. That is to say, the AHP is not capable of addressing statistical interactions or feedback dependency between different hierarchies of a decision making problem [22, 23]. Another major drawback lies on its inability to translate the imprecision of the decision maker's perceptions [24]. The exact nine-point AHP scale used in pairwise comparisons may fail to capture the imprecision or vagueness in the mind of respondents [25].

In response to these drawbacks, there have been many research attempts on incorporating interval uncertainty into the AHP. It has been well accepted that decision makers are more comfortable and confident to give interval judgments rather than to evaluate pairwise comparisons using single numeric values. Islam developed a lexicographic goal programming (LGP) approach in estimating weight vectors from interval pairwise comparison matrices (IPCMs) [5]. Wang et al. stated that fuzzy inputs can also be addressed by IPCMs using α-level sets and the extension principle [26]. Chandran et al. presented a method to estimate the weights of IPCMs based on linear programming [27]. Yu et al. advanced the LGP method by using multiplicative constraints to cope with the inherent deficiencies. On the other hand, to reflect the statistical characteristics of the traditional AHP, pairwise comparison elements were suggested to be viewed as random variables and computed via Monte Carlo simulation [9]. The triangular distribution is the most commonly used distribution for modeling expert judgment in the AHP [28, 29]. It is advantageous over normal distribution and lognormal distribution due to its bounded nature. However, it may place too much emphasis on the most likely value [22]. It is possible to overcome this disadvantage by using the uniform distribution, which is not much affected by the lack of information. To date, there has been no study specifically investigating how to handle both interval and probabilistic uncertainty in the AHP. Therefore, the objective of this study is to address such issue by integrating interval judgments, probabilistic distribution, the LGP method, and Monte Carlo simulation as a hybrid stochastic-interval analytic hierarchy process (SIAHP) approach. A case study of prioritizing the strategies of reusing treated wastewater from a WWTP in the city of Shuangcheng, China, was carried out to verify the feasibility and efficiency of the proposed approach.

2. Methodology

The proposed SIAHP approach uses expert knowledge as interval judgments and aggregates the lower and upper bounds into two independent arrays. For each nondiagonal element in the upper portion of each IPCM, the uniform distribution is assumed on both arrays such that random lower and upper bounds can be generated using Monte Carlo simulation. The lexicographic goal programming (LGP) method is then employed to estimate the priorities of each IPCM. The detailed steps are summarized as follows.

Step 1. Define the problem and structure the hierarchy from the top (i.e., goal) to the bottom (i.e., decision alternatives).

Step 2. Construct IPCMs for alternatives (or criteria) on each hierarchy level in terms of their performance against the ones on the level immediately above. Note that the IPCMs are reciprocal matrices which means judgments are required only for the upper portion:

$$\begin{bmatrix} 1 & a_{12} & a_{13} & \cdots & a_{1n} \\ \frac{1}{a_{12}} & 1 & a_{23} & \cdots & a_{2n} \\ \frac{1}{a_{13}} & \frac{1}{a_{23}} & 1 & \cdots & a_{3n} \\ \vdots & \vdots & \vdots & \cdots & \vdots \\ \frac{1}{a_{1n}} & \frac{1}{a_{2n}} & \frac{1}{a_{3n}} / & \cdots & 1 \end{bmatrix}. \tag{1}$$

Step 3. Expert opinions are collected as intervals through questionnaires, interviews, surveys, and round-table discussion (2). The upper and lower bounds should not exceed the standard preference scale where 1 represents equal importance and 9 stands for absolute importance

$$\begin{bmatrix} 1 & [l_{12}, u_{12}] & [l_{13}, u_{13}] & \cdots & [l_{1n}, u_{1n}] \\ \left[\frac{1}{u_{12}}, \frac{1}{l_{12}}\right] & 1 & [l_{23}, u_{23}] & \cdots & [l_{2n}, u_{2n}] \\ \left[\frac{1}{u_{13}}, \frac{1}{l_{13}}\right] & \left[\frac{1}{u_{23}}, \frac{1}{l_{23}}\right] & 1 & \cdots & [l_{3n}, u_{3n}] \\ \vdots & \vdots & \vdots & \cdots & \vdots \\ \left[\frac{1}{u_{1n}}, \frac{1}{l_{1n}}\right] & \left[\frac{1}{u_{2n}}, \frac{1}{l_{2n}}\right] & \left[\frac{1}{u_{3n}}, \frac{1}{l_{3n}}\right] & \cdots & 1 \end{bmatrix}, \tag{2}$$

where l and u are the lower and upper bounds of interval judgments, respectively.

Step 4. For each expert-assessed nondiagonal element in the upper portion of each IPCM (e.g., $a_{12} = [l_{12}, u_{12}]$), the lower and upper bounds of different opinions are categorized into two individual arrays, respectively. For both arrays, their maximum and minimum values are determined such that the uniform distribution can be employed in between. Note that the uniform distribution is assumed because the number of participating experts is usually limited. If more experts are involved in the evaluation process, many other distributions

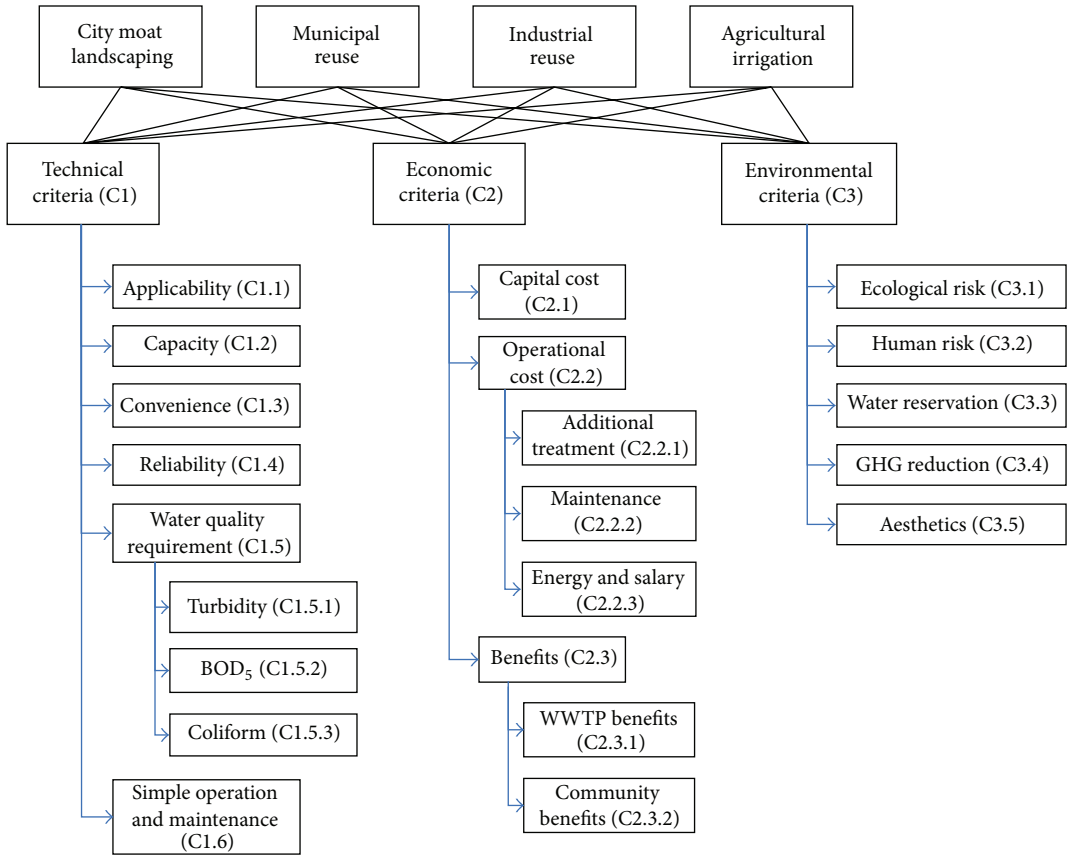

Figure 1: Criteria hierarchy for the selection of wastewater reuse alternatives.

Table 1: Quantitative database for reclaimed wastewater reuse.

Subcriteria	Description	Units	Alternatives				Reference
Reclaimed wastewater reuse			CML	MR	IR	AI	
C1.5.1	Turbidity	NTU	3	2	3	2	[30]
C1.5.2	BOD_5	mg/L	20	10	20	10	[30]
C1.5.3	Coliform	/100 mL	23	2.2	23	14	[30]
C2.1	Capital cost	$/ton	110	350	350	110	[31]
C2.2.2	Maintenance	$/ton	0.03	0.09	0.09	0.03	[31]
C2.3.1	WWTP benefits	$/ton	0.05	0.2	0.16	0.03	[30]

(e.g., normal, beta) that require more precise knowledge can be used.

Step 5. For each aforementioned upper portion element (e.g., $a_{12} = [l_{12}, u_{12}]$), generate uniformly distributed pseudorandom numbers and map them to the ranges of the two arrays (i.e., the lower and upper bounds) predefined in Step 4. Note that the ranges may intersect and hence the random upper bound must be greater than or equal to the random lower bound. The lower portion of each IPCM can be determined by taking the reciprocal values of the corresponding upper portion. At the end of this step, a series of random IPCMs are obtained such that their non-diagonal elements are random intervals.

Step 6. The lexicographic goal programming (LGP) method is used to estimate the weight vector [23], $W = (w_1, \ldots, w_n)$, of each IPCM of rank n. The interval judgments contained in the IPCMs can be defined by the following inequality:

$$l_{ij} w_j - p_{ij} \le w_i \le u_{ij} w_j + q_{ij}, \tag{3}$$

where l_{ij} and u_{ij} are the randomly generated lower and upper bounds of each element, respectively, w_i and w_j are real numbers representing the weights of the ith and jth entries, and deviation variables p_{ij} and q_{ij} are nonnegative real numbers. The weight vector can be derived by minimizing the inconsistency of the upper portion of the interval comparison

matrix, in other words, a summation of all deviation variables p_{ij} and q_{ij} as stated in the following:

$$\text{Min } Z = \sum_{i=1}^{n-1} \sum_{j=i+1}^{n} \left(p_{ij} + q_{ij}\right)$$

subject to

$$\begin{aligned} & w_i - w_j u_{ij} - q_{ij} \le 0 \\ & -w_i + w_j l_{ij} - p_{ij} \le 0 \\ & \sum_{i=1}^{n} w_i = 1 \\ & w_i \ge 0, \qquad p_{ij} \ge 0, \qquad q_{ij} \ge 0. \end{aligned} \tag{4}$$

Step 7. As with the traditional AHP, the inconsistency of judgements needs to be examined in order to ensure the validity of the random IPCMs. In this approach, the summations of all deviation variables Z are expected to be less than or equal to 0.1; otherwise, the IPCM should be declined and regenerated.

Step 8. The final scores of each decision alternative can be calculated by aggregating the weights throughout the hierarchy as follows:

$$A_{k(\text{Score})} = \sum_{j=1}^{p} \left(b_{kj} \cdot W_j\right), \tag{5}$$

where $A_{k(\text{Score})}$ is the final performance score for the kth alternative, b_{kj} is the merit of the kth alternative with regard to the jth criterion on the preceding level, p is the number of criteria, and W_j is the normalized weight of the jth criterion against the goal.

Step 9. Repeat Steps 5 through 8 using Monte Carlo simulation for a number of replications. The overall scores of decision alternatives can be obtained as probability density functions.

3. Case Study

3.1. The WWTP of the City of Shuangcheng. The study area (the city of Shuangcheng) is located at the southern end of Heilongjiang province, northeastern China, approximately 45 kilometers southwest from the provincial capital Harbin. As one of the major cities in the province, the city of Shuangcheng has a population of 830 thousand with 640 thousand people dependent on agriculture. An advanced wastewater treatment plant associated with a drainage system was built in 2009 and has been operated since then to treat sewage and wastewater from individual residences, businesses, schools, and so forth. This wastewater treatment plant has a daily treatment capacity of 30,000 tonnes, which is sufficient for population growth and any future expansion demand. However, some important issues with regard to the operation of the treatment plant have been emerging, such as how to optimize the operating parameters to adapt to varying environmental conditions, how to effectively use the treated effluent, sludge, and other byproducts, and particularly how to efficiently operate this plant in a sustainable manner. In this case study, the local government invited experts to evaluate wastewater reuse options in order to explore the possibility of saving natural water resources in the future.

Table 2: Alternatives' normalized scores for quantitative criteria.

Subcriteria	Description	Normalized scores of alternatives			
Reclaimed wastewater reuse		CML	MR	IR	AI
C1.5.1	Turbidity	0.300	0.200	0.300	0.200
C1.5.2	BOD_5	0.333	0.167	0.333	0.167
C1.5.3	Coliform	0.370	0.035	0.370	0.225
C2.1	Capital cost	−0.120	−0.380	−0.380	−0.120
C2.2.2	Maintenance	−0.125	−0.375	−0.375	−0.125
C2.3.1	WWTP benefits	0.114	0.455	0.364	0.068

Table 3: Uniform distributions (in MATLAB) of the PCM with regard to human risk.

	Min	Max	Uniform distribution
l_{12}	1/2	4	1/2 + rand × (4 − 1/2)
l_{13}	1/6	1	1/6 + rand × (1 − 1/6)
l_{14}	1	1	1 + rand × (1 − 1)
l_{23}	1/9	1/4	1/9 + rand × (1/4 − 1/9)
l_{24}	1/7	3	1/7 + rand × (3 − 1/7)
l_{34}	2	6	2 + rand × (6 − 2)
u_{12}	3	7	3 + rand × (7 − 3)
u_{13}	1/3	3	1/3 + rand × (3 − 1/3)
u_{14}	5	7	5 + rand × (7 − 5)
u_{23}	1/6	2	1/6 + rand × (2 − 1/6)
u_{24}	1	6	1 + rand × (6 − 1)
u_{34}	4	8	4 + rand × (8 − 4)

3.2. Management of the WWTP Effluent

3.2.1. Goal, Decision Alternatives, and Evaluation Criteria. The goal of this case study was to select the best alternative for WWTP effluent management and to provide the local government with a more systematic overview of sustainable development. Four reclaimed water reuse alternatives including city moat landscaping (CML), municipal reuse (MR), industrial reuse (IR), and agricultural irrigation (AI) were chosen based on the literature review and discussion with experts from local authorities and educational institutions (Figure 1). The city of Shuangcheng is surrounded by a city moat that uses a large amount of water every day to maintain water level and water quality. It is not just a landmark of the city's history but also a tourist attraction. Treated wastewater can be safely discharged into the moat to replenish its water supply and to improve water quality on a daily basis. Treated wastewater can be reused for certain restricted municipal purposes such as firefighting, irrigation of parks and golf courses, street cleaning, groundwater recharging,

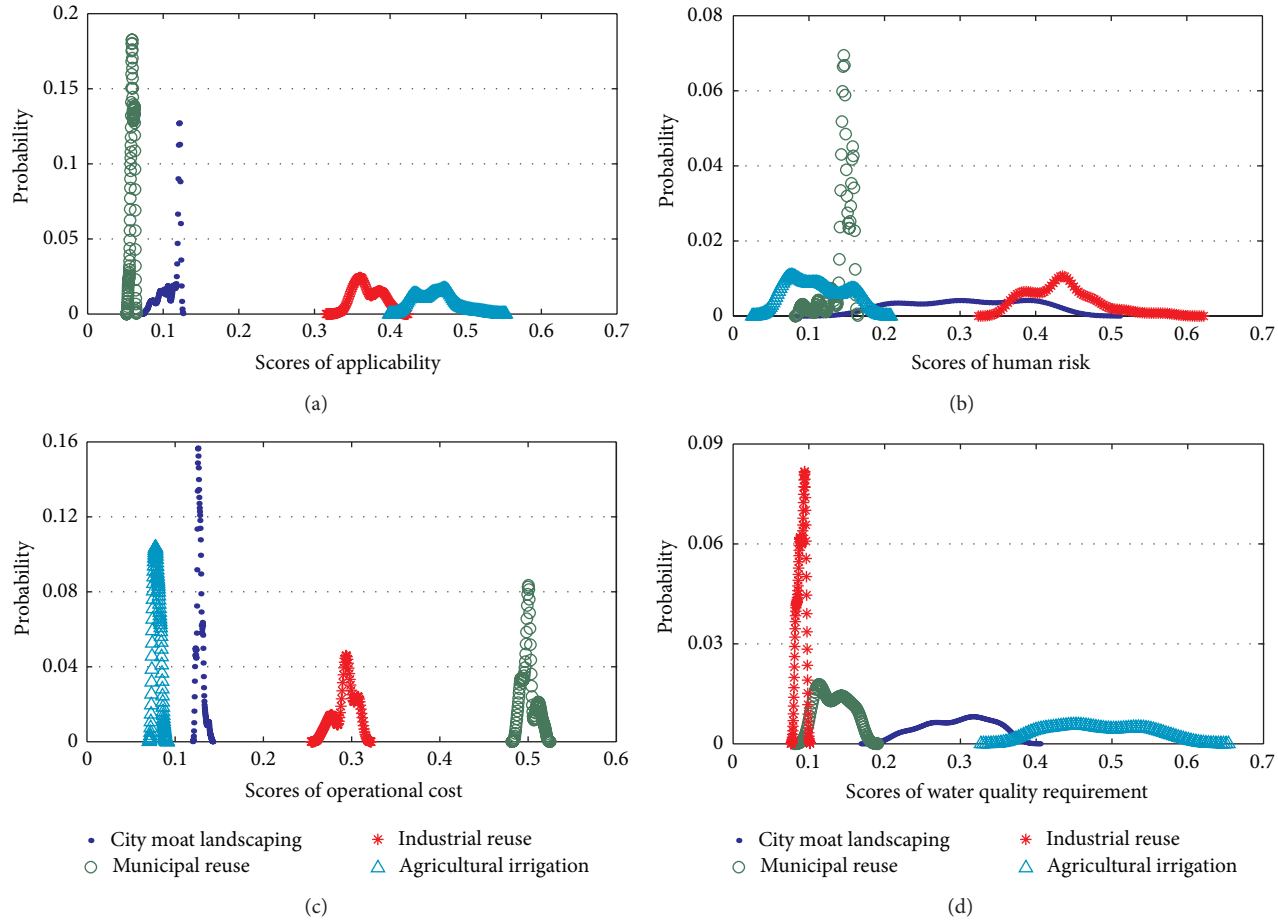

FIGURE 2: Probability density estimates of alternative scores with regard to the subcriterion of (a) applicability, (b) human risk, (c) operational cost, and (d) water quality requirement.

and flushing toilets in public buildings and households. It should be noted that effluent from the WWTP usually needs to be further disinfected to such an extent that is safe from a microbiological point of view. Reclaimed water may also serve industrial processes (e.g., cooling, boiler feed, and process water) after proper treatment to prevent scaling, corrosion, bacterial fouling, and foaming issues. However, its feasibility and economic applicability vary from case to case. For example, the electroplating process requires water of high quality to wash circuit boards while tanneries can use low-quality water for washing hides. Lastly, agricultural irrigation using treated wastewater (reclaimed water) is becoming a common practice in arid and semiarid regions. Treated wastewater can be directly or indirectly (e.g., after disinfection) applied for irrigation depending on its quality and usage. As depicted in Figure 1, these four alternatives were evaluated based on technical, economic, and environmental criteria adopted from the literature and expert recommendations [7].

3.2.2. Data Acquisition. Both quantitative and qualitative data were collected through questionnaire survey and the literature review. Key numbers such as capital cost and operational cost were obtained from different sources as shown in Table 1. They were normalized using a linear value function as follows:

$$b_k = \pm \frac{x_k}{\sum_{k=1}^{m} x_k}, \tag{6}$$

where b_k is the normalized performance score of the kth alternative in terms of a criterion, m is the number of alternatives, and x_k is the numerical value of the kth alternative. It should be noted that quantitative data has either increasing (e.g., benefit) or decreasing (e.g., cost, risk) behavior. Therefore, positive scores (between 0 and 1) were given to those with increasing values, while negative scores (between −1 and 0) were assigned to the decreasing values. Normalized values for different alternatives with respect to reclaimed wastewater reuse are reported in Table 2. In the absence of available quantitative data, expert subjective rankings were used to evaluate the alternatives in terms of other criteria. Five experts from local authorities (Bureau of Environmental Protection) and educational institutions (professors and graduate students at Memorial University of Newfoundland) were asked to assess the hierarchy with interval judgments. Equation (7) and Table 3 show an example of expert assessments in regard to human risk. The number of Monte Carlo iterations used in

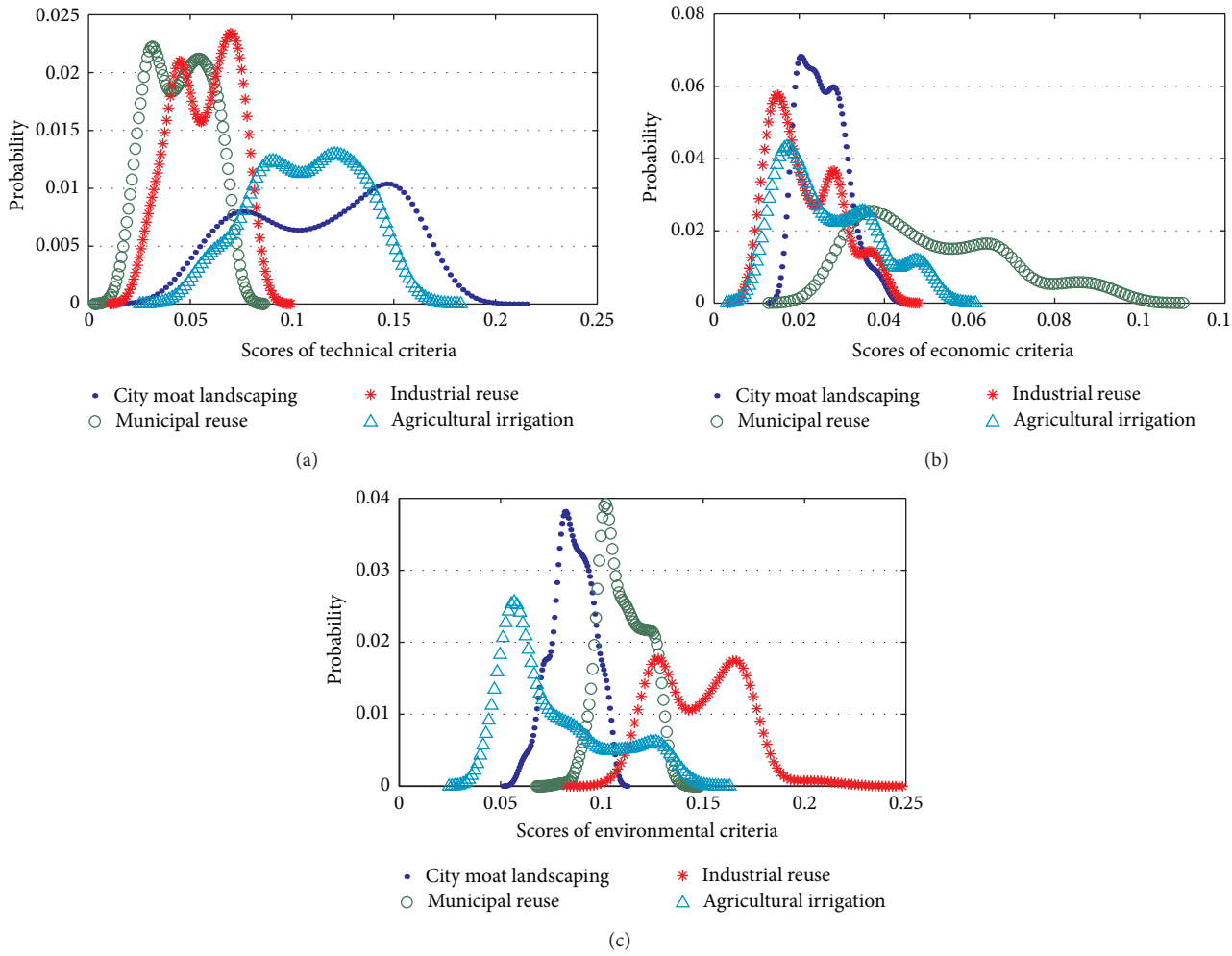

FIGURE 3: Probability density estimates of the overall alternative scores with regard to (a) technical criteria, (b) economic criteria, and (c) environmental criteria.

this case study was set as 1000 by considering time constraints and convergence speed.

$$\begin{array}{c} \\ CML \\ MR \\ IR \\ AI \end{array} \begin{array}{c} \begin{array}{cccc} CML & MR & IR & AI \end{array} \\ \begin{bmatrix} 1 & [l_{12}, u_{12}] & [l_{13}, u_{13}] & [l_{14}, u_{14}] \\ \left[\frac{1}{u_{12}}, \frac{1}{l_{12}}\right] & 1 & [l_{23}, u_{23}] & [l_{24}, u_{24}] \\ \left[\frac{1}{u_{13}}, \frac{1}{l_{13}}\right] & \left[\frac{1}{u_{23}}, \frac{1}{l_{23}}\right] & 1 & [l_{34}, u_{34}] \\ \left[\frac{1}{u_{14}}, \frac{1}{l_{14}}\right] & \left[\frac{1}{u_{24}}, \frac{1}{l_{24}}\right] & \left[\frac{1}{u_{34}}, \frac{1}{l_{34}}\right] & 1 \end{bmatrix} \end{array}. \quad (7)$$

4. Results and Discussion

As shown in Figure 2, the alternative priorities with respect to some subcriteria are depicted in the form of probability density estimates using the kernel-smoothing method. It clearly shows that most density estimates have two major peaks, indicating that the optimization results obtained from the LGP method tend to be concentrated within a certain interval possibly due to the randomly generated interval judgments. A few density estimates appear to be smooth and continuous over a large span while many others are steep and bell shaped. This may be attributable to expert assessments which diverge on unfamiliar knowledge (e.g., the application of city moat landscaping) but converge on some commonly agreed upon principles.

The overall alternative priorities with regard to the whole sets of technical, economic, and environmental criteria are synthesized in Figure 3. City moat landscaping and agricultural irrigation have the best technical performance in most replications mainly due to their ease of operation and maintenance. Their overlaps with other alternatives are not statistically significant (Figure 3(a)); however, their own overlap reveals itself with a strong correlation coefficient of (0.956). Municipal reuse is seemingly preferred over the other options in terms of economic concerns (Figure 3(b)). This is more or less in agreement with the reality that reusing

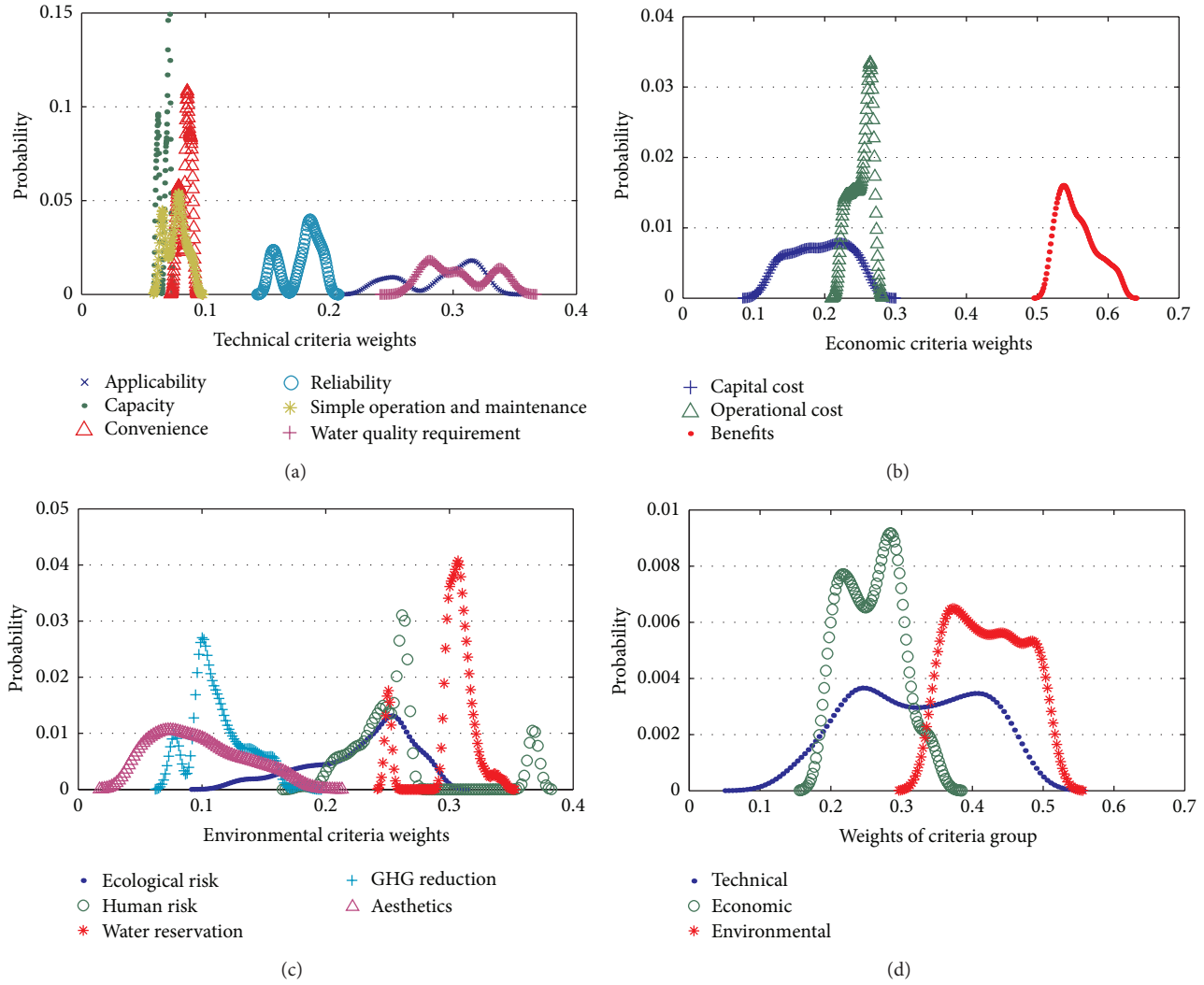

Figure 4: Probability density estimates of the relative weights between each (a) technical subcriterion, (b) economic sub-criterion, (c) environmental subcriterion, and (d) criteria group.

reclaimed water for municipal purposes can save extra costs of posttreatment and therefore creates more economic benefits. The correlation coefficients between the alternatives are all above 0.950 which suggests that their performance is positively correlated such that the increase of one is associated with the increase of the others. This can be further interpreted that the alternatives are not well distinguishable in terms of economic considerations; therefore, the significance of economic criteria is attenuated as demonstrated in Figures 3(b) and 4(d). From the perspective of environmental conservation, industrial reuse dominates the others in more than 95% of the replications (Figure 3(c)). This seems to fit the way most people think because using treated wastewater in industrial sectors can hardly cause any environmental issues or raise human health concerns.

The probability density distributions of subcriterion weights are demonstrated in Figure 4 using the kernel-smoothing method. Applicability and water quality requirement are the most influential technical subcriteria, followed by reliability. Benefit absolutely dominates other two economic subcriteria with the confidence level of 100%. Environmental subcriteria are to some extent tangle with each other while water reservation manages to lead in 89.2% of the replications. These aforementioned subcriteria should be prioritized and further considered in the decision making process if the final alternative scores are too close. The final scores of each decision alternative are plotted in Figure 5. It appears that industrial reuse (0.18–0.3) is more preferred over municipal reuse (0.16–0.25) or agricultural irrigation (0.17–0.26) though the existence of overlaps may contradict this assertion. Further analysis indicates that industrial reuse takes the first or second places in over 88.6% of the replications while this number for the other two options is somewhere between 20% and 30% (Table 4). Another worthy mentioned finding is related to the final score of city moat landscaping which spans over a large range from 0.11 to 0.31 (Figure 5). This range is larger than those of other alternatives mainly because of the great divergence of expert opinions.

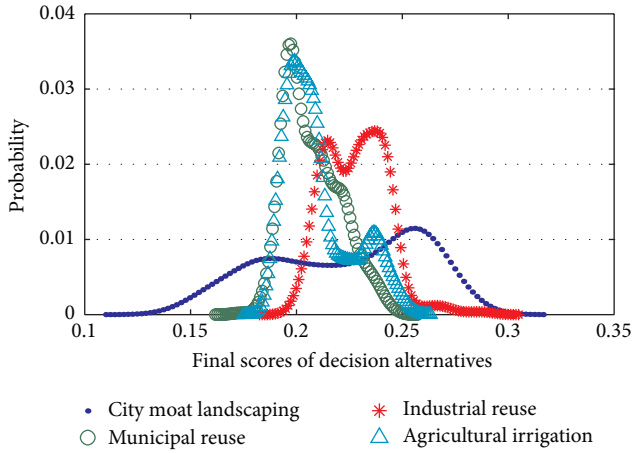

Figure 5: Probability density estimates of the final scores of decision alternatives.

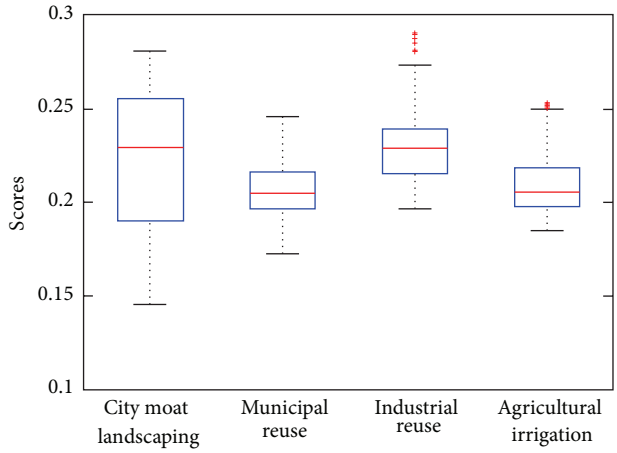

Figure 6: Box plots of overall scores of each alternative.

Table 4: Summary of the evaluation results of the SIAHP approach.

Decision alternative	Rank			
	1	2	3	4
City moat landscaping	542	80	25	353
Municipal reuse	1	206	468	325
Industrial reuse	397	489	106	8
Agricultural irrigation	60	225	401	314
Total	1000	1000	1000	1000

In other words, some experts may favor city moat over the others (in 54.2% replications), whereas some experts may rank it as the least preferable solution (in 35.3% replications) (Table 4). Figure 6 confirms these observations by using box plot to graphically illustrate the minimum, lower quartiles, medians, upper quartiles, and maximum of alternative overall scores. It can be argued that choosing industrial reuse seems to give the best overall account of technical, economic, and environmental concerns.

It is worth discussing the correlations between the final scores as this can help decision makers further interpret the experts' preferences. City moat landscaping and industrial reuse are in conflict with each other as their correlation coefficient is −0.858, implying that experts tend not to choose both options as their favorite (Figure 7(a)). The correlation coefficients between industrial reuse and municipal reuse, industrial reuse and agricultural irrigation, and municipal and agricultural irrigation are 0.701, 0.508, and 0.835, respectively, which agrees with the positive correlations shown in Figures 7(b)–7(d). That is to say, when either one of these three is favored by an expert, it is highly probable that the other two are also more or less favored.

5. Conclusions

This paper presents a hybrid stochastic-interval analytic hierarchy process (SIAHP) approach to address uncertainty issues in the decision making procedure by integrating interval judgments, probabilistic distributions, the lexicographic goal programming method, and Monte Carlo simulation. A case study of selecting the best effluent reuse strategy for a WWTP in the city of Shuangcheng, China, was carried out to verify the feasibility and efficiency of the proposed approach. Four candidate alternatives including city moat landscaping, municipal reuse, industrial reuse, and agricultural irrigation were evaluated by five experts from local authorities and educational institutions. Technical, economic, and environmental criteria and their associated sub-criteria were considered to investigate the performance of the alternatives. The results show that a few density estimates of alternative performance with regard to several subcriteria appear to be smooth and continuous over a large span while many others are steep and bell shaped. This may be attributable to expert assessments that diverge on unfamiliar knowledge but converge on some commonly agreed upon principles. City moat landscaping and agricultural irrigation have the best technical performance in most replications mainly due to their ease of operation and maintenance. Their own overlap is evident with a strong correlation coefficient of 0.956. Municipal reuse is seemingly preferred over the other options in terms of economic concerns while the correlation coefficients between all alternatives are above 0.950. This can be further interpreted that the alternatives are not well distinguishable in terms of economic considerations; therefore, the significance of economic criteria is attenuated. Industrial reuse seems to be the best option in terms of environmental reservation. Based on the final overall scores, industrial reuse (0.18–0.3) is more preferred than municipal reuse (0.16–0.25) or agricultural irrigation (0.17–0.26) in most replications. The final score of city moat landscaping ranges from 0.11 to 0.31 which is larger than those of other alternatives mainly because of the great divergence of expert opinions. In other words, some experts may favor it over the others (in 54.2% replications), whereas some experts may rank it as the least preferable solution (in 35.3% replications). It can be concluded that choosing industrial reuse seems to give the best overall account of technical, economic, and

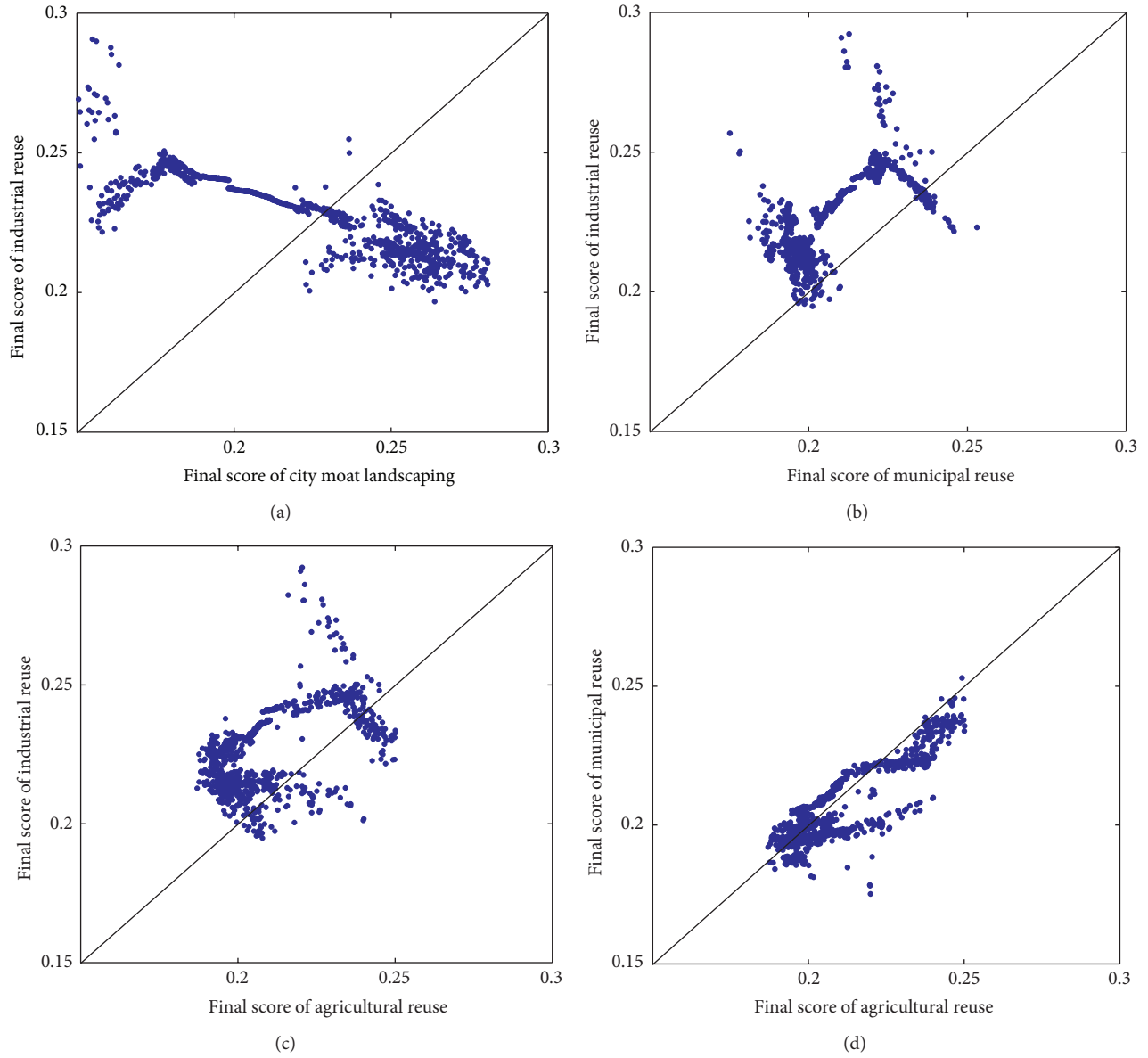

Figure 7: Scatter plots of the final scores of (a) city moat landscaping versus industrial reuse, (b) municipal reuse versus industrial reuse, (c) agricultural reuse versus industrial reuse, and (d) agricultural reuse versus municipal reuse.

environmental concerns. The proposed SIAHP approach can aid group decision making by accommodating linguistic information and dealing with insufficient information or biased opinions.

Acknowledgments

The study was supported by the National Natural Science Foundation of China (nos. 51179070 and 51209089), the Natural Science and Engineering Research Council of Canada, and the United Nations Development Programme (UNDP) as well as the China International Center for Economic and Technical Exchanges (CICETE) of the Ministry of Commerce of China.

References

[1] G. O. Engin, B. S. Ucar, and E. Senturk, "Reuse feasibility of pre-treated grey water and domestic wastewater with a compact household reverse osmosis system," *Desalination and Water Treatment*, vol. 29, no. 1–3, pp. 103–109, 2011.

[2] L. Jing and B. Chen, "Hydrological monitoring and modelling of the Deer River Watershed with SLURP," *Journal of Environmental Informatics*, vol. 17, no. 1, pp. 36–45, 2011.

[3] B. Chen, L. Jing, B. Y. Zhang, and S. Liu, "Wetland monitoring, characterization and modeling under changing climate in the Canadian subarctic," *Journal of Environmental Informatics*, vol. 18, no. 2, pp. 55–64, 2011.

[4] Y. R. Fan and G. H. Huang, "A robust two-step method for solving interval linear programming problems within an

environmental management context," *Journal of Environmental Informatics*, vol. 19, no. 1, pp. 1–9, 2012.

[5] S. Agidi, S. Vedachalam, K. Mancl, and J. Lee, "Effectiveness of onsite wastewater reuse system in reducing bacterial contaminants measured with human-specific IMS/ATP and qPCR," *Journal of Environmental Management*, vol. 115, pp. 167–174, 2013.

[6] E. Friedler, O. Lahav, H. Jizhaki, and T. Lahav, "Study of urban population attitudes towards various wastewater reuse options: Israel as a case study," *Journal of Environmental Management*, vol. 81, no. 4, pp. 360–370, 2006.

[7] S. J. You and D. C. Wu, "Potential for reuse of high cellulose containing wastewater after membrane bioreactor treatment," *Desalination*, vol. 249, no. 2, pp. 721–728, 2009.

[8] H. Kon and M. Watanabe, "Construction of a treated wastewater reuse system for renewal of a water cycle mechanism in urban areas—modeling analysis of reclamation treatment processes corresponding to target water quality by use," *Desalination and Water Treatment*, vol. 6, no. 1–3, pp. 5–11, 2009.

[9] L. Jing, B. Chen, B. Y. Zhang, P. Li, and J. S. Zheng, "Monte Carlo simulation-aided analytic hierarchy process approach: case study of assessing preferred non-point source pollution control best management practices," *ASCE Journal of Environmental Engineering*, 2013.

[10] J. R. Yu, Y. W. Hsiao, and H. J. Sheu, "A multiplicative approach to derive weights in the interval analytic hierarchy process," *International Journal of Fuzzy Systems*, vol. 13, no. 3, pp. 225–231, 2011.

[11] B. Chen, G. H. Huang, and Y. F. Li, "Pesticide-loss simulation and risk assessment during flooding season—a study in the Auglaize-Blanchard Watershed," *Water Internationalno*, vol. 30, no. 1, pp. 88–98, 2005.

[12] B. Chen, H. C. Guo, G. H. Huang et al., "ASRWM: an arid/semiarid region water management model," *Engineering Optimization*, vol. 37, no. 6, pp. 609–631, 2005.

[13] L. Jing, B. Chen, B. Y. Zhang, and H. X. Peng, "A review of ballast water management practices and challenges in harsh and arctic environments," *Environmental Reviews*, vol. 20, pp. 83–108, 2012.

[14] P. Li and B. Chen, "FSILP: fuzzy-stochastic-interval linear programming for supporting municipal solid waste management," *Journal of Environmental Management*, vol. 92, pp. 1198–1209, 2011.

[15] T. L. Saaty, *The Analytic Hierarchy Process: Planning, Priority Setting and Resource Allocation*, McGraw-Hill, New York, NY, USA, 1980.

[16] M. P. Amiri, "Project selection for oil-fields development by using the AHP and fuzzy TOPSIS methods," *Expert Systems With Applications*, vol. 37, no. 9, pp. 6218–6224, 2010.

[17] S. Chowdhury and T. Husain, "Evaluation of drinking water treatment technology: an entropy-based fuzzy application," *Journal of Environmental Engineering ASCE*, vol. 132, no. 10, pp. 1264–1271, 2006.

[18] T. Kaya and C. Kahraman, "An integrated fuzzy AHP-ELECTRE methodology for environmental impact assessment," *Expert Systems With Applications*, vol. 38, pp. 8553–8562, 2011.

[19] R. Sadiq and S. Tesfamariam, "Environmental decision-making under uncertainty using intuitionistic fuzzy analytic hierarchy process (IF-AHP)," *Stochastic Environmental Research and Risk Assessment (SERRA)*, vol. 23, no. 1, pp. 75–91, 2009.

[20] E. Tolga, M. L. Demircan, and C. Kahraman, "Operating system selection using fuzzy replacement analysis and analytic hierarchy process," *International Journal of Production Economics*, vol. 97, no. 1, pp. 89–117, 2005.

[21] E. S. Rosenbloom, "A probabilistic interpretation of the final rankings in AHP," *European Journal of Operational Research*, vol. 96, no. 2, pp. 371–378, 1997.

[22] R. Banuelas and J. Antony, "Modified analytic hierarchy process to incorporate uncertainty and managerial aspects," *International Journal of Production Research*, vol. 42, no. 18, pp. 3851–3872, 2004.

[23] D. Carlucci and G. Schiuma, "Applying the analytic network process to disclose knowledge assets value creation dynamics," *Expert Systems with Applications*, vol. 36, no. 4, pp. 7687–7694, 2009.

[24] T. C. Wang and Y. H. Chen, "Applying consistent fuzzy preference relations to partnership selection," *Omega*, vol. 35, pp. 384–388, 2007.

[25] A. Andronikidis, A. C. Georgiou, K. Gotzamani, and K. Kamvysi, "The application of quality function deployment in service quality management," *TQM Journal*, vol. 21, no. 4, pp. 319–333, 2009.

[26] Y.-M. Wang, J.-B. Yang, and D.-L. Xu, "A two-stage logarithmic goal programming method for generating weights from interval comparison matrices," *Fuzzy Sets and Systems*, vol. 152, no. 3, pp. 475–498, 2005.

[27] B. Chandran, B. Golden, and E. Wasil, "Linear programming models for estimating weights in the analytic hierarchy process," *Computers and Operations Research*, vol. 32, no. 9, pp. 2235–2254, 2005.

[28] T. Rezaei Taziani, M. Sanei, G. R. Jahanshahloo, J. Jablonsky, and M. R. Mozaffari, "Ranking bank branches with interval data by IAHP," *International Journal of Mathematical Analysis*, vol. 3, no. 17–20, pp. 971–983, 2009.

[29] T.-H. Hsu and F. F. C. Pan, "Application of Monte Carlo AHP in ranking dental quality attibutes," *Expert System With Applications*, vol. 36, pp. 2310–2316, 2009.

[30] U.S. EPA, *"Guidelines For Water Reuse*, Municipal Support Division, Office of Wastewater Management, Office of Water, Washington, DC, USA, 2004.

[31] H. Yang and K. C. Abbaspour, "Analysis of wastewater reuse potential in Beijing," *Desalination*, vol. 212, no. 1–3, pp. 238–250, 2007.

Hindawi Publishing Corporation
Mathematical Problems in Engineering
Volume 2013, Article ID 672936, 7 pages
http://dx.doi.org/10.1155/2013/672936

Research Article

Numerical Solution of Advection-Diffusion Equation Using a Sixth-Order Compact Finite Difference Method

Gurhan Gurarslan,[1] Halil Karahan,[1] Devrim Alkaya,[1] Murat Sari,[2] and Mutlu Yasar[1]

[1] *Department of Civil Engineering, Faculty of Engineering, Pamukkale University, 20070 Denizli, Turkey*
[2] *Department of Mathematics, Faculty of Art and Science, Pamukkale University, 20070 Denizli, Turkey*

Correspondence should be addressed to Gurhan Gurarslan; gurarslan@pau.edu.tr

Received 15 February 2013; Accepted 25 March 2013

Academic Editor: Guohe Huang

This study aims to produce numerical solutions of one-dimensional advection-diffusion equation using a sixth-order compact difference scheme in space and a fourth-order Runge-Kutta scheme in time. The suggested scheme here has been seen to be very accurate and a relatively flexible solution approach in solving the contaminant transport equation for Pe ≤ 5. For the solution of the present equation, the combined technique has been used instead of conventional solution techniques. The accuracy and validity of the numerical model are verified through the presented results and the literature. The computed results showed that the use of the current method in the simulation is very applicable for the solution of the advection-diffusion equation. The present technique is seen to be a very reliable alternative to existing techniques for these kinds of applications.

1. Introduction

Problems of environmental pollution can always be reduced to the solution of a mathematical model of advection diffusion. The unknown quantity in these cases is the concentration, C, a scalar physical quantity, which represents the mass of a pollutant or the salinity or temperature of the water [1]. Advection-diffusion equation (ADE) illustrates many quantities such as mass, heat, energy, velocity, and vorticity [2]. The ADE has been used as a model equation in many engineering problems such as dispersion of tracers in porous media [3], pollutant transport in rivers and streams [4], the dispersion of dissolved material in estuaries and coastal seas [5, 6], contaminant dispersion in shallow lakes [7], long-range transport of pollutants in the atmosphere [8], thermal pollution in river systems [9], and flow in porous media [10]. The advection-diffusion transport equation in one-dimensional case without source terms is as follows:

$$\frac{\partial C}{\partial t} + U\frac{\partial C}{\partial x} - D\frac{\partial^2 C}{\partial x^2} = 0, \quad 0 \le x \le L,\ 0 < t \le T, \tag{1}$$

with initial condition

$$C(x, t = 0) = C_0(x) \tag{2}$$

and boundary conditions

$$C(x = 0, t) = f_0(t),$$
$$C(x = L, t) = f_L(t) \quad \text{or} \quad -D\frac{\partial C(L, t)}{\partial x} = g(t), \tag{3}$$

where t is time, x is space coordinate, D is diffusion coefficient, $C(x, t)$ is concentration, $U(x, t)$ is velocity of water flow, and L is length of the channel, respectively. Here C_0, f_0, f_L, and g are prescribed functions, whilst C is the unknown function. Notice that $D > 0$ and $U > 0$ are considered to be positive constants quantifying the diffusion and advection processes, respectively.

It is known that the use of the standard finite difference and finite element method is not effective and often leads to unreal results. For that reason, several alternative methods are proposed in the literature for solving the ADE with high accuracy [11]. These include method of characteristic with

Galerkin method (MOCG) [11], finite difference method [12–14], high-order finite element techniques [15], high-order finite difference methods [16–24], Green-element method [25], cubic B-spline [26], cubic B-spline differential quadrature method (CBSDQM) [27], method of characteristics integrated with splines (MOCS) [28–30], Galerkin method with cubic B-splines (CBSG) [31], Taylor-Collocation (TC) and Taylor-Galerkin (TG) methods [32], B-spline finite element method [33], Least squares finite element method (FEMLSF and FEMQSF) [34], Lattice Boltzmann method [35], Taylor-Galerkin B-spline finite element method [36], and meshless method [37, 38].

Utility of higher-order numerical methods in solving many problems accurately is required. Lately, a noticeable interest in the development and application of CD methods for solving the Navier-Stokes [39–41] and other partial differential equations [42–46] has been renovated. Narrower stencils are required in the CD schemes, and by a comparison to classical difference schemes, they have less truncation error. In the current paper, accurate solutions of the ADE are obtained by using a sixth-order compact difference (CD6) [47], a fourth-order Runge-Kutta (RK4) schemes in space and time, respectively.

2. The Compact Finite Difference Method

CD methods are very popular in the fluid dynamics community because of their high accuracy and advantages associated with stencils [48]. These methods are efficient for higher accuracies without any increase in a stencil, while traditional high-order finite difference methods use larger stencil sizes that make boundary treatment hard. It can also be noted that the CD schemes have been demonstrated to be more precise and computationally economic. Use of smaller stencil sizes in the CD methods is useful when dealing with nonperiodic boundary conditions.

A uniform one-dimensional mesh is considered, consisting of N points: $x_1, x_2, \ldots, x_{i-1}, x_i, x_{i+1}, \ldots, x_N$ with the mesh size $h = x_{i+1} - x_i$. The first-order derivatives of the unknown function can be given at interior nodes as follows [47]:

$$\alpha C'_{i-1} + C'_i + \alpha C'_{i+1} = b\frac{C_{i+2} - C_{i-2}}{4h} + a\frac{C_{i+1} - C_{i-1}}{2h} \quad (4)$$

leading to an α-family of fourth-order tridiagonal schemes with

$$a = \frac{2}{3}(\alpha + 2), \qquad b = \frac{1}{3}(4\alpha - 1). \quad (5)$$

A sixth-order tridiagonal scheme is obtained by $\alpha = 1/3$,

$$C'_{i-1} + 3C'_i + C'_{i+1} = \frac{1}{12h}\left(C_{i+2} + 28C_{i+1} - 28C_{i-1} + C_{i-2}\right). \quad (6)$$

Approximation formulae for the derivatives of nonperiodic problems can be derived with the consideration of one-sided schemes for the boundary nodes. Interested readers are referred to the work of Lele [47] for details of the derivations for the first- and second-order derivatives.

The third-order formula at boundary point 1 is as follows:

$$C'_1 + 2C'_2 = \frac{1}{h}\left(-\frac{5}{2}C_1 + 2C_2 + \frac{1}{2}C_3\right). \quad (7)$$

The fourth-order formula at boundary points 2 and $N - 1$ is as follows:

$$C'_{i-1} + 4C'_i + C'_{i+1} = \frac{3}{h}\left(C_{i+1} - C_{i-1}\right). \quad (8)$$

The third-order formula at boundary point N is as follows:

$$2C'_{N-1} + C'_N = \frac{1}{h}\left(\frac{5}{2}C_N - 2C_{N-1} - \frac{1}{2}C_{N-2}\right). \quad (9)$$

Use of the above formulae leads to following matrix equation:

$$\mathbf{B}C' = \mathbf{A}C, \quad (10)$$

where $C = (C_1, \ldots, C_n)^T$. Consideration of the first-order operator twice will give us the second-order derivative terms; that is,

$$\mathbf{B}C'' = \mathbf{A}C'. \quad (11)$$

The RK4 scheme is considered to obtain the temporal integration in the present study. Utility of the CD6 technique to (1) gives rise to the following differential equation in time:

$$\frac{dC_i}{dt} = LC_i, \quad (12)$$

where L indicates a spatial linear differential operator. The spatial and temporal terms are approximated by the CD6 and the RK4 schemes, respectively. The semidiscrete equation (12) is solved using the RK4 scheme, through the following operations:

$$C^{(1)} = C^n + \frac{1}{2}\Delta t L\left(C^n\right),$$

$$C^{(2)} = C^n + \frac{1}{2}\Delta t L\left(C^{(1)}\right),$$

$$C^{(3)} = C^n + \Delta t L\left(C^{(2)}\right),$$

$$C^{n+1} = C^n + \frac{1}{6}\Delta t\left[L\left(C^n\right) + 2L\left(C^{(1)}\right) + 2L\left(C^{(2)}\right) + L\left(C^{(3)}\right)\right]. \quad (13)$$

To obtain the approximate solution of (1) with the boundary and initial conditions using the CD6-RK4, the domain $[0, L]$ is first discretized such that $0 = x_1 < x_2 < \cdots < x_N = L$ where N is the number of grid points.

3. Numerical Illustrations

Let us consider the advection-diffusion equation with the initial and boundary conditions. The numerical results are compared with the exact solutions. The differences between the computed solutions and the exact solutions are shown in Tables 1–5. Three examples for which the exact solutions

Table 1: Peak concentration values at $t = 9600$ s for various Cr numbers ($\Delta t = 50$ s).

Cr	0.25	0.50	0.75	1.00
MOCS [28]	9.677	9.756	9.805	10.000
MOCG [11]	9.816	9.836	9.934	10.000
CBSG [31]	9.986	9.986	9.993	9.986
FEMLSF [34]	9.647	9.864	9.918	9.943
FEMQSF [34]	9.926	9.932	9.949	9.961
TC [32]	9.940	9.984	9.993	9.986
TG [32]	9.989	9.991	9.996	9.991
CD6	9.999	10.000	10.000	10.000
Exact	10.000	10.000	10.000	10.000

Table 2: Error norms for various Cr values at $t = 9600$ s.

Cr	h	CSDQM [27]		FEMLSF [34]		FEMQSF [34]		CD6	
		L_2	L_∞	L_2	L_∞	L_2	L_∞	L_2	L_∞
0.1250	200	34.734	1.156	32.874	1.350	12.555	0.518	0.8511	0.4293
0.2500	100	2.685	0.136	10.596	0.494	7.951	0.376	0.0218	0.0100
0.5000	50	0.170	0.008	7.984	0.380	7.908	0.373	0.0024	0.0008
1.0000	25	0.023	0.001	7.881	0.377	7.908	0.379	0.0029	0.0007

Table 3: Comparison between numerical solutions and the exact solution.

x	MOCS [28]	MOCG [11]	CBSG [31]	FEMLSF [34]	FEMQSF [34]	TC [32]	TG [32]	CD6		Exact
								$\Delta t = 10$ s	$\Delta t = 1$ s	
0	1.000	1.000	1.000	1.000	1.000	1.000	1.000	1.000	1.000	1.000
18	1.000	1.000	1.000	1.000	1.000	1.000	1.000	1.000	1.000	1.000
19	1.000	0.999	1.000	1.000	1.000	0.999	0.999	0.999	0.999	0.999
20	1.000	0.998	0.999	0.999	1.000	0.999	0.998	0.998	0.998	0.998
21	1.000	0.996	0.996	0.997	0.999	0.999	0.996	0.996	0.996	0.996
22	1.000	0.990	0.991	0.993	0.996	0.998	0.991	0.992	0.991	0.991
23	1.000	0.978	0.981	0.985	0.989	0.994	0.980	0.982	0.982	0.982
24	1.000	0.957	0.961	0.970	0.974	0.987	0.960	0.965	0.964	0.964
25	1.000	0.922	0.927	0.943	0.946	0.972	0.926	0.936	0.935	0.934
26	0.996	0.870	0.874	0.902	0.900	0.945	0.874	0.891	0.889	0.889
27	1.013	0.799	0.800	0.842	0.832	0.902	0.800	0.827	0.824	0.823
28	1.047	0.708	0.706	0.763	0.743	0.838	0.705	0.743	0.739	0.738
29	0.897	0.602	0.596	0.666	0.638	0.755	0.595	0.641	0.637	0.636
30	0.457	0.488	0.479	0.556	0.524	0.653	0.479	0.528	0.523	0.523
31	0.067	0.375	0.366	0.442	0.411	0.541	0.366	0.413	0.408	0.408
32	−0.036	0.272	0.265	0.332	0.306	0.427	0.264	0.306	0.301	0.301
33	−0.010	0.185	0.181	0.235	0.218	0.320	0.181	0.212	0.208	0.208
34	0.002	0.118	0.118	0.156	0.147	0.227	0.117	0.138	0.135	0.135
35	0.000	0.070	0.072	0.096	0.095	0.152	0.072	0.084	0.082	0.082
36	0.000	0.038	0.042	0.055	0.058	0.096	0.041	0.048	0.047	0.046
37	0.000	0.020	0.023	0.030	0.034	0.057	0.023	0.025	0.025	0.024
38	0.000	0.009	0.012	0.015	0.019	0.032	0.012	0.012	0.012	0.012
39	0.000	0.004	0.006	0.007	0.010	0.017	0.006	0.006	0.005	0.005
40	0.000	0.002	0.003	0.003	0.005	0.008	0.002	0.002	0.002	0.002
41	0.000	0.001	0.001	0.001	0.003	0.004	0.001	0.001	0.001	0.001
42	0.000	0.000	0.001	0.000	0.001	0.001	0.000	0.000	0.000	0.000

Table 4: A comparison of the peak errors of different solution techniques for Pe = 4 with $h = 0.025$.

Cr	Δt	CN [12]	FD3 [17]	CD6
0.016	0.0005	$1.54E-03$	$9.13E-04$	$5.64E-09$
0.032	0.001	$1.51E-03$	$9.31E-04$	$5.64E-09$
0.064	0.002	$1.47E-03$	$9.73E-04$	$5.78E-09$
0.08	0.0025	$1.44E-03$	$9.96E-04$	$5.99E-09$
0.16	0.005	$1.34E-03$	$1.13E-03$	$1.10E-08$
0.32	0.01	$1.20E-03$	$1.47E-03$	$8.18E-08$
0.64	0.02	$1.12E-03$	$2.26E-03$	$9.02E-07$
0.80	0.025	NA	NA	$1.79E-06$

Table 5: A comparison of analytical and CD6 solutions for various values of x with $h = 0.025$, $\Delta t = 0.005$, Cr = 0.16, and Pe = 4.

x	Exact	CD6	Absolute error
3.50	0.0000000	0.0000000	$3.78E-13$
4.00	0.0000159	0.0000159	$1.02E-09$
4.50	0.0201770	0.0201769	$1.94E-08$
5.00	0.2182179	0.2182179	$1.10E-08$
5.50	0.0201770	0.0201770	$2.51E-08$
6.00	0.0000159	0.0000160	$9.45E-10$
6.50	0.0000000	0.0000000	$4.40E-13$

are known are used to test the method described for solving the advection-diffusion equation. The technique is applied to solve the ADE with $C_0(x)$, $f_0(t)$, $f_L(t)$, and $g(t)$ prescribed. To test the performance of the proposed method, L_2 and L_∞ error norms are used as follows:

$$L_\infty = \max_i \left| c_i^{\text{exact}} - c_i^{\text{numerical}} \right|,$$
$$L_2 = \sqrt{\sum_{i=1}^{N} \left| c_i^{\text{exact}} - c_i^{\text{numerical}} \right|^2}. \tag{14}$$

Example 1. Here, pure advection equation is considered in an infinitely long channel of constant cross-section and bottom slope, and velocity is taken to be $U = 0.5$ m/s. Concentration is accepted to be the Gaussian distribution of $\rho = 264$ m, and initial peak location is $x_0 = 2000$ m. The initial distribution is transported downstream in a long channel without change in shape by the time $t = 9600$ s. Exact solution of this problem is as follows [11]:

$$C(x,t) = 10 \exp\left[-\frac{(x - x_0 - Ut)^2}{2\rho^2} \right]. \tag{15}$$

At the boundaries the following conditions are used:

$$C(0,t) = 0,$$
$$-D\left(\frac{\partial c}{\partial x}\right)(9000,t) = 0. \tag{16}$$

Initial conditions can be taken from exact solution. The initial Gaussian pulse at $t = 0$, the concentration distribution obtained using the CD6 solution, and concentration distribution obtained using exact solution at $t = 9600$ s are compared in Figure 1. Both quantitative and qualitative agreements between the exact and the CD6 solutions are excellent (see Tables 1 and 2, Figure 1).

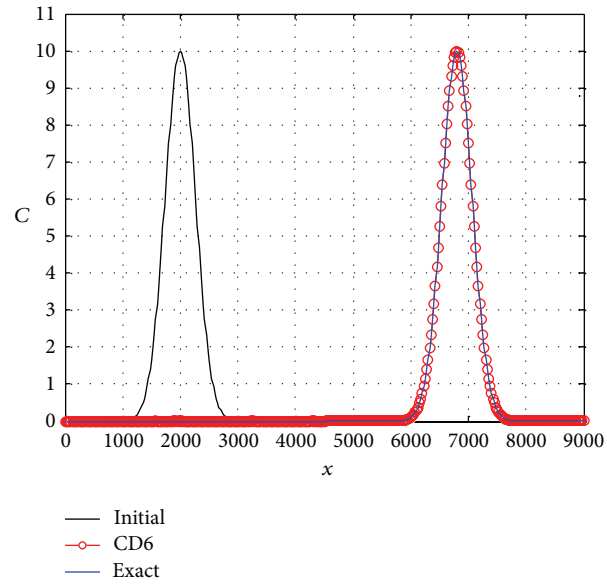

Figure 1: Comparison of the exact solution and the numerical solution obtained with CD6 scheme for $h = 25$ and $\Delta t = 50$ s.

As seen from Table 1, the CD6 method has given the closest result to the exact peak concentration value. Note that, since an explicit time integration scheme RK4 is used in this study, the CD6 scheme cannot produce any result for Cr > 1. To show the accuracy of the obtained results, L_2 and L_∞ error norms have been calculated using the CD6 scheme and exhibited in Table 2. As seen in the corresponding table, the CD6 solution is better than its rivals.

Example 2. Flow velocity and diffusion coefficient are taken to be $U = 0.01$ m/s and $D = 0.002$ m^2/s in this experiment. Let the length of the channel be $L = 100$ m and be divided into 100 uniform elements. The Pe number is accepted to be 5. The Cr numbers are selected as 0.01, 0.1, and 0.6 for the present work. Exact solution of the current problem is [11]

$$C(x,t) = \frac{1}{2}\operatorname{erfc}\left(\frac{x - Ut}{\sqrt{4Dt}}\right) + \frac{1}{2}\exp\left(\frac{Ux}{D}\right)\operatorname{erfc}\left(\frac{x + Ut}{\sqrt{4Dt}}\right). \tag{17}$$

At the boundaries the following conditions are used:

$$C(0,t) = 1,$$
$$-D\left(\frac{\partial c}{\partial x}\right)(L,t) = 0. \tag{18}$$

Initial conditions can be taken from exact solution. Comparison between numerical solutions and the exact solution is given in Table 3. In the calculation of the exact results given by Szymkiewicz [11], there has erroneously been a

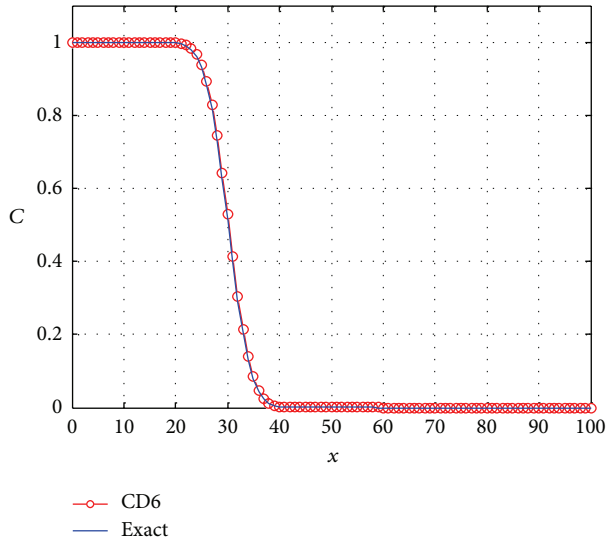

FIGURE 2: Comparison of the exact solution and the numerical solution obtained with CD6 scheme for $h = 1$ m and $\Delta t = 10$ s.

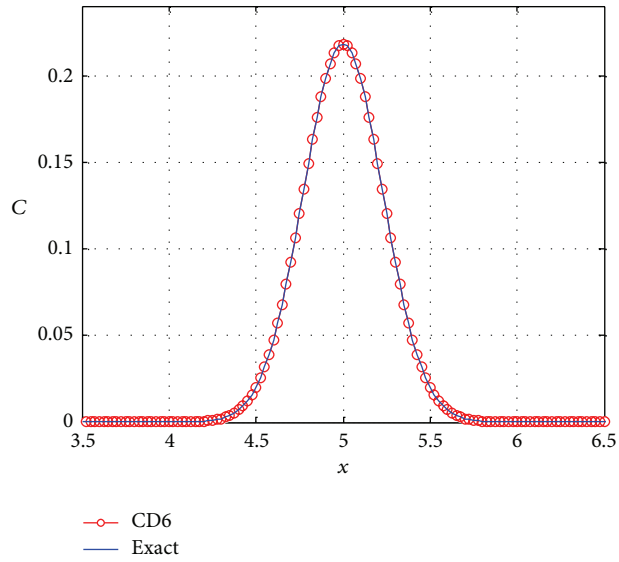

FIGURE 3: Comparison of analytical and CD6 solutions for transport of one-dimensional Gaussian pulse.

mistake. Therefore the exact results have been recalculated in MATLAB. As seen in Table 3, the solutions produced by other researchers [11, 28, 31, 32, 34] for Cr = 0.6 do not converge enough. This case proves that the selected time step ($\Delta t = 60$ s) is greater than it needs to be. Note also that the CD6 scheme gives stable results for Cr = 0.6, and the computed results are nearly as good as in FEMQSF [34]. Since this problem cannot be solved accurate enough for $\Delta t = 60$ s, the calculations have been repeated for the cases $\Delta t = 10$ s (Cr = 0.1) and $\Delta t = 1$ s (Cr = 0.01), and the corresponding results have been given in Table 3. The results produced by the CD6 scheme for $\Delta t = 1$ s are the same as with the exact solution, while the results of the CD6 scheme for $\Delta t = 10$ s are seen to be acceptable level. Comparison of the exact solution and the numerical solution obtained with CD6 scheme for $h = 1$ m and $\Delta t = 10$ s is shown in Figure 2. As can be seen in Figure 2, there is an excellent agreement between CD6 and exact solutions.

Example 3. Consider the quantities $U = 0.8$ m/s and $D = 0.005$ m^2/s in (1). The following exact solution for this example can be found in [49]:

$$C(x,t) = \frac{1}{\sqrt{4t+1}} \exp\left[-\frac{(x-1-Ut)^2}{D(4t+1)}\right]. \quad (19)$$

At the boundaries the following conditions are used:

$$C(0,t) = \frac{1}{\sqrt{4t+1}} \exp\left[-\frac{(-1-Ut)^2}{D(4t+1)}\right],$$
$$C(9,t) = \frac{1}{\sqrt{4t+1}} \exp\left[-\frac{(8-Ut)^2}{D(4t+1)}\right]. \quad (20)$$

Initial conditions can be taken from exact solution. The distribution of the Gaussian pulse at $t = 5$ s is computed using the exact solution and compared with the concentration distribution obtained using the CD6 solution as shown in Figure 3. As can be seen in Table 4, the CD6 results in Example 3 are far more accurate comparison to Crank-Nicolson (CN) scheme [12] and third-order finite difference (FD3) scheme [17]. In Table 5, a comparison of analytical and CD6 solutions is carried out for various values of x with $h = 0.025$, $\Delta t = 0.005$, Cr = 0.16, and Pe = 4.

4. Conclusions

This paper deals with the advection-diffusion equation using the CD6 scheme in space and the RK4 in time. The combined method worked very well to give very reliable and accurate solutions to these processes. The CD6 scheme provides an efficient and alternative way for modeling the advection-diffusion processes. The performance of the method for the considered problems was tested by computing L_2 and L_∞ error norms. The method gives convergent approximations for the advection-diffusion problems for Pe $\leq$ 5. Note that numerical solution cannot obtained while Pe $>$ 5 and Cr $>$ 1. To overcome these disadvantages, upwind compact schemes and implicit time integration need to be used. For further research, special attention can be paid on the use of compact difference schemes in computational hydraulic problems such as sediment transport in stream and lakes, contaminant transport in groundwater, and flood routing in river and modeling of shallow water waves.

References

[1] C. G. Koutitas, *Elements of Computational Hydraulics*, Pentech Press, London, UK, 1983.

[2] B. J. Noye, *Numerical Solution of Partial Differential Equations*, Lecture Notes, 1990.

[3] Q. N. Fattah and J. A. Hoopes, "Dispersion in anisotropic homogeneous, porous media," *Journal of Hydraulic Engineering*, vol. 111, no. 5, pp. 810–827, 1985.

[4] P. C. Chatwin and C. M. Allen, "Mathematical models of dispersion in rivers and estuaries," *Annual Review of Fluid Mechanics*, vol. 17, pp. 119–149, 1985.

[5] F. M. Holly and J. M. Usseglio-Polatera, "Dispersion simulation in two-dimensional tidal flow," *Journal of Hydraulic Engineering*, vol. 110, no. 7, pp. 905–926, 1984.

[6] J. R. Salmon, J. A. Liggett, and R. H. Gallagher, "Dispersion analysis in homogeneous lakes," *International Journal for Numerical Methods in Engineering*, vol. 15, no. 11, pp. 1627–1642, 1980.

[7] H. Karahan, "An iterative method for the solution of dispersion equation in shallow water," in *Water Pollution VI: Modelling, Measuring and Prediction*, C. A. Brebbia, Ed., pp. 445–453, Wessex Institute of Technology, Southampton, UK, 2001.

[8] Z. Zlatev, R. Berkowicz, and L. P. Prahm, "Implementation of a variable stepsize variable formula method in the time-integration part of a code for treatment of long-range transport of air pollutants," *Journal of Computational Physics*, vol. 55, no. 2, pp. 278–301, 1984.

[9] M. H. Chaudhry, D. E. Cass, and J. E. Edinger, "Modeling of unsteady-flow water temperatures," *Journal of Hydraulic Engineering*, vol. 109, no. 5, pp. 657–669, 1983.

[10] N. Kumar, "Unsteady flow against dispersion in finite porous media," *Journal of Hydrology*, vol. 63, no. 3-4, pp. 345–358, 1983.

[11] R. Szymkiewicz, "Solution of the advection-diffusion equation using the spline function and finite elements," *Communications in Numerical Methods in Engineering*, vol. 9, no. 3, pp. 197–206, 1993.

[12] H. Karahan, "Implicit finite difference techniques for the advection-diffusion equation using spreadsheets," *Advances in Engineering Software*, vol. 37, no. 9, pp. 601–608, 2006.

[13] H. Karahan, "Unconditional stable explicit finite difference technique for the advection-diffusion equation using spreadsheets," *Advances in Engineering Software*, vol. 38, no. 2, pp. 80–86, 2007.

[14] H. Karahan, "Solution of weighted finite difference techniques with the advection-diffusion equation using spreadsheets," *Computer Applications in Engineering Education*, vol. 16, no. 2, pp. 147–156, 2008.

[15] H. S. Price, J. C. Cavendish, and R. S. Varga, "Numerical methods of higher-order accuracy for diffusion-convection equations," *Society of Petroleum Engineers*, vol. 8, no. 3, pp. 293–303, 1968.

[16] K. W. Morton, "Stability of finite difference approximations to a diffusion-convection equation," *International Journal for Numerical Methods in Engineering*, vol. 15, no. 5, pp. 677–683, 1980.

[17] H. Karahan, "A third-order upwind scheme for the advection-diffusion equation using spreadsheets," *Advances in Engineering Software*, vol. 38, no. 10, pp. 688–697, 2007.

[18] Y. Chen and R. A. Falconer, "Advection-diffusion modelling using the modified QUICK scheme," *International Journal for Numerical Methods in Fluids*, vol. 15, no. 10, pp. 1171–1196, 1992.

[19] M. Dehghan, "Weighted finite difference techniques for the one-dimensional advection-diffusion equation," *Applied Mathematics and Computation*, vol. 147, no. 2, pp. 307–319, 2004.

[20] C. Man and C. W. Tsai, "A higher-order predictor-corrector scheme for two-dimensional advection-diffusion equation," *International Journal for Numerical Methods in Fluids*, vol. 56, no. 4, pp. 401–418, 2008.

[21] M. Dehghan and A. Mohebbi, "High-order compact boundary value method for the solution of unsteady convection-diffusion problems," *Mathematics and Computers in Simulation*, vol. 79, no. 3, pp. 683–699, 2008.

[22] G. Gurarslan and H. Karahan, "Numerical solution of advection-diffusion equation using a high-order MacCormack scheme," in *Proceedings of the 6th National Hydrology Congress*, Denizli, Turkey, September 2011.

[23] M. Sari, G. Gürarslan, and A. Zeytinoğlu, "High-order finite difference schemes for solving the advection-diffusion equation," *Mathematical and Computational Applications*, vol. 15, no. 3, pp. 449–460, 2010.

[24] A. Mohebbi and M. Dehghan, "High-order compact solution of the one-dimensional heat and advection-diffusion equations," *Applied Mathematical Modelling*, vol. 34, no. 10, pp. 3071–3084, 2010.

[25] A. E. Taigbenu and O. O. Onyejekwe, "Transient 1D transport equation simulated by a mixed green element formulation," *International Journal for Numerical Methods in Fluids*, vol. 25, no. 4, pp. 437–454, 1997.

[26] R. C. Mittal and R. K. Jain, "Numerical solution of convection-diffusion equation using cubic B-splines collocation methods with Neumann's boundary conditions," *International Journal of Applied Mathematics and Computation*, vol. 4, no. 2, pp. 115–127, 2012.

[27] A. Korkmaz and I. Dag, "Cubic B-spline differential quadrature methods for the advection-diffusion equation," *International Journal of Numerical Methods for Heat & Fluid Flow*, vol. 22, no. 8, pp. 1021–1036, 2012.

[28] F. M. Holly and A. Preissmann, "Accurate calculation of transport in two dimensions," *Journal of Hydraulic Division*, vol. 103, no. 11, pp. 1259–1277, 1977.

[29] T. L. Tsai, J. C. Yang, and L. H. Huang, "Characteristics method using cubic-spline interpolation for advection-diffusion equation," *Journal of Hydraulic Engineering*, vol. 130, no. 6, pp. 580–585, 2004.

[30] T. L. Tsai, S. W. Chiang, and J. C. Yang, "Examination of characteristics method with cubic interpolation for advection-diffusion equation," *Computers and Fluids*, vol. 35, no. 10, pp. 1217–1227, 2006.

[31] L. R. T. Gardner and I. Dag, "A numerical solution of the advection-diffusion equation using B-spline finite element," in *Proceedings International AMSE Conference, 'Systems Analysis, Control & Design'*, pp. 109–116, Lyon, France, July 1994.

[32] I. Dağ, A. Canivar, and A. Şahin, "Taylor-Galerkin method for advection-diffusion equation," *Kybernetes*, vol. 40, no. 5-6, pp. 762–777, 2011.

[33] S. Dhawan, S. Kapoor, and S. Kumar, "Numerical method for advection diffusion equation using FEM and B-splines," *Journal of Computational Science*, vol. 3, pp. 429–437, 2012.

[34] I. Dağ, D. Irk, and M. Tombul, "Least-squares finite element method for the advection-diffusion equation," *Applied Mathematics and Computation*, vol. 173, no. 1, pp. 554–565, 2006.

[35] B. Servan-Camas and F. T. C. Tsai, "Lattice Boltzmann method with two relaxation times for advection-diffusion equation: third order analysis and stability analysis," *Advances in Water Resources*, vol. 31, no. 8, pp. 1113–1126, 2008.

[36] M. K. Kadalbajoo and P. Arora, "Taylor-Galerkin B-spline finite element method for the one-dimensional advection-diffusion equation," *Numerical Methods for Partial Differential Equations*, vol. 26, no. 5, pp. 1206–1223, 2010.

[37] M. Zerroukat, K. Djidjeli, and A. Charafi, "Explicit and implicit meshless methods for linear advection-diffusion-type partial differential equations," *International Journal for Numerical Methods in Engineering*, vol. 48, no. 1, pp. 19–35, 2000.

[38] J. Li, Y. Chen, and D. Pepper, "Radial basis function method for 1-D and 2-D groundwater contaminant transport modeling," *Computational Mechanics*, vol. 32, no. 1-2, pp. 10–15, 2003.

[39] Y. V. S. S. Sanyasiraju and V. Manjula, "Higher order semi compact scheme to solve transient incompressible Navier-Stokes equations," *Computational Mechanics*, vol. 35, no. 6, pp. 441–448, 2005.

[40] Z. Tian and Y. Ge, "A fourth-order compact finite difference scheme for the steady stream function-vorticity formulation of the Navier-Stokes/Boussinesq equations," *International Journal for Numerical Methods in Fluids*, vol. 41, no. 5, pp. 495–518, 2003.

[41] Z. Tian, X. Liang, and P. Yu, "A higher order compact finite difference algorithm for solving the incompressible Navier-Stokes equations," *International Journal for Numerical Methods in Engineering*, vol. 88, no. 6, pp. 511–532, 2011.

[42] M. Sari and G. Gürarslan, "A sixth-order compact finite difference scheme to the numerical solutions of Burgers' equation," *Applied Mathematics and Computation*, vol. 208, no. 2, pp. 475–483, 2009.

[43] M. Sari, G. Gürarslan, and I. Dağ, "A compact finite difference method for the solution of the generalized burgers-fisher equation," *Numerical Methods for Partial Differential Equations*, vol. 26, no. 1, pp. 125–134, 2010.

[44] M. Sari and G. Gürarslan, "A sixth-order compact finite difference method for the one-dimensional sine-Gordon equation," *International Journal for Numerical Methods in Biomedical Engineering*, vol. 27, no. 7, pp. 1126–1138, 2011.

[45] G. Gürarslan, "Numerical modelling of linear and nonlinear diffusion equations by compact finite difference method," *Applied Mathematics and Computation*, vol. 216, no. 8, pp. 2472–2478, 2010.

[46] M. Sari, "Solution of the porous media equation by a compact finite difference method," *Mathematical Problems in Engineering*, vol. 2009, Article ID 912541, 13 pages, 2009.

[47] S. K. Lele, "Compact finite difference schemes with spectral-like resolution," *Journal of Computational Physics*, vol. 103, no. 1, pp. 16–42, 1992.

[48] J. C. Kalita and A. K. Dass, "High-order compact simulation of double-diffusive natural convection in a vertical porous annulus," *Engineering Applications of Computational Fluid Dynamics*, vol. 5, no. 3, pp. 357–371, 2011.

[49] S. Sankaranarayanan, N. J. Shankar, and H. F. Cheong, "Three-dimensional finite difference model for transport of conservative pollutants," *Ocean Engineering*, vol. 25, no. 6, pp. 425–442, 1998.

Hindawi Publishing Corporation
Mathematical Problems in Engineering
Volume 2013, Article ID 692103, 10 pages
http://dx.doi.org/10.1155/2013/692103

Research Article

A Model for Urban Environment and Resource Planning Based on Green GDP Accounting System

Linyu Xu, Bing Yu, Wencong Yue, and Xiaodong Xie

State Key Joint Laboratory of Environmental Simulation and Pollution Control, School of the Environment, Beijing Normal University, 19 Xinjiekouwai Street, Haidian District, Beijing 100875, China

Correspondence should be addressed to Linyu Xu; xly@bnu.edu.cn

Received 5 December 2012; Accepted 8 March 2013

Academic Editor: Yongping Li

The urban environment and resources are currently on course that is unsustainable in the long run due to excessive human pursuit of economic goals. Thus, it is very important to develop a model to analyse the relationship between urban economic development and environmental resource protection during the process of rapid urbanisation. This paper proposed a model to identify the key factors in urban environment and resource regulation based on a green GDP accounting system, which consisted of four parts: economy, society, resource, and environment. In this model, the analytic hierarchy process (AHP) method and a modified Pearl curve model were combined to allow for dynamic evaluation, with higher green GDP value as the planning target. The model was applied to the environmental and resource planning problem of Wuyishan City, and the results showed that energy use was a key factor that influenced the urban environment and resource development. Biodiversity and air quality were the most sensitive factors that influenced the value of green GDP in the city. According to the analysis, the urban environment and resource planning could be improved for promoting sustainable development in Wuyishan City.

1. Introduction

During the process of rapid urbanisation, many countries or regions excessively pursue economic development goals like gross domestic product (GDP) (GDP, an important indicator of the economic development level of a country, is the monetary value of all final goods and services produced in a country over a period of 1 year), while ignoring the integrity of the urban ecosystem. As a result, cities are confronted with increasingly relevant biophysical limitations due to the deterioration of natural resources and the environment during these periods of impressive economic growth [1]. Because of this deterioration, various regulations have targeted the urban environment and resource protection to make cities more ecologically resilient [2–5]. Within the relevant studies, the general idea of urban ecological regulation is to recognise the main ecological problems during urban development and then solve them through ecological planning [6, 7]. However, there are few efficient quantitative methods for coordinating the relationship between urban economic development and environmental resource protection in previous studies.

In fact, it is efficient to manage the environment and resources by methods of economic regulation. In this vein, green GDP is a general indicator of economic regulation for environmental protection and resource protection. Measuring green GDP can also be used by environmentalists to track the provision of nature's benefits over time to hold governments accountable or to compare environmental conditions among different cities [8].

Green GDP accounting conventions can be classified into two main groups [9]. Type I green GDP takes into account the difference between GDP and the cost of environmental pollution and resource depletion, but the value of natural ecosystem services is ignored. Heal noted that national economic accounts need to present income statements and balance sheets that reflect the value of ecosystem services [10]. In this context, more scholars have begun to account for the value of ecosystem services and include it in GDP accounting, which we refer to as type II green GDP. Type I green GDP can promote the control of emissions by pollution producers, and therefore is suitable for accounting for green GDP for typical polluted cities. Type II green GDP encourages households

to protect the ecoenvironment and is therefore suitable for application to typical cities with better natural environmental conditions. Of the two types, type II green GDP includes the benefits from the protection of natural ecosystems and has been widely studied in recent years.

The original notion of type II green GDP accounting came from research by Costanza et al. in which the value of global ecosystem services was compared with global GNP. After that, the idea of including ecoservice valuation in traditional economic accounting systems was proposed and gradually developed [11–13]. In 2005, the Millennium Ecosystem Assessment [14] used the notion of ecosystem services to research type II green GDP accounting, and in 2007, Boyd and Banzhaf [15] defined the concept of final ecosystem services and used these as standardised environmental accounting units. However, type II green GDP accounting is still in its infancy, and the approach used to define and calculate final ecosystem services is a key issue.

As argued in a report by the Commission on the Measurement of Economic Performance and Social Progress [16], "green GDP constitutes only one aspect of sustainability, and more research on sustainability assessment is required." On one hand, these green GDP accounting methods, especially the type II method, need to be further improved. Existing accounting methods have focused on accounting for ecoservices, but cannot be easily combined with traditional GDP accounting systems. In China, green GDP accounting systems have included the value of ecosystem services [17], but the accuracy and rationality of ecosystem services accounting do not meet requirements for green GDP accounting. On the other hand, most studies of green GDP still focus on value accounting methods rather than their application. The importance of green GDP should not be limited to calculating a numerical value. Rather, approaches for applying green GDP to reality, such as in urban ecosystem construction or environmental management, should be the focus of more studies.

In this context, a traditional GDP accounting system was decomposed in the present study according to the character of the national economic accounting system in China; it was adapted into a green GDP accounting system including direct ecosystem services; this system was the basis for the urban environment and resource regulation model in this paper. The AHP method and a modified Pearl curve model were then used to identify the key factors in the green GDP accounting system for urban environment and resource regulation; dynamic evaluation was performed, where a higher value of green GDP was the planning target. In this paper, these efforts were demonstrated by a case study of Wuyishan City, and six effective ecological projects were put forward to promote its urban sustainable development.

2. Methodology

2.1. Green GDP Accounting System. Traditional GDP in China was calculated for 20 different industry categories (e.g., agriculture, forestry, animal husbandry, fishing, and Appendix) according to the National Bureau of Statistics. These industries can be classified into three types according to their features, and thus GDP can be divided into three parts:

$$k_1\text{GDP} + k_2\text{GDP} + k_3\text{GDP} = \text{GDP}, \tag{1}$$

where k_1, k_2, and k_3 represent the proportion of GDP generated by economic, social, and resource systems, respectively. However, the environment, which is very important for urban development, is not considered in this equation. Thus, green GDP may be a more suitable metric and can be decomposed as follows:

$$\text{Green GDP}_2 = k_1\text{GDP} + k_2\text{GDP} + k_3\text{GDP} + \text{DES}, \tag{2}$$

$$\text{DES} + \text{ES}_1 + \text{ES}_2 = \text{ESP}, \tag{3}$$

where green GDP_2 is type II green GDP and DES is direct ecosystem services, which can be calculated as final consumption of GDP using the expenditure method. ESP is ecosystem services product, ES_1 is ecosystem benefits for other creatures, and ES_2 is ecosystem benefits for future generations. Therefore, (2) can be simplified to

$$\text{Green GDP}_2 = \text{GDP} + \text{DES}. \tag{4}$$

Because the proportion of the components can differ over time and for different cities or regions, k_1, k_2, and k_3 are not constant and need to be determined for specific cases. DES is part of the total ecosystem services; thus, we need to first determine the DES types (Figure 1) that should be selected. The selection principles are as follows.

(1) Both humans and other creatures will enjoy ecological benefits provided by the natural ecosystem. Therefore, ecosystem services to humans and other creatures should be treated separately in green GDP accounting.

(2) The ecosystem services selected must be end products consumed by humans within a certain period of time to meet GDP accounting requirements. In this study, services are only considered for humans.

Ecosystem services can be divided into those yielding contemporaneous human benefits, descendant benefits, and benefits for all creatures. The benefits for contemporary human included the ecosystem services which were consumed by mankind only in the present. The benefits for all creatures referred to the ecosystem services which can be enjoyed by all creatures, not limited to mankind. The benefits for descendant were the supports for sustainable development provided by ecosystem services.

Based on the selection principles, only the part of services yielding benefits for all creatures should be included in green GDP. Services that yield future human benefits belong to neither DES nor to green GDP. Services accounted for in GDP, such as food production, water supply, and raw material supply, should be excluded. This is a general division of the ecosystem, and the division can be varied for different regions or different periods.

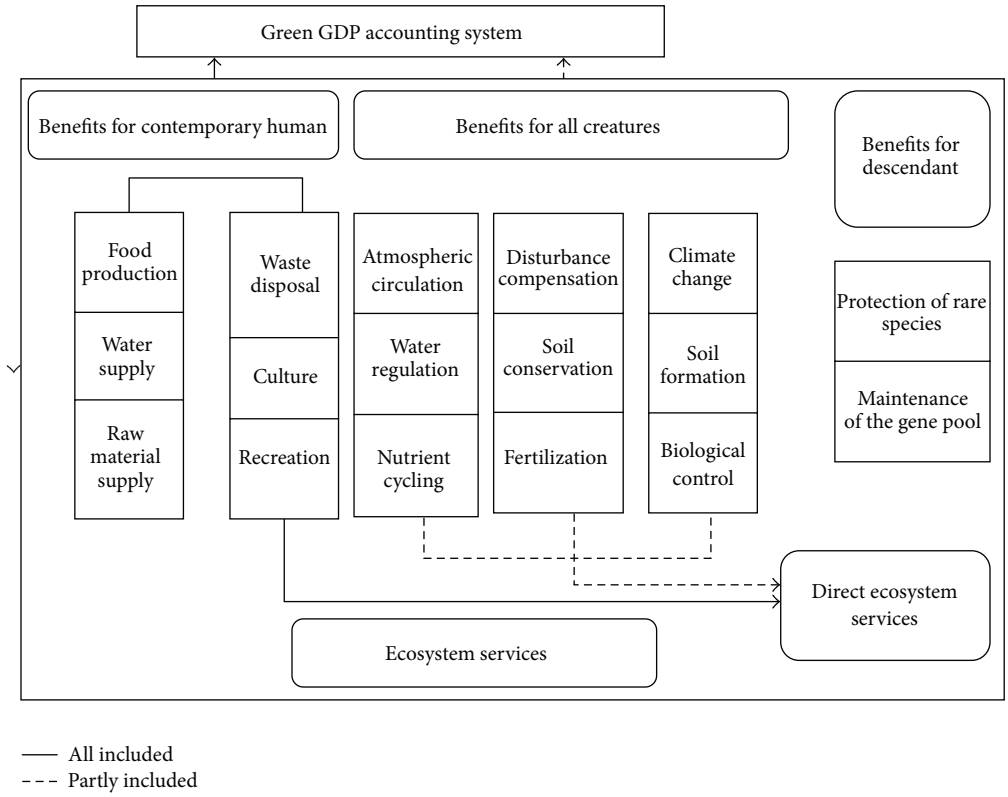

Figure 1: Green GDP accounting system.

Reasonable accounting methods are chosen to calculate the value of direct ecosystem services, such as the hedonic price method for aesthetic valuation and the market price method for water conservation. Thus, the value of DES and green GDP can be obtained.

2.2. Environment and Resource Regulation Model

2.2.1. Key Factors Analysis with AHP Method. The value of green GDP is influenced by multiple factors in environmental, social, and economic systems. Therefore, beyond accounting for values, a comprehensive analysis should be done by various influenced factors. We selected key factors and analysed them using AHP method (see Figure 2).

2.2.2. Sensitivity Analysis with Pearl Curve Model. The interactions among social, economic, environmental managerial, regulatory, and lifestyle factors are complicated and change over time [18]. Therefore, to identify improvements in ecosystem services and human activities, the impact of human activities on ecological factors and green GDP should be analysed dynamically. The Pearl curve model was widely used to show the variations [19, 20], mathematically expressed as:

$$l = \frac{L}{1 + ae^{-bt}}, \tag{5}$$

where l is the variation index for the factor, L is its maximum value, a and b are constants, and t is a parameter reflecting differences in the factor over time.

With reference to the form of Pearl curve, we established a modified Pearl curve model to express the influence of ecological factors and ecosystem services, mathematically expressed as:

$$l = \frac{L}{1 + e^{-t}} - \frac{1}{2}. \tag{6}$$

In this model, it insured that in the beginning ($t = 0$), when the situation of human activities and the ecological situations was retention (R), the change were equal to 0. Moreover, the model was symmetric about the x-axis, in order to make the influence of ecological factors and ecosystem services more clear and comparative.

Therefore, the models for changes in ecological factors and green GDP are:

$$\begin{aligned} l_1 &= \frac{L_1}{1 + e^{-t_1}} - \frac{1}{2}, \\ l_2 &= \frac{L_2}{1 + e^{-t_2}} - \frac{1}{2}, \end{aligned} \tag{7}$$

where l_1 is the change in ecological factor, L_1 is the maximum value for the ecological factor, and t_1 denotes the situation for human activities, with $t_1 = -3, -2, -1, 0, 1, 2$ and 3 indicating high deterioration (HD), moderate deterioration (MD), slight deterioration (SD), retention (R), slight improvement (SI), improvement (I), and entire improvement (EI), respectively. Similarly, l_2 is the change in green GDP, L_2 is

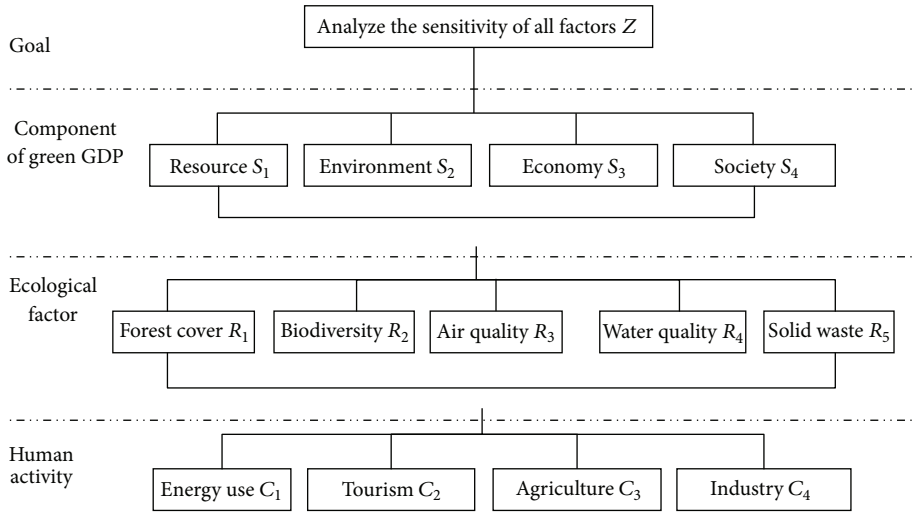

Figure 2: Hierarchical structure for key factors in green GDP accounting.

the maximum value of green GDP, and t_2 denotes the situation for ecological factors, with $t_2 = -3, -2, -1, 0, 1, 2$ and 3 indicating HD, MD, SD, R, SI, I, and EI, respectively.

According to the key factors analysis and sensitivity analysis for green GDP accounting, the relationships between human activities and green GDP and ecological factors and green GDP can be revealed; thus, environmental and resource planning can be proposed for improving green GDP.

3. Case Study

3.1. Study Area. Wuyishan City is located in the northwest of Fujian Province, China, and consists of three districts and seven towns. It covers a total area of approximately 2802.77 km^2 (Figure 3). It is a popular with tourists because of Mount Wuyi, which is included on the UNESCO World Heritage List (http://whc.unesco.org/en/list/911). Wuyishan Nature Reserve has the largest existing and best-preserved subtropical native forest ecosystem. To protect this important ecological environment, the authorities in Wuyishan City have limited industrial development, despite the GDP benefits of industrial production.

For Wuyishan City, the environmental externality mainly came from its good ecoenvironment; the valuation of its forest ecosystem services should be accounted well with type II green GDP. Therefore, type II green GDP accounting is suitable for encouraging the government and households of Wuyishan City to protect the natural environment.

3.2. Green GDP Accounting for Wuyishan City. The DES selection was based on the analysis of leading industries and the opinions of local residents. It not only considers current social economic situation, but also the individual's ecological consciousness. This process can also provide a reference for analysis of the key factors in green GDP accounting and ecological regulation in subsequent research.

3.2.1. Leading Industries. A ratio method can be used to select the leading industry according to the following:

$$SV_{ij} = \frac{\left(V_{ij}/V_i\right)}{\left(V_j/V\right)}, \tag{8}$$

where SV_{ij} is an index representing the status of an industry in the regional economy, V_{ij} is the value added by industry j in region i, V_i is the total value added for region i, V_j is the total value added by industry j, and V is the national gross value added. $SV_{ij} > 1$ means that industry j is a leading industry in region i.

According to (8), the value of SV_{ij} for each industry in Wuyishan City is shown in Table 1.

The data in Table 1 show that tourism has the highest SV_{ij} value, which reflects the predominant role of tourism in the economy of Wuyishan City. Manufacturing industry has the lowest SV_{ij} value, which confirms that local industrial development is low. These results properly reflect the character of Wuyishan City, which has strict environmental protection requirements. Hence, type II green GDP accounting, which reflects changes in the welfare of local residents and fully internalized market externalities for Wuyishan City, is more appropriate than type I green GDP.

3.2.2. Opinion of Local Residents. Based on the meaning of ESI, the DES was determined according to the urban ecosystem characteristics and the opinions of local residents. Through questionnaire surveys, the residents' attitudes toward and understanding of local ecosystem services were elicited.

Researchers conducted questionnaire surveys over a period of 15 days to investigate the ecological and environmental consciousness of the residents in Wuyishan City. Respondents were randomly selected from different towns within Wuyishan City and 361 questionnaires were returned. The third and fourth questions in the questionnaire focused

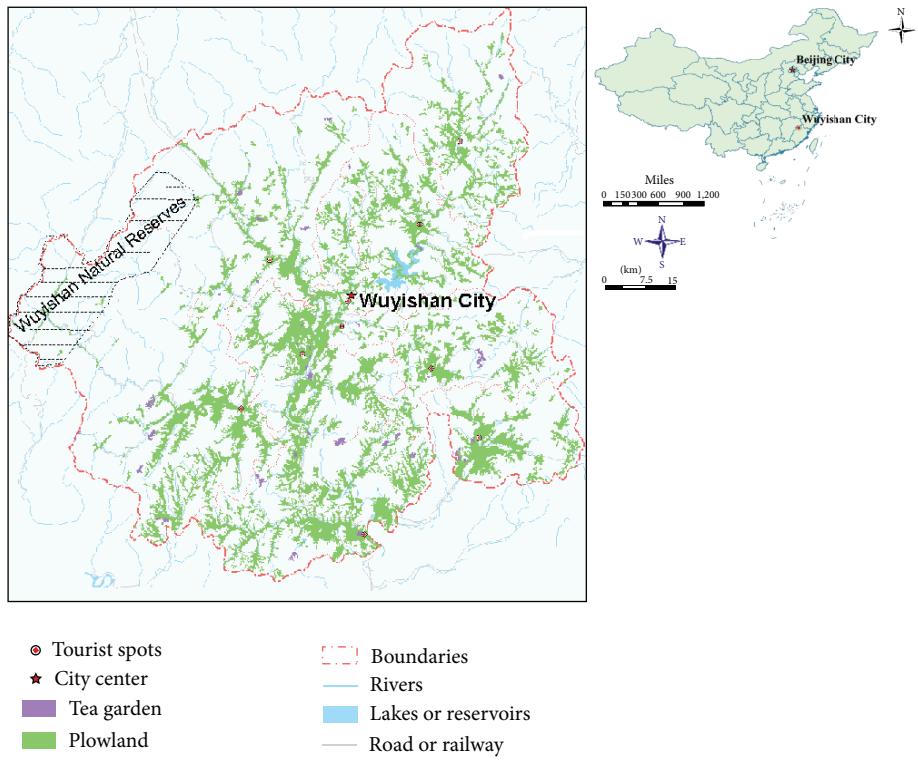

Figure 3: Location of Wuyishan City, China.

Table 1: SV_{ij} for each industry in Wuyishan City.

Item	National (10^8 yuan)	Wuyishan city (10^4 yuan)	SV_{ij}
GDP	335353	556423	—
Primary industry	35477	109709	1.863771
Secondary industry	156958	178303	0.684656
Manufacturing industry	134625	114603	0.513059
Construction	22333	63700	1.719054
Tertiary industry	142918	278411	1.174077
Tourism	10184	303200	17.94353

on attitudes toward and understanding of ecosystem services (Figure 4).

Some 35.3% of the respondents hoped that local tourism would be a priority for development, and 31.5% believed that parks should be built in vacant lots. These responses indicate that local residents are concerned about the recreation services provided by Wuyishan Scenic Spots and Nature Reserve.

According to the analysis and questionnaire results, the importance of six human benefit types (food production, water supply, aesthetic, health guarantee, reduced waste treatment costs, and culture) was confirmed. Because the first two were already included in the traditional GDP accounting system, they were excluded to avoid repeat accounting. The other four benefits were included in green GDP. The DES composition is shown in Figure 5.

After collecting relevant data, the accounting methods listed in Table 2 [21] were used to calculate the value of direct ecosystem services for Wuyishan City (Table 3).

Among DES types, the largest value was observed for water conservation (65%), followed by gas regulation (29%). This shows that the natural landscape of Wuyishan City not only promotes local tourism development but also provides many benefits for residents that cannot be ignored in GDP accounting systems. Therefore, protection of the natural environment should be strengthened when focusing on the development of local tourism.

According to the type II green GDP accounting model, the green GDP of Wuyishan City from 2005 to 2010 was calculated in Table 4.

The green GDP in Wuyishan City has risen gradually in the past years. As the direct ecosystem service value of Wuyishan City has changed little, the trend growth of green GDP and GDP kept pace. The results indicated that the economic development in Wuyishan City has coordinated with its environment and resource protection. But it is necessary to pay more attention to protect its environment and resources to increase its green GDP.

3.3. Environment and Resource Regulation for Wuyishan City. Using an analytic hierarchy process (AHP) method, we built the hierarchical structure (Figure 5) to analyse the correlations among resources, environment, economy, and society that form the important aspects of ecological factors and human activity. According to the hierarchical structure,

Table 2: Accounting method for each direct ecosystem service (DES).

DES	Method	Formula
Aesthetic	Hedonic pricing	Trees can increase real estate prices by 5–10%, which can be a basis for accounting for aesthetic value
Water conservation	Market price	$DES_1 = (R - E) \times A \times Ep$, where DES_1 is the water restoration per unit area, yuan/(hm^2·yr), R is average rainfall, mm/yr, E is average evaporation, mm/yr, A is the study area (hm^2), and Ep is the shadow price of water, 0.67 yuan/m^3
Gas regulation		
SO_2 absorption	Shadow price	$DES_2 = Qd_2 \times Cd_2 \times S$, where DES_2 is the value of absorbing SO_2 of per unit area of ecosystem, yuan/(hm^2·yr), Qd_2 is ability of SO_2 absorption of per unit area of ecosystem, ton/(hm^2·yr), Cd_2 is the engineering cost for reducing SO_2, 1 090 yuan/ton, and S is the study area acreage (hm^2).
Reducing particulate matter (PM)	Substitute cost	$DES_3 = Qd_3 \times Cd_3 \times S$, where DES_3 is the value of reducing PM per unit area, yuan/(hm^2·yr), Qd_3 is the ability to reduce PM per unit area, t/(hm^2·yr), Cd_3 is the cost of reducing PM, 170 yuan/ton, and S is the study area (hm^2)
Cultural	—	The average scientific cultural value of the global temperate forest ecosystem is 99 yuan/(hm^2·year)

Table 3: Value of direct ecosystem services in Wuyishan City in 2010.

Type of service	Value (10^4 yuan)
Aesthetic	6164
Water conservation	93670
Gas regulation	41605
Cultural	2269
Total value	143708

The total forest area in Wuyishan City was 229191.33 hm^2 in 2010 (land use plan of Wuyishan City, 2006–2020).

Table 4: Green GDP in Wuyishan City from 2005 to 2010 (10^4 yuan).

Year	2005	2006	2007	2008	2009	2010
DES	138947	139505	139837	141125	141858	143708
GDP	301818	339237	416641	493920	556423	657789
Green GDP	440765	478742	556478	635045	698281	801497

Data resource: Statistical bulletin of national economic and social development in Wuyishan, China (2005–2010); land use plan of Wuyishan City, 2006–2020.

Table 5: Value of direct ecosystem services in Wuyishan City in 2010.

Item	Energy use	Agriculture	Tourism	Industry
Forest cover	0.201	0.441	0.455	0.231
Biodiversity	0.078	0.062	0.455	0.077
Air quality	0.520	0.166	0.000	0.231
Water quality	0.000	0.166	0.000	0.231
Solid waste	0.201	0.166	0.091	0.231

the pairwise comparison matrices for each layer were constructed based on our survey conducted in Wuyishan City. The weights for the impact of human activities on ecological factors and of ecological factors on green GDP are presented in Tables 5 and 6.

The impact weights can be divided into four grades: 0–0.25 (no influence), grade I; 0.26–0.5 (slight influence), grade II; 0.51–0.75 (large influence), grade III; and 0.76–1 (enormous influence), grade IV.

The standards for human activities and ecological factors changes were classified according to (6) and are shown in Table 7.

The effects of changes in human activities on ecological factors can be calculated based on Tables 5 and 7; the data are multiplied by the corresponding numerical values. The results are shown in Table 8 and Figure 6.

Similarly, the effects of changes in ecological factors on green GDP can be calculated based on Tables 6 and 7. According to the weight for green GDP components (Table 9), the results are shown in Table 10 and Figure 7.

According to the results in Tables 8 and 10, human activities impact green GDP. These effects are shown in Table 11 and Figure 8.

According to our analysis, green GDP was most sensitive to biodiversity and energy use, followed by air quality and tourism. The results suggest that human activities have a significant influence on the green GDP of Wuyishan City and could be considered as key factors in ecological regulation. Based on these key factors, ecological projects can be carried out to regulate the ecological functioning of the region and increase the value of green GDP; some examples of possible projects include nature reserve division construction, corridor building restoration of ecological landscapes, rural biogas planning, vehicle control and improvements, and regulation of industrial energy.

3.4. Discussion. In this case study, we calculated Wuyishan City's green GDP in recent past years and applied the proposed models to identify the key factors of environment and resource planning for its ecological construction. Although

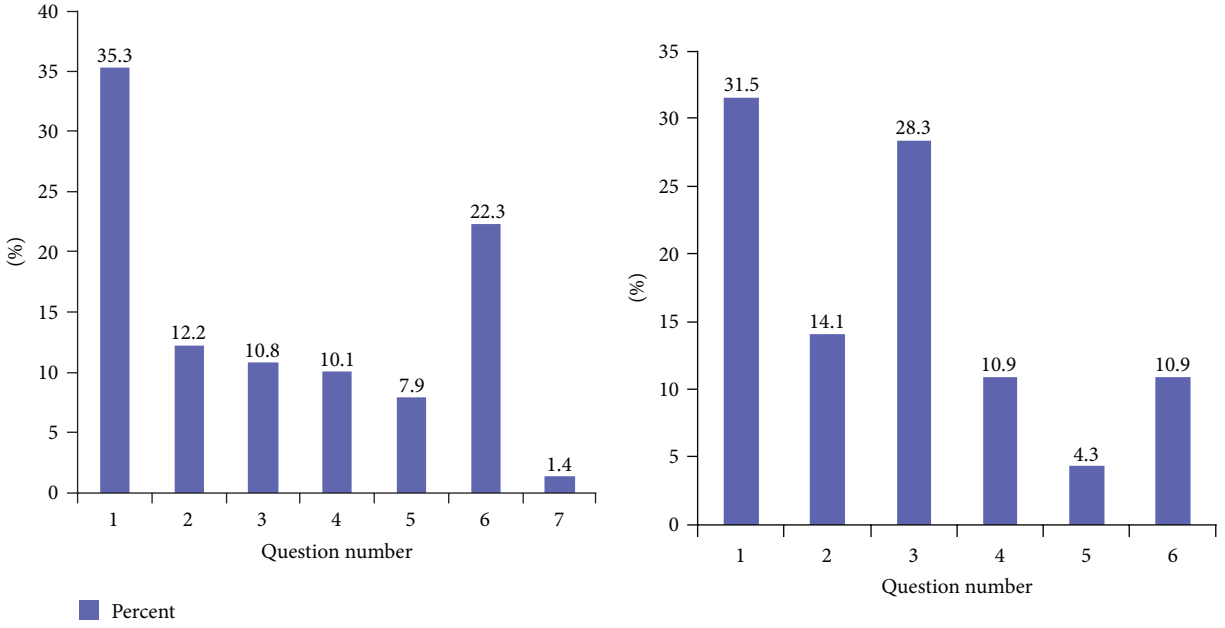

Q3. What would you prefer to be continuously developed in Wuyishan City after 5 years:

(1) Tourism
(2) Industry
(3) Agriculture
(4) Service industry
(5) Transportation
(6) Education
(7) Other

(a)

Q4. If you owned a piece of land in Wuyishan City, what would you build?

(1) Park
(2) Housing
(3) Factory
(4) Farmstead
(5) Other
(6) Not sure

(b)

Figure 4: The third and fourth questions in the questionnaire.

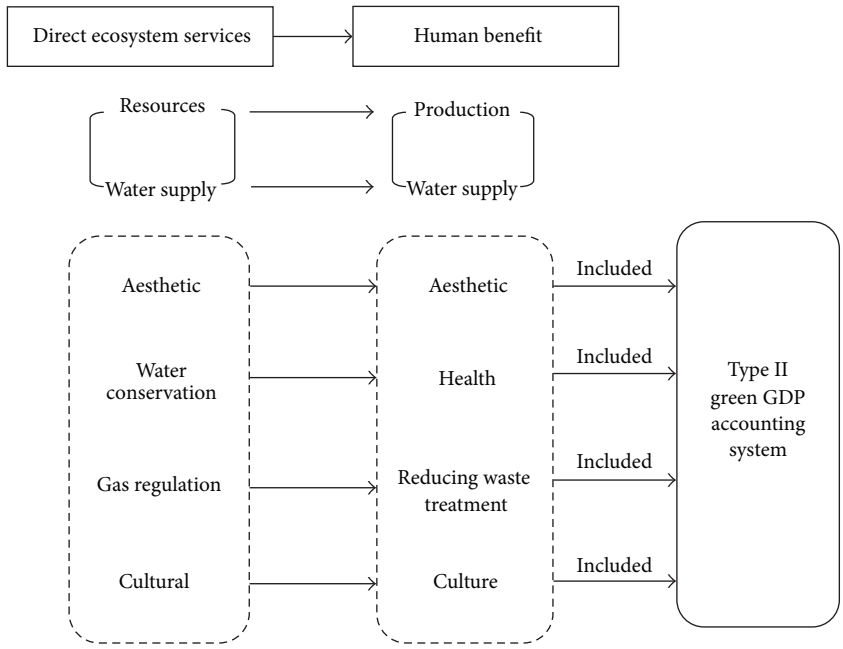

Figure 5: Direct ecosystem services for Wuyishan City.

Table 6: Weights for the impact of ecological factors on green GDP components.

Item	Forest cover	Biodiversity	Air quality	Water quality	Solid waste
Resource	0.138	0.086	0.105	0.375	0.109
Environment	0.545	0.153	0.159	0.125	0.109
Economy	0.233	0.522	0.512	0.375	0.297
Society	0.084	0.239	0.225	0.125	0.484

Table 7: Standards for changes in factors.

Change y	Impact grade			
	I	II	III	IV
HD y_7	−0.4517	−0.9033	−1.3550	−1.8066
MD y_6	−0.3794	−0.7587	−1.1381	−1.5175
SD y_5	−0.2297	−0.4595	−0.6892	−0.9189
R y_4	0.0000	0.0000	0.0000	0.0000
SI y_3	0.2297	0.4595	0.6892	0.9189
I y_2	0.3794	0.7587	1.1381	1.5175
EI y_1	0.4517	0.9033	1.3550	1.8066

Table 8: Standards for changes in ecological factors as a function of human activities.

	Changes in ecological factors			
	Energy use	Agriculture	Tourism	Industry
HD (−3)	$-0.921L_1$	$-0.651L_1$	$-0.863L_1$	$-0.452L_1$
MD (−2)	$-0.774L_1$	$-0.547L_1$	$-0.725L_1$	$-0.380L_1$
SD (−1)	$-0.469L_1$	$-0.331L_1$	$-0.439L_1$	$-0.230L_1$
R (0)	$0.000L_1$	$0.000L_1$	$0.000L_1$	$0.000L_1$
SI (1)	$0.469L_1$	$0.331L_1$	$0.439L_1$	$0.230L_1$
I (2)	$0.774L_1$	$0.547L_1$	$0.725L_1$	$0.380L_1$
EI (3)	$0.921L_1$	$0.651L_1$	$0.863L_1$	$0.452L_1$

Table 9: Proportion for green GDP components in 2010.

Component	Value (10^4 yuan)	Proportion (%)
Resource S_1 (k_3GDP)	206569	25.8
Environment S_2 (DES)	143708	17.9
Economy S_3 (k_1GDP)	399199	49.8
Society S_4 (k_2GDP)	52021	6.5
Green GDP	801497	100

Date source is based on Nanping monthly statistics in Fujian Province, China, 2010.

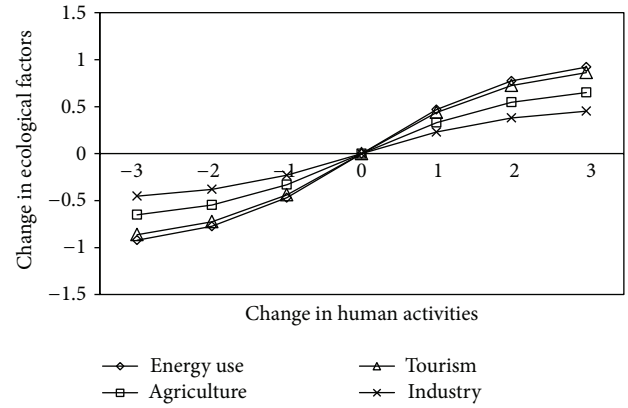

Figure 6: Changes in ecological factors as a function of human activities.

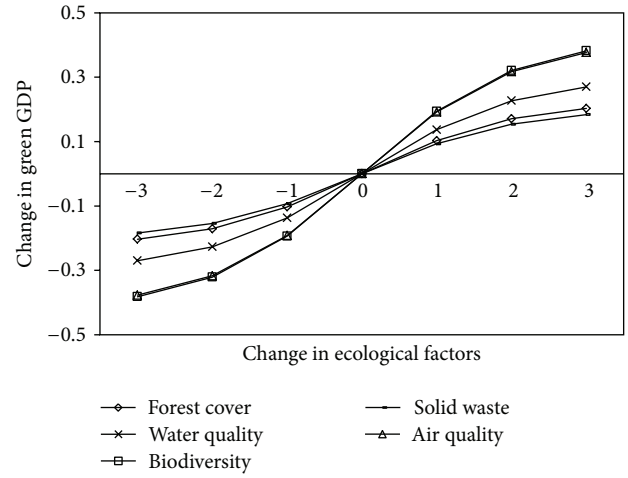

Figure 7: Changes in green GDP as a function of changes in ecological factors.

we have got the specific results, some uncertainties and limitation need to further discussion.

For green GDP accounting system, as it mentioned that the division of direct ecosystem services can be varied for different regions or different periods. In the case study, according to Wuyishan City's geographical feature, the DES selection was largely due to its typical forest ecosystem, and we assumed that in the past 6 years, from 2005 to 2010, the local people's ecological consciousness changed little.

In the regulation model, the key factors for environment and resource planning were identified by the AHP method; further, the sensitivities of the key factors were analysed using a modified Pearl curve model. Firstly, this model was especially suitable for cities with a better environment, and we chose Wuyishan City as the case study. The industrialized city with heavy environmental pollution is not applicable in this model. Moreover, the AHP method may have some subjective as using scoring, and its combination with Pearl curve model is to realize the dynamic qualitative analysis. The quantitative analysis needs further study.

Table 10: Standards for changes in green GDP as a function of ecological factors.

	Green GDP changes for Wuyishan City				
	Forest cover	Biodiversity	Air quality	Water quality	Solid waste
HD (−3)	$-0.203L_2$	$-0.382L_2$	$-0.377L_2$	$-0.270L_2$	$-0.184L_2$
MD (−2)	$-0.171L_2$	$-0.321L_2$	$-0.317L_2$	$-0.227L_2$	$-0.154L_2$
SD (−1)	$-0.103L_2$	$-0.194L_2$	$-0.192L_2$	$-0.137L_2$	$-0.093L_2$
R (0)	$0.000L_2$	$0.000L_2$	$0.000L_2$	$0.000L_2$	$0.000L_2$
SI (1)	$0.103L_2$	$0.194L_2$	$0.192L_2$	$0.137L_2$	$0.093L_2$
I (2)	$0.171L_2$	$0.321L_2$	$0.317L_2$	$0.227L_2$	$0.154L_2$
EI (3)	$0.203L_2$	$0.382L_2$	$0.377L_2$	$0.270L_2$	$0.184L_2$

Table 11: Changes in green GDP as a function of changes in human activities.

	Green GDP changes for Wuyishan City			
	Energy use	Agriculture	Tourism	Industry
HD (−3)	−0.257	−0.182	−0.241	−0.126
MD (−2)	−0.182	−0.129	−0.170	−0.089
SD (−1)	−0.067	−0.047	−0.062	−0.033
R (0)	0.000	0.000	0.000	0.000
SI (1)	0.067	0.047	0.062	0.033
I (2)	0.182	0.129	0.170	0.089
EI (3)	0.257	0.182	0.241	0.126

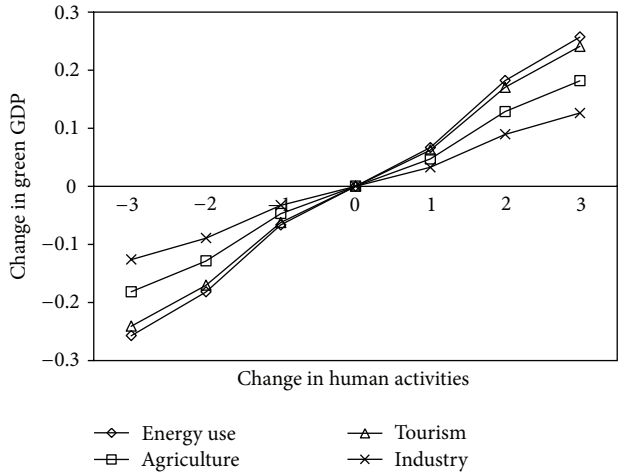

Figure 8: Changes in green GDP for Wuyishan City as a function of changes in human activities.

4. Conclusion

We proposed a model of the environment and resources planning and management based on a mathematical green GDP accounting method, which incorporated ecosystem services. This method can reflect the comprehensive state of a city, both in terms of the economy and environment, as well as understanding their implications for urban ecological regulation. This method is more suitable for cities with better natural environmental conditions; in this paper, the method was used to calculate the green GDP for Wuyishan City.

The DES value for Wuyishan City increased less, which was from 1.39 billion yuan in 2005 to 1.43 billion yuan in 2010. While the green GDP in Wuyishan City has risen much, which was from 4.41 billion yuan in 2005 to 8.01 billion yuan in 2010.

To improve the urban environment and resource development, a model for identification of sensitive urban factors was put forward based on green GDP accounting. The sensitivity analysis of factors influencing the green GDP of Wuyishan City was conducted using an AHP method and the Pearl curve model. The results show that energy use is the key factor that influences the ecological function of the Wuyishan urban ecosystem. Moreover, biodiversity and air quality are the most important factors influencing green GDP in terms of ecosystem services. Guided by the analysis, six ecological projects were put forward for ecological function regulation to promote urban sustainable development; these proposed projects were water system corridor construction, special park construction, ecological landscapes restoration, rural biogas planning, vehicle control and improvement, and industrial energy structure adjustment. If these projects are implemented, the green GDP of Wuyishan City should gradually increase in the future.

In conclusion, green GDP can be considered as an indicator of the degree of sustainable urban development. The sensitivity analysis model based on green GDP accounting can be used in the context of urban environmental and resource planning.

Appendix

The 20 industry categories of the National Bureau of Statistics (NBS) are as follows.

(A) Agriculture, forestry, animal husbandry, and fishery.

(B) Mining.

(C) Manufacture.

(D) Electricity, gas and water production, and supply industry.

(E) Construction.

(F) Traffic transportation, storage, and postal services.

(G) Information transmission, computer services, and software industry.

(H) Wholesale and retail business.

(I) Hotels, and catering services.

(J) Banking business.

(K) Realty business.

(L) Leasing and business services.

(M) Scientific research, technical services, and geological investigation industry.

(N) Water conservation, environmental, and public facilities management.

(O) Resident services and other services.

(P) Education.

(Q) Sanitation, social security, and social welfare.

(R) Culture, sports, and entertainment.

(S) Public administration and social organizations.

(T) International organizations.

Acknowledgments

This project is supported by the Fund for Innovative Research Group of the National Natural Science Foundation of China (Grant no. 51121003) and the National Science & Technology Pillar Program, China (no. 2012BAC05B02).

References

[1] X. H. Yuan, X. Ji, H. Chen, B. Chen, and G. Q. Chen, "Urban dynamics and multiple-objective programming: a case study of Beijing," *Communications in Nonlinear Science and Numerical Simulation*, vol. 13, no. 9, pp. 1998–2017, 2008.

[2] M. Alberti, *Advances in Urban Ecology: Integrating Humans and Ecological Processes in Urban Ecosystems*, Springer, New York, NY, USA, 2008.

[3] M. J. McDonnell, A. Hahs, and J. Breuste, *Ecology of Cities and Towns: A Comparative Approach*, Cambridge University Press, New York, NY, USA, 2009.

[4] Y. P. Cai, G. H. Huang, and Q. Tan, "An inexact optimization model for regional energy systems planning in the mixed stochastic and fuzzy environment," *International Journal of Energy Research*, vol. 33, no. 5, pp. 443–468, 2009.

[5] Q. Tan, G. H. Huang, and Y. P. Cai, "A superiority-inferiority-based inexact fuzzy stochastic programming approach for solid waste management under uncertainty," *Environmental Modelling and Assessment*, vol. 15, no. 5, pp. 381–396, 2010.

[6] E. S. Svendsen and L. Campbell, "Urban ecological stewardship: understanding the structure, function and network of community-based urban land management," *Cities and the Environment*, vol. 1, no. 1, pp. 1–32, 2008.

[7] M. Ignatieva, G. H. Stewart, and C. Meurk, "Planning and design of ecological networks in urban areas," *Landscape and Ecological Engineering*, vol. 7, no. 1, pp. 17–25, 2011.

[8] J. Boyd, "Nonmarket benefits of nature: what should be counted in green GDP?" *Ecological Economics*, vol. 61, no. 4, pp. 716–723, 2007.

[9] L. Y. Xu, B. Yu, and W. C. Yue, "A method of green GDP accounting based on eco-service and a case study of Wuyishan, China," *Procedia Environmental Sciences*, vol. 2, pp. 1865–1872, 2010.

[10] G. Heal, "Environmental accounting for ecosystems," *Ecological Economics*, vol. 61, no. 4, pp. 693–694, 2007.

[11] R. Costanza, R. d'Arge, R. de Groot et al., "The value of the world's ecosystem services and natural capital," *Nature*, vol. 387, no. 6630, pp. 253–260, 1997.

[12] R. Costanza, "Social goals and the valuation of ecosystem services," *Ecosystems*, vol. 3, no. 1, pp. 4–10, 2000.

[13] R. Costanza, I. Kubiszewski, D. Ervin et al., "Valuing ecological systems and services," *F1000 Biology Reports*, vol. 3, no. 1, article 14, 2011.

[14] *Millennium Ecosystem Assessment, Ecosystems and Human Well-Being: Synthesis*, Island Press, Washington, DC, USA, 2005.

[15] J. Boyd and S. Banzhaf, "What are ecosystem services? The need for standardized environmental accounting units," *Ecological Economics*, vol. 63, no. 2-3, pp. 616–626, 2007.

[16] J. E. Stiglitz, A. Sen, and J. P. Fitoussi, "Report of the commission on the measurement of economic performance et social progress," 2009, http://www.stiglitz-sen-fitoussi.fr/en/index.htm.

[17] SEPA, "Report on green national economic accounting in China, 2004," *Environmental Protection*, vol. 18, pp. 22–29, 2006 (Chinese).

[18] D. Guan, W. Gao, W. Su, H. Li, and K. Hokao, "Modeling and dynamic assessment of urban economy-resource-environment system with a coupled system dynamics—geographic information system model," *Ecological Indicators*, vol. 11, no. 5, pp. 1333–1344, 2011.

[19] V. Mahajan and R. A. Peterson, "Integrating time and space in technological substitution models," *Technological Forecasting and Social Change*, vol. 14, no. 3, pp. 231–241, 1979.

[20] J. Baker, X. Ruan, A. Alcantara et al., "Density-dependence in urban housing unit growth: an evaluation of the Pearl-Reed model for predicting housing unit stock at the census tract level," *Journal of Economic and Social Measurement*, vol. 33, no. 2-3, pp. 155–163, 2008.

[21] W. C. Yue, L. Y. Xu, and X. Zhao, "Research of green GDP accounting in Wuyishan City based on ecosystem services," *Ecological Economy*, vol. 2, pp. 11–12, 2009 (Chinese).

Hindawi Publishing Corporation
Mathematical Problems in Engineering
Volume 2013, Article ID 929383, 11 pages
http://dx.doi.org/10.1155/2013/929383

Research Article

Analysis of Variation Trends in Precipitation in an Upstream Catchment of Huai River

Peng Shi,[1,2] Xinxin Ma,[2] Xi Chen,[1,2] Simin Qu,[1,2] and Zhicai Zhang[2]

[1] *State Key Laboratory of Hydrology-Water Resources and Hydraulic Engineering, Nanjing 210098, China*
[2] *College of Water Resources and Hydrology, Hohai University, Nanjing 210098, China*

Correspondence should be addressed to Peng Shi; ship@hhu.edu.cn

Received 8 December 2012; Accepted 12 February 2013

Academic Editor: Yongping Li

We analyzed the variation trends in precipitation according to the observed data in the Shaying River catchment, upstream of the Huai River from 1951 to 2010, using the linear regression method and Mann-Kendall test. Further study was made by introducing *R/S* analysis, and the corresponding Hurst Exponent was estimated to predict the future trends of rainfall. The results suggested that the changing trends in precipitation for different time series in the whole catchment were relatively complex and not obvious. The annual precipitation showed a slightly increasing trend over the past 60 years, and in the future it would be antipersistent. For the 38 rainfall stations, the trends in spring and autumn precipitation time series were mostly negative; on the contrary, the trends in summer and winter were mostly positive. The results also indicated that the annual precipitation series showed positive trends in the northern region and negative trends in the southern region. Moreover, the relationships of H-Z and H-β of the 38 stations were analyzed. The results indicated that the greater the absolute values of Z the stronger the persistent nature. Meanwhile, for most of the H values were close to 0.5, the randomness of the future trends could not be ignored.

1. Introduction

Climate variability and human activities have become major concerns among societies and governments, as global warming arising from the anthropogenic-driven emissions of greenhouse gases has emerged in the last two decades and other water-related issues rendering the necessity of studying changes in hydrological processes [1, 2]. Knowledge of trends and variations of current and historical hydro-climatological variables is pertinent to the future development and sustainable management of water resources of a given region [3]. It is convinced that precipitation is one of the most important factors influencing water resources because changes in precipitation patterns may lead to floods or droughts in different areas. Understanding the spatial and temporal variability of precipitation series is of profound significance from both the scientific and practical point of view [4–7]. However, precipitation is not uniform and varies considerably from place to place and time to time, even on small scales, hence it is particularly hard to gauge the precipitation changes.

So far, many studies have focused on the analysis of precipitation variability at different temporal scales (from daily to annual) and in different parts of the world. Mosmann et al. [8] examined summer precipitation series of mainland Spain in 333 rainfall stations from 1961 to 1990 and found a statistically significant trend in wide areas. Cislaghi et al. [9] analyzed the long daily rainfall data in Italy. There results showed that the annual precipitation exhibited a negative trend in the first half of 20th century, with a subsequent positive trend in northern Italy. Conversely, the dataset for southern Italy displayed only a negative trend. Coulibaly [10] described spatial and temporal variability in Canadian seasonal precipitation for the period 1900–2000 and gained further insights into the dynamic relationship between the seasonal precipitation modes of climate variability in the Northern Hemisphere. Liu et al. [11] studied annual precipitation during 1961–2006 in Yellow River Basin, China. The results revealed that the precipitation possessed longitude zonality and had no clearly linear relationship with the latitude, most of the precipitation stations showed a decreasing trend in the basin. Ellouze et al. [12] checked

the spatial and temporal variability of rainfall characteristics over Southern Tunisia. Rainfall variability is shown to be dependent on seasonal conditions. Spatial patterns of shorter rainfall series (annual) are governed mainly by topography and coastal influence. Nastos and Zerefos [13] found out the spatial and temporal variability of the dry and wet spells in Greece, during the period 1958–2007. Kumar and Jain [1] investigated seasonal and annual rainfall and rainy days at five stations in Kashmir Valley to decipher rainfall trends. Afzal et al. [14] summarized trends and variability in daily precipitation from 28 weather stations with up to 80 years in Scotland.

Besides, there are a number of ongoing techniques to measure trends in hydrological and climatological time series. The Mann-Kendall (M-K) test has been widely used as an effective method to evaluate a presence of a statistically significant trend [15–17]. Tabari and Talaee [7] determined the annual and seasonal precipitation trends of 41 stations in Iran for the period 1966–2005 using the M-K test, the Sen's slope estimator, and the linear regression method. Wang et al. [18] reviewed the hydro-climatic trends for the lower reach of the Shiyang River Basin in the NW China using the wavelet analysis and the M-K test. In order to identify the optimal combination of the hydro-climatic data series in the discrete wavelet transform (DWT), the results from DWT were tested by the M-K test. Yang et al. [19] concluded temperature and precipitation trends in the Zhangweinan River Basin, based on monthly mean data for 53 years, from 1957 to 2009. They applied Mann-Kendall test method and cumulative anomaly method to analyze the long-term trends.

Another concern for precipitation change is the detection of the possible presence of long memory in the data, for example, if the change has occurred, whether and how the change persists. Hurst [20] heuristically detected the presence of long range dependence (or long memory) in the well-known series of annual minima of the Nile River. A Hurst Exponent value H between 0.5 and 1 indicates "persistent behavior," that is the time series is trending. Many researchers believe that a decrease or increase trend will tend to follow a decrease or increase for H between 0.5 and 1 (e.g, [19, 21]). Montanari et al. [22] examined six rainfall time series in various sites in Italy. However, they found a decreasing trend, though not statistically significant, in each of their records, but significant long memory in only two of them.

In Huai River basin, the majority of the previous studies in precipitation changes were focused on the whole Huai River based on sparsely observed climate data [2, 23–26]. They showed that no statistically significant trends of precipitation in the upper and middle Huai River Basins were detected at the annual scale and the trend of precipitation decreased significantly only in April. As we know, detection of changes in the precipitation and hydrological series is dependent on length and location of the observation data. In this study, the Shaying River, one of the first order tributaries in the upstream of the Huai River was selected to investigate the precipitation trends and its persistency. The linear regression method, Mann-Kendall test, and the rescaled range analysis (R/S analysis) were used for the period of 1951–2010 using data from 38 observation stations.

2. Materials and Methods

2.1. Study Area and Data. Shaying River, originated in the western mountainous area of Henan province, is the first tributary in the upstream of Huai River. It flows into the western of Anhui province through the central part of the Henan from northwest to southeast and falls into Huai River in the Mo River mouth of Fuyang city in Anhui province. Shaying River is located between 111.95° and 114.03°E in longitude and 33.07° and 34.42°N in latitude (Figure 1). The catchment area above the Luohe station is 12150 km^2, and the mountainous area accounts for 75%. The terrain of the catchment tilts from northwest to southeast, and plains in the southeast area were flat and open. The catchment is adjacent to the Yellow River Basin and the Yangtze River Basin and has a continental monsoon climate. The annual average temperature is within 10.7~12.9°C in the western mountains and within 14.5°C~14.9°C in the eastern plains. The annual precipitation is between 650 and 1400 mm. The annual distribution of rainfall is extremely uneven because its climate belongs to the south-north climate transition straps [27]. Nearly 42% of total rainfall concentrates on rainy season from June to September, and most between July and August.

Daily precipitation data from 38 rainfall stations in the study area were obtained to analyze the trend in annual, seasonal, and monthly scales, and the arithmetic average method was used to get catchment average precipitation. Considering the integrity and reliability of the source material, combined with observation of actual situation in the catchment, different time series in each station were selected, the longest series is 60 years (1951–2010), and the shortest series is 45 years. Thus, we have based our analysis on the period 1951–2010. The geographical location of the stations is shown in Figure 1.

2.2. Methods

2.2.1. Linear Regression Method. The method of linear regression is widely used in detecting and analyzing the variation trends in time series, which has an advantage that it provides a measure of significance based on the hypothesis test on the slope and also gives the magnitude of the rate of change [28]. The slope, which is the main statistical parameter drawn from the regression analysis, is the very index quantifying the trend of the temporal change in the studied period [29]. In details, positive values of the slope indicate increasing trends while negative values refer to decreasing trends. The total change during the period under observation is obtained with multiplying the slope with the number of years [7, 28, 30].

2.2.2. Mann-Kendall Test. The Mann-Kendall test is a non-parametric test, which was highly recommended for general use by the World Meteorological Organization [31]. There are two advantages for the test. The first one is that it does not require the data to be distributed normally; the second one is its low sensitivity to abrupt break due to inhomogeneous time series [7]. According to the test, the null hypothesis H_0 states that there is no trend in the analyzed records,

Figure 1: Study area and location of the gauge stations.

while the alternative hypothesis of a two-sided test is that the series displays change trend [32]. For a time series $X = \{x_1, x_2, \ldots, x_n\}$, the test statistic, S, is given by

$$S = \sum_{i=1}^{n-1} \sum_{j=i+1}^{n} \operatorname{sign}\left(x_j - x_i\right)$$
$$\operatorname{sign}\left(x_j - x_i\right) = \begin{cases} 1 & \text{if } x_j - x_i > 0 \\ 0 & \text{if } x_j - x_i = 0 \\ -1 & \text{if } x_j - x_i < 0, \end{cases} \quad (1)$$

where n is the number of data points. Under the assumption that the data are independent and randomly ordered, the mean of S is zero and the variance is given by [33]

$$\operatorname{Var}(S) = \frac{n(n-1)(2n+5) - \sum_{i=1}^{m} t_i (t_i - 1)(2t_i + 5)}{18}, \quad (2)$$

where m is the number of groups of tied ranks (equal observations), each with t_i tied observations.

Kendall [33] also shows that the distribution of S tends to normality as the number of observations becomes large. In cases where the sample size $n > 10$, the standard normal variable Z is computed by

$$Z = \begin{cases} \dfrac{(S-1)}{\sqrt{\operatorname{Var}(S)}} & S > 0 \\ 0 & S = 0 \\ \dfrac{(S+1)}{\sqrt{\operatorname{Var}(S)}} & S < 0. \end{cases} \quad (3)$$

Positive values of Z indicate increasing trends while negative values show decreasing trends. When testing increasing or decreasing monotonic trend at the α significance level, the null hypothesis was rejected for an absolute value of Z greater than $Z_{1-\alpha/2}$ obtained from the standard normal cumulative distribution tables. In this research, significance level of $\alpha = 0.1, 0.05, 0.01$ was applied, while the corresponding values of $Z_{1-\alpha/2}$ are 1.64, 1.96, and 2.58, respectively.

Another useful indicator is the Kendall slope β, which is used to quantify the changing trend, indicating the direction and the size of trend [19]. When $\beta > 0$, it indicates an upward trend, while $\beta < 0$ indicates a downward trend. The formulization of β is as follows:

$$\beta = \operatorname{Median}\left[\frac{x_i - x_j}{i - j}\right], \quad \forall j < i, \quad (4)$$

where $1 < j < i < n$. The higher the absolute value of β the greater the degree of the change.

2.2.3. R/S Analysis. R/S analysis was also called the Rescaled Range Analysis, which was the eldest and best-known method to estimate Hurst Exponent [34]. The exponent was originally proposed by Hurst [20] to analyze the time series flow data of Nile River, which was theoretically improved by Mandelbrot and Willis (1969).

The basic idea of the R/S analytical method could be described as follows [35, 36].

For the time series of a certain physical quantity $\{x(\tau)\}$ $(\tau = 1, 2, \ldots, n)$, the average value of $x(t)$ is

$$x_\tau = \frac{1}{\tau}\sum_{t=1}^{\tau} x(t). \tag{5}$$

The cumulative deviation is

$$X(t,\tau) = \sum_{t=1}^{\tau}\left(x(t) - x_\tau\right), \quad 1 \le t \le \tau. \tag{6}$$

The range sequence is

$$R(\tau) = \max_{1\le t\le\tau} X(t,\tau) - \min_{1\le t\le\tau} X(t,\tau). \tag{7}$$

The standard deviation sequence is

$$S(\tau) = \sqrt{\left(\frac{1}{\tau}\sum_{t=1}^{\tau}\left(x(t) - x_\tau\right)^2\right)}. \tag{8}$$

Finally they defined the nondimensional ratio R/S as follows:

$$\frac{R(\tau)}{S(\tau)} = (\alpha\tau)^H. \tag{9}$$

Hurst described $\ln(R/S)$ with $\ln\tau$ and found that the points in the data group almost lie on a straight line with perfect regularity [37]. The slope of the line is called the Hurst Exponent (H). When $H = 0.5$, it means that the time series is an independent random process, which indicates that the current trend will not affect the future trend. When $0.5 < H < 1$, it describes a dynamically persistent, or trend reinforcing series; with the greater the H value, the stronger the persistent. When $0 < H < 0.5$, it describes an antipersistent, or a mean reverting system; the smaller the H value, the stronger the antipersistent [29].

3. Results and Discussion

3.1. Trend Analysis by Linear Regression Method. Figure 2 showed the trends of the catchment average precipitation from 38 observation stations in time intervals of annual and seasonal scales. Since the R^2 values were small, the trends of seasonal and annual precipitation were all not significant. The analyses were just a reference in the study area. During the period between 1951 and 2010, the annual precipitation showed a slightly positive trend and a large fluctuation (Figure 2(a)). The annual precipitation increased in a rate of 0.0425 mm/year. Large fluctuations of the annual precipitation occurred in 1960s and late 1990s.

Table 1: Values of Z of the M-K test, the Kendall slope β, and H of the R/S analysis for monthly, seasonal, and annual series.

Time	Z	β (mm/a)	H
January	−0.74	−0.036	0.452
February	0.48	0.037	0.556
March	0.13	0.015	0.689
April	−1.32	−0.269	0.754
May	1.41	0.489	0.634
June	1.51	0.546	0.534
July	1.21	0.760	0.562
August	−0.17	−0.131	0.512
September	0.82	0.205	0.687
October	−0.68	−0.168	0.623
November	−1.26	−0.240	0.546
December	−0.34	−0.026	0.641
Spring (3–5 month)	0.13	0.077	0.595
Summer (6–8 month)	0.49	0.637	0.596
Autumn (9–11 month)	−0.29	−0.177	0.620
Winter (12–2 month)	0.03	0.012	0.560
Flood season (6–9 month)	−0.08	−0.232	0.595
Major flood season (7-8 month)	0.18	0.158	0.595
Nonflood season (10–5 month)	−0.41	−0.269	0.615
Annual	0.08	0.050	0.447

The linear regression analysis was further applied to detect the seasonal trends of precipitation for the whole catchment (Figures 2(b), 2(c), 2(d), and 2(e)). During 1951–2010, a decreasing trend was found from the precipitation time series in spring and autumn, with the change rates of −0.011 mm/year and −0.365 mm/year, respectively. In summer and winter, the precipitation series had positive trends at the rates of 0.241 mm/year and 0.051 mm/year, respectively. Comparing with the change rates, we know that precipitation changes in the summer and autumn were relatively significant but they were in opposite change directions, resulting in a small change in the annual precipitation.

3.2. Mann-Kendall Test for Precipitation Trends. The Mann-Kendall test was applied for testing the trends of the precipitation time series in different time scales of the catchment average precipitation (Table 1). Under the 90% significant level, the value of $Z_{1-\alpha/2}$ equals to 1.64. Compared with the standard normal variant Z in the value of 1.64, Z values in Table 1 indicated that no significant trends were detected for the catchment averaged precipitation in monthly, seasonal, and annual time scales.

According to positive and negative values of Z and β in Table 1, for monthly precipitation series, six months including January, April, August, October, November, and September showed decreasing trends. The Kendall slope β varied from −0.026 mm/year in September to −0.269 mm/year in April. Meanwhile, the left six months present increasing trends. These increase trends in May, June, and July were relatively more significant than those of other months. The β values in May, June, and July were 0.490, 0.546, and 0.760 mm/year,

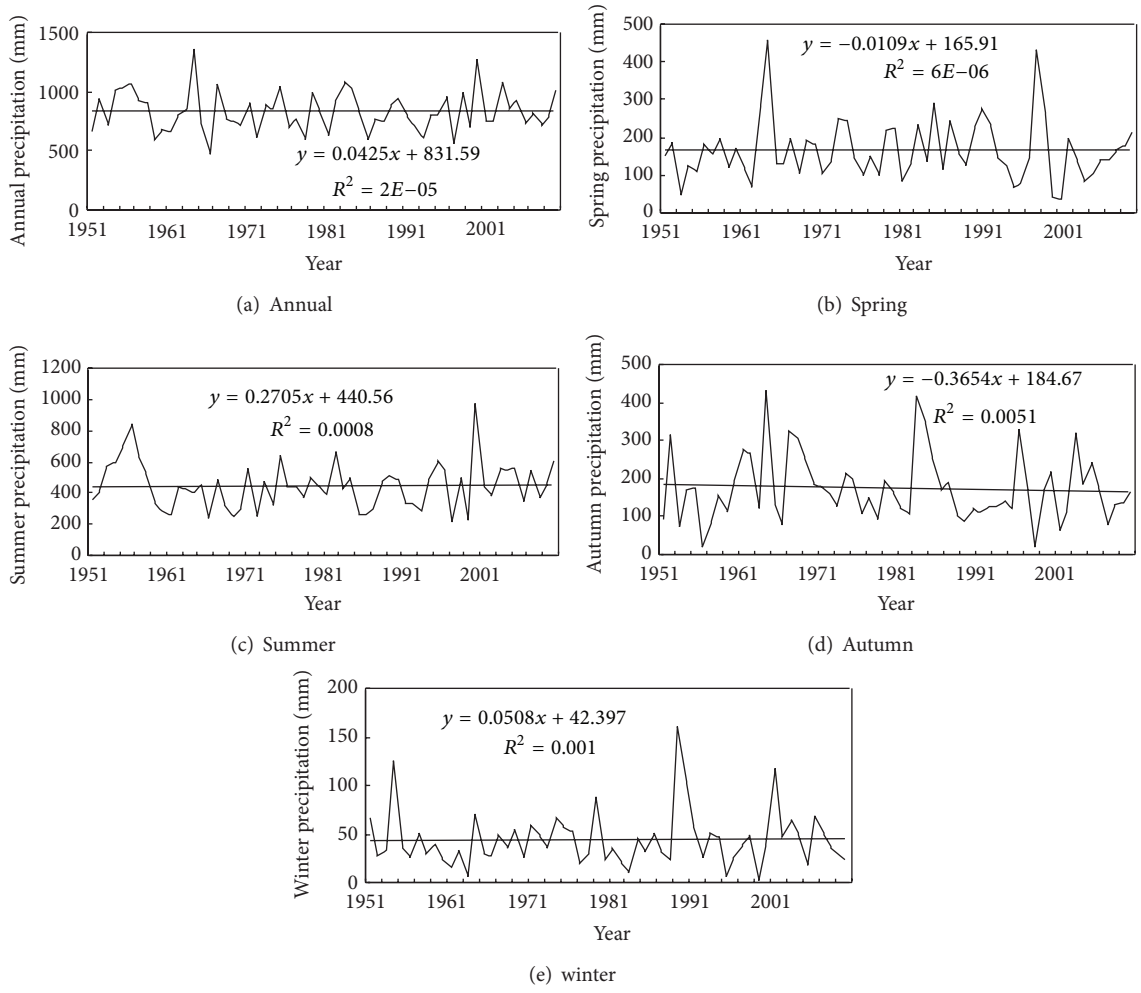

Figure 2: Trends for annual and seasonal precipitation during the period 1951–2010 by linear regression method.

respectively. For seasonal and annual precipitation series, the precipitation trends detected by M-K test were similar to those by the linear regression analysis though the magnitude of their changes was not different. The positive trend in summer was relatively significant, with the β value of 0.637 mm/year. In the major flooding season (7-8 month), the β value was 0.158 mm/year.

The results of M-K test using observed time series of individual station were shown in Table 2 and Figure 2. The number of the stations with increasing trends was almost same as that with decreasing trends in annual precipitation scale. Only three stations indicated that the trends were statistically significant. The annual precipitation in Jizhong and Zhiping stations showed increasing trends at the 90% and 99% confidence levels, respectively, while in Lianghekou station, the decreasing trend was found at the 95% confidence level.

On the seasonal scale, the trends detected significantly at the 90%, 95%, and 99% confidence levels were mostly positive and these significant positive trends occurred in spring, summer, and winter. Among all 38 stations in Table 2 and Figure 2, the number of stations with positive trends in spring, summer, and winter was 1, 8, and 2, respectively. It is found that significant positive trends for the eight stations in summer are located in the downstream of the study catchment, including Baiguishan, Baohe, Handian, Penghe, Silidian, Xiagushan, Zhaopingtai, and Zhiping. Meanwhile, only one station of Jiliaojie showed a significant negative trend for precipitation in autumn. The results also indicated that the majority of the precipitation trends in spring and autumn were negative, accounting for about 68% and 89% of the total number of stations, respectively. However, most of the trends were positive in summer and winter, accounting for 63% and 71% of the total number of stations, respectively. The increase trends in summer, particularly in the plain area of downstream station, would result in increasing flood occurrences in the study region.

Further analysis was executed in three subcatchments of the Beiru River, Sha River, and Li River in the south, middle, and north of the study catchment, respectively (Figure 1). Table 3 showed that the absolute values of statistics Z were all lower than 1.64, which means no significant trends were detected by the M-K test in the three regions for seasonal and annual series. However, the change trends presented regional

Table 2: Values of Z of the M-K test and the Kendall slope β for annual and seasonal precipitation in different stations.

Station	Spring		Summer		Autumn		Winter		Annual	
	Z	β (mm/a)	Z	β (mm/a)	Z	β (mm/a)	Z	β (mm/a)	Z	β (mm/a)
Baicaoping (BCP)	−0.06	−0.031	0.08	0.104	−0.72	−0.441	−0.25	−0.038	−0.46	−0.909
Baiguishan (BGS)	−0.39	−0.310	2.34**	3.016	−1.40	−1.017	1.43	0.195	0.89	1.199
Baofeng (BF)	−0.63	−0.525	0.95	1.331	−1.33	−0.931	0.18	0.049	−0.01	−0.008
Baohe (BH)	−0.16	−0.185	1.74*	3.648	−1.30	−1.133	0.68	0.190	0.82	2.050
Dadian (DD)	−0.09	−0.027	0.78	1.411	0.01	0.000	0.65	0.114	0.54	1.071
Daying (DY)	−0.36	−0.224	0.95	1.061	−1.14	−0.758	0.63	0.139	0.17	0.340
Dushu (DS)	−0.21	−0.144	0.51	0.587	−0.36	−0.278	−0.19	−0.019	0.11	0.114
Erlangmiao (ElM)	−0.19	−0.125	−0.81	−1.372	−0.30	−0.239	0.20	0.041	−1.14	−2.235
Fudian (FD)	0.00	0.000	−0.89	−1.152	−0.07	−0.037	0.91	0.133	−0.99	−1.605
Guaihe (GH)	−0.83	−0.523	1.63	2.369	−0.90	−0.719	0.37	0.064	0.38	0.704
Guanzhai (GZ)	−1.12	−0.686	0.78	1.278	−1.15	−0.941	−0.15	−0.054	0.23	0.355
Handian (HD)	−0.59	−0.477	1.82*	2.242	−2.17	−1.239	1.05	0.203	0.99	1.575
Hekou (HK)	−0.76	−0.536	1.31	1.712	−0.50	−0.334	0.10	0.028	0.35	0.830
Huangzhuang (HZ)	−0.80	−0.456	−1.26	−1.355	0.27	0.089	0.30	0.052	−1.48	−1.863
Jizhong (JZ)	0.96	0.745	1.55	2.512	−0.83	−0.683	1.14	0.245	1.69*	4.332
Jiliaojie (JLJ)	−0.85	−0.700	−0.58	−0.717	−2.14**	−1.689	0.34	0.076	−1.28	−3.251
Jiaxian (JX)	0.03	0.026	−0.44	−0.528	−0.79	−0.428	0.49	0.070	−0.47	−0.519
Jintangzhai (JTZ)	−0.06	−0.034	1.35	1.721	−0.56	−0.423	−0.53	−0.089	0.52	0.885
Lianghekou (LHK)	−0.96	−0.405	−1.24	−1.163	−0.79	−0.512	−0.45	−0.059	−2.13**	−2.384
Linruzhen (LRZ)	−0.62	−0.268	−0.67	−0.624	−0.12	−0.059	0.83	0.117	−0.70	−0.856
Louzigou (LZG)	−0.78	−0.376	−0.88	−0.774	−0.41	−0.290	0.24	0.031	−0.93	−1.523
Lushan (LS)	−0.06	−0.048	0.54	0.736	−0.03	−0.017	−0.18	−0.043	−0.21	−0.412
Luohe (LH)	−0.83	−0.492	0.25	0.221	−0.57	−0.384	−1.08	−0.224	−0.98	−1.662
Penghe (PH)	−0.28	−0.307	2.53**	4.911	−1.19	−1.342	0.31	0.068	1.03	2.532
Pinggou (PG)	−1.58	−2.410	0.59	1.218	−1.48	−1.490	0.17	0.069	−0.37	−1.023
Ruzhou (RZ)	−0.33	−0.167	−0.17	−0.135	−0.07	−0.046	−0.30	−0.039	−0.25	−0.213
Shenhou (SH)	0.16	0.125	−0.84	−1.083	−0.22	−0.111	0.57	0.090	−0.82	−1.253
Silidian (SLD)	−0.32	−0.151	1.90*	3.167	0.18	0.095	1.24	0.254	1.14	2.539
Wawu (WW)	0.57	0.315	−0.64	−0.868	−0.09	−0.032	0.94	0.166	−0.97	−1.436
Xiagushan (XGS)	0.03	0.024	1.82*	3.033	−1.39	−1.175	0.15	0.022	0.90	1.635
Xiatang (XT)	0.19	0.139	0.76	1.307	0.01	0.003	0.03	0.004	0.27	0.521
Xiaoshidian (XSD)	−0.55	−0.257	0.26	0.466	−1.02	−0.700	−0.13	−0.027	−0.27	−0.549
Xiangcheng (XC)	−0.25	−0.098	−0.67	−0.768	−0.73	−0.475	−0.41	−0.065	−0.96	−1.116
Zhaopingtai (ZPT)	0.42	0.317	3.01***	4.444	−0.82	−0.726	0.61	0.153	1.62	3.347
Zhiping (ZP)	2.34**	2.087	2.20**	4.200	−0.44	−0.347	4.82***	1.217	2.98***	7.476
Zhiyang (ZY)	0.12	0.090	−0.11	−0.101	−0.23	−0.197	1.68*	0.292	0.04	0.027
Zhongtang (ZT)	0.00	0.000	0.75	1.123	−1.35	−1.100	0.00	0.000	0.01	0.000
Ziluoshan (ZLS)	0.32	0.114	0.00	0.000	−0.15	−0.105	1.18	0.165	−0.22	−0.289

*Trends statistically significant at the 90% confidence level, **trends statistically significant at the 95% confidence level, ***trends statistically significant at the 99% confidence level.

Table 3: Values of Z of the M-K test and the Kendall slope β for annual and seasonal precipitation in three subcatchments.

Subcatchments	Spring		Summer		Autumn		Winter		Annual	
	Z	β	Z	β	Z	β	Z	β	Z	β
Beiru River	−0.22	−0.150	−0.62	−0.602	−0.35	−0.202	0.30	0.046	−0.90	−1.004
Sha River	0.47	0.268	0.52	0.579	−0.06	−0.029	0.21	0.045	0.21	0.297
Li River	−0.16	−0.078	0.86	1.364	−0.59	−0.349	−0.08	−0.025	0.17	0.274

Table 4: Values of H of the R/S analysis for annual and seasonal precipitation in different stations.

Station	H				
	Spring	Summer	Autumn	Winter	Annual
BCP	0.560	0.640	0.636	0.668	0.532
BGS	0.513	0.572	0.633	0.658	0.399
BF	0.488	0.612	0.662	0.714	0.478
BH	0.401	0.529	0.664	0.558	0.418
DD	0.659	0.672	0.673	0.542	0.338
DY	0.547	0.648	0.643	0.666	0.468
DS	0.499	0.617	0.610	0.515	0.485
ELM	0.491	0.614	0.672	0.624	0.487
FD	0.511	0.748	0.659	0.569	0.669
GH	0.616	0.655	0.655	0.550	0.461
GZ	0.511	0.530	0.588	0.607	0.401
HD	0.503	0.651	0.712	0.547	0.542
HK	0.461	0.595	0.678	0.536	0.430
HZ	0.560	0.691	0.629	0.637	0.611
JZ	0.744	0.629	0.581	0.653	0.740
JLJ	0.541	0.736	0.722	0.690	0.586
JX	0.572	0.762	0.609	0.658	0.609
JTZ	0.501	0.661	0.554	0.633	0.540
LHK	0.430	0.698	0.679	0.587	0.649
LRZ	0.551	0.675	0.717	0.622	0.506
LZG	0.575	0.609	0.611	0.576	0.596
LS	0.614	0.710	0.712	0.640	0.587
LH	0.445	0.557	0.670	0.678	0.637
PH	0.602	0.649	0.579	0.502	0.511
PG	0.522	0.642	0.710	0.533	0.453
RZ	0.595	0.633	0.758	0.626	0.463
SH	0.565	0.629	0.756	0.544	0.541
SLD	0.566	0.669	0.663	0.601	0.503
WW	0.618	0.682	0.716	0.567	0.465
XGS	0.543	0.620	0.708	0.636	0.564
XT	0.564	0.651	0.668	0.540	0.465
XSD	0.428	0.647	0.678	0.635	0.593
XC	0.547	0.716	0.625	0.624	0.643
ZPT	0.508	0.651	0.673	0.596	0.364
ZP	0.611	0.629	0.696	0.673	0.851
ZY	0.605	0.669	0.653	0.662	0.427
ZT	0.549	0.612	0.682	0.606	0.569
ZLS	0.564	0.607	0.582	0.603	0.463

differences. The average precipitation in Beiru River generally showed negative trends in spring, summer and autumn and in annual series, except a slightly positive trend in winter. In Sha River, the average precipitation showed positive trends in spring, summer and winter and in annual series and a slightly negative trend was only found in autumn. In Li River, although negative trends for the precipitation series occurred in three seasons of spring, autumn, and winter, a positive trend was found in an annual series because the positive trend in summer was relatively significant. The results indicated that the annual precipitation series showed positive trends in the northern region and negative trends in the southern region.

3.3. R/S Analysis for Future Trends. The Hurst Exponent (H) values estimated by R/S analysis in monthly, seasonal, and annual scales were shown in Table 1 for precipitation series in catchment average, Table 4 and Figure 4 for individual station, and Figure 5 for three subcatchments. From Table 1, the H values during March–May, September and October, and December were far larger than 0.5. It indicated trend reinforcing series for these months. The increase trends in March, May, and September and decrease trends in April, October, and December were enhanced. This trend reinforcing was found in spring and summer with an increasing trend and in autumn in a decreasing trend. The annual H value was close to 0.5, which indicated a randomness of the time series.

Table 4 and Figure 4 presented that the H values for all precipitation series of the 38 rainfall stations were on the upper side of the value of 0.5 in summer, autumn, and winter. Because most of the trends were positive in summer and winter, it again validated that these positive trends were reinforced. From Figure 5, we can see that all the H values of the annual and seasonal precipitation series in Beiru River were greater than 0.5, which means the dependence of future trends on previous ones. In Sha River, in spite of the consistency of future trends in seasonal precipitation, the H value of the annual time series was 0.420, which referred to an antipersistent nature. In Li River, all of the H values except the one in spring were found to be greater than 0.5, indicating a continuous nature for the future precipitation. The results were similar to the analysis for the stations.

Figures 6(a) and 6(b) show the relationship between Z and H values, and between β and H values according to values in Tables 2 and 4. The following results were obtained from Figures 6(a) and 6(b): (1)persistent exists ($H >$ 0.5 or <0.5) though the trend is not statistically significant ($Z < 1.64$); (2) when for the increasing trend ($Z > 0$ or $\beta > 0$ in Figures 6(a) and 6(b)), the greater the Z values or β values, the stronger the persistent; that is to say, the increasing trends will be reinforced in the future; (3) for the decreasing trends ($Z < 0$ or $\beta < 0$ in Figures 6(c) and 6(d)), the greater the absolute values of Z or β, the stronger the persistent; that is to say, the decreasing trends will be reinforced as well; (4) both the slopes in Figures 6(c) and 6(d) were relatively smaller than the corresponding ones in Figures 6(a) and 6(b), indicating that the future changes of precipitation in the whole area will be stronger in positive trends than in negative trends.

4. Conclusions

In this paper, trends of precipitation were investigated using the linear regression method, the Mann-Kendall test, and the R/S analysis based on daily data from 38 rainfall stations in the study area during the period 1951–2010 (Figure 3). The following conclusions were obtained.

The results show that the trends in precipitation were relatively not significant in catchment average even though

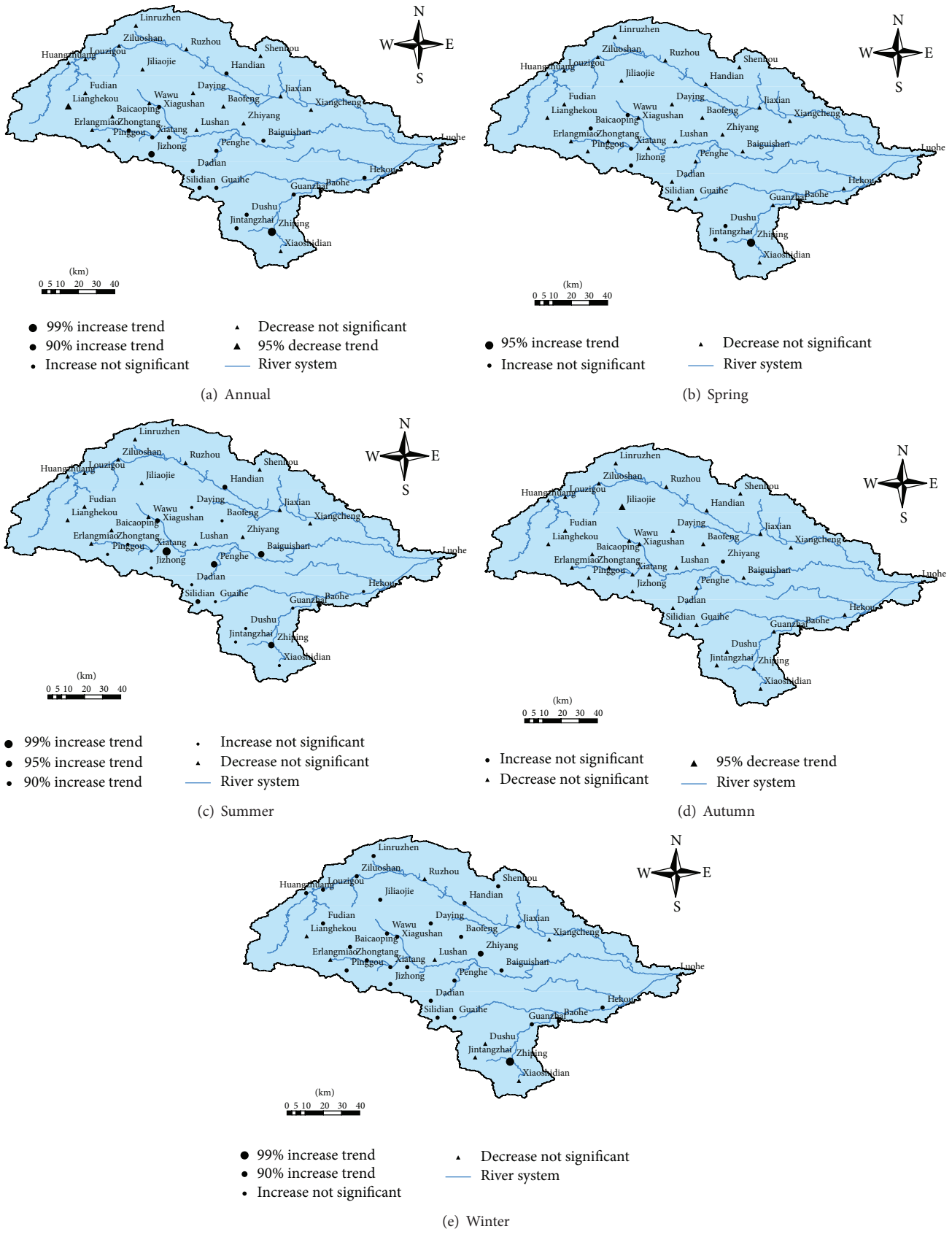

Figure 3: Trends for annual and seasonal precipitation in the 38 stations during the period 1951–2010.

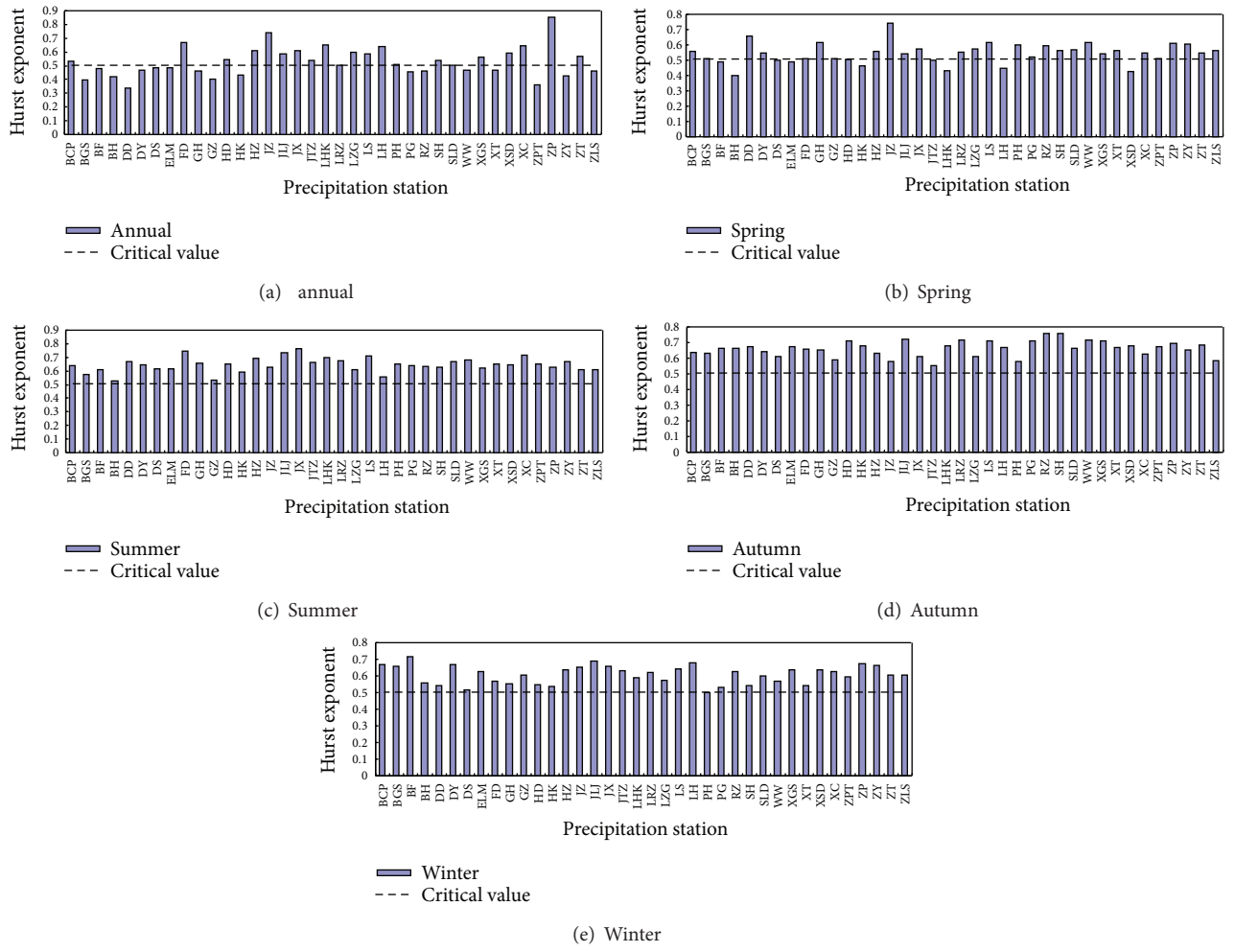

FIGURE 4: Values of H of the R/S analysis for annual and seasonal precipitation in the 38 stations.

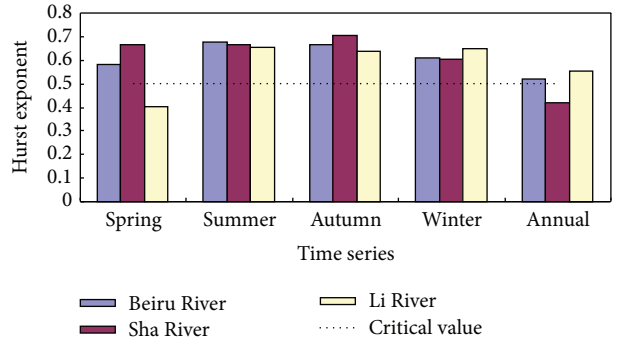

FIGURE 5: Values of H of the R/S analysis for annual and seasonal precipitation in three subcatchments.

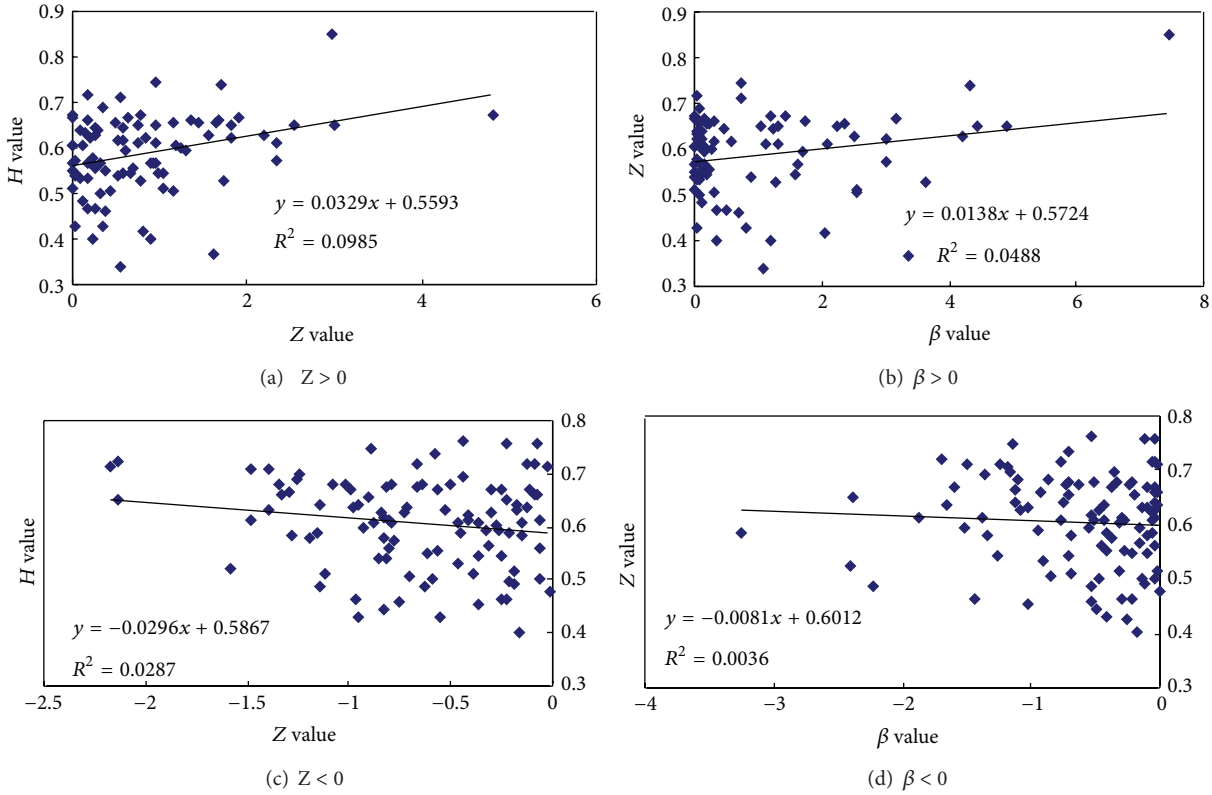

Figure 6: The relationship analysis of H-Z and H-β.

significant trends in some observation stations were found. The annual precipitation in the whole catchment represented a slightly increase trend in the past 60 years, with the rate of 0.042 mm/year. Precipitation series in spring and autumn presented decrease trend in a rate of −0.011 and −0.365 mm/year, respectively, and presented increase trend in a rate of 0.241 and 0.051 mm/year, respectively.

Increase trend in summer is relatively significant. Significant trends in summer account for 21% of the stations. Meanwhile, most of stations with significant increase trends were located in the downstream of the catchment. This increase trends in summer, particularly in the plain area of downstream station, would result in increase of flood occurrences in the study region.

According to calculated Hurst Exponent values, the future precipitation in January and annual series was anticipated to be antipersistent with the past, the rest time series showed persistent trends in the future, and the future precipitation trends were enhanced in all of the 38 rainfall stations in summer, autumn, and winter. The majority of the stations with an antipersistent nature in annual series were concentrated in the central area of the catchment, which probably related to the three large reservoirs (Zhaopingtai, Baiguishan, and Gushitan) in the central region. The three reservoirs were all started to construct in the year 1958 and completed in the 1960s.

The relationships of H-Z and H-β of the 38 stations indicated that persistent exists though the trend is not statistically significant ($Z < 1.64$). Meanwhile, the increase and decrease trends will be reinforced in the future as the increase and decrease trends tend to be more and more significant. Generally, the future changes of precipitation in the whole area will be stronger in positive trends than in negative trends.

However, as the data series are not long enough, the question of whether we are facing long-term climatic trends or whether the observed trends are only a part of long-term variability remains unanswered, and the understanding of influence of the reservoirs is not thorough clearly. In addition, it is also suggested to explore other hydrological and meteorological variables available in the study area. Further studies would be interesting to investigate the interrelationship between different variables.

Acknowledgments

The first author thanks the following financial support: Major Program of National Natural Science Foundation of China (51190091); the National 973 Project under Grant no. 2010CB951102; and the National Natural Science Foundation of China (no. 41001011/40901015/41101018).

References

[1] V. Kumar and S. K. Jain, "Trends in seasonal and annual rainfall and rainy days in Kashmir Valley in the last century," *Quaternary International*, vol. 212, no. 1, pp. 64–69, 2010.

[2] Y. F. Zhang, D. X. Guan, C. J. Jin, A. Z. Wang, J. B. Wu, and F. G. Yuan, "Analysis of impacts of climate variability and human activity on streamflow for a river basin in northeast China," *Journal of Hydrology*, vol. 410, no. 3-4, pp. 239–247, 2011.

[3] P. G. Oguntunde, B. J. Abiodun, and G. Lischeid, "Rainfall trends in Nigeria, 1901–2000," *Journal of Hydrology*, vol. 411, no. 3-4, pp. 207–218, 2011.

[4] I. A. Tošić, "Spatial and temporal variability of winter and summer precipitation over Serbia and Montenegro," *Theoretical and Applied Climatology*, vol. 77, no. 1-2, pp. 47–56, 2004.

[5] O. I. Abdul Aziz and D. H. Burn, "Trends and variability in the hydrological regime of the Mackenzie River Basin," *Journal of Hydrology*, vol. 319, no. 1–4, pp. 282–294, 2006.

[6] T. Jiang, B. D. Su, and H. Hartmann, "Temporal and spatial trends of precipitation and river flow in the Yangtze River Basin, 1961–2000," *Geomorphology*, vol. 85, no. 3-4, pp. 143–154, 2007.

[7] H. Tabari and P. H. Talaee, "Temporal variability of precipitation over Iran: 1966–2005," *Journal of Hydrology*, vol. 396, no. 3-4, pp. 313–320, 2011.

[8] V. Mosmann, A. Castro, R. Fraile, J. Dessens, and J. L. Sánchez, "Detection of statistically significant trends in the summer precipitation of mainland Spain," *Atmospheric Research*, vol. 70, no. 1, pp. 43–53, 2004.

[9] M. Cislaghi, C. de Michele, A. Ghezzi, and R. Rosso, "Statistical assessment of trends and oscillations in rainfall dynamics: analysis of long daily Italian series," *Atmospheric Research*, vol. 77, no. 1–4, pp. 188–202, 2005.

[10] P. Coulibaly, "Spatial and temporal variability of Canadian seasonal precipitation (1900–2000)," *Advances in Water Resources*, vol. 29, no. 12, pp. 1846–1865, 2006.

[11] Q. Liu, Z. F. Yang, and B. S. Cui, "Spatial and temporal variability of annual precipitation during 1961–2006 in Yellow River Basin, China," *Journal of Hydrology*, vol. 361, no. 3-4, pp. 330–338, 2008.

[12] M. Ellouze, C. Azri, and H. Abida, "Spatial variability of monthly and annual rainfall data over Southern Tunisia," *Atmospheric Research*, vol. 93, no. 4, pp. 832–839, 2009.

[13] P. T. Nastos and C. S. Zerefos, "Spatial and temporal variability of consecutive dry and wet days in Greece," *Atmospheric Research*, vol. 94, no. 4, pp. 616–628, 2009.

[14] M. Afzal, M. G. Mansell, and A. S. Gagnon, "Trends and variability in daily precipitation in Scotland," *Procedia Environmental Sciences*, vol. 6, pp. 15–26, 2011.

[15] M. Cannarozzo, L. V. Noto, and F. Viola, "Spatial distribution of rainfall trends in Sicily (1921–2000)," *Physics and Chemistry of the Earth*, vol. 31, no. 18, pp. 1201–1211, 2006.

[16] K. H. Hamed, "Trend detection in hydrologic data: the Mann-Kendall trend test under the scaling hypothesis," *Journal of Hydrology*, vol. 349, no. 3-4, pp. 350–363, 2008.

[17] I. Pal and A. Al-Tabbaa, "Trends in seasonal precipitation extremes—an indicator of 'climate change' in Kerala, India," *Journal of Hydrology*, vol. 367, no. 1-2, pp. 62–69, 2009.

[18] H. Q. Wang, M. S. Zhang, H. Zhu, X. Y. Dong, Z. Yang, and L. H. Yin, "Hydro-climatic trends in the last 50 years in the lower reach of Shiyang River Basin, NW China," *Catena*, vol. 95, pp. 33–41, 2012.

[19] X. L. Yang, L. R. Xu, K. K. Liu, C. H. Li, J. Hu, and X. H. Xia, "Trends in temperature and precipitation in the Zhangweinan River Basin during the last 53 Years," *Procedia Environmental Sciences*, vol. 13, pp. 1966–1974, 2012.

[20] H. Hurst, *Long Term Storage Capacity of Reservoirs*, vol. 6, Transactions of the American Society of Civil Engineers, 1951.

[21] H. J. Li, Z. Q. Xia, J. Zhang, and N. Zhang, "Analysis of time series of annual precipitation in Irtysh River Basin," *Water Resources Protection*, vol. 26, no. 5, pp. 29–32, 2010.

[22] A. Montanari, R. Rosso, and M. S. Taqqu, "Some long-run properties of rainfall records in Italy," *Journal of Geophysical Research D*, vol. 101, no. 23, pp. 29431–29438, 1996.

[23] G. Y. Wang and S. B. Dai, "Variation of water resource and its quality of Huaihe River in the past half century," *Journal of Anhui Normal University (Natural Science)*, vol. 31, no. 1, pp. 75–78, 87, 2008 (Chinese).

[24] S. Wang, W. S. Xie, W. A. Tang, Y. Tao, and X. Ding, "Change characteristics of day and night precipitation in Huaihe River Basin in 1961–2009," *Chinese Journal of Ecology*, vol. 30, no. 12, pp. 2881–2887, 2011 (Chinese).

[25] W. Q. Xing, W. G. Wang, Y. Q. Wu, and G. Y. An, "Change properties of precipitation concentration in Huaihe River Basin," *Water Resources and Power*, vol. 29, no. 5, pp. 1–5, 2011 (Chinese).

[26] C. H. Xu, Y. Luo, and Y. Xu, "Projected changes of precipitation extremes in river basins over China," *Quaternary International*, vol. 244, no. 2, pp. 149–158, 2011.

[27] X. P. Wang, "Characteristics analysis of rainfall in the upper reaches of the Shaying River Basin," *Hydrology*, vol. 20, no. 1, pp. 53–55, 2000 (Chinese).

[28] H. Tabari, S. Marofi, and M. Ahmadi, "Long-term variations of water quality parameters in the Maroon River, Iran," *Environmental Monitoring and Assessment*, vol. 177, no. 1–4, pp. 273–287, 2011.

[29] J. Peng, Z. H. Liu, Y. H. Liu, J. S. Wu, and Y. N. Han, "Trend analysis of vegetation dynamics in Qinghai-Tibet Plateau using Hurst Exponent," *Ecological Indicators*, vol. 14, no. 1, pp. 28–39, 2012.

[30] H. Tabari and P. H. Talaee, "Analysis of trends in temperature data in arid and semi-arid regions of Iran," *Global and Planetary Change*, vol. 79, no. 1-2, pp. 1–10, 2011.

[31] J. M. Mithell, B. Dzerdzeevskii, H. Flohn et al., "Climatic change. (Report of a working group of the Commission for Climatology)," WMO Technical Note No. 79, World Meteorological Organization, 1966.

[32] K. Chaouche, L. Neppel, C. Dieulin et al., "Analyses of precipitation, temperature and evapotranspiration in a French Mediterranean region in the context of climate change," *Comptes Rendus Geoscience*, vol. 342, no. 3, pp. 234–243, 2010.

[33] M. G. Kendall, *Rank Correlation Methods*, Griffin, London, UK, 1975.

[34] Z. Sánche, J. E. Trinidad, and P. J. García, "Some comments on Hurst exponent and the long memory processes on capital markets," *Physica A*, vol. 387, no. 22, pp. 5543–5551, 2008.

[35] X. L. Wang, B. Q. Hu, and J. Xia, "R/S analysis method of trend and aberrance point on hydrological time series," *Engineering Journal of Wuhan University*, vol. 35, no. 2, pp. 10–12, 2002 (Chinese).

[36] Y. S. Yu and X. W. Chen, "Analysis of future trend characteristics of hydrological time series based on R/ S and Mann-Kendall methods," *Journal of Water Resources & Water Engineering*, vol. 19, no. 3, pp. 41–44, 2008 (Chinese).

[37] Q. M. Bu, J. Bi, Z. W. Yuan, and L. Huang, "R/S method for evaluation of pollutant time series in environmental quality assessment," *Water Science and Engineering*, vol. 1, no. 4, pp. 82–88, 2008.

Hindawi Publishing Corporation
Mathematical Problems in Engineering
Volume 2013, Article ID 731042, 9 pages
http://dx.doi.org/10.1155/2013/731042

Research Article

Nonsmooth Dynamic Behaviors Inherited from an Ecohydrological Model: Mutation, Bifurcation, and Chaos

Mu Lin,[1,2] Fuqiang Tian,[2] Heping Hu,[2] and Dengfeng Liu[3]

[1] *School of Applied Mathematics, Central University of Finance and Economics, Beijing 100081, China*
[2] *Department of Hydraulic Engineering, State Key Laboratory of Hydroscience and Engineering, Tsinghua University, Beijing 100084, China*
[3] *Key Laboratory of Northwest Water Resources and Environmental Ecology of MOE, Xi'an University of Technology, Xi'an 710048, China*

Correspondence should be addressed to Fuqiang Tian; tianfq@tsinghua.edu.cn

Received 17 December 2012; Accepted 28 January 2013

Academic Editor: Yongping Li

The existence of nontrivial dynamic behaviors in a hydrological system is intensively discussed in the literature. However, most of the work has been done from the nonlinear data analysis perspective, with only a few exceptions, due to the mathematical difficulties for theoretical analysis. In this study, a simple but comprehensive enough ecohydrological model with the pulsed atmospheric forcing was developed from the process analysis perspective. The model was then utilized to analyze the non-trivial dynamic behaviors in a coupled ecohydrological system qualitatively and numerically. Our results confirm the existence of multiple stationary states discussed by many researchers. Furthermore, parameter bifurcation was studied and the phenomenon of mutation is found to be rather common. Also, the chaotic characteristic of the system state is obtained under some specific parameters. Parts of these behaviors were seldom reported through the deterministic dynamic analysis done previously.

1. Introduction

As stated by Peterson et al. [1], the dynamic behavior of a hydrological system is always assumed to be primary in traditional hydrology; that is, at the cessation of a transient hydrological disturbance of any magnitude, the system will return to the same stable state and thus show an infinite resilience. This hypothesis is challenged by the dynamic theory, especially the nonlinear theory raised in meteorology [2]. In fact, quite a few studies have been devoted to the "nontrivial" dynamic characters in hydrological systems in the past several decades [3–5]. For example, chaos has been intensively studied in many hydrology-related processes including rainfall, river flow, rainfall-runoff, lake volume, temperature, pressure, and wind velocity (see the summary by Sivakumar [6]). These studies are, however, principally based on the nonlinear data analysis method alone, which can obtain the statistical features from the existing data but cannot indicate the causal relationship between physical processes and dynamic phenomena.

Another point of view, as this study mainly concerns, uses process-based model incorporating intertwined interactions and feedbacks to explore the nontrivial dynamic behaviors. For example, considering the coupled system including the upper soil layer and the atmosphere planetary boundary layer, D'Andrea et al. [7] found the bimodal distribution of soil moisture resulting from the existence of multiple equilibria in the continental water balance. Ridolfi et al. [8] developed a conceptual framework to study the interaction and positive feedback in wetland forests and riparian ecosystems, which shows that the feedbacks may lead to the emergence of multiple stable states. Based on the field observations from savanna ecosystems in Kalahari, D'Odorico et al. [9] found that the difference between the soil moisture in the canopy and intercanopy spaces is related to the aridity level, and the system may exhibit two stable states corresponding to the conditions with and without tree canopy cover. With positive feedbacks between vegetation and soil moisture in arid ecosystems, Borgogno et al. [10] found that random rainfall fluctuation may turn the bistable deterministic system

into a stochastic system with only one statistically stable state in an analytical model. In order to challenge the potentially significant assumption of the single stable state in the ecohydrological models, Peterson et al. [1] developed a numerical distributed ecohydrological model and found that the multiple stable states may arise from the reduction of leaf area index as the saline water table approaches the surface. Also, they employed limit cycle continuation to locate the unstable stationary state in the phase space. Runyan and D'Odorico [11] developed a modeling framework relating vegetation-soil salinity feedbacks to the emergence of multiple stable states in the underlying dynamics and the results show that the presence of a strong feedback can result in bistable dynamics for a wide range of environmental conditions.

The above process-based work demonstrates the existence of multiple stationary states in some specific ecohydrological systems, which depends on no particular data or conditions. But more sophisticated dynamic behaviors, such as mutation and chaos, have not been explored yet. Nevertheless, Rodriguez-Iturbe and the collaborators [12, 13] conducted a study with the similar purpose but for the hydrometeorological system operating at the climate scales (i.e., continental spatial scale and annual temporal scale). They analyzed the soil moisture balance equation and demonstrated that soil moisture states could present abundant nontrivial dynamic behaviors including bimodal states, fixed points, limit cycles, and chaos due to the feedback between soil moisture and precipitation (i.e., local recycling of moisture). For the ecohydrological system running at much smaller spatial and temporal scales interested in this study, the dominating feedback is not the local recycle of moisture, but the vegetation growth fed by soil moisture. The evolution of ecohydrological system has recently drawn a lot of attentions and its dynamic behavior deserves further study, which is the purpose of this study.

The remainder of this paper is organized as follows. In Section 2, a simple but comprehensive enough ecohydrological model is established under pulsed atmospheric forcing. Dynamic analysis follows in Section 3, and the so-called nontrivial dynamic behaviors are explored by the way of numerical simulation. The paper is concluded in Section 4.

2. Framework of the Ecohydrological Model

2.1. Functional Expression of Nonsmooth Rainfall Process. As mentioned above, Rodriguez-Iturbe et al. conducted the notable work in the dynamic analysis of hydrometeorologic process. However, the annual rainfall amount in their analysis is regarded as a simple function (in the mathematical sense) of advective precipitation, local evaporation, and local soil moisture, and hence the smaller scale rainfall variability and nonsmooth feature (see below) are ignored. Such description of rainfall process is inapplicable to ecohydrological system running at a smaller spatiotemporal scale. For the detail study of hydrological processes at the finer scale, the Poisson process with white noise is often utilized to describe the stochastic properties of rainfall [14, 15]. However, such stochastic manner will go against the qualitative analysis of the dynamic process due to the mathematical complexity.

A deterministic functional expression of rainfall with moderate complexity is necessary for dynamic analysis of hydrological process. From the mathematical perspective, the rainfall intensity is a nonsmooth function of time [16]; that is, a pulsing function which means the time derivative is not continuous everywhere. In general, nonsmooth modeling has been widely used in many different areas [17–19] for its intuitional advantage; although nonsmooth terms can introduce additional mathematical difficulties for dynamic analysis [20, 21]. In hydrology, a simplified nonsmooth function, that is, a rectangular pulsing function, is frequently used for theoretical analysis of ecohydrological or hydrometeorologic processes. For example, a simple step function was used to describe the pulsing rainfall forcing by Collins and Bras [22] to examine how the gradient of mean annual precipitation is weaved in the topography of water-limited ecosystems; an ideal quasiperiodic pulsing precipitation was utilized by Lu [23] to study the physical basis of daily flood and drought index; a periodic step function was adopted by Robinson and Sivapalan [15] to identify different hydrological regimes according to the interactions between rainfall variability and catchment response time within a theoretical framework. Following these studies, a quasiperiodical rectangular pulsing function was chosen to represent real stochastic rainfall process by keeping between-storm temporal structure while ignoring more variability for a preliminary dynamic analysis of ecohydrological system.

Remarkably, the chosen pulsing function is just like the water application manner in an automatic irrigation system under the equilibrium state, see also Section 3 and Figure 8(c). The so-called automatic irrigation [24] means the duration of irrigation is controlled by the real-time observation on soil moisture content, with the switching bounds predetermined. As the dynamic analysis in this study focuses on the equilibrium state of ecohydrological system, we will use automatic irrigation scheme to represent the quasiperiodical pulsing function. Mathematically, such substitution of automatic irrigation scheme for stochastic rainfall process can ensure that the model is deterministic and autonomous in the resultant ordinary differential equations (ODEs), and therefore the dynamic phenomena discovered in the model depends not on any particular selection of external rainfall time series but on the internal system configuration. Practically, the automation has been widely used in water-saving irrigation systems [25, 26] under dry as well as wet conditions [27], and therefore we can assume a no-rainfall area and focus on the automatic irrigation system only, for the irrigation amount is much larger than the rainfall in the arid especially hyperarid regions [28].

2.2. Ecohydrological Model. An ecohydrological model is then introduced as follows. The schematic diagram is shown as Figure 1. As mentioned above, it can be assumed to be in the hyperarid area where water supply comes from irrigation alone. Our work imitates the tank model [29] to describe the storage and release of aquifer.

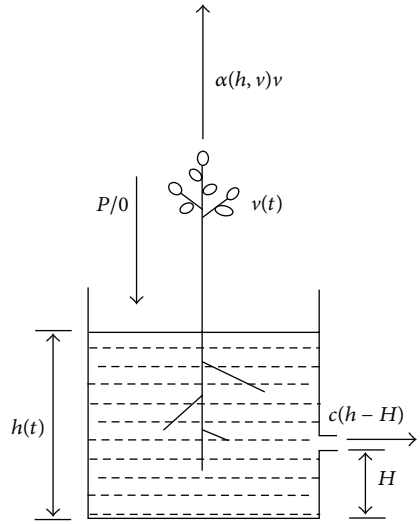

Figure 1: The schematic diagram of the model.

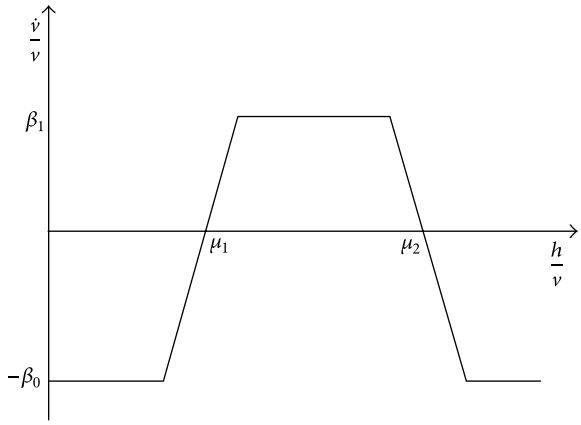

Figure 2: The schematic diagram of an ideal β function.

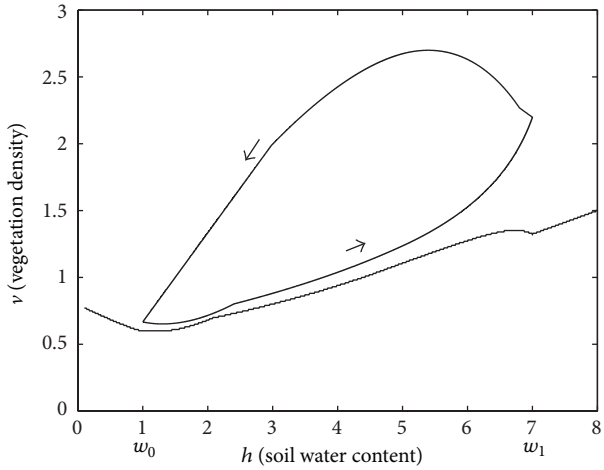

Figure 3: Typical multiple stationary states.

As shown in Figure 1, the height $h(t)$ (cm) stands for the storage per unit area at time t (d). Roughly speaking, it is equivalent to water content in the soil. The tank has only one side outlet with height H (cm). The side runoff from tank is assumed to be linear with respect to tank water storage excess relative to initial height H, defined by a positive coefficient c. The surface runoff is ignored. The term $v(t)$ (quantity of grasses per square meter) stands for biomass, that is, the vegetation density per unit surface area at time t. Generally, the evaporation and transpiration are related to biomass by $\alpha(h, v)v$. Assume that α is constant for a preliminary study here. Then, the dynamical equation of water storage can be written as follows:

$$\begin{aligned} \dot{h} &= p - \alpha v - \begin{cases} c\,(h - H), & \text{if } h \geq H, \\ 0, & \text{if } h < H, \end{cases} \quad \text{if } i\,(t) = 1, \\ \dot{h} &= -\alpha v - \begin{cases} c\,(h - H), & \text{if } h \geq H, \\ 0, & \text{if } h < H, \end{cases} \quad \text{if } i\,(t) = -1. \end{aligned} \tag{1}$$

Here we divide the whole process into two phases and introduce a variable $i(t)$ with value domain $\{-1, +1\}$ to depict them; that is, $i(t) = 1$ means irrigation at time t, with constant intensity p (cm/d), while $i(t) = -1$ means no irrigation at time t, that is, irrigation intensity is 0.

Another important dynamical equation is the evolution equation of the vegetation, which can be described as

$$\dot{v} = \beta\,(h, v)\, v, \tag{2}$$

where $\beta(h, v)$ indicates the varying rate per unit vegetation. It is a complicated problem to describe β function in ecology. However, a qualitative function can be described approximatively as follows:

$$\text{with } \beta\,(h, v) = \begin{cases} -\beta_0, & \text{if } \dfrac{h}{v} \in [0, \mu_1 - \delta_1), \\ \dfrac{\beta_0 + \beta_1}{\delta_1 + \delta_2}\left(\dfrac{h}{v} - \mu_1\right), & \text{if } \dfrac{h}{v} \in [\mu_1 - \delta_1, \mu_1 + \delta_2), \\ \beta_1, & \text{if } \dfrac{h}{v} \in [\mu_1 + \delta_2, \mu_2 - \delta_3), \\ -\dfrac{\beta_0 + \beta_1}{\delta_3 + \delta_4}\left(\dfrac{h}{v} - \mu_2\right), & \text{if } \dfrac{h}{v} \in [\mu_2 - \delta_3, \mu_2 + \delta_4), \\ -\beta_0, & \text{if } \dfrac{h}{v} \in [\mu_2 + \delta_4, +\infty). \end{cases} \tag{3}$$

The framework is similar to (the linearization of) the work in [30]. It means that the plants would die down when h/v is too large or too small, that is, $\dot{v} < 0$ [8]. A sketch map of relation between "breed" rate and available water amount (for unit plant) is shown as Figure 2. Here $\beta_1\,(\mathrm{d}^{-1})$ is the maximum growth rate per unit grass, while $-\beta_0\,(\mathrm{d}^{-1})$ is the rate of natural death. Also, there are two equilibrium states $h/v = \mu_1$ (cm/n), and $h/v = \mu_2$ (cm/n) during which the grass density keeps constant. Positive coefficients δ_k (cm/n), $k = 1, 2, 3, 4$, are used for separating the suitable growth parameter region.

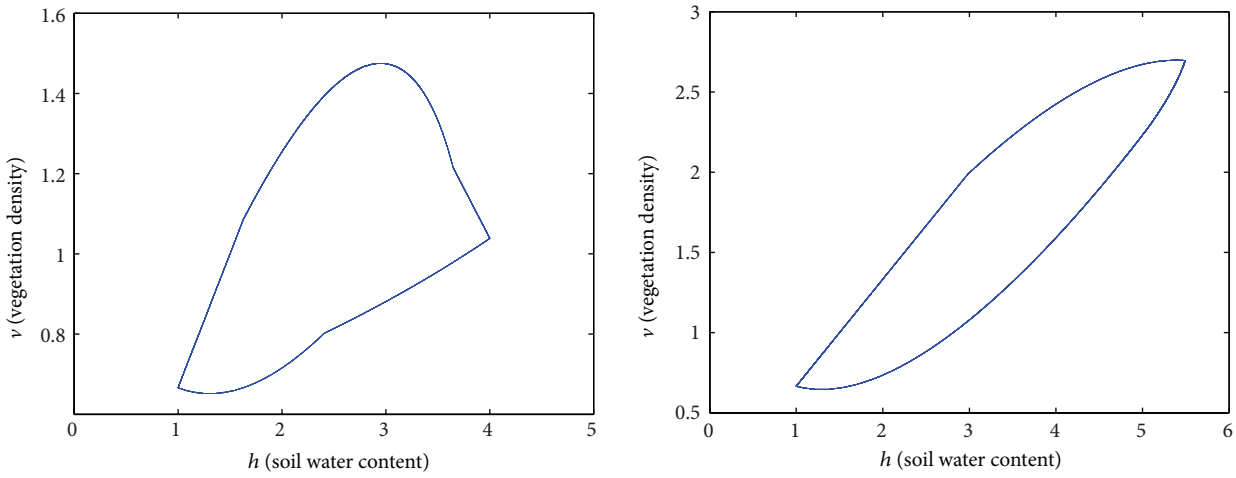

(a) $(w_0, w_1, p) = (1, 4, 4)$ (b) $(w_0, w_1, p) = (1, 7, 3)$

Figure 4: Different types of multiple stationary states.

2.3. Automatic Irrigation Scheme. To summarize, the model has three critical variables: $h(t)$, $v(t)$, and $i(t)$. The value sets of $h(t)$ and $v(t)$ are continuous with their dynamic functions (1)–(3), while the value set of $i(t)$ has only two discrete elements 1 and −1. We only have to define a dynamic function of $i(t)$ to complete our model. As mentioned in Section 2.1, we use a scheme of automatic irrigation switching rule based on the soil moisture content indicated by h:

$$i\left(t^{+}\right) = \begin{cases} -i\left(t\right), & \text{if } i\left(t\right) = -1,\ h\left(t\right) \le w_0, \\ & \text{or } i\left(t\right) = 1,\ h\left(t\right) \ge w_1, \\ i\left(t\right), & \text{else,} \end{cases} \tag{4}$$

where $i(t^+) = \lim_{\Delta t \to 0^+} i(t + \Delta t)$. Bounds of water content w_0 (cm) and w_1 (cm) are introduced, $w_0 < w_1$. In agricultural water management practice, w_0 could be chosen near the wilting point, and w_1 could be chosen near the field capacity [31]. Automatic control can be realized by combining the equipments of soil moisture monitoring, pipe irrigation, and switching [25]. Finally, an executable conceptual ecohydrological model is obtained by combining (1)–(4) together.

2.4. Qualitative Analysis on the Model. Plotting a trajectory $\{(h(t), v(t), t) \mid t \geqslant 0\}$ starting from $(h(0), v(0))$ in h-v space, we get a phase diagram; for example, see Figure 3. Thereinto, the state point is the pair $(h(t), v(t))$, and the limit stationary state (the state when $t \to +\infty$) appears as a period "circle" motion between $h \in [w_0, w_1]$. Generally, there are two stable stationary states. $v(t) \equiv 0$ is always a stationary state, which means that given plants cannot be generated without progenitor. Note the motion $\{(w_0, 0) \to (w_1, 0) \to (w_0, 0)\}$ as the zero circle. However in most cases there should be another periodic orbit with $v \neq 0$ for some parameters and initial values. It means that plants can be grown steadily under certain conditions. Note this stable stationary state as the nonzero circle. Because the vegetation density changes periodically, we concern the average vegetation density in a period of nonzero circle, noted as $\overline{v}$. Furthermore, note the average water supply and the average outflow in a nonzero circle as $\overline{p}$ and $\overline{Q}$. They are two important efficiency indices.

Efforts for theoretical analysis can be done after sufficient simplification of (1)–(3). For example, the Fourier series of the irrigation intensity of the limit cycle can be computed as follows (assume that $i(0^-) = -1$ and $i(0) = 1$):

$$p\left(t\right) = p\eta + 2\Sigma_{n=1}^{\infty} \sin\left(n\pi\eta\right) \cos\left(n\pi\eta - \frac{2n\pi\eta t}{T}\right), \tag{5}$$

where T is the time length of a period, and η is the proportion of irrigating time length in a period. Also restricting $h < H$, $v < \mu_1$, for all h, v, the first-order derivative of the so-called Poincaré map [2] at (w_0, v) is

$$f'(v)\,|_{(w_0,v)} = \frac{w_1}{\alpha\left(w_1 - w_0\right)} \frac{\beta_0 + \beta_1}{\delta_1 + \delta_2} + \frac{w_1}{\alpha\left(p - \alpha v\right)^2} \left(\frac{\beta_0 + \beta_1}{\delta_1 + \delta_2}\right)^2 \left(\alpha w_0 v - \mu_1 p\right). \tag{6}$$

This map indicates the iterative mapping of vegetation density after a loop of irrigation-nonirrigation. It transforms the different equations into the iterative equations and may be convenient to solve some problems; for example, the stationary state of the differential equations corresponds to the equilibrium of $f(v)$. But generally, solving $f(v)$ without any constraint is quite difficult and beyond the scope of this study. Numerical experiment is then carried out to explore the potential nontrivial dynamic behaviors.

3. Analysis of Nontrivial Dynamic Behaviors through Numerical Experiments

Generally speaking, for a given research area and particular vegetation, $c, H, \alpha, \beta, \delta_i$, $i = 1, 2, 3, 4, \mu_1, \mu_2$ are constants,

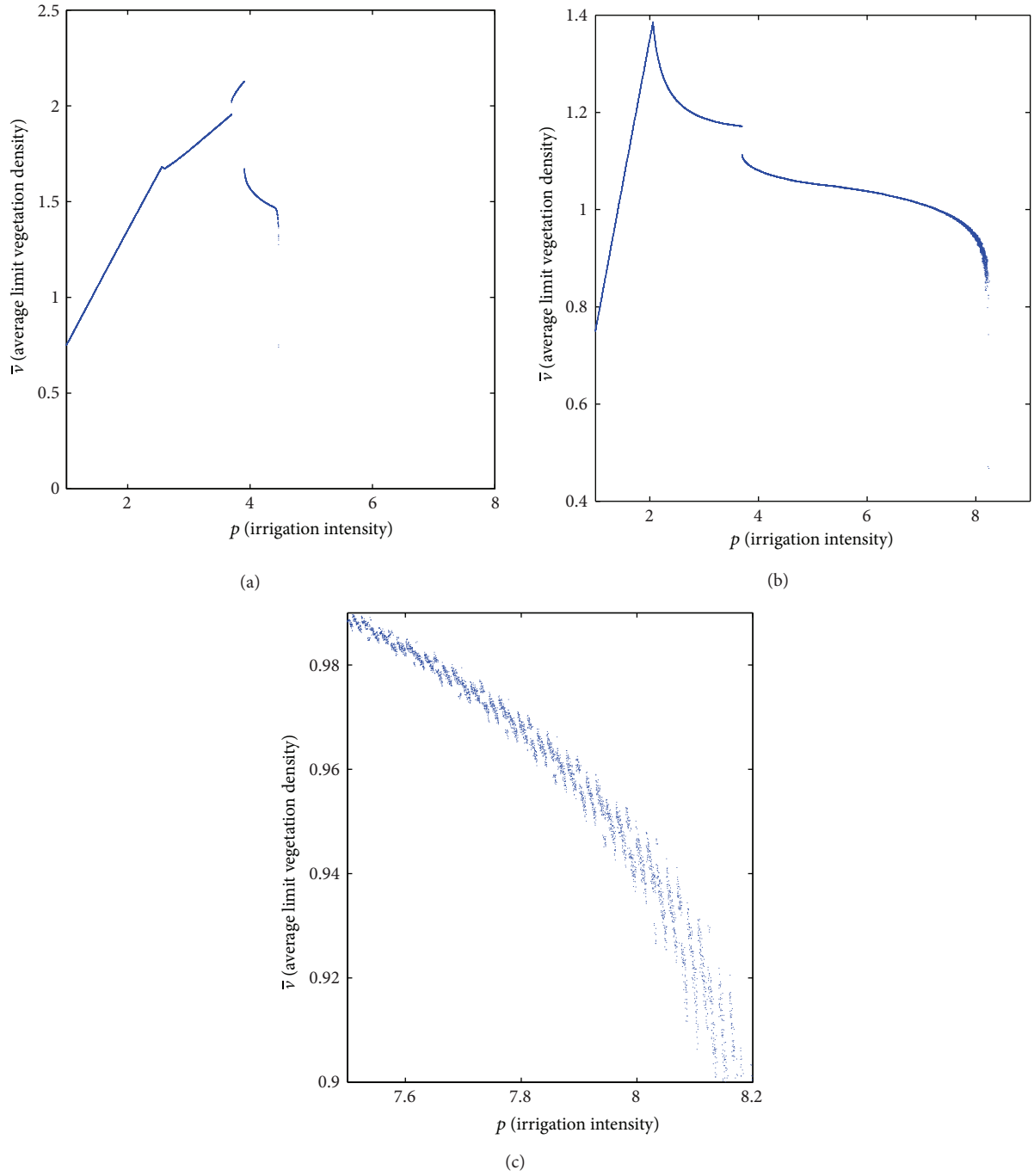

FIGURE 5: Bifurcation map with $\overline{v}$ and p. Here $(w_0, w_1) = (1, 7)$ in (a) and $(w_0, w_1) = (1, 4)$ in ((b), (c)). (c) is a locally magnified (b).

and p, w_0, w_1 are artificial parameters. Furthermore, the adjustment range of w_0 and w_1 is quite small for they should be near to the wilting point and field capacity, respectively, in the irrigation application. Of course, they can also be extended when we move beyond the irrigation problem, see also the discussion in the conclusion section. During the following discussion, we choose $\alpha = 1\,(\text{cm} \cdot \text{n}^{-1} \cdot \text{d}^{-1})$, $c = 0.5\,(\text{d}^{-1})$, $H = 5\,(\text{cm})$, $\beta_0 = 1\,(\text{d}^{-1})$, $\beta_1 = 0.5\,(\text{d}^{-1})$, $\delta_1 = \delta_3 = 0.5\,(\text{cm} \cdot \text{n}^{-1})$, $\delta_2 = \delta_4 = 1\,(\text{cm} \cdot \text{n}^{-1})$, $\mu_1 = 2\,(\text{cm} \cdot \text{n}^{-1})$, and $\mu_2 = 5\,(\text{cm} \cdot \text{n}^{-1})$ as a numerical testing environment, tune w_0 (cm) and w_1 (cm) coarsely, and consider the dynamic behaviors as depending on fine tuning of p (cm/d). (Here n stands for the quantity of grasses.)

There are three stationary states in Figure 3. Here $(w_0, w_1, p) = (1, 7, 4)$. The two thick "circles" are the two stable stationary states, and the thin line divide the first quadrant into two domains of attraction. Points starting from the upper region converge to the upper thick circle, while points starting from the lower region converge to the zero circle. Furthermore, the thin line between $[w_0, w_1]$ is also a

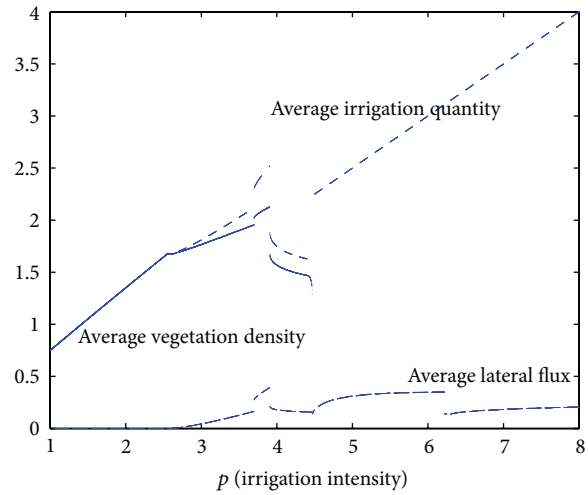

FIGURE 6: Bifurcation map of $\overline{v}$, $\overline{p}$, and $\overline{Q}$ with p.

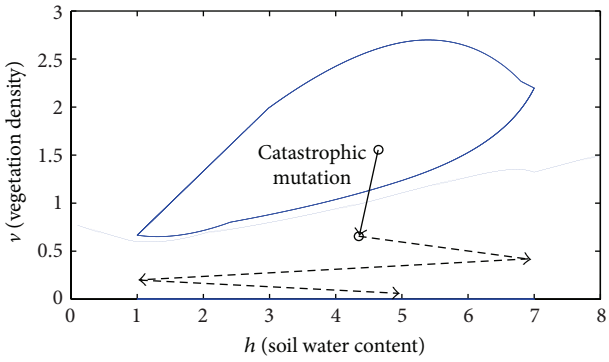

FIGURE 7: Influence of catastrophic mutation—a fire case.

half part of a stationary state (from $h = w_0$ to $h = w_1$), and it is unstable, that is, any tiny disturbance would lead the trajectory to leave this stationary state.

Figure 4 shows some other types of the nonzero stable states for different parameters. The hysteresis is similar with the famous LotkaVolterra predator-prey models raised in the First World War [32]; that is, during different regions, vegetation intensity and soil moisture content can either be of positive correlation or negative correlation, similar to the relationship between cartilaginous fishes and food fishes in the Mediterranean.

Also for some arbitrary parameters w_0, w_1, p, the nonzero stable circle vanishes, which means all plants will die after sufficiently long time. The alteration of the number of stationary states is identified as typical bifurcation. As other parameters fixed, the bifurcation map with p and $\overline{v}$ can be drawn as in Figure 5. Bifurcations with other variables are omitted for conciseness. From the bifurcation map, we can see, as p increased, that the steady vegetation coverage vanishes at $p \approx 4.4$ (Figure 5(a)) and $p \approx 8.3$ (Figure 5(b)), respectively. That means overlarge irrigation intensity will lead plants to die out.

Another important dynamic phenomenon presented in Figure 5 is the mutation, or so-called jump. The long-term behavior of our ecohydrological system is continuous with the parameter p for most of the time but jumps at some individual points. For example, in Figure 5(a), $\overline{v}$ varies continually with p for most time and jumps near $p = 3.7, 3.9, 4.4$. So along with the continuous increase of irrigation intensity, the limit vegetation density may suddenly go up or drop down discretely. A rough interpretation of this phenomenon is the mutation parameters collide the border of continuity intervals of the vegetation growth Equations (2) and (3) [21].

Further experiments are worthy to be done to verify the reliability of numerical analysis. In nature, the independent evolution events with the same parameters will never be repeated, and therefore these dynamical phenomena could not be directly verified by field observations. Nevertheless, the independent repeated artificial experiments could be conducted for the demonstration of these phenomena including the automatic irrigation experiments.

Analysis on the nontrivial dynamic behaviors can be used to guide human practice. For example, under the text condition, we plot the bifurcation maps $\overline{v}$, $\overline{p}$, $\overline{Q}$ (stand for the average vegetation coverage, irrigation quantity, and lateral flux, resp.) with p in a same figure, see Figure 6. From the computation we can see that the maximal stable vegetation coverage is at $p \approx 3.8$, and the unit water consumption is also the least economical at this time.

Another typical example in which dynamic research plays a key role in practical problems is to qualitative study the influence of catastrophic mutation. For example, a fire can push the system from the attracting basin of the nonzero circle to the attracting basin of the zero circle, such as Figure 7.

Moreover, deterministic chaos also occurs in this model, for example, when $p \in [7.8, 8.3]$, as shown in Figures 5(b) and 5(c). The chaotic limit set in h-v space when $p = 8.2$ is shown in Figure 8(a). In the scenario, with the constant irrigation strategy, the vegetation would not converge to a unique circle and the vegetation is "fluctuating" forever. Meanwhile, some chaotic characteristic can be computed. Consider the Poincaré map at the point (w_0, v), the Lyapunov exponent [2] of the Poincaré map is larger than zero, as shown in Figure 8(b), which confirms the existence of chaos. The time series of irrigation can be drawn as in Figure 8(c). To be noted, the graph of irrigation time series indicates a quasiperiodic rectangular pulsing function (see Section 2.1). As mentioned above, planar chaos is a specific behavior of nonsmooth dynamic system, which maybe more natural to depict hydrology process. The possible cause of this behavior is that the observation of soil water content of automatic irrigation system is discrete. The scenario should be designed (or avoided) to depend on the purpose of the irrigation system in the practice.

4. Conclusion

An ideal ecohydrological model convenient for dynamic analysis was established in this paper. Compared with traditional models, the nonsmooth property is emphasized. Pulsing function was used to describe the rainfall intensity with a practical interpretation of automatic irrigation. Under this approach, the deterministic process-based ecohydrological

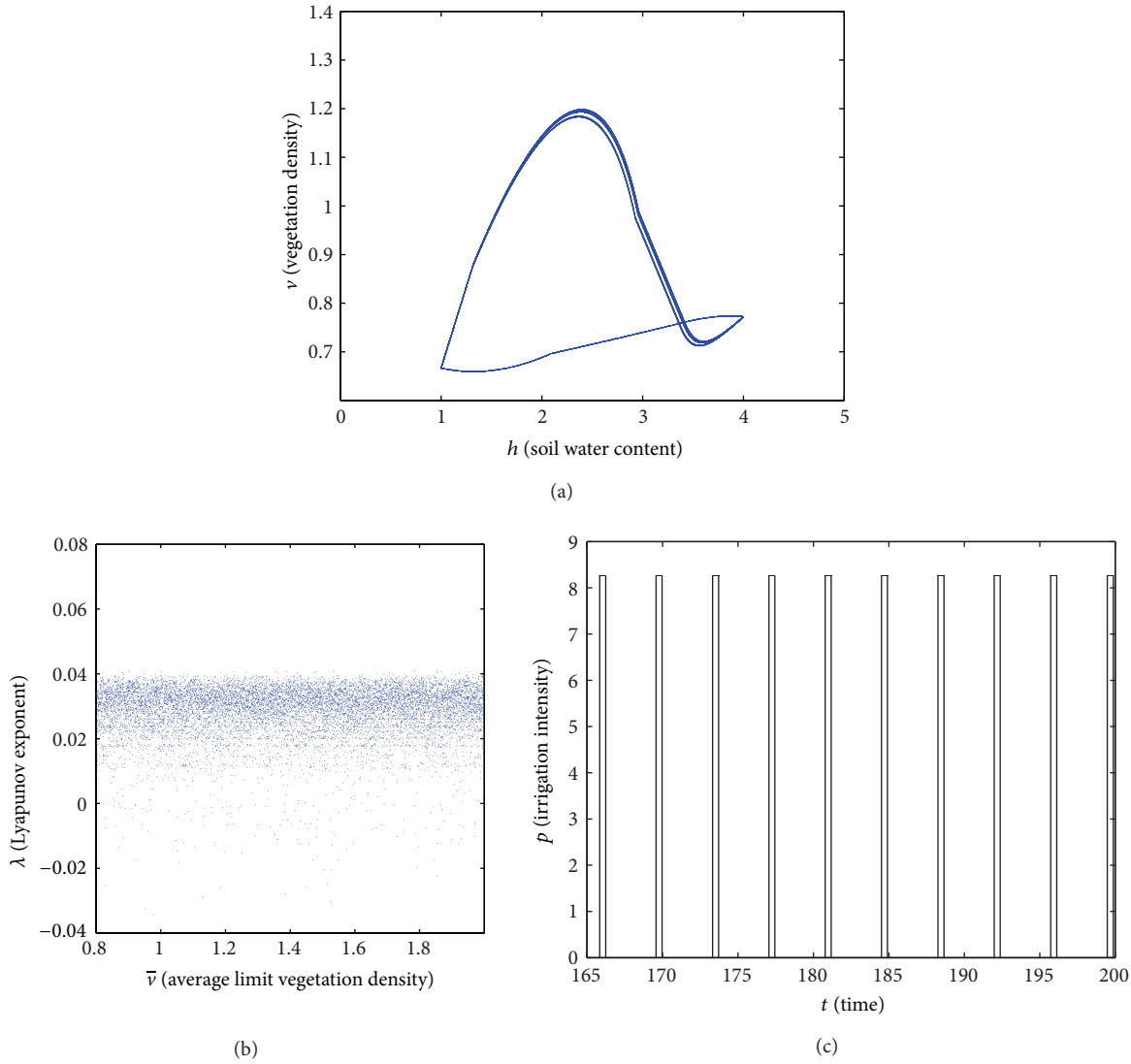

Figure 8: (a) The chaotic phase diagram; (b) The Lyapunov exponent. Here $(w_0, w_1, p) = (1, 4, 8.2)$; (c) the irrigation time series.

model was analyzed theoretically. Based on the model, some deterministic nontrivial dynamic phenomena are revealed. For example, the existence of multiple stationary states, mutation, bifurcation, and chaos was discussed under numerical simulation, with an overview on their possible application in optimization, avoiding the influence of catastrophic mutation, and so on.

This work can be seen as a kind of demonstration to show the existence of some complicated dynamic phenomena in ecohydrological process. Further observational study should be done to determine the scope of parameters in the real world which has nontrivial dynamic phenomena, probably starting from hyperarid area just as Liu et al. [33] have done to validate ecohydrological feedbacks in hyperarid Tarim River. Noticing that for the convenience of theoretical study, we used a step function to indicate the atmospheric forcing term, instead of considering the stochastic features of rainfall. Actually, one can change the switching policy (4) to a more complicated one, for example, through fixing the time length of $i(t) = 1$ corresponding to a timing irrigation, or randomizing the time length of $i(t) = 1$ corresponding to a stochastic irrigation. A bold hypothesis is that if we understand the rainfall mechanism thoroughly, a proper switching policy can be invented to simulate the fully stochastic features of real rainfall process by introducing additional oceanic and climatic variables, as implicated by the simple formulation of local recycling rainfall in [12, 13]. Also, the model could be further improved by refining the existing feedbacks between hydrological and ecological processes and by incorporating more feedbacks among hydrological, atmospheric, and other related processes.

Nomenclature

c: Side outlet coefficient (d^{-1})
h: Storage of aquifer (cm)

H: Height of the side outlet of the tank (cm)
i: Irrigation state $i \in \{\pm 1\}$
p: Irrigation intensity (cm/d)
Q: Side outlet intensity (cm/d)
t: Time (d)
T: Time length of a period (d)
v: Biomass (n) ((n) is short for quantity of grasses)
w_0, w_1: Bounds of storage of aquifer (cm)
α: Transpiration coefficient (cm/(d · n))
β_0, β_1: Bounds of evolution rate (d^{-1})
$\delta_{1\sim4}$: Distance between kickpoints and equilibria in (3) (n)
μ_1, μ_2: Equilibria of evolution (n)
η: The proportion of irrigating time length in a period (100%)
$\dot{x}$: dx/dt, x stands for any variable
$\overline{x}$: Average x in a nonzero circle, x stands for any variable.

Acknowledgments

This research was funded by the National Science Foundation of China (NSFC51179084, 51190092, 51222901, and 11072274), the foundation of State Key Laboratory of Hydroscience and Engineering of Tsinghua University (2012-KY-03), and the Scientific Research Foundation for the Returned Overseas Chinese Scholars, State Education Ministry.

References

[1] T. J. Peterson, R. M. Argent, A. W. Western, and F. H. S. Chiew, "Multiple stable states in hydrological models: an ecohydrological investigation," *Water Resources Research*, vol. 45, no. 3, Article ID W03406, 2009.

[2] H. G. Schuster and W. Just, *Deterministic Chaos, An Introduction*, Wiley-VCH, 2005.

[3] P. Kumar, "Variability, feedback, and cooperative process dynamics: elements of a unifying hydrologic theory," *Geophysical Compass*, vol. 1, no. 6, pp. 1338–1360, 2007.

[4] F. Laio, A. Porporato, L. Ridolfi, and I. Rodriguez-Iturbe, "Plants in water-controlled ecosystems: active role in hydrologie processes and responce to water stress II. Probabilistic soil moisture dynamics," *Advances in Water Resources*, vol. 24, no. 7, pp. 707–723, 2001.

[5] B. Sivakumar, "Chaos theory in hydrology: important issues and interpretations," *Journal of Hydrology*, vol. 227, no. 1–4, pp. 1–20, 2000.

[6] B. Sivakumar, "Chaos theory in geophysics: past, present and future," *Chaos, Solitons and Fractals*, vol. 19, no. 2, pp. 441–462, 2004.

[7] F. D'Andrea, A. Provenzale, R. Vautard, and N. De Noblet-Decoudre, "Hot and cool summers: multiple equilibria of the continental water cycle," *Geophysical Research Letters*, vol. 33, no. 24, Article ID L24807, 2006.

[8] L. Ridolfi, P. D'Odorico, F. Laio, S. Tamea, and I. Rodriguez-Iturbe, "Effect of vegetation-water table feedbacks on the stability and resilience of plant ecosystems," *Water Resources Research*, vol. 42, no. 1, Article ID W01201, 2006.

[9] P. D'Odorico, K. Caylor, G. S. Okin, and T. M. Scanlon, "On soil moisture-vegetation feedbacks and their possible effects on the dynamics of dryland ecosystems," *Journal of Geophysical Research*, vol. 112, no. G4, Article ID G04010, 2007.

[10] F. Borgogno, P. D'Odorico, F. Laio, and L. Ridolfi, "Effect of rainfall interannual variability on the stability and resilience of dryland plant ecosystems," *Water Resources Research*, vol. 43, no. 6, Article ID W06411, 2007.

[11] C. W. Runyan and P. D'Odorico, "Ecohydrological feedbacks between salt accumulation and vegetation dynamics: the role of vegetation-groundwater interactions," *Water Resources Research*, vol. 46, no. 11, Article ID W11561, 2010.

[12] I. Rodriguez-Iturbe, D. Entekhabi, and R. L. Bras, "Nonlinear dynamics of soil moisture at climate scales, 1. Stochastic analysis," *Water Resources Research*, vol. 27, no. 8, pp. 1899–1906, 1991.

[13] I. Rodriguez-Iturbe, D. Entekhabi, J.-S. Lee, and R. L. Bras, "Nonlinear dynamics of soil moisture at climate scales, 2. Chaotic analysis," *Water Resources Research*, vol. 27, no. 8, pp. 1907–1915, 1991.

[14] F. Laio, S. Tamea, L. Ridolfi, P. D'Odorico, and I. Rodriguez-Iturbe, "Ecohydrology of groundwater-dependent ecosystems: 1. Stochastic water table dynamics," *Water Resources Research*, vol. 45, no. 5, Article ID W05419, 2009.

[15] J. S. Robinson and M. Sivapalan, "Temporal scales and hydrological regimes: implications for flood frequency scaling," *Water Resources Research*, vol. 33, no. 12, pp. 2981–2999, 1997.

[16] M. A. Ghorbani, R. Khatibi, B. Sivakumar, and L. Cobb, "Study of discontinuities in hydrological data using catastrophe theory," *Hydrological Sciences Journal*, vol. 55, no. 7, pp. 1137–1151, 2010.

[17] A. van der Schaft and H. Schumacher, *An Introduction to Hybrid Dynamical Systems*, vol. 251, Springer, Berlin, Germany, 2000.

[18] M. Bernardo, J. Chris, R. Alan et al., "Numerical simulation of finite dimensional multibody nonsmooth mechanical systems," *ASME Applied Mechanics Reviews*, vol. 55, pp. 107–150, 2002.

[19] S. A. Matveev and V. A. Savkin, *Qualitative Theory of Hybrid Dynamical Systems*, Berlin, Germany, 2000.

[20] M. di Bernardo, C. J. Budd, A. R. Champneys et al., "Bifurcations in nonsmooth dynamical systems," *SIAM Review*, vol. 50, no. 4, pp. 629–701, 2008.

[21] M. Kunze, *Non-Smooth Dynamical Systems*, vol. 1744, Springer, Berlin, Germany, 2000.

[22] D. B. G. Collins and R. L. Bras, "Climatic and ecological controls of equilibrium drainage density, relief, and channel concavity in dry lands," *Water Resources Research*, vol. 46, no. 4, Article ID W04508, 2010.

[23] E. Lu, "Determining the start, duration, and strength of flood and drought with daily precipitation: rationale," *Geophysical Research Letters*, vol. 36, no. 12, Article ID L12707, 2009.

[24] B. Singh, J. Boivin, G. Kirkpatrick, and B. Hum, "Automatic irrigation scheduling system (AISSUM): principles and applications," *Journal of Irrigation & Drainage Engineering—ASCE*, vol. 121, no. 1, pp. 43–56, 1995.

[25] N. Abraham, P. S. Hema, E. K. Saritha, and S. Subramannian, "Irrigation automation based on soil electrical conductivity and leaf temperature," *Agricultural Water Management*, vol. 45, no. 2, pp. 145–157, 2000.

[26] M. Yildirim, "The performance of irrigation automation system based on soil moisture level for pepper (*Capsicum annuum* L.) growth," *Journal of Food, Agriculture and Environment*, vol. 8, no. 3-4, pp. 629–634, 2010.

[27] B. Cardenas-Lailhacar, M. D. Dukes, and G. L. Miller, "Sensor-Based automation of irrigation on bermudagrass, during wet weather conditions," *Journal of Irrigation and Drainage Engineering*, vol. 134, no. 2, pp. 120–128, 2008.

[28] Z. Ruisen, D. Xinguang, and M. Yingjie, "Sustainable water saving: new concept of modern agricultural water saving, starting from development of Xinjiang's agricultural irrigation over the last 50 years," *Irrigation and Drainage*, vol. 58, no. 4, pp. 383–392, 2009.

[29] M. Sugawara, "Automatic calibration of the tank model," *Hydrological Sciences Bulletin*, vol. 24, no. 3, pp. 375–388, 1979.

[30] T. F. M. Chui, S. Y. Low, and S.-Y. Liong, "An ecohydrological model for studying groundwater—vegetation interactions in wetlands," *Journal of Hydrology*, vol. 409, no. 1-2, pp. 291–304, 2011.

[31] R. G. Allen, L. S. Pereira, D. Raes, and M. Smith, *Crop Evapotranspiration: Guidelines for Computing Crop Water Requirements*, vol. 56 of *Irrigation and Drainage*, 1998.

[32] D. N. Burghes and M. S. Borrie, *Modelling with Differential Equations*, Horwood, Chichester, UK, 1981.

[33] D. Liu, F. Tian, H. Hu, M. Lin, and Z. Cong, "Ecohydrological evolution model on riparian vegetation in hyper-arid regions and its validation in the lower reach of Tarim River," *Hydrological Processes*, vol. 26, no. 13, pp. 2049–2060, 2012.

Hindawi Publishing Corporation
Mathematical Problems in Engineering
Volume 2013, Article ID 837919, 9 pages
http://dx.doi.org/10.1155/2013/837919

Research Article

Bilevel Multiobjective Programming Applied to Water Resources Allocation

Shiqi Fang,[1] Ping Guo,[1,2] Mo Li,[1] and Liudong Zhang[1,3]

[1] *Centre for Agricultural Water Research in China, China Agricultural University, Beijing 100083, China*
[2] *Environmental Science and Engineering Program, University of Northern British Columbia, Prince George, BC, Canada V2N 4Z9*
[3] *College of Water Conservancy, Hydropower and Architecture Engineering, Yunnan Agricultural University, Kunming 650201, China*

Correspondence should be addressed to Ping Guo; guop@cau.edu.cn

Received 28 November 2012; Accepted 3 February 2013

Academic Editor: Yongping Li

Water allocation is an essential programming to support the sustainable development of Wuwei Basin, Gansu Province, China. To satisfy the demands of the decision makers (DMs) of each subarea and the total area, a bilevel multiobjective linear programming (BLMOLP) model is proposed. In the BLMOLP, DMs have a hierarchy of two levels—the upper level and the lower level DMs. In this paper, a fuzzy goal programming (FGP) approach is applied to solve the BLMOLP. Firstly, the upper level is solved and used as the tolerance for the lower level. Then the weights of each objective function in the lower level are evaluated. Finally, a satisfied optimization solution of the problem was calculated. The result suggests that the FGP is a simple and feasible approach to BLMOLP problems. The proposed method was applied to a case study for water resources allocation in Wuwei Basin. For four scenarios under consideration, the model can effectively balance the benefits among all regions and sections according to the priority of the upper level decision makers. The results indicate that comprehensive solutions have been obtained.

1. Introduction

Water is essential for all forms of life and is a fundamental resource, which has benefited both people and their socioeconomies for many centuries [1, 2]. The services provided by water systems are multiple. Yet, the overgrowing population and the droughts are putting water resources under pressure, especially in arid and semiarid areas. Solutions to the problem depend on many factors among which rational water planning and management is essential [3]. Water resources management has been a popular problem since the 1990s. Many researchers have promoted many concepts and methods for sustainable water resources management, such as virtual water and water foot print.

To balance the conflicts among water users, researchers have introduced optimization models for the allocation of water resources. The earlier water resource optimization models have been applied to multiarid and semiarid areas all over the world, from Arizona [4] to southern California [5] from Africa [6, 7] to Asia [8]. There are different methods introduced in the literature for optimization models of water resources allocation, such as dynamic programming [9], genetic algorithm [10], and game theoretic approach [11]. In the progress of decision making, problems are often compounded by uncertainties, such as the rainfall and the runoff appeared random values. In recent years, to tackle these uncertainties, several scientists proposed kinds of novel approaches. Messner et al. [12] proposed a multicriteria decision support under uncertainty, to deal with the water allocation conflict in the watershed of the German Spree River. To handle uncertainties existing in the water resources management systems, Li et al. [13] applied a multistage fuzzy-stochastic programming (MFSP) model to the planning of sustainable water resources management. In water allocation problem, Sadegh et al. [14] developed new methodologies based on game theories for optimal allocation of interbasin water resources, and Sadegh and Kerachian [15] then developed two new concepts Fuzzy Least Core and Fuzzy Weak Least Core to solve the water allocation model with fuzzy cooperative games. Shao et al. [16] combined conditional value-at-risk (CVaR) model with inexact two-stage stochastic programming and applied it to a reservoir water allocation

system. Jin et al. [17] applied a dynamic dual interval programming (DDIP) to the irrigation water allocation systems. It is composed of potato, wheat, and alfalfa users with different requirements of water demand, value, and penalty cost under uncertainty. However, these methods have seldom been applied in practical cases for water resources allocation because of their complexity.

In practical cases, research area contains several subareas with multiwater users, such as irrigation, industry, domesticity, and ecology users. Competition for scare water resources by these users demands more well-developed methods to solve the conflicts, thus the researchers turned to multiobjective programming. Xevi and Khan [18] developed a multicriteria decision-making (MCDM) framework under multiconstraints, using the goal programming (GP) to solve the multiple objective problems. Singh et al. [19] presented an interactive fuzzy multiobjective linear programming (IFMOLP) model to improve the water quality and reduce the treatment cost. Fasakhodi et al. [20] were concerned with multiobjective linear fractional programming for optimizing sustainable water resources management. Many of them might encounter with the problem that it is difficult to select the target values and weights for the different goals.

However, water users and water managers always belong to two different groups in water system, especially in China. So there are not only conflicts between water users but also conflicts between water users and managers. And all the users have a hierarchical organization, so we need a multilevel or a bilevel programming to solve such a problem. Multilevel programming and bilevel programming were first proposed by Candler and Norton in their report [21]. Multi-level programming (MLP) is identified as mathematical programming that solves decentralized planning problems with multiple executors in a multi-level or hierarchical organization [22]. A bilevel programming problem is a special MLP that bilcontains decision makers (DMs) in two levels. Bilevel programming has been used in water exchange in eco-industrial parks [23], manufacturer-retailer supply chain problems [24], and lot-sizing problems [25]. Considering a water resources allocation problem that involves multisources and multiusers, Lv et al. [26] developed an interval fuzzy bilevel approach (IFBP) to solve the problems, from which decision makers had a characteristic of hierarchy and conflicted with each other. However, there are few researches to address the bilevel approach within multiobjective framework under uncertainty for the water resources allocation. Especially when managers need to make a choice among multiprofits, traditional mathematical programming cannot deal with such dilemma under a hierarchical structure.

Based on the above discussions, in water allocation behavior, different interest users and different interest managers have different objectives which may be conflicting and incommensurable. When water managers considered water allocation problem referring to targets on different levels, a bilevel programming can be used for different profit preference. Such as in the Wuwei Basin, environment and ecology deterioration is the most prominent problem, so the decision makers on the upper level can place particular emphasis on the ecology benefit. To coordinate their interests, a bilevel approach within multiobjective framework under uncertainty for the water resources allocation needs to be considered. In this research, a bilevel multiobjective linear programming (BLMOLP) is proposed to solve water resources allocation for multiusers, which were characterized as hierarchical structure. The detailed research tasks include the following. In Section 2, the general formulation and the solution methods are introduced. The fuzzy goal programming approach is mainly discussed and used to solve the problem. In Section 3, the general situation of the study area is presented, and the formulation of the problem is solved. Four scenarios are calculated for different goals, and the results will help the decision makers to balance the water allocation in the area. In Section 4, the conclusion is given, and the future work is proposed.

2. Methodology

2.1. Bilevel Programming

2.1.1. General Formulation. The general formulation of a bilevel programming problem (BLPP) is as follows [27]:

(upper level)

$$\begin{aligned} \max_{x\in X,y} \quad & F(x,y) \\ \text{s.t.} \quad & G(x,y)\le 0, \end{aligned} \tag{1}$$

where y can be solved from

(lower level)

$$\begin{aligned} \max_{y} \quad & f(x,y) \\ \text{s.t.} \quad & g(x,y)\le 0, \end{aligned} \tag{2}$$

where $x \in \mathbf{R}^{n_1}$ and $y \in \mathbf{R}^{n_2}$. The variables of problem (1), (2), (3), (4), and (5) are divided into two classes, namely, the upper level variables $x \in \mathbf{R}^{n_1}$ and the lower level variables $y \in \mathbf{R}^{n_2}$. The upper level decision maker (ULDM) controls over vector x, and the lower level decision maker (LLDM) controls over vector y.

Through introducing the bilevel programming into the multiobjective framework, the bilevel multiobjective linear programming (BLMOLP) can be expressed as

(upper level)

$$\begin{aligned} \max_{x\in X,y} \quad & F(x,y) \\ \text{s.t.} \quad & G(x,y)\le 0, \end{aligned} \tag{3}$$

where y can be solved from

(lower level)

$$\begin{aligned} \max_{y} \quad & \{f_1(x,y),\ldots,f_i(x,y),\ldots,f_n(x,y),\} \\ \text{s.t.} \quad & g_i(x,y)\le 0. \end{aligned} \tag{4}$$

2.1.2. Solution Methods. So far, many classical approaches to solve bilevel programming (BLP), especially for bilevel linear

programming, were developed. The Kth-best algorithm was first proposed by Candler and Townsley [28]. Shi et al. [29] proposed an extended Kth-best approach for linear BLP. Bialas and Karwan [30] first used complementary pivots approach for linear BLPPs. Also, Bard and Moore [31] proposed the branch and bound algorithm to solve bilevel programming. This algorithm has been applied with remarkable success in linear bilevel programming, but its performance is dependent on the linear form of the upper level constraint functions.

One of the most efficient approaches was the fuzzy goal programming (FGP), which is an extension of the conventional goal programming (GP) introduced by Charnes and Cooper [32]. Fuzzy goal programming (FGP) approach to BLP has been recently studied by many researchers [33–35].

2.2. Fuzzy Goal Programming to BLMOLP. In BLMOLP problems, if one level is assigned to each of the objectives, then these fuzzy objectives are termed as fuzzy goals. They are to be characterized by the associated membership functions by defining the tolerance limits for the achievement of each level. And the solution procedure appears as the following [22, 36, 37].

2.2.1. Construction of Membership Functions. If the two levels share the same constrains, all the DMs are interested in maximizing their own objective functions over the same feasible region, then the optimal solutions of both of them calculated in isolation can be taken as the aspiration levels of their associated fuzzy goals.

Let (x^U, y^U, F^U) and (x^L, y^L, f^L) be the optimal solutions of the upper level and lower level, respectively, when calculated in isolation. Then the fuzzy goals of leader and subordinates appear as

$$F \gtrsim F^L, \qquad f_i \gtrsim f_i^U. \tag{5}$$

It may be noticed that the two solutions (x^U, y^U, F^U) and (x^L, y^L, f^L) are usually different because the objectives of all DMs are conflicting in nature. Therefore, it can be assumed reasonably that the values $F^L [= F(x^L, y^L)] < F^U$ and all values $F(x, y) < F^L$ are absolutely unacceptable to the upper level. $f(x^m, y^m)$ can be considered as the tolerance limit of the fuzzy objective goal of the upper level. Similarly, $f^U [= f(x^U, y^U)] < f^L$ can be considered as the lower tolerance limit of the fuzzy objective goal of the lower level.

Let $x^m (x^L < x^m < x^U)$ be the tolerance limit of the fuzzy decision goal of the leader. Then, the membership functions of the defined fuzzy goals can be formulated as follows:

$$\mu_F [F(x, y)] = \begin{cases} 1 & \text{if } F(x, y) > F^U, \\ \dfrac{F^L - F(x, y)}{F^U - F^L} & \text{if } F^L < F(x, y) < F^U, \\ 0 & \text{if } F(x, y) < F^L. \end{cases} \tag{6}$$

Let t^l and t^R be the maximum negative and positive tolerance values on the decision vectors considered by the upper level DM. The tolerances t^l and t^R are not necessarily the same:

$$\mu_x (x) = \begin{cases} \dfrac{x - \left(x^U - t^L\right)}{t^L} & \text{if } x^U - t^L < x < x^U, \\ \dfrac{\left(x^U + t^R\right) - x}{t^R} & \text{if } x^U < x < x^U + t^R, \\ 0 & \text{if otherwise,} \end{cases} \tag{7}$$

$$\mu_{f_i} [f_i (x, y)] = \begin{cases} 1 & \text{if } f_i (x, y) > f_i^L, \\ \dfrac{f_i^L - f_i (x, y)}{f_i^L - f_i^U} & \text{if } f_i^U < f_i (x, y) < f_i^L, \\ 0 & \text{if } f_i (x, y) < f_i^U. \end{cases} \tag{8}$$

2.2.2. Fuzzy Goal Programming Approach. In fuzzy programming approaches, the highest degree of membership function is one. According to [38], for the defined membership functions in (6) and (7), the flexible membership goals with the upper level can be presented as

$$\begin{aligned} \mu_F [F(x, y)] + d_F^- - d_F^+ &= 1, \\ \mu_x (x) + d_F^- - d_F^+ &= 1 \end{aligned} \tag{9}$$

or equivalently as

$$\begin{aligned} \frac{F(x, y) - F^L}{F^U - F^L} + d_F^- - d_F^+ &= 1, \\ \frac{x - \left(x^U - t^L\right)}{t^L} + d_F^{L-} - d_F^{L+} &= 1, \\ \frac{\left(x^U + t^R\right) - x}{t^R} + d_F^{R-} - d_F^{R+} &= 1, \end{aligned} \tag{10}$$

where $d_F^- = (d_F^{L-}, d_F^{R-})$, $d_F^+ = (d_F^{L+}, d_F^{R+})$, and $d_F^-, d_F^{L-}, d_F^{R-}$, $d_F^+, d_F^{L+}, d_F^{R+}$ with $d_F^- \times d_F^+ = 0$, $d_F^{L-} \times d_F^{L+} = 0$ and $d_F^{R-} \times d_F^{R+} = 0$, represent the under and over deviations, respectively, from the aspired levels.

Then, the proposed fuzzy bilevel multiobjective linear goal programming model of the problem can be presented under the framework of min-sum goal programming as follows:

upper level DM FGP model:

$$\max Z = \omega_F^+ d_F^+ \tag{11}$$

subject to

$$\frac{F(x,y)-F^L}{F^U-F^L}+d_F^- - d_F^+ = 1, \tag{12}$$

$$G(x,y)\le 0, \qquad g_i(x,y)\le 0, \tag{13}$$

$$d_F^-, d_F^+ \ge 0, \qquad d_F^- \times d_F^+ = 0, \tag{14}$$

lower level DM FGP model:

$$\max Z = \omega_F^+ d_F^+ + \sum_{i=1}^{n}\omega_{2i}^+ d_{2i}^+ + \omega_F^L\left(d_F^{L-}+d_F^{L+}\right) + \omega_1^R\left(d_F^{R-}+d_F^{R+}\right) \tag{15}$$

subject to

$$\frac{F(x,y)-F^L}{F^U-F^L}+d_F^- - d_F^+ = 1, \tag{16}$$

$$\frac{x-\left(x^U-t^L\right)}{t^L}+d_F^{L-}-d_F^{L+}=1, \tag{17}$$

$$\frac{\left(x^U+t^R\right)-x}{t^R}+d_F^{R-}-d_F^{R+}=1, \tag{18}$$

$$G(x,y)\le 0, \qquad g_i(x,y)\le 0, \tag{19}$$

$$d_F^-, d_F^+ \ge 0, \qquad d_F^- \times d_F^+ = 0, \tag{20}$$

$$d_F^{L-}, d_F^{L+} \ge 0, \qquad d_F^{L-} \times d_F^{L+} = 0, \tag{21}$$

$$d_F^{R-}, d_F^{R+} \ge 0, \qquad d_F^{R-} \times d_F^{R+} = 0, \tag{22}$$

where Z represents the fuzzy achievement function consisting of the weighted over-deviational variables d_F^+ of the fuzzy goals F^L, and the under-deviational and the over-deviational variables $d_F^{R-}, d_F^{R+}, d_F^{L-}$ and d_F^{L+} for the fuzzy goals of all the decision variables for the upper level. The numerical weights $\omega_F^+, \omega_{2i}^+, \omega_F^L$, and ω_1^R represent the relative importance of the respective fuzzy goals subject to the constraints set in the decision situation.

To assess the relative importance of the fuzzy goals properly, the weighting scheme suggested by Mohamed—decision makers can rank the K objectives according to their priority [38]—can be used to assign the values to $\omega_F^+, \omega_{2i}^+, \omega_F^L$ and ω_1^R. In the present formulation, these values are determined as

$$\omega_F^+ = \frac{1}{\left(F^U-F^L\right)}, \qquad \omega_{2i}^+ = \frac{1}{\left(f_i^L-f_i^U\right)}, \tag{23}$$

$$\omega_F^L = \frac{1}{t^L}, \qquad \omega_1^R = \frac{1}{t^R}. \tag{24}$$

Using the fuzzy goal programming approach referred above, the calculating procedure is expressed as in the following steps.

Step 1. Calculate the individual values (minimum $F^L [= F(x^L, y^L)]$ and maximum $f^U [= f(x^U, y^U)]$) of all objective functions for the upper level and lower level under the given constraints.

Step 2. Set the goals and tolerances limits and evaluate the weights ω_F^+ for the objective function of the upper level.

Step 3. Elicit the membership function $\mu_F[F(x,y)]$ and formulate the transformed upper level model (15), (16), (17), (18), (19), (20), (21), and (22).

Step 4. Solve the transformed upper level model.

Step 5. Set the tolerance for $d_F^-, d_F^{L-}, d_F^{R-}, d_F^+, d_F^{L+}$, and d_F^{R+} and evaluate the weights ω_F^L, ω_1^R.

Step 6. Elicit the membership function $\mu_{f_i}[f_i(x,y)]$ and formulate the transformed lower level model (23), (24).

Step 7. Solve the transformed lower level model to get the satisfactory solution of the BLMOP problem.

3. Case Study

3.1. Overview of the Study Area. The Wuwei Basin, Gansu Province, China (Figure 1), which is located in the eastern part of the Hexi Corridor (near Lanzhou, Qinghai, and Inner Mongolia), is an oasis-desert ecotone that links the Loess Plateau, Tibetan Plateau, and Mongolia-Xinjiang Plateau. [39, 40]. Wuwei is a typical continental climate region, with its average temperature of 7.80°C per year, average sunshine of 2968.2 hours per year, and frost-free period of 158 days per year. The rainfall is 161 mm, and its evaporation is 2020 mm per year. The distribution of rainfall is uneven which accounted for 59.4% of the annual precipitation from July to September.

Due to the particular geography and the influence of human activities in Shiyang River Basin, the vegetation coverage of water conservation forest is decreasing, and the shortage of surface water resources is coming. The contradiction between supply and demand of water resources is increasing. Conflicts arise in the allocation of limited water resources among multiple competing interests, because each region prefers to maximize its own net benefit. But for the upper level decision makers, to balance the benefits of each region (lower level decision makers) is more important. Thus, bilevel programming is considered for the research area.

According to statistics annual reports published by Wuwei Water Affairs Bureau, the values per 1000 cube meters of water of each area are calculated (Table 2), which will be used as the coefficient of the upper level programming; the water price is selected as the coefficient of the lower level programming. Therefore, the upper level goal is the total benefit of Wuwei, and the lower level goal was the profit of water resources of each area.

According to Gansu Water Resources Bulletin (2009), the total amount of water supplied in 2009 is 1.91436 billion m^3. Considering five-year (2005–2009) water resources datum, water demand numbers were calculated by trend forecasting method. The maximum and minimum water demands of each area are in Table 1.

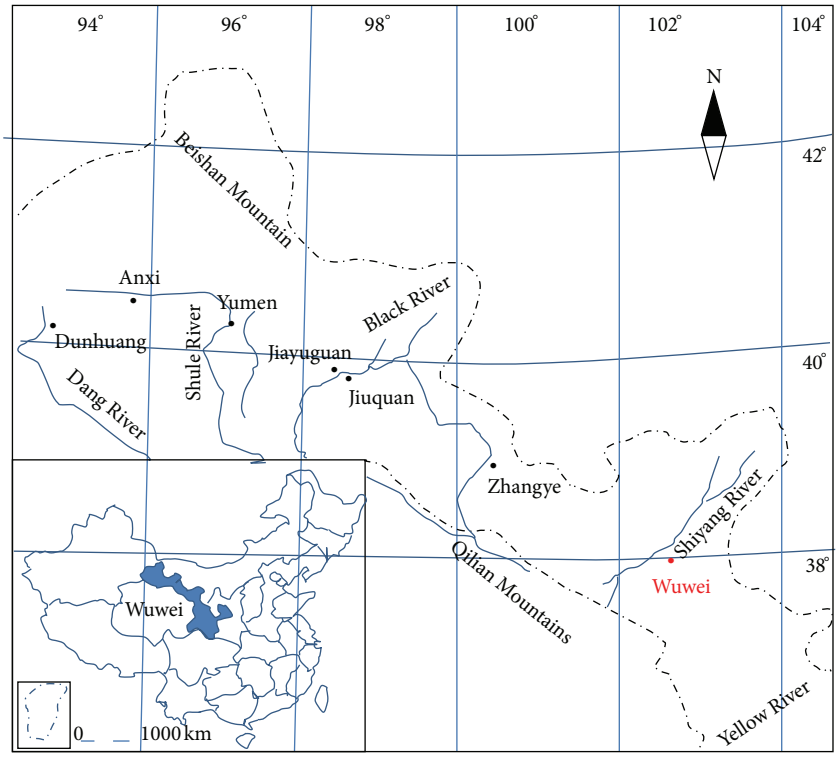

Figure 1: Location of the study area in Gansu Province.

Table 1: Water demand of each area.

Demand 10^6	Area	Irrigation	Industry	Domesticity	Ecology
Maximum	Liangzhou	983.913	89.880	63.034	92.884
	Minqin	573.518	3.804	18.693	43.575
	Gulang	164.666	3.144	11.453	16.032
	Tianzhu	101.183	8.412	11.962	2.957
Minimum	Liangzhou	648.912	60.257	42.604	68.481
	Minqin	379.506	2.555	12.546	28.306
	Gulang	109.096	2.110	7.634	10.808
	Tianzhu	67.315	5.619	7.999	2.141

Table 2: Coefficients of the upper-level and lower-level programming.

Area	ULP coefficient Yuan/(1000 m^3)	LLP coefficient (Yuan/m^3)			
	C_i	Irrigation	Industry	Domesticity	Ecology
Liangzhou	139.28	0.11	1.9	1.85	0.11
Minqin	54.66	0.208	3.5	1.8	0.15
Gulang	132.45	0.13	2.8	1.8	0.13
Tianzhu	163.28	0.1	0.15	1.1	0.13

3.2. Modeling Formulation and Calculating Procedure. The problem under consideration is how to allocate water resources. The upper level decision makers wanted to get the maximum benefits of the whole system, while the lower level decision makers would like to maximize their own profits. Then the objects of the problem are shown as follows:

(upper level)

$$\max F = \sum_{i=1}^{4} \left(C_i \cdot \sum_{j=1}^{4} x_{ij} \right), \tag{25}$$

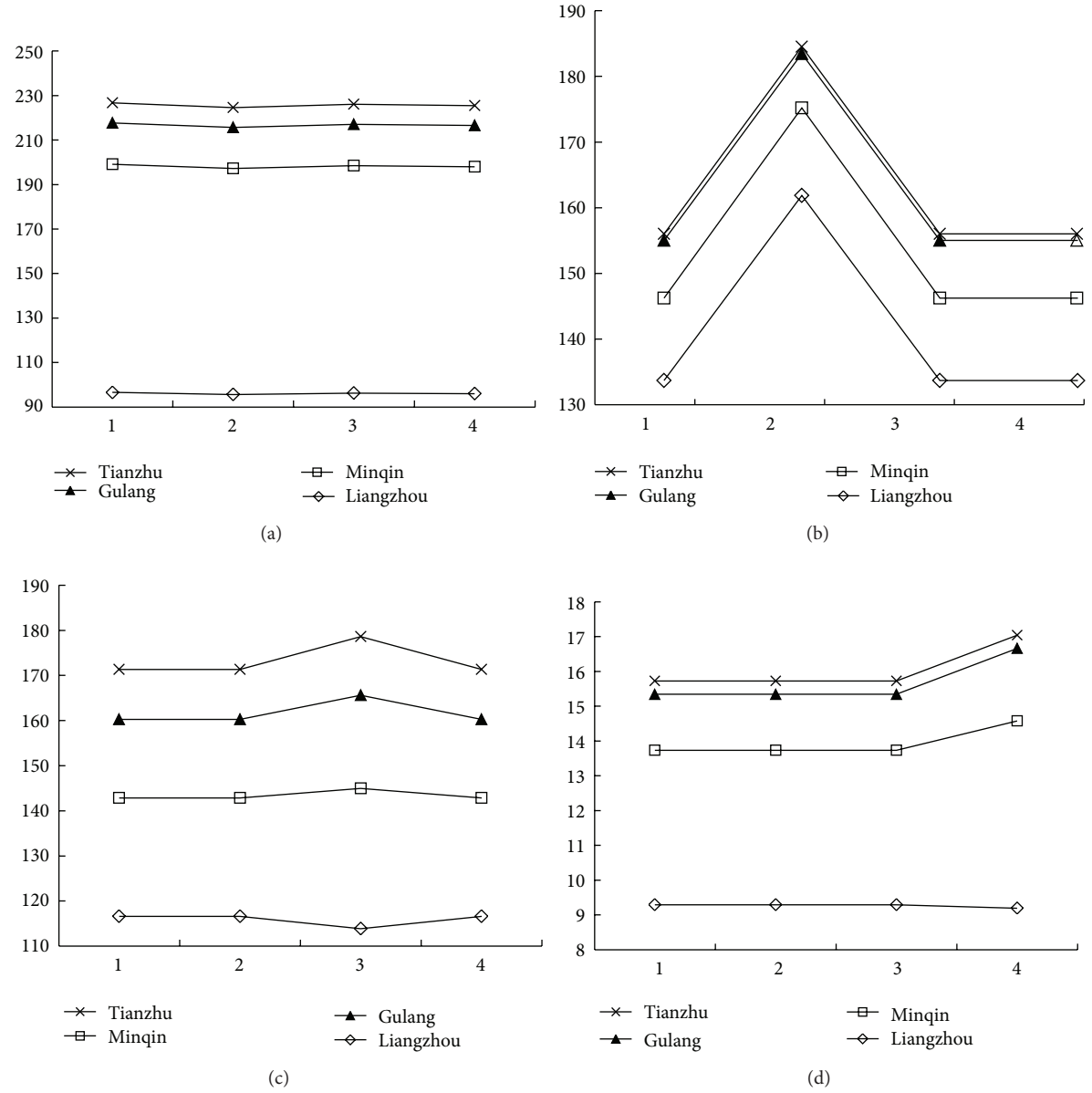

Figure 2: Different benefits (10^9 Yuan) accumulated diagrams under different scenarios. (a) Irrigation benefits accumulated diagram under different scenarios. (b) Industry benefits accumulated diagram under different scenarios. (c) Domesticity benefits accumulated diagram under different scenarios. (d) Ecology benefits accumulated diagram under different scenarios.

(lower level)

$$\max f_i = \sum_{j=1}^{4} d_{ij} \cdot x_{ij} \tag{26}$$

subject to

(1) total amount not more than available water supply

$$\sum_{i=1}^{4} \sum_{j=1}^{4} x_{ij} \le T, \tag{27}$$

(2) not less than minimum water supply

$$x_{ij} \ge x_{\min ij}, \tag{28}$$

(3) not more than maximum water supply

$$x_{ij} \le x_{\max ij}, \tag{29}$$

(4) regional coordination development

$$\mu \ge \mu^*, \tag{30}$$

(5) nonnegative constraints

$$x_{ij} \ge 0, \tag{31}$$

Table 3: Results of the regional water resources allocation.

Areas	Allocated water (10^6 m^3)				
	Irrigation	Industry	Domesticity	Ecology	Total
Scenario 1 irrigation priority					
Liangzhou	877.709	70.360	63.034	84.486	1095.589
Minqin	492.959	3.584	14.565	29.584	540.692
Gulang	143.280	3.144	9.685	12.384	168.493
Tianzhu	89.940	6.654	10.035	2.957	109.586
Scenario 2 industry priority					
Liangzhou	868.851	85.200	63.034	84.486	1101.572
Minqin	488.531	3.804	14.565	29.584	536.484
Gulang	141.951	2.943	9.685	12.384	166.963
Tianzhu	89.054	7.295	10.035	2.957	109.342
Scenario 3 domesticity priority					
Liangzhou	874.984	70.360	61.543	84.486	1091.373
Minqin	491.597	3.584	17.291	29.584	542.055
Gulang	142.871	3.144	11.453	12.384	169.851
Tianzhu	89.667	6.654	11.803	2.957	111.081
Scenario 4 ecology priority					
Liangzhou	872.559	70.360	63.034	83.576	1089.529
Minqin	490.384	3.584	14.565	35.903	544.437
Gulang	142.507	3.144	9.685	16.032	171.369
Tianzhu	89.425	6.654	10.035	2.911	109.026

where

x_{ij} are decision variables, water allocated to each users, 10^6 are cube meters (10^6 m^3),

F are benefits of upper level programming, Yuan,

f_i are profits of lower level programming, Yuan,

C_i are values per 1000 cube meters, Yuan per 1000 cube meters,

d_{ij} is water price per cube meter, Yuan/m^3,

T is total amount of available water supplement,

$x_{\min ij}$ is minimum water demand of each area, 10^6 m^3,

$x_{\max ij}$ is maximum water demand of each area, 10^6 m^3,

μ is regional coordination value, dimensionless.

According to the procedure above, four scenarios are set, and the satisfactory solutions are shown in Table 3. In scenario 1, the decision makers emphasise on irrigation benefits, and in scenario 2 to scenario 4, DMs emphasise on the industry benefits, domesticity benefits, and ecology benefits, respectively.

4. Results Analysis

The detailed satisfactory solutions in Table 3 are parts of the optimal solutions of the BLMOLP model for water resources allocation. Because the different tolerance limit had a corresponding solution for the model, multioptimal solutions will emerge. However, the deviation of each result is tiny. The progress of the solution suggests that fuzzy goal programming is a user friendly method. For a specific target, there is a little alteration in the objective goal.

Irrigation water allocated is about 84% of the total amount of water on average and is nearly the same as the figure of the former 5 years. In scenario 1, irrigation water allocated is about 5×10^6 m^3 more than the other three scenarios on average. While DMs give priorities to the industry users (scenario 2), the water allocated for industry is over 16×10^6 m^3 more than the other three scenarios on average. The probable reason for this is that the coefficient of industry water use is higher than the coefficient of irrigation water use. In other words, even if the DMs prefer the irrigation users, the water allocated to the department would not increase too much. In this regard, in the Minqin area, the coefficient of ecology is higher than the other areas, so in scenario 4 the water allocated increases a lot. However, in scenario 4, the other areas' water allocation decreases a bit. It is because the model needs to balance the net water allocation. We also notice that in scenario 2 Liangzhou gets the highest water allocation, and the result is coherent to actual circumstances. Liangzhou is the main area of industry output, so a slight change would influence the result, especially, when DMs emphasise on industry. Figure 2 shows the benefit variousness under different scenarios for different users. For irrigation users, the benefits keep a constant level in the limited increase due to

the upper level objects' constrains. And the variousness of the industry users' benefits reflects the adaptability of the lower-level decision makers to the upper level decision changes. According to Figure 2, although the upper level decision makers emphasise on domesticity and ecology water users, there are a slight decrease in Liangzhou. This also inflects the upper level constrains to the lower level objects, because the total benefits reflect an upward trend. However, the results also indicate the subjectivity of the bilevel programming. When the upper level decision maker cannot choose the specific benefits he/she cared for, the result of the programming is confusing for the lower level decision makers. Another disadvantage of fuzzy goal programming is that the determination of numerical weights is difficult. Based on the fuzzy membership functions, there is not too much complicated calculation. Anyway, fuzzy goal programming is flexible for bilevel programming.

5. Conclusions

A bilevel multiobjective linear programming (BLMOLP) model is discussed in this paper and applied to Wuwei Basin in Shiyang River, Gansu Province, China. Water resources allocation involved several decision makers including the leaders and the subordinates. Using the fuzzy goal programming to solve the problem, by setting the tolerance value, the result could be calculated easily. Fuzzy goal programming approach is developed to minimize the group regret of degree of satisfactions of all DMs. In this research, the deviational variables of the defined membership functions are minimized to achieve the highest degree. The result of the BLMOLP model can be used for the water allocation in the Wuwei area; meanwhile, the model also can be generalized to a broader area. However, the formulation is a typical linear programming in this research. In practical situations, the water resources system may be nonlinear, and the relationship between the water users or the decision makers is more complicated. Therefore, nonlinear programming will be studied in the future, and the fuzzy goal approach also can be used. As well, a bilevel multiobjective nonlinear programming (BLMONLP) model can be studied for the water resources system, even for the energy system, waste disposal problem.

Acknowledgments

This research was supported by the National Natural Science Foundation of China (nos. 71071154 and 91125017), National High Technology Research and Development Program of China (863 Program) (no. 2011AA100502), the Government Public Research Funds for Projects of Ministry of Agriculture (no. 201203077), and the Ministry of Water Resources (nos. 201001060 and 201001061).

References

[1] D. Prinz and A. K. Singh, "Water resources in arid regions and their sustainable management," *Annals of Arid Zone*, vol. 39, no. 3, pp. 251–271, 2000.

[2] D. P. Loucks, E. van Beek, J. R. Stedinger et al., *Water Resources Systems Planning and Management: An Introduction to Methods, Models and Applications*, UNESCO, Paris, France, 2005.

[3] A. K. Biswas, "Integrated water resources management: a reassessment," *Water International*, vol. 29, no. 2, pp. 248–256, 2004.

[4] W. O. Maddaus and J. M. McGill, "Development and application of a water resource allocation model.," *Water Resources Research*, vol. 12, no. 4, pp. 767–774, 1976.

[5] R. P. Lejano and C. A. Davos, "Cost allocation of multiagency water resource projects: game theoretic approaches and case study," *Water Resources Research*, vol. 31, no. 5, pp. 1387–1393, 1995.

[6] E. F. Y. Gakpo, L. A. D. Plessis, and M. F. Viljoen, "Towards institutional arrangements to ensure optimal allocation and security of South Africa's water resources," *Agrekon*, vol. 40, no. 1, pp. 87–103, 2001.

[7] H. Lévite, H. Sally, and J. Cour, "Testing water demand management scenarios in a water-stressed basin in South Africa: application of the WEAP model," *Physics and Chemistry of the Earth*, vol. 28, no. 20-27, pp. 779–786, 2003.

[8] I. Fischhendler, "Institutional conditions for IWRM: the Israeli case," *Ground Water*, vol. 46, no. 1, pp. 91–102, 2008.

[9] G. N. Paudyal and H. B. Manguerra, "Two-step dynamic programming approach for optimal irrigation water allocation," *Water Resources Management*, vol. 4, no. 3, pp. 187–204, 1990.

[10] R. Wardlaw and K. Bhaktikul, "Application of a genetic algorithm for water allocation in an irrigation system," *Irrigation and Drainage*, vol. 50, no. 2, pp. 159–170, 2001.

[11] L. Z. Wang, L. Fang, and K. W. Hipel, "Water resources allocation: a cooperative game theoretic approach," *Journal of Environmental Informatics*, vol. 2, no. 2, pp. 11–22, 2003.

[12] F. Messner, O. Zwirner, and M. Karkuschke, "Participation in multi-criteria decision support for the resolution of a water allocation problem in the Spree River basin," *Land Use Policy*, vol. 23, no. 1, pp. 63–75, 2006.

[13] Y. P. Li, G. H. Huang, Y. F. Huang, and H. D. Zhou, "A multistage fuzzy-stochastic programming model for supporting sustainable water-resources allocation and management," *Environmental Modelling and Software*, vol. 24, no. 7, pp. 786–797, 2009.

[14] M. Sadegh, N. Mahjouri, and R. Kerachian, "Optimal inter-basin water allocation using crisp and fuzzy Shapley games," *Water Resources Management*, vol. 24, no. 10, pp. 2291–2310, 2010.

[15] M. Sadegh and R. Kerachian, "Water resources allocation using solution concepts of fuzzy cooperative games: fuzzy least core and fuzzy weak least core," *Water Resources Management*, vol. 25, no. 10, pp. 2543–2573, 2011.

[16] L. G. Shao, X. S. Qin, and Y. Xu, "A conditional value-at-risk based inexact water allocation model," *Water Resources Management*, vol. 25, no. 9, pp. 2125–2145, 2011.

[17] L. Jin, G. H. Huang, Y. R. Fan et al., "A hybrid dynamic dual interval programming for irrigation water allocation under uncertainty," *Water Resources Management*, vol. 26, no. 5, pp. 1183–1200, 2012.

[18] E. Xevi and S. Khan, "A multi-objective optimisation approach to water management," *Journal of Environmental Management*, vol. 77, no. 4, pp. 269–277, 2005.

[19] A. P. Singh, S. K. Ghosh, and P. Sharma, "Water quality management of a stretch of river Yamuna: an interactive fuzzy multiobjective approach," *Water Resources Management*, vol. 21, no. 2, pp. 515–532, 2007.

[20] A. A. Fasakhodi, S. H. Nouri, and M. Amini, "Water resources sustainability and optimal cropping pattern in farming systems; a multi-objective fractional goal programming approach," *Water Resources Management*, vol. 24, no. 15, pp. 4639–4657, 2010.

[21] W. Candler and R. D. Norton, "Multi-level programming," World Bank, 1977.

[22] H. S. Shih, Y. J. Lai, and E. S. Lee, "Fuzzy approach for multi-level programming problems," *Computers & Operations Research*, vol. 23, no. 1, pp. 73–91, 1996.

[23] K. B. Aviso, R. R. Tan, A. B. Culaba, and J. B. Cruz, "Bi-level fuzzy optimization approach for water exchange in eco-industrial parks," *Process Safety and Environmental Protection*, vol. 88, no. 1, pp. 31–40, 2010.

[24] A. N. Sadigh, M. Mozafari, and B. Karimi, "Manufacturer-retailer supply chain coordination: a bi-level programming approach," *Advances in Engineering Software*, vol. 45, no. 1, pp. 144–152, 2012.

[25] J. Wonga, C. Su, and C. Wang, "Stochastic dynamic lot-sizing problem using bi-level programming base on artificial intelligence techniques," *Applied Mathematical Modelling*, vol. 36, no. 5, pp. 2003–2016, 2012.

[26] Y. Lv, G. H. Huang, Y. P. Li, Z. F. Yang, Y. Liu, and G. H. Cheng, "Planning regional water resources system using an interval fuzzy bi-level programming method," *Journal of Environmental Informatics*, vol. 16, no. 2, pp. 43–56, 2010.

[27] B. Colson, P. Marcotte, and G. Savard, "Bilevel programming: a survey," *4OR*, vol. 3, no. 2, pp. 87–107, 2005.

[28] W. Candler and R. Townsley, "A linear two-level programming problem," *Computers & Operations Research*, vol. 9, no. 1, pp. 59–76, 1982.

[29] C. Shi, J. Lu, and G. Zhang, "An extended Kth-best approach for linear bilevel programming," *Applied Mathematics and Computation*, vol. 164, no. 3, pp. 843–855, 2005.

[30] W. F. Bialas and M. H. Karwan, "Two-level linear programming," *Management Science*, vol. 30, no. 8, pp. 1004–1020, 1984.

[31] J. F. Bard and J. T. Moore, "A branch and bound algorithm for the bilevel programming problem," *Siam Journal on Scientific and Statistical Computing*, vol. 11, no. 2, pp. 281–292, 1990.

[32] A. Charnes and W. W. Cooper, "Management models and industrial applications of linear programming," *Management Science*, vol. 4, no. 1, pp. 38–91, 1957.

[33] B. Moitra and B. Pal, "A fuzzy goal programming approach for solving bilevel programming problems," *Advances in Soft Computing-Afss*, vol. 2275, pp. 415–421, 2002.

[34] B. B. Pal and B. N. Moitra, "A fuzzy goal programming procedure for solving quadratic bilevel programming problems," *International Journal of Intelligent Systems*, vol. 18, no. 5, pp. 529–540, 2003.

[35] S. Pramanik and T. K. Roy, "Fuzzy goal programming approach to multilevel programming problems," *European Journal of Operational Research*, vol. 176, no. 2, pp. 1151–1166, 2007.

[36] S. R. Arora and R. Gupta, "Interactive fuzzy goal programming approach for bilevel programming problem," *European Journal of Operational Research*, vol. 194, no. 2, pp. 368–376, 2009.

[37] I. A. Baky, "Solving multi-level multi-objective linear programming problems through fuzzy goal programming approach," *Applied Mathematical Modelling*, vol. 34, no. 9, pp. 2377–2387, 2010.

[38] R. H. Mohamed, "The relationship between goal programming and fuzzy programming," *Fuzzy Sets and Systems*, vol. 89, no. 2, pp. 215–222, 1997.

[39] F. You, Y. Li, and S. C. Dong, "Environmental sustainability and scenarios of urbanization in arid area: a case study in Wuwei City of Gansu Province," *Chinese Geographical Science*, vol. 15, no. 2, pp. 120–130, 2005.

[40] J. Ma, Z. Ding, G. Wei, H. Zhao, and T. Huang, "Sources of water pollution and evolution of water quality in the Wuwei basin of Shiyang river, Northwest China," *Journal of Environmental Management*, vol. 90, no. 2, pp. 1168–1177, 2009.

Hindawi Publishing Corporation
Mathematical Problems in Engineering
Volume 2013, Article ID 647569, 10 pages
http://dx.doi.org/10.1155/2013/647569

Research Article

Applying an Extended Fuzzy Parametric Approach to the Problem of Water Allocations

T. Y. Xu[1] and X. S. Qin[1,2]

[1] *School of Civil & Environmental Engineering, Nanyang Technological University, Blk N1-01c-82, 50 Nanyang Avenue, Singapore 639798*
[2] *Earth Observatory of Singapore (EOS), Nanyang Technological University, Singapore 639798*

Correspondence should be addressed to X. S. Qin; xsqin@ntu.edu.sg

Received 22 November 2012; Accepted 22 January 2013

Academic Editor: Songlin Nie

An extended fuzzy parametric programming (EFPP) model was proposed for supporting water resources allocation problems under uncertainty. EFPP deals with flexible constraints (i.e., fuzzy relationships) by allowing violation of constraints at certain satisfaction degrees (i.e., α levels) and employs fuzzy ranking method to handle trapezoidal-shaped fuzzy coefficients. The objective function is defuzzified by using β cuts and weighting factors. The applicability of EFPP was demonstrated by a numerical example and a water resources allocation case. A series of decision alternatives at various satisfaction degrees were obtained. Generally, the higher the α level, the lower the system benefit. In comparison, the β level in the objective function posed less sensitive impacts on both objective function and model solutions. The reliability of EFPP was tested by comparing its solutions with those from fuzzy chance constrained programming (FCCP). The results indicated that EFPP performed equally well with FCCP in addressing parameter uncertainties, but it demonstrated a wider applicability due to its extended capacity of handling fuzzy relationships in the model constraints.

1. Introduction

Water resources allocation is an important task for distributing water resources to various users for ensuring healthy socioeconomic development and ecoenvironmental protection. The task is especially critical for areas that are currently suffering from water scarcity problems and facing even greater challenges under future climate change. The conflict among different water users is hardly avoidable, but application of management models, that fully consider the uneven spatial and temporal distributions of water resources, the interactions between water supply and demand, and the regulatory requirement of local authorities, will surely benefit the related allocation and planning processes. In recent years, it has been recognized that the intrinsic uncertainties linking with many system components in water resources allocation could also affect the effectiveness of management strategies that are normally made based on deterministic conditions. These uncertainties could be related to water availability (e.g., fluctuating hydrological condition), water demand (e.g., growing population and changing weather), transportation/storage loss, water prices, and even human judgment (e.g., regulatory policies).

The previous research efforts relied heavily on stochastic, fuzzy and interval techniques in tackling uncertainties [1–6]. Among various alternatives, fuzzy mathematical programming (FMP) was found effective in dealing with uncertainties caused by measurement errors, implicit knowledge, and ambiguous human judgment. The definition of the fuzzy parameters in FMP has less strict data requirement than that of stochastic ones, and the fuzzy parameters contain richer distribution information than interval numbers [7, 8]. For decades, many types of FMP models were proposed for solving water resources management problems [9–11]. Depending on the way of handling uncertainties, FMP can be categorized into fuzzy flexible (e.g., fuzzy parametric programming) (FF) [12–14], fuzzy possibilistic (FP) (e.g., fuzzy chance constrained programming) [15–17], and fuzzy

robust (FR) [18, 19] programming models. Maqsood et al. [20] incorporated fuzzy flexible programming into a two-stage stochastic optimization framework, which embedded risk information into the constraints and objective function. Nie et al. [21] advanced a water management model based on fuzzy robust programming approach for water quality problem, where the model could reflect a compromise between system stability and optimality. Xu and Qin [5] proposed a double-sided fuzzy chance-constrained model and applied it to an agricultural water quality management problem. The proposed model could tackle uncertainties expressed as possibilistic distributions in the constraints and allow system violations at predetermined confidence levels.

The above-mentioned fuzzy approaches have specific scopes of applicability, in the sense of handling (i) fuzziness in objective function and/or constraints and (ii) fuzziness of relationship and/or model parameters. FF programming allows flexibility and elasticity to be reflected in the objective function and constraints but is relatively weak in dealing with ambiguous coefficients [8, 22]. FP programming tackles fuzzy coefficients in objective function and/or constraints, but is less capable of dealing with fuzzy relationships [8, 22]. FR programming is designed for handling highly uncertain variables (i.e., dual uncertainties) which are expressed as fuzzy boundary intervals [19, 21]; it is generally not suitable to be used for reflecting vague relationships or objective functions [5]. In water resources allocation problems, uncertainty could exist in many system components and their relationships. To benefit general-purpose applications, it is desired that a sophisticated model that could handle all possible fuzzy conditions mentioned above will be available.

Herrera and Verdegay [23] gave a general introduction of three models of fuzzy parametric linear programming. These models have shown advantages in dealing with fuzzy-relation-based constraints, fuzzy coefficients in system objective, and fuzzy parameters in model constraints. Although the different types of fuzziness were treated individually, the parametric models did show a potential to be coupled together for handling more complicated cases. This further topic was not discussed in the previous studies, and the applicability of such a method in engineering problems has yet to be explored. In addition, the models were developed for triangular-shaped fuzzy sets and were incapable of reflecting more general cases. Thus, an extended fuzzy parametric programming (EFPP) method, which is based on the models proposed by Herrera and Verdegay [23], will be developed in this study. A numerical example and a water resources allocation problem will be used for demonstration.

2. Methodology

2.1. Extended Fuzzy Parametric Programming. A fuzzy linear programming (FLP) problem in consideration of fuzziness under a general condition can be written as follows [24]:

$$\text{Max } z = \sum_{j=1}^{J} \widetilde{c}_j x_j \tag{1a}$$

subject to

$$\sum_{j=1}^{J} \widetilde{a}_{ij} x_j \lesssim \widetilde{b}_i, \quad \forall i, \tag{1b}$$

$$\sum_{j=1}^{J} d_{jk} x_j \le e_k, \quad \forall k, \tag{1c}$$

$$x_j \ge 0, \quad \forall j, \tag{1d}$$

where $\widetilde{c}_j$, $\widetilde{a}_{ij}$, and $\widetilde{b}_i$ are fuzzy coefficients (or parameters); x_j is deterministic decision variable, d_{jk} and e_k are deterministic coefficients; j is the index of decision variable; J is the number of decision variables; i is the index of fuzzy constraint; k is the index of deterministic constraint; the symbols $\lesssim$ denote fuzzy inequality. The fuzzy coefficients for trapezoidal fuzzy sets could be expressed as $\widetilde{c}_j = (c_j^1, c_j^2, c_j^3, c_j^4)$, $\widetilde{a}_{ij} = (a_{ij}^1, a_{ij}^2, a_{ij}^3, a_{ij}^4)$, and $\widetilde{b}_i = (b_i^1, b_i^2, b_i^3, b_i^4)$, respectively. In this study, we consider the trapezoidal shape a relatively general shape of a fuzzy membership function. It could address the minimum, maximum, and most possible range of an uncertain variable. The triangular-shaped fuzzy membership function is a special case of trapezoidal ones when the most possible range converges to a single point.

Assume the flexibility of the constraints could be represented by fuzzy sets. When the constraints are fully satisfied, the membership degree of the constraints would be 1, when the constraints are totally violated, the membership degree of the constraints would be 0. Let a fuzzy number $\widetilde{\theta}_i$ represent the allowable maximum violation of the constraints, that is, to be determined by decision makers. The membership degree of constraints $\mu_i(x)$ would linearly decrease over the interval $(\widetilde{b}_i, \widetilde{b}_i + \widetilde{\theta}_i)$, and could be expressed as follows [23]:

$$\mu_i(x) = \begin{cases} 1, & \text{if } \sum \widetilde{a}_{ij} x_j \lesssim \widetilde{b}_i, \\ \dfrac{\left[\left(\widetilde{b}_i + \widetilde{\theta}_i\right) - \sum \widetilde{a}_{ij} x_j\right]}{\widetilde{\theta}_i}, & \text{if } \widetilde{b}_i \lesssim \sum \widetilde{a}_{ij} x_j \lesssim \widetilde{b}_i + \widetilde{\theta}_i, \\ 0, & \text{if } \sum \widetilde{a}_{ij} x_j \gtrsim \widetilde{b}_i + \widetilde{\theta}_i, \end{cases} \tag{2}$$

where the fuzziness could exist in both the fulfillment of the constraints and the coefficients in constraints. For simplicity, $\sum_{j=1}^{J}(\cdot)$ is represented by $\sum(\cdot)$. To deal with fuzzy relationship, the fuzzy ranking method (FRM), studied by many researchers [25–28], will be employed. FRM has the following definitions [23]:

$$\text{FR}\left(\widetilde{A}\right) \ge \text{FR}\left(\widetilde{B}\right) \Longrightarrow \widetilde{A} \gtrsim \widetilde{B}, \tag{3a}$$

$$\text{FR}\left(\widetilde{A} + \widetilde{B}\right) = \text{FR}\left(\widetilde{A}\right) + \text{FR}\left(\widetilde{B}\right), \tag{3b}$$

$$\text{FR}\left(r\widetilde{A}\right) = r \cdot \text{FR}\left(\widetilde{A}\right), \tag{3c}$$

where FR$(\cdot)$ is defined as a fuzzy ranking function; $\widetilde{A}$ and $\widetilde{B}$ are fuzzy numbers; r is a deterministic coefficient. Examples of fuzzy ranking functions include Chang's index [25] and

Yager's first, second, and third indexes [26, 27]. In this study, we use Yager's first index to deal with fuzzy coefficients. Therefore, $\mu_i(x)$ in (2) can be transformed to [29]:

$$\mu_i(x) = \frac{\left[\left(\tilde{b}_i + \tilde{\theta}_i\right) - \sum \tilde{a}_{ij}x_j\right]}{\tilde{\theta}_i} \Longrightarrow \mu_i(x) = \frac{\mathrm{FR}\left[\left(\tilde{b}_i + \tilde{\theta}_i\right) - \sum \tilde{a}_{ij}x_j\right]}{\mathrm{FR}\left(\tilde{\theta}_i\right)}. \tag{4}$$

To handle fuzzy parameters, a satisfaction degree (i.e., α) is introduced. If the decision makers prefer a confidence level of constraint satisfaction to be α, the membership degree of the constraints $\mu_i(x)$ should be higher than α, where $\alpha \in [0, 1]$. Then the constraint (1b) could be further transformed to the following [29]:

$$\begin{aligned} &\frac{\mathrm{FR}\left(\tilde{b}_i + \tilde{\theta}_i - \sum \tilde{a}_{ij}x_j\right)}{\mathrm{FR}\left(\tilde{\theta}_i\right)} \\ &\geq \alpha \Longrightarrow \left[\frac{\mathrm{FR}\left(\tilde{b}_i\right) + \mathrm{FR}\left(\tilde{\theta}_i\right) - \mathrm{FR}\left(\sum \tilde{a}_{ij}x_j\right)}{\mathrm{FR}\left(\tilde{\theta}_i\right)}\right] \\ &\geq \alpha \Longrightarrow \mathrm{FR}\left(\sum \tilde{a}_{ij}x_j\right) \leq \mathrm{FR}\left(\tilde{b}_i\right) + (1-\alpha)\cdot \mathrm{FR}\left(\tilde{\theta}_i\right). \end{aligned} \tag{5}$$

Consider the fuzziness in the objective function, the membership degree of the objective function $\mu(z)$ could be expressed in the following trapezoidal form:

$$\mu(z) = \begin{cases} 0, & \text{if } z \leq c_j^1 x_j,\ z \geq c_j^4 x_j, \\ \dfrac{z - c_j^1 x_j}{c_j^2 x_j - c_j^1 x_j}, & \text{if } c_j^1 x_j \leq z \leq c_j^2 x_j, \\ 1, & \text{if } c_j^2 x_j \leq z \leq c_j^3 x_j, \\ \dfrac{c_j^4 x_j - z}{c_j^4 x_j - c_j^3 x_j}, & \text{if } c_j^3 x_j \leq z \leq c_j^4 x_j. \end{cases} \tag{6}$$

Equation (6) can be converted into crisp sets using β-cut, where the range under β-cut represents the aspiration range of the objective function values that the decision makers would accept. The membership degree $\mu(z)$ should be higher than β, then we can obtain the following relationship:

$$\mu(z) \geq \beta \Longrightarrow L(\beta) \leq \sum c_j x_j \leq U(\beta), \tag{7}$$

where $L(\beta) = (1-\beta)\sum c_j^1 x_j + \beta \sum c_j^2 x_j$, and $U(\beta) = \beta \sum c_j^3 x_j + (1-\beta)\sum c_j^4 x_j$.

Then, it turns into a problem with interval-type objective function, which can be written as [23, 30]:

$$\mathrm{Max}\left\{z \mid z \in \left[L(\beta), U(\beta)\right], \beta \in [0,1]\right\}. \tag{8}$$

A simple way to handle the interval objective function is to assign a weight vector ε to both $L(\beta)$ and $U(\beta)$. In this study, we assume an equal importance of $L(\beta)$ and $U(\beta)$ and use their average as the following objective function:

$$\mathrm{Max}\, z = \frac{1}{2}\left[L(\beta) + U(\beta)\right]. \tag{9}$$

Then, the fuzzy parametric model can be written as follows:

$$\mathrm{Max}\, z = \frac{1}{2}\left[(1-\beta)\cdot\left(\sum_{j=1}^{J} c_j^1 x_j + \sum_{j=1}^{J} c_j^4 x_j\right) + \beta\cdot\left(\sum_{j=1}^{J} c_j^2 x_j + \sum_{j=1}^{J} c_j^3 x_j\right)\right], \tag{10a}$$

subject to

$$\mathrm{FR}\left(\sum_{j=1}^{J} \tilde{a}_{ij}x_j\right) \leq \mathrm{FR}\left(\tilde{b}_i\right) + (1-\alpha)\cdot \mathrm{FR}\left(\tilde{\theta}_i\right), \quad \forall i, \tag{10b}$$

$$\sum_{j=1}^{J} d_{jk}x_j \leq e_k, \quad \forall k, \tag{10c}$$

$$x_j \geq 0, \quad \alpha, \beta \in [0,1], \tag{10d}$$

where α reflects the satisfaction degree of constraints. The selection of α depends on the preference of decision makers. The higher the values of α, the higher the satisfaction degree of constraints. If decision makers are willing to make a conservative plan, higher values of α should be selected; conversely, if they prefer a higher objective function value (normally this may lead to higher risk of system violation), lower values of α should be chosen. The parameter β represents the level of the aspiration range of objective function. The higher the level of β, the narrower the range of $[L(\beta), U(\beta)]$. To examine the influence of β on the objective function, we could assume that β has an increment of $\Delta\beta$. Then, the objective function becomes as follows:

$$\begin{aligned} \mathrm{Max}\, z' = {} & \frac{1}{2}(\beta + \Delta\beta) \\ & \cdot\left[\left(\sum c_j^2 x_j + \sum c_j^3 x_j\right) - \left(\sum c_j^1 x_j + \sum c_j^4 x_j\right)\right] \\ & + \frac{1}{2}\left(\sum c_j^1 x_j + \sum c_j^4 x_j\right). \end{aligned} \tag{11}$$

The equation shows that the influence of β on the objective function value relies heavily on the distribution of the fuzzy coefficients. The trend is generally linear provided that the decision variables do not have significant variations.

Figure 1 shows the EFPP's general framework. The steps of using EFPP are as follows: (i) identify fuzzy uncertain parameters and obtain the fuzzy membership function of each variable; (ii) determine the maximum violation of constraints that the decision maker would accept; (iii) establish the aspiration level to the objective function and assign a weight vector to objective function (or use average); (iv) establish

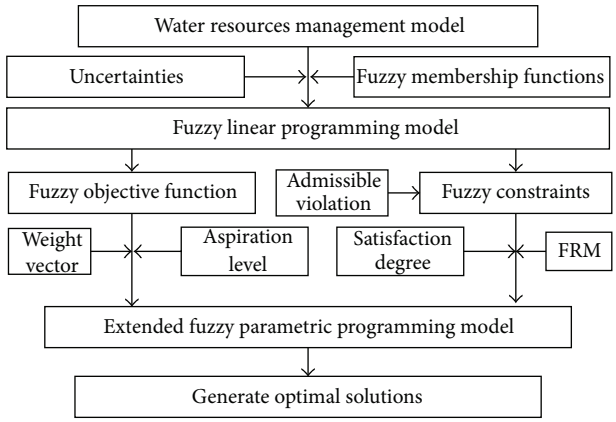

Figure 1: General framework of EFPP.

the satisfaction degree to the constraints and transform constraints using FRM; (v) formulate the fuzzy parametric linear programming model and generate the final optimal solutions.

2.2. Numerical Example. Consider the following numerical problem:

$$\text{Max } f = \tilde{c}_1 x_1 + \tilde{c}_2 x_2 \tag{12a}$$

subjective to

$$\tilde{a}_{11} x_1 - \tilde{a}_{12} x_2 \gtrsim \tilde{b}_1, \tag{12b}$$

$$\tilde{a}_{21} x_1 + \tilde{a}_{22} x_2 \lesssim \tilde{b}_2, \tag{12c}$$

$$x_j \geq 0, \tag{12d}$$

where $c_1 = (1, 2, 3, 11)$, $c_2 = (3, 7, 8, 9)$, $a_{11} = (1, 2, 2.5, 3)$, $a_{12} = (1, 2.5, 3.5, 4)$, $b_1 = (2, 3, 5, 6)$, $a_{21} = (1.5, 3.5, 4, 6)$, $a_{22} = (3, 4, 6, 7.5)$, $b_2 = (29, 35, 36, 40)$.

According to (7),

$$\begin{aligned} l_1(\beta) &= 1 + \beta, & u_1(\beta) &= 11 - 8\beta, \\ l_2(\beta) &= 3 + 4\beta, & u_2(\beta) &= 9 - \beta. \end{aligned} \tag{13}$$

The objective function could be written as follows:

$$\text{Max } f = \left[(1+\beta) x_1 + (3+4\beta) x_2, (11-8\beta) x_1 + (9-\beta) x_2\right]. \tag{14}$$

Assume that $\tilde{\theta}_1 = (1, 1.5, 3, 4.5)$ and $\tilde{\theta}_2 = (3, 5, 5.5, 7)$ are the admissible violations, and a linear ranking function based on the first index of Yager [27] is used. Then the fuzzy parametric model can be written as follows:

$$\text{Max } f = \frac{1}{2}\left[(12 - 7\beta) x_1 + (12 + 3\beta) x_2\right] \tag{15a}$$

subject to

$$2.125 x_1 - 2.75 x_2 \geq 4 - 2.5(1 - \alpha), \tag{15b}$$

$$3.75 x_1 + 5.125 x_2 \leq 35 + 5.125(1 - \alpha), \tag{15c}$$

$$x_j \geq 0, \tag{15d}$$

$$\alpha, \beta \in [0, 1], \tag{15e}$$

where α and β are the satisfaction degree of the constraints and the aspiration level of the objective function, respectively. At a β level of 0.9, the results of (f, x_1, x_2) obtained from EFPP under α levels of 0.9, 0.6, and 0.3 are (36.99, 5.51, 2.89), (39.15, 5.53, 3.18), and (41.31, 5.55, 3.47), respectively. At an α level of 0.9, the results of (f, x_1, x_2) at β levels of 0.9, 0.6, 0.3 are (36.99, 5.51, 2.89), (41.48, 5.51, 2.89), and (46.88, 9.47, 0.315), respectively. The results indicate that, as α and β levels decrease, the objective function values would both increase. The decision variables would not change until the β level drops below 0.3, which implies that, β may only show notable impact on the model solutions when its influence on the objective function reaches a certain threshold.

3. Application in Water Resources Allocation Problem

3.1. Case Background and Model Formulation. The same method will be used to a hypothetical water allocation problem [20, 31], where two reservoirs are serving as water sources for three users, including municipality, agriculture, and industry. A target water allocation amount to each consuming sector is assigned for each reservoir. Generally, an excessively high water target could lead to water shortage problems when the water availability is low; the corresponding penalties could also be high. Conversely, a too low target may cause waste of water resources during high-flow seasons. Therefore, an optimal water allocation scheme from reservoirs to water users is desired. Thus, the problem under consideration is how to allocate water from various water sources (i.e., reservoirs) to three competing users over three periods so that the overall system benefit can be maximized, while, at the same time, the restrictions of water availability and regulatory requirement should be met.

In such a water resources allocation system, the available water amount is influenced by many factors such as the annual and seasonal variation of rainfall, runoff, and evaporation, as well as groundwater interaction; the values of net benefit and the penalty rely on the market condition and human judgment; the water loss rate is affected by transferring condition (e.g., soil absorption) and infrastructure reliability. Problems of data procurement, survey methods, equipment failure, and human judgment could cause large errors about these parameters. In real-world applications, efforts should be made to ensure an accurate quantification of these uncertainties. In this study, we assume the uncertain parameters be expressed as trapezoidal-shaped fuzzy sets (listed in Tables 1 and 2).

Table 1: Parameters of water demand, reservoir capacity, and water loss rate.

	Time period		
	$t = 1$	$t = 2$	$t = 3$
Water demand ($\times 10^6$ m^3)			
Municipality	9.7	10	11
Agriculture	13	13.5	14.5
Industry	11.5	12	12.5
Capacity ($\times 10^6$ m^3)			
Reservoir 1	(5, 5.5, 6, 6.5)	(5.5, 6, 6.5, 7)	(4, 4.5, 5, 6)
Reservoir 2	(3.5, 4.5, 5, 5.5)	(4, 4.5, 5.5, 6)	(3, 3.5, 4, 5)
Loss rate	Municipality	Agriculture	Industry
Reservoir 1	(0.1, 0.15, 0.18, 0.2)	(0.2, 0.23, 0.25, 0.3)	(0.25, 0.3, 0.35, 0.4)
Reservoir 2	(0.05, 0.08, 0.1, 0.15)	(0.1, 0.15, 0.2, 0.25)	(0.15, 0.2, 0.25, 0.3)

Table 2: Parameters of unit net benefit and penalty.

	Time period		
	$t = 1$	$t = 2$	$t = 3$
Unit net benefit (\$/m^3)			
Reservoir 1			
Municipality	(8, 10, 11, 12)	(8.5, 11, 11.5, 12.5)	(10, 11, 12, 14)
Agriculture	(3, 4.2, 4.3, 5)	(3.5, 4.3, 4.5, 5.5)	(3.5, 4.7, 5, 6.5)
Industry	(6, 8, 8.3, 10)	(7, 8, 9, 10)	(7, 8.5, 9, 11)
Reservoir 2			
Municipality	(7, 9, 9.5, 11)	(8, 9.5, 10.5, 12)	(9, 10.5, 11, 13)
Agriculture	(2, 3.5, 3.7, 4)	(2, 3.5, 4, 4.5)	(3, 4, 4.5, 5)
Industry	(5, 7, 7.5, 9)	(6, 7.5, 8, 9.5)	(6, 8, 8.5, 10)
Unit penalty (\$/m^3)			
Municipality	(15.5, 16, 18, 20)	(16.5, 18, 20, 22)	(18, 20, 22, 24)
Agriculture	(5.5, 6, 7, 7.5)	(6, 6.5, 7, 7.5)	(6.5, 7, 7.5, 8)
Industry	(11.5, 13, 14, 15)	(12.5, 13, 15, 16.5)	(13.5, 15, 16, 18)

The model for this water allocation problem can then be formulated as follows:

$$\text{Maximize} f = \sum_{i=1}^{I}\sum_{j=1}^{J}\sum_{t=1}^{T} N\widetilde{B}_{ijt} \cdot TG_{ijt} - \sum_{i=1}^{I}\sum_{t=1}^{T}\sum_{j=1}^{J} C\widetilde{T}_{it} \cdot DL_{ijt} \tag{16a}$$

subject to

$$\sum_{j=1}^{J} TG_{ijt} = TTG_{it}, \quad \forall i, t, \tag{16b}$$

$$\sum_{i=1}^{I} \left(1 + \widetilde{\eta}_{ij}\right) \cdot \left(TG_{ijt} - DL_{ijt}\right) \lesssim I\widetilde{N}F_{jt}, \quad \forall j, t, \tag{16c}$$

$$\sum_{i=1}^{I}\sum_{j=1}^{J} \widetilde{\eta}_{ij} \cdot \left(TG_{ijt} - DL_{ijt}\right) \lesssim T\widetilde{W}L, \quad \forall t, \tag{16d}$$

$$DL_{ijt} \le TG_{ijt}, \quad \forall i, j, t, \tag{16e}$$

$$TG_{ijt} \ge 0, \quad DL_{ijt} \ge 0, \quad \forall i, j, t, \tag{16f}$$

where i = index of water users, and $i = 1, 2, \ldots, I$ ($I = 3$); j = index of reservoirs, and $j = 1, 2, \ldots, J$ ($J = 2$); t = index of periods, and $t = 1, 2, \ldots, T$, ($T = 3$); η_{ij} = water loss rate from reservoir j to user i; NB_{ijt} = unit net benefit of water delivered from reservoir j to user i at period t (\$/m^3); TG_{ijt} = water allocation target of reservoir j to user i at period t (10^6 m^3); CT_{it} = unit penalty of not satisfying the target of user i at period t (\$/m^3); DL_{ijt} = water amount failed to be delivered (i.e., deficit) from reservoir j to user i at period t (10^6 m^3); TTG_{it} = water allocation target for user i at period t (10^6 m^3); TWL = total allowable water loss (10^6 m^3); INF_{jt} = available water amount for reservoir j at period t (10^6 m^3).

The objective function (16a) is to obtain the maximum system benefit of allocating water from two reservoirs to three consumers. Constraint (16b) means that the total allocation target of reservoirs to each water user should be equal to the demand of each user; constraint (16c) denotes that the total allocated water from each reservoir should be smaller than its available capacity; constraint (16d) means that the total amount of water loss should be lower than the allowable water loss; constraint (16e) denotes that the shortage should

Table 3: Solutions from EFPP.

		$\alpha, \beta = 0.95$			$\alpha, \beta = 0.9$			$\alpha, \beta = 0.8$			$\alpha, \beta = 0.7$		
		$t = 1$	$t = 2$	$t = 3$	$t = 1$	$t = 2$	$t = 3$	$t = 1$	$t = 2$	$t = 3$	$t = 1$	$t = 2$	$t = 3$
Target from reservoirs to users ($\times 10^6$ m^3)													
M	R1	5.32	5.59	7.30	5.36	5.79	7.14	5.75	6.18	6.82	6.13	6.57	6.50
	R2	4.38	4.41	3.70	4.34	4.21	3.86	3.95	3.82	4.17	3.57	3.43	4.50
A	R1	8.91	9.10	11.1	8.77	8.95	10.9	8.47	8.65	10.6	8.17	8.35	10.3
	R2	4.09	4.40	3.45	4.23	4.55	3.60	4.53	4.85	3.89	4.83	5.15	4.19
I	R1	7.58	7.78	9.19	7.44	7.63	9.05	7.15	7.35	8.77	6.87	7.06	8.48
	R2	3.92	4.22	3.31	4.06	4.37	3.45	4.35	4.65	3.73	4.63	4.94	4.02
Water deficit for users ($\times 10^6$ m^3)													
M	R1	0.15	0	2.90	0	0	2.54	0	0	1.83	0	0	1.12
	R2	0	0	0	0	0	0	0	0	0	0	0	0
A	R1	4.12	3.89	6.96	3.79	3.57	6.63	3.13	2.91	5.97	2.47	2.25	5.31
	R2	0	0	0	0	0	0	0	0	0	0	0	0
I	R1	3.07	2.89	5.34	2.76	2.58	5.03	2.13	1.95	4.41	1.51	1.33	3.78
	R2	0	0	0	0	0	0	0	0	0	0	0	0

M: municipality; A: agriculture; I: industry; R1: reservoir 1; R2: reservoir 2.

not exceed a predefined target; constraint (16f) stipulates the nonnegativity of all decision variables. The fuzzy parameters are associated with unit benefits, unit penalties, water loss rates, allowable water losses, and available water amounts. The fuzzy relations in constraints (16c) and (16d) mean that the total allocation amounts and water loss amounts are not strictly restricted by the policy regulations and violations are allowable to a certain degree (i.e., satisfaction degree). Constraints (16c) and (16d) can be transformed to:

$$\sum_{i=1}^{I} \left(1 + \widetilde{\eta}_{ij}\right) \cdot \left(TG_{ijt} - DL_{ijt}\right) \lesssim I\widetilde{N}F_{jt} + (1-\alpha) \cdot \widetilde{\theta}_{jt}^{\inf} \tag{17a}$$

$$\sum_{i=1}^{I}\sum_{j=1}^{J} \widetilde{\eta}_{ij} \cdot \left(TG_{ijt} - DL_{ijt}\right) \lesssim T\widetilde{W}L + (1-\alpha) \cdot \widetilde{\theta}^{twl}, \tag{17b}$$

where $\widetilde{\theta}_{jt}^{\inf}$ and $\widetilde{\theta}^{twl}$ are the acceptable tolerances of water availability and total water loss amount, respectively. Constraint (17a) shows that if the total allocated water from reservoir is higher than its total water availability, the satisfaction degree would decrease. It would not be acceptable if the total allocated water amount exceeds the tolerance of water availability (i.e., $I\widetilde{N}F_{jt} + \widetilde{\theta}_{jt}^{\inf}$). Constraint (17b) shows a similar treatment for water losses.

3.2. Results. For simplicity of demonstration, we firstly assume the aspiration level of the objective function is identical to the satisfaction degree of constraints. The fuzzy parameters in constraints are dealt with by the first index of Yager [26, 27]. Table 3 lists the solution of the allocated target and shortage under various satisfaction degrees. For reservoir 1, the water target assigned to agriculture is the highest, followed by industry and municipality. For example, at period 1, under satisfaction degree of 0.9, the target amounts from reservoir 1 to municipality, agriculture, and industry are 5.36, 8.77, and 7.44 ($\times 10^6$ m^3), respectively. This is because the demand of agriculture is the highest and the available flow of reservoir 1 is higher than that of reservoir 2; consequently, more water would be allocated to satisfy the demand of agriculture from reservoir 1. Table 3 also shows that, as the satisfaction degree decreases, the target amount from reservoir 1 to municipality would increase. For example, at period 2, as the satisfaction decreases from 0.95 to 0.7, the target allocation amount from reservoir 1 to municipality would increase from 5.32 to 6.13 ($\times 10^6$ m^3). This is due to the fact that a lower satisfaction level corresponds to a higher violation degree; reservoir 1, which has a higher net benefit, would be preferred to supply more water.

The total shortages of municipality, agriculture, and industry over periods 1 to 3 under various satisfaction degrees have been plotted in Figure 2. The total shortage amount of municipality is the lowest and that of agriculture is the highest. It means that the target of municipality would be satisfied first, and that of agriculture would be of least priority. This is due to the highest net benefit the municipality could bring in and also the highest penalty if the target of municipality could not be satisfied. It also shows that as α level decreases, the shortage amount of the three users would decrease. For example, at period 3, under satisfaction degrees of 0.95, 0.9, 0.8, and 0.7, the total water shortage amount of agriculture are 6.96, 6.63, 5.97, and 5.31 ($\times 10^6$ m^3), respectively. This implies that, under a lower satisfaction degree (i.e., higher risk of constraint violation), the decision makers would be more optimistic about the water availability and prefer to allocate more water and avoid more shortage problem.

Figure 3 shows the total target and water allocation amount from reservoirs 1 and 2. It demonstrates that the total target amount from reservoir 2 is lower than that from reservoir 1; correspondingly, the total allocated amount would be

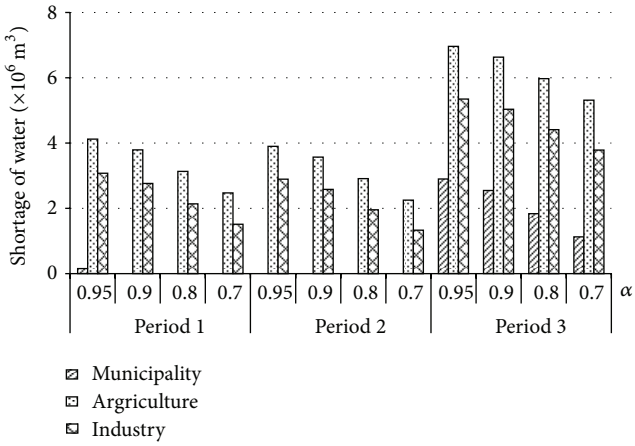

Figure 2: Water shortages of municipality, agriculture and industry.

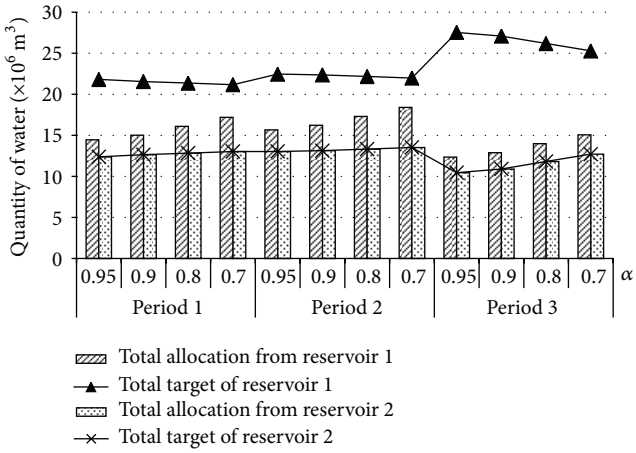

Figure 3: Total target and allocation amounts from reservoirs 1 and 2.

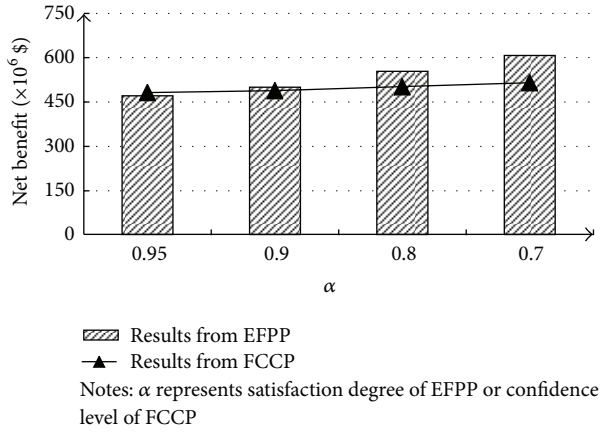

Figure 4: System benefits obtained from EFPP and FCCP.

lower. For example, at period 1, under satisfaction degree of 0.9, the total target from reservoirs 1 and 2 is 21.56 and 12.64 ($\times 10^6$ m^3), respectively, and the total allocation is 15.02 and 12.63 ($\times 10^6$ m^3), respectively. This is because reservoir 1 has higher net benefit and capacity. It also shows that, as α decreases, the total target from reservoir 1 would decrease and the total allocation amount from reservoir 1 would increase. For example, at period 2, as the satisfaction degree drops from 0.95 to 0.7, the total target of reservoir 1 would decrease from 22.5 to 22.0 ($\times 10^6$ m^3), and the allocation from reservoir 1 would increase from 15.7 to 18.4 ($\times 10^6$ m^3). This is because, as the satisfaction degree decreases, the allowable violation of the constraints (i.e., constraints of water available and loss) would increase, and the discrepancy between water target and allocation (i.e., shortage amount) would reduce; this could lead to a higher system benefit.

Figure 4 presents the net benefits of the system at various satisfaction degrees. A higher satisfaction degree has an obvious lower system benefit but a lower risk of system reliability, and vice versa. Generally, the results obtained through EFPP demonstrate that the approach is capable of (i) tackling uncertainties in water allocation problems as fuzzy sets; (ii) dealing with fuzzy parameters in both objective function and constraints; (iii) handling fuzzy relationship by allowing violation of the accomplishment of the constraints; (iv) helping decision makers understand the balance between system benefit and reliability.

3.3. Comparison with FCCP. To verify the reliability of the solutions from EFPP, the fuzzy chance constrained programming (FCCP) model, proposed by Liu and Iwamura [32], is applied to solve the same problem after a few modifications. As FCCP could only tackle fuzzy parameters, the treatment of fuzzy relationship is not considered. For simplicity, the fuzzy objective function has been converted to its deterministic version by averaging the upper and lower bounds of the fuzzy coefficients. The fuzzy parameters in the constraints are still expressed as trapezoidal-shaped fuzzy sets. We use confidence levels of 0.95, 0.9, 0.8, and 0.7 for the FCCP model; they are deemed equivalent to the satisfaction degrees used in EFPP. The objective-function values obtained from both FCCP and EFPP are shown in Figure 4, and decision variables are shown in Figure 5. At a high satisfaction degree or confidence level (i.e., 0.95), the system benefit obtained from EFPP is slightly lower than that from FCCP. As the satisfaction degree decreases, the system benefits from EFPP would outstrip the results at the same confidence level from FCCP. For example, under satisfaction degrees of 0.9, 0.8, and 0.7, the system benefits from EFPP would be 498.26, 551.79, and 605.18 ($\times 10^6$\$), respectively; those from FCCP at confidence levels of 0.9, 0.8, and 0.7 are 488.90, 502.13, and 515.48 ($\times 10^6$\$), respectively.

Figure 5 shows the values of decision variables obtained from FCCP and EFPP. It is obvious that the solutions from both models are fairly close to each other at the same levels of satisfaction or confidence. For instance, at period 3, at a satisfaction degree of 0.7, the target amounts from reservoir 1 to municipality, agriculture, and industry from EFPP are 6.50, 10.3, and 8.48 ($\times 10^6$ m^3), respectively, and at a confidence level of 0.7, the target amounts obtained from FCCP are 6.99, 10.7,

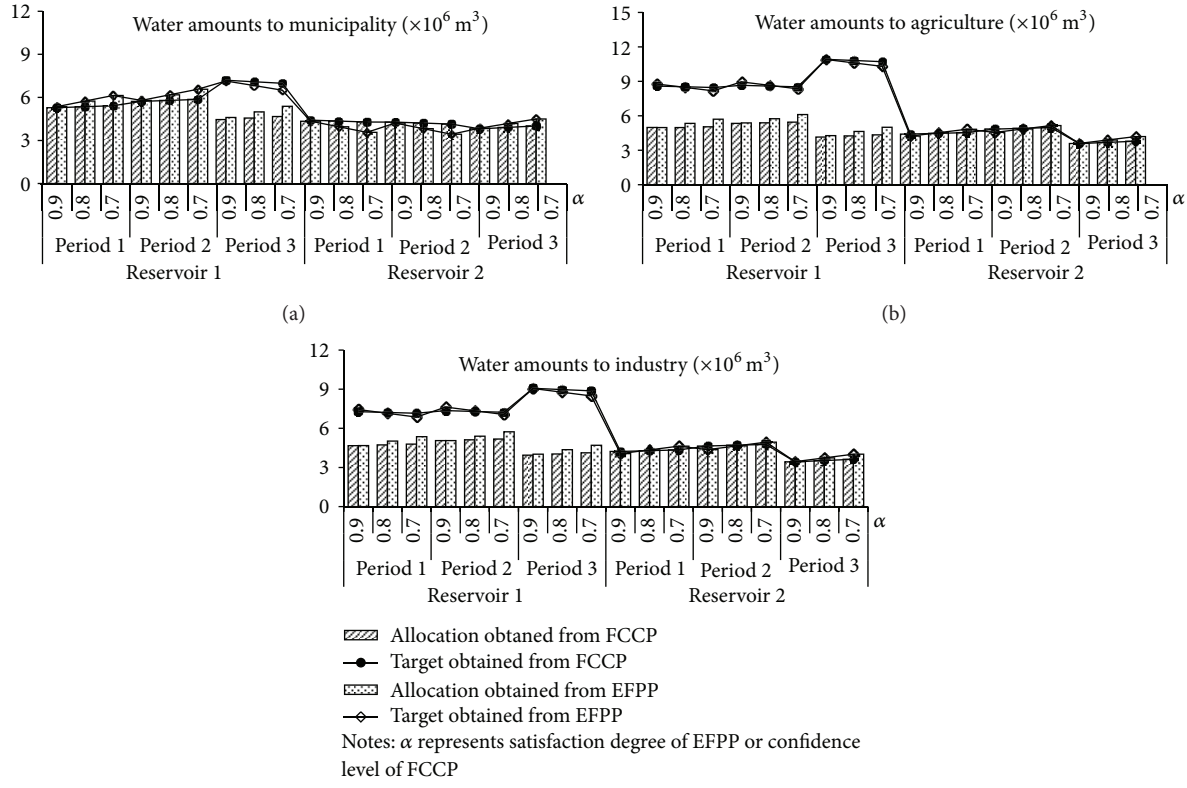

Figure 5: Comparison between FCCP and EFPP.

and 8.87 ($\times 10^6$ m^3), respectively. The solutions of allocation from EFPP are somewhat higher than those obtained from FCCP when α level is lower than 0.8; this explains the higher benefits of EFPP shown in Figure 4. From the comparison results, it appears that FCCP and EFPP are both capable of reflecting the balance of system benefit and reliability and could lead to comparable solutions under the same model settings. Obviously, EFPP has a wider applicability due to its extended capacity of handling fuzzy relationships in the model constraints.

3.4. Solutions under Different α and β Levels. Figure 6 shows the net benefits under various α and β levels. Obviously, the higher the α value, the more reliable the system and the lower the system benefit. For instance, when $\beta = 0.9$, the net benefit would increase from 498.26 to 793.68 ($\times 10^6$\$) when α level decreases from 0.9 to 0.1. Figure 6 also shows that the objective function is more sensitive to α than β. For example, when $\alpha = 0.9$, the difference of net benefits between $\beta = 0.9$ and 0.1 is 9.23 ($\times 10^6$\$), when $\beta = 0.9$, the difference of net benefits between $\alpha = 0.9$ and 0.1 is 295.42 ($\times 10^6$\$). It is also found that the values of decision variables would not vary with the change of β for this study case. This is due to the fact that the distributions of fuzzy coefficients in the objective function only cause negligible influence on model solutions; this is consistent with what we have explained in the numerical example section.

3.5. Applicability of EFPP to Other Engineering Management Problems. The proposed method has a potential to be applied to many other engineering management problems, where uncertainties could be described by fuzzy sets. For example, water quality management is also complicated with uncertainties existed among many socioeconomic, environmental, and technical factors, as well as their interactions. The optimization model for water quality management may include environmental constraints, such as the pollutant loading restrictions. The estimation of pollutant loads and maximum allowable discharge amounts involves experience of experts, model estimation errors, and data shortage, and the related parameter uncertainties could be described by fuzzy sets. The decision makers may also accept a certain level of exceedance of environmental constraints, and the unit cost associated with the water quality treatment may also vary with market conditions and subject to uncertainties. EFPP would be most suitable for such type of problems, provided that the model structures and parameters be specifically designed and estimated.

4. Conclusion

An extended fuzzy parametric programming (EFPP) approach was developed in this study and applied to a water resource allocation problem. The proposed method could deal with fuzzy parameters with trapezoidal-shaped

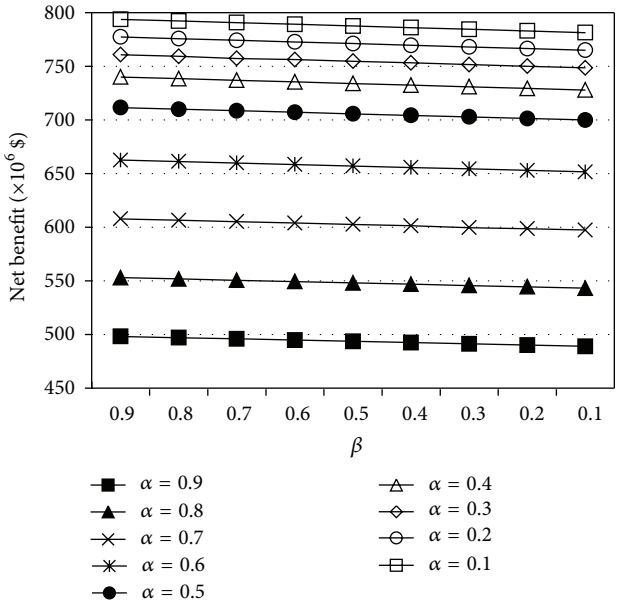

Figure 6: Net benefits under different α and β values.

distribution functions in the model, and also fuzzy relationships in the constraints. The results obtained from a water allocation problem showed that EFPP was capable of tackling a wide range of fuzziness in the management model and allowed water managers to analyze the balance of system benefit and risk of failure. Compared with conventional FCCP method, EFPP was flexible in handling the fuzzy relationship and fuzzy parameters in both objective function and constraints and had a more general applicability.

The EFPP method also showed a number of limitations. Firstly, EFPP was restricted to fuzzy variables with triangular- or trapezoidal-shaped membership functions. For more general-shape fuzzy variables, heuristic techniques may be employed [32]. Secondly, the value of using EFPP should also be compared with methods with multiple uncertainty-analysis techniques such as coupled fuzzy-stochastic theory [20, 31] as some particular forms of uncertainty may be better described by other algorithms like interval or stochastic ones. Nevertheless, the proposed method was proved effective in simple water allocation problems, and further applications and verifications in a wider range of engineering fields with more complicated conditions are expected.

Acknowledgment

This research was supported by Singapore's Ministry of Education (MOM) AcRF Tier 1 Project (M4010973.030).

References

[1] G. H. Huang, "IPWM: an interval parameter water quality management model," *Engineering Optimization*, vol. 26, no. 2, pp. 79–103, 1996.

[2] G. H. Huang, "A hybrid inexact-stochastic water management model," *European Journal of Operational Research*, vol. 107, no. 1, pp. 137–158, 1998.

[3] B. Abolpour and M. Javan, "Optimization model for allocating water in a river basin during a drought," *Journal of Irrigation and Drainage Engineering—ASCE*, vol. 133, no. 6, pp. 559–572, 2007.

[4] H. W. Chen and N. B. Chang, "Using fuzzy operators to address the complexity in decision making of water resources redistribution in two neighboring river basins," *Advances in Water Resources*, vol. 33, no. 6, pp. 652–666, 2010.

[5] Y. Xu and X. S. Qin, "Agricultural effluent control under uncertainty: an inexact double-sided fuzzy chance-constrained model," *Advances in Water Resources*, vol. 33, no. 9, pp. 997–1014, 2010.

[6] M. R. Nikoo, R. Kerachian, and H. Poorsepahy-Samian, "An interval parameter model for cooperative inter-basin water resources allocation considering the water quality issues," *Water Resources Management*, vol. 26, no. 11, pp. 3329–3343, 2012.

[7] C. Baudrit, D. Guyonnet, and D. Dubois, "Postprocessing the hybrid method for addressing uncertainty in risk assessments," *Journal of Environmental Engineering—ASCE*, vol. 131, no. 12, pp. 1750–1754, 2005.

[8] M. Inuiguchi and J. Ramík, "Possibilistic linear programming: a brief review of fuzzy mathematical programming and a comparison with stochastic programming in portfolio selection problem," *Fuzzy Sets and Systems*, vol. 111, no. 1, pp. 3–28, 2000.

[9] R. Slowinski, "A multicriteria fuzzy linear programming method for water supply system development planning," *Fuzzy Sets and Systems*, vol. 19, no. 3, pp. 217–237, 1986.

[10] J. Kindler, "Rationalizing water requirements with aid of fuzzy allocation model," *Journal of Water Resources Planning & Management—ASCE*, vol. 118, no. 3, pp. 308–323, 1992.

[11] C. S. Lee and S. P. Chang, "Interactive fuzzy optimization for an economic and environmental balance in a river system," *Water Research*, vol. 39, no. 1, pp. 221–231, 2005.

[12] R. M. Faye, S. Sawadogo, and F. Mora-Camino, "Flexible management of water resource systems," *Applied Mathematics and Computation*, vol. 167, no. 1, pp. 516–527, 2005.

[13] J. Mula, R. Poler, and J. P. Garcia, "MRP with flexible constraints: a fuzzy mathematical programming approach," *Fuzzy Sets and Systems*, vol. 157, no. 1, pp. 74–97, 2006.

[14] R. R. Tan, "Fuzzy optimization model for source-sink water network synthesis with parametric uncertainties," *Industrial and Engineering Chemistry Research*, vol. 50, no. 7, pp. 3686–3694, 2011.

[15] B. Julien, "An extension to possibilistic linear programming," *Fuzzy Sets and Systems*, vol. 64, no. 2, pp. 195–206, 1994.

[16] H. Tanaka, P. Guo, and H. J. Zimmermann, "Possibility distributions of fuzzy decision variables obtained from possibilistic linear programming problems," *Fuzzy Sets and Systems*, vol. 113, no. 2, pp. 323–332, 2000.

[17] C. Riverol, M. V. Pilipovik, and C. Carosi, "Assessing the water requirements in refineries using possibilistic programming," *Chemical Engineering and Processing*, vol. 45, no. 7, pp. 533–537, 2006.

[18] C. Xu and I. C. Goulter, "Optimal design of water distribution networks using fuzzy optimization," *Civil Engineering and Environmental Systems*, vol. 16, no. 4, pp. 243–266, 1999.

[19] H. Zhu, G. H. Huang, P. Guo, and X. S. Qin, "A fuzzy robust nonlinear programming model for stream water quality management," *Water Resources Management*, vol. 23, no. 14, pp. 2913–2940, 2009.

[20] I. Maqsood, G. H. Huang, and J. S. Yeomans, "An interval-parameter fuzzy two-stage stochastic program for water resources management under uncertainty," *European Journal of Operational Research*, vol. 167, no. 1, pp. 208–225, 2005.

[21] X. H. Nie, G. H. Huang, D. Wang, and H. L. Li, "Robust optimisation for inexact water quality management under uncertainty," *Civil Engineering and Environmental Systems*, vol. 25, no. 2, pp. 167–184, 2008.

[22] S. A. Torabi and E. Hassini, "An interactive possibilistic programming approach for multiple objective supply chain master planning," *Fuzzy Sets and Systems*, vol. 159, no. 2, pp. 193–214, 2008.

[23] F. Herrera and J. L. Verdegay, "Three models of fuzzy integer linear programming," *European Journal of Operational Research*, vol. 83, no. 3, pp. 581–593, 1995.

[24] M. Delgado, J. L. Verdegay, and M. A. Vila, "A general model for fuzzy linear programming," *Fuzzy Sets and Systems*, vol. 29, no. 1, pp. 21–29, 1989.

[25] W. Chang, "Ranking of fuzzy utilities with triangular membership functions," in *Proceedingd of International Conference on Policy Analysis and Information Systems*, pp. 263–272, 1981.

[26] R. R. Yager, "Ranking fuzzy subsets over the unit interval," in *Proceedings of the International Conference on Decision and Control (CDC '78)*, pp. 1435–1437, San Diego, Calif, USA, 1978.

[27] R. R. Yager, "A procedure for ordering fuzzy subsets of the unit interval," *Information Sciences*, vol. 24, no. 2, pp. 143–161, 1981.

[28] R. R. Yager, "Mathematical programming approach to inference with the capability of implementing default rules," *International Journal of Man-Machine Studies*, vol. 29, no. 6, pp. 685–714, 1988.

[29] J. M. Cadenas and J. L. Verdegay, "Using fuzzy numbers in linear programming," *IEEE Transactions on Systems, Man, and Cybernetics, Part B: Cybernetics*, vol. 27, no. 6, pp. 1016–1022, 1997.

[30] H. Ishibuchi and H. Tanaka, "Multiobjective programming in optimization of the interval objective function," *European Journal of Operational Research*, vol. 48, no. 2, pp. 219–225, 1990.

[31] Y. P. Li, G. H. Huang, and S. L. Nie, "An interval-parameter multi-stage stochastic programming model for water resources management under uncertainty," *Advances in Water Resources*, vol. 29, no. 5, pp. 776–789, 2006.

[32] B. Liu and K. Iwamura, "Chance constrained programming with fuzzy parameters," *Fuzzy Sets and Systems*, vol. 94, no. 2, pp. 227–237, 1998.

Hindawi Publishing Corporation
Mathematical Problems in Engineering
Volume 2013, Article ID 404327, 9 pages
http://dx.doi.org/10.1155/2013/404327

Research Article

Simulation of Multiphase Flow of the Oil-Water Separation in a Rotating Packed Bed for Oil Purification

Xiaojun Zhang, Yun Cheng, Songlin Nie, Hui Ji, and Laiguo Liu

College of Mechanical Engineering and Applied Electronics Technology, Beijing University of Technology, Beijing 100124, China

Correspondence should be addressed to Songlin Nie; niesonglin@tom.com

Received 12 December 2012; Accepted 22 January 2013

Academic Editor: Xiaosheng Qin

HIGEE (High Gravity Rotary Device) rotating oil purifier which consists of two parts: hydrocyclone separator and rotating packed bed (abbr. RPB) is considered to be capable of removing the solid particle contaminant, moisture and gas simultaneously. As the major unit of HIGEE, the RPB uses centrifugal force to intensify mass transfer. Because of the special structure of RPB, the hydraulic characteristics of the RPB are very important. In this study, the multiphase flow model in porous media of the RPB is presented, and the dynamical oil-water separation in the RPB is simulated using a commercial computational fluid dynamics code. The operating conditions and configuration on the hydraulic performance of the RPB are investigated. The results have indicated that the separation efficiency of HIGEE rotating oil purifier is predominantly affected by operating conditions and the configurations. The best inlet pressure is 0.002 MPa. When the liquid inlet is placed in the outside of the lower surface of RPB; oil outlet is placed in the upper surface, where it is near the rotation axis; and water outlet is placed in the middle of the RPB, where it is far away from the oil outlet, the separating efficiency is the best.

1. Introduction

The pollution of hydraulic engineering equipment is the mainly responsible for the trouble of hydraulic system, and it is the key of maintenance. Contaminant particles can bring about a number of detrimental effects on the hydraulic system components as well as the fluid itself. One of the key problems of hydraulic contamination control is to design and maintain system reasonably reducing the contamination level of key point as low as possible. There are various kinds of purification technologies to improve the contamination control level of fluid power system (FPS), such as oil filter, electrostatic oil cleaner, oil vacuum cleaning, magnetic field pulse filtration, and other coalescence methods [1]. However, most of traditional purification technologies can only remove individual contamination while there are solid particle contaminant, moisture, and gas simultaneously in the FPS. A novel hydraulic oil purifier is developed to be capable of removing the solid particle contaminant, moisture, and gas simultaneously, which consists of two parts: hydrocyclone separator and rotating packed bed (RPB) as shown in Figure 1.

Rotating packed beds (RPBs) intensify mass transfer by using centrifugal force to realize separation, which has been applied to distillation, absorption, striping, polymer devolatilization, bio-oxidation, and so on [2–6]. HIGEE (high gravity rotary device) rotating oil purifier is based on the traditional oil purification, which is developed on the introduction of the HIGEE technology. The fluid from preliminary purification goes into the internal space of rotating bed along the axis of rotation and rotates at high speed with the rotating packed bed driven by the motor. The function of packing is increasing the speed of fluid, and huge shear force overcomes surface forces, increasing contact area between different phases, tearing fluid into spray of micron order. In the action of HIGEE, when the droplet contains spray through the voids of the layers of packing which rotates at high speed, which is bend, narrow, and varied, which is also filled with very thin spray and very small droplet, the inertia settlement ability of spray and droplet will be enhanced. It will form rapid collision for effective coagulation between droplet and spray, in the action of different physical properties of packing which are hydrophilic or hydrophobic to droplet and spray; finally the media of different density

Figure 1: 3D plot of HIGEE rotating oil purifier.

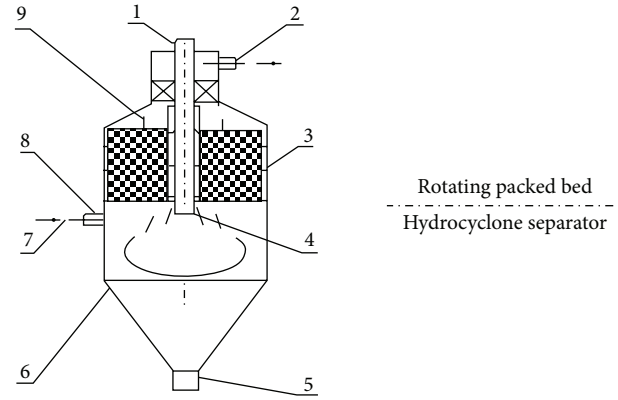

Figure 2: Sectional drawing of HIGEE rotating oil purifier. 1: connecting motor shaft; 2: the hydraulic oil outlet; 3: packing; 4: vortex finder; 5: underflow outlet; 6: shell; 7: tangential nozzle; 8: contaminated oil inlet; 9: parting face.

are separated out in the action of centrifugal force [7].

The hydraulic characteristics of the RPB have been reported in many studies, such as the liquid holdup, the pressure drop, flooding, residence time distribution, and visualized liquid flow [8–11]. Ramshaw and Mallinson conducted a water-oxygen absorption system in an RPB and found that the mass transfer coefficient was 27–44 times higher than that in conventional packed columns [12]. Tung and Mah theoretically proposed a correlation for the mass transfer coefficient in an RPB [13]. Munjal et al. proposed a correlation in an RPB theoretically and experimentally studied for the absorption of CO_2 from air into NaOH [14, 15]. Kumar and Gardner obtained mass transfer coefficients in an RPB packed with aluminum foam metal of various specific surface areas in a CO_2-water system [16]. In 1990, Kumar and Rao performed experiments of absorption of CO_2 from air into NaOH solution in an RPB and found that the mass transfer coefficient changed with increasing liquid rates and rotation speeds [17]. Singh et al. investigated the mass transfer in an RPB for air stripping of volatile organic compounds from groundwater [18]. Chen et al. also did a lot of research on the RPB, they evaluated the mass transfer coefficient of an oxygen-water absorption system [19], and they investigated the influence of liquid viscosity on the mass transfer rate for both Newtonian and non-Newtonian fluids in an RPB [20]. Further, they evaluated the end effects of an RPB by varying the radii of the packed bed [21]. Burns and Ramshaw took the visual study of liquid flow in RPBs under different rotating speeds. They observed the spiral of liquid and severe liquid maldistribution on radial orientation; in contrast the liquid wandered slightly laterally and consequently led to a relatively uniform distribution on the tangential orientation [22]. Similar results were reached by the researchers [7] in Beijing University of Chemical Technology [11].

Many studies have been investigated by theory or experiment. However, many physical experiments are very expensive and time-consuming, and there are no precise experimental data about the flow in RPBs. Hence, using mathematical models as design tools can contribute to a better understand of the hydraulic characteristics of the RPB with the fast development of the computer technology. Computational fluid dynamics (CFD) is a good design and analysis tool to simulate the flow of mass and momentum throughout a fluid continuum. It is an advantage method to study the hydraulics characteristics of RPB. Numerical simulation by using FLUENT software will be conducted in this research. The multiphase flow in porous media of RPB will be numerically studied. The effects of operating conditions and configuration on the hydraulic performance of RPB are investigated to increase the separation efficiency of HIGEE rotating oil purifier.

2. Mathematical Methods

2.1. Physical Model. According to the introduction of HIGEE rotating oil purifier (Figure 1), Figure 2 shows the geometrical diagram of HIGEE rotating oil purifier designed for this research, which consists of two parts: hydrocyclone separator and rotating packed bed (RPB). The hydraulic characteristics of RPB are very important. In this study, the multiphase flow model in porous media of RPB is presented.

The 3D model (Figure 3) is developed for the RPB considered using a commercial code Gambit. The diameter of the RPB is 110 mm, and its height is 60 mm. The whole rotating packed bed is taken as the object of study in this research. In Figure 3, the whole rotating packed bed is a cylinder. There are three small cylinders at the upper and lower surfaces of the RPB. The oil and water outlets are at the upper surface and the oil-water mixture inlet is at the lower surface.

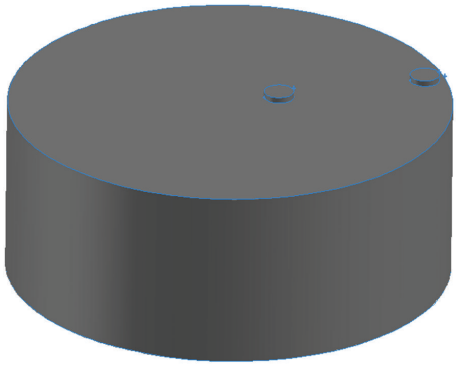

Figure 3: 3D model of the RPB.

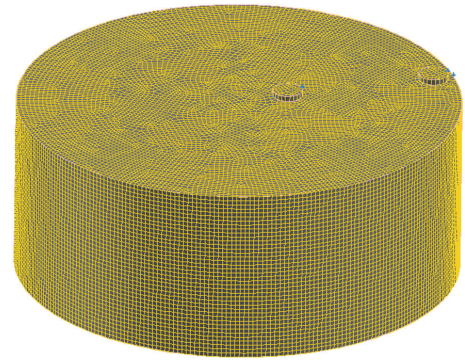

Figure 4: Mesh generation of the 3D model.

2.2. Mathematical Model. In this research, the Eulerian multiphase model is applied. The phases are water and oil. The description of multiphase flow as interpenetrating continua incorporates the concept of phasic volume fractions which is defined by α_q in this paper. Because there is no temperature gradient, so only the mass conservation and the momentum equations are used. Volume fractions represent the space occupied by each phase, and the laws of conservation of mass and momentum are satisfied by each phase individually [23].

The volume of phase q is V_q, which is defined by

$$V_q = \int_V \alpha_q dV, \tag{1}$$

where

$$\sum_{q=1}^{n} \alpha_q = 1. \tag{2}$$

The effective density of phase q is

$$\widehat{\rho_q} = \alpha_q \rho_q, \tag{3}$$

where ρ_q is the physical density of phase q. Continuity equation is shown as

$$\nabla \cdot \left(\widehat{\rho_q} v\right) = 0, \tag{4}$$

where v is the vector velocity of the liquid. Momentum balance equation is shown as

$$\nabla \cdot \left(\widehat{\rho_q} vv\right) = -\nabla \times P + \nabla \cdot \left(\mu \left(\nabla \times v + (\nabla \times v)^T\right)\right), \tag{5}$$

where P is the static pressure, and μ is the viscosity. Porous media are simulated by adding a momentum source term S_i to the standard fluid flow equations; therefore the momentum balance in the porous media could be defined as

$$\nabla \cdot \left(\widehat{\rho_q} vv\right) = -\nabla \times P + \nabla \cdot \left(\mu \left(\nabla \times v + (\nabla \times v)^T\right)\right) + S_i \quad (i = x, y, z), \tag{6}$$

where S_i is the source term for the momentum equation, which is composed of two parts: a viscous loss term (the first term on the right-hand side of (7)), and inertial loss term (the second term on the right-hand side of (7)):

$$S_i = -\left(\sum_{j=1}^{3} D_{ij} \mu v_i + \sum_{j=1}^{3} C_{ij} \frac{1}{2} \widehat{\rho_q} |v_i| v_i\right) \quad (i = x, y, z), \tag{7}$$

where D and C are viscous resistance and inertia loss coefficient matrices respectively. When the case is simple homogeneous porous media, the source term is shown as

$$S_i = -\left(\frac{\mu}{\alpha} v_i + C_2 \frac{1}{2} \hat{\rho}_q |v_i| v_i\right) \quad (i = x, y, z), \tag{8}$$

where α is the permeability and C_2 is the inertial resistance coefficient. D and C are simply specified as diagonal matrices with $1/\alpha$ and C_2, respectively [24, 25].

In this paper, the Ergun equation is used to derive porous media input for a packed bed, and the laminar flow through the porous media is simulated, which is similar to a packed bed in this paper and easy to simulate on existing computers. The permeability and inertial loss coefficients in each component direction could be identified as

$$\alpha = \frac{d^2}{150} \frac{\varepsilon^3}{(1-\varepsilon)^2}, \qquad C_2 = \frac{3.5}{d} \frac{(1-\varepsilon)}{\varepsilon^3}, \tag{9}$$

where d is the mean particle diameter, and ε is the void fraction [26].

2.3. Grid Generation and Boundary Condition. To solve the governing equations, appropriate grid generation and boundary conditions are specified at all external boundaries based on the following. The 3D model (Figure 3) is meshed into tetrahedral grid (Figure 4), which has about 920538 elements and 164675 nodes for the 3D computational grid. The mesh density is increased appropriately to improve the computational convergent velocity. The technique of finite volume is selected to solve the governing equations. Frequently, suitable values of the underrelaxation factors are adopted to assure the smooth convergence of the numerical solution. In the

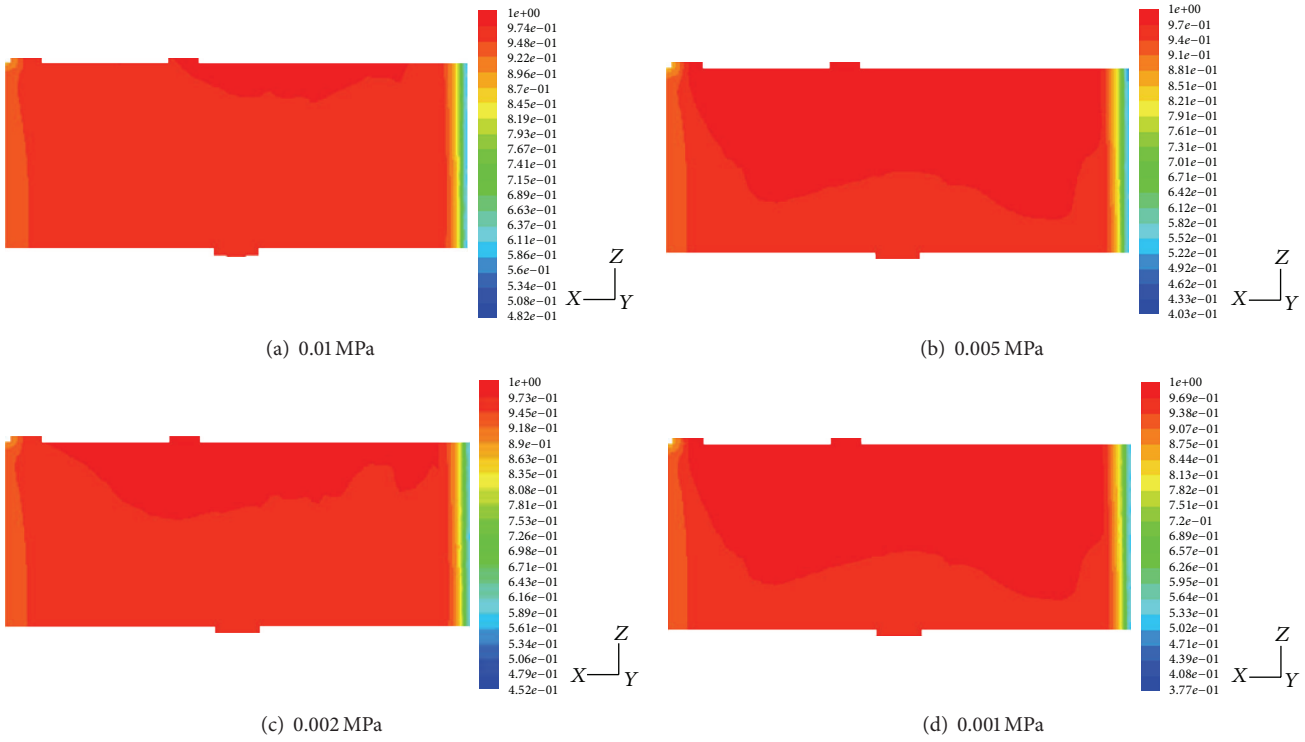

Figure 5: Contours of the outlet volume fraction of oil in the outlet with different pressures.

Table 1: Material properties of the model.

Parameter	Unit	Water	Oil
Volume fraction	—	5%	95%
Density	kg/m^3	1000	780
Viscosity	kg/ms	0.001003	0.0024

Table 2: Boundary conditions of the model.

Description	Type
Porosity of porous medium	0.5
Mean particle diameter of porous medium	0.05 mm
Flow condition of the oil-water mixture	Turbulence
Viscous model	K-ε model
Inlet of the oil-water mixture	Pressure inlet
Outlet of oil or water	Pressure inlet

oil-water two-phase flow, the material properties [27] and boundary conditions [28, 29] in this research can be seen in Tables 1 and 2.

The material properties and boundary conditions are selected reasonably. The standard K-ε model is selected, where robustness, economy, and reasonable accuracy for a wide range of turbulent flows explain its popularity in industrial flow and heat transfer simulations.

3. Results and Discussion

The multiphase flow in porous media of RPB will be numerical simulated. The effects of operating conditions and configuration on the hydraulic performance of the RPB are investigated to increase the separation efficiency of HIGEE rotating oil purifier.

3.1. Effect of the Inlet Pressure. To understand the feature distribution of inner hydrocyclone separator more clearly, the outlet pressure of hydrocyclone separator is 0.002 MPa which is considered a reference. The static pressure is firstly to be simulated as shown. This example is identified as follows: the configuration of the RPB is certain. The oil-water mixture inlet is set near to the middle of the lower surface of the RPB, whose diameter is 15 mm. The outlet for water and oil is set in the upper surface, where the oil outlet is in the middle, while the water outlet is in the edge. The diameter of outlets is 10 mm. The rotation speed is 1500 rpm. The other conditions are constant. This research investigated the separation efficiency of HIGEE rotating oil purifier by changing the inlet pressure. The sectional drawings are extracted. Contour plot and graph of the outlet volume fraction of oil in the outlet with different pressures are shown in Figures 5 and 6.

Figure 5 displays contour plots of the outlet volume fraction of oil in the outlet with different pressures. As shown in Figure 5(a), the liquid inlet pressure is 0.01 MPa. The volume fraction of oil in the oil outlet is not entirely 100%, and the fraction of oil in the water outlet can be about 96%. In Figure 5(b), the liquid inlet pressure is 0.005 MPa.

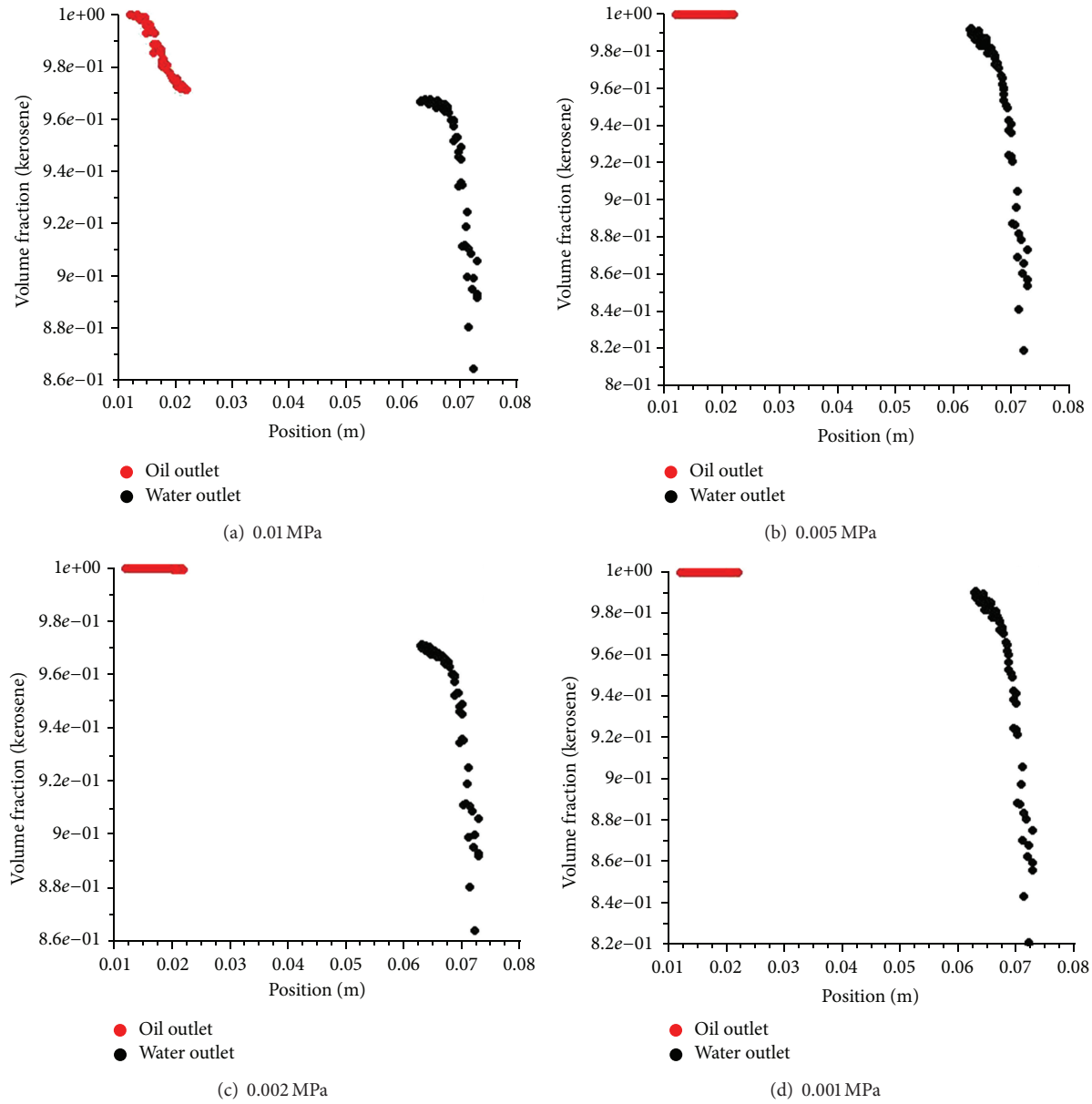

Figure 6: Graphs of the outlet volume fraction of oil in the outlet with different pressures.

The volume fraction of oil in the oil outlet can be up to 100%, and the fraction of oil in the water outlet can also be about 99%. However, when the liquid inlet pressure is 0.002 MPa, the volume fraction of oil in the oil outlet can be up to 100%, as seen in Figure 5(c), and the fraction of oil in the water outlet can also be about 96%. When the liquid inlet pressure is 0.001 MPa, the volume fraction of oil in the oil outlet can be up to 100%, which is shown in Figure 5(d), and the fraction of oil in the water outlet can also be about 98%.

Figure 6 displays graphs of the outlet volume fraction of oil in the outlet with different pressures. The volume fraction of oil in the oil outlet can be up to 100%, but it is not entirely 100%, as shown in Figure 6(a), and the fraction of oil in the water outlet can also be about 96%. In Figure 6(b), the volume fraction of oil in the oil outlet can be up to 100%, and it is entirely 100%, but the fraction of oil in the water outlet can also be about more than 99%. When the liquid inlet pressure is 0.002 MPa, the volume fraction of oil in the oil outlet can be up to 100%, as shown in Figure 6(c), and it is entirely 100%, but the fraction of oil in the water outlet can also be about less than 96%. As shown in Figure 6(d), the volume fraction of oil in the oil outlet can be up to 100%, and it is entirely 100%, but the fraction of oil in the water outlet can also be about more than 98%.

It can be seen from the simulation results that the inlet pressure has a big effect on the separation efficiency of HIGEE rotating oil purifier. The separation efficiency of HIGEE rotating oil purifier improves with the decreasing of inlet pressure; in particular when the inlet pressure is 0.002 MPa, the separation efficiency is the best. The volume fraction of

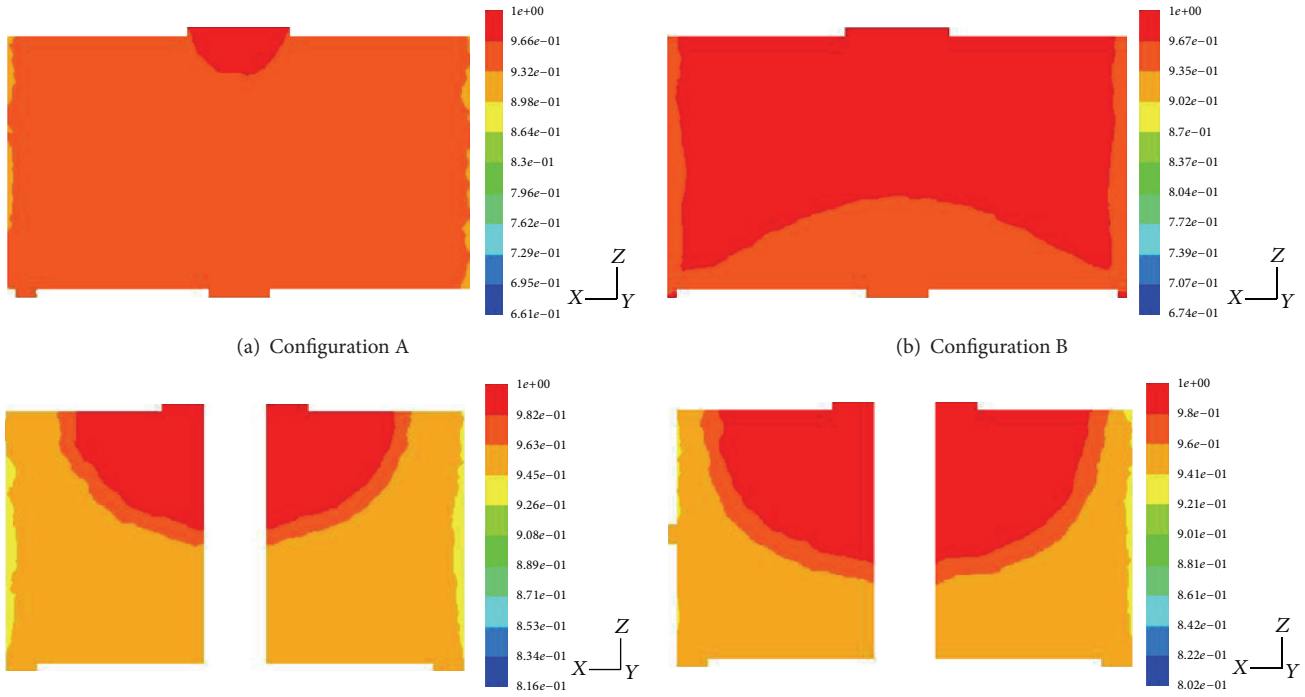

Figure 7: Contours of the volume fraction of oil in the outlet with different configurations.

oil in the oil outlet can be up to 100%, and it is entirely 100%, and the fraction of oil in the water outlet can also be about less than 96%, which is better than other inlet pressures.

3.2. Effect of the Configuration. In order to investigate the effect of the configuration, the example is identified as follows. The rotation speed is 1500 rpm. The inlet pressure is 0.002 MPa with the other boundary conditions unchanged. This research investigated the separation effect of HIGEE rotating oil purifier by changing the configuration, such as the location of the oil-water mixture inlet, oil outlet, and water outlet in the RPB.

Based on previous theoretical and experimental results, fluids of different densities will concentrate on different places accordingly under rotation speed. The fluid of high density concentrates close to the rotation axis, while the fluid of low density concentrates away from the rotation axis. Therefore, four different configurations are investigated in this research. *Configuration A*. The oil-water mixture inlet is placed in the middle of the lower surface of RPB, whose diameter is 15 mm, the water outlet is placed in the outside of the lower surface, whose diameter is 5 mm, and the oil outlet is placed in the middle of the upper surface, whose diameter is 20 mm. *Configuration B*. The water outlet is also placed in the outside of the lower surface, but its width is 2.5 mm, which is different from Configuration A. *Configuration C*. The oil-water mixture inlet is placed in the outside of the lower surface, whose width is 7.5 mm, the water outlet is placed in the side of upper, whose diameter is 5 mm, and the oil outlet is placed in the middle of the upper face, whose width is 10 mm. *Configuration D*. The water outlet is placed in the side of middle, which is different from Configuration C. The sectional drawings are extracted. Contour plot and graph of the outlet volume fraction of oil in the outlet with different configurations are shown in Figures 7 and 8.

Figure 7 displays contour plots of the outlet volume fraction of oil in the outlet with different configurations. As shown in Figure 7(a), the volume fraction of oil in the oil outlet can be up to 100%, and the fraction of oil in the water outlet can also be about 95%. In Figure 7(b), the volume fraction of oil in the oil outlet can be up to 100%, and the fraction of oil in the water outlet can also be about more than 98%. Corresponding to the Configuration C, the volume fraction of oil in the oil outlet can be up to 100%, and the fraction of oil in the water outlet can also be about more than 95% (Figure 7(c)). The volume fraction of oil in the oil outlet can be up to 100%, which is shown in Figure 7(d), and the fraction of oil in the water outlet can also be about less than 95%.

Figure 8 displays graphs of the outlet volume fraction of oil in the outlet with different configurations. The volume fraction of oil in the oil outlet can be up to 100%, but it is not entirely 100%, which is shown in Figure 8(a). And the fraction of oil in the water outlet can also be about 95%. In Figure 8(b), the volume fraction of oil in the oil outlet can be up to 100%, and it is entirely 100%, but the fraction of oil in the water outlet can also be about more than 98%. Corresponding to Configuration C, the volume fraction of oil in the oil outlet can be up to 100%, and it is entirely 100%, but the fraction of oil in the water outlet can also be about more than 95% (Figure 8(c)). As shown in Figure 8(d), the volume fraction of oil in the oil outlet can be up to 100%, and it is entirely

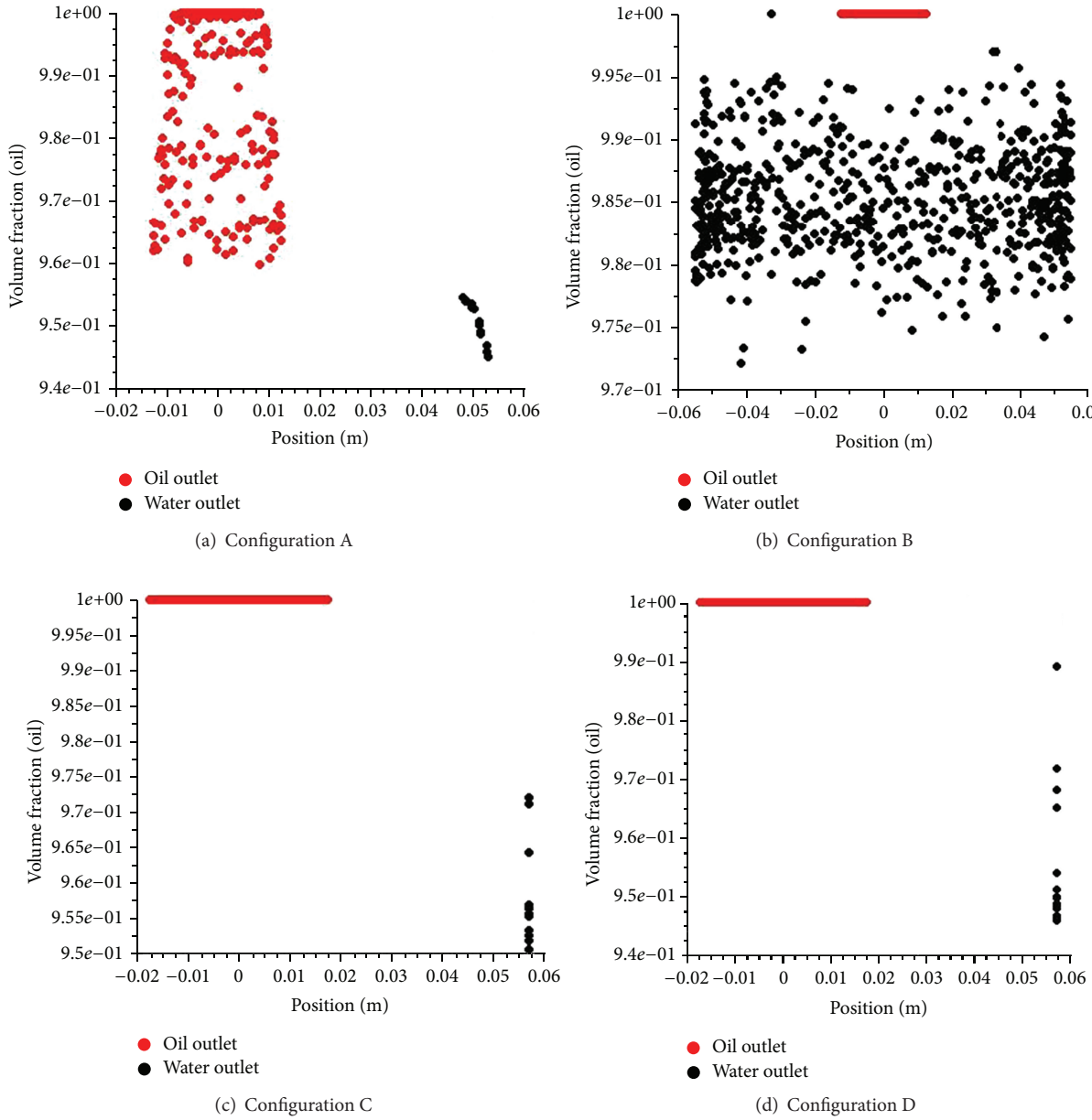

Figure 8: Graphs of the volume fraction of oil in the outlet with different configurations.

100%, but the fraction of oil in the water outlet can also be about less than 95%.

Simulation results show that the simulation results indicate that the separating efficiency of HIGEE rotating oil purifier is greatly affected by the configuration; Configuration D is the best configuration. In Configuration D, the volume fraction of oil in the oil outlet can be up to 100%, and it is entirely 100%, but the fraction of oil in the water outlet can also be about less than 95%.

3.3. Discussion. Simulation results show that because of different densities, when the oil from preliminary purification goes through the HIGEE field, the oil-which has a low density outflows from the oil outlet in the middle, where it is near the rotation axis, while water which has a high density outflows from the water outlet is in the edge, where it is far away from the oil outlet.

Applying the inlet pressure is for applying an inlet velocity to the oil from preliminary purification. When the inlet pressure is small, which can increase the residence time of the oil-water mixture, therefore, the fluid from preliminary purification can make a good contact with hydrophilic material in the RPB to get better separation efficiency. The separation efficiency of HIGEE rotating oil purifier increases with the decreasing of inlet pressure; in particular when the inlet pressure is 0.002 MPa, the separation efficiency is the best. However, a small pressure is not the best choice for the

inlet pressure. The working hours will last long when the inlet velocity is very small.

The separating efficiency of HIGEE rotating oil purifier is greatly affected by the configurations. Configuration D is the best configuration. The layout of liquid inlet, oil outlet, and water outlet of the RPB significantly affected the separating efficiency. When the liquid inlet is placed in the outside of the lower surface of RPB; oil outlet is placed in the upper surface, where it is near the rotation axis; and water outlet is placed in the middle of the side of the RPB, where it is far away from the oil outlet, the corresponding separating efficiency was the best. In Configuration D the volume fraction of oil in the oil outlet can be up to 100%, and it is entirely 100%, but the fraction of oil in the water outlet can also be about less than 95%, which is better than other configurations.

4. Conclusions

Unlike previous experimental research, numerical simulation is employed in this paper to analyze the flow characteristics inside the RPB, and related conclusions are got.

(1) The oil-water two-phase flow is simulated based on the 3D model of the RPB which is established in Gambit.

(2) The operating conditions on the hydraulic performance of the RPB are investigated. Inlet pressure has big effect on the separation efficiency of HIGEE rotating oil purifier. The separation efficiency of HIGEE rotating oil purifier increases with the decreasing of inlet pressure; in particular when the inlet pressure is 0.002 MPa, the separation efficiency is the best.

(3) Simulation results also show that the separating efficiency of HIGEE rotating oil purifier is greatly affected by the configuration, especially the layout of liquid inlet, oil outlet, and water outlet in the RPB. When the liquid inlet is placed in the outside of the lower surface of RPB; oil outlet is placed in the upper surface, where it is near to the rotation axis; and water outlet is placed in the middle of the side of the RPB, which it is far away from the oil outlet, the corresponding separating efficiency is the best.

Compared with theoretical analysis and experimental research, numerical simulation has provided an easy and effective method to design and optimize the HIGEE rotating oil purifier and other mechanical devices, which was widely used in resources and environmental systems. In order to certificate the numerical results, corresponding experiments need to be investigated in the future work.

Acknowledgments

This research was funded by the Natural Science Foundations of China (no. 51075007), National High-tech R&D (863) Program (no. 2012AA091103), and The Importation and Development of High-Caliber Talents Project of Beijing Municipal Institutions (CIT&TCD 20130316).

References

[1] Z. X. Xia, *Contamination Control of Hydraulic System*, China Machine Press, Beijing, 1992.

[2] C. Ramshaw, "'HiGee' distillation-An example of process intensification," *Chemical Engineering Science*, vol. 389, pp. 13–14, 1983.

[3] M. Keyvani and N. C. Gardner, "Operating characteristics of rotating beds," *Chemical Engineering Progress*, vol. 85, no. 9, pp. 48–52, 1989.

[4] H. S. Liu, C. C. Lin, S. C. Wu, and H. W. Hsu, "Characteristics of a rotating packed bed," *Industrial and Engineering Chemistry Research*, vol. 35, no. 10, pp. 3590–3596, 1996.

[5] D. P. Rao, A. Bhowal, and P. S. Goswami, "Process intensification in rotating packed beds (HIGee): an Appraisal," *Industrial and Engineering Chemistry Research*, vol. 43, no. 4, pp. 1150–1162, 2004.

[6] X. Li, Y. Liu, Z. Li, and X. Wang, "Continues distillation experiment with rotating packed bed," *Chinese Journal of Chemical Engineering*, vol. 16, no. 4, pp. 656–662, 2008.

[7] H. Ji, S. L. Nie, H. M. Sun, and X. H. Tang, "Research on on-line purification of hydraulic oil based on high gravity technology," *Chinese Hydraulics & Pneumatics*, no. 11, pp. 1–6, 2011.

[8] C. Zheng, K. Guo, Y. Feng, C. Yang, and N. C. Gardner, "Pressure drop of centripetal gas flow through rotating beds," *Industrial and Engineering Chemistry Research*, vol. 39, no. 3, pp. 829–834, 2000.

[9] A. Basic and M. P. Dudukovic, "Liquid holdup in rotating packed beds: examination of the film flow assumption," *AIChE Journal*, vol. 41, no. 2, pp. 301–316, 1995.

[10] M. J. Lockett, "Flooding of rotating structured packing and its application to conventional packed columns," *Trans IChemE*, vol. 73, pp. 379–384, 1995.

[11] K. Guo, F. Guo, Y. Feng, J. Chen, C. Zheng, and N. C. Gardner, "Synchronous visual and RTD study on liquid flow in rotating packed-bed contractor," *Chemical Engineering Science*, vol. 55, no. 9, pp. 1699–1706, 2000.

[12] C. Ramshaw and R. H. Mallinson, "Mass transfer process," U.S. Patent 4, vol. 283, no. 255, 1981.

[13] H. H. Tung and R. S. H. Mah, "Modeling liquid mass tranfer in HIGee separtion process," *Chemical Engineering Communications*, vol. 39, no. 1–6, pp. 147–153, 1985.

[14] S. Munjal, M. P. Duduković, and P. Ramachandran, "Mass-transfer in rotating packed beds-I. Development of gas-liquid and liquid-solid mass-transfer correlations," *Chemical Engineering Science*, vol. 44, no. 10, pp. 2245–2256, 1989.

[15] S. Munjal, M. P. Duduković, and P. Ramachandran, "Mass-transfer in rotating packed beds-II. Experimental results and comparison with theory and gravity flow," *Chemical Engineering Science*, vol. 44, no. 10, pp. 2257–2268, 1989.

[16] M. Kumar and N. C. Gardner, "Operating characteristics of rotating beds," *Chemical Engineering Science*, vol. 85, no. 9, pp. 48–52, 1989.

[17] M. P. Kumar and D. P. Rao, "Studies on a high-gravity gas-liquid contactor," *Industrial Engineering Chemistry Research*, vol. 29, no. 5, pp. 917–920, 1990.

[18] S. P. Singh, J. H. Wilson, R. M. Counce et al., "Removal of volatile organic compounds from groundwater using a rotary air stripper," *Industrial and Engineering Chemistry Research*, vol. 31, no. 2, pp. 574–580, 1992.

[19] Y. H. Chen, C. Y. Chang, W. L. Su et al., "Modeling ozone contacting process in a rotating packed bed," *Industrial and Engineering Chemistry Research*, vol. 43, no. 1, pp. 228–236, 2004.

[20] Y. S. Chen, C. C. Lin, and H. S. Liu, "Mass tranfer in a rotationg packed bed with viscous newtonian and non-newtonian fluids," *Industrial Engineering Chemistry Research*, vol. 44, no. 4, pp. 1043–1051, 2005.

[21] Y. S. Chen, C. C. Lin, and H. S. Liu, "Mass tranfer in a rotationg packed bed with viscous radii of the bed," *Industrial Engineering Chemistry Research*, vol. 44, no. 20, pp. 7868–7875, 2005.

[22] J. R. Burns and C. Ramshaw, "Process intensification: visual study of liquid maldistribution in rotating packed beds," *Chemical Engineering Science*, vol. 51, no. 8, pp. 1347–1352, 1996.

[23] L. J. Guo, *Two-Phase and multiPhase Hydrodynamics*, Xi'an Jiaotong University Press, Xi'an, China, 2002.

[24] X. Y. Kong, *Advanced Mechanics of Fluid Flow in Porous Media*, Chinese Science and Technology University Press, Hefei, China, 2010.

[25] L. S. Cheng, *Advanced Mechanics of Fluid Flow in Porous Media*, Petroleum Industry Press, Beijng, China, 2010.

[26] L. Fan, R.T. Hai, W. X. Wang, Z. Lu, and Z. M. Yang, "Application of computational fluid dynamic to model the hydraulic performance of subsurface flow wetlands," *Journal of Environmental Sciences*, vol. 20, no. 12, pp. 1415–1422, 2008.

[27] Z. Wen, L. C. Shi, and Y. R. Ren, *The Flent Computational Dynamics Application Guide*, Tsinghua University Press, Beijing, China, 2009.

[28] J. C. Sheng, *Hydraulic Fluid Mechanics*, Mechanical Industry Press, Beijing, China, 1980.

[29] Y. Yu, J. M. Zhang, and L. T. Jiang, *Fluent Introductory and Advanced Course*, Beijing Institute of Technology Press, Beijing, China, 2011.

Hindawi Publishing Corporation
Mathematical Problems in Engineering
Volume 2012, Article ID 704989, 14 pages
doi:10.1155/2012/704989

Research Article

Suitable Environmental Flow Release Criteria for Both Human and Riverine Ecosystems: Accounting for the Uncertainty of Flows

Jian Tang, Xinan Yin, ChunXue Yu, and Zhifeng Yang

State Key Laboratory of Water Environment Simulation, School of Environment, Beijing Normal University, Beijing 100875, China

Correspondence should be addressed to Xinan Yin, yinxinan@163.com
and Zhifeng Yang, zfyang@bnu.edu.cn

Received 16 November 2012; Accepted 11 December 2012

Academic Editor: Yongping Li

Environmental flow (e-flow) release criteria are key parameters in water resources management and riverine ecosystem protection. The previous methods for e-flow criterion determination are based on the historical flow time series without the consideration of flow uncertainty. Due to low possibility of reoccurrence of the historical flows and the uncertainty of future flows, the flow uncertainty needs to be integrated in the process of determining e-flow release criteria. In this research, a new method is proposed to determine the optimal e-flow release criteria under flow uncertainty accounting for both the human and riverine ecosystem needs. In the new method, the scenario tree method is applied to generate the scenarios of flows, which can cover most of possible flow conditions and can effectively reflect the uncertainty of flows; the Range of Variability Approach (RVA), a most commonly used method to assess the flow regime alteration, is refined by incorporating the uncertainty of flows. The Tang River in Northern China is taken as a case study to test the effectiveness of the new method. The results show that the previous method obviously overestimates the optimal e-flow release criteria and the new method can get more suitable criteria that are suitable for both human and riverine ecosystems.

1. Introduction

One-third of the world's population are under the pressure of water scarcity and estimates suggest that by 2050 more countries will experience water shortage [1]. Increasing water supply has become an urgent task in the world [2, 3]. Rivers as the major sources for water supply are expected to provide more water to humans. However, rivers also need water to sustain their health [4, 5]. The overwithdrawal of water from rivers has led to severe

degradation of riverine ecosystems in the world [6–8]. To address the conflict between human and riverine ecosystems, it is necessary to conduct research on how to balance the water requirements between the two users [9–12].

The concept of environmental flows (e-flows) is developed to direct water allocation between humans and rivers. Sustaining e-flows has become a basic principle for water resources management [1, 5, 13–15]. E-flows are defined as the volume of water that should remain in a river and its variation over time to sustain specified ecosystem conditions [16]. Many methods have been developed to determine the e-flows, such as hydrological methods, hydraulic rating methods, habitat simulation methods, and holistic methods [17–22]. Among them, many methods try to determine one or several fixed values of e-flows [20, 21]. After the development of several decades, scientists found that the full range of natural intra- and interannual variability of hydrological regimes, and the associated characteristics of flow magnitude, frequency, duration, timing, and rate of change, are critical in determining the structures and functions of riverine ecosystems [17, 23, 24]. It is widely acknowledged that e-flow provision should try to maintain natural flow regimes rather than only to ensure one or several fixed values [25–27]. Thus, the reduction of natural flow regime alteration has become the key principle for e-flow assessment and provision. This principle has contributed to the implementation of e-flow management on thousands of rivers worldwide [22, 28].

The e-flows reflect the characteristics of riverine ecosystems. In real-world water resources management and e-flow provision, the e-flows must be balanced with the water requirements of humans [11, 12]. Thus, after determining the e-flow requirements, the e-flow release criteria need to be further determined. The release criteria directly specify the volume of water used for e-flow provision. The e-flow release criteria can be equal to, greater than or less than the e-flow requirements. They need to be determined accounting for both the human and riverine ecosystem needs. Much research has been done to determine the e-flow release criteria to downstream rivers. Most of the research only tried to maintain the minimum e-flows and regarded the difference between the mean annual flows and the minimum e-flows as the planned water diversion to humans [20, 29]. These methods are easy to apply in real-world water resources management, but they have not taken into account the maintenance of natural flow regimes. To effectively account for natural flow regimes, Shiau and Wu applied the Range of Variability Approach (RVA) to investigate the effect of e-flow release criteria on restoring the natural flow regime downstream and evaluated the tradeoffs between the ecosystem and human needs associated with various combinations of water withdrawal and e-flow release criteria [30]. Further, they used a compromise programming methodology to identify the optimal e-flow release criteria that simultaneously assured the water supply reliability and sustained the natural flow variability [31]. The innovative research is useful to balance e-flow release and water diversion. In the research, the historical flow time series were used to calibrate the e-flow release and water diversion models and got the optimal values for e-flow release criteria. When the optimized values are used to direct water resources management in the future, the underlying assumption is that the historical flow time series will occur again in the future. In fact, the flows in the future are quite uncertain [32, 33], and the reoccurrence possibility of the historical flows is very low [34–39]. Thus, the values optimized based on historical flows may be not optimal for the future flow conditions [40, 41]. In addition, uncertainty is a basic characteristic of flows. The use of historical flow data for e-flow release criteria determination neglects the uncertainty of flows [42]. It is necessary to establish new methods to optimize e-flow release criteria accounting for flow uncertainty.

Shiau and Wu's research was performed for the rivers regulated by weirs. It is just a simple scenario in e-flow release criterion determination, but it can serve as a significant

foundation for future research on more complex river conditions with cascade dams. In this research, we also consider this basic scenario and extend the previous research by accounting for flow uncertainty. To incorporate the uncertainty of flows into the process of e-flow criterion determination, in the method section the scenario tree method is applied to generate flow scenarios that can effectively cover the possible conditions of flows. The RVA is refined to suit the uncertainty of flows and is used to measure the degree of flow regime alteration. The metric for water supply reliability is also refined due to the flow uncertainty. In the case study section, the Tang River in Northern China is applied to test the effectiveness of the new method.

2. Method

2.1. Scenario Tree

Scenario tree approach is a commonly used method to generate the possible scenarios of flows. It is effective to realize the twin goals of covering the possible scenarios of flows and reducing the computing time for optimizing water resources management parameters by combining and reducing similar flow scenarios. It is widely used in water resources management, and is also adopted in this research [43–46].

A scenario tree may be represented by a finite set of nodes. It starts from the root node at the first period and eventually branches into nodes at the next period. Each node has a unique predecessor node, but possibly several successors. The branching continues up to nodes at the final period whose number corresponds to the number of scenarios. Each possible discrete outcome is called a scenario. The generated set of scenarios, with the corresponding probabilities, can be viewed as a representation of the underlying probability distribution [47].

Constructing the scenario tree involves two steps, that is, scenario generation and scenario reduction. In the step of scenario generation, a scenario tree is firstly generated which can represent sufficiently well the historical data. Sampling from historical time series or from statistical models is the most popular method for generating scenarios. The resulting tree may be much larger than the desired size, because too many scenarios may lead to a dimensionality problem. So in the step of scenario reduction, the number of scenarios is reduced to reach the size limit that is still a sufficient good approximation of the original one [44]. The reduction algorithms based on Kantorovich distance not only consider distances, but also the probabilities of the scenarios, in order to avoid the important information might be lost. Scenarios are deleted if the Kantorovich distance near to some other scenario. In each step one scenario is deleted and the probability of the deleted scenario is added to the nearest scenarios. This deleting procedure is applied iteratively, until a given number of scenarios is remaining. The details for scenario generation and reduction can refer to Brand et al. [48].

Based on the scenario tree approach, a specified number of scenarios of flows can be generated. In this research, one scenario is the daily flows for one year. The sum of all probabilities of the remaining scenarios should remain equal to 1.

2.2. Refined RVA under Flow Uncertainty

The RVA is the most commonly used method to assess the degree of flow regime alteration. In RVA, 32 Indicators of Hydrological Alteration (IHAs) are adopted (Table 1). These IHAs are

divided into five groups, that is, magnitude, duration, timing, frequency, and rate of change [17]. According to the RVA, a range of variation for each IHA is derived from the natural hydrological time series and is set as the flow management target. The range of the 25th and 75th percentiles of the natural daily flows has been recommended as the management target [18]. The degree of alteration, D_m, is used to measure the deviation of the impacted flow regime from the natural one for the mth hydrological indicator, which is defined by

$$D_m = \left| \frac{N_{o,m} - N_{e,m}}{N_{e,m}} \right| \times 100\%, \tag{2.1}$$

where $N_{o,m}$ is the observed number of postimpact years in which the value of the mth hydrological indicator falls within its RVA target range; $N_{e,m}$ is the expected number of post-impact years in which the indicator value falls within the RVA target range.

Equation (2.1) is from the original RVA, which does not account for the possibility of the flow time series in each year. To take into account the possibility of flows of each year, (2.1) could be replaced by the following equation:

$$D_m = \left| \frac{N_{o,m}/N_m - N_{e,m}/N_m}{N_{e,m}/N_m} \right| \times 100\% = \left| \frac{p_{o,m} - 50\%}{50\%} \right| \times 100\%, \tag{2.2}$$

where N_m is the observed number of post-impact years; $p_{o,m}$ is the possibility of post-impact years in which the value of the mth hydrological indicator falls within its RVA target range. $N_{e,m}/N_m$ is replaced by 50%, because the expected possibility of post-impact years in which the value of the mth hydrological indicator falls within 25th and 75th percentile is equal to 50%.

Equation (2.2) could be further replaced by (2.3) by incorporating the possibility of the flow time series in each year

$$D_m = \left| \frac{\sum p_{i,m} - 50\%}{50\%} \right| \times 100\%, \tag{2.3}$$

where $p_{i,m}$ is the possibility of the ith flow scenario under which the value of the mth hydrological indicator falls within its RVA target range. $\sum p_{i,m}$ is not equal to 1 in this formula, because the indicator values of only a few post-impacted flow scenarios can fall within 25th and 75th percentiles.

Then, the overall degree of hydrologic alteration (D_o) is defined as follows:

$$D_o = \frac{1}{32} \sum_{m=1}^{32} D_m. \tag{2.4}$$

The degree of flow regime alteration could be further categorized into three levels: low alterations (values of D between 0 and 0.33), moderate alterations (values of D between 0.33 and 0.67), and high alterations (values of D between 0.67 and 1.0) [49].

Table 1: Hydrological alterations corresponding to the optimal e-flow release criterion under flow uncertainty.

IHA group	IHA	Values
Group 1: magnitude of monthly flow conditions	Mean flow in January	1
	Mean flow in February	1
	Mean flow in March	1
	Mean flow in April	1
	Mean flow in May	1
	Mean flow in June	1
	Mean flow in July	0.71
	Mean flow in August	0.68
	Mean flow in September	0.82
	Mean flow in October	1
	Mean flow in November	1
	Mean flow in December	1
Group 2: magnitude and duration of annual extreme flow conditions and base flow condition	Annual 1-day minimum flow	0.11
	Annual 1-day maximum flow	0.22
	Annual 3-day minimum flow	0.17
	Annual 3-day maximum flow	0
	Annual 7-day minimum flow	0.02
	Annual 7-day maximum flow	0.56
	Annual 30-day minimum flow	0.11
	Annual 30-day maximum flow	0.84
	Annual 90-day minimum flow	1
	Annual 90-day maximum flow	1
	7-day minimum flow divided by mean flow in each year	0.78
Group 3: timing of annual extreme flow conditions	Date of annual 1-day maximum flow	0.11
	Date of annual 1-day minimum flow	0.12
Group 4: frequency and duration of high and low pulses	Number of high pulses in each year	0.13
	Number of low pulses in each year	0.3
	Mean duration of high pulse in each year	0.02
	Mean duration of low pulse in each year	0.01
Group 5: rate and frequency of flow condition changes	Mean of all positive differences between consecutive daily flows	0.45
	Mean of all negative differences between consecutive daily flows	0.45
	Number of flow reversals	1

2.3. *Refined Metric for Water Supply Reliability*

The water supply reliability is defined as the ratio of the overall actual water supply to humans and the overall planned water supply over a planned period [11]. Equation (2.5) is the previous metric for water supply reliability, which does not account for the flow uncertainty

$$R = \frac{\sum_{j=1}^{T} \sum_{i=1}^{365} RW_{ij}}{\sum_{j=1}^{T} \sum_{i=1}^{365} PW_{ij}}, \tag{2.5}$$

where R is the water supply reliability; T is the number of years during the planned water supply period; RW_{ij} is the actual water supply to humans for the ith day jth year; PW_{ij} is the planned water supply to humans for the ith day jth year.

Based on (2.5), we could further develop the metric for water supply reliability accounting for the possibility of flow scenarios (see (2.6)). Here, we assume the planned water supply for each year is the same. In fact, many cases of real-world water supplies meet this assumption during a planned horizon [4, 11]

$$R = \frac{\sum_{j=1}^{T} \sum_{i=1}^{365} RW_{ij}}{T \sum_{i=1}^{365} PW_{ij}} = \frac{\sum_{j=1}^{T} R_j}{T} = \sum_{k=1}^{N} p_k \times R_k, \tag{2.6}$$

where R_j is the water supply reliability for year j; N is the scenario number after scenario reduction; R_k is the water supply reliability for flow scenario k; p_k is the possibility of flow scenario k.

2.4. Water Diversion Model

In this research, we consider the rivers regulated by weirs. The priority-based weir management model is suitable for water diversion management [4]. We adopt the water diversion model by Shiau and Wu [30, 31, 50, 51] for e-flow release and water diversion. The model is as follows:

$$\begin{aligned}
&\text{If } Q_{N,k} < Q_{\text{IF}}, \text{ then } Q_{E,k} = Q_{N,k}, \text{ and } RQ_{U,k} = 0,\\
&\text{If } Q_{\text{IF}} \le Q_{N,k} < D_{U,k} + Q_{\text{IF}}, \text{ then } Q_{E,k} = Q_{\text{IF}}, \text{ and } RQ_{U,k} = Q_{N,k} - Q_{\text{IF}},\\
&\text{If } Q_{N,k} \ge D_{U,k} + Q_{\text{IF}}, \text{ then } Q_{E,k} = Q_{N,k} - D_{U,k}, \text{ and } RQ_{U,k} = D_{U,k},
\end{aligned} \tag{2.7}$$

where $Q_{N,k}$ is the inflow to the diversion on day k; Q_{IF} is the e-flow release criterion, which is employed to meet environmental flow requirement, and this parameter will be optimized in this paper; $Q_{E,k}$ is the actual flow released to the downstream river on day k; $D_{U,k}$ is the planned water supply to human beings on day k; $RQ_{U,k}$ is the actual water supply to human beings on day k.

2.5. Objective of E-Flow Release Criterion Optimization

Increasing water supply reliability and reducing the degree of flow regime alteration are the two conflicting objectives for water resources management. It is a typical multiobjective optimization. To find the optimal e-flow release criteria, it is necessary to integrate the two objectives into one objective. Based on the method of compromise programming [42, 51–53], the combined objective is as follows:

$$\text{Min} \left[w_D \left(\frac{D_o - D_{o,\min}}{D_{o,\max} - D_{o,\min}} \right)^2 + w_R \left(\frac{R_{\max} - R}{R_{\max} - R_{\min}} \right)^2 \right]^{1/2}, \tag{2.8}$$

where $D_{o,\max}$ and $D_{o,\min}$ are the maximum and minimum values of the overall degree of hydrological alteration. $R_{\max}$ and $R_{\min}$ are the maximum and minimum values of water supply reliability. W_D and W_R are weighting factors for hydrological alteration and water supply reliability, respectively. As an example, in this research they are set at 0.5, indicating an equal position for human and riverine ecosystems.

3. Case Study

The Tang River is an important river in northern China. It is about 123 km long, with a drainage area of 1462 km^2. The river is mainly used for water supply. It provides water for four major water users: the Liaoning Chemical Industry Group, the Anshan Domestic Water Supply Company, the Liaoyang Domestic Water Supply Company, and the Gongchangling Mine Industry Company. The current planned water supplies for these users are 54.8×10^6, 73×10^6, 36.5×10^6, and 18.3×10^6 m^3 each year, respectively. It is the main drinking water source of Liaoyang City. Due the diversion of large amount of water for the river, severe degradation has occurred in the river ecosystem. It is urgent to balance the water requirements of human beings and rivers. To demonstrate the methods established above, we assume all the planned water supplies are withdrawn from a weir on the river. The daily runoff data from 1950 to 1969 at the Tanghe gauge station are used in this paper.

4. Results

Based on the historical runoff data, the scenario tree approach is applied to generate the possible scenarios of flows. 2000 scenarios of flows are generated and are then reduced to 200 scenarios. In this research, the e-flow release criterion Q_{IF} is assumed to be constant for each month. The optimal value for Q_{IF} is determined by exploring all the values of Q_{IF} between 0 m^3/s and the 5.8 m^3/s (the mean annual flow) with an increment of 0.1 m^3/s and evaluating the effects of different Q_{IF} on the hydrological alterations and water supply reliability. Under the present water supply of 5.8 m^3/s, the minimum and maximum water supply reliabilities are 0.2 and 0.58, and the minimum and maximum degrees of flow regime alteration are 0.48 and 0.81, respectively. According to (2.8), the optimal e-flow release criterion is 1.2 m^3/s. The corresponding overall hydrological alteration and water supply reliability are 0.58 and 0.47, respectively. The very low reliability of water supply is due to the high planned water supply (approaching to the mean annual water supply) and the inability of weir to store water. The flow alteration degrees for the 32 IHAs are listed in Table 1.

Hydrological Alterations of Indicators in Group 1

The alteration degrees for the indicators related to monthly magnitude are all in the category of high alteration. It is due to the high planned water supply to humans. The ecological functions closely related to the monthly flows, such as the provision of habitat in river channels, will be severely disturbed. Interestingly, the alteration degrees for the monthly flows in July, August, and September are relatively lower. It is because the three months are in the flood season and many high flows could be released following the present water diversion and e-flow release model during these three months.

Hydrological Alterations of Indicators in Group 2

The alteration degrees for 1-, 3-, 7-, and 30-day minimum flows and the 1-, 3-, and 7-day maximum flows are all in the category of low alterations. It indicates the ecological functions related to extreme flow magnitude could be effectively maintained. The other indicators are in the category of moderate or high alterations because these indicators are similar to the monthly flows that are significantly influenced by the high planned yield.

Hydrological Alterations of Indicators in Group 3

The alteration degrees for the date of extreme flows are all in the categories of low flows. The timing of annual extremes significantly influence the start of life cycle of aquatic organisms. Maintaining the timing of annual extremes are possibly more important than the maintenance of the magnitude of annual extreme in terms of the life cycle of aquatic organisms [25, 54].

Hydrological Alterations of Indicators in Group 4

The alterations degrees for the indicators of frequency and duration of high and low pulses are all in the category of low alteration. The low alteration of these indicators is significant to sustain the ecological functions related to the high flow pulses such as the provision of access by fish to floodplains for feeding, spawning, and nursery areas and the determination of the streambed substrate size, and the functions related to extreme low flows such as the elimination of exotic species.

Hydrological Alterations of Indicators in Group 5

The indicators related to the rate of flow changes and flow reversals are in moderate or high degree. It mainly stems from the reduction of flow reversal when the flows are between the e-flow release criteria and the sum of the release criteria and the planned yield.

5. Discussion

5.1. Comparison of the Optimal Results with and without Considering the Flow Uncertainty

In the above section, the planned water supply is $5.8\,m^3/s$. We further set the planned yield between $1\,m^3/s$ and $6\,m^3/s$ with an increment of $1\,m^3/s$. Under these planned yields, the optimal e-flow criteria and the corresponding degree of flow regime alteration and water supply reliability are determined with and without accounting for flow uncertainty, respectively. The results are shown in Table 2.

Table 2 shows the optimal e-flow criteria under flow uncertainty are obviously lower than those without taking into account the flow uncertainty. Thus, without taking into account the flow uncertainty, the water resources managers tend to sustain more water in the river ecosystems. The obvious difference of e-flow criteria under the two conditions further demonstrates the needs of considering flow uncertainty. The degrees of flow regime alteration under the flow uncertainty will be in the category of moderate alteration, while the alteration degrees without considering the flow uncertainty are all in the category of low alteration. The higher alteration degree stems from the lower e-flow release criteria. It indicates that

Table 2: The optimal results for different planned water supplies.

Planned water supply (m^3/s)	Flow uncertainty			Historical data		
	E-flow release criterion (m^3/s)	Hydrological alteration	Water supply reliability	E-flow release criterion (m^3/s)	Hydrological alteration	Water supply reliability
1	1.2	0.37	0.69	4.4	0.11	0.65
2	1	0.49	0.66	3.2	0.12	0.70
3	1	0.52	0.60	3.4	0.15	0.65
4	1.2	0.52	0.54	3.9	0.19	0.58
5	1.2	0.54	0.50	3.7	0.22	0.56
6	1.8	0.54	0.41	4.1	0.22	0.51

without taking into account the flow uncertainty the optimized e-flow criteria will be positive to the maintenance of natural flow regime and consequently the better protection of riverine ecosystems. The water supply reliabilities under the two scenarios generally do not show obvious difference. It indicates the major influence of incorporating flow uncertainty is on e-flow release criteria and the corresponding degree of flow regime alteration, while the influence on human water supply is very limited.

Because it is too tedious to compare the difference of alteration degree for each of the 32 IHAs between the uncertain and certain flows, we compare the difference for the average values for the five groups. The results are shown in Figure 1. Under inflow uncertainty, the alteration degree for the magnitude of monthly flows (group 1), magnitude and duration of annual extreme flows (group 2), timing of annual extreme flow conditions (group 3) and rate and frequency of flow condition changes (group 5) are always greater than that under the certain flows (the historical data), while only the frequency and duration of high and low pulses (group 4) show lower alteration degrees for some planned yields.

5.2. Effects of Changing Both E-Flow Release Criteria and Planned Yields

Besides the optimal e-flow criteria which have been discussed above, the water resources managers are also interested in the effects of different combination of e-flow criteria and planned yields on water supply reliability and flow regime alteration. Here, we further determine the water supply reliability and flow regime alteration under different combination of e-flow criteria and planned yields. Both the planned water supply and the e-flow release criteria vary from 0 to 6.3 m^3/s (average runoff from 1950 to 1969 at Tanghe gauge station) with an increment of 0.1 m^3/s, which forms 4096 e-flow criteria and water diversion scenarios.

Figure 2 shows the water supply reliability under various combinations of e-flow release criteria and planned water diversion. Higher water supply reliability mainly locates in the lower left corner of the contour map, that is, low e-flow release criteria and low planned water supply. Despite the high water supply reliability, these combinations of e-flow and water supply are not recommended due to the low volume of the total water supply. Lower water supply reliability appears in the upper right corner of the contour map, that is, high e-flow release criteria and high planned water supply. Besides, the distance between two contour curves decreases with the increase of the reliability. It indicates that under the high

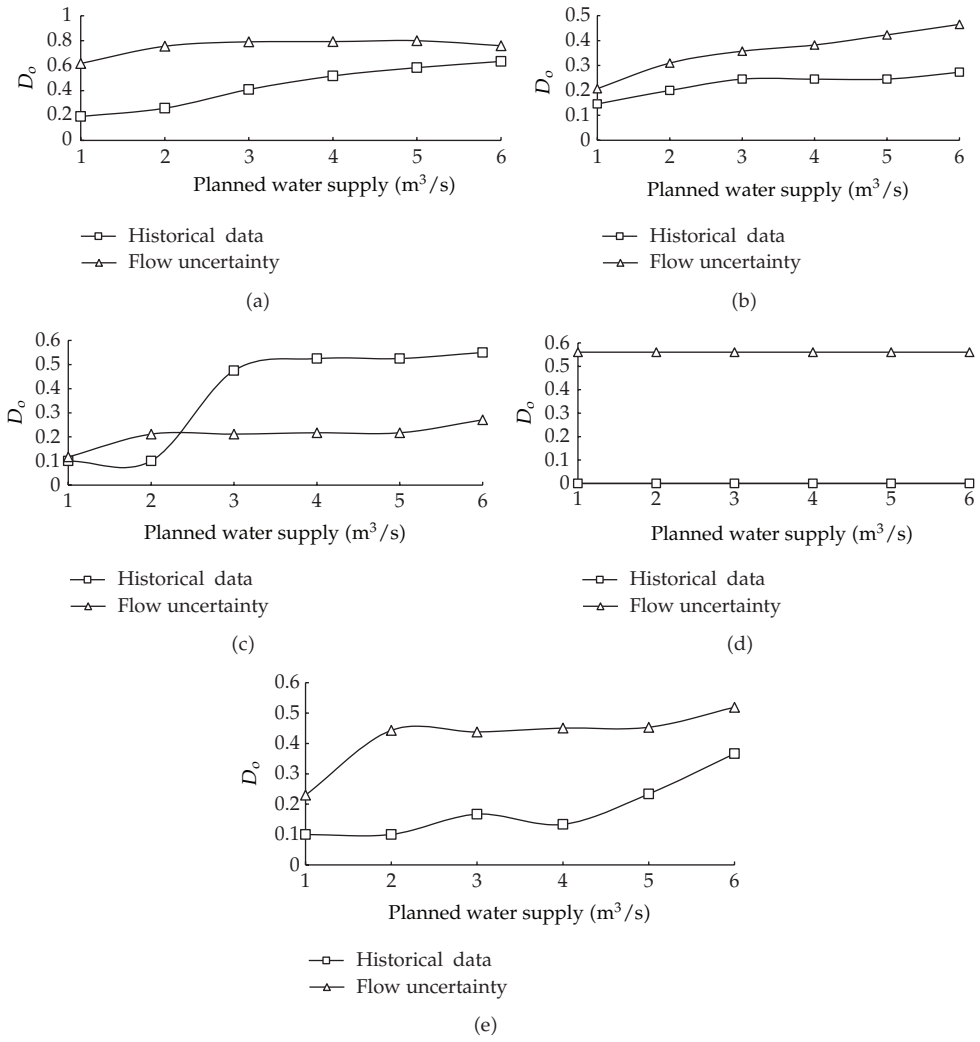

Figure 1: The average hydrological alteration degree of each group of IHAs with and without the consideration of flow uncertainty. (a) group 1; (b) group 2; (c) group 3; (d) group 4; (e) group 5.

water supply reliability the reliability is more sensitive to the change of e-flow criteria and planned water supply than that under low reliability.

Figure 3 shows the overall hydrological alteration for different e-flow criteria and planned water supply. When the planned water supply is no more than 2.8 m^3/s, the degree of flow regime alteration will be always in the category of low alteration (less than 0.33). From the perspective of riverine ecosystem protection, it is recommended to set the planned water supply no more than 2.8 m^3/s. In addition, when the e-flow release criterion is less than 1 m^3/s and the planned water supply is greater than 1.3 m^3/s, the degree of flow regime alteration is always in the category of high alterations. The e-flow release and water supply combination within this region should be avoided to protect the riverine ecosystem. Thus, although the planned water supply and e-flow release criteria can influence the degree of flow regime alteration simultaneously, the low and high alteration degree is corresponding to

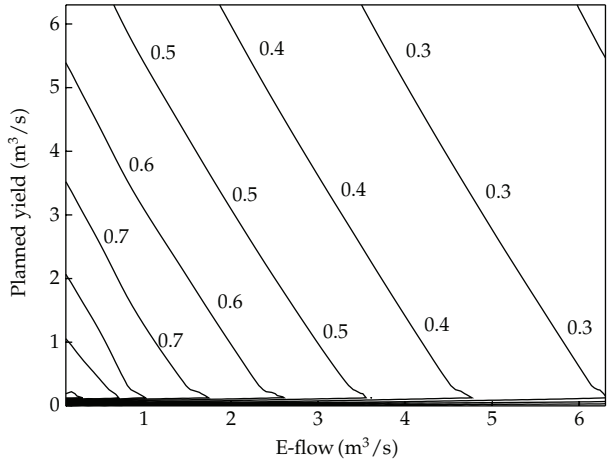

Figure 2: Contour map of the water supply reliabilities under different e-flow release criteria and planned yields.

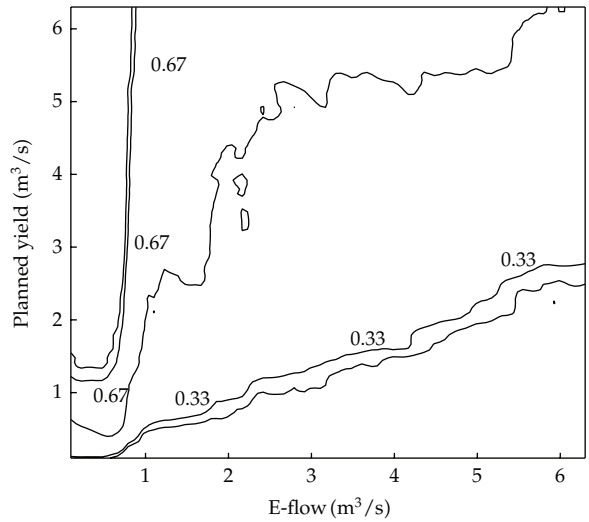

Figure 3: Contour map of the degree of flow regime alteration under different e-flow release criteria and planned yields.

limited ranges of e-flow release criteria and planned water supply. The identified ranges are helpful for the water resources managers to design suitable combinations of planned water supply and e-flow release criteria.

6. Conclusions

In this study, a method is developed to determine the optimal e-flow release criteria accounting for the uncertainty of flows. The scenario tree method is applied to generate the scenarios of flows and to reduce the flow scenarios to specified number of scenarios. The reduced scenarios can sufficiently cover the possible flow conditions and can effectively

reflect the uncertainty of flows. The RVA, a widely used method to assess the flow regime alteration, is refined by incorporating the uncertainty of flows. The metric for water supply reliability is also modified through the incorporation of the possibility of each flow scenarios. The new method is applied to the Tang River to demonstrate its effectiveness. The following conclusions are drawn.

(i) The previous method for e-flow criteria determination is based on the historical flow time series without the consideration of flow uncertainty. The case study shows the previous method obviously overestimates the optimal e-flow release criteria suitable for both humans and ecosystems. Because the historical flow time series will not occur again and the future flows are still uncertain, the flow uncertainty needs be integrated in the process of e-flow release criteria.

(ii) Although the planned water supply and e-flow release criteria can influence the degree of flow regime alteration simultaneously, the low and high alteration degree may be corresponding to limited ranges of e-flow release criteria and planned water supply. For example, in this research, the low degree of the overall flow regime alteration is mainly corresponding to the planned yield no more than $2.8\,m^3/s$, while the high alteration degree is mainly corresponding to the e-flow release criteria less than $1\,m^3/s$. The identified ranges can help the water resources managers design suitable combinations of planned water supply and e-flow release criteria.

Acknowledgments

The authors thank the International Science and Technology Cooperation Program of China (no. 2011DFA72420), the National Science Foundation for Innovative Research Group (no. 51121003), and National Natural Science Foundation of China (no. 50939001) for their financial support.

References

[1] G. E. Petts, "Instream flow science for sustainable river management," *Journal of the American Water Resources Association*, vol. 45, no. 5, pp. 1071–1086, 2009.

[2] R. A. Wurbs, "Modeling river/reservoir system management, water allocation, and supply reliability," *Journal of Hydrology*, vol. 300, no. 1–4, pp. 100–113, 2005.

[3] B. Rajagopalan, K. Nowak, J. Prairie et al., "Water supply risk on the Colorado River: can management mitigate?" *Water Resources Research*, vol. 45, no. 8, Article ID W08201, 2009.

[4] X. A. Yin and Z. F. Yang, "Development of a coupled reservoir operation and water diversion model: balancing human and environmental flow requirements," *Ecological Modelling*, vol. 222, no. 2, pp. 224–231, 2011.

[5] S. K. Jain, "Assessment of environmental flow requirements," *Hydrological Processes*, vol. 26, no. 22, pp. 3472–3476, 2012.

[6] M. A. Palmer, C. A. Reidy Liermann, C. Nilsson et al., "Climate change and the world's river basins: anticipating management options," *Frontiers in Ecology and the Environment*, vol. 6, no. 2, pp. 81–89, 2008.

[7] P. B. McIntyre, S. Glidden, S. E. Bunn, C. A. Sullivan, C. R. Liermann, and P. M. Davies, "Global threats to human water security and river biodiversity," *Nature*, vol. 467, no. 7315, pp. 555–561, 2010.

[8] K. H. Bowmer, "Water resource protection in Australia: links between land use and river health with a focus on stubble farming systems," *Journal of Hydrology*, vol. 403, no. 1-2, pp. 176–185, 2011.

[9] R. M. Vogel, J. Sieber, S. A. Archfield, M. P. Smith, C. D. Apse, and A. Huber-Lee, "Relations among storage, yield, and instream flow," *Water Resources Research*, vol. 43, no. 5, Article ID W05403, 2007.

[10] Z. F. Yang, T. Sun, B. S. Cui, B. Chen, and G. Q. Chen, "Environmental flow requirements for integrated water resources allocation in the Yellow River Basin, China," *Communications in Nonlinear Science and Numerical Simulation*, vol. 14, no. 5, pp. 2469–2481, 2009.
[11] X.-A. Yin, Z.-F. Yang, and G. E. Petts, "Reservoir operating rules to sustain environmental flows in regulated rivers," *Water Resources Research*, vol. 47, no. 8, Article ID 7206, 2011.
[12] N.-S. Hsu, C.-H. Chiang, W.-M. Cheng, and C.-C. Wei, "Study on the trade-off between ecological base flow and optimized water supply," *Water Resources Management*, vol. 26, no. 11, pp. 3095–3112, 2012.
[13] M. R. Su, Z. F. Yang, G. Y. Liu, and B. Chen, "Ecosystem health assessment and regulation for urban ecosystems: a case study of the yangtze river delta urban cluster, China," *Journal of Environmental Informatics*, vol. 18, no. 2, pp. 65–74, 2011.
[14] C. Zheng, W. Yang, and Z. F. Yang, "Strategies for managing environmental flows based on the spatial distribution of water quality: a case study of Baiyangdian Lake, China," *Journal of Environmental Informatics*, vol. 18, no. 2, pp. 84–90, 2011.
[15] L. Jing and B. Chen, "Field investigation and hydrological modelling of a subarctic wetland-the Deer River watershed," *Journal of Environmental Informatics*, vol. 17, no. 1, pp. 36–45, 2011.
[16] M. C. Acreman and A. J. D. Ferguson, "Environmental flows and the European Water Framework Directive," *Freshwater Biology*, vol. 55, no. 1, pp. 32–48, 2010.
[17] B. D. Richter, "A method for assessing hydrologic alteration within ecosystems," *Conservation Biology*, vol. 10, no. 4, pp. 1163–1174, 1996.
[18] B. D. Richter, J. V. Baumgartner, R. Wigington, and D. P. Braun, "How much water does a river need?" *Freshwater Biology*, vol. 37, no. 1, pp. 231–249, 1997.
[19] M. J. Kennard, B. J. Pusey, J. D. Olden, S. J. MacKay, J. L. Stein, and N. Marsh, "Classification of natural flow regimes in Australia to support environmental flow management," *Freshwater Biology*, vol. 55, no. 1, pp. 171–193, 2010.
[20] D. L. Tennant, "Instream flow regimens for fish, wildlife, recreation and related environmental resources," *Fisheries*, vol. 1, no. 4, pp. 6–10, 1976.
[21] K. D. Bovee, B. L. Lamb, J. M. Bartholow, C. B. Stalnaker, J. G. Taylor, and J. Henriksen, *Stream Habitat Analysis Using the Instream Flow Incremental Methodology*, US. Fish and Wildlife Service, 1998.
[22] N. L. Poff, B. D. Richter, A. H. Arthington et al., "The ecological limits of hydrologic alteration (ELOHA): a new framework for developing regional environmental flow standards," *Freshwater Biology*, vol. 55, no. 1, pp. 147–170, 2010.
[23] O. T. Gorman and J. R. Karr, "Habitat structure and stream fish communities," *Ecology*, vol. 59, pp. 507–515, 1978.
[24] N. L. Poff and J. V. Ward, "Physical habitat template of lotic systems: recovery in the context of historical pattern of spatiotemporal heterogeneity," *Environmental Management*, vol. 14, no. 5, pp. 629–646, 1990.
[25] D. A. Lytle and N. L. Poff, "Adaptation to natural flow regimes," *Trends in Ecology and Evolution*, vol. 19, no. 2, pp. 94–100, 2004.
[26] A. H. Arthington, S. E. Bunn, N. L. Poff, and R. J. Naiman, "The challenge of providing environmental flow rules to sustain river ecosystems," *Ecological Applications*, vol. 16, no. 4, pp. 1311–1318, 2006.
[27] N. L. Poff and J. K. H. Zimmerman, "Ecological responses to altered flow regimes: a literature review to inform the science and management of environmental flows," *Freshwater Biology*, vol. 55, no. 1, pp. 194–205, 2010.
[28] S. Postel and B. Richter, *Rivers for Life: Managing Water for People and Nature*, Island Press, Washington, DC, USA, 2003.
[29] A. F. Casper, B. Dixon, J. Earls, and J. A. Gore, "Linking a spatially explicit watershed model (SWAT) with an in-stream fish habitat model (PHABSIM): a case study of setting minimum flows and levels in a low gradient, sub-tropical river," *River Research and Applications*, vol. 27, no. 3, pp. 269–282, 2011.
[30] J. T. Shiau and F. C. Wu, "Feasible diversion and instream flow release using range of variability approach," *Journal of Water Resources Planning and Management*, vol. 130, no. 5, pp. 395–404, 2004.
[31] J. T. Shiau and F. C. Wu, "Compromise programming methodology for determining instream flow under multiobjective water allocation criteria," *Journal of the American Water Resources Association*, vol. 42, no. 5, pp. 1179–1191, 2006.
[32] J. W. Labadie, "Optimal operation of multireservoir systems: state-of-the-art review," *Journal of Water Resources Planning and Management*, vol. 130, no. 2, pp. 93–111, 2004.
[33] N. K. Ajami, G. M. Hornberger, and D. L. Sunding, "Sustainable water resource management under hydrological uncertainty," *Water Resources Research*, vol. 44, no. 11, Article ID W11406, 2008.

[34] Y. P. Li and G. H. Huang, "Fuzzy-stochastic-based violation analysis method for planning water resources management systems with uncertain information," *Information Sciences*, vol. 179, no. 24, pp. 4261–4276, 2009.
[35] Y. P. Li, G. H. Huang, Y. F. Huang, and H. D. Zhou, "A multistage fuzzy-stochastic programming model for supporting sustainable water-resources allocation and management," *Environmental Modelling and Software*, vol. 24, no. 7, pp. 786–797, 2009.
[36] Y. P. Li, G. H. Huang, and S. L. Nie, "Planning water resources management systems using a fuzzy-boundary interval-stochastic programming method," *Advances in Water Resources*, vol. 33, no. 9, pp. 1105–1117, 2010.
[37] Y. P. Li and G. H. Huang, "Inexact joint-probabilistic stochastic programming for water resources management under uncertainty," *Engineering Optimization*, vol. 42, no. 11, pp. 1023–1037, 2010.
[38] Y. P. Li, G. H. Huang, S. L. Nie, and X. Chen, "A robust modeling approach for regional water management under multiple uncertainties," *Agricultural Water Management*, vol. 98, no. 10, pp. 1577–1588, 2011.
[39] M. Q. Suo, Y. P. Li, and G. H. Huang, "An inventory-theory-based interval-parameter two-stage stochastic programming model for water resources management," *Engineering Optimization*, vol. 43, no. 9, pp. 999–1018, 2011.
[40] Y. O. Kim, H. I. Eum, E. G. Lee, and I. H. Ko, "Optimizing operational policies of a Korean multireservoir system using sampling stochastic dynamic programming with ensemble streamflow prediction," *Journal of Water Resources Planning and Management*, vol. 133, no. 1, pp. 4–14, 2007.
[41] M. J. Kennard, S. J. Mackay, B. J. Pusey, J. D. Olden, and N. Marsh, "Quantifying uncertainty in estimation of hydrologic metrics for ecohydrological studies," *River Research and Applications*, vol. 26, no. 2, pp. 137–156, 2010.
[42] J. T. Shiau and F. C. Wu, "A histogram matching approach for assessment of flow regime alteration: application to environmental flow optimization," *River Research and Applications*, vol. 24, no. 7, pp. 914–928, 2008.
[43] H. Liu, C. Jiang, and Y. Zhang, "Portfolio management of hydropower producer via stochastic programming," *Energy Conversion and Management*, vol. 50, no. 10, pp. 2593–2599, 2009.
[44] K. Høyland and S. W. Wallace, "Generating scenario trees for multistage decision problems," *Management Science*, vol. 47, no. 2, pp. 295–307, 2001.
[45] D. W. Watkins Jr., D. C. McKinney, L. S. Lasdon, S. S. Nielsen, and Q. W. Martind, "A scenario-based stochastic programming model for water supplies from the highland lakes," *International Transactions in Operational Research*, vol. 7, no. 3, pp. 211–230, 2000.
[46] S. Wang and G. H. Huang, "Identifying optimal water resources allocation strategies through an interactive multi-stage stochastic fuzzy programming approach," *Water Resources Management*, vol. 26, no. 7, pp. 2015–2038, 2012.
[47] J. Dupačová, G. Consigli, and S. W. Wallace, "Scenarios for multistage stochastic programs," *Annals of Operations Research*, vol. 100, pp. 25–53, 2000.
[48] H. Brand, E. Thorin, and C. Weber, "Scenario reduction algorithm and creation of multi-stage scenario trees," Optimization of Cogeneration Systems in a Competitive Market Environment, Discussion Paper no. 7, 2002.
[49] B. D. Richter, J. V. Baumgartner, D. P. Braun, and J. Powell, "A spatial assessment of hydrologic alteration within a river network," *River Research and Applications*, vol. 14, no. 4, pp. 329–340, 1998.
[50] J. T. Shiau and F. C. Wu, "Assessment of hydrologic alterations caused by chi-chi diversion weir in Chou-Shui Creek, Taiwan: opportunities for restoring natural flow conditions," *River Research and Applications*, vol. 20, no. 4, pp. 401–412, 2004.
[51] J. T. Shiau and F. C. Wu, "Pareto-optimal solutions for environmental flow schemes incorporating the intra-annual and interannual variability of the natural flow regime," *Water Resources Research*, vol. 43, no. 6, Article ID W06433, 2007.
[52] O. Marinoni, A. Higgins, S. Hajkowicz, and K. Collins, "The multiple criteria analysis tool (MCAT): a new software tool to support environmental investment decision making," *Environmental Modelling and Software*, vol. 24, no. 2, pp. 153–164, 2009.
[53] P. Fattahi and S. Fayyaz, "A compromise programming model to integrated urban water management," *Water Resources Management*, vol. 24, no. 6, pp. 1211–1227, 2010.
[54] G. E. Petts, *Impounded Rivers: Perspectives for Ecological Management*, Environmental Monographs and Symposia Series, John Wiley and Sons, Chichester, UK, 1984.